DESIGN OF MICROWAVE FILTERS,

IMPEDANCE-MATCHING NETWORKS, AND COUPLING STRUCTURES

VOLUME II

By: G. L. Matthaei   Leo Young   E. M. T. Jones

STANFORD RESEARCH INSTITUTE

MENLO PARK, CALIFORNIA   *SRI

402 930

DESIGN OF MICROWAVE FILTERS,

IMPEDANCE-MATCHING NETWORKS, AND COUPLING STRUCTURES

VOLUME II

Prepared for:

By: G. L. Matthaei   Leo Young   E. M. T. Jones

SRI Project No. 3527

*Objective: To advance the state of the art in the field of microwave filters
and coupling structures through applied research and development.*

Approved:

G. L. MATTHAEI, MANAGER   ELECTROMAGNETIC TECHNIQUES LABORATORY

D. R. SCHEUCH, DIRECTOR   ELECTRONICS AND RADIO SCIENCES DIVISION

ABSTRACT OF VOLUMES I AND II.

This book presents design techniques for a wide variety of low-pass, band-pass, high-pass, and band-stop microwave filters; for multiplexers; and for certain kinds of directional couplers. The material is organized to be used by the designer who needs to work out a specific design quickly, with a minimum of reading, as well as by the engineer who wants a deeper understanding of the design techniques used, so that he can apply them to new and unusual situations.

Most of the design procedures described make use of either a lumped-element low-pass prototype filter or a step-transformer prototype as a basis for design. Using these prototypes, microwave filters can be obtained which derive response characteristics (such as a Tchebyscheff attenuation ripples in the pass band) from their prototype. Prototype filter designs are tabulated, and data is given relevant to the use of prototype filters as a basis for the design of impedance-matching networks and time-delay networks. Design formulas and tables for step-transformer prototypes are also given.

The design of microwave filter structures to serve as impedance-matching networks is discussed, and examples are presented. The techniques described should find application in the design of impedance-matching networks for use in microwave devices such as tubes, parametric devices, antennas, etc., in order to achieve efficient broad-band operation. The design of microwave filters to achieve various time-delay (or slow-wave) properties is also discussed.

Various equations, graphs, and tables are collected together relevant to the design of coaxial lines, strip-lines, waveguides, parallel-coupled lines between common ground planes, arrays of lines between ground planes, coupling and junction discontinuities, and resonators. Techniques for measuring the Q's of resonators and the coupling coefficients between resonators are also discussed, along with procedures for tuning filters. Equations and principles useful in the analysis of filters are collected

together for easy reference and to aid the reader whose background for
the subject matter of this book may contain some gaps.

Directional filters have special advantages for certain applica-
tions, and are treated in detail in a separate chapter, as are high-
power filters. Tunable filters of the kind that might be desired for
preselector applications are also treated. Both mechanically tunable
filters and filters using ferrimagnetic resonators, which can be tuned
by varying a biasing magnetic field, are discussed.

The organization of this book has three general objectives. The first objective is to present fundamental concepts, techniques, and data that are of general use in the design of the wide range of microwave structures discussed in this book. The second objective is to present specialized data in more or less handbook form so that a designer can work out practical designs for structures having certain specific configurations, without having to recreate the design theory or the derivation of the equations. (However, the operation of most of the devices discussed herein is sufficiently complex that knowledge of some of the basic concepts and techniques is usually important.) The third objective is to present the theory upon which the various design procedures are based, so that the designer can adapt the various design techniques to new and unusual situations, and so that researchers in the field of microwave devices may use some of this information as a basis for deriving additional techniques. The presentation of the material so that it can be adapted to new and unusual situations is important because many of the microwave filter techniques described in this book are potentially useful for the design of microwave devices not ordinarily thought of as having anything to do with filters. Some examples are tubes, parametric devices, and antennas, where filter structures can serve as efficient impedance-matching networks for achieving broad-band operation. Filter structures are also useful as slow-wave structures or time-delay structures. In addition, microwave filter techniques can be applied to other devices not operating in the microwave band of frequencies, as for instance to infrared and optical filters.

The three objectives above are not listed in any order of importance, nor is this book entirely separated into parts according to these objectives. However, in certain chapters where the material lends itself to such organization, the first section or the first few sections discuss general principles which a designer should understand in order to make best use of the design data in the chapter, then come sections giving design data

for specific types cf structures, and the end of the chapter discusses the derivations of the various design equations. Also, at numerous places cross references are made to other portions of the book where information useful for the design of the particular structure under consideration can be found. For example, Chapter 11 describes procedures for measuring the unloaded Q and external Q of resonators, and for measuring the coupling coefficients between resonators. Such procedures have wide application in the practical development of many types of band-pass filters and impedance-matching networks.

Chapter 1 of this book describes the broad range of applications for which microwave filter structures are potentially useful. Chapters 2 through 6 contain reference data and background information for the rest of the book. Chapter 2 summarizes various concepts and equations that are particularly useful in the analysis of filter structures. Although the image point of view for filter design is made use of only at certain points in this book, some knowledge of image design methods is desirable. Chapter 3 gives a brief summary of the image design concepts which are particularly useful for the purposes of this book. Chapters 1 to 3 should be especially helpful to readers who background for the material of this book may have some gaps.

Most of the filter and impedance-matching network design techniques described later in the book make use of a low-pass prototype filter as a basis for design. Chapter 4 discusses various types of lumped-element, low-pass, prototype filters, presents tables of element values for such filters, discusses their time-delay properties, their impedance-matching properties, and the effects of dissipation loss upon their responses. In later chapters these low-pass prototype filters and their various properties are employed in the design of low-pass, high-pass, band-pass, and band-stop microwave filters, and also in the design of microwave impedance-matching networks, and time-delay networks.

Various equations, graphs, and tables relevant to the design of coaxial line, strip-line, waveguide, and a variety of resonators, coupling structures, and discontinuities, are summarized for easy reference in Chapter 5. Chapter 6 discusses the design of step transformers and presents tables of designs for certain cases. The step transformers in Chapter 6 are not only for use in conventional impedance-transformer

applications, but also for use as prototypes for certain types of band-pass or pseudo high-pass filters discussed in Chapter 9.

Design of low-pass filters and high-pass filters from the semi-lumped-element point of view are treated in Chapter 7. Chapters 8, 9, and 10 discuss band-pass or pseudo-high-pass filter design using three different design approaches. Which approach is best depends on the type of filter structure to be used and the bandwidth required. A tabulation of the various filter structures discussed in all three chapters, a summary of the properties of the various filter structures, and the section number where design data for the various structures can be found, are presented at the beginning of Chapter 8.

Chapter 11 describes various additional techniques which are useful to the practical development of microwave band-pass filters, impedance-matching networks, and time-delay networks. These techniques are quite general in their application and can be used in conjunction with the filter structures and techniques discussed in Chapters 8, 9, and 10, and elsewhere in the book.

Chapter 12 discusses band-stop filters, while Chapter 13 treats certain types of directional couplers. The TEM-mode, coupled-transmission-line, directional couplers discussed in Chapter 13 are related to certain types of directional filters discussed in Chapter 14, while the branch-guide directional couplers can be designed using the step-transformer prototypes in Chapter 6. Both waveguide and strip-line directional filters are discussed in Chapter 14, while high-power filters are treated in Chapter 15. Chapter 16 treats multiplexers and diplexers, and Chapter 17 deals with filters that can be tuned either mechanically or by varying a biasing magnetic field.

It is hoped that this book will fill a need (which has become in-creasingly apparent in the last few years) for a reference book on design data, practical development techniques, and design theory, in a field of engineering which has been evolving rapidly.

ACKNOWLEDGMENTS

x

CONTENTS .

VOLUME II

CONTENTS

CONTENTS

BAND-PASS FILTERS, CONTINUED
(WIDE-BAND AND NARROW-BAND BAND-PASS FILTERS CONSISTING OF TRANSMISSION LINES WITH REACTIVE DISCONTINUITIES)

SEC. 9.01, INTRODUCTION

The band-pass filter design techniques discussed in this chapter
are based on the quarter-wave transformer prototype circuit (Chapter 6).
They apply to band-pass filters with transmission line resonators
alternating between coupling elements which are series capacitances or
shunt inductances. The design bandwidths may range from narrow-band on
up to such wide bandwidths that the filters can be used for microwave
high-pass applications. Filters of these general types were also
discussed in Secs. 8.05 to 8.08, using the design view point of Chapter 8,
which is applicable to narrow and moderate bandwidths. The design view
point of this chapter was developed to obtain a design method which would
hold for wider bandwidths, and for smaller pass-band Tchebyscheff ripples,
as well.

Section 9.02 introduces the quarter-wave transformer prototype
circuit, and Sec. 9.03 gives basic design formulas for synchronously
tuned filters.

Section 9.04 treats narrow-band filters from the view point of this
chapter, showing the connection with the lumped-constant low-pass
prototype used in Chapter 8. It has been found that the design technique
of Sec. 9.04 and Chapter 8 for narrow-band filters generally works well
up to fractional bandwidths of about 20 percent or more (compare Sec. 8.01),
provided that the pass-band ripple is not too small: the ripple VSWR
should exceed about $1 + (2w)^2$, where w is the fractional bandwidth of
the narrow-band filter, if it is to be derivable from a lumped-constant
low-pass prototype.

The remainder of this chapter, from Sec. 9.05 on, is concerned
mainly with the design of wide-band and pseudo-high-pass filters, for
which the method of the quarter-wave transformer prototype is principally
intended.

Section 9.05 deals with the realization of the reactive discontin-
uities (for filters of any bandwidth). In Sec. 9.06 some standardized
designs are given which can be adapted for many high-pass applications,
and experimental results are given in Sec. 9.07.

The basic theory, design data, and examples will be found in
Secs. 9.08 through 9.11. Finally, Section 9.12 deals briefly with
reactance-coupled quarter-wave filters.

In this chapter the frequency is introduced everywhere as the
normalized frequency, usually denoted by f/f_0, the ratio of the frequency
f to the synchronous frequency f_0. For waveguide filters the "normalized
frequency" is to be understood to refer to the quantity λ_{g0}/λ_g, the ratio
of the guide wavelength λ_{g0} at the frequency of synchronous tuning, to
the guide wavelength λ_g. (For example, an experimental waveguide filter
is described in Sec. 9.07.)

SEC. 9.02, FILTERS WITH IMPEDANCE STEPS AND
            IMPEDANCE INVERTERS

Stepped-impedance filters (quarter-wave transformers and half-wave
filters) have been treated in Chapter 6. This section points out their
equivalence to filters with impedance inverters, and, serves as an
introduction to the design of wide-band reactance-coupled half-wave
filters.

An impedance (or admittance) step [Fig. 9.02-1(a)] can always be re-
placed by an impedance (or admittance) inverter [Fig. 9.02-1(b) and (c)]
without affecting the filter response curve, provided that the input and
output ports are properly terminated. Thus the two types of circuit in
Fig. 9.02-1 are entirely equivalent as a starting point for the design
of filters. The impedance-inverter (or admittance-inverter) point of
view [Fig. 9.02-1(b) and (c)] was the more natural one to adopt in
Chapter 8 to convert the lumped-constant low-pass prototype of Chapter 4
into a transmission-line filter; whereas in this chapter a stepped-
impedance-filter point of view is more convenient to utilize directly the
design data of Chapter 6.

The stepped-impedance filter is turned into a reactance-coupled filter
by replacing each impedance step with a reactance having the same
discontinuity-VSWR and spacing the reactances to obtain synchronous tuning
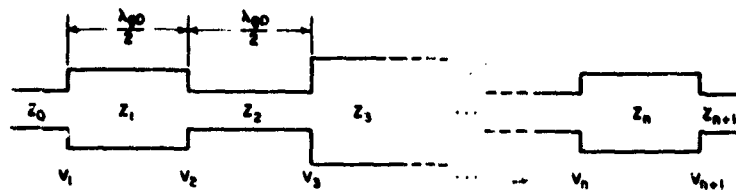
V_i = STEP VSWR = $\dfrac{Z_i}{Z_{i-1}}$ OR $\dfrac{Z_{i-1}}{Z_i}$ > 1

(EQUIVALENTLY, USE ADMITTANCES Y_i = $1/Z_i$)

(a) HALF-WAVE FILTER WITH STEPPED IMPEDANCES
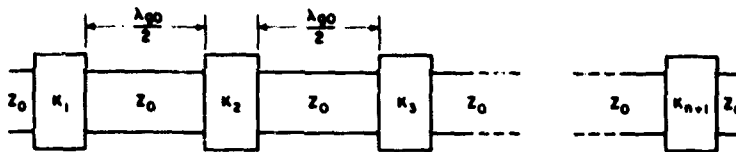
K_i = IMPEDANCE INVERTER PARAMETER = $\dfrac{Z_0}{\sqrt{V_i}}$

(b) HALF-WAVE FILTER WITH IDEAL IMPEDANCE INVERTERS
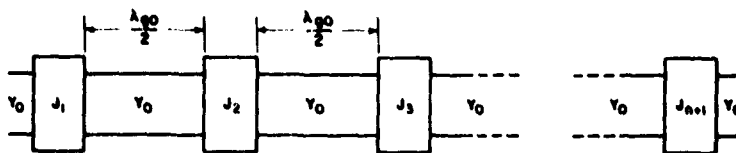
J_i = ADMITTANCE INVERTER PARAMETER = $\dfrac{Y_0}{\sqrt{V_i}}$

(c) HALF-WAVE FILTER WITH IDEAL ADMITTANCE INVERTERS

FIG. 9.02-1   A STEPPED-IMPEDANCE HALF-WAVE FILTER, AND
EQUIVALENT FILTERS USING IMPEDANCE OR
ADMITTANCE INVERTERS

(Sec. 9.03). The step-VSWRs will generally be obtained from Chapter 6. For narrow-band filters Eq. (6.09-2) may be used. This is equivalent (through Fig. 9.07-1) to the formulas in Fig. 8.05-1 for the normalized inverter parameters $K_{j,j+1}/Z_0$. Other equivalent circuits for impedance inverters suitable for narrow-band filter design are given in Sec. 8.03, but we shall be concerned in this chapter only with the shunt-inductance of Fig. 8.03-1(c) and the series-capacitance of Fig. 8.03-2(d).

One important difference in approach between this chapter and Chapter 8 is that in this chapter the starting point or prototype circuit is one of the circuits in Fig. 9.02-1 (whose synthesis is precisely controlled), whereas in Chapter 8 the exact synthesis is pushed back one stage to the lumped-constant prototype circuit of Chapter 4. For example, the performance of the circuits shown in Fig. 9.02-1(b), (c), having ideal inverters, would not give exactly the prescribed response if designed by the methods of Chapter 8 (although the approximations would be very close for narrow or moderate bandwidths). However, the circuits in Fig. 9.02-1(b), (c) have transmission characteristics identical to those of the half-wave filter in Fig. 9.02-1(a).

The other important difference over the previous chapter is that the frequency-behavior of the reactive discontinuities (shunt-inductances or series-capacitances) is examined in detail. The behavior of the discontinuities leads to increasing distortion of the filter response (e.g., pass-band bandwidth and stop-band attenuation), as the frequency spread is increased. This type of consideration can be left out in the design of narrow-band filters thereby simplifying the design process considerably. However, it is important to predict the distortion for filters having large bandwidths.

A quarter-wave transformer and the notation associated with it is shown in Fig. 9.02-2. The characteristics of maximally flat and Tchebyscheff quarter-wave transformers are sketched in Fig. 9.02-3. Closely related to the quarter-wave transformer is the stepped-impedance half-wave filter (Sec. 6.03) sketched in Fig. 9.02-4. Its characteristics, shown in Fig. 9.02-5 are similar to those of the quarter-wave transformer, shown in Fig. 9.02-3. If the impedance steps or junction VSWRs $V_i (i = 1, 2, \ldots, n+1)$ of a quarter-wave transformer and a stepped-impedance half-wave filter are the same, then the characteristics of the latter can be obtained from those of the former by a linear change of
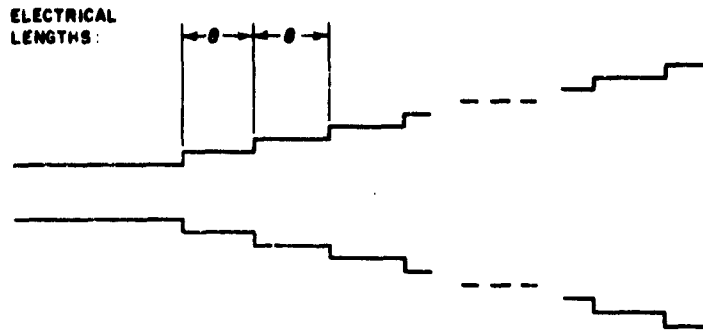
JUNCTION VSWR s: V_1 V_2 V_3 · · · V_n V_{n+1}

PRODUCT, V_1 $V_2 \cdots V_{n+1}$ • R • OUTPUT / INPUT IMPEDANCE RATIO.

ALL ELECTRICAL LENGTHS θ ARE 90 DEGREES AT THE

SYNCHRONOUS FREQUENCY, WHICH IS ALSO THE CENTER FREQUENCY.

A-3527-364

FIG. 9.02-2 QUARTER-WAVE TRANSFORMER USED AS
PROTOTYPE CIRCUIT

(a) MAXIMALLY FLAT

NORMALIZED FREQUENCY f/f_0, OR, NORMALIZED RECIPROCAL GUIDE WAVELENGTH λ_{g0}/λ_g

(b) TCHEBYSCHEFF

NORMALIZED FREQUENCY f/f_0, OR, NORMALIZED RECIPROCAL GUIDE WAVELENGTH λ_{g0}/λ_g

A-3527-295R
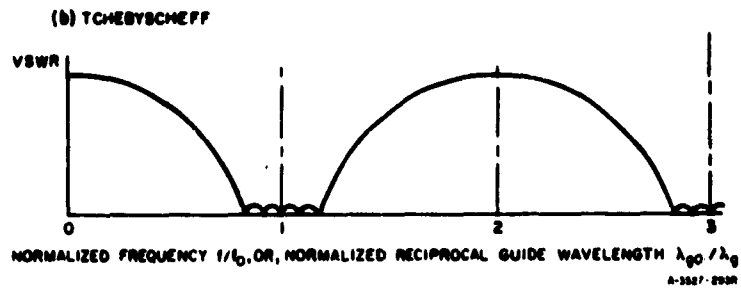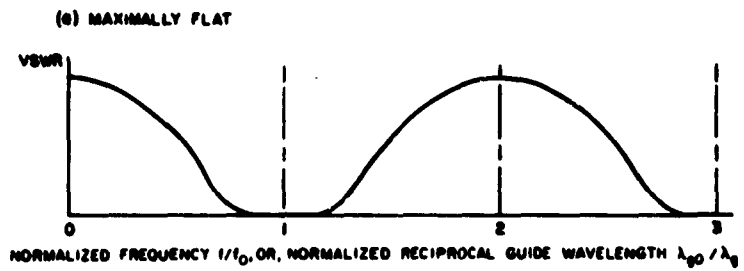
FIG. 9.02-3 QUARTER-WAVE TRANSFORMER CHARACTERISTICS

521

ELECTRICAL
LENGTHS:
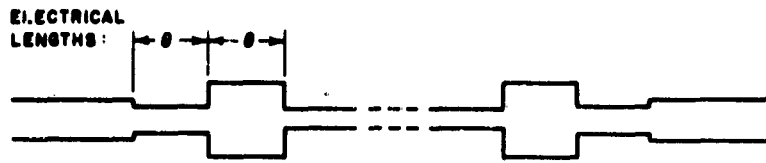
JUNCTION
VSWR s: V_1 V_2 V_3 $\cdots$ V_n V_{n+1}

PRODUCT $V_1 V_2 \cdots V_{n+1}$ = R DETERMINES PEAK ATTENUATION.

ALL ELECTRICAL LENGTHS θ ARE 180 DEGREES AT THE

SYNCHRONOUS FREQUENCY, WHICH IS ALSO THE CENTER FREQUENC..

A-352 -365

FIG. 9.02-4   STEPPED HALF-WAVE FILTER USED AS PROTOTYPE
              CIRCUIT

(a) MAXIMALLY FLAT

VSWR

NORMALIZED FREQUENCY f/f_0, OR, NORMALIZED RECIPROCAL GUIDE WAVELENGTH λ_{g0}/λ_g

(b) TCHEBYSCHEFF

VSWR

NORMALIZED FREQUENCY f/f_0, OR, NORMALIZED RECIPROCAL GUIDE WAVELENGTH λ_{g0}/λ_g
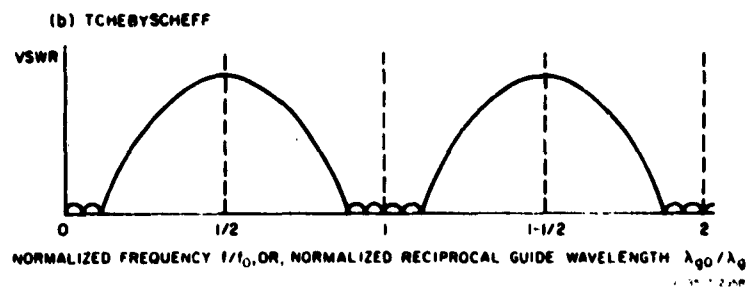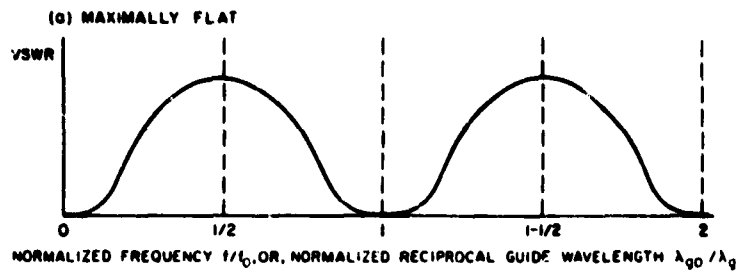
FIG. 9.02-5   STEPPED HALF-WAVE FILTER CHARACTERISTICS

522

scale on the frequency axis; the stepped-impedance half-wave filter bandwidth becomes one-half the quarter-wave transformer bandwidth.

The parameter R is again defined as the product of the discontinuity VSWRs [compare Eq. (6.03-4)]:

$$R = V_1 V_2 \ldots V_{n+1} \quad . \tag{9.02-1}$$

If the fractional bandwidth w is less than about 20-percent, and if, by Eq. (6.09-1),

$$R \gg \left(\frac{1}{w}\right)^n \tag{9.02-2}$$

then the filter may be considered narrow-band; this case will be treated in Sec. 9.04.

The quarter-wave transformer prototype circuit is suitable for designing reactance-coupled filters up to very large bandwidths. As a result, it is subject to certain limitations that do not complicate narrow-band design-procedures. It is well to understand these differences at the outset. Basically they arise from the fact that it is not possible to convert the specified performance of the filter into the performance of the appropriate prototype transformer over large frequency bands by means of simple equations or tabulated functions. Instead, the frequency variations of the reactive couplings have been used to modify the known response functions of quarter-wave transformers to predict the performance of the derived filters (Fig. 9.02-1) over large frequency ranges. Thus it is possible from the graphs to quickly calculate the principal filter characteristics from the transformer characteristics, but not the other way around, as would be more desirable. In the case of wide-band designs where the variation of reactive coupling across the pass band is appreciable, it is necessary first to guess what prototype should be used, and then to match the predicted filter performance against the specified filter performance; if they are not close enough, the process must be repeated with another prototype. What makes this method feasible and practical is the speed with which, by means of the design graphs, this prediction can be made. Most of these design graphs will be presented in Sec. 9.08.

Band-pass filters of the two configurations shown in Fig. 9.03-1
are of considerable practical importance since they are easily realized
in practice. These two circuits are duals of each other: the first,
shown in Fig. 9.03-1(a), consists of a number of series capacitances
alternating with a number of transmission-line sections; the second,
shown in Fig. 9.03-1(b), consists of a number of shunt inductances alter-
nating with a number of transmission-line sections. Both filters shown
in Fig. 9.03-1 will be called reactance-coupled *half-wave* filters, in
the sense that all line lengths between reactances approach one-half
wavelength (or a multiple thereof) as the couplings become weak. Each
line length between discontinuities constitutes a resonator, so that the
filters in Fig. 9.03-1 have n resonators. Notice that the series elements
in Fig. 9.03-1(a) are stipulated to be capacitances, that is, their sus-
ceptances are supposed to be positive and proportional to frequency.
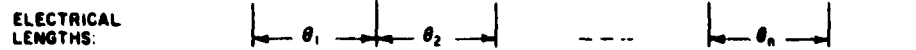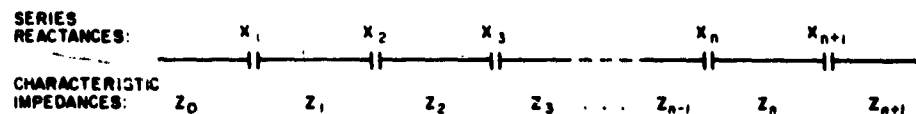
$$X_i = \frac{-1}{\omega C_i} = \frac{-1}{B_{i-1,i}} \quad (i=1,2, \quad ,n+1)$$

(a) With Series Capacitances
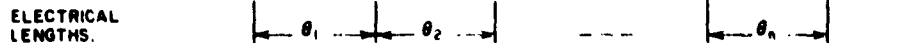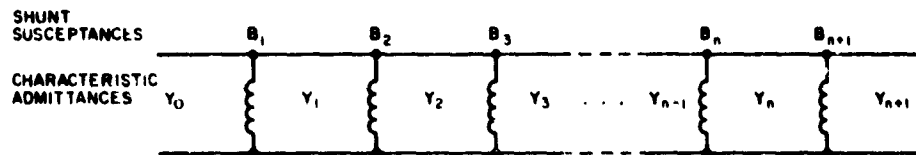
$$B_i = \frac{-1}{\omega L_i} = \frac{-1}{X_{i-1,i}} \quad (i=1,2, \quad ,n+1)$$

(b) With Shunt Inductances

A-3527-354

FIG. 9.03-1 REACTANCE-COUPLED HALF-WAVE FILTERS

Similarly, the shunt elements in Fig. 9.03-1(b) are stipulated to be inductances, that is, their reactances are supposed to be positive and proportional to frequency. (If the transmission line is dispersive, these statements are to be modified by replacing frequency by reciprocal guide wavelength.)

All the filters described in this chapter are synchronously tuned as defined in Sec. 6.01; that is, all discontinuities are so spaced that the reflections from any two adjacent discontinuities are phased to give maximum cancellation at a fixed frequency (the synchronous frequency) in the pass band. At the synchronous frequency the filter is interchangeable with a stepped-impedance half-wave filter (Sec. 6.03), and the ith reactive discontinuity has the same discontinuity VSWR, V_i, as the ith impedance step.[1,2] Impedances are shown for the series-reactance coupled filter in Fig. 9.03-1(a), and admittances for the shunt-susceptance coupled filter in Fig. 9.03-1(b); then, let

$$h_i = \frac{Z_i}{Z_{i-1}} \quad \text{or} \quad \frac{Y_i}{Y_{i-1}} \qquad (9.03\text{-}1)$$

and

$$u_i = \frac{X_i}{Z_{i-1}} \quad \text{or} \quad \frac{B_i}{Y_{i-1}} \qquad (9.03\text{-}2)$$

Most frequently $h_i = 1$, since usually this is mechanically the most convenient. Sometimes it may be advantageous for electrical or mechnical reasons to make some of the characteristic impedance ratios h_i different from unity. For instance, it may be desirable to combine the filter with an impedance transformer instead of cascading a filter with a separate transformer; also, in some cases the filter performance can be improved appreciably when the values of h_i are selected carefully, as in Sec. 9.11.

The u_i of the reactance-coupled filter are obtained from the V_i of the stepped-impedance filter (Chapter 6), and the h_i, from

$$u_i = \sqrt{\left(V_i + \frac{1}{V_i}\right)h_i - (1 + h_i^2)} \quad . \qquad (9.03\text{-}3)$$
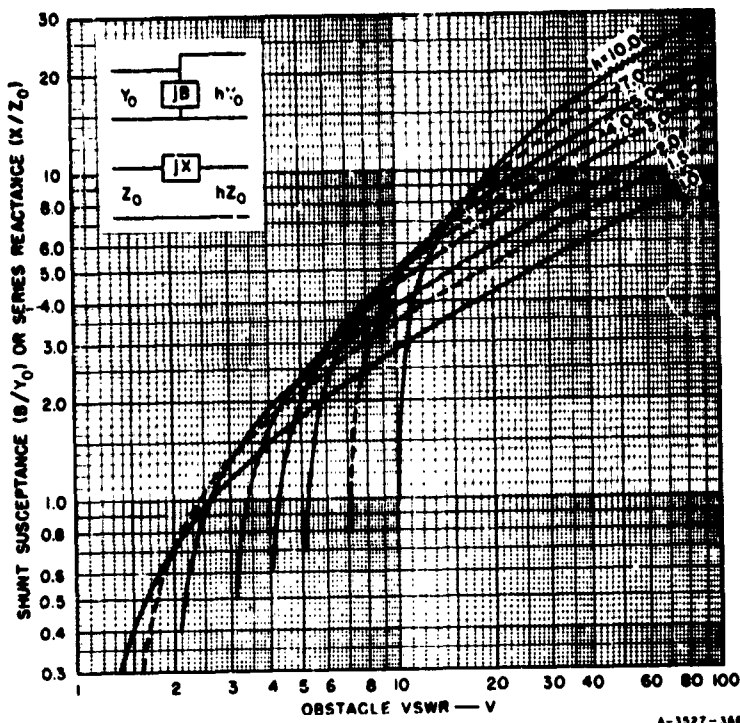
FIG. 9.03-2 SHUNT SUSCEPTANCE (or Series Reactance) AS A
FUNCTION OF DISCONTINUITY VSWR FOR SEVERAL
CHARACTERISTIC ADMITTANCE (or Impedance)
RATIOS, h

The graph of Fig. 9.03-2 gives some solutions of this equation. Generally
it will be most convenient to select $h_i = 1$ (that is, all Z_i or Y_i equal),
and then Eq. (9.03-3) simplifies to

$$u_i = \sqrt{V_i} - \frac{1}{\sqrt{V_i}} . \tag{9.03-4}$$

The spacings θ_i in Fig. 9.03-1 are determined as follows:[1,2] A single
discontinuity of a series-reactance coupled filter is shown in Fig. 9.03-3.
(A similar notation, but with Y for Z and B for X, applies to a shunt sus-
ceptance coupled filter.) It represents the ith discontinuity of the
filter (Fig. 9.03-1). If the reflection coefficients of this discontinuity

526

in the two reference planes
shown are to be pure imaginary
quantities,[42] then one has to set

$$\psi'_i = \frac{1}{2} \arctan\left(\frac{u_i^2 + h_i^2 - 1}{2u_i}\right)$$

(9.03-5)
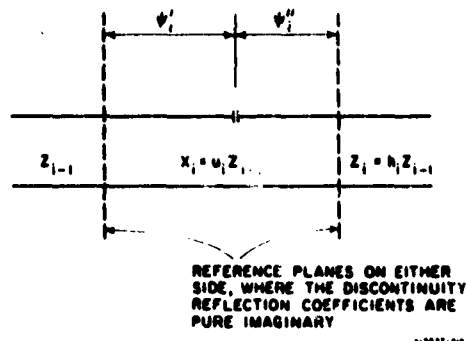
FIG. 9.03-3 SERIES-REACTANCE COUPLING
OF TWO LINES WITH DIFFERENT
CHARACTERISTIC IMPEDANCES

$$\psi''_i = \frac{1}{2} \arctan\left(\frac{u_i^2 + 1 - h_i^2}{2h_i u_i}\right) .$$

(9.03-6)

The spacings θ_i in Fig. 9.03-1 are now given (in radians) by

$$\theta_i = \frac{\pi}{2} + \psi''_i + \psi'_{i+1}$$

(9.03-7)

When $h_i = 1$, these equations reduce to

$$\psi'_i = \psi''_i = \psi_i = \frac{1}{2} \arctan\left(\frac{u_i}{2}\right)$$

(9.03-8)

and then*

$$\left.\begin{aligned}
\theta_i &= \frac{\pi}{2} + \psi_i + \psi_{i+1} \\
&= \frac{\pi}{2} + \frac{1}{2}\left[\arctan\left(\frac{u_i}{2}\right) + \arctan\left(\frac{u_{i+1}}{2}\right)\right] \\
&= \pi - \frac{1}{2}\left[\arctan\left(\frac{2}{u_i}\right) + \arctan\left(\frac{2}{u_{i+1}}\right)\right] .
\end{aligned}\right\}$$

(9.03-9)

---

* These equations are equivalent to Eqs. (5) of Figs. 8.05-1 and 8.06-1.

527

SEC. 9.04, NARROW-BAND HALF-WAVE FILTERS

The main application of this chapter is to wide-band filters. However, since the design of narrow-band filters is simpler, it will be convenient to use the narrow-band case to illustrate the method in its simplest form.

When the impedance-steps of a narrow-band (Sec. 9.01) stepped-impedance half-wave filter (Sec. 6.03) are replaced by reactances having the same discontinuity-VSWRs, and the filter is again synchronously tuned (Sec. 9.03), then there is little change in the characteristics of the filter in and near the pass-band region. All the formulas necessary to carry out this conversion have been given in Sec. 9.03. It is not necessary to maintain uniform line impedance (all Z_i or Y_i the same), but it is usually convenient to do so.

For narrow-band filters, both quarter-wave transformers and lumped-constant low-pass filters will serve as a prototype, and the conversion from either prototype into the actual filter is equally convenient. The choice of prototype depends on two factors:

    (1)   Which prototype results in a filter that meets the design specifications more closely, and

    (2)   Which prototype design is more readily available.

The quarter-wave transformer is better as regards Point (1), but the difference in accuracy is usually negligible for *narrow-band* filters; the lumped-constant low-pass filter, on the other hand, is generally more convenient as regards (2). The reason for this is that explicit formulas exist for the lumped-constant low-pass filter of n elements (Chapter 4), whereas the numerical design of transformers demands great arithmetical accuracy, and becomes convenient·only for those cases where the solutions have been tabulated (Chapter 6).

A lumped-constant low-pass filter (Chapter 4) can serve as a prototype circuit for a narrow-band stepped-impedance half-wave filter. Equations (6.09-2) with the substitution $w_q = 2w$, reduce to

$$\left.\begin{array}{l} V_1 \cdot V_{n+1} \quad \dfrac{2}{n}\, g_0\, \dfrac{g_1 \omega_1'}{w} \\[2em] V_i = \dfrac{4}{n^2}\, \dfrac{\omega_1'^2}{w^2}\, g_{i-1} g_i, \qquad \text{when } 2 \leq i \leq n \end{array}\right\} \qquad (9.04\text{-}1)$$

where w is the fractional bandwidth of the narrow-band half-wave filter. The reactances are then obtained from Eq. (9.03-3) or (9.03-4) and the spacings from Eq. (9.03-5) through (9.03-9). The low-pass prototype filter is here assumed to be either symmetric or antimetric (Sec. 4.05), and element values for maximally flat and Tchebyscheff prototypes of this type can be found in Sec. 4.05. The parameter ω_1' is the cutoff frequency of the low-pass prototype filter.

Example—It is desired to design a reactance-coupled half-wave filter to have a pass-band VSWR of better than 1.10 over a 10-percent bandwidth, and to have at least 25 db of attenuation at a frequency 10 percent above band center (i.e., twice as far out as the desired band-edge).

This filter can be considered narrow-band, and may be based on a low-pass prototype circuit (Sec. 4.05), since the ripple VSWR of 1.10 exceeds the quantity $1 + (2w)^2 = 1.04$, as mentioned in Sec. 9.01.

We must next determine the minimum number of resonators with which these specifications can be met. Selecting a quarter-wave transformer of fractional bandwidth $w_q = 0.20$, since $w = 0.10$, and with $V_r = 1.10$, the attenuation at twice the band-edge frequency-increment (see the first example in Sec. 6.09) is 24.5 db for $n = 5$ sections and 35.5 db for $n = 6$ sections. Since the filter attenuation at the corresponding frequency above the pass-band will be somewhat less than it was, $n = 5$ is certainly not enough resonators. We then tentatively select $n = 6$. It will be shown in Sec. 9.08 that the attenuation in the stop band of the narrow-band reactance-coupled half-wave filter of Fig. 9.03-1 differs from the attenuation of the narrow-band stepped-impedance half-wave filter of Sec. 6.09 by approximately

$$\Delta L_A = 20\ (n + 1)\ \log_{10}\left(\frac{f_0}{f}\right) \quad \text{db} \qquad (9.04\text{-}2)$$

where f/f_0 is the normalized frequency (the ratio of the frequency f to the center frequency f_0). This ΔL_A has to be added to the attenuation of the stepped-impedance filter to give the attenuation of the reactance-coupled filter.

Let us, for instance, calculate the attenuation of the filter at $f/f_0 = 1.10$. Using Eq. (9.04-2), with $n = 6$,

$$\Delta L_A = -20 \times 7 \times \log_{10}\ (1.1) = -5.8\ \text{db} \qquad (9.04\text{-}3)$$

529

which shows that the filter attenuation is 5.8 db less than the atten-
uation of the half-wave stepped filter at $f = 1.1\ f_0$, that is, -
35.5 - 5.8 = 29.7 db. This exceeds the 25-db attenuation specified,
which confirms our choice of $n = 6$. The discontinuity VSWRs are then
given by Eq. (6.09-4). Taking the shunt-inductance-coupled filter of
Fig. 9.03-1, with all Y_i equal to Y_0, yields

$$
\left.\begin{array}{rcl}
\dfrac{B_1}{Y_0} = \dfrac{B_7}{Y_0} &=& -1.780 \\[3ex]
\dfrac{B_2}{Y_0} = \dfrac{B_6}{Y_0} &=& -6.405 \\[3ex]
\dfrac{B_3}{Y_0} = \dfrac{B_5}{Y_0} &=& -9.544 \\[3ex]
\dfrac{B_4}{Y_0} &=& -10.154
\end{array}\right\}
\qquad (9.04\text{-}4)
$$

and from Eq. (9.03-9),

$$
\left.\begin{array}{rcl}
\theta_1 = \theta_6 &=& 147.16 \text{ degrees} \\[2ex]
\theta_2 = \theta_5 &=& 165.41 \text{ degrees} \\[2ex]
\theta_3 = \theta_4 &=& 168.51 \text{ degrees} \cdot
\end{array}\right\}
\qquad (9.04\text{-}5)
$$

    This filter was analyzed and its computed response is shown in
Fig. 9.04-1 (solid line) together with the computed response of the
stepped-impedance half-wave filter (broken line). (The stepped-impedance
half-wave filter has the same characteristics as the quarter-wave trans-
former, except for a linear change of scale, by a factor of 2 along the
frequency axis.) It is seen that the band edges of the filter and its
stepped-impedance half-wave filter prototype very nearly coincide, and
that the peak ripples in the two pass bands are nearly the same height.

The VSWR ripple in the pass band is very close to 1.10. The quarter-wave transformer design is itself only approximate, and the ripple heights (broken line, top of Fig. 9.04-1) are not exactly the same, since the transformer was designed from a lumped-constant low-pass prototype (first example in Sec. 6.09). The causes of imperfection in the filter response in Fig. 9.04-1 may in this case be ascribed partly to (1) the imperfect quarter-wave transformer response, since the transformer was derived by an approximation from a lumped-constant circuit, and partly to (2) the further approximation involved in deriving the filter with its unequal spacings and frequency-sensitive couplings from the transformer.

With regard to the imperfect quarter-wave transformer response, there is clearly little room for improvement, as can be seen from Fig. 9.04-1. As for the further approximations involved, one could adjust the line characteristic impedances to improve the performance (as is explained in

FIG. 9.04-1 CHARACTERISTICS OF A SIX-RESONATOR FILTER AND ITS STEPPED-IMPEDANCE HALF-WAVE FILTER PROTOTYPE

Sec. 9.11), but this would also result in only a very small improvement. These adjustments were not considered further in the present example.

The attenuation of the filter at $f/f_0 = 1.1$ had been predicted from Eq. (9.04-2) to be 29.7 db. This gives one of the circle points in Fig. 9.04-1, and falls very close to the curve computed by analysis of the filter (solid line); other points predicted using Eq. (9.04-2) also fall very close to this computed curve.

531

SEC. 9.05, PRACTICAL REALIZATION OF REACTIVE COUPLINGS

Series Capacitances[4]—Series-capacitive coupling can be realized easily in coaxial line or strip transmission line by breaking the inner conductor as shown in Fig. 9.05-1. The gap-spacing is controlled to produce the desired capacitance. When air dialectric is used, filters coupled by series capacitances should have lower dissipation losses than
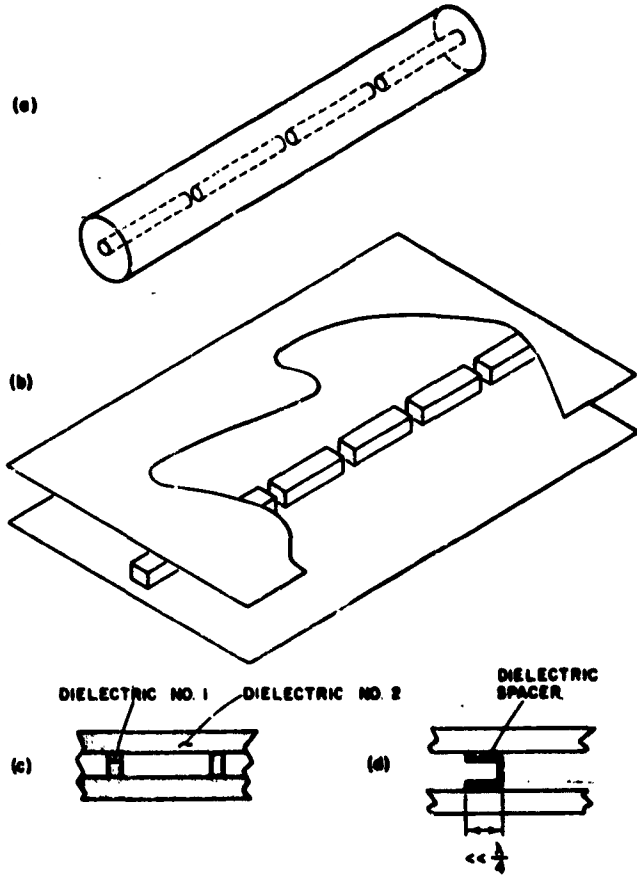
(a)

(b)

DIELECTRIC NO. I   DIELECTRIC NO. 2   DIELECTRIC
                                                  SPACER

(c)   (d)

$\ll \frac{\lambda}{4}$

A-3527-300

FIG. 9.05-1   REALIZATION OF SERIES-CAPACITANCE
              REACTANCE-COUPLED HALF-WAVE FILTERS
              (a) Filter in Coaxial Line
              (b) Filter in Strip Transmission Line
              (c) and (d)   Series Capacitance in Coaxial Line

filters using shunt inductive posts or irises (considered below), because of their ohmic losses.

The gap spacing that will produce the desired coupling can be determined either experimentally or theoretically. Experimentally one can proceed as follows: The desired VSWR of each discontinuity is, by definition, equal to the junction VSWR of the corresponding step of the prototype transformer. The VSWR-versus-gap-spacing curve can be determined experimentally by direct measurement, or by measuring attenuation, or by using two identical gaps to obtain resonance and measuring the 3 db bandwidth. The curve can then be plotted for the particular transmission line at the synchronous frequency of the pass band. The desired gap spacings are read off from this curve.

In general it would be difficult to calculate the capacitance of a gap for arbitrary cross-sectional shape. However good approximations for the circular inner conductor inside a circular outer conductor (Fig. 9.05-1) can be obtained in the following two ways.

The first approximation is as follows: The inside diameter of the outer tube is b inches; the diameter of the concentric inner conductor is a inches; and the gap spacing is s inches, as shown in Fig. 9.05-2.
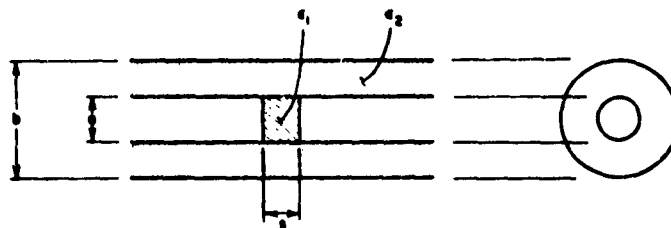
a = INNER CONDUCTOR DIAMETER

b = OUTER CONDUCTOR DIAMETER

s = GAP SPACING

ϵ_1 = DIELECTRIC CONSTANT IN GAP

ϵ_2 = DIELECTRIC CONSTANT IN COAXIAL LINE

A-3627-300

FIG. 9.05-2 NOTATION FOR SERIES CAPACITIVE GAP IN COAXIAL LINE

The following formula is adapted from an approximate formula given by Marcuvitz[5] which is valid when $(b - a) < \lambda$, $s \ll \lambda$, and $s \ll (b - a)$, where λ is the free-space wavelength. Then

$$C = C_p + C_f \qquad (9.05\text{-}1)$$

where

$$C_p = \frac{0.1764 \, \epsilon_{r1} a^2}{s} \text{ picofarads} \qquad (9.05\text{-}2)$$

is the parallel-plate capacitance,

$$C_f = 0.2245 \, \epsilon_{r1} a \, \ln\left(\frac{b - a}{s}\right) \text{ picofarads} \qquad (9.05\text{-}3)$$

is the fringing capacitance, and ϵ_{r1} and ϵ_{r2} are the relative dielectric constants of the materials (Fig. 9.05-2). Equations (9.05-2) and (9.05-3) are given also in mks units in Ref. 4.

Second, a more accurate, but still approximate, estimate of the capacitance in Fig. 9.05-2 can be obtained[6] by Fig. 5.05-9: use the curve for $t/b = 0$ and determine the quantity $\Delta C/\epsilon$ using the same s/b (Fig. 9.05-2) on the abscissa. In Fig. 5.05-9 ϵ is our present ϵ_2, which is the absolute dielectric constant for Dielectric 2 in Fig. 9.05-2. Then the capacitance is given by Eqs. (9.05-1) and (9.05-2) but with Eq. (9.05-3) replaced by

$$C_f = 0.353 \, \epsilon_{r2} a \left(\frac{\Delta C}{\epsilon}\right)_G \text{ picofarads} \qquad (9.05\text{-}4)$$

where $(\Delta C/\epsilon)_G$ is the quantity $\Delta C/\epsilon$ in Fig. 5.05-9. Both Eqs. (9.05-3) and (9.05-4) tend to underestimate the true capacitance. For $d/b < 0.1$, the two approximate formulas for the total capacitance C agree to within 5 percent.

Numerical data for a rectangular strip transmission line with a strip cross section 0.184 inch by 0.125 inch is given in Fig. 8.05-3.

Example—Find the capacitance of a gap in a coaxial line whose dimensions (Fig. 9.05-2) are $b = 0.575$ inch, $a = 0.250$ inch, $s = 0.025$ inch.

The relative dielectric constant in the gap is $\epsilon_{r_1} = 2.0$ and the relative dielectric constant between the conductors is $\epsilon_{r_2} = 2.5$. Then find the normalized reactance at a frequency of 1.3 Gc. From Eq. (9.05-2),

$$C_p = 0.882 \text{ picofarad} \tag{9.05-5}$$

and from Eq. (9.05-3)

$$C_f = 0.371 \text{ picofarad} \quad . \tag{9.05-6}$$

Thus the total capacitance is

$$C = C_p + C_f = 1.253 \text{ picofarads} \quad . \tag{9.05-7}$$

The line impedance is

$$Z_0 = \frac{60}{\sqrt{\epsilon_{r_2}}} \ln \frac{b}{a} = 31.6 \text{ ohms} \tag{9.05-8}$$

and therefore the normalized reactance at 1.3 Gc is

$$\left. \begin{aligned} \frac{X}{Z_0} &= \frac{10^{12}}{2\pi \times 1300 \times 10^6 \times 1.253 \times 31.6} \\[2mm] &= 3.08 \quad \cdot \end{aligned} \right\} \tag{9.05-9}$$

In this case, by Eqs. (9.05-5) and (9.05-6), about three-tenths of the total capacitance is due to the fringing fields; as the gap is reduced, both C_p and C_f increase, but an increasingly higher proportion of the total capacitance is due to C_p.

Filters with series-capacitance couplings were also treated in Sec. 8.05, and have been discussed by Cohn,[7] Ragan,[8] and Torgow.[9] The sleeve-like coupling shown in Fig. 9.05-1(d) is a short, open-circuited stub rather than a lumped capacitance. When its length is increased to one-quarter wavelength at center frequency, and the connecting lines are also made one-quarter wavelength long at center frequency, then a different type of filter, although still with somewhat similar electrical characteristics, results from this change. This type of filter has been treated by Matthaei,[10] and constructional details have also been given by Bostick.[11]

Shunt Inductances—Shunt-inductive couplings can easily be realized
in coaxial line, strip transmission line, and waveguide. Some of the
common structures are shown in Fig. 9.05-3. Numerical data on some of
them have been given in Sec. 8.06, and a few further references will be
mentioned here.
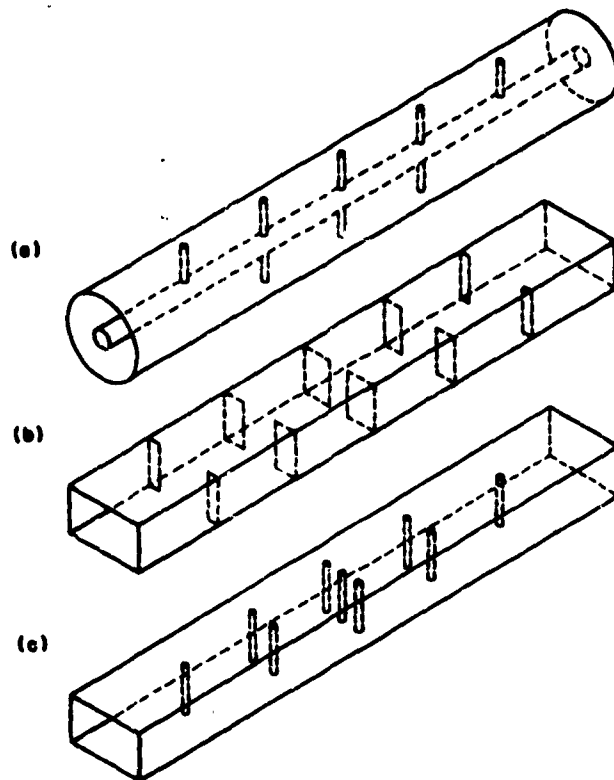
FIG. 9.05-3   REALIZATION OF SHUNT-INDUCTANCE
REACTANCE-COUPLED HALF-WAVE FILTER
(a) In Coaxial Line; (b) and (c) In Waveguide

As long as the obstacles are thin in an axial direction, their re-
actances are nearly proportional to frequency, or reciprocal guide wave-
length in dispersive waveguide. In addition, short-circuit stubs also
behave approximately as inductances when their lengths are well below
one-quarter wavelength. In this case, however, the stub equivalent cir-
cuit is more complicated than a simple shunt inductance, since the T-
junction reference plane positions and the coupling ratio all change

with frequency, and the stub can then be approximated by a single in-
ductance only over a limited frequency band.

Numerical data are available for a single post, for double posts,
and for four posts in coaxial line,[12,13] as shown in Figs. 9.05-3(a) and
9.05-4. Data on shunt-inductive irises [Fig. 9.05-3(b)] and a single
center post in waveguide are graphed in Figs. 8.06-2 and 8.06-3. As
shown in Fig. 9.05-3(c), one can also use double symmetrical posts,[14]
equally spaced triple posts,[15] and even more than three equally spaced
posts[16] in waveguide. Data on strip-line shunt-inductive stubs are
given in Figs. 8.08-2(a), (b) to 8.08-4(a), (b).

(a)   (b)   (c)
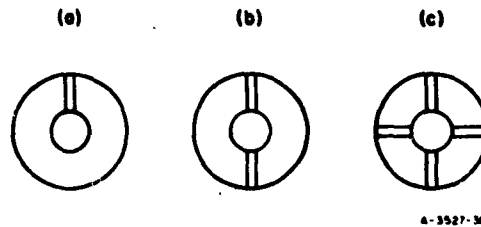
FIG. 9.05-4 CROSS-SECTIONAL VIEW OF ROUND SHUNT-
            INDUCTIVE POSTS IN COAXIAL LINE
            (a) Single Post, (b) Two Posts, (c) Four Posts

As long as all of these discontinuities can be represented by shunt
inductances—that is to say by positive reactances whose reactance values
are proportional to frequency or to reciprocal guide wavelength—the de-
sign data reported here apply up to very large bandwidths.

SEC. 9.06, SOME STANDARDIZED PSEUDO-HIGH-PASS FILTER DESIGNS

A problem frequently encountered is the design of a high-pass filter
with capacitive couplings of the type shown in Fig. 9.03-1. Actually,
this filter is not high-pass but band-pass; however, for large bandwidths
the upper stop band becomes vestigial, because the series reactances di-
minish rapidly with increasing frequency. Such a filter may therefore be
called *pseudo-high-pass*. In the past it has usually been designed on an
image-impedance basis (See Chapter 3), often leading to increasing ripple
amplitude in the pass band near the cutoff frequency (lower band edge).
An equal-ripple characteristic would generally be preferable; a systematic
design procedure for equal-ripple wide-band filters is given in this chapter.

537

The fractional bandwidth, w, of nondispersive filters is defined as in Chapter 6, by

$$w = 2\left(\frac{f_2 - f_1}{f_2 + f_1}\right) \qquad (9.06\text{-}1)$$

$$= 2\left(\frac{\lambda_1 - \lambda_2}{\lambda_1 + \lambda_2}\right) \qquad (9.06\text{-}2)$$

where f_1 and f_2 are the lower and upper pass-band edge frequencies, and λ_1, and λ_2 are the corresponding wavelengths. For dispersive filters, guide wavelength has to be substituted in Eq. (9.06-2), and then

$$w = 2\left(\frac{\lambda_{g1} - \lambda_{g2}}{\lambda_{g1} + \lambda_{g2}}\right) . \qquad (9.06\text{-}3)$$

The design of an eight-resonator (i.e, $n = 8$) filter with 0.1-db pass-band ripple and fractional bandwidth 0.85 is treated in the last example of Sec. 9.09. (A fractional bandwidth of 0.85 corresponds to $f_2/f_1 = 2.5$.) Its normalized series reactances X_i/Z_0 (or shunt susceptances B_i/Y_0) were found to be -0.2998, -0.4495, -0.613, -0.700, -0.725, -0.700, 0.613, 0.4495 and -0.2998. Since the three central elements were so nearly alike, they were each set equal to 0.710 for the present purpose. The responses of several filters with normalized series reactances (or shunt susceptances) -0.2998, -0.4495, -0.613, -0.710, -0.710, ... -0.710, 0.613, -0.4495, -0.2998 were then analyzed numerically on a digital computer. Since all Z_i are the same, then by Eq. (9.03-9) the line lengths are 100.60, 104.85, 108.29, 109.54, ..., 109.54, 108.29, 104.85, and 100.60 electrical degrees. When eight or more resonator lines are used, involving three or more identical central elements, the filter may be thought of as a periodic structure with three (instead of the usual one) impedance-matching resonators at each end. The performance of five such filters with eight, nine, ten, twelve, and fifteen resonators is shown in Figs. 9.06-1 and 9.06-2. It is seen that the computed performance closely meets the predicted one: only in the fifteen-resonator filter (which contains ten identical coupling reactances) are there any ripples appreciably greater than 0.1 db, and even then there are only two large ripples, one just inside each band edge (Fig. 9.06-1).
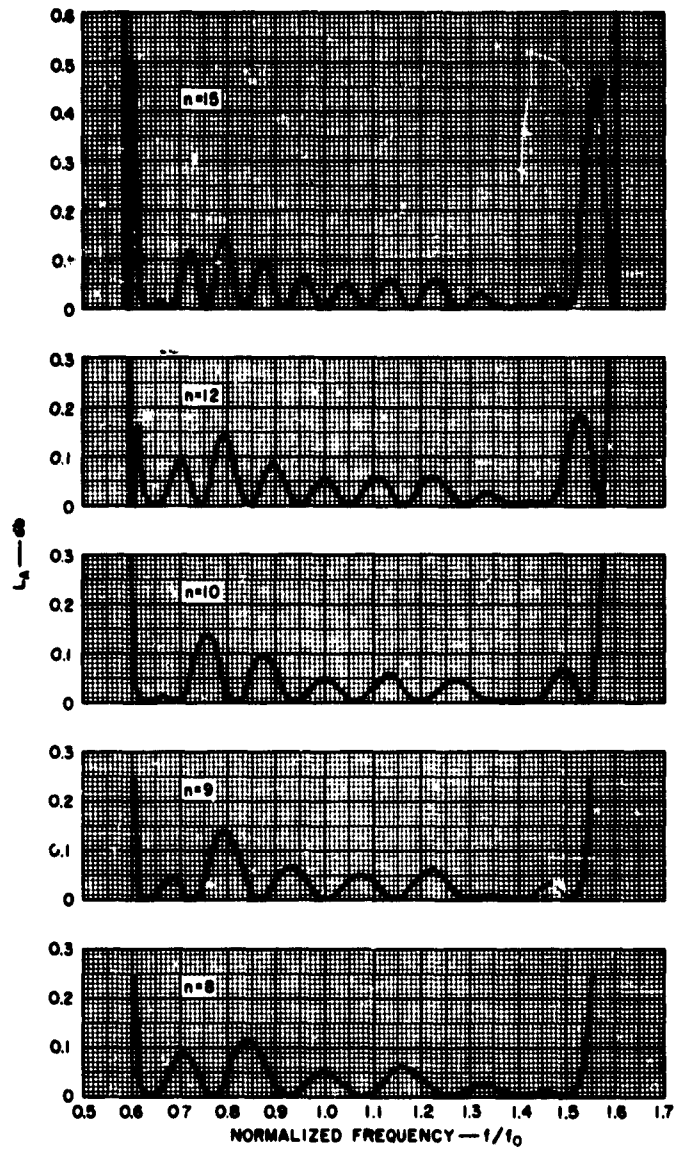
538

FIG. 9.06-1   PASS-BAND RESPONSE OF FIVE PSEUDO-HIGH-PASS FILTERS
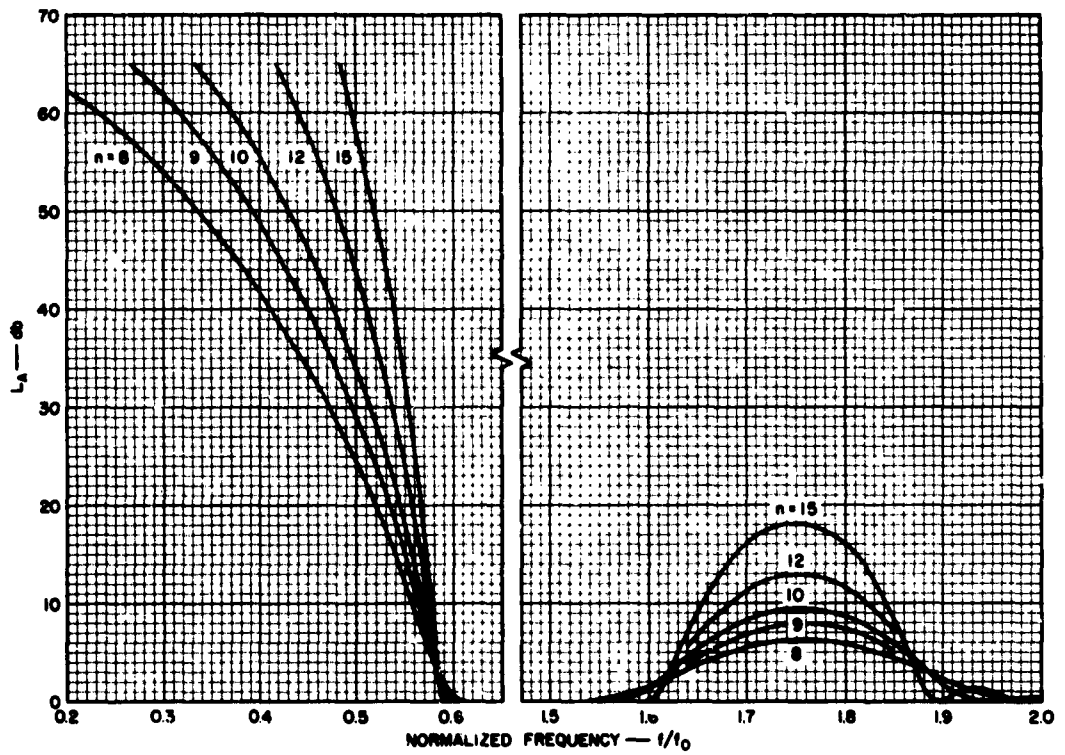
B-3527-357

FIG. 9.06-2   STOP·BAND RESPONSE OF FIVE PSEUDO-HIGH·PASS FILTERS

540

The rate of cutoff (skirt selectivity) improves as the number of resonators is increased, as can be seen from Fig. 9.06-2, increasing by approximately the same number of decibels per resonator added. Since the upper stop band is not particularly useful, these filters will find application as high-pass rather than as band-pass filters.

SEC. 9.07, AN EXPERIMENTAL WIDE-BAND WAVEGUIDE FILTER

In order to test the performance of the pseudo-high-pass filter described in Sec. 9.06, a six-cavity filter derived from the eight-cavity design of Sec. 9.09 was constructed in waveguide. Because all of the central cavities have been removed, the six-cavity design is the smallest possible filter of the group of periodic structures with three matching resonators on each end. The end three shunt susceptances, the single shunt susceptance in the center, and the line lengths are unchanged.

A photograph of the waveguide filter is shown in Fig. 9.07-1. For this design, WR-137 waveguide (1.372 inches × 0.622 inch I.D.) was used and the lower cutoff frequency was chosen to be 5.4 Gc, which is well above the waveguide cutoff frequency of 4.3 Gc. The upper band edge is 9.0 Gc and the design center frequency is 6.8 Gc. The shunt susceptances are symmetrical irises 0.020 inch thick designed with the aid of graphs in Fig. 8.06-2(b).

An empirical adjustment was made to allow for the iris thickness, namely, the aperture d (Fig. 8.06-2) was increased by 0.020 inch (an amount equal to the iris thickness). It is known that the shunt susceptance of a waveguide iris is not an exact linear function of guide wavelength; the iris inductances cannot therefore be treated as constants independent of frequency. Since the most important single frequency of a high-pass filter is the lower cutoff frequency, the iris susceptances were made to coincide with the values of the design susceptances at 5.4 Gc (the lower band-edge or cutoff frequency) rather than at 6.8 Gc (the band center). The response of the filter was then computed using the curves in Fig. 8.06-2(b) to obtain the numerical values of the shunt susceptances at each frequency. It was found that the computed difference in performance between the physically more realistic filter [based on Fig. 8.06-2(b)] and the one assuming constant iris inductance (i.e., susceptance proportional to guide wavelength) could hardly have been detected experimentally. We therefore conclude that the irises might equally well have been designed to have the correct values at the band center.

541
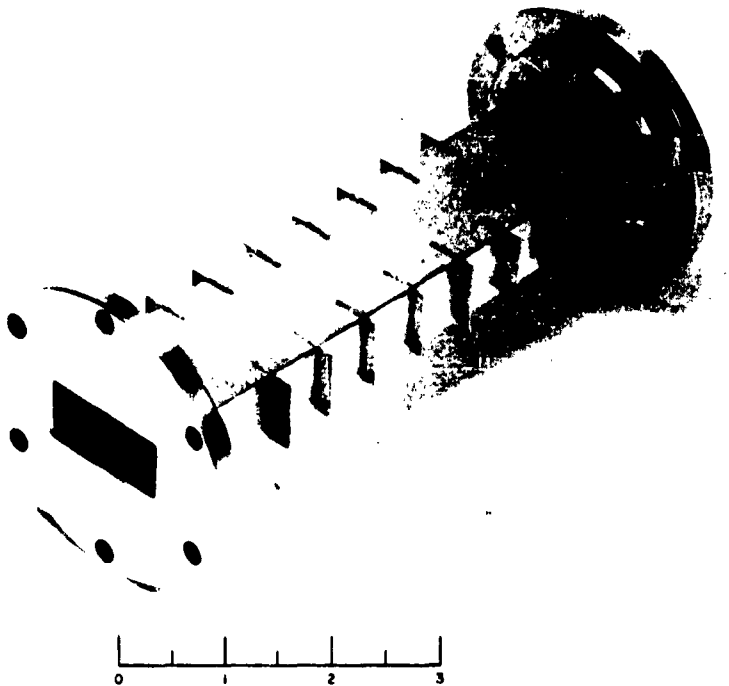
FIG. 9.07-1   EXPERIMENTAL WAVEGUIDE FILTER FOR C-BAND

The widths of the iris-openings for the experimental six-cavity filter (starting at one end and going towards the center) are 1.026, 0.958, 0.898, and 0.870 inch, respectively. The cavity lengths (again starting from one end) are 0.626, 0.653, and 0.674 inch, respectively. Insertion loss and VSWR measurements were made, and the results were as shown in Fig. 9.07-2. While the general shape of the computed response curve* was followed remarkably well by the measured points, a slight shift toward the higher-frequency region is evident. This may be due in part to the fact that cavity lengths were measured between center lines of the 0.020-inch irises with no allowance for iris thickness.

---

* The computed curve shown was programmed for constant inductance, i.e., susceptance directly proportional to guide wavelength.
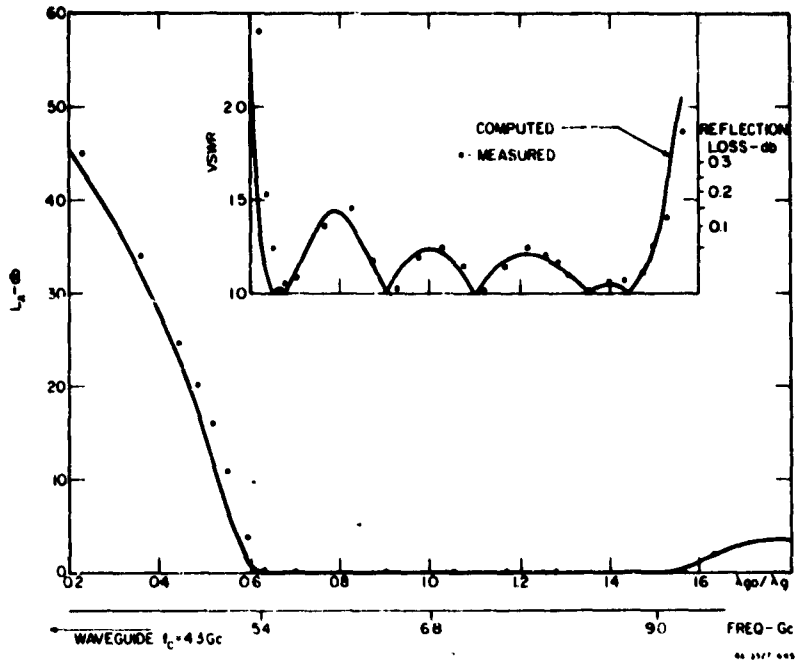
FIG. 9.07-2   COMPUTED AND MEASURED PASS-BAND RESPONSE OF
SIX-RESONATOR EXPERIMENTAL FILTER FOR C-BAND

SEC.   9.08,   DESIGN FOR SPECIFIED BAND EDGES AND STOP-BAND
ATTENUATION

Typical characteristics of a quarter-wave transformer and the reac-
tively coupled filter derived from it are shown in Fig. 9.08-1. The
transformer prototype has a symmetrical response (broken line) on a fre-
quency scale. Denoting its band edges by f_1' and f_2' (Fig. 9.08-1), the
frequency of synchronous operation (Sec. 9.03) is also the mean or center
frequency,

$$f_0 = \frac{f_1' + f_2'}{2}$$ (9.08-1)

The response is symmetrical about f_0. When the impedance steps of the
transformer (Chapter 6) are replaced by series capacitances or shunt in-
ductances, then the new response is as indicated by the solid line in
Fig. 9.08-1. The following general changes should be noted:

543

FILTER

QUARTER—WAVE
TRFR. PROTOTYPE
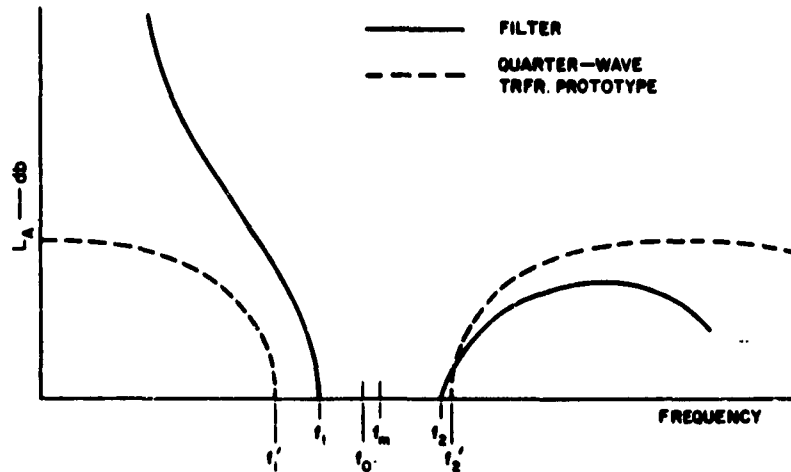
SYNCHRONOUS FREQUENCY : $f_0 = \frac{1}{2}(f_1' + f_2')$

FILTER MEAN FREQUENCY : $f_m = \frac{1}{2}(f_1 + f_2)$

A-3527-369

FIG. 9.08-1 GENERAL CHARACTERISTICS OF REACTANCE-COUPLED
HALF-WAVE FILTER AND QUARTER-WAVE TRANSFORMER
WITH SAME DISCONTINUITY VSWRs AND SAME
SYNCHRONOUS FREQUENCY

(1) The bandwidth has contracted. (For small bandwidths this
is the only change of major concern.)

(2) The lower band edge has contracted (f_1' to f_1) more than the
upper band edge (f_2' to f_2). If both the transformer and
the filter have the same synchronous frequency f_0, then
the new mean frequency (defined as the arithmetic mean of
f_1 and f_2)

$$f_m = \frac{f_1 + f_2}{2} \qquad (9.08-2)$$

is greater than f_0, the frequency of synchronous tuning.
Also, the two curves in the upper stop band cross each
other, and the response is not symmetrical about f_m.

(3) The ripple amplitude inside the pass band, for a
Tchebyscheff filter, has not changed appreciably. (This
is not indicated in Fig. 9.08-1.)

544

Bandwidth Contraction—We shall define the fractional bandwidth w of the filter in the usual way by

$$w = \frac{f_2 - f_1}{f_a} \quad . \tag{9.08-3}$$

The fractional bandwidth w_q of the transformer is

$$w_q = \frac{f_2' - f_1'}{f_0} \quad . \tag{9.08-4}$$

The bandwidth contraction factor β is then defined by

$$\beta = \frac{w}{w_q} \tag{9.08-5}$$

and can be obtained from the graphs given in Fig. 9.08-2 as a function of R, the ratio (greater than one) of the output impedance to the input impedance of the transformer prototype. For narrow bandwidths, the pass band is nearly symmetrical on a frequency scale, and so the bandwidth also determines the band edges. (For narrow-band filters, β will be close to 0.5, as in the example in Sec. 9.04.) For wide-band filters, the band-width contraction does not give the whole story, and one has to consider the movement of the two band edges separately, as will now be shown.

Pass-Band Distortion—It will be shown in Sec. 9.10 that one would expect the response to be approximately symmetrical when plotted not against frequency, but against the quantity

$$x = \frac{\Delta f}{(f//f_0)^\alpha} = \frac{f - f_0}{(f//f_0)^\alpha} \tag{9.08-6}$$

as shown in Fig. 9.08-3, and that for highly selective filters (filters corresponding to large transformer output-to-input impedance ratio, R), the exponent α is given approximately by

$$\alpha \approx 1 + \frac{1}{n} \quad \text{(large } R\text{)} \tag{9.08-7}$$
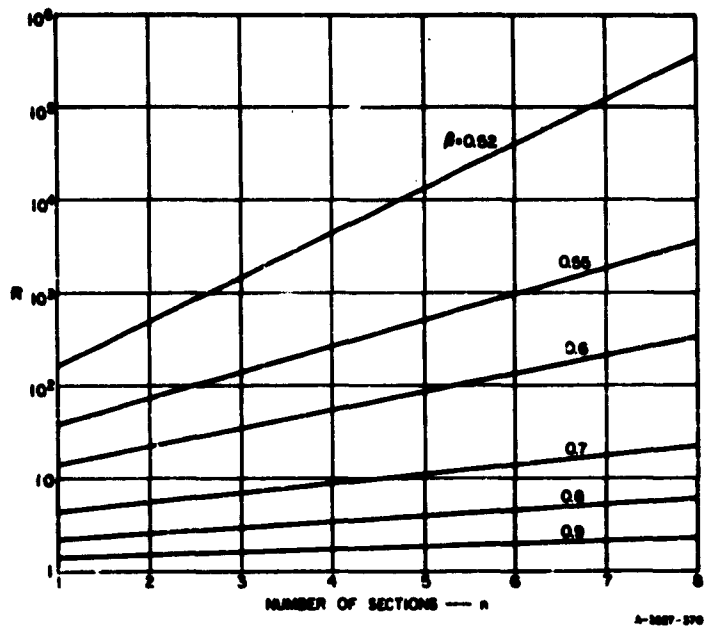
FIG. 9.08-2   BANDWIDTH CONTRACTION FACTCR β AS A
FUNCTION OF n (Number of Resonators) AND R
(Discontinuity-VSWR Product)
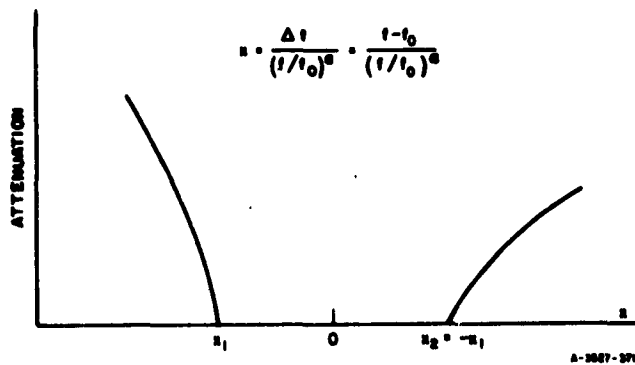
FIG. 9.08-3   A METHOD OF TRANSFORMING THE
FREQUENCY VARIABLE TO OBTAIN AN
APPROXIMATELY SYMMETRICAL FILTER
CHARACTERISTIC

where n is the number of transformer sections or filter resonators. (The case $\alpha \approx 1$, corresponding to large n, leads to a symmetrical response on a wavelength scale, as previously noted by Cohn,[3] using different arguments.)

When R approaches unity, α will approach zero for synchronous filters for all n, regardless of the frequency dependence of the couplings. Thus any curve in Fig. 9.08-4 must pass through the origin. Similarly, Eq. (9.08-7) supplies the asymptotes for the graph of Fig. 9.08-4. Equation (9.08-6) can be made exact for the two band-edge frequencies, f_1 and f_2, by defining

$$\alpha = \frac{\log \,(\Delta f_2 / \Delta f_1)}{\log \,(f_2 / f_1)} \qquad (9.08\text{-}8)$$
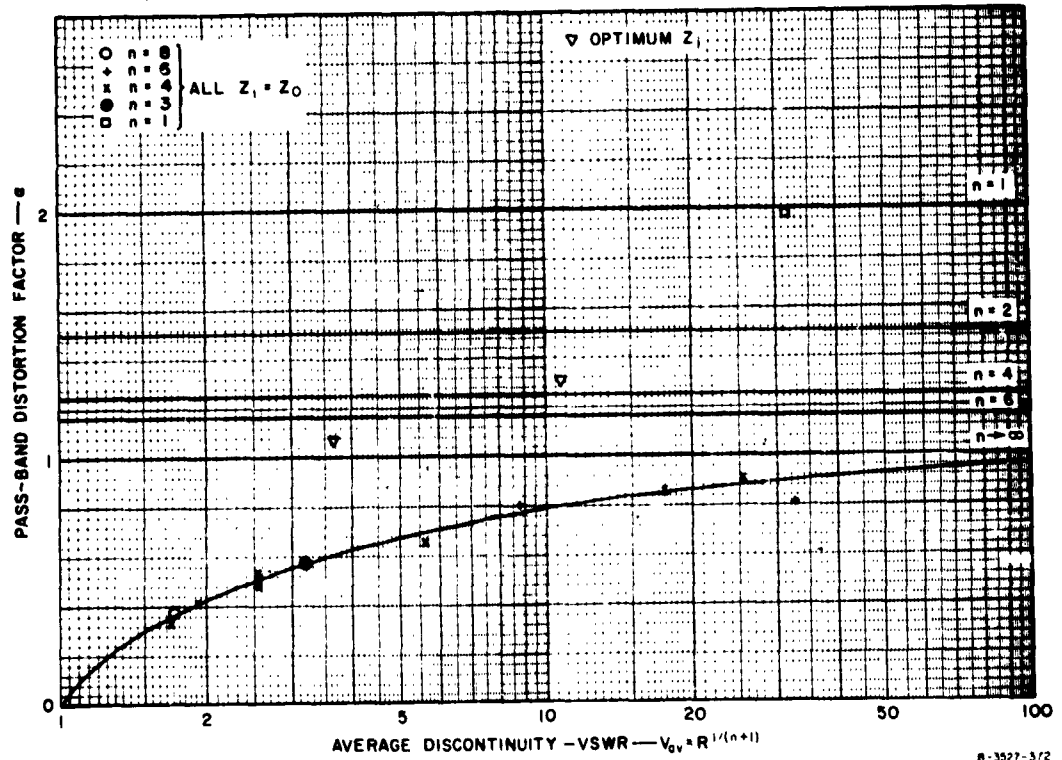
FIG. 9.08-4 PASS-BAND DISTORTION FACTOR, γ, VERSUS AVERAGE DISCONTINUITY VSWR, V_{av}, SHOWING THE SOLUTIONS FOR FOURTEEN PARTICULAR CASES JOINED BY A SMOOTH CURVE

where

$$\Delta f_2 = f_2 - f_0$$
$$\Delta f_1 = f_0 - f_1$$

$$(9.08-9)$$

Equation (9.08-8) will henceforth be used as the definition of α. The parameter α was thus calculated for fourteen widely different filters whose response curves had been computed, having from $n = 3$ to 8 resonators plus one with $n = 1$ resonator, and for bandwidths varying from narrow (10 percent) through medium to wide (85 percent). These fourteen points are plotted in Fig. 9.08-4 against the average discontinuity VSWR,

$$V_{av} = R^{1/(n+1)} \quad .$$

$$(9.08-10)$$

It is seen that eleven points can be joined by a smooth curve running through or very close to them. The three exceptions are explained as follows: One is for $n = 1$ (see Sec. 9.10), and then by Eq. (9.08-7) one would expect $\alpha = 2$, which is indeed the case. The other two points, shown by triangles, correspond to non-uniform-impedance filters, to be dealt with in Sec. 9.11. It may be concluded that the curve in Fig. 9.08-4 can generally be used to obtain the pass-band distortion factor α for filters with uniform line impedances (all Z_i equal to Z_0 in Fig. 9.03-1), and having more than about $n = 3$ resonators.

It can be shown from Eqs. (9.08-8) and (9.08-9) that the frequency displacement $f_a - f_0$ is given by

$$\delta = \frac{f_a - f_0}{f_a} = \frac{\Delta f_2 - \Delta f_1}{2 f_a} = \left(\frac{A-1}{A+1}\right)\frac{w}{2}$$

where

$$\log A = \log(\Delta f_2 / \Delta f_1)$$
$$= \alpha \log(f_2 / f_1)$$
$$= \alpha \log\left(\frac{2+w}{2-w}\right) .$$

$$(9.08-11)$$

This equation is *exact* when Eq. (9.08-8) is regarded as a definition as it is here. Equation (9.08-11) is plotted in Fig. 9.08-5, showing the relative mean-to-synchronous frequency displacement, $(f_a - f_0)/f_a$ as a function of the fractional bandwidth, w, for several values of the parameter α. [When $\alpha = 0$, the displacement $(f_a - f_0)$ is zero.]

This completes the discussion of the effect on the pass-band edges of changing the discontinuities from impedance steps to reactive elements. We shall now show how the stop-band attenuation is affected by this change.
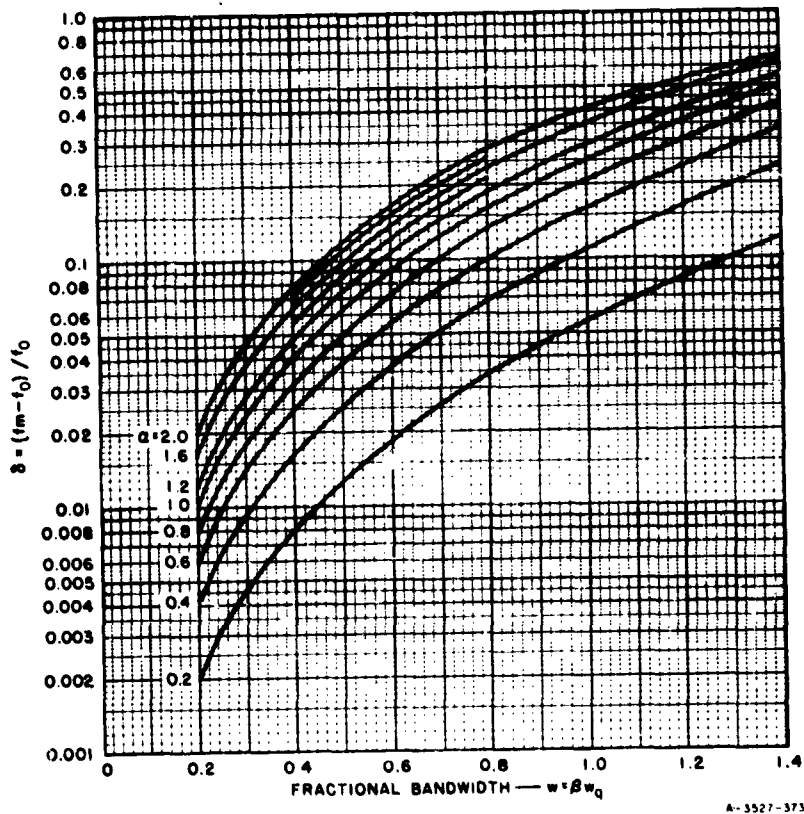
FIG. 9.08-5 RELATIVE DISPLACEMENT OF MEAN FREQUENCY FROM SYNCHRONOUS FREQUENCY, δ, AS A FUNCTION OF FRACTIONAL BANDWIDTH FOR SEVERAL VALUES OF α

549

Stop-Band Attenuation--A simple procedure will be developed for pre-
dicting the skirt of the filter response. The approximations made are
such that this prediction holds closely over most of the rising portion
of the skirt, but will be relatively less accurate very close to the band
edge, as well as past the first attenuation maximum above the pass band;
these are not serious limitations in practice. (The accuracy obtainable
will be illustrated by several examples in Secs. 9.09 and 9.11.)

The excess loss, $\mathcal{E}$, of a stepped-impedance half-wave filter is (see
Sec. 6.03)

$$\mathcal{E} = \frac{P_{available}}{P_{load}} - 1 = \frac{(R-1)^2}{4R} \frac{T_n^2(\sin\theta/\mu_0)}{T_n^2(1/\mu_0)} \qquad (9.08-12)$$

where R is the product of the discontinuity VSWRs

$$R = V_1 V_2 V_3 \dots V_{n+1} \qquad (9.08-13)$$

Here, T_n is a Tchebyscheff polynomial of order n and μ_0 is a constant
(Sec. 6.02),

$$\mu_0 = \sin\left(\frac{\pi w_q}{4}\right) . \qquad (9.08-14)$$

The response of the reactive-element filter is also given by
Eq. (9.08-12) except that R is no longer constant, since the V_i become
functions of frequency, as a result of the changing susceptances or re-
actances. Therefore at any frequency f [and for the shunt-susceptance
filter of Fig. 9.03-1(b)]

$$V_i(f) = \frac{[4 + (B_i/Y_0)^2(f_0/f)^2]^{1/2} + (B_i/Y_0)(f_0/f)}{[4 + (B_i/Y_0)^2(f_0/f)^2]^{1/2} - (B_i/Y_0)(f_0/f)} \qquad (9.08-15)$$

when all the line impedances are equal. [For the series-reactance filter
of Fig. 9.02-1(a), substitute (X_i/Z_0) for (B_i/Y_0).] For large enough V_i and
B_i, Eq. (9.08-15) reduces approximately to

$$V_i(f) = (B_i f_0/f)^2 . \qquad (9.08-16)$$

This equation is accurate to within 20 percent for $|B| > 3$; 8 percent for $|B| > 5$; 2 percent for $|B| > 7$; and 1 percent for $|B| > 8$. For smaller $|B|$, Eq. (9.08-15) should be used. The numerical solution of Eq. (9.08-15) for $f = f_0$ is the curve marked $h = 1$ in Fig. 9.03-2.

The attenuation of the filter on both skirts of the response curve may be estimated simply and fairly accurately from the known attenuation of the transformer prototype. Using Eq. (9.08-16), R becomes a function of frequency such that approximately

$$R \propto (f_0/f)^{2(n+1)} \tag{9.08-17}$$

and by Eq. (9.08-12) the attenuation will be multiplied by the same factor when R is large. [More accurately Eq. (9.08-15) rather than Eq. (9.08-16) should be used when some of the V_i are small.] Thus to estimate the filter attenuation at a specified frequency not too close to the band edge, we may first find the transformer attenuation in decibels at the corresponding frequency and then add $20(n + 1) \log_{10} (f_0/f)$ decibels, as already stated in Eq. (9.04-2).

By the *corresponding frequency*, we here mean that frequency on the quarter-wave transformer characteristic, f', (Fig. 9.08-1) which is obtained from a linear scaling

$$\frac{f'}{f'_1} = \frac{f}{f_1} \tag{9.08-18}$$

or

$$\frac{f'}{f'_2} = \frac{f}{f_2} \tag{9.08-19}$$

depending on whether the frequency f is below the lower band edge, f_1, or above the upper band edge, f_2 (Fig. 9.08-1).

The stop-band attenuation of the filter can thus be predicted fairly accurately from the prototype transformer characteristic. More often the reverse problem has to be solved. Thus the quantities specified may include the stop-band attenuation of the *filter* at some frequency, besides (for instance) the pass-band ripple and bandwidth; it is then required to find the minimum number of resonators, n, to meet these specifications.

This problem can be solved explicitly only for the prototype circuit
(Chapter 6). To find the number of resonators, n, for the reactively
coupled half-wave filter to meet a specified pass-band ripple, band-
width, and skirt selectivity (stop-band attenuation) requires trial
solutions in which numbers are assumed for n until the filter meets the
specifications. Where Eqs. (9.08-17) and (9.04-2) are valid, this can
be worked out quickly, as illustrated in the example of Sec. 9.04.
Otherwise Eqs. (9.08-13) and (9.08-15) should be used; the numerical
solution is facilitated by the graph in Fig. 9.03-2. Usually it is not
necessary to solve for all the V_i, but to solve only for one average
discontinuity VSWR, $V_{a,v}$, given by Eq. (9.08-10), which saves time in
making the calculations; this method is used in the last example of
Sec. 9.09.

This completes the necessary background material required for the
selection of transformer prototypes which will lead to filters of speci-
fied characteristics. The design procedure will now be summarized.

Summary of Design Procedure--The design procedure to be followed
then consists of the following steps:

(1) From the filter specifications select a quarter-wave
     transformer prototype that may be expected to yield
     a filter with nearly the desired performance. (The
     selected transformer will have the same pass-band
     ripple as specified for the filter.)

(2) Determine β from Fig. 9.08-2, and so estimate
     $w = \beta w_q$. If w is not as specified, repeat with
     another transformer with different bandwidth w_q
     until this specification is met.

(3) Determine α from Fig. 9.08-4, and then $\delta = (f_a - f_0)/f_a$
     from Fig. 9.08-5. If $(f_a - f_0)$ is small enough to be
     neglected (as will generally be the case for filters
     below about 10-percent bandwidth), omit Steps 4 and 5.

(4) If $(f_a - f_0)$ is significant, find f_0 from

$$f_0 = (1 - \delta)f_a \ . \qquad\qquad (9.08-20)$$

     This is the synchronous frequency, which is also the
     center frequency of the transformer.

(5) The upper and lower band-edges, f_2 and f_1, are next found from

$$
\left.
\begin{aligned}
f_2 &= f_a\left(1 + \frac{w}{2}\right) \\
    &= f_0\left(\frac{1 + w/2}{1 - \delta}\right) \\[2em]
\text{and} \qquad\qquad & \\[1em]
f_1 &= f_a\left(1 - \frac{w}{2}\right) \\
    &= f_0\left(\frac{1 - w/2}{1 - \delta}\right) \; .
\end{aligned}
\right\}
\qquad (9.08\text{-}21)
$$

(6) The values of the reactances or susceptances and their spacings are given in Eqs. (9.03-1) through (9.03-9), and must be determined at the synchronous frequency f_0.

SEC. 9.09, EXAMPLES OF FILTERS HAVING MEDIUM AND LARGE BANDWIDTHS

In this section, two further examples will be given, illustrating the design of a medium-bandwidth (20 percent), and a large-bandwidth (85 percent) filter (all of the type shown in Fig. 9.03-1). Their predicted and analyzed performances will be compared to show how accurate the method may be expected to be.

A 20-Percent-Bandwidth Filter—It is required to design a filter with four resonators to have a pass-band VSWR of better than 1.10 over a 20-percent bandwidth.

Thus $n = 4$, $w = 0.20$, $V_r = 1.10$.

Here $V_r = 1.10$ is less than $1 + (2w)^2 = 1.16$, but not very much less; reference to Sec. 9.01 suggests that this is a borderline case, for which the low-pass prototype will not work too well, but is worth trying. Using Eqs. (9.04-1) and (9.03-4), one obtains*

---

* These results could also be obtained using Eqs. (1) to (5) of Fig. 8.06-1 with $\lambda = w$ and $X_{j,j+1}/Z_0 = Y_0/B_{j+1}$.

$$\left. \begin{array}{l} \dfrac{B_1}{Y_0} = \dfrac{B_5}{Y_0} = -0.842 \\[2ex] \dfrac{B_2}{Y_0} = \dfrac{B_4}{Y_0} = -2.607 \\[2ex] \dfrac{B_3}{Y_0} = -3.758 \end{array} \right\} \qquad (9.09\text{-}1)$$

with

$$\left. \begin{array}{l} \theta_1 = \theta_4 = 127.67 \text{ degrees} \\[1ex] \theta_2 = \theta_3 = 147.24 \text{ degrees} \end{array} \right\} \qquad (9.09\text{-}2)$$

which also corresponds to a quarter-wave transformer or half-wave filter that would have

$$\left. \begin{array}{l} V_1 = V_5 = 2.27 \\[1ex] V_2 = V_4 = 8.67 \\[1ex] V_3 = 16.07 \end{array} \right\} \qquad (9.09\text{-}3)$$

The product $R = V_1 V_2 \ldots V_5$ is equal to 6215 which is only about ten times $(1/w)^n = (1/0.2)^4 = 625$, which confirms that this is a borderline case. [See Eq. (9.02-2) and Sec. 6.09.]

The analyzed performance curves of the filter defined by Eqs. (9.09-1) and (9.09-2), and the stepped-impedance half-wave filter defined by Eq. (9.09-3), are plotted in Fig. 9.09-1. Neither characteristic meets the specifications very closely, because the narrow-band condition, Eq. (9.09-2), is not satisfied well enough.

Let us re-design the prototype quarter-wave transformer, or stepped-impedance half-wave filter, and derive the reactance-coupled filter from the quarter-wave transformer prototype. Selecting $n = 4$, $w_q = 0.40$, $V_r = 1.10$, which by Table 6.02-1 gives $R = 5625$, yields

$$\left. \begin{array}{l} V_1 = V_5 = 2.398 \\[1ex] V_2 = V_4 = 8.45 \\[1ex] V_3 = 13.71 \end{array} \right\} \qquad (9.09\text{-}4)$$
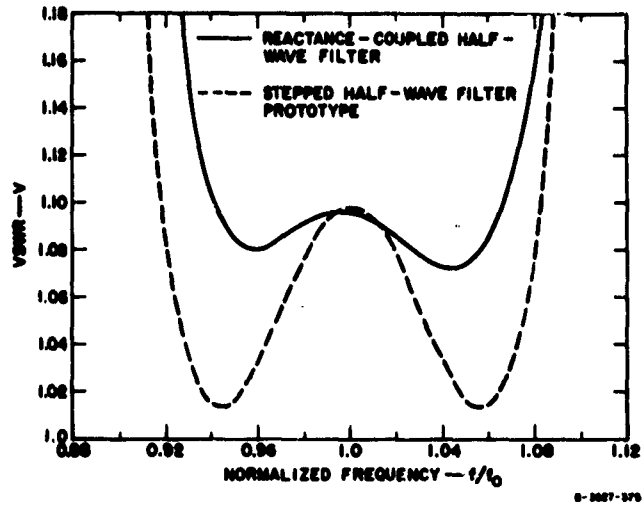
FIG. 9.09-1 CHARACTERISTICS OF A FOUR-RESONATOR
FILTER AND ITS STEPPED HALF-WAVE
FILTER PROTOTYPE, BOTH BASED ON AN
EQUAL-RIPPLE LOW-PASS LUMPED-
CONSTANT PROTOTYPE

These VSWRs do not seem to differ greatly from those in Eq. (9.09-3),
yet they will be enough to turn the broken-line characteristic in
Fig. 9.09-1 into an equi-ripple prototype response and greatly improved
filter response.

From Fig. 9.08-2 for $n \sim 4$ and $R = 5625$, one obtains $\beta = 0.52$, so
that we would expect the reactance-coupled filter bandwidth to be
$w = \beta w_q = 0.52 \times 0.40 = 0.208$. From Fig. 9.08-4, for

$$V_{s v} = R^{(1/n+1)} = (5625)^{1/5} = 5.65 \qquad (9.09-5)$$

we read off $\alpha = 0.65$. Hence, from Fig. 9.08-5, $\delta = 0.0064$. Then, from
Eq. (9.08-21)

$$\left.\begin{array}{l} f_2 = 1.110 \, f_0 \\ \\ f_1 = 0.902 \, f_0 \end{array}\right\} \qquad (9.09-6)$$

where f_0 is the synchronous frequency.

555

For the reactance-coupled filter derived from Eqs. (9.09-4) using Eqs. (9.03-4) and (9.03-9) (which assume that $h_i = 1$)

$$\left.\begin{array}{l}
\dfrac{B_1}{Y_0} = \dfrac{B_5}{Y_0} = -0.902 \\[2em]
\dfrac{B_2}{Y_0} = \dfrac{B_4}{Y_0} = -2.563 \\[2em]
\dfrac{B_3}{Y_0} = -3.436
\end{array}\right\} \qquad (9.09-7)$$

and therefore

$$\left.\begin{array}{l}
\theta_1 = \theta_4 = 128.15 \text{ degrees} \\[1em]
\theta_2 = \theta_3 = 145.92 \text{ degrees}
\end{array}\right\} \qquad (9.09-8)$$

The analyzed response of the stepped-impedance half-wave filter prototype corresponding to the exact Tchebyscheff transformer design Eq. (9.09-4) is shown by the broken line in Fig. 9.09-2, and the reactance-coupled filter response is shown by the solid line in that figure. This is an appreciable improvement on the performance of the preceding filter and transformer design based on the first procedure using the lumped-constant low-pass prototype. The analyzed performance of the filter shows that $f_1 = 0.909 \ f_0$ (compare 0.902 f_0 predicted) and $f_2 = 1.103 \ f_0$ (compare 1.110 f_0 predicted). The fractional bandwidth w is 0.193 (compare 0.208 predicted), and the relative mean-to-synchronous frequency displacement $\delta = (f_a - f_0)/f_a$ is 0.006 (just as predicted).

It is clear, comparing the solid and broken lines of Fig. 9.09-2, that there is still room for improvement. The main discrepancy between predicted and analyzed performance is in the bandwidth, which is 1.5 percent less than predicted. The reason for this is the difference in the frequency sensitivities of the resonator lengths; this difference is typical of filters in which some of the discontinuity VSWRs are in the neighborhood of 2.0 and others differ appreciably from the value 2.0 [see Eq. (9.09-4)]. The reason for this will be explained in Sec. 9.10.
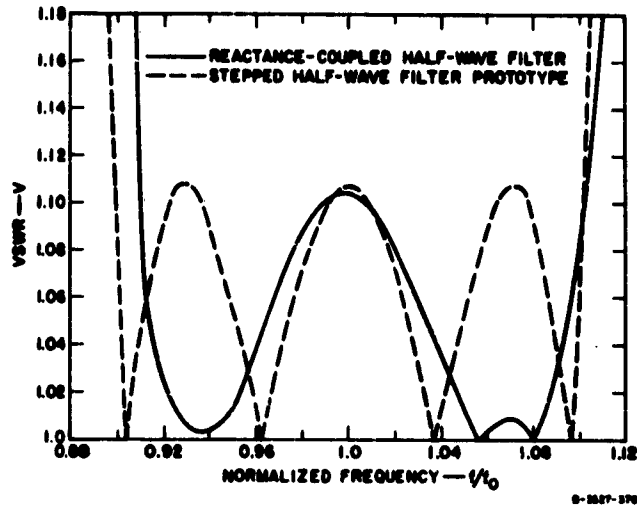
FIG. 9.09-2 CHARACTERISTICS OF A FOUR-RESONATOR
FILTER AND ITS EQUAL-RIPPLE STEPPED
HALF-WAVE FILTER PROTOTYPE

This example will then be continued in the first example of Sec. 9.11,
where it will be shown that the line-length frequency-sensitivities can
be equalized by optimizing the line impedances (instead of setting them
all equal to each other). This generally leads to a very nearly equal-
ripple characteristic with slightly more than the predicted bandwidth.

An 85-Percent-Bandwidth Filter—A pseudo-high-pass filter of eight
sections is to be designed to have a pass-band frequency ratio, f_2/f_1,
of approximately 2.5:1, and a pass-band attenuation (reflection-loss) of
less than 0.1 db.

Since $f_2/f_1 = 2.5$,

$$w = 2\left(\frac{f_2 - f_1}{f_2 + f_1}\right) = 0.85 \quad . \qquad (9.09-9)$$

We design a quarter-wave transformer prototype by the modified first-
order theory of Sec. 6.07, specifying $w_q = 1.40$, and a 0.2 db pass-band
attenuation ripple. (This approximate method always gives slightly less
bandwidth, and slightly less ripple, than specified.) The modified first-
order theory gives

557

$$\left.\begin{array}{rcl} V_1 & = & V_9 = 1.348 \\ V_2 & = & V_8 = 1.561 \\ V_3 & = & V_7 = 1.829 \\ V_4 & = & {}_6 = 1.985 \\ & & V_5 = 2.034 \end{array}\right\} \qquad (9.09\text{-}10)$$

The computed response is shown by the broken line in Fig. 9.09-3, and it is seen that it has a pass-band attenuation of less than 0.12 db over a 135-percent bandwidth ($w_q = 1.35$). The quarter-wave transformer output-to-input impedance ratio, R, is

$$R = V_1 V_2 \ldots V_9 = 118.4 \qquad . \qquad (9.09\text{-}11)$$
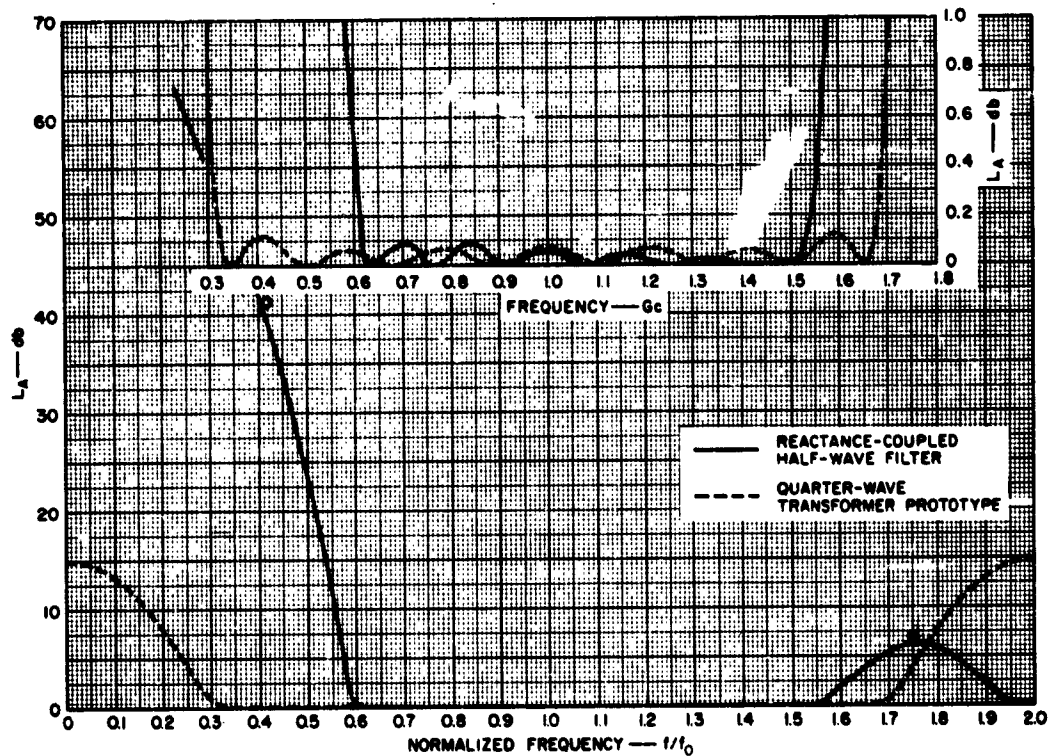
FIG. 9.09-3 CHARACTERISTICS OF AN EIGHT-RESONATOR FILTER AND ITS QUARTER-WAVE TRANSFORMER PROTOTYPE

From Fig. 9.08-2, the bandwidth contraction factor is $\beta = 0.63$, and the expected fractional bandwidth of the filter is therefore $w = \beta w_q = 0.85$, which is the specified bandwidth.

We also find from Fig. 9.08-4 that for $V_{av} = (118.4)^{1/9} = 1.70$, $\alpha = 0.36$. Then, from Fig. 9.08-5, one obtains $\delta = 0.06$. Therefore, by Eq. (9.08-21), we shall expect

$$\left. \begin{array}{l} f_2 = 1.52\ f_0 \\ \\ f_1 = 0.61\ f_0 \end{array} \right\} \tag{9.09-12}$$

For the reactance-coupled filter derived from Eq. (9.09-10) by use of the equations in Sec. 9.03 with $h_1 = 1$,

$$\left. \begin{array}{ll} \dfrac{B_1}{Y_0} = \dfrac{B_9}{Y_0} = -0.2998 \\ \\ \dfrac{B_2}{Y_0} = \dfrac{B_8}{Y_0} = -0.4495 \\ \\ \dfrac{B_3}{Y_0} = \dfrac{B_7}{Y_0} = -0.613 \\ \\ \dfrac{B_4}{Y_0} = \dfrac{B_6}{Y_0} = -0.700 \\ \\ \dfrac{B_5}{Y_0} = -0.725 \end{array} \right\} \tag{9.09-13}$$

and

$$\left. \begin{array}{l} \theta_1 = \theta_9 = 100.60 \text{ degrees} \\ \\ \theta_2 = \theta_7 = 104.85 \text{ degrees} \\ \\ \theta_3 = \theta_6 = 108.17 \text{ degrees} \\ \\ \theta_4 = \theta_5 = 109.61 \text{ degrees} \end{array} \right\} \tag{9.09-14}$$

The response of this filter was analysed and is shown by the solid line in Fig. 9.09-3. It is seen that the attenuation in the pass band is everywhere less than 0.1 db, the fractional bandwidth w is 0.85, the band edges are $f_2 = 1.53$ and $f_1 = 0.62$, and the relative mean-to-synchronous frequency displacement is 0.075; all of these are very close to the predicted values.

The stop-band attenuation was worked out at two frequencies, as explained in Sec. 9.08; Fig. 9.03-2, based on Eq. (9.08-15), was utilised in this calculation. These two points are shown by the small rings in Fig. 9.09-3, and fall very close to the curve obtained by analysis on a digital computer.

This filter was used to obtain the "standardized" pseudo-high-pass filters of Sec. 9.06. The three central elements, which are nearly equal (0.700, 0.725, 0.700), were averaged and each set equal to 0.710. This element was then repeated periodically as explained in Sec. 9.06, with the results shown in Figs. 9.06-1 and 9.06-2.

SEC. 9.10, DERIVATION OF THE DATA FOR BANDWIDTH CONTRACTION AND PASS-BAND DISTORTION

The basic ideas on the conversion of the quarter-wave transformer prototype into a filter with reactive elements have already been explained. The design procedure and numerical data were presented—mostly without proof. We now proceed to fill in the details of the over-all picture presented thus far.

Bandwidth Contraction—The frequency-sensitivity[1,2] (and hence bandwidth) of the reactance-coupled filters of Fig. 9.03-1 is strongly influenced by the angles ψ' and ψ'', in Fig. 9.03-3, which correspond to the electrical distances between the coupling reactance and the two reference planes with pure imaginary reflection coefficient on either side of it. Both reference planes move closer to the reactance as the frequency increases, partly (1), because a given *electrical* separation shrinks in *physical* length as the frequency increases; and partly (2) because the *electrical* lengths ψ' and ψ'' do not remain constant, but decrease with increasing frequency for shunt inductances (or series capacitances), since their susceptance (or reactance) values decrease with frequency. The movement of the reference planes is measured quantitatively by two parameters d' and d'' defined by

$$d' = \frac{4}{\pi}\left[\psi' - \frac{d\psi'}{d(f//f_0)}\right]_{f=f_0} \tag{9.10-1}$$

$$d'' = \frac{4}{\pi}\left[\psi'' - \frac{d\psi''}{d(f//f_0)}\right]_{f=f_0} \tag{9.10-2}$$

where the first term in the square brackets corresponds to Cause (1), and the second term to Cause (2). The parameters d' and d'' measure the rate of change with frequency of the reference planes in Fig. 9.03-3 as compared to the rate of change of a 45-degree line length. The spacings θ_i (Fig. 9.03-1) between reactances are given at band center by Eq. (9.03-7). The spacings are thus always longer electrically than 90-degrees, and accordingly increase with frequency faster than does a quarter-wave line length. The bandwidth of the filter is therefore always less than the bandwidth of its quarter-wave transformer prototype by a factor β. The bandwidth contraction factor associated with the ith resonator or line-section, β_i, is given by

$$\frac{1}{\beta_i} = \frac{2}{\pi}\left[\frac{d\theta_i}{d(f//f_0)}\right]_{f=f_0} = 1 + \frac{d''_i + d'_{i+1}}{2} \tag{9.10-3}$$

If all the β_i, defined in Eq. (9.10-3) were the same for a particular filter, then its bandwidth would be

$$w = \beta w_q \quad , \tag{9.10-4}$$

where w_q is the quarter-wave transformer bandwidth. Usually the β_i are not all equal; the smallest of the β_i should then be used for β in the above equation since the most frequency-sensitive resonator tends to determine the filter bandwidth.

To cover both the series-reactance-coupled and the shunt-susceptance-coupled filter in Fig. 9.03-1, we shall use the word *immittance* when we mean impedance for the former [Fig. 9.03-1(a)] or admittance for the latter [Fig. 9.03-1(b)]. When the line immittances are all equal, then $d'_i = d''_i$, but when the line immittances are not all equal, the d'_i and d''_i

are not equal: The larger d_i is associated with the ψ_i in the line with lower immittance, and is given by the solid lines in Fig. 9.10-1; conversely, the smaller d_i is associated with the ψ_i in the line with higher immittance, and is given by the broken lines in Fig. 9.10-1. The curves in Fig. 9.10-1 were worked out for infinitesimal bandwidths, following Eqs. (9.10-1) and (9.10-2). The curves in Fig. 9.10-2 were worked out for several finite bandwidths, replacing the differential terms in Eqs. (9.10-1) and (9.10-2) by finite increment ratios; only filters with uniform line immittances ($h_i = 1$) are shown in Fig. 9.10-2. Figure 9.08-2 was then worked out[1] with the aid of the curve $h = 1$ in Fig. 9.10-1, which is the same as the curve $v = 0$ in Fig. 9.10-2.

It has been found that Fig. 9.08-2 has predicted bandwidths closely for all the filters analyzed. The accuracy is least for filters that have a considerable spread among their β_i. According to Eq. (9.10-3) and Fig. 9.10-1 or 9.10-2, this occurs when the discontinuity VSWRs in one filter range into and out of the neighborhood of 2.0, where d can change appreciably in either direction (see Figs. 9.10-1 or 9.10-2). In that case it may be worthwhile to optimize the line impedances, as in Sec. 9.11.

Pass-Band Distortion—The distinction has already been made between the synchronous frequency, f_0, and the arithmetic mean frequency, f_a, which is always greater than f_0, since the portion of the pass band above the synchronous frequency is greater than the portion below. This phenomenon is due to the declining discontinuity VSWRs with increasing frequency when series capacitances or shunt inductances are used, and may be put on a quantitative footing as follows.

The excess loss has already been cited in Eq. (9.08-12). Consider now the case of large R, so that the approximation Eq. (9.09-16) holds. The largest term of the Tchebyscheff polynomial well inside the stop-band is the highest power of $(\sin \theta / \mu_0)$, and then Eq. (9.08-12) reduces to

$$\mathcal{E} = \frac{P_{avail}}{P_{load}} - 1 = const. \ \frac{\sin^{2n}\theta}{(f/f_0)^{2(n+1)}} \tag{9.10-5}$$

$$\approx const. \left[\frac{\Delta f}{(f/f_0)^{1+1/n}} \right]^{2n} \tag{9.10-6}$$

562
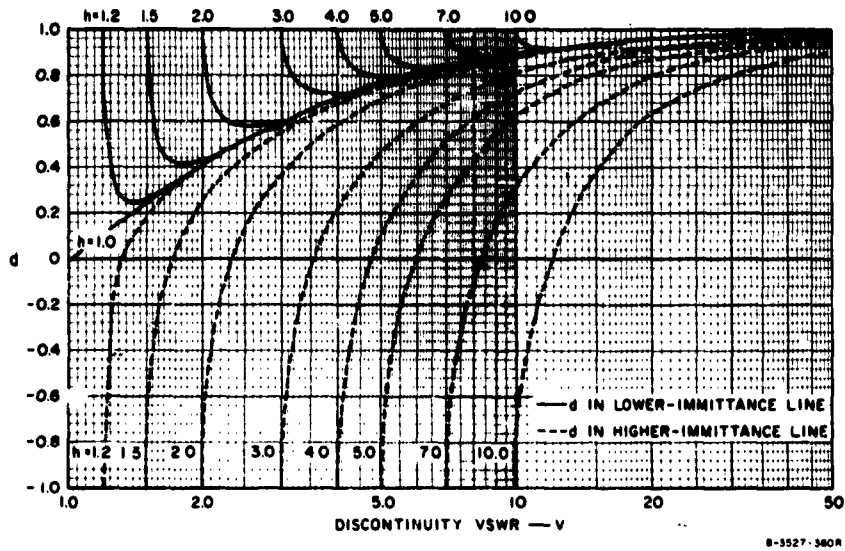
FIG. 9.10-1   CHART DETERMINING FREQUENCY SENSITIVITIES OF INDIVIDUAL
RESONATORS OVER SMALL FREQUENCY BANDS
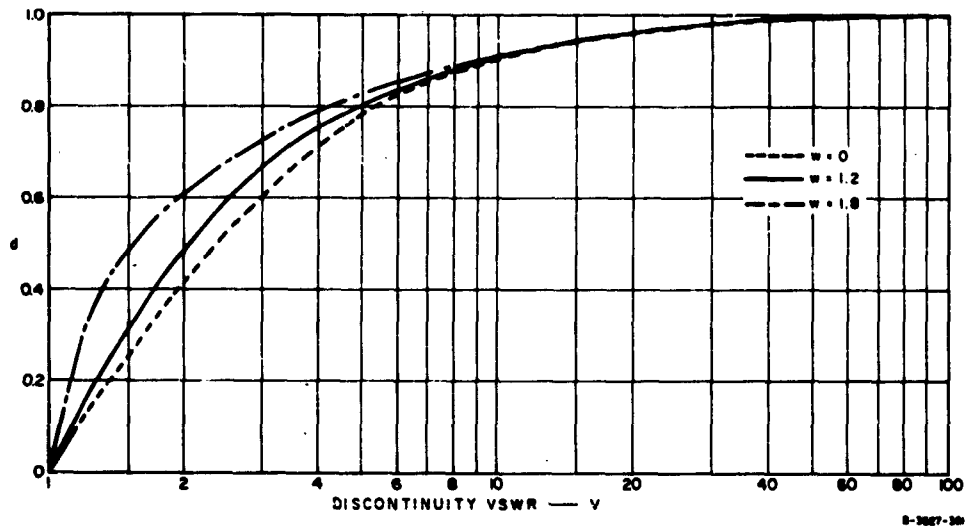
FIG. 9.10-2   CHART DETERMINING FREQUENCY SENSITIVITIES OF INDIVIDUAL
RESONATORS OVER VARIOUS FRACTIONAL BANDWIDTHS, w, WHEN
THE LINE IMPEDANCES ARE CONSTANT

563
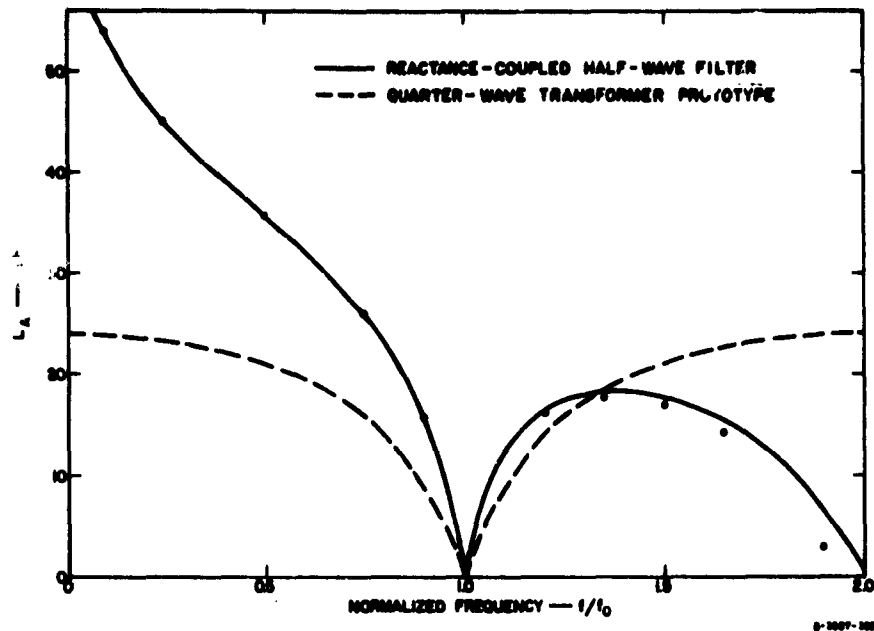
FIG. 9.10-3   CHARACTERISTICS OF A SINGLE-SECTION FILTER AND ITS
QUARTER-WAVE TRANSFORMER PROTOTYPE

where $\Delta f = f - f_0$. This proves the result stated in Eqs. (9.08-6) and
(9.08-7); for large n and large R, the exponent of (f/f_0) reduces to
unity, leading to a more symmetrical response on a wavelength (rather
than frequency) scale. As a counter-example, a single-resonator filter
($n = 1$) was analyzed and α calculated from Eq. (9.08-8). The response
of this filter ($n = 1$, $R = 1000$) is plotted in Fig. 9.10-3, and it was
found that (using the 14-db band edges for convenience) $\alpha = 1.97$, which
is close to $1 + 1/n = 2.0$ as required for $n = 1$. This point is the square
one in Fig. 9.08-4.

The circle points in Fig. 9.10-3 were calculated using the approximate
Eq. (9.04-2) in conjunction with the prototype characteristic. This method
is seen once again to give excellent results.

The choice of mapping or frequency distortion by a function of the
form $\Delta f/(f/f_0)^a$, was based on the above considerations, and is further
developed in Sec. 9.08.

564

SEC. 9.11, OPTIMIZING THE LINE IMPEDANCES

It was pointed out in Sec. 9.10 that different line sections of a single filter yield different bandwidth contraction factors β_i, because the quantities d'_i, d''_i vary from resonator to resonator. So far we have only considered examples of filters with uniform line impedances, where all Z_i are equal to Z_0. In deriving the discontinuity parameters, the discontinuity VSWR is always set equal to the corresponding step-VSWR of the prototype transformer; this VSWR can be obtained in the filter by an infinity of combinations of reactances with impedance ratios, since the two parameters h and u (Fig. 9.03-3) produce the desired discontinuity VSWR. Thus, if V_i is given and h_i is selected, X_i or B_i is determined from Eqs. (9.03-2) and (9.03-3). The problem is now to select h_i, V_i being given, so that all the β_i are the same. This can easily be done with the aid of Fig. 9.10-1, and is best illustrated by an example.

A 20 Percent-Bandwidth Filter with Optimized Line Impedances—it is required to improve the performance of the filter defined by Eqs. (9.09-7) and (9.09-8) and shown by the solid line in Fig. 9.09-2.

We see from Eq. (9.09-4) that the V_i range in numerical value from about 2 to nearly 14. Thus the different resonators have appreciably different β_i, and we might expect a noticeable deviation from an equal-ripple response, as already pointed out for this situation.

Here we have a four-resonator filter. The two central resonators, Nos. 2 and 3, are each flanked by discontinuity VSWRs of 8.45 and 13.71, according to Eq. (9.09-4). Keeping the characteristic admittances of the lines forming the four resonators the same. we find from Fig. 9.10-1 that $d''_2 = 0.88$ (corresponding to $h = 1$, $V = 8.45$) and $d'_3 = 0.93$ (corresponding to $h = 1$, $V = 13.71$), so that for the two central resonators,

$$\frac{d''_2 + d'_3}{2} = \frac{d''_3 + d'_4}{2} = 0.905 \qquad (9.11\text{-}1)$$

If we kept the input and output admittances the same also, so that $h = 1$ at both the first and last discontinuities, then for $V = 2.398$ [Eq. (9.09-4)] we would have $d''_1 = 0.50$, which is considerably different from the other d. Since $d'_2 = d''_2 = 0.88$, this would yield $(d''_1 + d'_2)/2 = 0.59$ for the outside resonators, which differs appreciably from 0.905 for the central resonators. Hence the relatively poor response shape in

Fig. 9.09-2. To obtain a value of $(d_1'' + d_2')/2$ equal to 0.905, as for the central resonators, requires $d_1'' = d_3' = 0.93$. We then find the value of h from Fig. 9.10-1. Finding the intersection of the horizontal line for $d = 0.93$ with the vertical line for $V = 2.398$ gives $h = 2.38$. One then obtains the following filter parameters:

$$\frac{Y_1}{Y_0} = \frac{Y_2}{Y_0} = \frac{Y_3}{Y_0} = \frac{Y_4}{Y_0} = \frac{1}{2.38} = 0.4202 \qquad (9.11\text{-}2)$$

$$\left. \begin{aligned} \frac{B_1}{Y_0} &= \frac{B_5}{Y_0} = -0.7895 \\[2em] \frac{B_2}{Y_1} &= \frac{B_4}{Y_1} = -2.564 \\[2em] \frac{B_3}{Y_1} &= -3.433 \end{aligned} \right\} \qquad (9.11\text{-}3)$$

$$\left. \begin{aligned} \theta_1 &= \theta_4 = 158.74 \quad \text{degrees} \\ \theta_2 &= \theta_3 = 145.92 \quad \text{degrees} \end{aligned} \right\} \qquad (9.11\text{-}4)$$

The predicted bandwidth is

$$w = \beta w_q = 0.40/1.905 = 0.210 \qquad . \qquad (9.11\text{-}5)$$

The appearance of such a filter with shur'-inductive irises in wave-guide, or with series-capacitive gaps in strip line, is shown in Fig. 9.11-1.

The analyzed performance of this filter is shown by the solid line (marked C) in Fig. 9.11-2. The original design obtained from a lumped-constant low-pass prototype through Eqs. (9.04-1) and (9.03-4) is shown for comparison (Curve A); the performance of the filter based on the same transformer prototype as Curve C, but with *uniform* line impedances (all $h_i = 1$: see Sec. 9.09) is also shown (Curve B). It is seen that the new

566

design, after optimizing the line impedances, gives an almost equal-ripple response. Its bandwidth is 21.8 percent, slightly more than the 21.0 percent predicted.

The distortion factor, α, worked out from Eq. (9.08-8) amounts to 1.33, and is shown by the upper triangle-point in Fig. 9.08-4. It does not fall in line with the points calculated for the constant-line-impedance filters. Most of the improvement in bandwidth is due to an increase in the upper band-edge frequency (Fig. 9.11-2) which has the effect of increasing α. A possible explanation is that V_1 and V_5 are largely determined by the impedance step, which is independent of frequency, whereas the other VSWRs (V_2, V_3, and V_4) are determined by reactances which decrease as the frequency rises. This corresponds, on the high-frequency side, to having the filter turn into a wider-band design, thus pushing the upper band edge even further up. The reverse holds

(a)

(b)
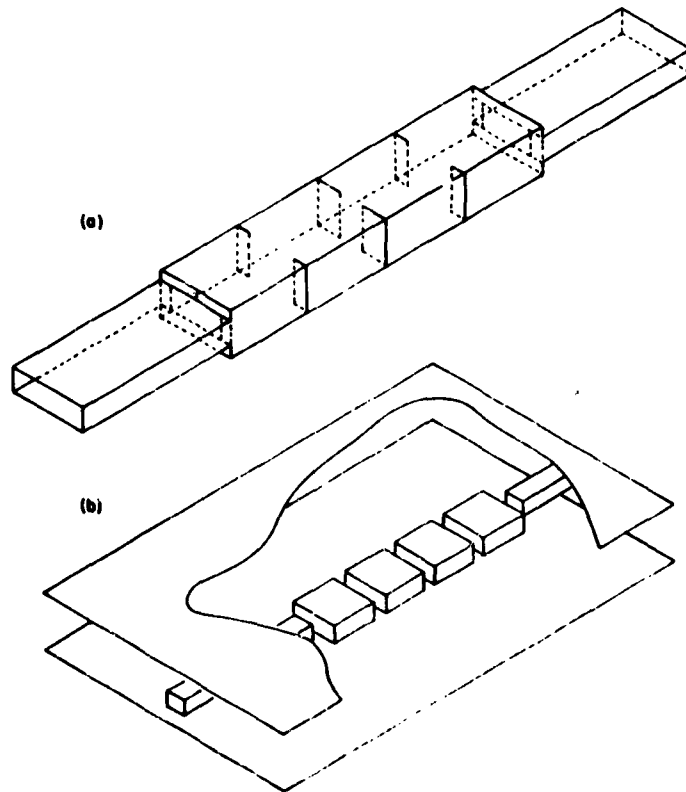
FIG. 9.11-1   FILTERS IN WHICH THE LINE IMPEDANCES CHANGE

567
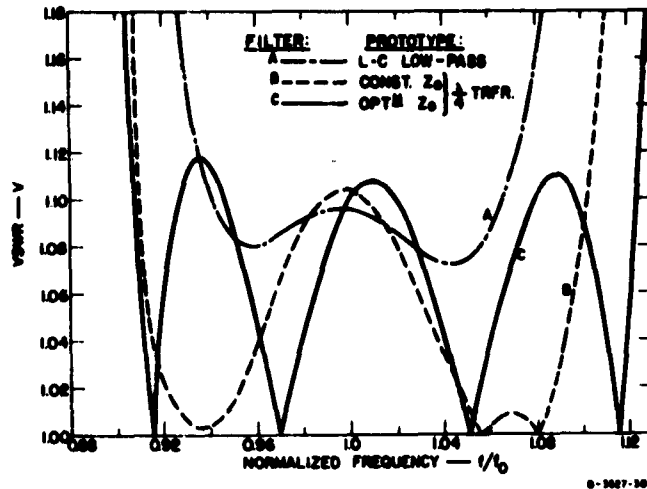
FIG. 9.11-2 CHARACTERISTICS IN THE PASS BAND OF
THREE FILTERS DESIGNED TO THE SAME
SPECIFICATIONS

(the V_i increase) below band center, which here partly cancels the improvement in bandwidth due to making all β_i equal to one another, and so the lower band edge moves less. Thus α increases by Eq. (9.08-8).

The pass- and stop-band responses of the two filters based on the same quarter-wave transformer prototype are shown in Fig. 9.11-3, along with the response of the transformer. The circle-points were calculated for the uniform-line impedance filter curve (B in Figs. 9.11-2 and -3) by the method described in Sec. 9.08.

A 30 Percent-Bandwidth Filter—The following example is worked the same way as the previous one, and only the results are given. It is based on the following prototype Tchebyscheff transformer:

$$
\left.
\begin{array}{rcl}
n & = & 4 \\
R & = & 100 \\
w_q & = & 0.6 \\
\text{Ripple VSWR} & = & 1.07
\end{array}
\right\}
\qquad (9.11\text{-}6)
$$

568

giving

$$V_1 = V_5 = 1.538$$
$$V_2 = V_4 = 3.111$$
$$V_3 = 4.368 .$$

$$(9.11\text{-}7)$$

Transformed into a filter with uniform line impedances, the reactance-parameters and line-lengths are

$$\frac{B_1}{Y_0} = \frac{B_5}{Y_0} = -0.4335$$

$$\frac{B_2}{Y_0} = \frac{B_4}{Y_0} = -1.1971$$

$$(9.11\text{-}8)$$

$$\frac{B_3}{Y_0} = -1.6115 .$$

$$\theta_1 = \theta_4 = 111.57 \quad \text{degrees}$$
$$\theta_2 = \theta_3 = 124.88 \quad \text{degrees} .$$

$$(9.11\text{-}9)$$
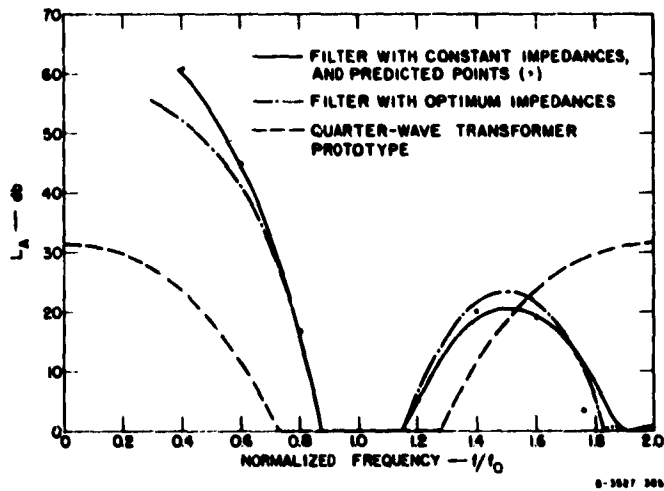
FIG. 9.11-3 CHARACTERISTICS IN THE STOP BAND OF THE
THREE FILTERS DESCRIBED IN FIG. 9.11-2

569
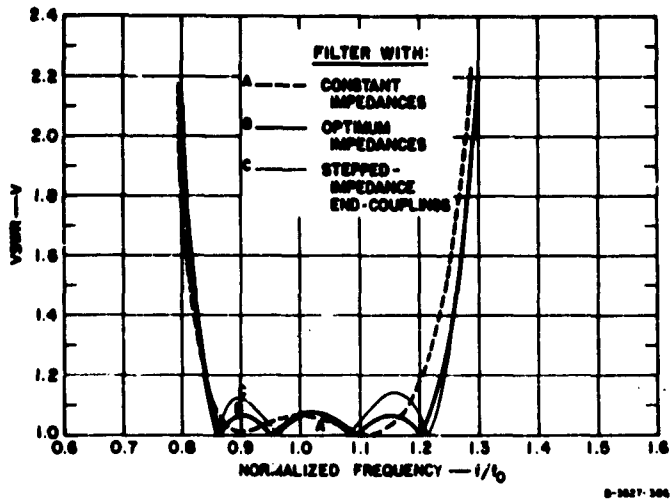
FIG. 9.11-4 PASS-BAND CHARACTERISTICS OF THREE
FILTERS DESIGNED FOR 30-PERCENT
BANDWIDTH

This example has been selected because of the appreciable spread of V_i about the numerical value 2.

With these values of V_i and all $Z_i = Z_0$, Fig. 9.10-1 shows a considerable variation in d_i from about 0.25 to 0.75, and we would expect these different frequency sensitivities to result in a poor response shape. This is borne out in Fig. 9.11-4, in which Curve A is the filter response analyzed on a digital computer. It has a bandwidth of 30.7 percent, compared to 34.7 percent predicted.

To optimize the line impedances, Fig. 9.10-1 determines $h = 1.5$ for the end-couplings, and one obtains

$$\frac{Y_1}{Y_0} = \frac{Y_2}{Y_0} = \frac{Y_3}{Y_0} = \frac{Y_4}{Y_0} = \frac{1}{1.5} = 0.6667 \qquad (9.11\text{-}10)$$

$$\left. \begin{array}{l} \dfrac{B_1}{Y_0} = \dfrac{B_5}{Y_0} = -0.1198 \\[2em] \dfrac{B_2}{Y_1} = \dfrac{B_4}{Y_1} = -1.1971 \\[2em] \dfrac{B_3}{Y_1} = -1.6115 \end{array} \right\} \qquad (9.11\text{-}11)$$

570

$$\left. \begin{array}{l} \theta_1 \ = \ \theta_4 \ = \ 142.62 \quad \text{degrees} \\[2mm] \theta_2 \ = \ \theta_3 \ = \ 124.88 \quad \text{degrees} \quad . \end{array} \right\} \qquad (9.11\text{-}12)$$

The physical appearance of this filter would again be as indicated in Fig. 9.11-1. The response of the filter was analyzed and is plotted as Curve B in Fig. 9.11-4. Again there is very nearly an equal-ripple response, and the bandwidth is 36.2 percent, which is slightly more than the 35.8 percent predicted. Most of the improvement in bandwidth occurs above the band-center. A possible explanation for this effect was offered in the previous example. The distortion factor α here equals 1.07 and is shown by the lower triangle-point in Fig. 9.08-4.

Most of the end-coupling VSWR of 1.538 is due to the impedance ratio of 1.50, and only a small part is due to the normalized susceptance of 0.1198. Since most of $V_1 = V_5 = 1.538$ is due to the 1.5:1 impedance step, it is of practical interest to investigate what happens to the performance when the reactances B_1 and B_5 are left out, and the impedance ratio is increased to 1.538:1 to achieve the desired V_1 and V_5. The result is

$$\frac{Y_1}{Y_0} \ = \ \frac{Y_2}{Y_0} \ = \ \frac{Y_3}{Y_0} \ = \ \frac{Y_4}{Y_0} \ = \ \frac{1}{1.538} \ = \ 0.6502 \qquad (9.11\text{-}13)$$

$$\left. \begin{array}{l} \dfrac{B_1}{Y_0} \ = \ \dfrac{B_5}{Y_0} \ = \ 0 \\[5mm] \dfrac{B_2}{Y_1} \ = \ \dfrac{B_4}{Y_1} \ = \ -1.1971 \\[5mm] \dfrac{B_3}{Y_1} \ = \ -1.6115 \end{array} \right\} \qquad (9.11\text{-}14)$$

$$\left. \begin{array}{l} \theta_1 \ = \ \theta_4 \ = \ 150.45 \quad \text{degrees} \\[2mm] \theta_2 \ = \ \theta_3 \ = \ 124.88 \quad \text{degrees} \quad . \end{array} \right\} \qquad (9.11\text{-}15)$$

571
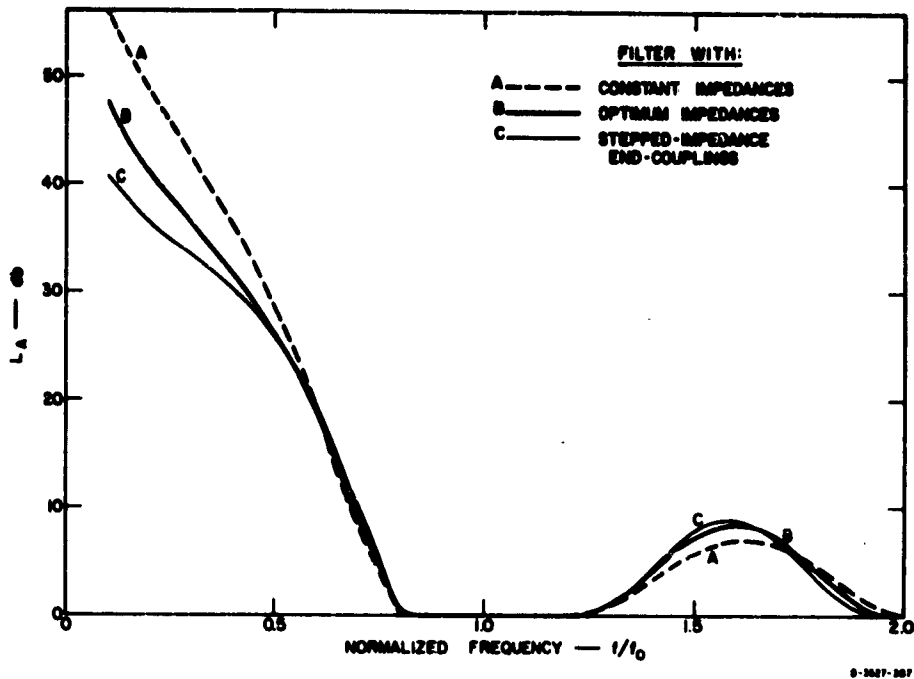
FIG. 9.11-5 STOP-BAND CHARACTERISTICS OF THREE FILTERS
DESIGNED FOR 30-PERCENT BANDWIDTH

The analyzed performance of this filter is shown in Fig. 9.11-4 by Curve C.
This filter has passed beyond the optimum performance; the peak reflection
has almost doubled in the pass band, and the ripples are no longer equal.
Even so, this performance is better than the first design with uniform
line impedances (Curve A).

The pass- and stop-band characteristics of all three filters are
shown in Fig. 9.11-5, and are in the expected relationships to each other,
since the end couplings of Design A have the most cap citance, and those
of Design C have none.

SEC. 9.12, REACTANCE-COUPLED QUARTER-WAVE FILTERS

The circuit of a reactance-coupled quarter-wave filter is shown in
Fig. 9.12-1. This circuit was described in Sec. 8.08, where it was
designed from a lumped-constant low-pass prototype. The method of
Chapter 8 holds up to about 20 percent bandwidths for reactance-coupled
half-wave filters, and up to about 40 percent bandwidths for

572

reactance-coupled quarter-wave filters, which generally have about twice the fractional bandwidth when the discontinuity VSWRs are the same.

The spacings between elements at the synchronous frequency are exactly one-quarter wavelength less than for a reactance-coupled half-wave filter (Fig. 9.03-1) having the same discontinuity VSWRs, and can thus be determined with the aid of Eq. (9.03-7) or Eq. (9.03-9). [The series reactances and shunt susceptances are still determined from the quarter-wave transformer prototype step-VSWRs using Eqs. (9.03-3) or (9.03-4).] The quantities d' and d'' can be determined from Fig. 9.10-1, but the new bandwidth contraction or expansion factor β' is given by

$$\frac{1}{\beta'_i} = \frac{d''_i + d'_{i+1}}{2} \qquad (9.12\text{-}1)$$

instead of Eq. (9.10-3). The bandwidth contraction factor β' for the quarter-wave reactance-coupled filter can also be determined from Fig. 9.08-2 by substituting

$$\beta' = \frac{1}{\frac{1}{\beta} - 1} = \frac{\beta}{1 - \beta} \qquad (9.12\text{-}2)$$

and may thus be expected to be greater than unity. This is in keeping with the fact that all discontinuities are separated by distances *less* than one-quarter wavelength at the synchronous frequency, and the bandwidth of the filter may therefore be expected to be greater than the bandwidth of its prototype quarter-wave transformer.

SHUNT SUSCEPTANCES
OR SERIES REACTANCES:

B_1 X_2 B_3 X_4

ELECTRICAL LENGTHS:

θ'_1 —— θ'_2 —— θ'_3

LAST ELEMENT: B_{n+1} OR X_{n+1}

A 3527 355
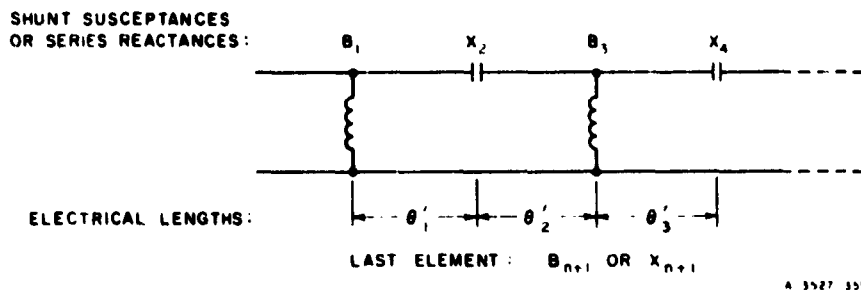
FIG. 9.12-1   REACTANCE-COUPLED QUARTER-WAVE FILTER

However, since a common 90-degree line-length (at the synchronous frequency) has been removed from each cavity, the remaining line lengths differ relatively more among themselves than before, so that one should expect less than the bandwidths predicted by Eq. (9.12-2) and Fig. 9.08-2. This will be so especially for strong couplings, when the small series reactances or shunt susceptances lead to close spacings (much less than 90 electrical degrees) between discontinuities. Then a small absolute difference in resonator lengths may amount to a large relative difference. Prediction by the previous method then becomes less and less accurate as the couplings become stronger (which usually means, as the bandwidth increases).

We shall now convert two half-wave reactance-coupled filters (one narrow-band and one wide-band) into quarter-wave reactance-coupled filters. The parameters of the filters are obtained on making the substitutions

$$\left. \begin{array}{l} \dfrac{B_1}{Y_0} \rightarrow \dfrac{B_1}{Y_0} \\[2em] \dfrac{B_2}{Y_0} \rightarrow \dfrac{X_2}{Z_0} \\[2em] \dfrac{B_3}{Y_0} \rightarrow \dfrac{B_3}{Y_0} \\[2em] \dfrac{B_4}{Y_0} \rightarrow \dfrac{X_4}{Z_0} \end{array} \right\} \text{, etc.} \tag{9.12-3}$$

and

$$\theta_i - \frac{\pi}{2} \rightarrow \theta_i' \quad , \tag{9.12-4}$$

(that is, all separations are reduced by 90 degrees). The numerical values will therefore not be repeated.

A 20 Percent Bandwidth Filter—It is desired to design a quarter-wave reactance-coupled filter to have a pass-band VSWR of better than 1.10 over a 20-percent bandwidth, and to have at least 22 db of attenuation at a frequency 20 percent above band center (i.e., twice as far out as the desired band edge).

574

A quarter-wave filter of sufficiently small bandwidth should have twice the fractional bandwidth of a half-wave filter with the same discontinuity VSWRs. Therefore the reactance-coupled quarter-wave filter specified above and the reactance-coupled half-wave filter of Sec. 9.04 will be derivable from the same prototype transformer, provided that the skirt selectivity requires the same number of resonators. The attenuation twice as far above band center as the band edge was specified as 25 db in the example of Sec. 9.04, but is only 22 db in the present example. We must expect a lower attenuation in the present example since by Eq. (9.08-17) R is reduced by a factor $(1.2)^{14}$ instead of $(1.1)^{14}$ as before. Therefore we may again try $n = 6$ resonators.

The pass-band response of this filter is shown in Fig. 9.12-2. Its bandwidth is almost twice (19.1 percent as compared with 9.7 percent) the bandwidth of the half-wave reactance-coupled resonator filter, which is also shown for comparison. This was expected. The deterioration in the response shape can be attributed to the relatively greater differences in the frequency sensitivities of the spacings.

The attenuation at $f/f_0 = 1.2$ may be calculated using Eq. (9.04-5),

$$(f/f_0)^{2(n+1)} = (1.2)^{14} = 12.8 , \qquad (9.12-5)$$

which shows that the attenuation is 11.1 db less than the attenuation of the quarter-wave transformer at $(f/f_0) = 1.2$, or the attenuation of the stepped-impedance half-wave filter at $f/f_0 = 1.1$, which are both 35.5 db as in Sec. 9.04. Therefore the attenuation is predicted to be 35.5 − 11.1 = 24.4 db at $(f/f_0) = 1.2$, as shown by the circle in Fig. 9.12-3. It lies almost right on the computed curve.

The stop-band response up to the fifth harmonic is also shown in Fig. 9.12-3. Notice that the first spurious response occurs at the third (rather than at the second) harmonic; the next occurs at the fifth; and so on.

A *High-Pass Filter*—This filter is based on the last example in Sec. 9.09, which had an 85-percent bandwidth. It is beyond the point where any reliable predictions can be made. The response of this filter is shown in Fig. 9.12-4. Compare this figure with Fig. 9.09-3, for the reactance-coupled half-wave filter. The element spacings are now all between 10 and 20 degrees, making this almost a lumped-constant high-pass
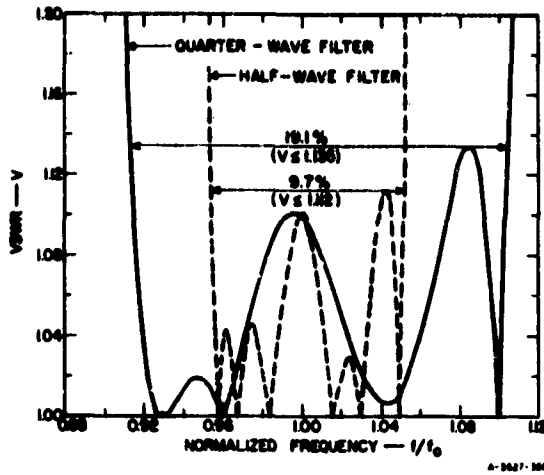
FIG. 9.12-2   PASS-BAND CHARACTERISTICS OF
             REACTANCE-COUPLED QUARTER-
             WAVE AND HALF-WAVE FILTERS
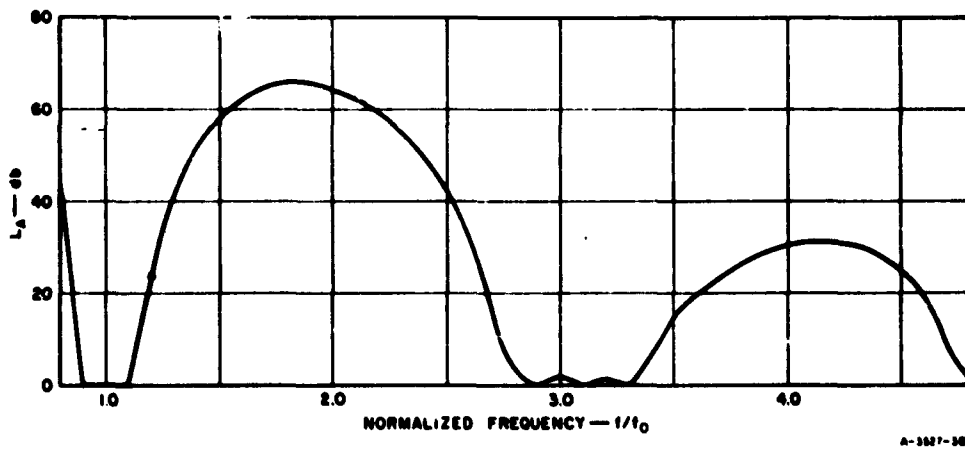
FIG. 9.12-3   STOP-BAND CHARACTERISTICS OF REACTANCE-COUPLED
             QUARTER-WAVE FILTER

576

filter. In fact, the general behavior of this filter at the low-frequency
end can be predicted most simply by treating it as a lumped-constant filter.
Its lower cutoff frequency, based on the formula $1/\sqrt{LC}$, is some sort of a
geometric mean of the numbers in Eq. (9.09-13), as a fraction of the syn-
chronous frequency. The actual cutoff frequency from Fig. 9.12-4 as a
fraction of the synchronous frequency lies between 0.4 and 0.5, whereas the
unweighted geometric mean of the numbers in Eq. (9.09-13) is 0.51.

   As the frequency increases, the first stop band should occur when the
element spacings are about 90 degrees. With spacings of from 10 to 20 degrees
at the synchronous frequency, this stop band is expected to be centered at
about 6 times the synchronous frequency. The peak attenuation will then be
determined by multiplying all the discontinuity VSWRs at this frequency, which
yields an input VSWR of 2.6. The peak attenuation should therefore fall just
short of 1 db. All this appears to be borne out by Fig. 9.12-4, as far as
it is plotted.
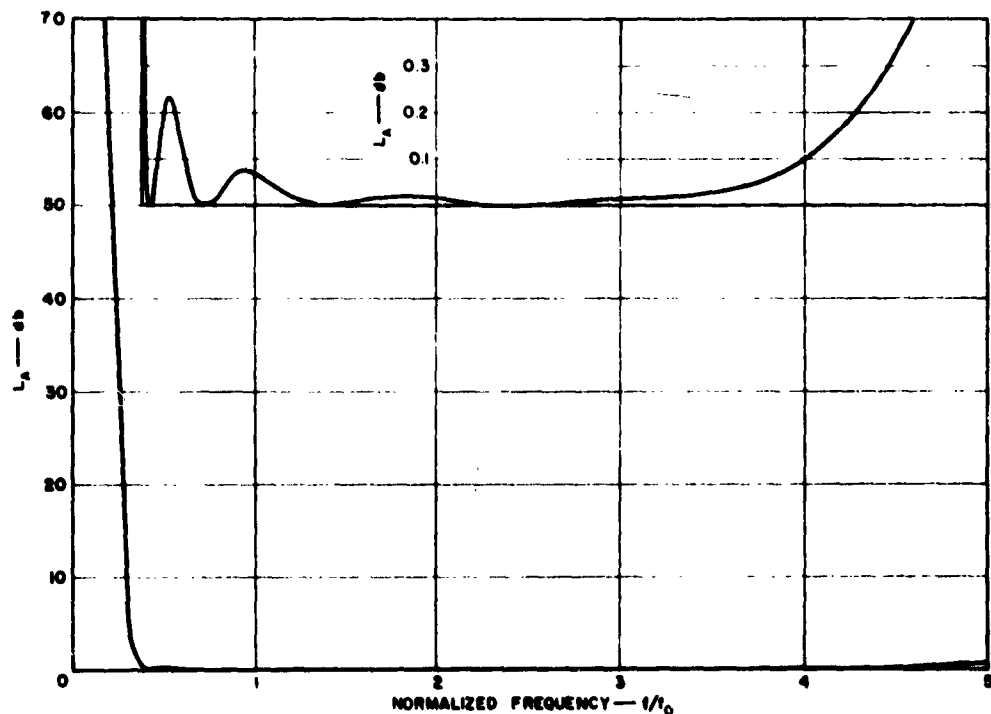
FIG. 9.12-4 CHARACTERISTICS OF A QUARTER-WAVE REACTANCE-COUPLED
            PSEUDO-HIGH-PASS FILTER

REFERENCES

1. G. L. Matthaei and Leo Young, "Microwave Filters and Coupling Structures, "Quarterly Progress Report 5, SRI Project 3527, Contract DA 36-039 SC-87398, Stanford Research Institute, Menlo Park, California (April 1962).

2. Leo Young, "The Quarter-Wave Transformer Prototype Circuit," IRE Trans. PGMTT-8, pp. 483-489 (September 1960).

3. S. B. Cohn, "Direct-Coupled-Resonator Filters," Proc. IRE 45, pp. 187-196 (February 1957). (See also Correspondence, p. 880, June 1957, for a discussion on the frequency dependence of the coupling elements.)

4. Leo Young, "The Practical Realization of Series-Capacitive Couplings for Microwave Filters," The Microwave Journal 5, No. 12, pp. 79-81 (December 1962).

5. N. Marcuvitz, Waveguide Handbook, MIT Rad. Lab. Series Vol. 10, p. 178, (McGraw-Hill Book Co., Inc., New York City, 1951).

6. W. J. Getsinger, "Coupled Rectangular Bars Between Parallel Plates," IRE Trans. PGMTT-10, pp. 65-72 (January 1962).

7. Harvard University, Radio Research Laboratory, Very High Frequency Techniques, Vol. 2, Chapter 26 and 27. (McGraw-Hill Book Company, Inc., New York City, 1947).

8. G. L. Ragan, Microwave Transmission, MIT Rad. Lab. Series Vol. 9, p. 641 (McGraw-Hill Book Co., Inc., New York City, 1948).

9. E. N. Torgow, "Microwave Filters," Electro-Technology 67, pp. 90-96 (April 1961).

10. G. L. Matthaei, "Design of Wide-Band (and Narrow-Band) Band-Pass Microwave Filters on the Insertion Loss Basis," IRE Trans. PGMTT-8, pp. 580-593 (November 1960).

11. Glyn Bostick, "Design Procedure for Coaxial, High-Pass Filters," Electronic Design, 8, pp. 66-69 (13 April 1960).

12. H. Smith, "Design of Symmetrical Bandpass Filters," Electronic Design (Microwaves Section), Vol. 10, pp. 40-43 (12 April 1962). (Note: These data apply only to 50-ohm line.)

13. C. E. Muehe, "The Inductive Susceptance of Round Metal Posts Mounted in Coaxial Line," Group Report 46-32, MIT Lincoln Laboratory (5 November 1958).

14. H. Gruenberg, "Symmetrically Placed Inductive Posts in Rectangular Waveguide," Canadian Journal of Physics 30, pp. 211-217 (1952).

15. G. Craven and L. Lewin, "Design of Microwave Filters with Quarter-Wave Couplings," Proc. IEE, (London), Vol. 103B, pp. 173-177 (March 1956).

16. J. C. Simon and G. Broussaud, "Les Filtres Passe-Bande, en hyperfréquence," Annales de Radioélectricité," Vol. 3, pp. 3-19 (1953).

17. Leo Young and B. M. Schiffman, "A Useful High-Pass Filter Design," The Microwave Journal 6, No. 2, pp. 78-80, (February 1963).

NOTE: Most of the material in this chapter is contained in the following paper, which was accepted for publication after this chapter had been completed:

18. Leo Young, "Direct-Coupled Cavity Filters for Wide and Narrow Bandwidths," to be published in the IRE Trans. PGMTT.

BAND-PASS FILTERS, CONTINUED
(BAND-PASS AND PSEUDO HIGH-PASS FILTERS CONSISTING OF LINES AND STUBS, OR PARALLEL-COUPLED ARRAYS OF LINES)

SEC. 10.01, CONCERNING THE FILTERS AND
DESIGN PROCEDURES IN THIS CHAPTER

A summary of the various filter structures described in this chapter, along with their various advantages and disadvantages as compared with the other types of band-pass filters in Chapters 8, 9, and 10 will be found in Sec. 8.01. Wide-band filters of some of the forms discussed in this chapter are also useful for microwave high-pass applications.

The design procedures in this chapter make use of the lumped-element low-pass prototype filters in Chapter 4, as did the procedures in Chapter 8. Though the procedures in Chapter 8 are relatively simple and quite versatile, they involve fixing the various filter parameters at the midband frequency, and as a result the design equations obtained are accurate only for filters of narrow c noderate bandwidth. The design procedures in this chapter fix various filter parameters at band-edge frequencies as well as at midband. For this reason, good results are insured when these procedures are used for either narrow- or wide-bandwidth designs. Though the method used for deriving the equations in this chapter is very general in its potential application, in most cases of wide-band filters consisting of lines with lumped-reactance couplings (such as the filters in Chapter 9), the design viewpoint of this chapter leads to simultaneous equations that are a combination of transcendental and algebraic functions, which are very tedious to solve. In such cases design from step-transformer prototypes, as described in Chapter 9, is easier. However, in many cases of filters consisting of lines and stubs or parallel arrays of lines, the methods of this chapter give equations that are very easy to use.

Using a low-pass prototype filter having a response as shown in Fig. 10.01(a), along with the methods of this chapter, a band-pass filter response approximately like that in Fig. 10.01(b) will be obtained.
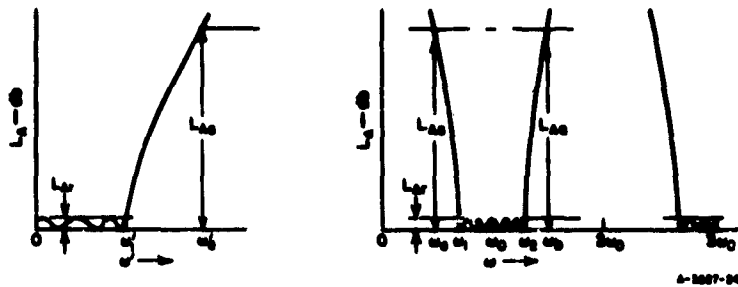
FIG. 10.01-1   LOW-PASS PROTOTYPE RESPONSE AND CORRESPONDING
BAND-PASS FILTER RESPONSE

Most of the filters in this chapter have additional pass bands centered at $3\omega_0$, $5\omega_0$, etc., though some (which will be noted) tend to have spurious pass bands also at $2\omega_0$, $4\omega_0$, etc., if they are not perfectly tuned.   The fractional bandwidth

$$w = \frac{(\omega_2 - \omega_1)}{\omega_0} \qquad (10.01\text{-}1)$$

of the band-pass filter pass band may be fixed by the designer as desired. As was done in Chapter 8, in order to estimate the rate of cutoff to be expected from the band-pass filter, approximate low-pass-to-band-pass transformations of the form

$$\frac{\omega'}{\omega_1'} = F(w, \omega/\omega_0) \qquad (10.01\text{-}2)$$

will be utilized, where the primed frequencies refer to Fig. 10.01-1(a) and the unprimed frequencies to Fig. 10.01-1(b).   The specific function $F(w, \omega/\omega_0)$ to be used will vary with the different filter structures considered.   For two frequencies, ω' and ω, which satisfy such a mapping, the attenuation is the same for both the prototype and the band-pass filter.   Hence, the low-pass prototype attenuation characteristics in Fig. 4.03-2 and Figs. 4.03-4 through 4.03-10 can be mapped into corresponding band-pass attenuation characteristics by use of such mappings. Readers who are unfamiliar with these procedures should find the example in Sec. 8.04 helpful.

SEC. 10.02, PARALLEL-COUPLED FILTERS WITH
$\lambda_0/2$ RESONATORS

Figure 10.02-1(a) shows a strip-line filter having n parallel-coupled resonators which are short-circuited at both ends and which are a half-wavelength long at midband. The filter may be viewed as being pieced together from $n + 1$ parallel-coupled sections $S_{k,k+1}$ which are a quarter-wavelength long in the medium of propagation at the midband frequency ω_0. The filter in Fig. 10.02-1(b), which uses open-circuits at the ends of its resonators, is the dual of the filter in Fig. 10.02-1(a). Both types of filter can have identical transmission characteristics, the main bases for choice between them being related to their method of fabrication.

Figure 10.02-2 shows a possible way of fabricating the filter in Fig. 10.01-1(a). In this structure the resonators consist of rectangular bars which are supported by the short-circuit blocks at their ends. This construction requires no dielectric material (hence it eliminates dielectric loss), and can easily achieve the tight coupling between resonator elements that is required for wide-band filters. The required bar dimensions can be obtained from the odd- and even-mode admittances calculated in this section with the aid of Figs. 5.05-9 through 5.05-13 and their accompanying discussion.

The filter in Fig. 10.02-1(b) is of the form discussed in Sec. 8.09. However, the design equations presented in Sec. 8.09 are not accurate for large bandwidths, while the equations discussed in this section give good accuracy for either narrow or wide bandwidths.

If the printed-circuit form discussed in Sec. 8.09 is used for design of wide-band filters, it will be found that unreasonably small gaps will be required between resonator elements. One way of avoiding this problem while still using printed-circuit construction is to use the interleaved construction shown in Fig. 10.02-3. In this construction alternate resonator strips are printed on two parallel strips of dielectric so that the resonators can be interleaved to achieve tight coupling. Since the structure is symmetrical about a centerline midway between the ground planes, no ground-plane modes will be excited. Interleaved resonators of this type can be designed from the odd- and even-mode impedances computed in this section with the aid of the information in Figs. 5.05-4 through 5.05-8 and their accompanying discussion. Since the propagation is in

$(Y_{oo}^a)_{01}$
$(Y_{oe}^a)_{01}$

Y_A a

S_{12}

END SECTIONS S_{01} AND $S_{n,n+1}$ MAY USE
LINES WITH UNEQUAL WIDTHS

b

S_{23}

$(Y_{oo}^b)_{01}$
$(Y_{oe}^b)_{01}$

S_{34}

S_{01}

$(Y_{oo})_{12}$
$(Y_{oe})_{12}$

$(Y_{oo})_{23}$
$(Y_{oe})_{23}$

$(Y_{oo}^b)_{n,n+1}$
$(Y_{oe}^b)_{n,n+1}$

$(Y_{oo})_{34}$
$(Y_{oe})_{34}$

b

a $Y_B = Y_A$

$(Y_{oo}^a)_{n,n+1}$
$(Y_{oe}^a)_{n,n+1}$

$S_{n,n+1}$

(a)

$(Z_{oe}^a)_{01}$
$(Z_{oo}^a)_{01}$

Z_A a

S_{12}

b

S_{23}

$(Z_{oe}^b)_{01}$
$(Z_{oo}^b)_{01}$

S_{34}

S_{01}

$(Z_{oe})_{12}$
$(Z_{oo})_{12}$

$(Z_{oe})_{23}$
$(Z_{oo})_{23}$

$(Z_{oe}^b)_{n,n+1}$
$(Z_{oo}^b)_{n,n+1}$

$(Z_{oe})_{34}$
$(Z_{oo})_{34}$

b

a $Z_B = Z_A$

END SECTIONS S_{01} AND $S_{n,n+1}$ MAY USE
LINES WITH UNEQUAL WIDTHS

$(Z_{oe}^a)_{n,n+1}$
$(Z_{oo}^a)_{n,n+1}$

$S_{n,n+1}$

(b)

B-3527-314R

FIG. 10.02-1   TWO FORMS OF PARALLEL-COUPLED FILTERS
WITH $\lambda_0/2$ RESONATORS
Each section $S_{k,k+1}$ is $\lambda_0/4$ long where λ_0 is the
wavelength at frequency ω_0
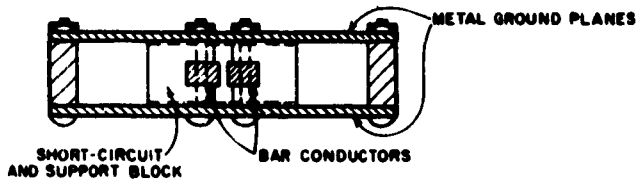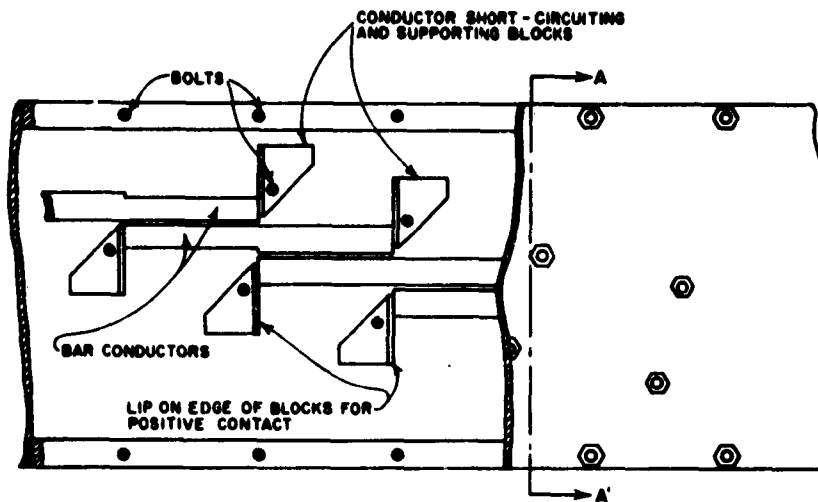
Labels within the figure:
CONDUCTOR SHORT - CIRCUITING AND SUPPORTING BLOCKS
BOLTS
A
BAR CONDUCTORS
LIP ON EDGE OF BLOCKS FOR POSITIVE CONTACT
A'
METAL GROUND PLANES
SHORT-CIRCUIT AND SUPPORT BLOCK
BAR CONDUCTORS

SECTION A - A'

FIG. 10.02-2   POSSIBLE MEANS FOR FABRICATING WIDE-BAND FILTERS OF
THE TYPE IN FIG. 10.02-1(a) IN BAR TRANSMISSION-LINE
CONSTRUCTION
The short-circuiting blocks support the bar conductors so that no
dielectric material is required
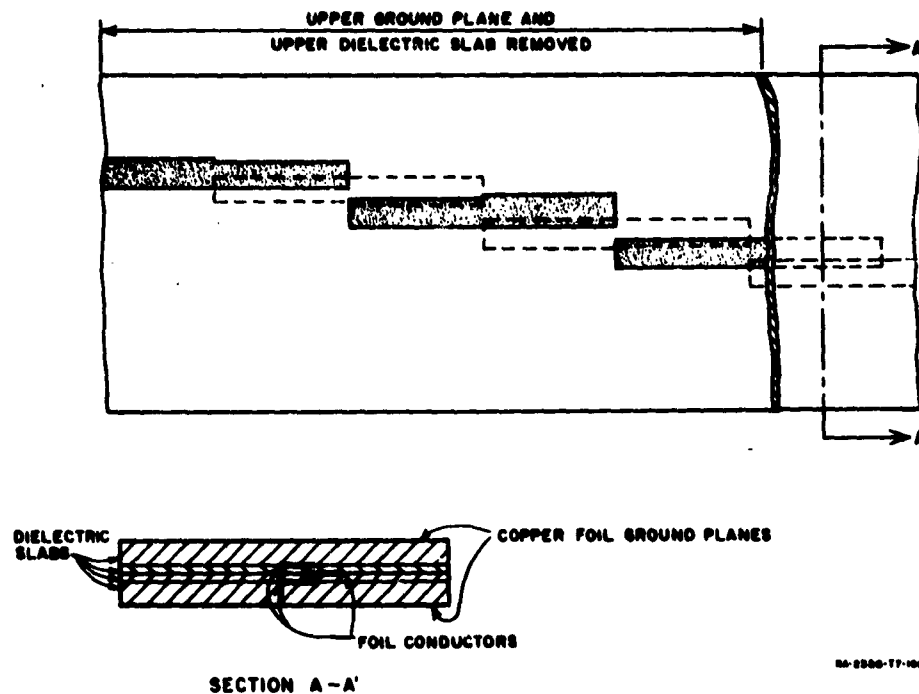
UPPER GROUND PLANE AND
UPPER DIELECTRIC SLAB REMOVED

SECTION A−A'

FIG. 10.02-3 POSSIBLE MEANS FOR FABRICATING WIDE-BAND FILTERS OF THE
TYPE IN FIG. 10.02-1(b) USING PRINTED CIRCUIT TECHNIQUES
In order to achieve tight coupling with reasonably large conductor spacings,
alternate conductor strips are made to be double so that conductor strips
can be interleaved

dielectric, the relative dielectric constant, ϵ_r, must be taken into
account, of course, in computing the lengths and widths of the resonator
elements. Each section having admittances $(Y_{oe})_{k,k+1}$ and $(Y_{oo})_{k,k+1}$ is
a quarter wavelength long in the medium of propagation at frequency ω_0,
and the $n + 1$ sections joined together operate as n half-wavelength
resonators (when designed by the methods described in this section).

A convenient and moderately accurate low-pass-to-band-pass mapping
(Sec. 10.01) which can be used to estimate the attenuation of the filters
in Fig. 10.02-1 from their low-pass prototypes is

$$\frac{\omega'}{\omega_1'} = \frac{2}{w}\left(\frac{\omega - \omega_0}{\omega_0}\right) \qquad (10.02\text{-}1)$$

where

$$w = \frac{\omega_2 - \omega_1}{\omega_0} \qquad (10.02\text{-}2)$$

$$\omega_0 = \frac{\omega_2 + \omega_1}{2} \qquad (10.02\text{-}3)$$

and ω', ω_1', ω, ω_1, and ω_2 are as indicated in Figs. 10.01-1(a)(b). A more accurate mapping is

$$\frac{\omega'}{\omega_1'} = \frac{-\cos\left(\frac{\pi}{2}\frac{\omega}{\omega_0}\right)\sqrt[n]{\left|\sin\left(\frac{\pi\omega_1}{2\omega_0}\right)\right|}}{\cos\left(\frac{\pi}{2}\frac{\omega_1}{\omega_0}\right)\sqrt[n]{\left|\sin\left(\frac{\pi}{2}\frac{\omega}{\omega_0}\right)\right|}} \qquad (10.02\text{-}4)$$

where

$$\frac{\omega_1}{\omega_0} = 1 - \frac{w}{2} \qquad (10.02\text{-}5)$$

and n is the number of reactive elements in the low-pass prototype. Examples indicating the relative accuracy of these two mappings will be shown later in this section.

After the low-pass to band-pass transformation has been used to estimate the number n of resonators required to achieve a desired rate of cutoff for the filter, low-pass prototype element values g_0, g_1, g_2, ..., g_{n+1} are obtained (see Chapter 4), along with the prototype cutoff frequency, ω_1'. The fractional bandwidth w and the terminating conductances, $Y_A = Y_B$, having been specified, the odd- and even-mode admittances for the various sections of the filter can be computed in a straightforward fashion by use of the equations in Table 10.02-1. In the table the parameter h is a dimensionless admittance scale factor which can be chosen arbitrarily to adjust the admittance level within the interior of the filter as may be desired, without affecting the filter response.

Table 10.02-1

DESIGN EQUATIONS FOR PARALLEL-COUPLED FILTER
IN FIG. 10.02-1(a)

Use mapping Eq. (10.02-1) or (10.02-4) to select low-pass prototype with required value of n. There will be $n + 1$ parallel-coupled sections for an n-reactive-element prototype.

END SECTIONS 0,1 AND n,n + 1

For $k = 0$ and $k = n$ compute:

$$\frac{J_{k,k+1}}{Y_A} = \frac{1}{\sqrt{g_k g_{k+1} \omega_1'}} \qquad (Y_{oo}^a)_{k,k+1} = Y_A\left(\frac{J_{k,k+1}}{Y_A}\sqrt{h} + 1\right)$$

$$(Y_{oo}^a)_{k,k+1} = 2Y_A - (Y_{oe}^a)_{k,k+1} \qquad \theta_1 = \frac{\pi \omega_1}{2\omega_0} = \frac{\pi}{2}\left(1 - \frac{w}{2}\right)$$

$$(Y_{oe}^b)_{k,k+1} = (Y_{oe}^a)_{k,k+1} + hY_A\left[\frac{\tan\theta_1}{2} + \left(\frac{J_{k,k+1}}{Y_A}\right)^2\right] - Y_A$$

$$(Y_{oo}^b)_{k,k+1} = (Y_{oe}^b)_{k,k+1} + (Y_{oo}^a)_{k,k+1} - (Y_{oe}^a)_{k,k+1}$$

The parameter h is a dimensionless scale factor which may be chosen arbitrarily so as to give a convenient admittance level in the filter (see text).

INTERIOR SECTIONS 1,2 TO n - 1,n

For $k = 1$ to $k = n - 1$ compute:

$$\frac{J_{k,k+1}}{Y_A} = \frac{1}{\omega_1' g_k g_{k+1}} \qquad N_{k,k+1} = \sqrt{\left(\frac{J_{k,k+1}}{Y_A}\right)^2 + \frac{\tan^2\theta_1}{4}}$$

$$(Y_{oo})_{k,k+1} = hY_A\left(N_{k,k+1} + \frac{J_{k,k+1}}{Y_A}\right)$$

$$(Y_{oe})_{k,k+1} = hY_A\left(N_{k,k+1} - \frac{J_{k,k+1}}{Y_A}\right)$$

586

A value for h which is usually satisfactory (and which makes at least the parallel-coupled section, S_{01}, of the filter have strips of equal width) is

$$h = \frac{1}{\dfrac{\tan \theta_1}{2} + \left(\dfrac{J_{01}}{Y_A}\right)^2} \qquad (10.02\text{-}6)$$

where θ_1 and J_{01}/Y_A are given in Table 10.02-1. When the symmetric or antimetric prototypes such as those in Tables 4.05-1(a), (b) and 4.05-2(a), (b) are used, the strip widths in both the end sections, S_{01} and $S_{n,n+1}$, will all be the same, if Eq. (10.02-6) is used. Other values of h may be chosen to obtain other more convenient admittance levels (and dimensions) for the resonators or to optimize the unloaded Q of the resonator elements. (At present the choice of resonator dimensions to obtain optimum unloaded Q for parallel-coupled resonators of this sort has not been determined.) As previously mentioned, after the odd- and even-mode admittances for the $n + 1$ sections of the filter are obtained, the dimensions of the various lines are obtained by use of the data in Sec. 5.05.

Table 10.02-2 summarizes the odd- and even-mode admittances for three designs obtained by use of Table 10.02-1 along with Eq. (10.02-6). All three were designed from a Tchebyscheff low-pass prototype filter

Table 10.02-2

SUMMARY OF THE ODD-MODE AND EVEN-MODE ADMITTANCE VALUES FOR THE FILTERS OF FIGS. 10.02-4 TO 10.02-6

They were designed by use of Table 10.02-1 and realized in the form in Fig. 10.02-1(a). Equation (10.02-6) was applied so that $(Y_{oo})^a_{01} = (Y_{oo})^b_{01}$ and $(Y_{oe})^a_{01} = (Y_{oe})^b_{01}$.

	FIG. 10.02-4 (5% Bandwidth)	FIG. 10.02-5 (30% Bandwidth)	FIG. 10.02-6 (2 to 1 Bandwidth)
$(Y_{oo})_{01} = (Y_{oo})_{67}$	1.251	1.540	1.716
$(Y_{oo})_{12} = (Y_{oo})_{56}$	0.996	1.023	1.142
$(Y_{oo})_{23} = (Y_{oo})_{45}$	0.981	0.937	0.954
$(Y_{oo})_{34}$	0.980	0.927	0.933
$(Y_{oe})_{01} = (Y_{oe})_{67}$	0.749	0.460	0.284
$(Y_{oe})_{12} = (Y_{oe})_{56}$	0.881	0.491	0.208
$(Y_{oe})_{23} = (Y_{oe})_{45}$	0.895	0.536	0.250
$(Y_{oe})_{34}$	0.896	0.542	0.255

All values normalized so that $Y_A = 1$.
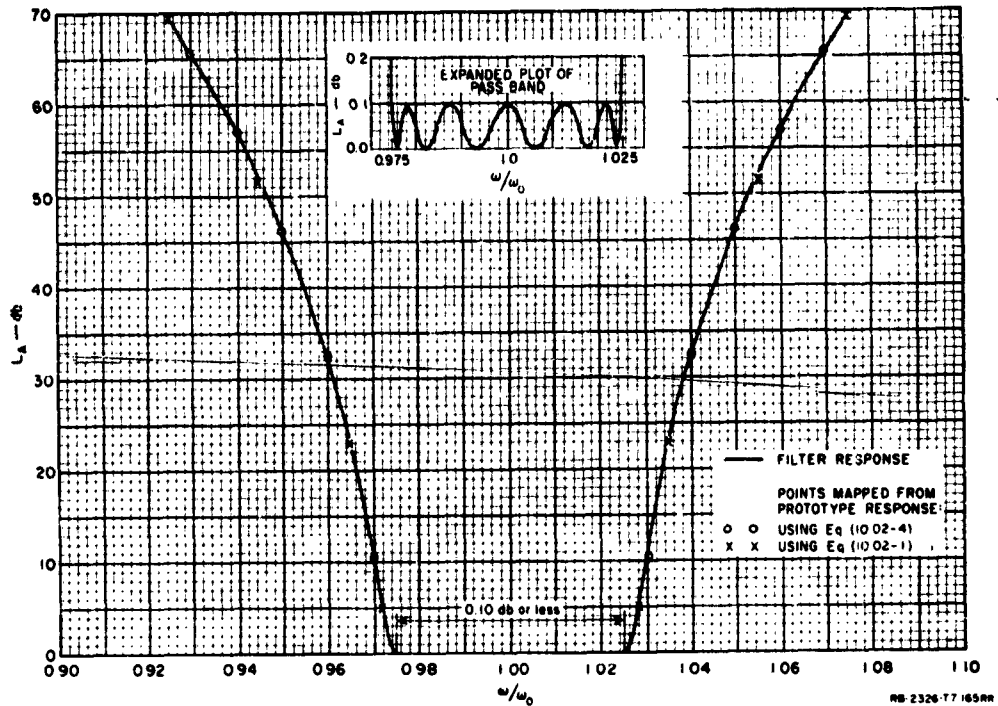
SOURCE: Final Report, Contract DA 36-039 SC-74862, SRI; reprinted in IRE Trans. PGMTT (see Ref. 1 by G. L. Matthaei).

FIG. 10.02-4 COMPUTED RESPONSE OF FILTERS DESIGNED AS
IN TABLE 10.02-1 TO HAVE 5 PERCENT BANDWIDTH
Design value for ω_1/ω_0 was 0.975. Prototype had
0.10-db Tchebyscheff pass-band ripple with n = 6
reactive elements

having 0.1-db ripple and n = 6 reactive elements [the element values being
obtained from Table 4.05-2(a)]. As is seen from Table 10.02-2, the designs
are for 5-percent, 30-percent, and an octave bandwidth; and the admittances
have been normalized so that Y_A = 1. Figures 10.02-4, 10.02-5, and 10.02-6
show the computed responses of these designs. Note that even the octave-
bandwidth design comes close to having the specified 0.1-db ripple in the
pass band, the main error being a slight shrinkage in bandwidth. Points
mapped from the low-pass prototype by use of the mapping of Eqs. (10.02-1)
and (10.02-4) are also shown. Note that for the 5- and 30-percent-
bandwidth designs the simple mapping in Eq. (10.02-1) gives quite good
results even up to quite high attenuations. However, in the case of the

octave-bandwidth design (Fig. 10.02-6), the more complicated Eq. (10.02-4) gives markedly better accuracy up around 60 db or above.

Design equations for the form of filter in Fig. 10.02-1(b) are obtained by applying duality to the equations in Table 10.02-1. Thus, the admittance quantities are replaced by impedance quantities as indicated below.

$$Y_A = Y_B \longrightarrow Z_A = Z_B$$

$$J_{b,b+1} \longrightarrow K_{b,b+1}$$

$$(Y_{oo})_{b,b+1} \longrightarrow (Z_{oo})_{b,b+1}$$
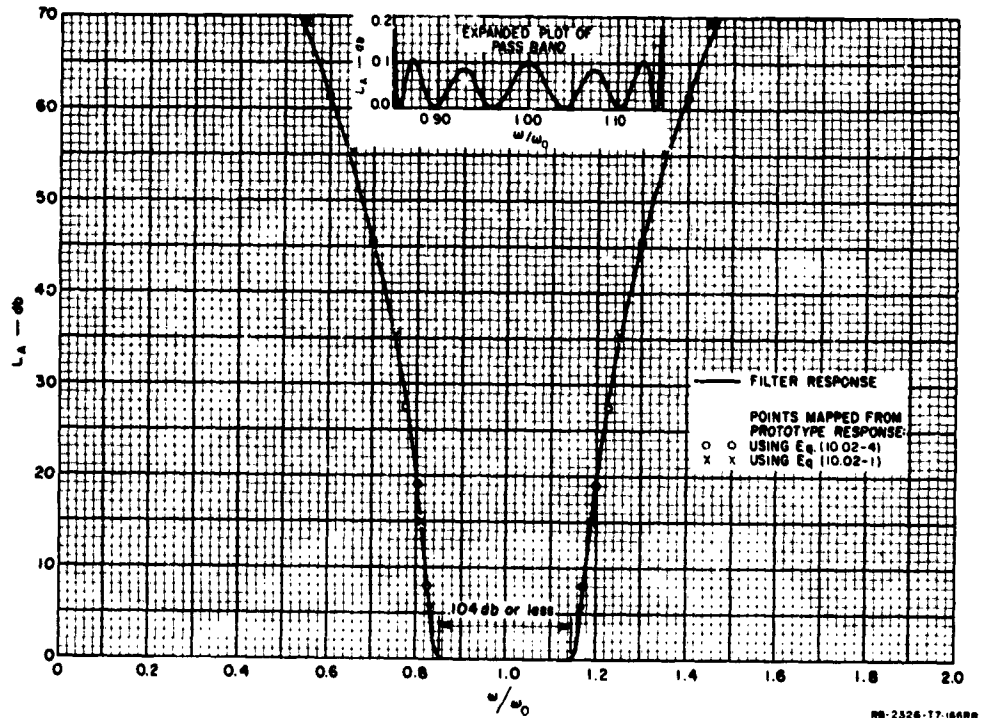
$$(Y_{oo})_{b,b+1} \longrightarrow (Z_{oo})_{b,b+1} \qquad .$$

(10.02-7)

FIG. 10.02-5 COMPUTED RESPONSE OF FILTERS DESIGNED AS IN TABLE 10.02-1 TO HAVE 30 PERCENT BANDWIDTH
Design value of ω_1/ω_0 was 0.850. Prototype same as for Fig. 10.02-4
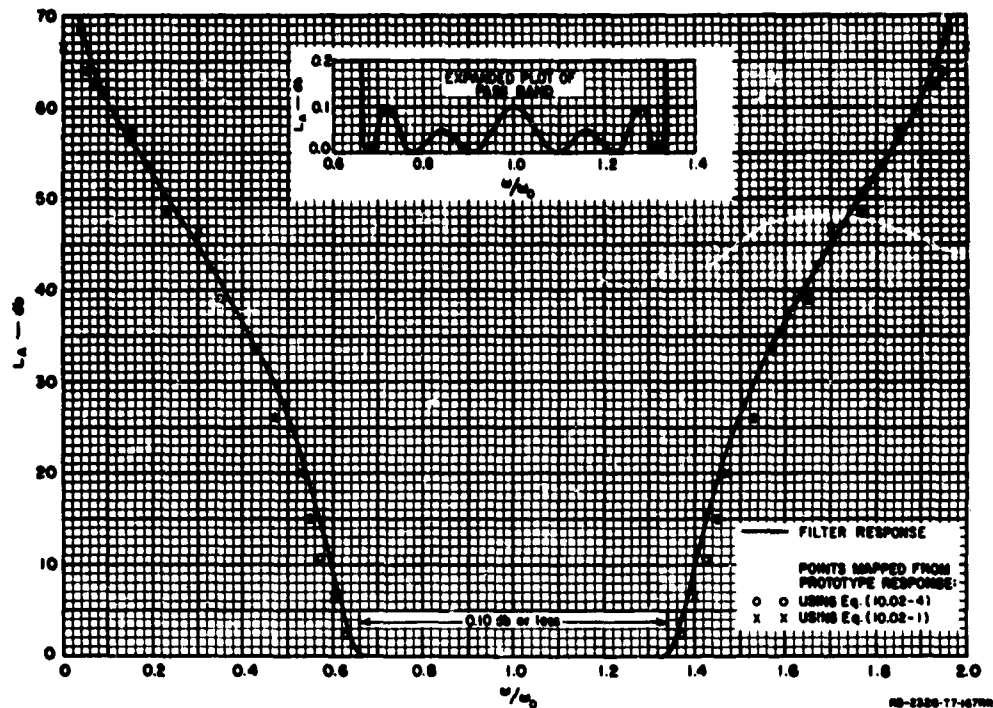
FIG. 10.02-6 COMPUTED RESPONSE OF FILTERS DESIGNED AS IN TABLE 10.02-1
TO HAVE APPROXIMATELY 2 TO 1 BANDWIDTH
Design value for ω_1/ω_0 was 0.650, which calls for ω_2/ω_1 = 2.077.
Prototype same as for Fig. 10.02-4

Note that the admittance inverter parameters $J_{k,k+1}$ are replaced by impedance inverter parameters, $K_{k,k+1}$; that odd-mode admittances $(Y_{oo})_{k,k+1}$ are replaced by even-mode impedances $(Z_{oe})_{k,k+1}$, and that even-mode admittances $(Y_{oe})_{k,k+1}$, are replaced by odd-mode impedances $(Z_{oo})_{k,k+1}$. The dimensionless scale factor, h, is used as before, except that in this case it scales the impedance level instead of the admittance level.

The filters in Figs. 10.02-1(a), (b) have their second pass band centered at $3\omega_0$, and in theory they have infinite attenuation at $2\omega_0$. However, the resonators are actually resonant at $2\omega_0$ (since the resonator strips are a wavelength long at that frequency), and the theoretical pole of attenuation arises only because the coupling regions between adjacent resonators are a half-wavelength long. (The coupling is maximum when the

590

coupling gaps are $\lambda/4$ long and zero when they are $\lambda/2$ long.) However, for this to work out in fact, for the attenuation to remain high at and near ω_0 all of the coupling regions throughout the filter must be exactly $\lambda/2$ long at exactly the same frequency, which must also be exactly the frequency for which all the resonators are resonant. Since this is almost impossible to achieve in practice, there are almost always narrow spurious responses in the vicinity of $2\omega_0$ for these types of filters.

SEC. 10.03, FILTERS WITH SHUNT OR SERIES $\lambda_0/4$ STUBS

By use of equivalences which were summarized in Figs. 5.09-2(a), (b), it can be shown that parallel-coupled strip-line filters of the form in Fig. 10.02-1(a) are electrically ~~exactly equivalent to stub filters of~~ the form in Fig. 10.03-1. Likewise, parallel-coupled strip-line filters of the form in Fig. 10.02-1(b) are exactly equivalent to stub filters of the form in Fig. 10.03-2. It would be possible to work out a parallel-coupled filter design by the procedures in Sec. 10.02 and then convert it to either the form in Fig. 10.03-1 or that in Fig. 10.03-2; however, parallel-coupled filter designs that have reasonable impedance levels and dimensions generally have quite unreasonable impedance levels when converted to a stub-filter form. Similarly, practical stub filter designs generally do not convert to practical parallel-coupled designs. For this reason the design equations in this section are based on a somewhat different design procedure than are those in Sec. 10.02. This procedure gives reasonable impedance levels in typical stub filters, and also makes complete use of all of the natural modes of vibration of the
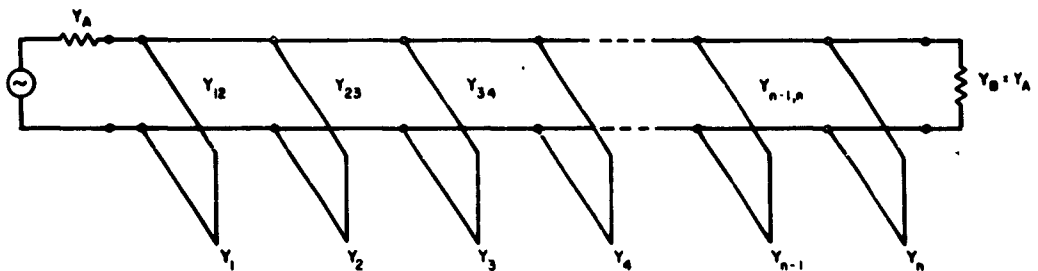
FIG. 10.03-1 A BAND-PASS FILTER USING $\lambda_0/4$ CONNECTING LINES
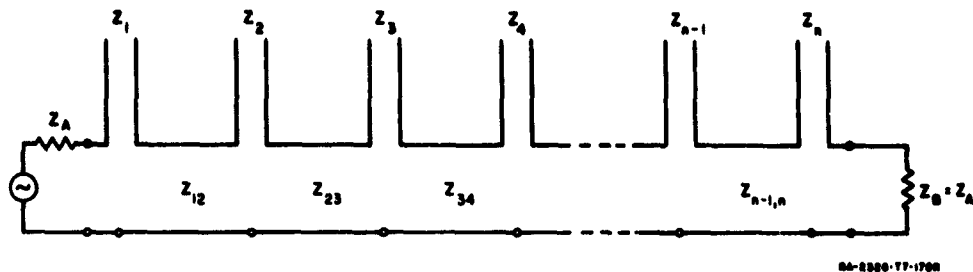
FIG. 10.03-2 A BAND-PASS FILTER USING $\lambda_0/4$ SERIES STUBS AND $\lambda_0/4$
CONNECTING LINES
This filter is the dual of that in Fig. 10.03-1 and can have
identical response characteristics

circuit (which the procedure in Sec. 10.02 does not, as a result of the
manner in which the end sections are designed).

Both the filter in Fig. 10.03-1 and that in Fig. 10.03-2 are com-
posed of stubs that are $\lambda_0/4$ long with connecting lines that are also
$\lambda_0/4$ long, where λ_0 is the wavel .gth in the medium of propagation at
the midband frequency ω_0. These two types of filters can be made to
have identical transmission properties. However, the form in Fig. 10.03-1
is the one that is most commonly used since the series stubs of the filter
in Fig. 10.03-2 are difficult to realize in a shielded structure. Since
the filter in Fig. 10.03-1 is the most important for practical applica-
tions, it will be discussed first.

In order to determine how many reactive elements are required in the
low-pass prototype in order to give a desired rate of cutoff, the low-pass
to band-pass mapping in Eq. (10.02-1) or Eq. (10.02-4) should be used.
Having the low-pass prototype parameters g_0, g_1, g_2, ..., g_{n+1} and ω_1',
and having specified the fractional bandwidth, w, and the terminating
conductances $Y_A = Y_B$, the designer can compute the characteristic admit-
tances of the stubs and connecting lines in a straightforward fashion
from the equations in Table 10.03-1. In the equations there is a dimen-
sionless constant d which may be chosen for some adjustment of the
admittance level in the interior of the filter. In the case of the
equations in Table 10.02-1 the choice of the admittance scale factor, h,
should have no effect on the transmission characteristics of the filter;
however, in the case of the equations in Table 10.03-1, the choice of d

Table 10.03-1

DESIGN EQUATIONS FOR FILTERS WITH SHUNT $\lambda_0/4$ STUBS
AND $\lambda_0/4$ CONNECTING LINES AS SHOWN IN FIG. 10.03-1

Use mapping Eq. (10.02-1) or (10.02-4) to select a low-pass prototype with the required value of n. The filter will have n shunt stubs for an n-reactive-element prototype.
Compute:

$$\theta_1 = \frac{\pi}{2}\frac{\omega_1}{\omega_0} = \frac{\pi}{2}\left(1 - \frac{w}{2}\right) \quad ,$$

$$\frac{J_{12}}{Y_A} = g_0\sqrt{\frac{C_a}{g_2}} \quad , \quad \frac{J_{k,k+1}}{Y_A}\bigg|_{k=2 \text{ to } n-2} = \frac{g_0 C_a}{\sqrt{g_k g_{k+1}}} \quad .$$

$$\frac{J_{n-1,n}}{Y_A} = g_0\sqrt{\frac{C_a g_{n+1}}{g_0 g_{n-1}}} \quad , \quad \text{where } C_a = 2dg_1$$

and d is a dimensionless constant (typically chosen to be 1.0) which can be chosen so as to give a convenient admittance level in the interior of the filter. (See text)

$$N_{k,k+1}\bigg|_{k=1 \text{ to } n-1} = \sqrt{\left(\frac{J_{k,k+1}}{Y_A}\right)^2 + \left(\frac{g_0\omega_1' C_a \tan\theta_1}{2}\right)^2}$$

The characteristic admittances of the shunt stubs are:

$$Y_1 = g_0 Y_A \omega_1'(1-d)g_1 \tan\theta_1 + Y_A\left(N_{12} - \frac{J_{12}}{Y_A}\right)$$

$$Y_k\bigg|_{k=2 \text{ to } n-1} = Y_A\left(N_{k-1,k} + N_{k,k+1} - \frac{J_{k-1,k}}{Y_A} - \frac{J_{k,k+1}}{Y_A}\right)$$

$$Y_n = Y_A\omega_1'(g_n g_{n+1} - dg_0 g_1) \tan\theta_1 + Y_A\left(N_{n-1,n} - \frac{J_{n-1,n}}{Y_A}\right)$$

The characteristic admittances of the connecting lines are:

$$Y_{k,k+1}\bigg|_{k=1 \text{ to } n-1} = Y_A\left(\frac{J_{k,k+1}}{Y_A}\right)$$

All stubs and connecting lines are $\lambda_0/4$ long, where λ_0 is the wavelength in the medium of propagation at the mid-band frequency ω_0.

Y_1	=	Y_8 = 1.042	Y_3	=	Y_6 = 2.049
Y_{12}	=	Y_{78} = 1.288	Y_{34}	=	Y_{56} = 1.292
Y_2	=	Y_7 = 2.050	Y_4	=	Y_5 = 2.087
Y_{23}	=	Y_{67} = 1.364	Y_{45}	=	1.277

may have some small effect on
the approximations upon which
the equations are based. To
date, only values of d of 0.5
and 1.0 have been tested in
this design procedure, but it
is probable that considerably
different values in the range
$0 < d \le 1$ would give satisfac-
tory results.

Table 10.03-2 summarizes
the line admittances for a de-
sign obtained using an n = 8-reactive element Tchebyscheff prototype with
0.10-db ripple [Table 4.05-2(a)]. The admittance level is normalized so
that $Y_A = Y_B = 1$, and $\omega_1/\omega_0 = 0.650$ which calls for slightly over an
octave bandwidth. Figure 10.03-3 shows the computed response of this de-
sign. Note that though the ripples at the edges of the pass band are
undersized, the pass-band performance is quite close to what was specified.
The x's and circles on the graph show points mapped from the low-pass pro-
totype response by use of Eqs. (10.02-1) and (10.02-4). Note that in this
case the more complicated Eq. (10.02-4) gives much better accuracy than
does Eq. (10.02-1), for attenuation above 30 db.

Note in Table 10.03-2 that the admittances of the end stubs are about
half of that for the stubs in the interior of the filter. For this reason
it is sometimes convenient to build this type of filter with double stubs
in the interior of the filter and with single stubs at the ends, as is
illustrated in Fig. 10.03-4. Table 10.03-3 summarizes the line impedances
for an n = 13 design which has the form in Fig. 10.03-4. This filter was
constructed and tested in rectangular-bar strip-line form and its important
dimensions are summarized in Figs. 10.03-5(a), (b), and (c). The filter
was designed for a band-center frequency of $\omega_0/2\pi$ = 3.6 Gc, and it was
necessary to take account of the junction effect where the stubs and main-
line meet, in order to properly determine the lengths of the stubs and the
connecting lines. It was assumed that the junction effect for a plus-
junction must be similar to that of the T-junctions in Figs. 5.07-6 to
5.07-9. From tests on the filter, the junction equivalent circuit and
reference planes were estimated to be about as indicated in Fig. 10.03-6.
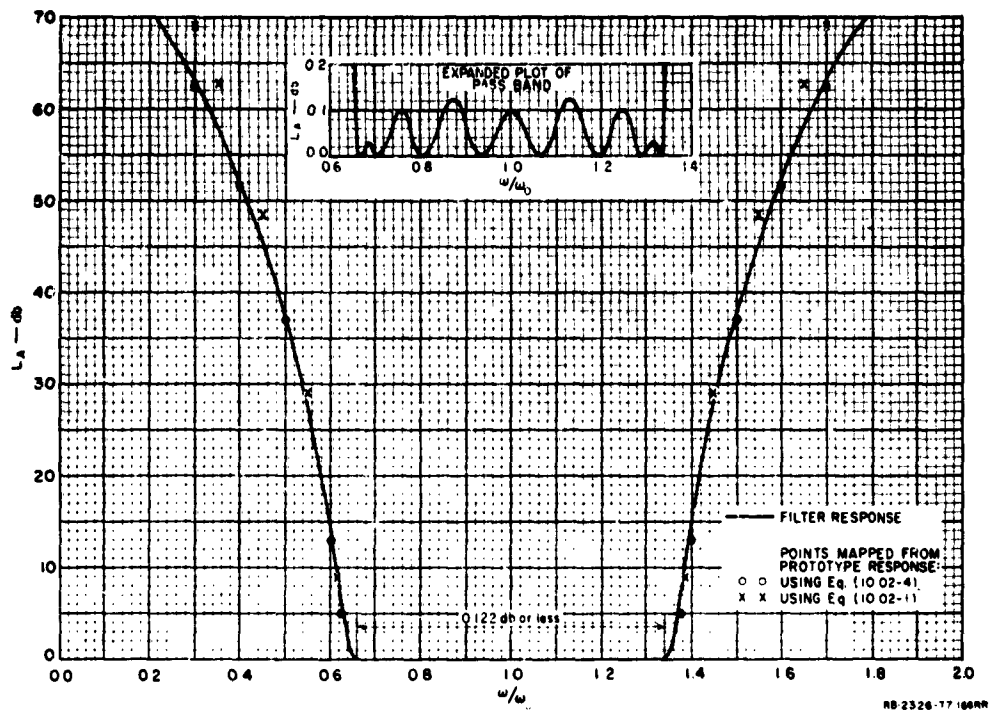
FIG. 10.03-3 COMPUTED RESPONSE OF A FILTER DESIGNED AS IN TABLE 10.03-1
TO HAVE APPROXIMATELY 2 TO 1 BANDWIDTH
Design value for ω_1/ω_0 was 0.650. Prototype had 0.10-db Tchebyscheff
pass-band ripple with n = 8 reactive elements
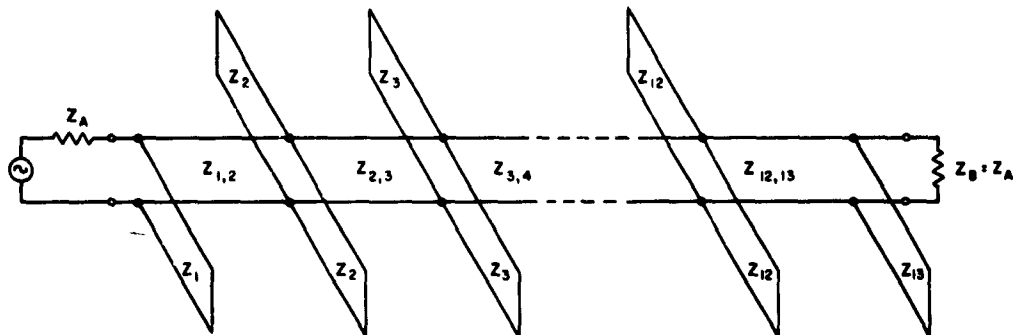
FIG. 10.03-4 OPEN-WIRE-LINE REPRESENTATION OF THE FILTER IN FIG. 10.03-5

Table 10.03-3

LINE IMPEDANCES FOR A BAND-PASS FILTER OF THE FORM IN FIG. 10.03-4
HAVING $n = 13$, A BAND-EDGE RATIO OF $f_2//f_1 = 2.175$, AND
APPROXIMATELY 0.1-db TCHEBYSCHEFF PASS-BAND RIPPLE

$Z_0 = 50$ ohms	$Z_4 = Z_{10} = 52.4$ ohms
$Z_1 = Z_{13} = 52.8$	$Z_{4,5} = Z_{9,10} = 39.6$
$Z_{1,2} = Z_{12,13} = 38.8$	$Z_5 = Z_9 = 52.1$
$Z_2 = Z_{12} = 53.7$	$Z_{5,6} = Z_{8,9} = 39.8$
$Z_{2,3} = Z_{11,12} = 36.7$	$Z_6 = Z_8 = 52.0$
$Z_3 = Z_{11} = 53.7$	$Z_{6,7} = Z_{7,8} = 39.8$
$Z_{3,4} = Z_{10,11} = 36.9$	$Z_7 = 52.0$

These line impedances were computed from an $n = 10$, 0.10-db ripple pro-
totype since at the time of this filter's design, tables of element
values for n larger than 10 were not available. The design was
augmented to $n = 13$ by adding additional lines and stubs at the center
of the filter, the added lines and stubs having impedances the same as
those at the center of the $n = 10$ design.
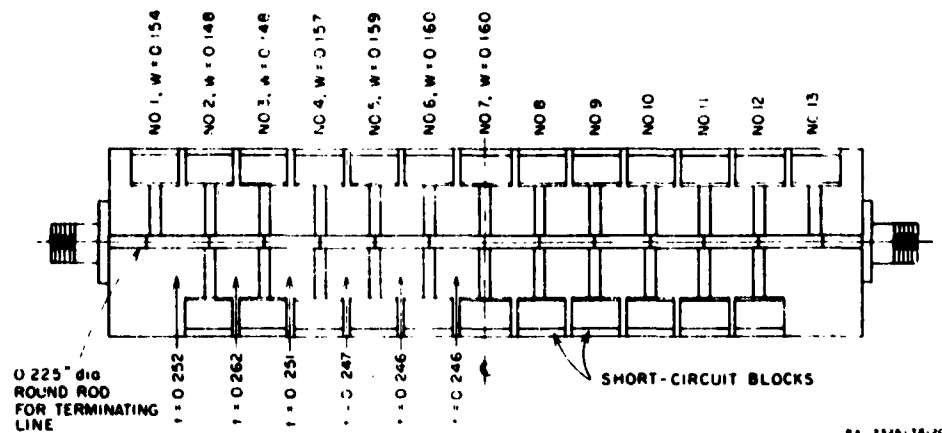
FIG. 10.03-5(a) LAYOUT OF STRIP TRANSMISSION LINE BAND-PASS FILTER WITH
UPPER GROUND PLANE REMOVED
See Fig. 10.03-5(b) for definitions of t and w as used here

CENTER CONDUCTOR

LIP FOR
PRESSURE
CONTACT

SHORT-CIRCUIT
BLOCKS

0.915"
BETWEEN
ALL STUBS

STUBS

0.205"

PARTIAL TOP VIEW
WITH UPPER GROUND PLANE REMOVED

GROUND PLANES

0.410"

0.205"

SCREWS TO
CLAMP SHORTING
BLOCKS TO STUB

ℓ = 1.005" FOR ALL DOUBLE STUBS
ℓ = 0.970" FOR THE SINGLE STUBS

PARTIAL CROSS-SECTIONAL VIEW

RA-2326-76-202
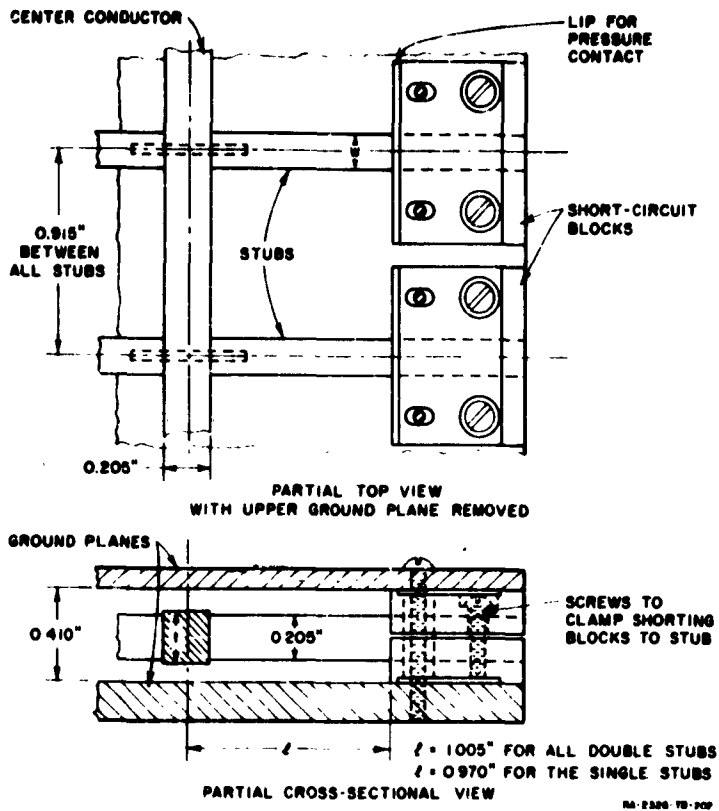
FIG. 10.03-5(b)   SOME CONSTRUCTION DETAILS OF THE BAND-PASS FILTER IN FIG. 10.03-5(a)

TRANSITION BLOCK

0.276"dia HOLE
IN TRANSITION BLOCK

0.120"dia ROUND
CENTER CONDUCTOR

GROUND
PLANES

STUB SHORT-CIRCUIT
BLOCK

0.035"

UG 58A/U
CONNECTOR WITH PROTRUDING
RETAINER BUTTON MACHINED OFF
OF BACK SIDE.

0.225"dia ROUND, 50-ohm
CENTER CONDUCTOR

RA-2326-76-203
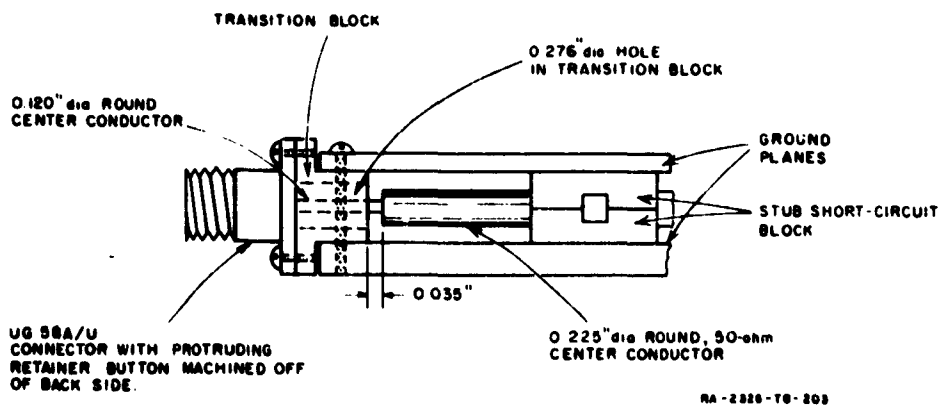
FIG. 10.03-5(c)   DETAILS OF TRANSITION FROM FILTER TO TYPE-N CONNECTOR

$Z_{02} = 52.0$ ohms

$w_2 = 0.156"$ $(0.156" \times 0.205"$ BAR)

$Z_{01} = 39.8$

P_2

$d_2 = 0.064"$

$Z_{01} = 39.8$ ohms

P_2

$d_1 = 0.049"$

$w = 0.205"(0.205 \times 0.246"$ BAR)

P_1 P_1

GROUND PLANE
SPACING 0.410"

$Z_{02} = 52.0$ ohms

(a)

Z_{02}

$1 : \sqrt{A_2}$

P_2

Z_{01}

Z_{01}

$\sqrt{A_1} : 1$

$1 : \sqrt{A_1}$

P_1 P_1

$\sqrt{A_2} : 1$

$jB_d = \dfrac{-j0.030}{\lambda}$ mhos WHERE λ = WAVELENGTH
IN AIR IN INCHES

Z_{02}

FOR $f \leq 5$ kMc

$A_1 \approx A_2 \approx 1$

P_2

(b)

RA-2520-73-304R
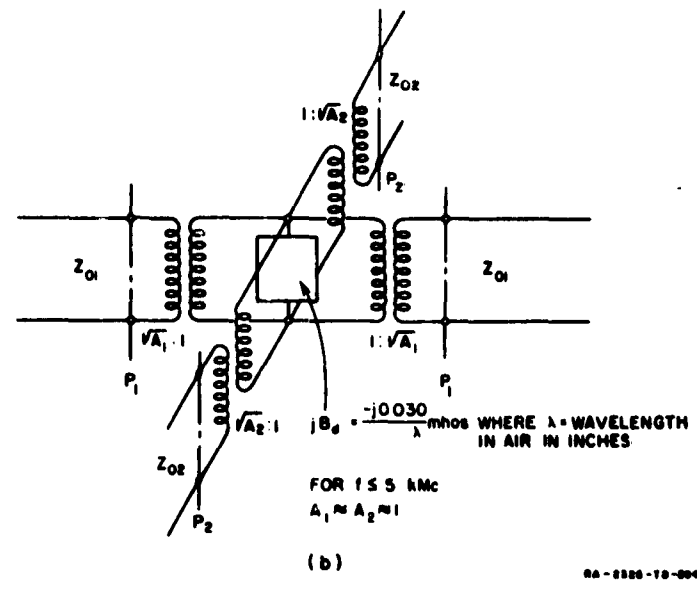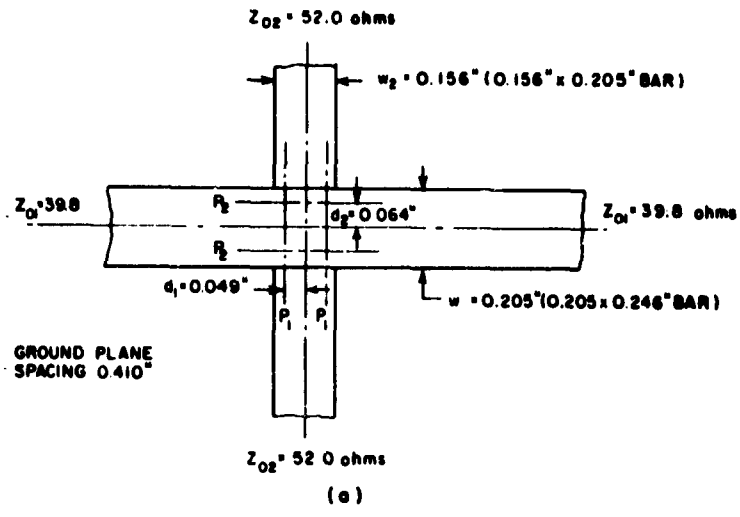
FIG. 10.03-6 ESTIMATED EQUIVALENT CIRCUIT FOR TYPICAL
PLUS-JUNCTION IN THE FILTER OF
FIGS. 10.03-5(a), (b), (c)

598

The $\lambda_0/4$ length for the stubs and the connecting lines was figured from the reference planes P_1 and P_2 indicated. The capacitive junction susceptance B_d is compensated for by reducing the lengths of each of the two side stubs by the amount

$$\Delta l = \frac{\lambda_0 B_d}{4\pi Y_s} , \qquad (10.03\text{-}1)$$

where Y_s is the characteristic admittance of each of the two stubs. (This equation effectively removes an amount of stub on each side so that each stub plus half of the small junction susceptance B_d will still be resonant at ω_0.) In the case of the T-junctions for the single stubs at the ends of the filter, the reference plane for determining the stub length was closer to the centerline of the main line so that the single, end stubs were made to be about 0.035 inch shorter than the double stubs in the interior of the filter.

Figure 10.03-7 shows the measured performance of this filter. The band-edge ratio, $\omega_2/\omega_1 = 2.21$, compared favorably with the 2.17 design value. In general, the performance is seen to be in excellent agreement with the design objective.

Design formulas for the filter in Fig. 10.03-2 can be obtained directly from the formulas in Table 10.03-1 by application of duality Thus, admittance quantities in Table 10.03-1 are simply replaced by corresponding impedance quantities as listed below:

$$
\begin{aligned}
Y_A &= Y_B \longrightarrow Z_A = Z_B \\
J_{k,k+1} &\longrightarrow K_{k,k+1} \\
Y_k &\longrightarrow Z_k \qquad\qquad (10.03\text{-}2) \\
Y_{k,k+1} &\longrightarrow Z_{k,k+1} \\
C_s &\longrightarrow L_s
\end{aligned}
$$

It would be possible to build a filter of the type in Fig. 10.03-2 shielded coaxial form by constructing the series stubs as stubs within the center conductor of the line, as shown in Fig. 10.03-8.
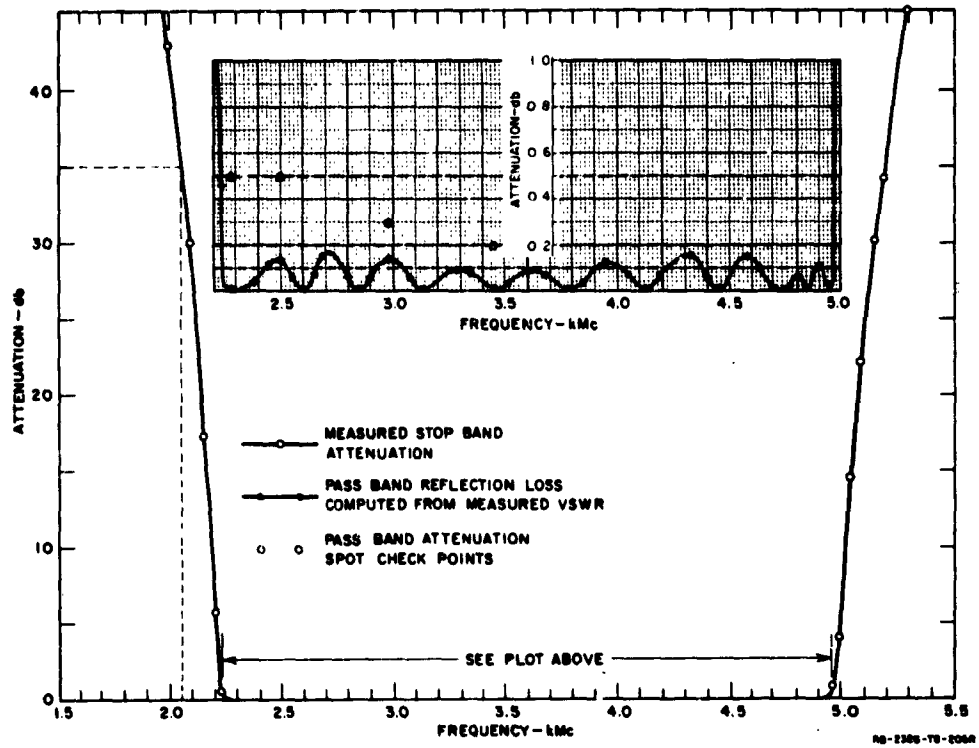
FIG. 10.03-7 MEASURED RESPONSE OF THE FILTER SHOWN IN FIGS. 10.03-5(a), (b), (c)
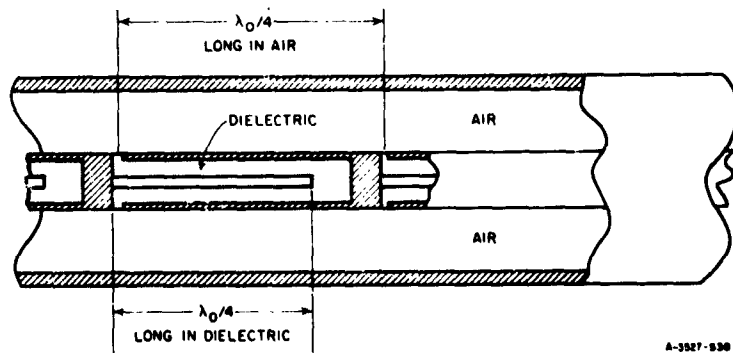
FIG. 10.03-8 POSSIBLE MEANS FOR REALIZING THE FILTER IN
FIG. 10.03-2 IN COAXIAL FORM

Just as with the parallel-coupled filters discussed in Sec. 10.02, the filters in Figs. 10.03-1 and 10.03·2 have their second pass band centered by $3\omega_0$, but they are very prone to have narrow spurious responses in the vicinity of $2\omega_0$ if there is the slightest mistuning. Filters of the forms in Figs. 10.03-1 and 10.03-2 are candidates for use primarily as wide-band filters, because if narrow-band filters are designed in this form, their stubs will have unreasonably low impedance levels in the case of Fig. 10.03-1, and unreasonably high impedance levels for the case of Fig. 10.03-2.

SEC. 10.04, FILTERS WITH $\lambda_0/2$ STUBS AND $\lambda_0/4$ CONNECTING LINES

The filter in Fig. 10.04-1, which uses open-circuited $\lambda_0/2$ stubs spaced $\lambda_0/4$ apart, can be made to have pass-band characteristics similar to those of the filter in Fig. 10.03-1, which uses short-circuited $\lambda_0/4$ stubs spaced $\lambda_0/4$ apa. (where λ_1 is th wavelength at the pass-band center frequency ω_0). However, the filter in Fig. 10.04-1 has quite different stop-band characteristics. If each $\lambda_0/2$ stub is of the same characteristic admittance throughout its length, then the stop-band will have infinite attenuation at the frequencies $\omega_0/2$ and $3\omega_0/2$. If the
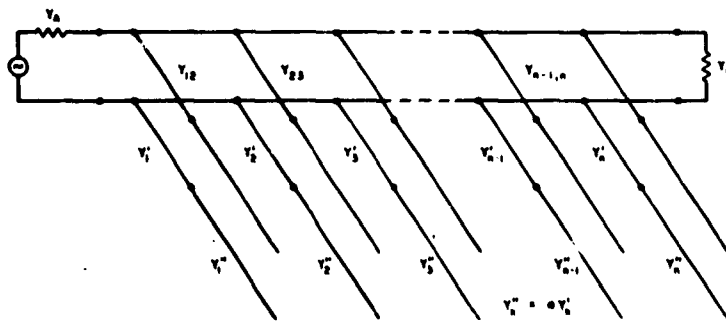
FIG. 10.04-1   BAND-PASS FILTER WITH HALF-WAVELENGTH SHUNT STUBS AND QUARTER-WAVELENGTH CONNECTING LINES
The reference wavelength is the propagation wavelength at the midband frequency, ω_0

outer half of each stub is made to have an admittance that is a constant times the admittance of the inner half of the stub, as indicated in Fig. 10.04-1, then the frequencies of infinite attenuation can be made to occur at frequencies other than $\omega_0/2$ and $3\omega_0/2$. This type of filter will have additional pass bands in the vicinity of $\omega = 0$ and $\omega = 2\omega_0$, and at other corresponding periodic frequencies.

Filters in the form shown in Fig. 10.04-1 can be readily designed by a modified use of Table 10.03-1. The design is carried out first to give a filter in the form in Fig. 10.03-1 with the desired pass-band characteristic and bandwidth. Then each shunt, quarter-wavelength, short-circuited stub of characteristic admittance Y_k is replaced as shown in Fig. 10.04-1 by a shunt, half-wavelength, open-circuited stub having an inner quarter-wavelength portion with a characteristic admittance

$$Y_k' = \frac{Y_k (a \tan^2 \theta_1 - 1)}{(a + 1) \tan^2 \theta_1} \qquad (10.04\text{-}1)$$

and an outer quarter-wavelength portion with a characteristic admittance

$$Y_k'' = a Y_k' \qquad (10.04\text{-}2)$$

The parameter a is fixed by

$$a = \cot^2 \left(\frac{\pi \omega_\infty}{2\omega_0}\right)\Bigg|_{(\omega_\infty/\omega_0) < (\omega_1/\omega_0)} \qquad (10.04\text{-}3)$$

where $\theta_1 = \pi\omega_1/2\omega_0$, and ω_∞ is a frequency at which the shunt lines present short circuits to the main line and cause infinite attenuation.* The principle upon which the above substitution is made is that Eqs. (10.04-1) through (10.04-3) are constrained to yield half-wavelength open-circuited stubs which have exactly the same susceptances at the band-edge frequency ω_1 as did the quarter-wavelength short-circuited stubs that they replace, while both kinds of stubs have zero admittance at ω_0.

To test out this procedure, a filter was designed as in Table 10.03-1 to give 30-percent bandwidth ($\omega_1/\omega_0 = 0.850$) using a 0.10-db Tchebyscheff

---

* Of course, in an actual filter the attenuation will be finite due to the losses in the stubs preventing the stub impedances from going to exactly zero.

prototype with $n = 8$. Then, choosing $\omega_\infty/\omega_0 = 0.500$, which gives $a = 1$, the quarter-wavelength stubs were replaced by half-wavelength stubs as described above, and the resulting computed response is shown in Fig. 10.04-2. Note that the pass band is almost exactly as prescribed, and that there are low-attenuation regions in the vicinity of $\omega = 0$ and $\omega = 2\omega_0$, which are to be expected. The element values for this filter are shown in Table 10.04-1.

The 2-to-1-bandwidth filter design (Fig. 10.03-1 and Table 10.03-2) was also converted to this form using $\omega_\infty/\omega_0 = 0.500$, and its response was computed. The features of the pass band looked much the same as those in the expanded plot in Fig. 10.03-3, while the stop bands consisted of
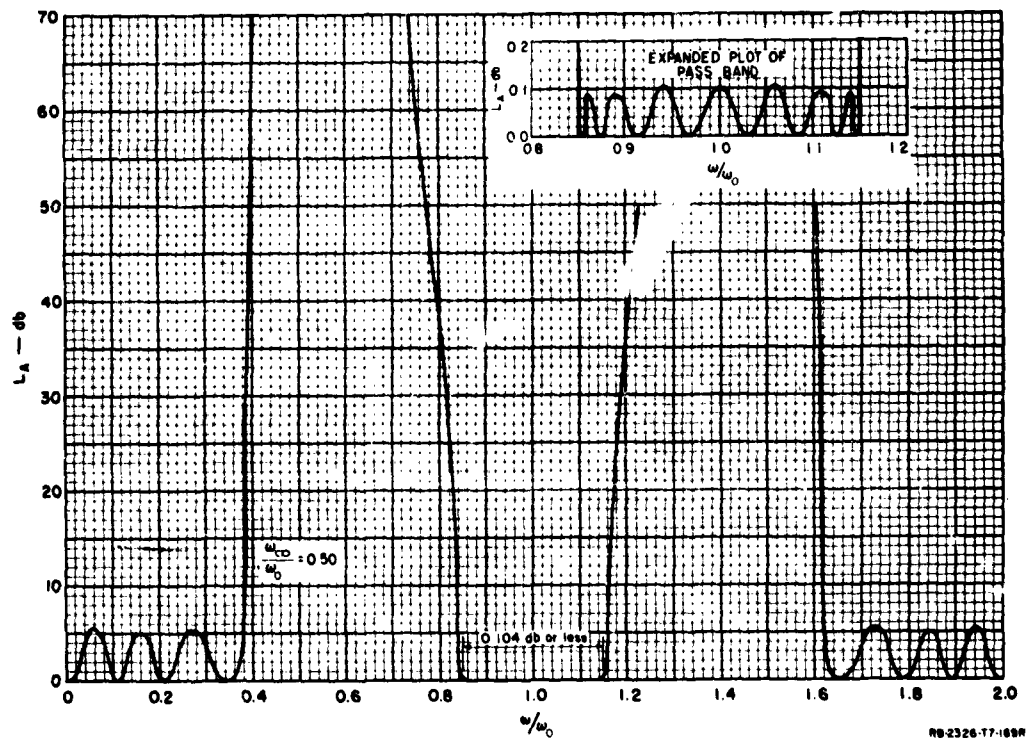
FIG. 10.04-2   COMPUTED RESPONSE OF A 30-PERCENT-BANDWIDTH BAND-PASS FILTER
DESIGNED IN THE FORM IN FIG. 10.04-1
Design value for $\omega_1/\omega_0 = 0.850$. Prototype had 0.10-db Tchebyscheff ripple
with $n = 8$ reactive elements

Y_1'	$= Y_8'$	$= 1.806$	Y_3'	$= Y_6'$	$= 3.584$
Y_{12}	$= Y_{78}$	$= 1.286$	Y_{34}	$= Y_{56}$	$= 1.292$
Y_2'	$= Y_7'$	$= 3.585$	Y_4'	$= Y_5'$	$= 3.614$
Y_{23}	$= Y_{67}$	$= 1.364$	Y_{45}	$= 1.277$	

very sharp attenuation spikes surrounding $\omega/\omega_0 = 0.500$, in a manner similar to that in Fig. 10.04-2, except that the attenuation bands were much narrower.

Filters of the form in Fig. 10.04-1 should be particularly useful where the pass bands around $\omega = 0$ and $\omega = 2\omega_0$ are not objectionable, and where there is a relatively narrow band of signals to be rejected. By the proper choice of ω_∞, the infinite attenuation point can be so placed as to give maximum effectiveness against the unwanted signals. Although using the same ω_∞ for all of the stubs should give the best pass-band response, it may be permissible to stagger the ω_∞ points of the stubs slightly to achieve broader regions of high attenuation. Filters of the form in Fig. 10.04-1 are practical for bandwidths narrower than those of filters of the form in Fig. 10.03-1 because of the larger susceptance slope of half-wavelength stubs for a given characteristic admittance. For example, in the case of Fig. 10.04-1, the shunt stubs for this filter as shown in Fig. 10.04-1 have characteristic admittances $Y_b' = Y_b''$ which are 0.471 times the characteristic admittances of the shunt stubs of the analogous filter in the form in Fig. 10.03-1 from which it was designed. Thus narrower bandwidths can be achieved without having the characteristic admittances of the shunt stubs become excessive.

No accurate low-pass-to-band-pass transformation has been developed for filters of the form in Fig. 10.04-1.

Since filters of the form in Fig. 10.04-1 do not involve any short-circuit connections, they are very easy to fabricate in printed-circuit strip-line form as suggested in Fig. 10.04-3.

SEC 10.05, FILTERS USING BOTH SERIES AND SHUNT STUBS

The filter in Fig. 10.05-1 makes use of short-circuited $\lambda_0/4$ stubs spaced $\lambda_0/4$ apart, which makes it similar to the filter in Fig. 10.03-1. However, the filter in Fig. 10.05-1 has, in addition, a $\lambda_0/2$ *series*
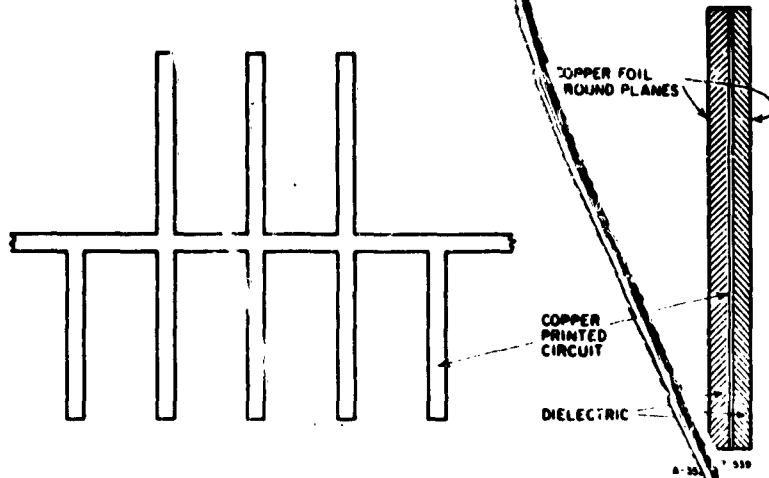
FIG. 10.04-3 A POSSIBLE PRACTICAL STRIP-LINE PRINTED-
CIRCUIT VERSION OF THE FILTER IN FIG. 10.04-
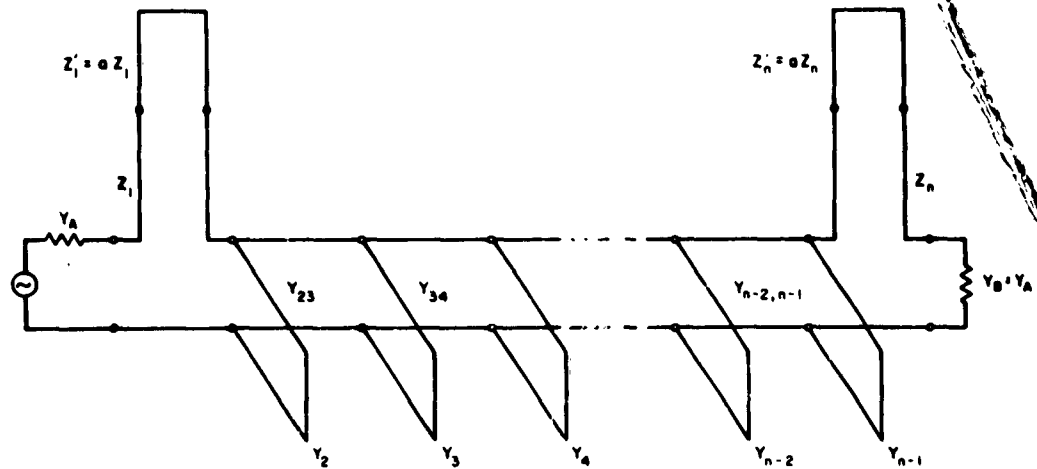
FIG. 10.05-1 BAND-PASS FILTER WITH QUARTER-WAVELENGTH SHUNT STUBS,
QUARTER-WAVELENGTH CONNECTING LINES, AND HALF-
WAVELENGTH SERIES STUBS AT THE ENDS
The reference wavelength is that at the midband frequency, ω_0

short-circuited stub at each end. These $\lambda_g/2$ stubs yield frequencies ω where "infinite" attenuation* occurs close to the pass band, similar to those of the filter in Fig. 10.04-2, but in this case the attenuation remains high at $\omega = 0$ and $\omega = 2\omega_0$ (except for possible narrow spurious responses at $2\omega_0$ which can result from any mistuning).

In this case a reasonably accurate low-pass-to-band-pass transformation (Sec. 10.01) is

$$\frac{\omega'}{\omega'_1} = \frac{F_n\left(\frac{\omega}{\omega_0}\right)}{F_n\left(\frac{\omega_1}{\omega_0}\right)} , \qquad (10.05\text{-}1)$$

where

$$F_n\left(\frac{\omega}{\omega_0}\right) = \frac{-\cos\left(\frac{\pi\omega}{2\omega_0}\right)}{{}^n\sqrt{\left|\sin\left(\frac{\pi\omega}{2\omega_0}\right)\right|\left[\sin\frac{\pi}{2}\frac{(\omega-\omega_\infty)}{\omega_0}\right]^2\left[\sin\frac{\pi}{2}\frac{(\omega-2\omega_0+\omega_\infty)}{\omega_0}\right]^2}}$$

$$(10.05\text{-}2)$$

$\omega_1/\omega_0 = 1 - w/2$, and ω_∞ is a stop-band frequency where infinite attenuation is desired.

After selection of a low-pass prototype with element values g_0, g_1, g_2, ..., g_{n+1} and cutoff frequency ω'_1, and after specification of Y_A, w (or ω_1/ω_0), and ω_∞/ω_0, the design can be carried out by making the calculations indicated in Table 10.05-1. As in Table 10.03-1, the dimensionless parameter d can be used to give some degree of freedom in establishing the impedance level in the interior of the filter. The choice of d will have some minor influence on the approximations involved in the design process, but values of d in the range $0 < d \leq 1$ should be usable (to date only the value $d = 0.5$ has been used in trial designs).

Table 10.05-2 shows the results of a trial design computed using an $n = 8$ reactive element and a 0.10-db ripple Tchebyscheff prototype, and using $\omega_1/\omega_0 = 0.650$, $\omega_\infty/\omega_0 = 0.500$, $Y_A = 1$, and $d = 0.50$. Figure 10.05-2

---

* Of course, as a result of dissipation in the circuit the attenuation will always be finite for frequencies ω, but L_A will typically go very high at frequencies where the $\lambda_g/2$ stubs are anti-resonant.

Table 10.05-1

DESIGN EQUATIONS FOR FILTERS OF THE FORM IN FIG. 10.05-1

Use mapping Eqs. (10.05-1) and (10.05-2) to select low-pass prototype with the required value of n.

Compute:

$$\theta_1 = \frac{\pi}{2}\frac{\omega_1}{\omega_0} = \frac{\pi}{2}\left(1 - \frac{w}{2}\right), \qquad C_a = 2d g_2$$

where $d \lesssim 1$ is a dimensionless constant (typically one-half or somewhat larger) which may be chosen to give a desired impedance level in the interior of the filter.

$$\frac{J_{23}}{Y_A} = \frac{\sqrt{g_2 C_a}}{g_0\sqrt{g_2 g_3}}, \qquad \left.\frac{J_{k,k+1}}{Y_A}\right|_{k=3 \text{ to } n-3} = \frac{C_a}{g_0\sqrt{g_k g_{k+1}}}$$

$$\frac{J_{n-2,n-1}}{Y_A} = \frac{1}{g_0}\sqrt{\frac{C_a g_0}{g_{n-2}g_{n+1}}}$$

$$\left.N_{k,k+1}\right|_{k=2 \text{ to } n-2} = \sqrt{\left(\frac{J_{k,k+1}}{Y_A}\right)^2 + \left(\frac{\omega_1' C_a \tan\theta_1}{2g_0}\right)^2}$$

$$\theta_\infty = \frac{\pi}{2}\frac{\omega_\infty}{\omega_0}, \qquad a = \cot^2\theta_\infty$$

where ω_∞ is a frequency of infinite attenuation as indicated in the example in Fig. 10.05-2.

Referring to Fig. 10.05-1, for the stubs:

$$Z_1 = \frac{[a(\tan\theta_1)^2 - 1]\omega_1' g_0 g_1}{Y_A(a+1)\tan\theta_1}, \qquad Z_1' = a Z_1$$

$$Y_2 = \frac{Y_A \omega_1'(1-d)g_2}{g_0}\tan\theta_1 + Y_A\left(N_{23} - \frac{J_{23}}{Y_A}\right)$$

$$\left.Y_k\right|_{k=3 \text{ to } n-2} = Y_A\left(N_{k-1,k} + N_{k+1,k} - \frac{J_{k-1,k}}{Y_A} - \frac{J_{k,k+1}}{Y_A}\right)$$

$$Y_{n-1} = \frac{Y_A\omega_1'(g_{n-1}g_0 - dg_2 g_{n+1})\tan\theta_1}{g_0 g_{n+1}} + N_{n-2,n-1} - \frac{J_{n-2,n-1}}{Y_A}$$

$$Z_n = \frac{[a(\tan\theta_1)^2 - 1]\omega_1' g_n g_{n+1}}{Y_A(a+1)\tan\theta_1}, \qquad Z_n' = a Z_n$$

For the connecting lines:

$$\left.Y_{k,k+1}\right|_{k=2 \text{ to } n-2} = \left(\frac{J_{k,k+1}}{Y_A}\right)Y_A$$

607

shows the computed response of
this filter (indicated by the
solid lines), while the circles
indicate points mapped from
the low-pass prototype response
using the mapping in
Eqs. (10.05-1) and (10.05-2).
Note that the 0.1-db point on
the left side of the pass band
is very nearly at $\omega/\omega_0 = 0.650$
as specified, and that the re-
sponse in general is, for most

Table 10.05-2

ELEMENT VALUES FOR THE FILTER OF FIG. 10.05-2
REALIZED AS SHOWN IN FIG. 10.05-1

Filter designed using Table 10.05-1 from a 0.10-db
ripple, n = 8, Tchebyscheff prototype using ω_1/ω_0 =
0.650, ω_∞/ω_0 = 0.500, and d = 0.5.

$Z_1 = Z_8 = 0.606$		$Y_3 = Y_6 = 1.235$
$Z_1' = Z_8' = 0.606$		$Y_{34} = Y_{56} = 0.779$
$Y_2 = Y_7 = 1.779$		$Y_4 = Y_5 = 1.258$
$Y_{23} = Y_{67} = 0.823$		$Y_{45} = 0.770$

Values normalized so that $Y_A = 1$.

SOURCE: Final Report, Contract DA 36-039 SC-74862,
SRI; reprinted in *IRE Trans. PGMTT* (see
Ref. 1 by G. L. Matthaei).
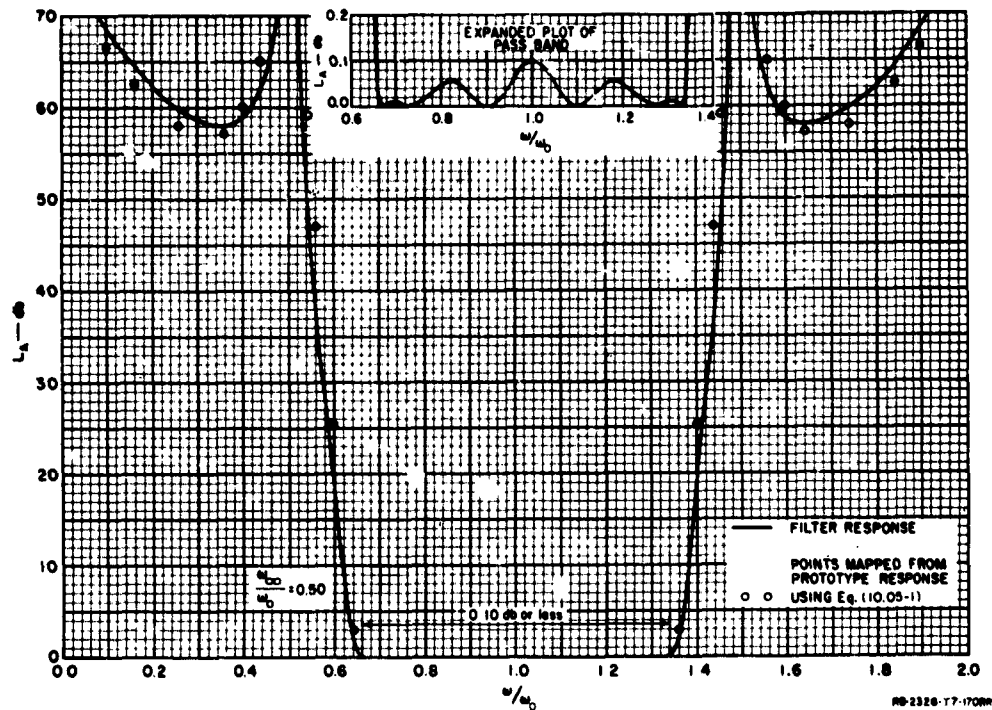
SOURCE: Final Report, Contract DA 36-039 SC-74862, SRI; reprinted
in *IRE Trans. PGMTT* (see Ref. 1 by G. L. Matthaei)

FIG. 10.05-2 COMPUTED RESPONSE OF A FILTER AS IN FIG. 10.05-1 WITH
APPROXIMATELY 2 TO 1 BANDWIDTH
Design value for ω_1/ω_0 was 0.650. Prototype had 0.10-db Tchebyscheff
ripple with n = 8 reactive elements. Parameters d and ω_∞/ω_0 were
both chosen as 0.500

engineering purposes, a satisfactory realization of the specified
performance.

Figure 10.05-3 shows a possible way for constructing filters of
the form in Fig. 10.05-1. The filter shown is in so-called split-block
coaxial construction. The round center conductors are within cylindrical
cavities machined from a solid split block. Note that the $\lambda_0/2$ series
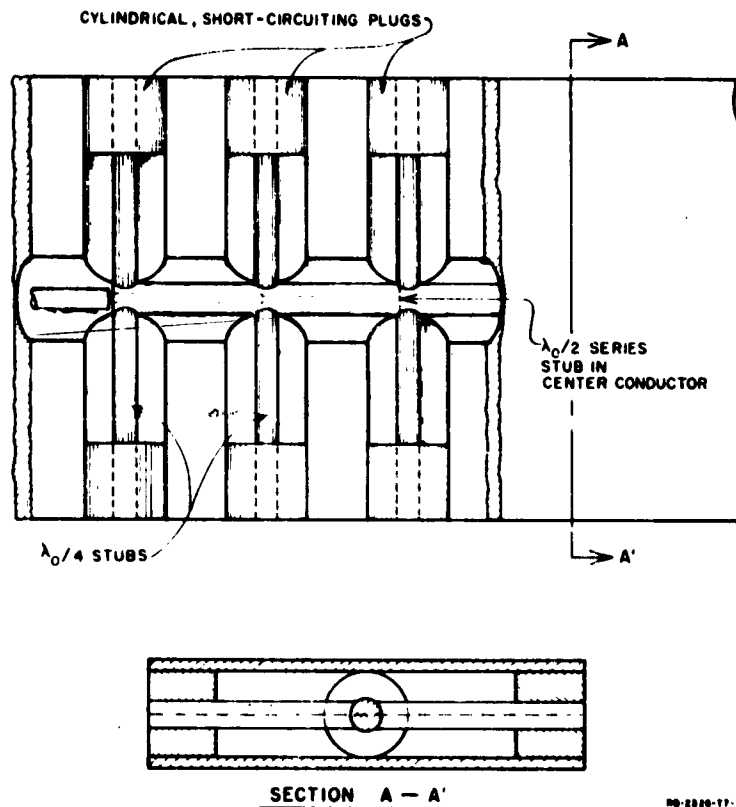
FIG. 10.05-3 POSSIBLE WAY FOR FABRICATING W'DE-BAND FILTERS
OF THE TYPE IN FIG. 10.05-1 IN SPLIT-BLOCK
CONSTRUCTION
The shunt, quarter-wavelength, short-circuited stubs are realized
in parallel pairs so that the characteristic admittance of each stub
will be cut in half, and so that the structure will be self-supporting.
The series, half-wavelength, short-circuited stubs are inside the
center conductor

stub at the input of the filter is realized as a coaxial stub within the main line of the filter.

SEC. 10.06, INTERDIGITAL-LINE FILTERS OF NARROW OR MODERATE BANDWIDTH

Figure 10.06-1 shows one type of interdigital filter to be discussed. The structure, as shown, consists of TEM-mode strip-line resonators between parallel ground planes. Each resonator element is a quarter-wavelength long at the midband frequency and is short-circuited at one end and open-circuited at the other end. Coupling is achieved by way of the fields fringing between adjacent resonator elements. Using the design procedure described in this section, Lines 1 to n in Fig. 10.06-1 serve as resonators. Lines 0 and $n + 1$, however, operate as impedance-transforming sections and not as resonators. Thus, using the procedures of this section, an n-reactive-element low-pass prototype will lead to an interdigital filter with $n + 2$ line elements.

If all of the coupling effects are accounted for, the mathematics that describe the performance of such interdigital filters as those discussed in this and the next section become quite unwieldy.[2] Since synthesizing a structure to have a prescribed response is a much more difficult problem than analyzing a given structure, and since an exact analysis of
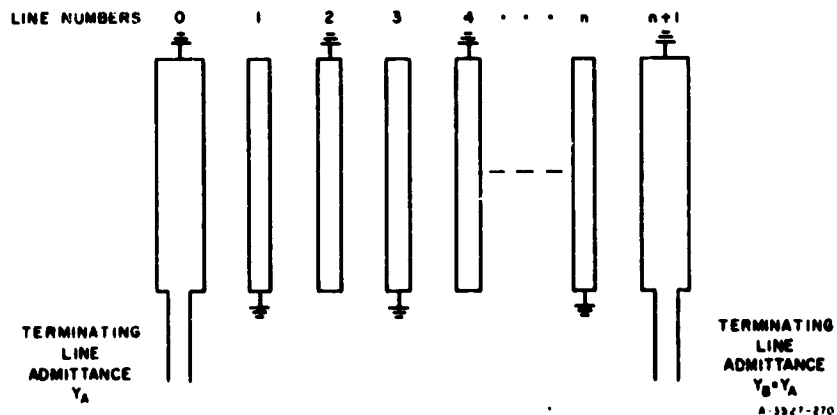
FIG. 10.06-1   INTERDIGITAL FILTER WITH SHORT-CIRCUITED LINES AT THE ENDS
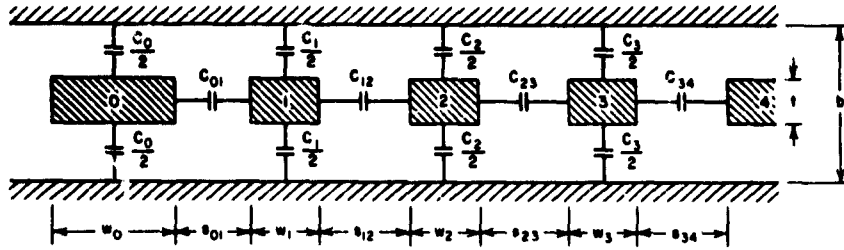
**FIG. 10.06-2 CROSS SECTION OF AN ARRAY OF PARALLEL-COUPLED LINES
BETWEEN GROUND PLANES**

such a structure is itself very tedious, the prospects of obtaining a
usable exact synthesis procedure appear to be dim. Thus, the synthesis
procedure given here involves several additional simplifying approxima-
tions (beyond those used for the procedures in Secs. 10.02 through 10.05)
that permit straightforward, easy-to-use design calculations. Although
the design formulas are approximate, the results of trial designs indi-
cate that they are sufficiently accurate for most practical applications.

Figure 10.06-2 shows an array of parallel-coupled lines such as is
used in an interdigital filter. The electrical properties of the structure
are characterized in terms of the self-capacitances, C_k, per unit length
of each bar with respect to ground, and the mutual capacitances, $C_{k,k+1}$,
per unit length between adjacent bars k and $k + 1$. This representation
is not always highly accurate; it is conceivable that a significant amount
of fringing capacitance could exist between a given line element and, say,
the line element beyond the nearest neighbor. However, at least for
geometries such as that shown, experience has shown this representation to
have satisfactory accuracy.

For designs of the interdigital-filter structures discussed herein,
equations will be given for the normalized self and mutual capacitances,
C_k/ϵ and $C_{k,k+1}/\epsilon$, for all the lines in the structure; where ϵ is the
dielectric constant of the medium of propagation. Having these normalized
capacitances the designer can obtain the dimensions of the bars, using the
data in Sec. 5.05.

A convenient and reasonably accurate low-pass-to-band-pass transformation (Sec. 10.01) to use for estimating the attenuation characteristics of interdigital filters is

$$\frac{\omega'}{\omega_1'} = \frac{2}{w} \left(\frac{\omega - \omega_0}{\omega_0} \right) \qquad (10.06\text{-}1)$$

where

$$w = \frac{\omega_2 - \omega_1}{\omega_0} \qquad (10.06\text{-}2)$$

$$\omega_0 = \frac{\omega_2 + \omega_1}{2} \qquad (10.06\text{-}3)$$

and ω', ω_1', ω_2', ω, ω_1, and ω_2 are as indicated in Figs. 10.01-1(a), (b).

Table 10.06-1 shows approximate design equations for interdigital filters of the form shown in Fig. 10.06-1. This type of design is most practical for filters having narrow or moderate bandwidth. Although no special investigation of this point has been made, it appears probable that one should consider the possibility of using the design equations in Sec. 10.07 when the bandwidth is of the order of 30 percent or more, instead of those in Table 10.06-1. Both sets of design equations are valid, however, for either narrow or wide bandwidths. The main drawback in applying the design procedure in this section to filters of wide bandwidth is that the gaps between Lines 0 and 1 and between Lines n and $n+1$ (see Fig. 10.06-1) tend to become inconveniently small when the bandwidth is large, and the widths of Bars 1 and n tend to become very small.

To use Table 10.06-1 for the design of an interdigital filter, first use Eqs. (10.06-1) through (10.06-3) and the charts in Sec. 4.03 to estimate the number, n, of reactive elements required in the low-pass prototype in order to give the desired rate of cutoff with the desired pass-band characteristics. When the prototype cutoff frequency ω_1' and element values g_0, g_1, $\cdots$, g_{n+1} have been obtained from the tables in Chapter 4, the design computations can begin. It is suggested that the filter fractional bandwidth, w, be specified to be 6 or 7 percent larger than is actually desired, since from the trial design described later it appears that there will be some shrinkage in bandwidth due to the approximate nature of the

612

Table 10.06-1

DESIGN EQUATIONS FOR INTERDIGITAL FILTERS OF THE FORM
IN FIG. 10.06-1

Use mapping in Eqs. (10.06-1) to (10.06-3) to select a low-pass
prototype with the required value of n. The input and output lines
in this filter do not count as resonators, so that there are $n + 2$
lines for an n-reactive-element prototype.

Compute:

$$\theta_1 = \frac{\pi}{2}\frac{\omega_1}{\omega_0} = \frac{\pi}{2}\left(1 - \frac{w}{2}\right)$$

$$\frac{J_{01}}{Y_A} = \frac{1}{\sqrt{g_0 g_1 \omega_1'}} \quad , \quad \left.\frac{J_{k,k+1}}{Y_A}\right|_{k=1 \text{ to } n-1} = \frac{1}{\omega_1'\sqrt{g_k g_{k+1}}}$$

$$\frac{J_{n,n+1}}{Y_A} = \frac{1}{\sqrt{g_n g_{n+1}}\,\omega_1'}$$

$$\left. N_{k,k+1}\right|_{k=1 \text{ to } n-1} = \sqrt{\left(\frac{J_{k,k+1}}{Y_A}\right)^2 + \frac{\tan^2\theta_1}{4}}$$

$$M_1 = Y_A\left(\frac{J_{01}}{Y_A}\sqrt{h} + 1\right) \quad , \quad M_n = Y_A\left(\frac{J_{n,n+1}}{Y_A}\sqrt{h} + 1\right)$$

where h is a dimensionless admittance scale factor to be specified
arbitrarily so as to give a convenient admittance level in the
filter. (See text.)

The normalized self capacitances C_k/ϵ per unit length for the line
elements are:

$$\frac{C_0}{\epsilon} = \frac{376.7}{\sqrt{\epsilon_r}}\left[2Y_A - M_1\right]$$

$$\frac{C_1}{\epsilon} = \frac{376.7}{\sqrt{\epsilon_r}}\left\{Y_A - M_1 + hY_A\left[\frac{\tan\theta_1}{2} + \left(\frac{J_{01}}{Y_A}\right)^2 + N_{12} - \frac{J_{12}}{Y_A}\right]\right\}$$

Table 10.06-1 *concluded*

$$\frac{C_h}{\epsilon}\bigg|_{h=2 \text{ to } n-1} = \frac{376.7}{\sqrt{\epsilon_r}} hY_A\left(N_{h-1,h} + N_{h,h+1} - \frac{J_{h-1,h}}{Y_A} - \frac{J_{h,h+1}}{Y_A}\right)$$

$$\frac{C_n}{\epsilon} = \frac{376.7}{\sqrt{\epsilon_r}}\left\{Y_A - M_n + hY_A\left[\frac{\tan \theta_1}{2} + \left(\frac{J_{n,n+1}}{Y_A}\right)^2 + N_{n-1,n} - \frac{J_{n-1,n}}{Y_A}\right]\right\}$$

$$\frac{C_{n+1}}{\epsilon} = \frac{376.7}{\sqrt{\epsilon_r}}\left[2Y_A - M_n\right]$$

where ϵ is the dielectric constant and ϵ_r is the relative dielectric constant in the medium of propagation.

The normalized mutual capacitances $C_{h,h+1}/\epsilon$ per unit length between adjacent line elements are:

$$\frac{C_{01}}{\epsilon} = \frac{376.7}{\sqrt{\epsilon_r}}\left[M_1 - Y_A\right] \quad,$$

$$\frac{C_{h,h+1}}{\epsilon}\bigg|_{h=1 \text{ to } n-1} = \frac{376.7 \, hY_A}{\sqrt{\epsilon_r}}\left(\frac{J_{h,h+1}}{Y_A}\right) \quad,$$

$$\frac{C_{n,n+1}}{\epsilon} = \frac{376.7}{\sqrt{\epsilon_r}}\left[M_n - Y_A\right] \quad.$$

---

design equations. However, the desired value of w should be used in the mapping Eqs. (10.06-1) through (10.06-3) for determining n. Note that $Y_A = Y_B$ is the characteristic admittance of the terminating lines.

After all of the J/Y_A and N parameters in Table 10.06-1 have been computed, the admittance scale factor, h, must be fixed. One of the prime considerations in the choice of h is that the line dimensions must be such that the resonators will have a high unloaded Q. The dimensions that give optimum resonator Q's in such structures as interdigital filters are not known. However, it is known that for air-filled, coaxial-line resonators the optimum Q will result when the line impedance is about 76 ohms, and various approximate studies suggest that the optimum impedance for thick, rectangular-bar, strip-line resonators such as those in Fig. 10.06-2 is not greatly different. Thus, it is suggested that in this case h be chosen to make the quantity

$$\frac{2C_{k-1,k}}{\epsilon} + \frac{C_k}{\epsilon} + \frac{2C_{k,k+1}}{\epsilon}\bigg|_{\substack{k=n/2 \text{ for } n \text{ even} \\ =(n+1)/2 \text{ for } n \text{ odd}}} = \text{(around 5.4)}$$

(10.06-4)

if air dielectric is used. If the quantity in Eq. (10.06-4) is set equal to 5.4 for the case of $\epsilon_r = 1$, this corresponds to making the line impedance 70 ohms for the resonator lines in the center of the filter, under the conditions that the adjacent lines are being excited with the same amplitude of voltage but with opposite phase (this is a generalized odd-mode admittance condition). A value for h, having been established, the remainder of the calculations follow in a straightforward manner. After the normalized capacitances, C_k/ϵ and $C_{k,k+1}/\epsilon$, have been computed, the line dimensions are determined as discussed in Sec. 5.05 [by use of Eqs. (5.05-33) through (5.05-35) and the accompanying charts].

A trial design was worked out using an $n = 6$ reactive-element Tchebyscheff prototype with $L_{Ar} = 0.10$ db. The prototype parameters were $g_0 = 1$, $g_1 = 1.1681$, $g_2 = 1.4039$, $g_3 = 2.0562$, $g_4 = 1.5170$, $g_5 = 1.9029$, $g_6 = 0.8618$, $g_7 = 1.3554$, and $\omega_1' = 1$. The design was worked out for a fractional bandwidth of $w = 0.10$ centered at $f_0 = 1.5$ Gc. Table 10.06-2 summarizes the various parameters used or computed in the calculations. The parameter h was chosen so that Eq. (10.06-4) would yield 5.4. The resulting circuit has symmetry in its dimensions because the Tchebyscheff prototype is antimetric (i.e., one half of the network is reciprocal to the other half as discussed in Sec. 4.05).

615

TABULATION OF QUANTITIES IN TABLE 10.06-1 AND IN FIG. 10.06-2 FOR A
10-PERCENT BANDWIDTH TRIAL DESIGN WITH $n = 6$

k	$J_{k,k+1}/Y_A$	$N_{k,k+1}$	$C_{k,k+1}/\epsilon$	$s_{k,k+1}$ (inches)	k	C_k/ϵ	w_k (inches)
0 and 6	0.9253		1.582	0.159*	0 and 7	5.950	0.405†
1 and 5	0.7809	6.401	0.301	0.419	1 and 6	3.390	0.152
2 and 4	0.5886	6.381	0.226	0.512	2 and 5	4.420	0.183
3	0.5662	6.379	0.218	0.520	3 and 4	4.496	0.183

$w = 0.10$ $Y_A = 0.020$ mho
$\theta_1 = 1.492$ $N_1 = N_6 = 0.02420$
$h = 0.05143$ $b = 0.625$ inch
$\epsilon_r = 1$ $t = 0.187$ inch

* Changed to 0.127 inch after laboratory tests.

† Changed to 0.437 inch after laboratory tests.

Figure 10.06-3 shows a photograph of the completed filter, while
Fig. 10.06-4 shows those dimensions of the filter not summarized in
Table 10.06-2. The short-circuiting side walls of the structure are
spaced exactly a quarter-wavelength apart at the midband frequency
$f_0 = 1.5$ Gc ($\lambda_0/4 = 1.968$ inches). Because of the capacitance between
the open-circuited ends of the resonator elements and the side walls,
it was necessary to foreshorten the resonators so as to maintain their
resonant frequency at 1.5 Gc. No very satisfactory means for accounting
for all of the fringing capacitances at the open-circuit ends of the
resonators has been devised, but some rough estimates were made using
fringing capacitance data in Sec. 5.05 and various approximations. The
estimated foreshortening for the resonators was 0.216 inch, but laboratory
tests showed this to be excessive since the pass-band center was 1.56
instead of 1.50 Gc. Although the filter pass band can always be lowered
in frequei .y by use of tuning screws, if the resonators had been fore-
shortened about 0.160 inch instead of 0.216 inch, the pass-band center
frequency would probably have been about right.

Although the structure included tuning screws, no effort was made
to lower the band-center frequency to 1.50 Gc. However, it was found
that since Resonators 1 and 6 have different fringing-capacitance

FIG. 10.06-3   A 10-PERCENT BANDWIDTH INTERDIGITAL FILTER WITH ITS COVER
PLATE REMOVED

conditions at their open-circuit ends than do the other resonators, it
was necessary to increase the capacitance at their open-circuit ends by
inserting the tuning screws. Before this was done, the pass-band re-
sponse was not symmetrical (this is indicative of mistuning of some of
the resonators with respect to the others).

When the filter was first tested, the pass-band VSWR reached peaks
of 2.2, which is somewhat high since 0.1-db Tchebyscheff ripples call
for VSWR peaks of only 1.3(Such conditions can usually be corrected
by altering the couplings between the terminations and the first reso-
nator on each end. Thus, a 0.032-inch-thick brass shim was added to the

SECTION A-A'

TOP VIEW, UPPER GROUND PLANE REMOVED

A-3527-277

FIG. 10.06-4   DRAWING OF THE 10-PERCENT BANDWIDTH
INTERDIGITAL FILTER
Part of the dimensions are as specified by Table 10.06-2
along with Fig. 10.06-2

input and output lines (Lines 0 and 7) to reduce the adjacent gaps from $s_{01} = s_{67} = 0.159$ inch to 0.127 inch. This reduced the input VSWR to 1.30 or less across the band. It appears desirable that, in working out the design of trial models of interdigital filters as described herein, some provision should be made for experimental adjustment of the size of coupling gaps at the ends, if the pass-band VSWR is to be closely controlled.

Figure 10.06-5 shows the measured attenuation characteristic of this filter, while Fig. 10.06-6 shows the measured VSWR. The measured fractional bandwidth is slightly less than the design value ($w = 0.0935$ instead of 0.100). Using $w = 0.0935$ and $f_0 = \omega_0/(2\pi) = 1.563$ Gc, the

618

measured attenuation was compared with that estimated by use of the
mapping Eqs. (10.06-1) through (10.06-3) along with Fig. 4.03-5. The
measured attenuation in the stop bands was found to be somewhat less
than that predicted for a Tchebycheff filter with L_{A_r} = 0.1-db ripple.
However, the pass-band VSWR in Fig. 10.06-6 is, for the most part, much
less than the 1.36 peak value corresponding to a 0.1-db Tchebycheff
ripple, and some of the VSWR amplitude shown may be due to the connectors
and slight mistuning.* The attenuation for a L_{A_r} = 0.01-db ripple filter
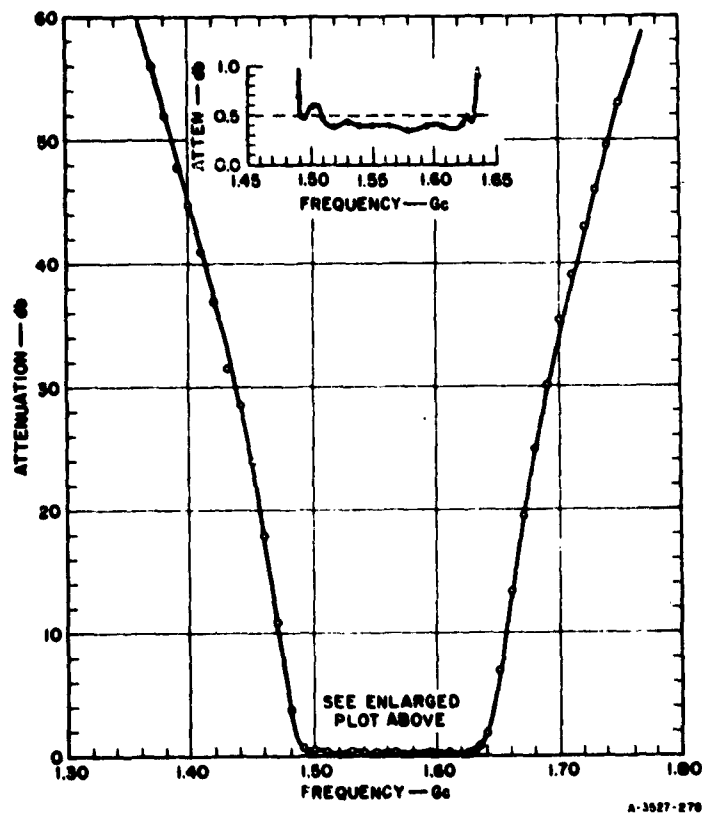
FIG. 10.06-5   MEASURED ATTENUATION CHARACTERISTIC OF
THE FILTER IN FIG. 10.06-3

---

* The pass-band VSWR is the most sensitive index of the correlation of the actual design as com-
pared to the pass-band characteristic of the prototype. The pass-band attenuation as determined
from through transmission measurements includes the additional attenuation due to dissipation
loss, which may be markedly greater than 0.1 db depending on the Q's of the resonators.
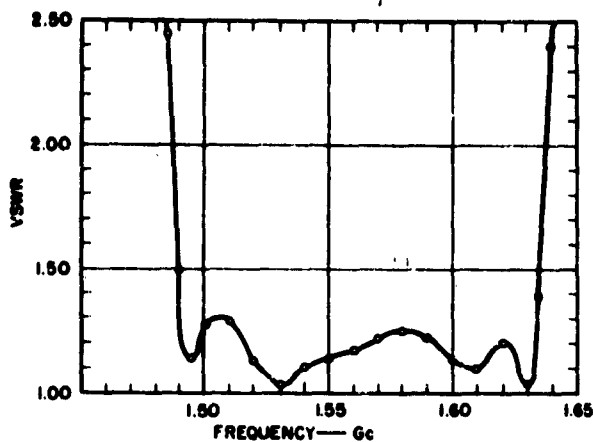
2.50
2.00
VSWR
1.50
1.00

1.50   1.55   1.60   1.65
FREQUENCY — Gc

A-3627-279

FIG. 10.06-6   MEASURED VSWR OF THE FILTER IN
FIG. 10.06-3

filter (VSWR = 1.1 peak) was also estimated, and the results are summarized
in Table 10.06-3. Note that in all cases the measured stop-band attenuation
is less than that computed for a 0.10-db ripple filter, but more than that
for a 0.01-db ripple filter. Thus, the given approximate mapping procedure
appears to be reasonably consistent with the measured results.

Table 10.06-3
COMPARISON OF MEASURED ATTENUATION IN
FIG. 10.06-5 WITH ATTENUATION PREDICTED
USING MAPPING EQS. (10.06-1) TO (10.06-3)
Computed values are for 0.01 and 0.10 db ripple,
$n = 6$, $w = 0.0935$, and $f_0 = \omega_0/(2\pi) = 1.563$ Gc

f, Gc	L_A, db FOR $L_{Ar} = 0.01$	L_A, db MEASURED	L_A, db FOR $L_{Ar} = 0.10$
1.440	25	29	35.5
1.686	25	28	35.5
1.380	49.5	52	59.5
1.746	49.5	52	59.5

The second pass band for inter-
digital filters is centered at $3\omega_0$
(where ω_0 is the center of the first
pass band). There are multiple-
order poles of attenuation
(Sec. 2.04) at $\omega = 0$, $2\omega_0$, $4\omega_0$,
etc., so the stop bands are very
strong. Unlike all the filters dis-
cussed earlier in this chapter,
interdigital filters cannot possibly
have any spurious responses near $2\omega_0$,
$4\omega_0$, etc., no matter how poorly they
may be tuned.

620

Calculating from the measured pass-band attenuation of the trial design, it is estimated that the unloaded Q's of the resonators in this filter are about 1100. Using copper for the structure instead of aluminum would theoretically give a value about 25 percent higher for the unloaded Q's. It is possible that a different impedance level within the filter might also give higher Q's for a given ground plane spacing. Polishing the resonator bars and the ground planes would also help to raise the resonator Q's.

The lines in the trial interdigital filter (Figs. 10.06-3 and 10.06-4) were fabricated by machining Lines 0, 2, 4, and 6 in comb form from a single piece of jig plate. Lines 1, 3, 5, and 7 were cut out similarly from a second piece of jig plate. (Actually, both comb structures were machined at once, back-to-back.) Then, interleaving the two comb structures between ground planes gave the desired interdigital structure.

Figure 10.06-7 shows an alternative form of interdigital filter structure that should be even less expensive to fabricate. In this case, the interdigital line structure is photo-etched on a copper-clad dielectric card, and the dielectric material removed from the region between the copper-foil lines. In order to provide good support for the lines, the
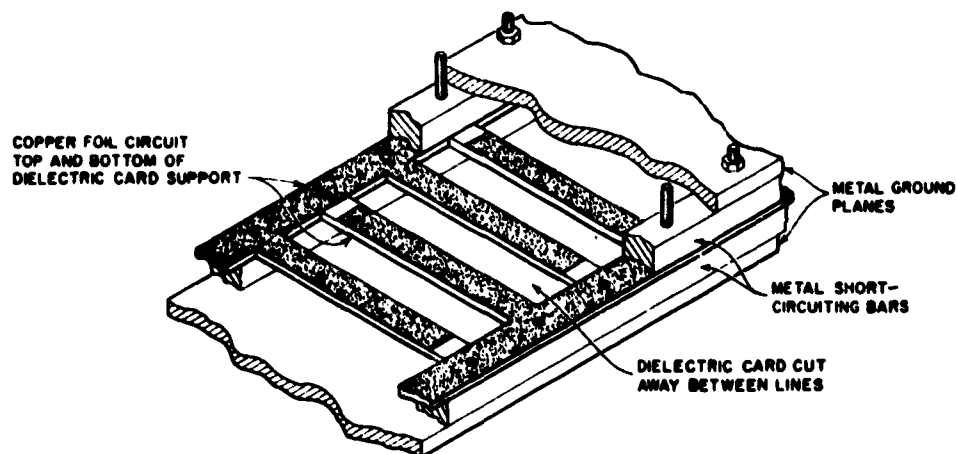
A-3527-280

FIG. 10.06-7   A PROPOSED LOW-COST CONSTRUCTION FOR INTERDIGITAL-LINE FILTERS

621

dielectric is not removed at the open-circuit ends of the lines, however,
With the use of this structure, the propagation is largely in air, which
should permit good performance; also, the dielectric-card line structures
should be quite inexpensive to mass produce.

Round rods between ground planes also provide an attractive form for
fabricating interdigital filters.[2] However, no data are yet available for
accurate determination of the rod diameters and spacings from specified
line capacitances.*

SEC. 10.07, INTERDIGITAL-LINE FILTERS HAVING WIDE BANDWIDTHS

In this section the interdigital band-pass filter discussion in
Sec. 10.06 is extended to cover the filter structure shown in Fig. 10.07-1.
Note that the structure in Fig. 10.07-1 differs from that in Fig. 10.06-1
in that the terminating lines are connected to open-circuited rather than
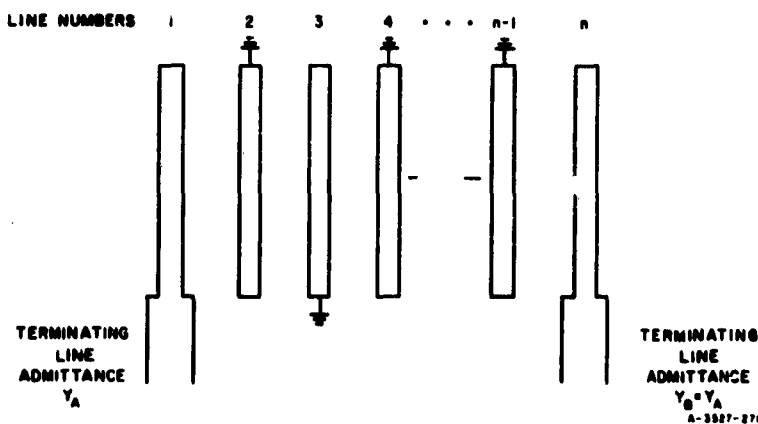
FIG. 10.07-1   INTERDIGITAL FILTER WITH OPEN-CIRCUITED
LINES AT THE ENDS

short-circuited line elements.   In the case of the structure in Fig. 10.07-1,
when it is designed by the methods of this section, all of the line elements
(including Lines 1 and n) serve as resonators.   Thus, when the procedure of
this section is used, an n-reactive-element, low-pass prototype will lead to
an interdigital filter with n interdigital line elements.

---

* Bolljahn and Matthaei (Ref. 2) give an approximate method for design of structures consisting of rods that are
all the same size and have the same spacings. A procedure for accurate design where varying diameters and
spacings are required has not as yet been obtained.

Table 10.07-1 presents approximate design equations for filters of
the form in Fig. 10.07-1. This type of filter is most practical for
designs having moderate or wide bandwidths (i.e., perhaps bandwidths of
around 30 percent or more), although the design procedure given is valid
for either narrow- or wide-band filters. The main drawback in applying
the procedure in Table 10.07-1 to narrow-band filters is that Lines 1 and
n will tend to attain extremely high impedance in such designs.

Except for the somewhat different design equations, the procedure for
the design of filters of the form shown in Fig. 10.07-1 is much the same as
that described for filters in Sec. 10.06. It is suggested that for use in
Table 10.07-1, w be made about 8 percent larger than the actual desired
fractional bandwidth, in order to allow for some bandwidth shrinkage.
Equation (10.06-4) is applicable when selecting a value for the admittance
scale factor, h.

A trial design was worked out using an $n = 8$ reactive-element
Tchebyscheff prototype with $L_{A_r} = 0.10$ db. The prototype parameters were
$g_0 = 1$, $g_1 = 1.1897$, $g_2 = 1.4346$, $g_3 = 2.1199$, $g_4 = 1.6010$, $g_5 = 2.1699$,
$g_6 = 1.5640$, $g_7 = 1.9444$, $g_8 = 0.8778$, $g_9 = 1.3554$, and $\omega'_1 = 1$. The design
was carried out for a fractional bandwidth of $w = 0.70$ centered at 1.50 Gc,
and the parameter h was chosen to make Eq. (10.06-4) equal to 5.86. (This
gives a generalized odd-mode impedance of 64.5 ohms for the middle lines.)
Table 10.07-2 summarizes some of the quantities computed in the course of
the design of this filter.

Figure 10.07-2 shows the completed filter, while the drawing in
Fig. 10.07-3 shows additional construction details and additional dimen-
sions not summarized in Table 10.07-2. The filter was fabricated in much
the same manner as the filter described in Sec. 10.06, except that the
resonator lines were foreshortened by 0.150 inch. The relatively small
cross-sectional dimensions of the resonator elements, unfortunately, made
0.150 inch excessive, so that the measured band-center frequency was
1.55 Gc instead of 1.50 Gc. It is probable that foreshortening the line
elements about 0.125 inch would have been about right.

When this filter was first tested, the VSWR was quite low across the
band (about 1.2 or less) except at band center where the VSWR peaked to
1.8. This situation was altered by increasing the s_{12} and s_{78} gaps from
0.087 inch to 0.092 inch, which caused the VSWR peaks across the band to
be more nearly even and to be 1.55 or less.

Table 10.07-1

DESIGN EQUATIONS FOR INTERDIGITAL FILTERS OF THE FORM
IN FIG. 10.07-1

Use mapping in Eqs. (10.06-1) to (10.06-3) to select low-pass
prototype with the required value of n. The input and output
lines in this filter count as resonators, so that there are n
line elements for an n-reactive-element prototype.

Compute:

$$\theta_1 = \frac{\pi}{2} \frac{\omega_1}{\omega_0} = \frac{\pi}{2}\left(1 - \frac{w}{2}\right)$$

$$\left.\frac{J_{k,k+1}}{Y_A}\right|_{k=2 \text{ to } n-3} = \frac{g_2}{g_0\sqrt{g_k g_{k+1}}} \quad , \quad \frac{J_{n-2,n-1}}{Y_A} = \frac{1}{g_0}\sqrt{\frac{g_2 g_0}{g_{n-2}g_{n+1}}}$$

$$\left.N_{k,k+1}\right|_{k=2 \text{ to } n-2} = \sqrt{\left(\frac{J_{k,k+1}}{Y_A}\right)^2 + \left(\frac{\omega_1' g_2 \tan\theta_1}{2g_0}\right)^2}$$

$$\frac{Z_1}{Z_A} = \omega_1' g_0 g_1 \tan\theta_1$$

$$\frac{Y_2}{Y_A} = \frac{\omega_1' g_2}{2g_0}\tan\theta_1 + N_{23} - \frac{J_{23}}{Y_A}$$

$$\left.\frac{Y_k}{Y_A}\right|_{k=3 \text{ to } n-2} = N_{k-1,k} + N_{k,k+1} - \frac{J_{k-1,k}}{Y_A} - \frac{J_{k,k+1}}{Y_A}$$

$$\frac{Y_{n-1}}{Y_A} = \frac{\omega'(2g_0 g_{n-1} - g_2 g_{n+1})\tan\theta_1}{2g_0 g_{n+1}} + N_{n-2,n-1} - \frac{J_{n-2,n-1}}{Y_A}$$

$$\frac{Z_n}{Z_A} = \omega_1' g_n g_{n+1}\tan\theta_1$$

The normalized self-capacitances, C_k/ϵ, per unit length for
the line elements are:

$$\frac{C_1}{\epsilon} = \frac{376.7}{\sqrt{\epsilon_r}} Y_A \frac{(1 - \sqrt{h})}{(Y_1/Z_A)}$$

Table 10.07-1 *concluded*

$$\frac{C_2}{\epsilon} = \frac{376.7}{\epsilon_r} Y_A h \left(\frac{Y_2}{Y_A}\right) - \sqrt{h} \frac{C_1}{\epsilon}$$

$$\left.\frac{C_k}{\epsilon}\right|_{k=3 \text{ to } n-2} = \frac{376.7}{\sqrt{\epsilon_r}} Y_A h \left(\frac{Y_k}{Y_A}\right)$$

$$\frac{C_{n-1}}{\epsilon} = \frac{376.7}{\sqrt{\epsilon_r}} Y_A h \left(\frac{Y_{n-1}}{Y_A}\right) - \sqrt{h} \frac{C_n}{\epsilon}$$

$$\frac{C_n}{\epsilon} = \frac{376.7}{\sqrt{\epsilon_r}} Y_A \frac{(1 - \sqrt{h})}{(Z_n/Z_A)}$$

where ϵ is the dielectric constant, ϵ_r is the relative dielectric constant in the medium of propagation, and h is a dimensionless admittance scale factor whose value should be chosen to give a convenient admittance level in the filter. (See Text.)

The normalized mutual capacitances $C_{k,k+1}/\epsilon$ per unit length between adjacent line elements are:

$$\frac{C_{12}}{\epsilon} = \frac{376.7}{\sqrt{\epsilon_r}} Y_A \frac{\sqrt{h}}{(Z_1/Z_A)}$$

$$\left.\frac{C_{k,k+1}}{\epsilon}\right|_{k=2 \text{ to } n-2} = \frac{376.7}{\sqrt{\epsilon_r}} Y_A h \left(\frac{J_{k,k+1}}{Y_A}\right)$$

$$\frac{C_{n-1,n}}{\epsilon} = \frac{376.7}{\sqrt{\epsilon_r}} Y_A \frac{\sqrt{h}}{(Z_n/Z_A)}$$
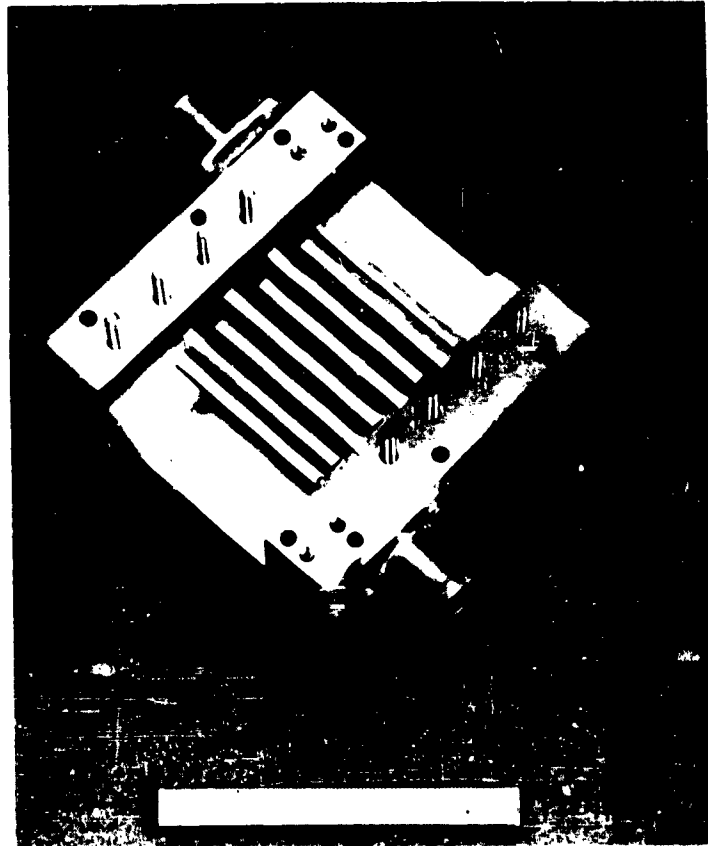
FIG. 10.07-2 OCTAVE BANDWIDTH INTERDIGITAL FILTER WITH
COVER PLATE REMOVED
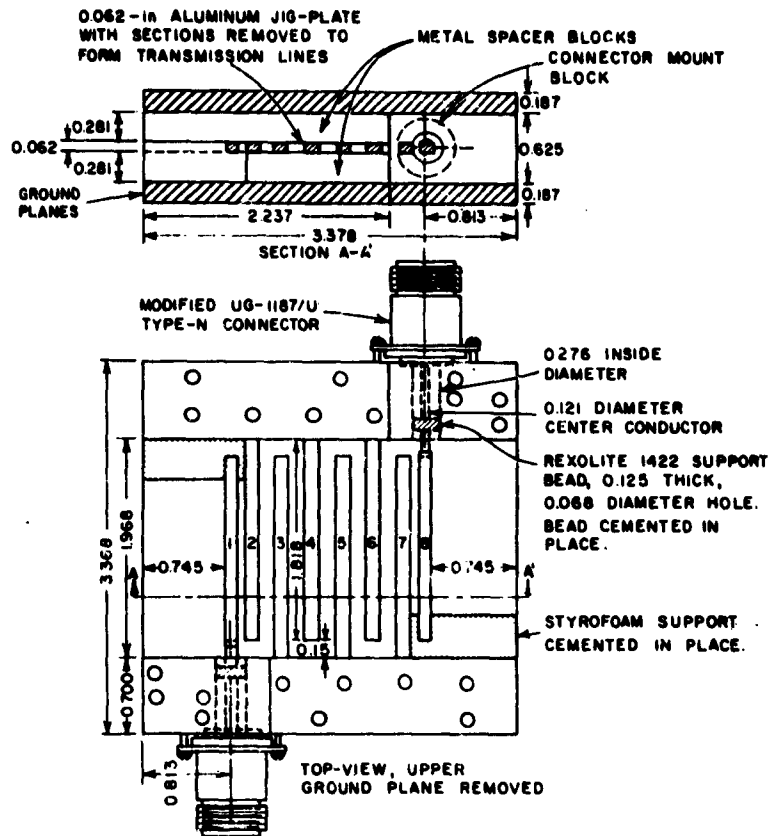
0.062-in ALUMINUM JIG-PLATE
WITH SECTIONS REMOVED TO
FORM TRANSMISSION LINES

METAL SPACER BLOCKS

CONNECTOR MOUNT
BLOCK

SECTION A-A

MODIFIED UG-1187/U
TYPE-N CONNECTOR

0.276 INSIDE
DIAMETER

0.121 DIAMETER
CENTER CONDUCTOR

REXOLITE 1422 SUPPORT
BEAD, 0.125 THICK,
0.068 DIAMETER HOLE.
BEAD CEMENTED IN
PLACE.

STYROFOAM SUPPORT
CEMENTED IN PLACE.

TOP-VIEW, UPPER
GROUND PLANE REMOVED

FIG. 10.07-3 DRAWING OF THE INTERDIGITAL FILTER
IN FIG. 10.07-2
Other dimensions not shown are as defined by
Fig. 10.06-2 and Table 10.07-2

627

Table 10.07-2

**TABULATION OF SOME OF THE PARAMETERS COMPUTED IN THE DESIGN OF
THE TRIAL OCTAVE-BANDWIDTH INTERDIGITAL FILTER**

The dimensions are as defined in Fig. 10.06-2

k	$J_{k,k+1}/Y_A$	$C_{k,k+1}/\epsilon$	$s_{k,k+1}$ (inches)	k	$\dfrac{Z_k}{Z_A}$ or $\dfrac{Y_k}{Y_A}$	C_k/ϵ	w_k (inches)
1 and 7		1.647	0.087*	1 and 8	1.941	2.235	0.126†
2 and 6	0.823	1.115	0.136	2 and 7	1.779	1.463	0.121†
3 and 5	0.779	1.056	0.143	3 and 6	1.235	1.675	0.126†
4	0.770	1.044	0.146	4 and 5	1.258	1.706	0.127†

w = 0.70	Y_A = 0.020 mho		
θ_1 = 1.021	b = 0.625 inch		
h = 0.18	t = 0.063 inch		
ϵ_r = 1			

* Changed to 0.092 inch after laboratory tests.

† Computed using Eq. (5.05-26) for width correction.

SOURCE: Quarterly Progress Report 4, Contract DA 36-039 SC-87398, SRI; reprinted in *IRE Trans. PGMTT* (see Ref. 3 by G. L. Matthaei.

Figure 10.07-4 shows the measured attenuation of this filter, while Fig. 10.07-5 shows its measured VSWR. The fractional bandwidth is 0.645 instead of the specified 0.700 value, which indicates a shrinkage of bandwidth of about 8 percent, as a result of the various approximations involved in the design equations. The attenuation characteristics in Fig. 10.07-4 was checked against the attenuation computed using the mapping Eqs. (10.06-1) through (10.06-3) with w = 0.645, and f_0 = $\omega_0/(2\pi)$ = 1.55 Gc, along with the n = 8 curve in Fig. 4.03-5. The resulting computed values are listed in Table 10.07-3, along with the corresponding measured values of attenuation. The agreement can be seen to be quite good.

Table 10.07-3

COMPARISON OF THE MEASURED
ATTENUATION IN FIG. 10.07-4 WITH
ATTENUATION PREDICTED USING MAPPING
EQS. (10.06-1) TO (10.06-3)
Computed values are for 0.10-db
ripple, n = 8, w = 0.645, and
f_0 = $\omega_0/(2\pi)$ = 1.55 Gc

f, Gc	L_A, db FOR L_{Ar} = 0.10	L_A, db MEASURED
0.90	32	31
2.23	32	33
0.70	56	55
2.43	56	57

SOURCE: Quarterly Progress Report 4, Contract DA 36-039 SC-87398, SRI; reprinted in *IRE Trans. PGMTT* (see Ref. 3 by G. L. Matthaei).

SEC. 10.08, DERIVATION OF THE DESIGN EQUATIONS FOR PARALLEL-COUPLED AND STUB FILTERS

The first step in deriving the design equations in Tables 10.02-1 through
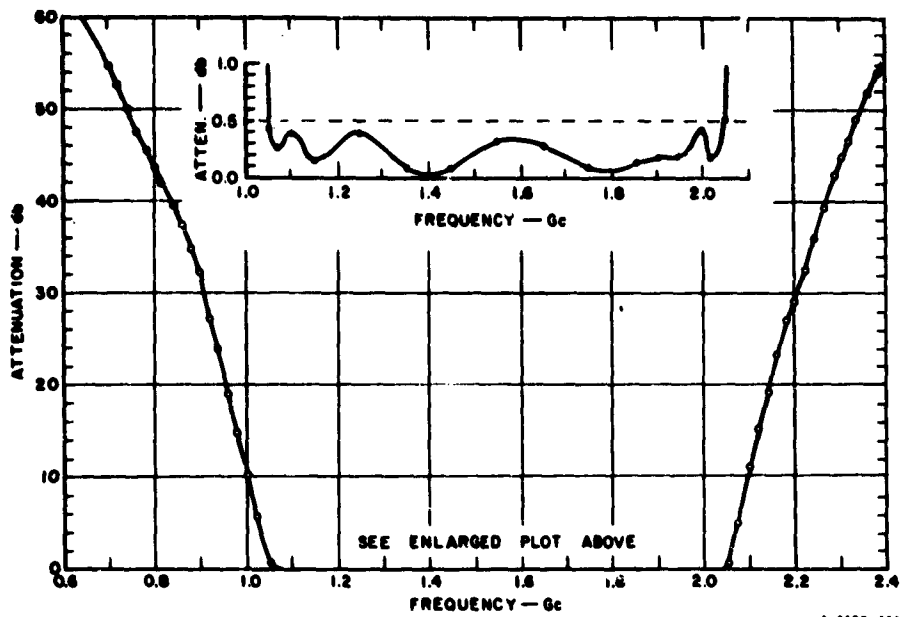
SEE ENLARGED PLOT ABOVE

A-3527-306

FIG. 10.07-4 MEASURED ATTENUATION CHARACTERISTIC OF THE
FILTER IN FIG. 10.07-2
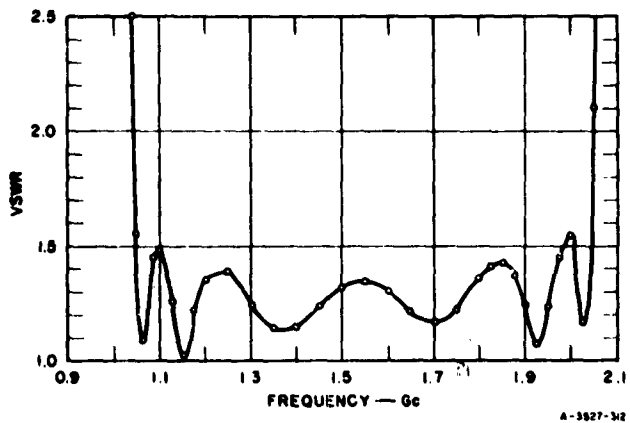
A-3527-312

FIG. 10.07-5 MEASURED VSWR OF THE FILTER
IN FIG. 10.07-2

629

Table 10.05-1 is to convert the low-pass prototype (Sec. 4.04) into the
modified form discussed in Sec. 4.12, which uses only one kind of reactive
element along with impedance or admittance inverters as shown in
Fig. 10.08-1, where the impedance and admittance inverters are assumed
to be frequency-independent and to have the properties summarized in
Fig. 10.08-2. It will be recalled that the low-pass prototype element
values g_0, g_1, g_2, ..., g_{n+1} having been specified for the circuit in
Fig. 10.08-1(a), the elements R_A, L_{a1}, L_{a2}, ..., L_{an}, R_B may be chosen
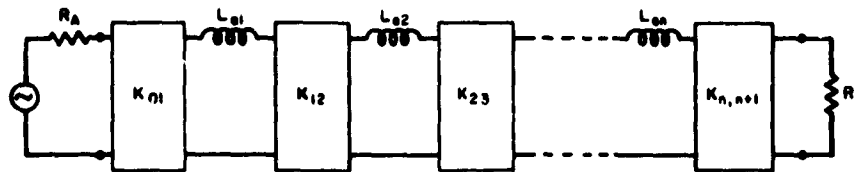
$$K_{01} = \sqrt{\frac{R_A L_{a1}}{g_0 g_1}} \quad , \quad K_{k,k+1}\bigg|_{k=1\ to\ n-1} = \sqrt{\frac{L_{ak}\ L_{a(k+1)}}{g_k\ g_{k+1}}} \quad , \quad K_{n,n+1} = \sqrt{\frac{L_{an} R_B}{g_n\ g_{n+1}}}$$

(a) MODIFIED PROTOTYPE USING IMPEDANCE INVERTERS
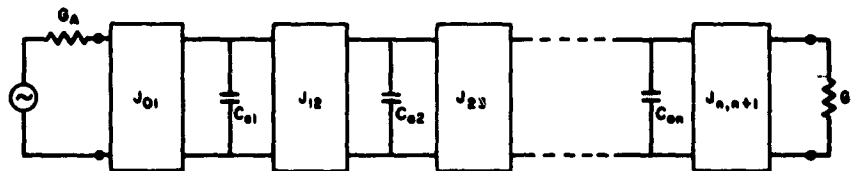
$$J_{01} = \sqrt{\frac{G_A C_{a1}}{g_0 g_1}} \quad , \quad J_{k,k+1}\bigg|_{k=1\ to\ n-1} = \sqrt{\frac{C_{ak}\ C_{a(k+1)}}{g_k\ g_{k+1}}} \quad , \quad J_{n,n+1} = \sqrt{\frac{C_{an} G_B}{g_n\ g_{n+1}}}$$

(b) MODIFIED PROTOTYPE USING ADMITTANCE INVERTERS

FIG. 10.08-1 LOW-PASS PROTOTYPES MODIFIED TO INCLUDE IMPEDANCE
INVERTERS OR ADMITTANCE INVERTERS
The g_0, g_1, ..., g_n, g_{n+1} are obtained from the original prototype
as in Fig. 4.04-1, while the R_A, L_{a1}, ..., L_{an}, and R_B or the G_A,
C_{a1}, ..., C_{an}, and G_B may be chosen as desired
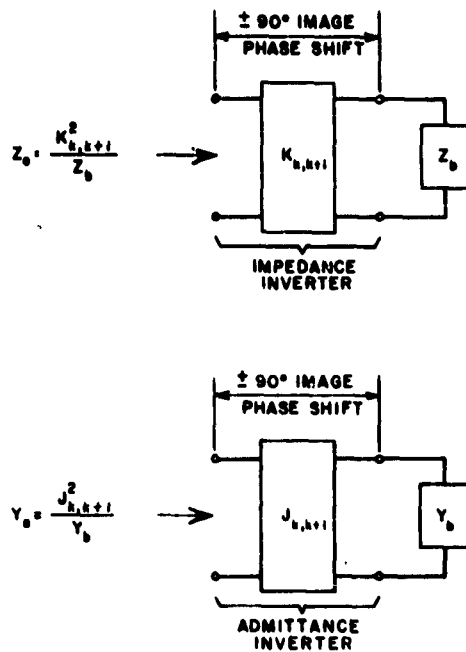
$$Z_a = \frac{K_{k,k+1}^2}{Z_b}$$

±90° IMAGE PHASE SHIFT

$K_{k,k+1}$ Z_b

IMPEDANCE INVERTER

$$Y_a = \frac{J_{k,k+1}^2}{Y_b}$$

±90° IMAGE PHASE SHIFT

$J_{k,k+1}$ Y_b

ADMITTANCE INVERTER

FIG. 10.08-2   DEFINITION OF IMPEDANCE
INVERTERS AND ADMITTANCE
INVERTERS

as desired. Then the circuit with impedance inverters and series induc-
tances will have exactly the same response as the original L-C ladder
prototype if the impedance inverter parameters are specified as indicated
by the equations in Fig. 10.08-1(a). An analogous situation also applies
for the dual circuit in Fig. 10.08-1(b).

The derivations of the design equations in this chapter are based on
the use of the converted prototypes in Fig. 10.08-1 using idealized,
frequency-independent impedance or admittance inverters. The procedure
will be to break up the modified prototype into symmetrical sections, and
then to relate the image *properties* (Chapter 3) of the modified prototype
sections to the image properties of corresponding sections of the actual
band-pass microwave filter structure.

631

Procedure for Deriving the Equations in Table 10.02-1—The design
equations in Table 10.02-1 are based on the modified prototype shown at
(b) in Fig. 10.08-1, while Fig. 10.08-3 shows the manner in which the
element values are specified, and the manner in which the prototype is
broken into sections. The image admittance, $Y_{k,k+1}^i(\omega')$, and phase,
$\beta_{k,k+1}$ (in the pass band) for each of the prototype interior sections
(S_{12}' to $S_{n-1,n}'$) are readily shown to be

$$Y_{k,k+1}^i(\omega') = J_{k,k+1}\sqrt{1 - \left[\frac{\omega'(C_a/2)}{J_{k,k+1}}\right]^2} \qquad (10.08\text{-}1)$$

and

$$\left.\beta_{k,k+1}\right|_{\omega' \leq \frac{J_{k,k+1}}{C_a/2}} = \sin^{-1}\left[\frac{\omega'(C_a/2)}{J_{k,k+1}}\right] \mp \frac{\pi}{2} \qquad (10.08\text{-}2)$$

where, in this case, $C_a = G_A/\omega_1'$ and ω_1' is the cutoff frequency for the
low-pass prototype. The choice of $\mp\pi/2$ in Eq. (10.08-2) depends on
whether the inverter is taken to have ±90-degree phase shift. The
equations in Fig. 5.09-1(b) can be adapted to show that the image admit-
tance and pass-band image phase for a parallel-coupled section, $S_{k,k+1}$
such as those in the filter in Fig. 10.02-1(a) is
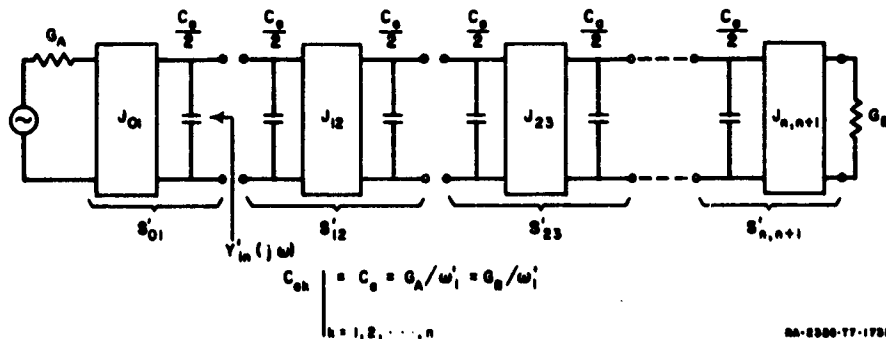
FIG. 10.08-3 MODIFIED PROTOTYPE FOR DERIVING THE DESIGN
EQUATIONS IN TABLE 10.02-1

$$Y_I = \frac{\sqrt{(Y_{oo} - Y_{oe})^2 + (Y_{oo} + Y_{oe})^2 \cos^2 \theta}}{2 \sin \theta} \qquad (10.08\text{-}3)$$

and

$$\beta = \cos^{-1}\left[\left(\frac{Y_{oo} + Y_{oe}}{Y_{oo} - Y_{oe}}\right) \cos \theta\right] \qquad (10.08\text{-}4)$$

where $\theta = \pi\omega/2\omega_0$ and Y_{oo} and Y_{oe} are the odd- and even-mode line admittances, respectively. The parameters of the parallel-coupled sections S_{12} to $S_{n-1,n}$ in Fig. 10.02-1(a) are related to sections S'_{12} to $S'_{n-1,n}$ of the prototype by forcing the following correspondences between the two structures:

(1) The image phase of the parallel-coupled sections when $\omega = \omega_0$ must be the same as the image phase of the prototype sections when $\omega' = 0$.

(2) The image admittances of the parallel-coupled sections when $\omega = \omega_0$ must be the same (within a scale factor h)* as the image admittances of the corresponding prototype sections when $\omega' = 0$.

(3) The image admittance of the parallel-coupled sections when $\omega = \omega_1$ must be the same (within a scale factor h)* as the image admittance of the corresponding prototype sections when $\omega' = \omega'_1$.

$$(10.08\text{-}5)$$

Correspondence (1) is fulfilled in this case by choosing the + sign in Eq. (10.08-2). Equating Eqs. (10.08-1) and (10.08-3) and evaluating each side at the appropriate frequencies indicated above, two equations are obtained from which the equations for interior sections in Table 10.02-1 may be derived (with the help of the information in Figs. 10.08-1 and 10.08-3) by solving for Y_{oo} and Y_{oe}.

The end sections, S_{01} and $S_{n,n+1}$, must be treated as a special case. If $Y_{i_a}(j\omega)$ is defined as the admittance seen looking in the right end of the parallel-coupled section S_{01} in Fig. 10.02-1(a), with the left end

---

* Taking $G_A = G_B = Y_A = Y_B$.

connected to the input line of admittance Y_A, the following correspondences are forced with respect to $Y'_{ia}(j\omega')$ indicated in Fig. 10.08-3:

(1) Re $Y_{ia}(j\omega_0)$ = Re $Y_{ia}(j\omega_1)$ for the parallel-coupled terminating circuit, just as Re $Y'_{ia}(j0)$ = Re $Y'_{ia}(-j\omega'_1)$ for the terminating circuit of the prototype.

(10.08-6)

(2) Im $Y_{ia}(j\omega_1)$/Re $Y_{ia}(j\omega_1)$ must equal B'/G' = Im $Y'_{ia}(-j\omega'_1)$/ Re $Y'_{ia}(-j\omega'_1)$ computed from the prototype.

In order to obtain additional degrees of freedom for adjusting the admittance level within the interior of the filter, the two parallel-coupled strips for the end sections S_{01} and $S_{n,n+1}$ were allowed to be of unequal width and the special constraint conditions summarized in Fig. 5.09-3(a) were used in computing $Y_{ia}(j\omega)$ for the actual filter. [The constraint $(Y^e_{oe})_{01} + (Y^e_{oe})_{01}$ = $2Y_A$ insures that Correspondence 1 in Eq. (10.08-6) will be satisfied.] From Fig. 10.08-3 it is easily seen that

$$Y'_{ia}(j\omega') \approx \frac{J^2_{01}}{G_A} + j\,\frac{\omega'C_a}{2} \quad . \tag{10.08-7}$$

The equations in Table 10.02-1 for design of the end sections S_{01} and $S_{n,n+1}$ of the parallel-coupled filter were then obtained by using $Y_{ia}(j\omega)$ computed using Fig. 5.09-3(a), and $Y'_{ia}(j\omega')$ from Eq. (10.08-7) in the correspondences (10.08-6) above. It should be noted that the admittance scale factor $h = 1/\sqrt{N}$, where N is the turns ratio in Fig. 5.09-3(a).

Procedure for Deriving the Equations in Table 10.03-1—The equations in Table 10.03-1 were derived using much the same point of view as discussed above for Table 10.02-1, except that the somewhat different modified prototype in Fig. 10.08-4 was used. Note that in this case the J_{01} and $J_{n,n+1}$ admittance inverters are eliminated, and that the circuit has been split into a cascade of symmetrical sections. Note that the symmetrical sections in Fig. 10.08-4 are the same as those in Fig. 10.08-3, and that their image admittance and phase are given by Eqs. (10.08-1) and (10.08-2). Now the stub filter in Fig. 10.03-1 can be pieced together as a cascade of symmetrical stub sections as shown in Fig. 10.08-5. Also, note from Fig. 5.09-1(b) that these stub sections are exactly equivalent to the parallel-coupled sections in the filter in Fig. 10.02-1(a). Due
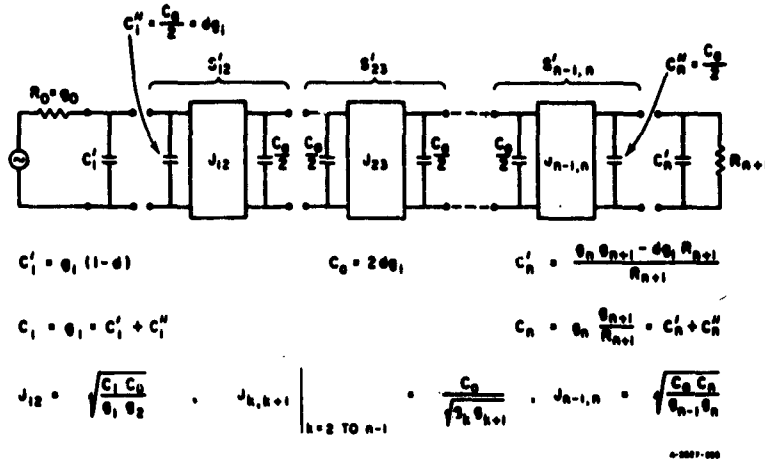
FIG. 10.08-4 MODIFIED PROTOTYPE FOR USE IN DERIVING THE
DESIGN EQUATIONS IN TABLE 10.03-1
The parameter d may be chosen arbitrarily within the
range $0 < d \leq 1$
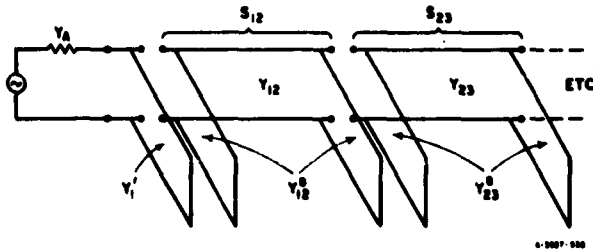
FIG. 10.08-5 THE FILTER IN FIG. 10.03-1 BROKEN
INTO SYMMETRICAL SECTIONS
The sections of this filter are designed
using the prototype sections in
Fig. 10.08-4 as a guide

635

to this equivalence, Eqs. (10.08-3) and (10.08-4) also apply for stub sections by substituting

$$(Y_{oe})_{k,k+1} = Y'_{k,k+1} \qquad (10.08\text{-}8)$$

and

$$(Y_{oo})_{k,k+1} = Y'_{k,k+1} + 2Y_{k,k+1} \qquad (10.08\text{-}9)$$

where $Y_{k,k+1}$ is the characteristic admittance of the $\lambda_0/4$ connecting line and $Y'_{k,k+1}$ is the characteristic admittance of the short-circuited $\lambda_0/4$ stubs in section $S_{k,k+1}$ of the filter (Fig. 10.08-5).

The sections $S'_{k,k+1}$ of the modified prototype in Fig. 10.08-4 were related to the corresponding sections $S_{k,k+1}$ (Fig. 10.08-5) of the band-pass filter by first setting $R_{n+1} = g_0$ (for Fig. 10.08-4) and then applying the correspondences (10.08-5) above. (Of course, in the statements of the correspondences "stub filter sections" should be used to replace "parallel-coupled sections.") The correspondences were first worked out using the admittance level of the prototype in Fig. 10.08-4; later the admittance level was altered by multiplying all admittances by $Y_{A}g_0$. Relating the prototype and band-pass filter sections made it possible to obtain equations for the line admittances in the band-pass filter sections, and then the final stub admittances for the filter in Fig. 10.03-1 were computed as the sums of the admittances of adjacent stubs, i.e., for the kth stub

$$Y_k \Big|_{k=2 \text{ to } n-1} = Y'_{k-1,k} + Y'_{k,k+1} \qquad (10.08\text{-}10)$$

The stub Y'_1 in Fig. 10.08-5 is related to C'_1 in Fig. 10.08-4 by the relation

$$\omega'_1 C'_1 R_0 = \frac{Y'_1 \operatorname{ctn} \theta_1}{Y_A} \qquad (10.08\text{-}11)$$

which forces the susceptance of the Y'_1 stub at the band-edge frequency, ω_1, to be the same as the susceptance of C'_1 of the modified prototype at the prototype band-edge frequency, ω'_1, (except for a possible admittance scale change in the microwave filter). Then the end stub Y_1 has the total admittance

636

$$Y_1 = Y_1' + Y_{12}' \qquad\qquad (10.08\text{-}12)$$

The other end stub, Y_n, is treated in similar fashion.

Procedure for Deriving the Equations in Table 10.05-1—The stub filter in Fig. 10.05-1 is much the same as that in Fig. 10.03-1, except that series $\lambda_0/2$ short-circuited stubs have been added at the ends of the filter. In order to accommodate the series stubs, the modified prototype in Fig. 10.08-6 is used, where it should be noted that there are now series inductances at both ends of the filter. The series stub Z_1 of the filter in Fig. 10.05-1 is related to the series element L_1 of the filter in Fig. 10.08-6. This relation forces the reactance of the series stub at the band-edge frequency ω_1 for the band-pass filter to be the same as the reactance $\omega_1' L_1$ of the prototype at the prototype band-edge frequency, ω_1' (within a possible impedance scale change for the microwave filter). The same was done for the series stub Z_n at the other end of the filter. In all other respects the derivation of the equations in Table 10.05-1 is much the same as the derivation for the equations for the stub filter in Fig. 10.03-1, as discussed above.
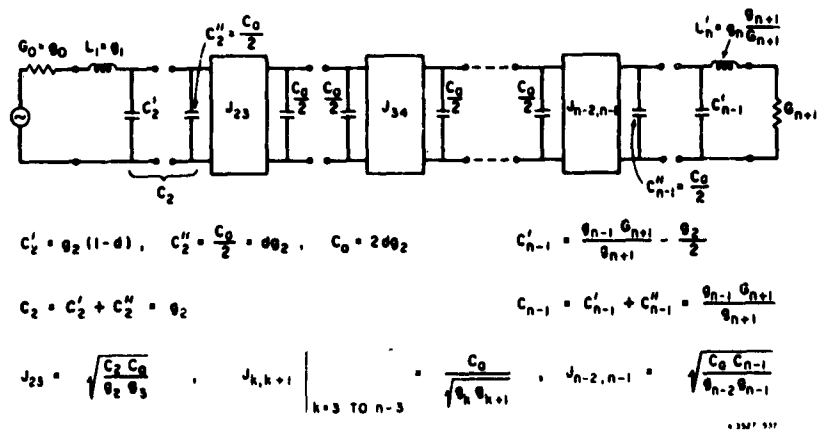
FIG. 10 08-6 MODIFIED PROTOTYPE FOR USE IN DERIVING THE EQUATIONS IN TABLE 10.05-1
The parameter d may be chosen arbitrarily within the range $0 < d \leq 1$

SEC. 10.09, DERIVATION OF THE DESIGN EQUATIONS FOR
INTERDIGITAL-LINE FILTERS

The derivation of design equations for filters of the form in
Fig. 10.09-1 was explained in Sec. 10.08. Filters of this type consist of
parallel-coupled resonators which are $\lambda_0/2$ long at the midband frequency.
There is a $\lambda_0/4$, short-circuited input and output coupling line at each
end of this filter; these are designed to serve only as part of an admit-
tance transforming section. An interdigital filter of the form in
Fig. 10.06-1 is obtained from the filter in Fig. 10.09-1 if each $\lambda_0/2$
line is cut in the middle and folded double to give the structure in
Fig. 10.09-2. It can be seen from Fig. 10.09-3 that this operation has
little effect on the currents and voltages on the lines, at least at
midband. Figure 10.09-3(a) shows the voltages and currents on a short-
circuited $\lambda_0/2$ resonator, while Fig. 10.09-3(b) shows the voltages and
currents after the resonator has been cut and folded. Note that the
voltages and currents on the a and b portions of the resonator are the
same in either case.

The circuits in Figs. 10.09-1 and 10.09-2 are clearly not electri-
cally the same. First, if the structure in Fig. 10.09-2 has significant
fringing capacitances extending beyond nearest-neighbor line elements,
the coupling mechanism becomes much more complicated than is implied by
the simple folding process. Second, the circuit in Fig. 10.09-1 can be
shown to have only a first-order pole of attenuation (Sec. 2.04) at
$\omega = 0$, $2\omega_0$, $4\omega_0$, etc., while the circuit in Fig. 10.09-2 has high-order
poles of attenuation at these frequencies. For this reason it was at
first believed that folding a filter as in Fig. 10.09-2 would have very
little effect on its response for frequencies near ω_0 (provided that
fringing beyond nearest neighbors is negligible)', but that the error
might be considerable at frequencies well removed from ω_0 (which would
imply that the folding shown in Fig. 10.09-2 might considerably disturb
the response of a wide-band filter). To check this point, the image
cutoff frequency predicted by the approximation in Figs. 10.09-1 and
10.09-2 was compared with a previous interdigital-line exact analysis[2]
for the case where there is no fringing beyond nearest neighbors.
Surprisingly enough, the image bandwidths were practically the same (to
slide rule accuracy) by either theory, even for bandwidths as great as
an octave. This unexpected result indicates that the folding process
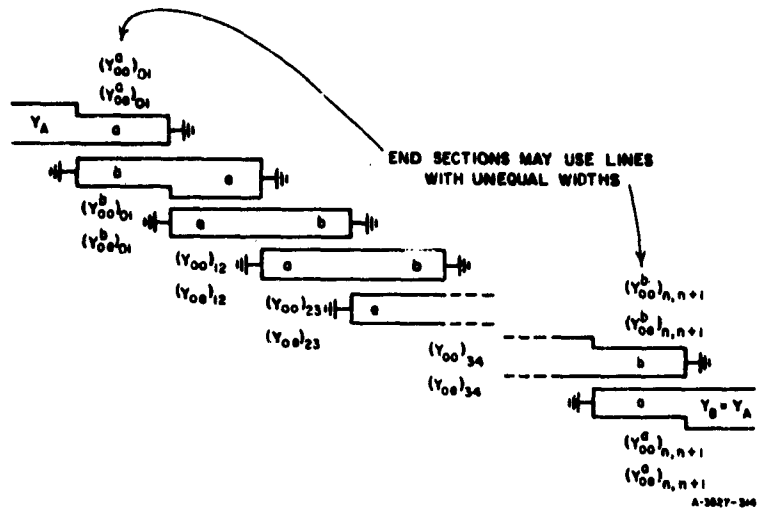
END SECTIONS MAY USE LINES
WITH UNEQUAL WIDTHS

A-3527-346

FIG. 10.09-1   A PARALLEL-COUPLED STRIP-LINE FILTER WITH
$\lambda_0/2$ RESONATORS
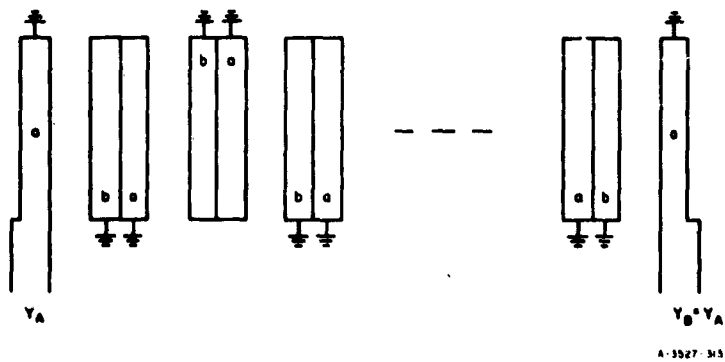
Y_A $Y_B = Y_A$

A-3527-345

FIG. 10.09-2   AN INTERDIGITAL FILTER FORMED FROM THE
FILTER IN FIG. 10.09-1
Each $\lambda_0/2$ resonator has been cut in two in the
middle and then folded double
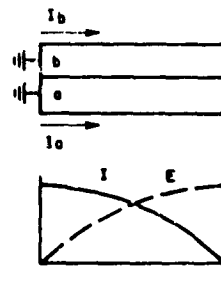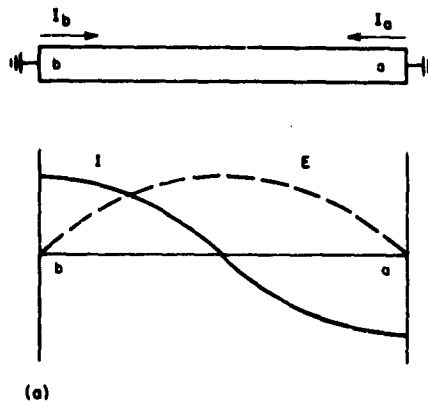
(a)

(b)

A - 3627-305

FIG. 10.09-3 EFFECT OF FOLDING A
$\lambda_g/2$ RESONATOR TO
MAKE A $\lambda_g/4$
RESONATOR

in Fig. 10.09-2 should not greatly disturb the response of filters of
the form in Fig. 10.09-1, even if the bandwidth is quite wide (provided
that fringing capacitances beyond nearest-neighbor line elements are
negligible). Experimental results show that in typical cases the fring-
ing capacitance beyond nearest neighbor has no serious effect.

The design equations in Table 10.06-1 were obtained directly from
those in Table 10.02-1 (which are for a filter of the form in Fig. 10.09-1),
along with the "folding" approximation in Fig. 10.09-2. Since the equations
for the filter in Fig. 10.09-1 were shown to be valid from narrow bandwidths
to at least bandwidths of the order of an octave, and since the folding ap-
proximation appears to be reasonably good to such bandwidths, the design

equations in Table 10.06-1 should, in principle, be good for large as well as for narrow bandwidths. However, the physical dimensions of wide-band filters of this type are not as desirable as those of the type shown in Fig. 10.07-1.

In order to derive design equations for interdigital filters with open-circuited terminating lines (Fig. 10.07-1), design equations were first derived for the type of filter shown in Fig. 10.09-4. This filter is nearly the same as the parallel-coupled filter in Fig. 10.09-1, except for the manner in which the terminating lines are coupled in. It is readily seen that if the folding process in Fig. 10.09-2 is applied to to the filter in Fig. 10.09-4, an interdigital filter with open-circuited input lines will result. It might seem at first that design equations for interdigital filters with open-circuited terminating lines could have been obtained by folding a parallel-coupled filter that had resonators open-circuited at the ends [Fig. 10.02-1(b)]. However, it will be seen that this cannot work, since the voltages at opposite ends of a $\lambda/2$ open-circuited resonator have opposite polarity.
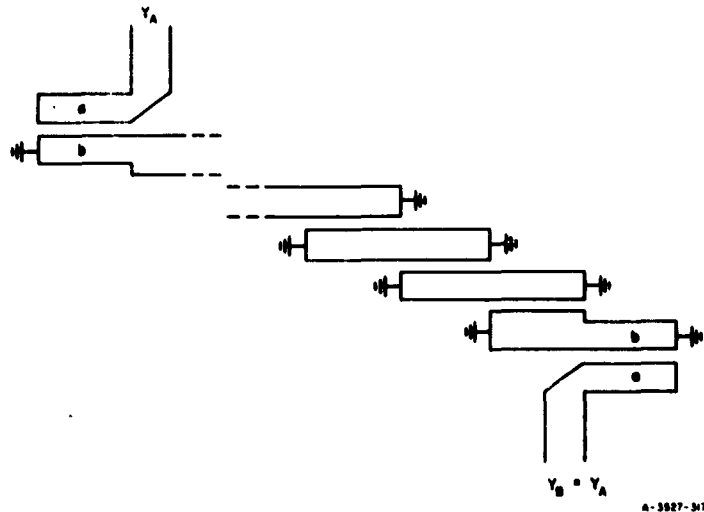
FIG. 10.09-4 A PARALLEL-COUPLED FILTER WITH $\lambda_0/2$ SHORT-CIRCUITED RESONATORS AND OPEN-CIRCUITED TERMINATING LINES

Design equations for the filter in Fig. 10.09-4 were derived in a manner much like that used for deriving the equations for the filter in Fig. 10.09-1, except that the parallel-coupled line information summarized in Fig. 5.09-2(c) was used in designing the end sections. Note that this section also has impedance-transforming properties so that the admittance scale factor $h = 1/\sqrt{N}$, where N is the turns ratio of the ideal transformer in Fig. 5.09-2(c). Note that, in the derivation of the equations for filters of the form in Fig. 10.09-1, the mathematical constraint and equivalent circuit in Fig. 5.09-3(a) were used. The constraint given there causes one natural mode (Sec. 2.03) of each end section to be stifled. When end sections as in Fig. 5.09-2(c) are used, all natural modes are fully utilized.

When the strip-line and open-wire line equivalences in Figs. 5.09-2(a) and 5.09-2(c) are used, it will be seen that the strip-line circuit in Fig. 10.09-4 is electrically identical to the open-wire line circuit in Fig. 10.09-5. The filter circuit in Fig. 10.09-5 is very similar to the filter in Fig. 10.05-1, for which design equations were presented in Table 10.05-1. The filters in Fig. 10.09-5 and in Fig. 10.05-1 become identical if we set $a = \infty$ in Fig. 10.05-1 and Table 10.05-1, and if we introduce an ideal transformer at each end of the filter while altering the impedance level within the filter to make the impedances looking into the ends of the filter the same as before the transformers were introduced. Design equations for the filter in Fig. 10.09-5 were obtained in this manner,
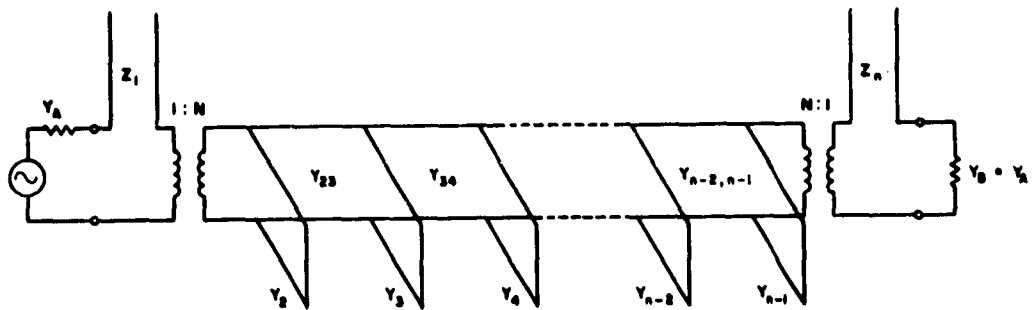
FIG. 10.09-5   AN OPEN-WIRE-LINE EQUIVALENT CIRCUIT OF THE FILTER IN FIG. 10.09-4
All stubs and connecting lines are $\lambda_0/4$ long at midband

and from these results equations for the equivalent filter in Fig. 10.09-4
were obtained. Then the equations for the corresponding interdigital
filter resulted from applying to the filter in Fig. 10.09-4 the folding
approximation illustrated in Fig. 10.09-2. The reader will be interested
to note that the $J_{k,k+1}$ in Table 10.07-1 correspond to characteristic
admittances $Y_{k,k+1}$ of the connecting lines in Fig. 10.09-5, while Z_1, Y_2,
Y_3, ..., Y_{n-1}, Z_n in Table 10.07-1 correspond to the characteristic imped-
ances or admittances of the stubs in Fig. 10.09-5, for the limiting case
where the transformer turns ratio is $N = 1$. For $N > 1$ the admittances
are scaled by the factor h.

SEC. 10.10, SELECTION OF MAPPING FUNCTIONS

The plots presented herin show that when the function in Eq. (10.02-1)
is used as indicated in Fig. 10.02-4 or 10.02-5 to map the response of a
low-pass prototype, it will predict quite accurately the response of band-
pass filters of the forms in Figs. 10.02-1 or 10.03-1 having narrow or
moderate bandwidth. Although the function in Eq. (10.02-1) is very useful,
it should not be expected to give high accuracy for wide-band cases because
it is not periodic (which the filter responses in Sec. 10.02 and 10.03 are),
nor does it go to infinity for $\omega = 0$, $2\omega_0$, $4\omega_0$, etc., which is necessary in
order to predict the infinite attenuation frequencies (Sec. 2.04) in the
response of the band-pass filter structure. It might at first seem that
the function

$$F_n\left(\frac{\omega}{\omega_0}\right) = -\cot\left(\frac{\pi\omega}{2\omega_0}\right)$$
(10.10-1)

would solve this problem nicely, since (1) it is periodic as desired,
(2) it varies similarly to Eq. (10.02-1) in the vicinity of ω_0, and (3)
it has poles at the desired frequencies, $\omega = 0$, $2\omega_0$, $4\omega_0$, etc. However,
if the structures in Figs. 10.02-1 and 10.03-1 are analyzed, it will be
seen that no matter what value of n is used, the poles of attenuation at
$\omega = 0$, $2\omega_0$, $4\omega_0$, etc., are always first-order poles.* Meanwhile, an
n-reactive-element prototype as in Fig. 4.04-1 (which will have an nth-
order pole at $\omega' = \infty$) will map so as to give nth order poles at $\omega = 0$,

---

* For example, for the filter form in Fig. 10.03-1, as $\omega \to 0$ the effect of all of the shunt stubs
can be reduced to that of a single, shunt, zero-impedance branch which would produce a first-
order pole of attenuation at $\omega = 0$. (One way in which higher-order poles can be generated is
to produce shunt, zero-impedance branches alternating with series branches having infinite
impedance. See Sec. 2.04.)

$2\omega_0$, etc., if the function in Eq. (10.10-1) is used. This important source of error is corrected in the case of Eq. (10.02-4) by replacing cot $(\pi\omega/2\omega_0)$ by cos $(\pi\omega/2\omega_0)/|\sin(\pi\omega/2\omega_0)|$, and then taking the nth root of the denominator. In this manner the poles generated by the zeros of $|\sin(\pi\omega/2\omega_0)|$ become of $1/n$ order, which causes the nth-order pole at $\omega' = \infty$ for the prototype response to map into first-order poles of the band-pass filter response at the desired frequencies.

In the case of the circuit in Fig. 10.05-1, the poles of attenuation at $\omega = 0$, $2\omega_0$, $4\omega_0$, etc., will again always be of first order regardless of the value of n used. However, the series stubs at each end produce second-order poles at the frequency ω_∞ and at other corresponding points in the periodic response.* Thus, the

$$\sqrt[n]{|\sin(\pi\omega/2\omega_0)|}$$

factor in the denominator of Eq. (10.05-2) assures that the nth-order poles at $\omega' = \infty$ in the prototype response will always map to first-order poles at $\omega = 0$, $2\omega_0$, etc., for the band-pass filter response. In addition, the factor

$$\sqrt[n]{\left[\sin\frac{\pi}{2}\left(\frac{\omega - \omega_\infty}{\omega_0}\right)\right]^2 \left[\sin\frac{\pi}{2}\left(\frac{\omega - \omega_0 + \omega_\infty}{\omega_0}\right)\right]^2}$$

is introduced to cause the nth-order pole at infinity in the prototype response to map to second-order poles at ω_∞ (and other periodic points) for the band-pass filter response. In this manner, all of the proper poles of attenuation are introduced with their proper order.

These principles can also be applied to the structure in Fig. 10.04-1, but this structure presents some new difficulties. It can be seen that this structure will develop nth-order poles of attenuation at ω_∞ and corresponding periodic points. However, the half-wavelength stubs also introduce additional natural modes of oscillation which create, in addition

---

* This can be seen as follows: For $\omega = \omega_\infty$, each of the series stubs represents an infinite-impedance series branch. For this single frequency, the interior part of the filter can be replaced by an equivalent T-section with a finite shunt impedance. Thus, the structure can be reduced (for the frequency ω_∞) to two, series, infinite-impedance branches separated by a finite, shunt-impedance branch. This can be seen to result in a second-order pole of attenuation. (If the impedance of the equivalent shunt branch had been zero, the pole of attenuation would have been raised to third order.)

644

to the desired pass band, a low-pass pass band (and corresponding periodic pass bands) as shown in the response in Fig. 10.04-2. This additional low-pass pass band approaches ω_∞ quite closely, with the result that, although the pole at ω_∞ is of relatively high order, its effectiveness is weakened by the close proximity of this low-pass pass band. The function

$$F_n\left(\frac{\omega}{\omega_0}\right) = \tan\left(\frac{\pi\omega}{\omega_0}\right) \qquad (10.10\text{-}2)$$

for the case of $\omega_\infty/\omega_0 = 0.50$ would map the prototype response to give a low-pass pass band, an nth-order pole at ω_∞, and the desired pass band centered at ω_0. However, it would not properly predict how close the low-pass pass band comes to ω_∞, nor could it account for the oversize attenuation ripples which occur in this band (see Fig. 10.04-2). As a result, the function in Eq. (10.10-2) predicts an overly optimistic rate of cutoff at the edges of the pass band centered at ω_0. It is probable that a useful approximation could be obtained by using a mapping function such as that in Eq. (10.10-2) with additional factors added which create zeros in $F_n(\omega/\omega_0)$, close to, but somewhat off of, the $j\omega$ axis (regarded from the complex-frequency point of view as discussed in Secs. 2.03 and 2.04). These zeros could then be located to extend the low-pass pass band upwards toward ω_∞, which should give the proper effect.

The mapping in Eqs. (10.06-1) through (10.06-3) was found to predict the responses of the trial, interdigital filters reasonably well, so no further study was made of mapping for use in the design of interdigital filters.

REFERENCES

1. Matthaei, G. L. "Design of Wide-Band (and Narrow-Band) Band-Pass Microwave Filters on the Insertion Loss Basis," *IRE Trans. PGMTT*-8, pp. 580-593 (November 1960).

2. Bolljahn, J. T., and Matthaei, G. L., "A Study of the Phase and Filter Properties of Arrays of Parallel Conductors Between Ground Planes," *Proc. IRE, 50*, pp. 299-311 (March 1962).

3. Matthaei, G. L., "Interdigital Band-Pass Filters," *IRE Trans. PGMTT*-10, pp. 479-491 (November 1962).

CHAPTER 11

SPECIAL PROCEDURES TO AID IN THE PRACTICAL DEVELOPMENT OF COUPLED-RESONATOR BAND-PASS FILTERS, IMPEDANCE-MATCHING NETWORKS, AND TIME-DELAY NETWORKS

SEC. 11.01, INTRODUCTION

The preceding three chapters have dealt with design information of different sorts for various specific types of band-pass filters, and also with general theory by which similar design information can be prepared for additional types of band-pass filters. This chapter continues the discussion of band-pass filters by treating various general techniques which are of considerable help in the practical development of filters. That is to say, this chapter introduces additional information of help in reducing theory to practice.

Sections 11.02 to 11.05 deal with laboratory procedures for determining the Q's of resonators, for adjusting their couplings to correspond to the couplings called for by the theory, and for the tuning adjustment of completed filters. Sections 11.06 and 11.07 discuss the effects of resonator losses and present special design information for applications where minimizing the midband loss of a band-pass filter is important. Sections 11.08 and 11.09 present supplementary information to aid in using the filter design methods of Chapters 8 and 10 for design of impedance-matching networks, and Sec. 11.10 explains how these same procedures can be used for design of coupling networks for negative-resistance devices. Section 11.11 is included to further clarify how the methods of Chapters 8 to 10 can be used for the design of band-pass filter networks with specified nominal time delay.

SEC. 11.02, MEASUREMENT OF Q_u, Q_e, AND Q_L OF A SINGLY LOADED RESONATOR

Figure 11.02(a) shows a resonator with impedance-inverter couplings K_1 and K_2. The inverter K_2 is open-circuited on its right, so that it reflects a short-circuit at its left side. As a result, the circuit in
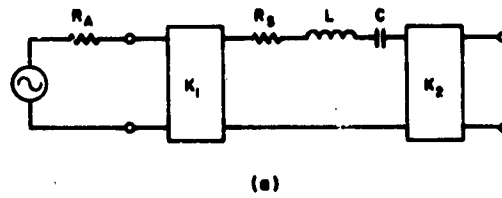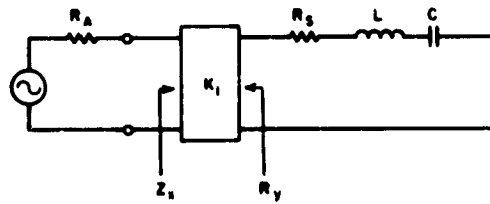
FIG. 11.02-1 TWO EQUIVALENT SINGLY
LOADED RESONATORS

Fig. 11.02-1(a) may be replaced with the circuit in Fig. 11.02-1(b).
The resonator as shown has a reactance slope parameter (Sec. 8.02) of

$$\alpha = \omega_0 L \qquad (11.02\text{-}1)$$

and an *unloaded* Q of

$$Q_a = \frac{\alpha}{R_s} \qquad (11.02\text{-}2)$$

The inverter K_1 reflects an impedance of $R_y = K_1^2/R_A$ to the resonator
which gives it a *loaded* Q of

$$Q_L = \frac{\alpha}{R_y + R_s} = \frac{\alpha}{\dfrac{K_1^2}{R_A} + R_s} \qquad (11.02\text{-}3)$$

648

The *external* Q of the resonator is defined as the Q with $R_s = 0$ (i.e., with $Q_u = \infty$), so that the resistive loading of the resonator is due only to R_y. Thus, the external Q is

$$Q_e \; = \; \frac{\alpha}{R_y} \; = \; \frac{\alpha}{\left(\dfrac{K_1^2}{R_A} \right)} \; . \tag{11.02-4}$$

Let us suppose that the resonator shown in Fig. 11.02-1(a), and its equivalent form in Fig. 11.02-1(b), symbolize a resonator which with its adjacent coupling discontinuities forms a resonator of a waveguide filter such as that in Fig. 8.06-1, or forms a resonator of a small-aperture-coupled cavity filter such as is discussed in Sec. 8.07. Let us further suppose that the resonator under consideration is the first resonator of the filter and its desired external Q has been computed by Eq. (6) of Fig. 8.02-3. The problem at hand then is to make measurements on the resonator to see if its external Q is as required by the calculations from the low-pass prototype element values.

Measurement of the values of Q_u, Q_L, and Q_e of a singly loaded resonator can be made by use of a slotted line of characteristic impedance $Z_0 = R_A$, along with procedures about to be explained. Since the resonator has some internal loss represented by the resistor R_s in Fig. 11.02-1, the VSWR at the resonant frequency f_0 will be finite. A plot of the VSWR in the vicinity of resonance will have a shape similar to that in Fig. 11.02-2.

FIG. 11.02-2 DEFINITION OF PARAMETERS OF THE VSWR CHARACTERISTIC FOR A SINGLY LOADED RESONATOR

If in Fig. 11.02-1(b)

$$\left. \frac{Z_s}{R_A} \right|_{f=f_0} = \frac{\dfrac{K_1^2}{R_s}}{R_A} > 1 \quad , \tag{11.02-5}$$

649

the resonator is said to be *overcoupled*. This condition will be evidenced by the fact that the locations of the voltage minima on the slotted line at the resonant frequency f_0 (minimum VSWR frequency) will be about a quarter-wavelength away from their locations when the frequency is appreciably off resonance.* When this condition holds, the VSWR at resonance is

$$V_0 = \frac{\dfrac{K_1^2}{R_s}}{R_A} .$$

(11.02-6)

For the so-called *undercoupled* case, the VSWR at resonance is

$$V_0 = \frac{R_A}{\dfrac{K_1^2}{R_s}} > 1 .$$

(11.02-7)

This situation will be evidenced by the fact that the voltage minima on the slotted line will be in approximately the same positions at a frequency appreciably off of resonance as they are at the resonant frequency.† If at resonance the VSWR is $V_0 = 1$, the resonator is said to be *critically coupled*.

The procedure for measuring the various Q's of a resonator is then to first measure the cavity's VSWR in the vicinity of resonance, and then make a plot such as that in Fig. 11.02-2. At the same time, by noting how the voltage minima on the slotted line shift as the frequency deviates from the resonant frequency it should be determined whether the resonator is over-coupled, or undercoupled (or if $V_0 = 1$ it is critically coupled). Then by use of Fig. 11.02-3(a) for the overcoupled case, or Fig. 11.02-3(b) for the undercoupled case, a parameter ΔV is picked from the chart for the

---

* This assumes that the width of the resonance is quite narrow, so that there is little change in the electrical length of the slotted line over the frequency range of interest. The shift in the voltage minima results from the reflection coefficient at the input coupling of the cavity being 180° different in phase at resonance from its phase well off resonance.

† The assumptions mentioned in the immediately preceding footnote also apply here. In this undercoupled case the reflection coefficient between the slotted line and the resonator input coupling has the same phase at resonance, as it does well off of resonance. As a result, the voltage minima will assume approximately the same positions on the slotted line at the resonant frequency as they will at frequencies well off resonance, provided the frequency has not been shifted so much as to greatly change the electrical length of the slotted line. If at the resonant and off-resonance frequencies the electrical distance between the resonator and the region of interest on the slotted line changes appreciably compared to a quarter wavelength, this fact should be taken into account when determining whether a resonator is overcoupled or undercoupled.

OVERCOUPLED CASE

(VOLTAGE MINIMA ON SLOTTED
LINE SHIFT ABOUT $\lambda_0/4$ BETWEEN
RESONANCE AND APPRECIABLY OFF
OF RESONANCE.)

$\Delta v = v_c - v_0$

v_0 — midband VSWR

B-3527-409
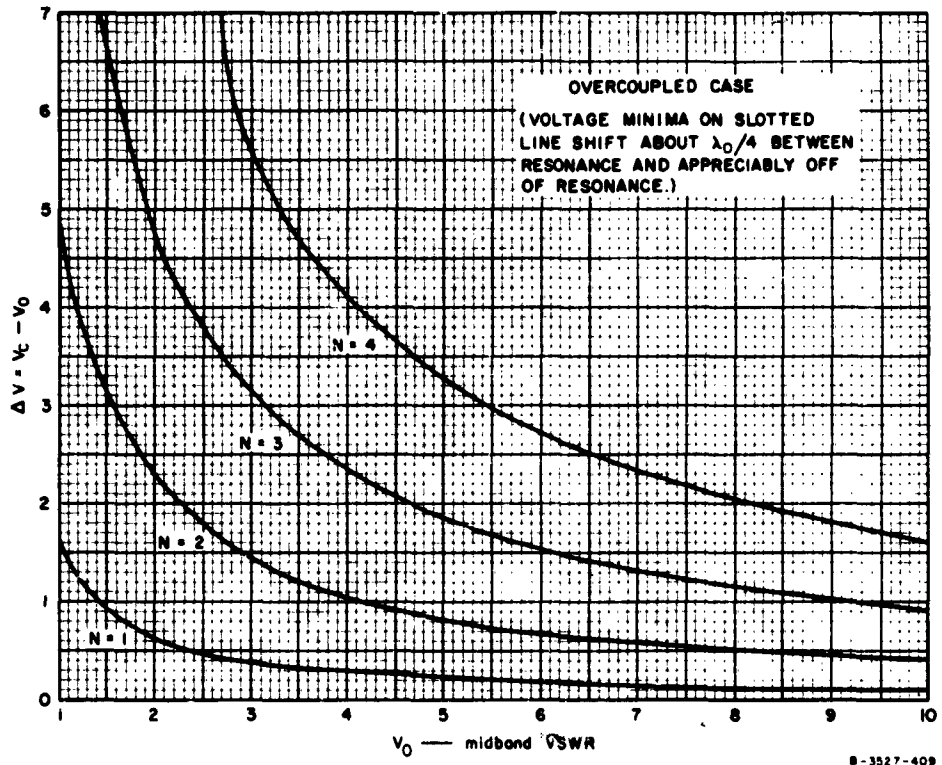
FIG. 11.02-3(a)   CHART FOR USE IN DETERMINING Q_u OF AN
OVER-COUPLED RESONATOR

651

The chart shows:
- Y-axis: $\Delta V = V_C - V_0$, from 0 to 7
- X-axis: V_0 —— midband VSWR, from 1 to 8

Text on chart:
FOR $V_0 > 7$
USE $\Delta V = V_0$

N = 1

UNDERCOUPLED CASE
(VOLTAGE MINIMA ON SLOTTED
LINE ARE IN ABOUT THE SAME
POSITION AT RESONANCE AS FOR
A FREQUENCY APPRECIABLY OFF
OF RESONANCE.)

A-3527-410
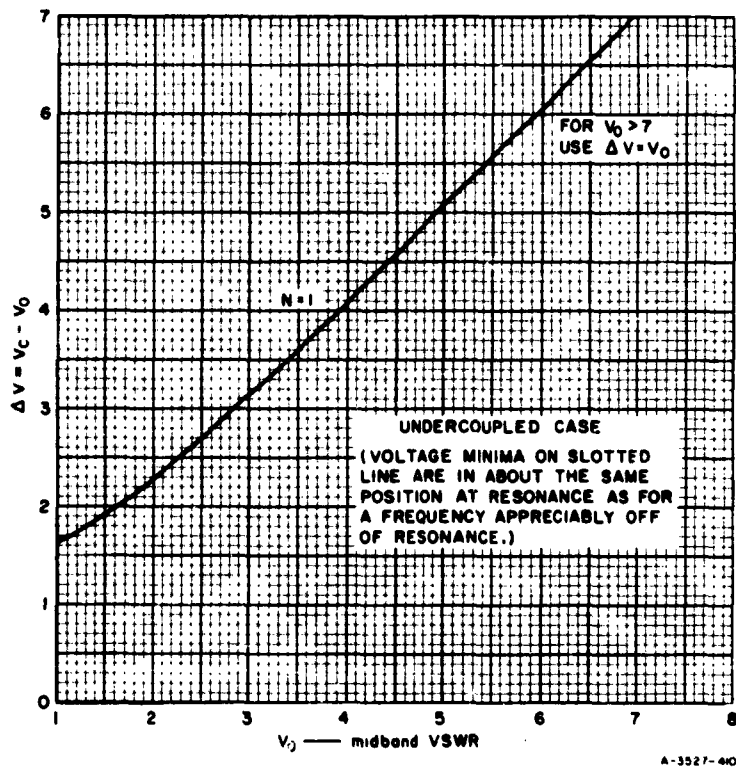
FIG. 11.02-3(b)   CHART FOR USE IN DETERMINING Q_u
OF AN UNDER-COUPLED RESONATOR

652

given midband VSWR value V_0 and for the value of N for the particular curve chosen. The choice of N is arbitrary, but it should be chosen large enough so that $V_C = V_0 + \Delta V$ will be appreciably different from V_0. In the undercoupled case V_0 and V_C are sufficiently different when $N = 1$, so that only the $N = 1$ case is shown in Fig. 11.02-3(b).*

When ΔV has been chosen,

$$V_C = V_0 + \Delta V \qquad (11.02\text{-}8)$$

is computed. Next, as indicated in Fig. 11.02-2, the bandwidth Δf at the points where the VSWR equals V_C is determined. Then the unloaded Q of the resonator is computed by the formula

$$Q_u = \frac{N f_0}{\Delta f} \qquad (11.02\text{-}9)$$

If the resonator is *overcoupled*, then the external Q is

$$Q_e = \frac{Q_u}{V_0} \qquad (11.02\text{-}10)$$

and the loaded Q is

$$Q_L = \frac{Q_u}{V_0 + 1} \qquad (11.02\text{-}11)$$

If the resonator is *undercoupled*, then the external Q is

$$Q_e = V_0 Q_u \qquad (11.02\text{-}12)$$

and the loaded Q is

$$Q_L = \frac{Q_u V_0}{V_0 + 1} \qquad (11.02\text{-}13)$$

---

* The significance of the value of N is as follows. The half-power point for the unloaded Q of a resonator occurs when the resonator reactance X equals the resonator resistance R_s. The curves in Fig. 11.02-3(a) correspond to the resonator reactance being equal to $X = N R_s$. For $N = 1$, Δf is the half-power bandwidth. For N other than one, $\Delta f = N$ times (half-power bandwidth).

If the resonator is critically coupled, the equations for both the over-coupled and the undercoupled cases will work.

To further clarify the use of these equations and charts, suppose that $V_0 = 7$ and it is found that the resonator is overcoupled. In order to make V_c significantly different from V_0, it is desirable to use the $N = 4$ curve in Fig. 11.02-3(a), and this value of N should be used in Eq. (11.02-8). If V_0 were even larger, it might be desirable to doubly load the resonator as described in the next section. Alternatively, measurements can be made on the singly loaded resonator by using the phase method described by Ginzton.[1]

The discussion so far has been phrased in terms of series-type resonators with couplings which simulate K-inverters. The same analysis on a dual basis applies to shunt-type resonators (which will have couplings that operate like J-inverters). As far as the laboratory procedures and the calculation of Q_u, Q_e, and Q_L from the laboratory data are concerned, there is no difference whatsoever.

The methods described above are very useful in determining if the couplings from the end resonators of a filter to their terminations are correct. After the external Q values are measured, they can be compared with the values computed from the lumped-element prototype elements by use of Eqs. (6) and (7) of Fig. 8.02-3 or 8.02-4. Equations (6) and (7) of Fig. 8.02-3 or 8.02-4, along with the laboratory procedures described in this section, are applicable to all of the filter types discussed in Chapter 8, as well as to numerous other possible forms of coupled-resonator filters. By these procedures the end couplings can be checked and adjusted to be correct to give a filter response corresponding to that of the low-pass prototype. The procedures of this section are also useful for checking the unloaded Q of resonators so that the over-all filter pass-band loss can be predicted.

If the reactance or susceptance slope parameter α or b of the resonators is known, this same procedure can be used for checking the couplings of all of the resonators of a filter. If a resonator with its adjacent couplings is removed from a filter and tested under singly loaded conditions as in Fig. 11.02-1(a), then it is easily shown that

$$\frac{K_1}{R_A} = \sqrt{\frac{\alpha}{R_A Q_e}} \ .$$

(11.02-14)

654

In the case of a filter with shunt-type resonance the dual equation

$$\frac{J_1}{G_A} = \sqrt{\frac{\theta}{G_A Q_e}} \qquad (11.02\text{-}15)$$

applies where G_A is the generator conductance, J_1 is the admittance-inverter parameter, and θ is the susceptance slope parameter.

As an example, consider the case of filters of the form in Fig. 8.05-1. By Eq. (8.13-16) the susceptance slope parameter of these resonators is $\theta = (\pi/2)Y_0$. Taking $G_A = Y_0$, Eq. (11.02-15) becomes

$$\frac{J_1}{Y_0} = \sqrt{\frac{\pi}{2Q_e}} . \qquad (11.02\text{-}16)$$

Thus, by measuring the Q_e of such a strip-line resonator connected as in Fig. 11.02-4, it is possible to determine the J/Y_0 value associated with a given size of capacitive coupling gap. Using a test unit such as that shown in Fig. 11.02-4, the proper coupling gaps to give the J/Y_0 values called for by Eqs. (1) to (3) of Fig. 8.05-1 can be determined. Analogous procedures will, of course, also work for other types of filters.
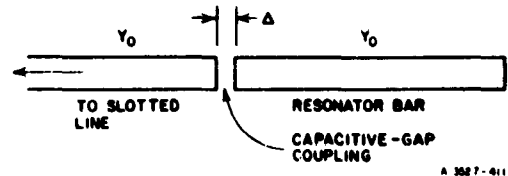
FIG. 11.02-4 A POSSIBLE ARRANGEMENT FOR EXPERIMENTALLY DETERMINING THE RESONATOR COUPLING GAPS FOR A STRIP-LINE FILTER OF THE FORM IN FIG. 8.05-1

The procedures described above concern themselves primarily with experimentally adjusting the resonator couplings to the proper values. The matter of obtaining the exactly correct resonant frequency will be treated in Sec. 11.05. Fortunately, tuning adjustments on resonators in typical cases has little effect on their couplings. The procedures of this section are most accurate when the Q's involved are relatively large. However, in some cases they can be helpful even when quite low Q's are involved (such as, say, 20 or so).

SEC. 11.03, TESTS ON SINGLE RESONATORS WITH LOADING AT BOTH ENDS

In some cases there is considerable advantage in testing a resonator under doubly loaded conditions as shown in Fig. 11.03-1, rather than under singly loaded conditions as shown in Fig. 11.02-1(a). The VSWRs to be measured will usually not be as high, and in some cases the resonant frequency of a single resonator will be exactly the same under doubly loaded conditions as it will be in a multiple-resonator filter. Thus, in such cases, both the couplings and the resonant frequency of resonators for a multiple-resonator filter can be checked by this procedure. The details concerning tuning will be discussed in Sec. 11.05. In order to check couplings other than the end couplings of a filter, it is necessary with this procedure to know the resonator slope parameters.

FIG. 11.03-1   A DOUBLY LOADED SINGLE RESONATOR

With respect to Fig. 11.03-1, the external Q, $(Q_e)_1$, will be defined as the Q when the circuit is loaded only by R_A on the left (i.e., R_A on the right is removed so as to leave an open circuit, and $R_e = 0$). Similarly, $(Q_e)_2$ is the external Q when the circuit is loaded only by R_A on the right. Note that if K_1 and K_2 are different, $(Q_e)_1$ and $(Q_e)_2$ will be different. The unloaded Q, Q_u, of the resonator is its Q when both of the R_A terminations on the left and right are removed, and the resonator's only resistive loading is that due to its internal loss (represented by R_g in Fig. 11.03-1).

The loaded Q, Q_L, of the doubly loaded resonator is

$$Q_L = \cfrac{1}{\cfrac{1}{(Q_e)_1} + \cfrac{1}{Q_u} + \cfrac{1}{(Q_e)_2}} \qquad (11.03\text{-}1)$$

$$= \frac{f_0}{(\Delta f)_{3 \text{ db}}} \qquad (11.03\text{-}2)$$

656

where f_0 is the resonant frequency of the resonator and $(\Delta f_0)_{3db}$ is here the bandwidth for which the attenuation for transmission through the resonator is up 3 db from that at resonance.

The attenuation through the resonator at resonance is

$$(L_A)_0 \; = \; 10 \; \log_{10} \; \left[\frac{(Q_e)_1 (Q_e)_2}{4 Q_L^2} \right] \quad . \qquad (11.03\text{-}3)$$

The definitions of $(Q_e)_1$, $(Q_e)_2$, Q_u, and Q_L mentioned above apply analogously to any resonator regardless of whether it is of the series- or shunt-resonance type. Equations (11.03-1) to (11.03-3) also apply regardless of the form of the resonator.

It is possible to check the couplings of a resonator by computing theoretical values for Q_L and $(L_A)_0$ and then by attenuation measurements compare the measured and computed $(\Delta f)_{3db}$ [which by Eq. (11.03-2) gives Q_L], and $(L_A)_0$. However, usually VSWR measurements are easier.

If the measurement procedures of Sec. 11.02 are applied by making VSWR measurements at the left side in Fig. 11.03-1, $(Q_e)_1$ can be determined along with an apparent unloaded Q which is equal to

$$(Q_u)_1 \; = \; \frac{1}{\dfrac{1}{Q_u} + \dfrac{1}{(Q_e)_2}} \quad . \qquad (11.03\text{-}4)$$

Similarly, if VSWR tests are made from the right side in Fig. 11.03-1, $(Q_e)_2$ and an apparent unloaded Q

$$(Q_u)_2 \; = \; \frac{1}{\dfrac{1}{Q_u} + \dfrac{1}{(Q_e)_1}} \qquad (11.03\text{-}5)$$

are obtained. The VSWR seen from the left at resonance will be

$$ (V_0)_1 \Big|_{\substack{\text{overcoupled} \\ \text{case}}} \quad \text{or} \quad \frac{1}{(V_0)_1} \Big|_{\substack{\text{undercoupled} \\ \text{case}}} = \frac{(Q_e)_2}{(Q_e)_1} \left[\frac{Q_u}{Q_u + (Q_e)_2} \right] . \qquad (11.03\text{-}6) $$

The VSWR seen from the right at resonance will be

$$ (V_0)_2 \Big|_{\substack{\text{overcoupled} \\ \text{case}}} \quad \text{or} \quad \frac{1}{(V_0)_2} \Big|_{\substack{\text{undercoupled} \\ \text{case}}} = \frac{(Q_e)_1}{(Q_e)_2} \left[\frac{Q_u}{Q_u + (Q_e)_1} \right] . \qquad (11.03\text{-}7) $$

Since $(Q_e)_1$ and $(Q_e)_2$ are obtained directly from the measurements as described above, it is possible to compute Q_u by use of Eq. (11.03-6) or (11.03-7). However, using single loading as described in Sec. 11.02 will usually give better accuracy for that purpose. If Q_u is known to be large compared to $(Q_e)_1$ and $(Q_e)_2$, it will be convenient to measure, say, $(Q_e)_1$ and then compute $(Q_e)_2$ from Eq. (11.03-6) using $Q_u = \infty$.
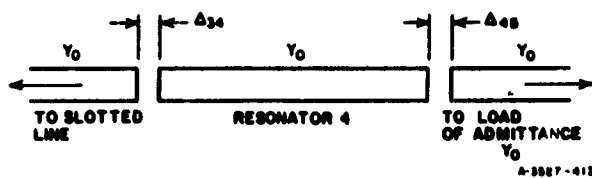
FIG. 11.03-2 AN ARRANGEMENT FOR TESTS ON
A STRIP-LINE RESONATOR USING
LOADING AT BOTH ENDS

Figure 11.03-2 shows how a resonator from a filter such as that in Fig. 8.05-1 can be tested using the procedure described above. The resonator shown is assumed to be Resonator 4, of a, say, six-resonator filter, and it is desired to see if the capacitive gaps Δ_{34} and Δ_{45} are correct to correspond to the J_{34}/Y_0 and J_{45}/Y_0 values computed by Eq. (2) of Fig. 8.05-1. By measurements as described above, external Q's $(Q_e)_{34}$ and $(Q_e)_{45}$ for loading at the left and right ends, respectively, of the

resonator as set up in Fig. 11.03-2 are obtained, and then the corresponding values of J_{34}/Y_0 and J_{45}/Y_0 can be computed by use of Eq. (11.02-16) in the form[*]

$$\frac{J_{j,j+1}}{Y_0} = \sqrt{\frac{\pi}{2(Q_e)_{j,j+1}}} \quad . \quad (11.03\text{-}8)$$

If the $J_{j,j+1}/Y_0$ values are incorrect, the gap spacings can be altered to produce the correct values. The resonator in Fig. 11.03-2 would have exactly the same resonant frequency when operated as shown as it would when operated in a multiple-resonator filter as shown in Fig. 8.05-1. For that reason, after the resonant frequency of the resonator has been checked with the proper coupling gaps, the length of the resonator bar can be corrected if necessary to give the desired resonant frequency. (See Sec. 11.05 for discussion of tuning corrections for other types of filters.)

This procedure is particularly handy for the bar-strip-line resonators discussed in Sec. 8.05, because the individual resonators can be easily tested separately and then later inserted together in the complete multiple-resonator filter. In cases such as the analogous waveguide filters in Sec. 8.06, it may be desirable to build a test resonator with the coupling irises mounted in waveguide coupling flanges. In this way the irises being checked can easily be removed and their dimensions altered as indicated by the tests.

SEC. 11.04, TESTS ON SYMMETRICAL PAIRS OF RESONATORS[†]

Most microwave filters are symmetrical. Then, for each resonator with given couplings at one end of the filter there is another identical resonator with identical couplings at the other end of the filter. It is often feasible to check the couplings within a filter (and sometimes also to check the tuning of the resonators precisely) by disassembling the filter , connecting the pairs of identical resonators together, and testing them a pair at a time. A special advantage of this procedure

---

[*] As indicated in Sec. 11.02, this equation is based on the resonator slope parameters being $b = (\pi/2)\, Y_0$ as is the case for filters of the form discussed in Sec. 8.05.

[†] Dishal has discussed a similar two-resonator technique in somewhat different terms. See Ref. 2.

over the procedures described in Secs. 11.02 and 11.03 is that the coefficient of coupling k (see Eqs. (8) of Fig. 8.02-3 and 8.02-4] for the coupling between resonators can be determined without specific knowledge of the slope parameters of the resonators. (See discussion in Sec. 11.02.) Also, in most cases, two sharp points of good transmission will be obtained, so that fewer measurements are required in order to get the desired information.

As an example, consider the symmetrical pair of cavity resonators shown in Fig. 11.04-1. In the discussion to follow, Q_u is the unloaded Q of either of the resonators by itself, Q_e is the external Q of either one of the resonators loaded by its adjacent termination (with Q_u equal to infinity), and k is the coefficient of coupling between the two resonators.

Cohn and Shimizu[3] have shown that the attenuation of a symmetrical pair of resonators i.[*]
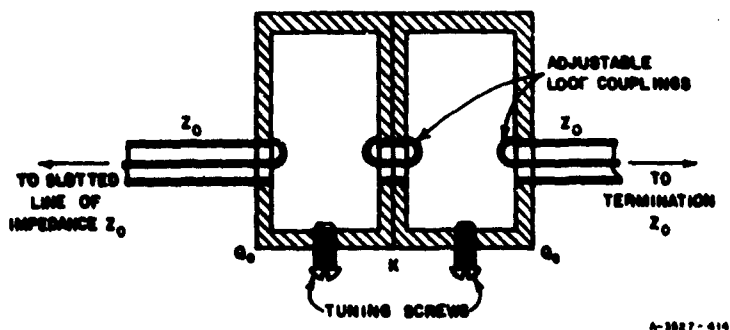
FIG. 11.04-1 SYMMETRICAL PAIR OF CAVITY RESONATORS
WITH LOOP COUPLINGS

$$L_A = 10 \log_{10} \left\{ \left[\frac{\left(1 + \dfrac{Q_e}{Q_u} \right)^2}{2kQ_e} + \frac{kQ_e}{2} \right]^2 \right.$$

$$\left. + 2 \left[\frac{\left(1 + \dfrac{Q_e}{Q_u} \right)^2}{k^2} - Q_e^2 \right] u^2 + \frac{4Q_e^2}{k^2} u^4 \right\} \quad \text{db}$$

$$(11.04\text{-}1)$$

where

$$u = \frac{f - f_0}{f_0}$$

f = frequency

f_0 = midband frequency .

At midband the attenuation is seen to be

$$(L_A)_0 = 20 \log_{10} \left[\frac{\left(1 + \dfrac{Q_e}{Q_u} \right)^2}{2kQ_e} + \frac{kQ_e}{2} \right] \quad \text{db} \quad .$$

$$(11.04\text{-}2)$$

If the condition

$$k > \left(\frac{1}{Q_e} + \frac{1}{Q_u} \right) \tag{11.04-3}$$

is satisfied the response will have a hump in the middle as shown in Fig. 11.04-2, and the resonators are said to be *overcoupled*. If

$$k = \left(\frac{1}{Q_e} + \frac{1}{Q_u} \right) \tag{11.04-4}$$

the resonators are said to be *critically coupled*, while if

661

$$k < \frac{1}{Q_e} + \frac{1}{Q_u} \qquad (11.04\text{-}5)$$

the resonators are said to be *undercoupled*. In the critically coupled and undercoupled cases the response has no hump in the middle, and the midband loss increases as the resonators become more undercoupled. It should be noted that this use of the terms overcoupled, critically coupled, and under-coupled is entirely different from the use of these terms in discussing single resonators (see Sec. 11.02).

FIG. 11.04-2 TYPICAL RESPONSE OF AN "OVERCOUPLED" SYMMETRICAL PAIR OF RESONATORS

A possible way of making tests on a pair of resonators such as those in Fig. 11.04-1 is to first make single-resonator tests on, say, the resonator on the left using the methods of Sec. 11.02, with the resonator on the right grossly mistuned by running its tuning screw well in. This would make the second resonator have negligible effect on the resonance of the first resonator. From these tests, values for Q_e and Q_u can be obtained. Then, if the resonators are tuned to the same frequency (see Sec. 11.05) and the midband attenuation $(L_A)_0$ is measured, the coupling coefficient k can be obtained by solving Eq. (11.04-2) for k.

In most cases when testing pairs of resonators from a multiple-resonator filter, the response will be greatly overcoupled. In such cases, rather than measure $(L_A)_0$, it may be more convenient to measure the frequencies f_a and f_b in Fig. 11.04-2 by finding the points of minimum VSWR. Then it can be shown that

$$k = \sqrt{w_a^2 + \left(\frac{1}{Q_e} + \frac{1}{Q_u}\right)^2} \qquad (11.04\text{-}6)$$

where

$$w_a = \frac{f_b - f_a}{f_0} \qquad (11.04\text{-}7)$$

662

Note that if Q_e and Q_u are both sizeable compared to $1/w_a$, rather large percentage errors in Q_e or in Q_u will cause little error in k.

The strip-line impedance- and admittance-inverter data in Figs. 8.05-3(a), (b), (c), and 8.08-2(a) to 8.08-4(b) were obtained by laboratory tests using symmetrical, two-resonator test sections with adjustable coupling discontinuities between resonators. The couplings at the ends were held fixed and were made to be quite loose so that Q_e would be quite large and so that the response would be greatly overcoupled (which made the low-VSWR points at f_a and f_b in Fig. 11.04-2 very sharp and distinct). After the coupling coefficient between resonators had been determined using the procedures described above, it was possible to determine the inverter parameters since

$$k_{j,j+1} = \frac{J_{j,j+1}}{\sqrt{b_j b_{j+1}}} \quad \text{or} \quad \frac{K_{j,j+1}}{\sqrt{x_j x_{j+1}}} \qquad (11.04\text{-}8)$$

as was discussed in Sec. 6.02, and since the resonator slope parameters in this case are $b_j = d(\pi/4)Y_0$ or $x_j = d(\pi/4)Z_0$, where d is an integer equal to the nominal number of quarter-wavelengths in the resonators (see Sec. 8.14).

Note that determining the inverter parameters from the coupling coefficients requires knowledge of the resonator slope parameters. The inverter description of a coupling is usually more useful for purposes of analysis because specification of the inverter parameter gives more information than does specification of a coupling coefficient. However, fixing the coupling coefficients $k_{j,j+1}$ between resonators and the external Q's of the resonators at the ends of a filter as called for by Eqs. (6) and (8) of Fig. 8.02-3 or 8.02-4 is adequate to fix the response of the filter as prescribed (i.e., at least if the filter is of narrow or moderate bandwidth, and if the resonators are all properly tuned to the same frequency). Thus, the procedures of this section along with those of Sec. 11.02 are sufficient to properly adjust the the couplings of a filter of narrow or moderate bandwidth, even though the resonators may be of some arbitrary form for which the resonator slope parameters are unknown. If the filter is of such a form that the resonators can easily be removed, it may be convenient to remove the resonators two at a time and test pairs of identical resonators

(assuming that the filter is symmetrical). If the resonators are not
easily removed, it may be desirable to construct a separate, symmetrical,
two-resonator test filter designed so that the couplings can easily be
altered. This test filter can then be used to check out the designs
of all of the couplings.

SEC. 11.05, TUNING OF MULTIPLE-RESONATOR BAND-PASS FILTERS

The word *tuning* as used herein refers to the process of adjusting
all of the resonators to resonate at the same midband frequency ω_0.
In general, synchronously tuned band-pass filters (of the sorts
discussed in Chapters 8, 9, and 10) which are properly tuned will have
a response that is symmetrical about the midband frequency ω_0, except
for some possible skew as a result of the variation of the couplings
with frequency [see, for example, the response in Fig. 8.08-5(b)].
In contrast, if a band-pass filter of this type has the resonators all
properly tuned, but the couplings are not correct, the response will
be nearly symmetrical, but it will otherwise have an improper shape
(for example, pass-band ripples of the wrong size, or improper
bandwidth).

*Alternating Short-Circuit and Open-Circuit Procedure**—A procedure
which is frequently very useful for tuning synchronously tuned filters
can be understood with the aid of Fig. 11.05-1. This figure shows a
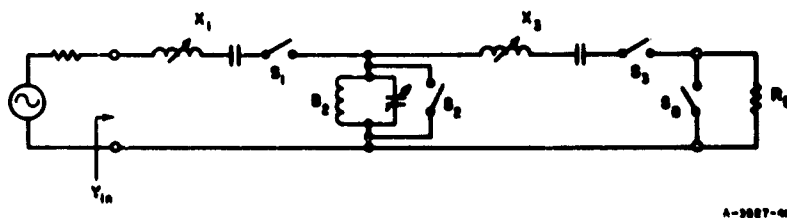
FIG. 11.05-1   A THREE-RESONATOR BAND-PASS FILTER
The switches are used to open-circuit the series resonators
and to short-circuit the shunt resonator during the tuning
process

---

* This procedure is the same as that described by Dishal in Ref. 2.

band-pass filter having two series and one shunt resonator, and switches are provided to open-circuit the series resonators and to short-circuit the shunt resonator. To start with, the series resonators are open-circuited by opening switches S_1 and S_3 while the shunt resonator is short-circuited by closing S_2. Then the admittance Y_{in} will be zero.

Next, a signal at the desired midband frequency ω_0 is applied, switch S_1 is closed, and Resonator 1 is tuned. Since Resonator 2 is still short-circuited, Resonator 1 will be tuned when $Y_{in} = \infty$. After Resonator 1 has been tuned it will present zero reactance and Resonator 2 can be tuned by opening S_2 and tuning Resonator 2 until $Y_{in} = 0$ (which occurs since S_2 is still open). Next, Resonator 3 is tuned (with S_3 still closed to short-circuit the load) until $Y_{in} = \infty$. Then S_3 is opened and the tuning process is complete.

Note that in the above process the series resonators were tuned to yield a *short-circuit* at the input while the shunt resonators were tuned to yield an *open-circuit* at the input.

Now let us consider the entirely equivalent filter in Fig. 11.05-2 which uses only shunt resonators separated by J-inverters. If the J-inverters are frequency invariant, this filter can have exactly the same Y_{in} and transmission characteristic as the filter in Fig. 11.05-1. However, since the resonators are in this case all in shunt, the tuning process is started with all of the resonators and the load on the right short-circuited. The tuning process then goes much the same as before and can be stated in general as follows:
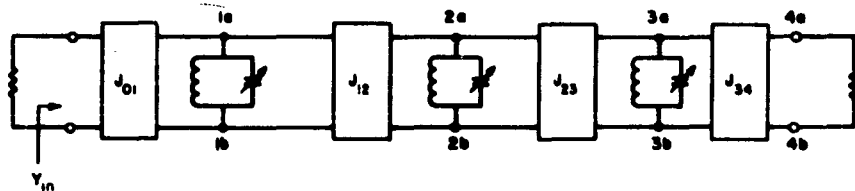
A-3527-417

FIG. 11.05-2   DIRECT-COUPLED BAND-PASS FILTER WITH SHUNT
RESONATORS
The J-inverters represent the couplings

665

(1) All of the shunt-resonators are short-circuited and an *open-circuit* is observed at the input (i.e., $Y_{i a} = 0$).

(2) The short-circuit is removed from Resonator 1, which is then tuned until a *short-circuit* is observed at the input at frequency ω_0.

(3) The short-circuit is removed from Resonator 2, which is then adjusted until an *open-circuit* is observed at the input at frequency ω_0.

(4) This process is repeated, tuning alternately for a short-circuit at the input when tuning one resonator, and for an open-circuit at the input when tuning the next. After the last resonator is tuned, the short-circuit is removed from the output.

If the filter uses series resonators and K-inverters, the procedure is essentially the same, except that all of the resonators must be open-circuited to start with, and for this condition the input will appear as a short-circuit.

As an example of how this procedure applies to microwave filters, let us consider capacitively coupled strip-line filters of the form discussed in Sec. 8.05. Tuning screws are added as shown in Fig. 11.05-3. To start the tuning process, the screws are screwed in all the way to short-out the resonators and the output line. The filter is connected to a slotted line and the position of a voltage minimum for frequency ω_0 is observed. Then the screws on the first resonator are backed-out and adjusted until the voltage minimum on the slotted line moves exactly a quarter wavelength. Next the second resonator is tuned to bring the minimum back to its original position. As consecutive resonators are tuned, the voltage minimum continues to move back and forth between the two points separated by $\lambda_0/4$.
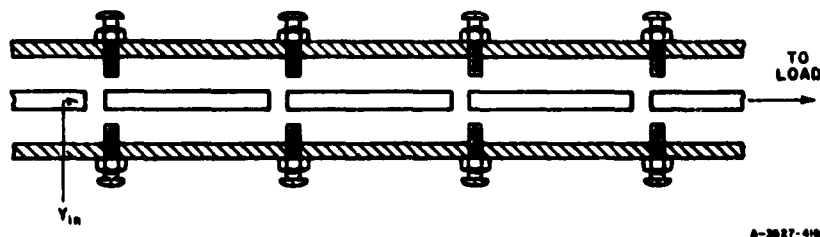
FIG. 11.05-3 A CAPACITIVELY COUPLED STRIP-LINE FILTER
WITH TUNING SCREWS

In the case of the waveguide filters in Sec. 8.06, which have resonators with series-type resonances and K-inverters, the procedure is essentially the same except for that the tuning screws are located in the middle of the $\lambda/2$ resonators instead of at the ends. (This reflects an open-circuit to the K-inverters when the screws are all the way in.) Also, the screw on the output should be placed a quarter-wavelength away from the output iris.

In practical situations, the accuracy of the procedure described above depends very much on how close the idealized circuit in Fig. 11.05-2 (or its dual) is approximated. That is, in Fig. 11.05-2 short-circuiting a resonator will also apply a short-circuit directly across the terminals of the adjacent J-inverters. However, in the circuit in Fig. 11.05-3, the inverters are of the form in Fig. 8.03-2(d). These inverters include a negative length of line which in the actual filter structure is absorbed into adjacent positive line length of the same impedance. For this reason, the actual terminals of the inverter are not physically accessible, and the tuning screws cannot short-out the resonators at the exactly correct spot for perfect tuning. For narrow-band filters, however, the coupling susceptances will be very small, the negative length of line in the inverter will be very short, and the exact locations of the short-circuits on the resonator bars will not be critical. In such cases, the above tuning procedure works well. Similar considerations arise in tuning other types of direct-coupled filters.

In direct-coupled filters, the resonators that are most likely to give trouble when using this procedure are the first and last resonator, since their couplings generally differ more radically from those of the other resonators. Thus, if the bandwidth of the filter is, say, around 10 percent and this tuning procedure does not yield a suitably symmetrical response, it may be possible to correct this by experimental adjustment of the tuning of the end resonators alone. This is often quite easy to do if a sweeping signal generator is available.

Tuning of Resonators Singly or in Pairs—For precision tuning of filters having more than around 10-percent bandwidth, the best method appears to be to test and adjust the resonators individually or in identical pairs as was discussed in Secs. 11.03 and 11.04. Even with such procedures, however, difficulties can occur if the resonator

667

couplings are at all tight. Filters such as those in Secs. 8.11, and
8.12 which use lumped-element couplings representable by the inverters
in Fig. 8.03-1(a) and 8.03-2(b), will tune somewhat differently when
connected to another resonator than they will when connected to resistor terminations.
In the case of lumped-element shunt resonators with series-capacitance
couplings, the coupling capacitors may be regarded as being part of
inverters of the form in Fig. 8.03-2(b). In such cases the negative
capacitance of the inverter can be absorbed into the shunt capacitances
of the adjacent resonators; but when coupling a resonator to a resistor
termination, the negative shunt capacitance next to the resistor cannot
be absorbed. For this reason the tuning effect due to capacitor coupling between
two lumped-element shunt resonators is different from that between a
resonator and a resistor. These matters were previously discussed with
regard to Eqs. (8.14-32) to (8.14-34). If the couplings are relatively
tight, a correction can be applied by tuning the individual resonators (when tested
individually while connected to resistor terminations) to a slightly
different frequency calculated by use of the principles discussed in
connection with Eqs. (8.14-32) and (8.14-34). If the couplings are rel-
atively loose (case of narrow bandwidth) the correction required will
be small and possibly negligible.

In the cases of the filter types in Figs. 8.05-1, 8.06-1, 8.07-3,
8.08-1, and 8.10-3, the difficulty described in the immediately
preceding paragraph does not occur. These filters all consist of
uniform transmission lines with appropriately spaced discontinuities.
The inverters in these cases are of the forms in Figs. 8.03-1(c),
8.03-2(d), or 8.03-3. The negative line lengths ϕ involved in these
inverters are of the same characteristic impedance as the resonator
lines and the termination transmission lines. Thus, these lines can
be absorbed equally well into the resonators or into the matched
terminating lines, and if a resonator of characteristic impedance Z_0
is removed from the interior of a multiple-resonator filter and tested
between matched terminating lines of the same characteristic impedance
Z_0, there will be no tuning error regardless of whether the couplings
are loose or tight. For example, the tuning of the resonators of
filters of the form in Fig. 8.05-4(a) can be checked by testing each
resonator individually as shown in Fig. 11.03-2, using exactly the same
coupling gaps at each end as will be used when each resonator is
installed in the multiple-resonator filter. The resonators in the filter

668

in Fig. 8.05-4(a) were actually tested in symmetrical pairs as discussed
in Sec. 11.04. Either the single- or double-resonator procedure gives
high accuracy. After the resonators were tested, the lengths of the
bars were corrected to give precisely the desired tuning frequency.
Using this procedure, no tuning screws are required, and in many cases
the tolerances required are reasonable enough that it should be
practical to mass-produce additional filters of the same design without
any tuning screws or adjustments.

Narrow-band parallel-coupled filters of the form in Fig. 8.09-1 can
be tuned using the slotted-line procedure described with reference to
Fig. 11.05-2. Figure 11.05-4 shows suggested locations for the tuning
screws for parallel-coupled filters. The screws on the output line
section $n,n+1$ should be backed-out flush with the ground planes after
Resonator n has been tuned. It should usually not be necessary to tune
relatively wide-band filters of this sort, since the accuracy of the
synchronous tuning becomes less critical as the bandwidth becomes
greater, and this type of filter tends to be relatively free of errors
in tuning of any one resonator with respect to the others. If the pass
band is not centered at the correct frequency, the lengths of all the
resonators should be altered by a fixed amount computed to give the
desired shift in pass-band center frequency.
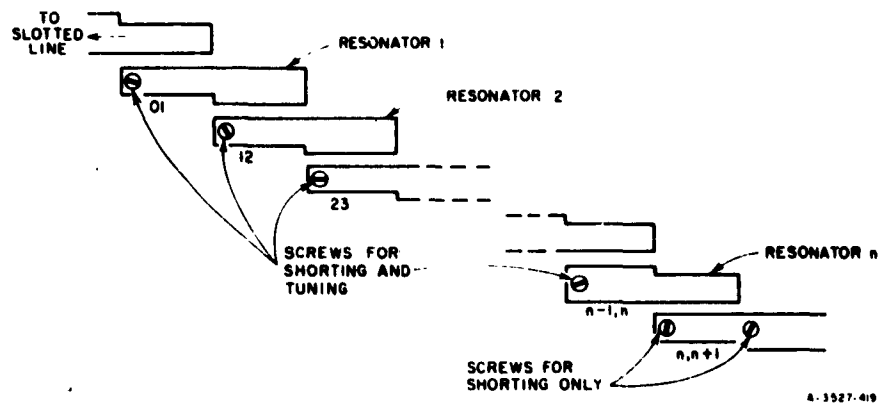
FIG. 11.05-4   ARRANGEMENT OF SCREWS FOR TUNING OF A NARROW-
              BAND PARALLEL-COUPLED FILTER

669

SEC. 11.06, CALCULATION OF THE MIDBAND DISSIPATION LOSS OF BAND-PASS FILTERS

The information necessary for computing the midband loss of band-pass filters was previously presented in Sec. 4.13, but an example in this chapter may be desirable. Let us suppose that a 10-percent-bandwidth, six-resonator, band-pass filter with a 0.10-db-ripple Tchebyscheff response is desired, and it is estimated that the resonator Q's will be about 1000 for the type of construction which is proposed. An estimate of the midband attenuation due to dissipation loss in the filter is desired. For this case, Fig. 4.13-2 is convenient, and from it for $n = 6$ and 0.10-db Tchebyscheff ripple we obtain $C_6 = 4.3$. By Eq. (4.13-2) the corresponding Q of the elements in the analogous low-pass prototype filter at the low-pass cutoff frequency ω_1' is

$$Q = wQ_{BP} = (0.10)(1000) = 100$$

where w is the band-pass filter fractional bandwidth; here $Q_{BP} = Q_u$ indicates the unloaded Q of the resonators of the band-pass filter. Then by Eq. (4.13-3) the dissipation factor is

$$d = \frac{\omega_1'}{Q} = \frac{1}{100} = 0.01$$

where, for the data in Fig. 4.13-2, the prototypes have been normalized so that $\omega_1' = 1$. Then by Eq. (4.13-8) the increase in attenuation at midband as a result of dissipation loss will be approximately

$$(\Delta L_A)_0 = 8.686C_n d = 8.686(4.3)(0.01) = 0.37 \quad db.$$

As was discussed in Sec. 4.13, the attenuation due to dissipation at the pass-band edge frequencies can be expected to be around two to three times this amount, or from around 0.74 to 1.1 db.

It should be noted that it is sometimes useful to make the above calculations in the reverse sequence in order to estimate the unloaded Q's of the resonators of a band-pass filter from the measured increase in filter midband attenuation resulting from dissipation loss.

From Sec. 4.13 we obtain

$$Q_u = Q_{uP} = \frac{8.686 C_n \omega_1'}{w(\Delta L_A)_0} \quad . \tag{11.06-1}$$

Estimates of the unloaded Q values to use in computing band-pass filter attenuation can be obtained in a number of ways. One is to use data obtained by computing from the measured midband loss of existing filters as suggested in the preceding paragraph. Another is to make laboratory tests on a resonator of the type to be used—utilizing the techniques described in Sec. 11.02 to determine the unloaded Q. Another is to compute the unloaded Q by use of the information given in Chapter 5 for coaxial-line, strip-line, and waveguide structures. It should be remembered, however, that the values of Q which are theoretically possible are rarely achieved in practice. This is due to surface roughness of the metal, corrosion, and due to additional losses in the coupling elements which are difficult to accurately predict. In some strip-line filter structures, the Q's realized are typically about half of the theoretical value. In the case of waveguide filters, the agreement between theory and practice appears to be somewhat better, but in general some allowance should be made for the fact that the Q's in typical operating filters will be less than the theoretical optimum.

Some further matters involving filter dissipation loss will be treated in the next section.

SEC. 11.07, DESIGN OF NARROW-BAND FILTERS FOR MINIMUM
MIDBAND LOSS AND SPECIFIED HIGH ATTENUATION
AT SOME NEARBY FREQUENCY

In various practical situations such as the design of preselectors for superheterodyne receivers, narrow-band filters are desired which have as little loss as possible at band center, with some specified high attenuation at some nearby frequency. For example, in a super-heterodyne receiver using a 30-Mc IF frequency, a preselector filter with high attenuation 60 Mc away from the pass-band center may be desired in order to suppress the image response. For microwave receivers of this sort the signal bandwidth is usually very small compared to the carrier frequencies involved. Thus, the design objectives for the preselector filter focus on obtaining minimum midband loss,

$$w_s = \frac{f_s - f_r}{f_0}$$

$(L_A)_s$

$(L_A)_0$

$L_A \longrightarrow dB$

$0 \qquad f_r \qquad f_1 \ f_0 \ f_2 \qquad f_s$

FREQUENCY — f

A-3527-420

**FIG. 11.07-1   DEFINITION OF TERMS USED
IN SEC. 11.07**
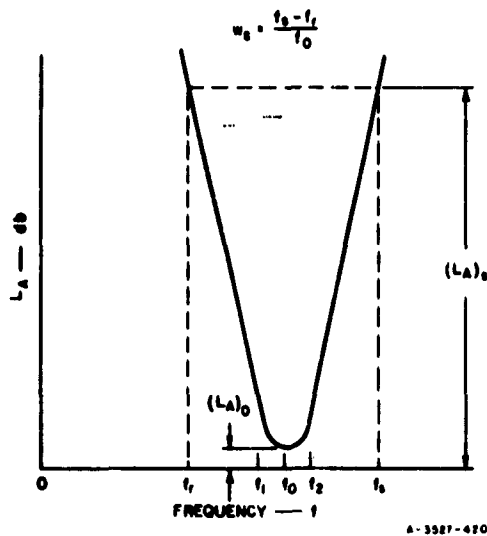
and specified high attenuation at some nearby frequency. Adequate pass-band width for the narrow signal spectrum to be received is virtually assured.

Figure 11.07-1 defines most of the symbols to be used in the following discussion. For the purposes of this analysis it will be assumed that the filters under discussion are of sufficiently narrow bandwidth so that the simplified low-pass to band-pass mapping

$$\frac{\omega'}{\omega_1'} = \frac{2}{w}\left(\frac{f - f_0}{f_0}\right)$$

where

$$w = \frac{f_2 - f_1}{f_0} \qquad\qquad (11.07\text{-}1)$$

and

$$f_0 = \frac{f_1 + f_2}{2}$$

will be valid regardless of the physical form of the resonators and couplings to be used. In Eq. (11.07-1), w is the fractional pass-band width at the pass-band edges corresponding to ω_1' of the prototype. Of more importance for this application is the fractional bandwidth w_s for which the attenuation is specified to have reached a specified high level $(L_A)_s$, as indicated in Fig. 11.07-1. The attenuation $(L_A)_0$ at midband is, of course, to be minimized.

Many low-pass prototype designs will lead to band-pass filter designs which will have $(L_A)_0 = 0$ *if the resonators of the*

672

band-pass filter are lossless. However, when the inevitable resonator losses are included $(L_A)_0$ will necessarily be non-zero. Under these conditions filters which all have the same w_s for a specified $(L_A)_s$, and which would all have $(L_A)_0 = 0$ for the case of no losses, may have considerably different $(L_A)_0$ values when losses are included.

Schiffman[4] has developed design data for filters having two or three resonators which will yield minimum midband loss for specified w_s and $(L_A)_s$ as mentioned above.* Cohn[5] has studied the general case for an arbitrary number of resonators and has found that designs with very nearly minimum $(L_A)_0$ will be obtained if the filter is designed from a low-pass prototype having the parameters

$$g_0 = g_1 = \ _{\angle} = \cdots = g_n = g_{n+1} = 1$$

and   (11.07-2)

$$\omega_1' = 1 \ .$$

The significance of these parameters is the same as in Sec. 4.04.

By use of Eqs. (11.07-2), (4.13-3), and (4.13-11), the midband loss for filters designed from the prototype element values in Eq. (11.07-2) is approximately

$$(L_A)_0 = \frac{4.343n}{wQ_u} \quad \text{db} \qquad (11.07-3)$$

where Q_u is the unloaded Q of the resonators. Here $(L_A)_0$ is practically the same as $(\Delta L_A)_0$ in Eq. (4.13-11), since this type of filter is perfectly matched at midband when no losses are present, and very nearly matched at midband when losses are included. The fractional bandwidth w in Eq. (11.07-3) is the pass-band fractional bandwidth corresponding to ω_1' for the prototype, and is the one to be used in the design equations of Chapters 8 to 11. However, the fractional bandwidth w_s is the one which is most useful for specifying the performance requirements for this application. By use of Eqs. (4.14-1), (11.07-1), and (11.07-2), w and w_s are found to be related by the approximate formula

---

* Taub and Bogner,[10] and Fubini and Guillemin[11] have studied true maximally flat and Tchebyscheff filters which have dissipation. It will be seen that, a true maximally flat or Tchebyscheff response in a filter having dissipation requires increased midband attenuation over that of the equal-element filters discussed in this section [i.e., for the same $(L_A)_s$, w_s and resonator $Q's$].

673

$$\frac{w_{\mathfrak{e}}}{w} = \text{antilog}_{10} \frac{(L_A)_{\mathfrak{e}} + 6.02}{20n} \qquad (11.07\text{-}4)$$

where $(L_A)_{\mathfrak{e}}$ is in decibels. Thus, by Eqs. (11.07-3) and (11.07-4)

$$(L_A)_0 = \frac{4.343n \text{ antilog}_{10} \left[\frac{(L_A)_{\mathfrak{e}} + 6.02}{20n} \right]}{w_{\mathfrak{e}} Q_{\mathfrak{u}}} \qquad db. \quad (11.07\text{-}5)$$

Figure 11.07-2 shows plots of data obtained from Eq. (11.07-5) for various values of $(L_A)_{\mathfrak{e}}$.[*] Note that $w_{\mathfrak{e}} Q_{\mathfrak{u}} (L_A)_0$ is plotted vs. the number, n, of resonators. Thus, for given $w_{\mathfrak{e}}$ and $Q_{\mathfrak{u}}$ the height of the curves is proportional to the midband loss that will occur. Observe that the optimum number of resonators needed to achieve minimum $(L_A)_0$ depends on the value of $(L_A)_{\mathfrak{e}}$ which has been specified. For $(L_A)_{\mathfrak{e}} = 30$ db the optimum number of resonators is four, while for $(L_A)_{\mathfrak{e}} = 70$ db, the optimum number of resonators is eight.

Equation (11.07-5) upon which Fig. 11.07-2 is based, involves a number of approximations such that the answers given will improve in accuracy as $(L_A)_{\mathfrak{e}}$ increases in size and as the product $Q_{\mathfrak{u}} w_{\mathfrak{e}}$ increases in size.[*] As a check on the accuracy of this equation, a typical trial design with moderate values of $(L_A)_{\mathfrak{e}}$ and $Q_{\mathfrak{u}} w_{\mathfrak{e}}$ will be considered. Let us suppose that $w_{\mathfrak{e}} = 0.03$ is required for $(L_A)_{\mathfrak{e}} = 40$ db, and that $Q_{\mathfrak{u}} = 1000$. Figure 11.07-2 shows that an $n = 4$ resonator design will be quite close to optimum. From the chart, for $n = 4$, $w_{\mathfrak{e}} Q_{\mathfrak{u}} (L_A)_0 = 65$. Thus, the estimated midband loss is

$$(L_A)_0 = \frac{65}{w_{\mathfrak{e}} Q_{\mathfrak{u}}} = \frac{65}{0.03(1000)} = 2.16 \quad db.$$

To check this result a lumped-element, $n = 4$, trial design of the form in Fig. 8.02-2(a) was worked out using $g_0 = g_1 = g_2 = g_3 = g_4 = g_5 = 1$, $\omega_1' = 1$, and $w = 0.007978$ [which was obtained from Eq. (11.07-4)]. The computed response of this design is shown in Fig. 11.07-3 for the cases of $Q_{\mathfrak{u}} = \infty$ (i.e., not losses), and $Q_{\mathfrak{u}} = 1000$.

---

[*] Examples due to Mr. L. A. Robinson indicate that these curves are reasonably accurate from $n = 1$ to where they flatten out, but, because of the approximations involved, they do not rise as fast as they should towards the right.
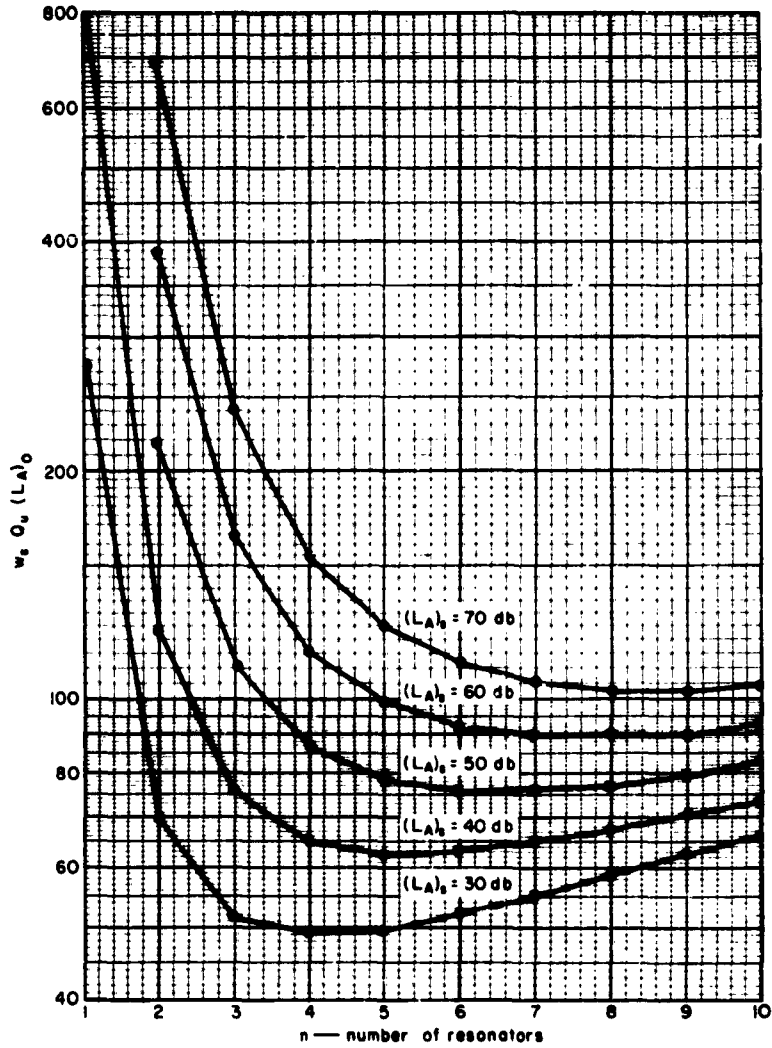
FIG. 11.07-2 DATA FOR DETERMINING THE PERFORMANCE OF
BAND-PASS FILTERS DESIGNED FROM EQUAL-
ELEMENT PROTOTYPES

Figure 11.07-3 shows the data in Fig. 11.07-2 to be satisfactory
for this case. Note that the midband loss when Q_u = 1000 is for practical
purposes exactly as predicted. The only noticeable error is that the
attenuation at the w_s = 0.03 fractional bandwidth points (i.e., the
points were ω/ω_0 = 0.85 and 1.15) is 1 db low on one side and 1.5 db
low on the other as compared to the specified $(L_A)_s$ = 40-db value.
Thus, Fig. 11.07-2 should be sufficiently accurate for most practical
applications of the sort under consideration.
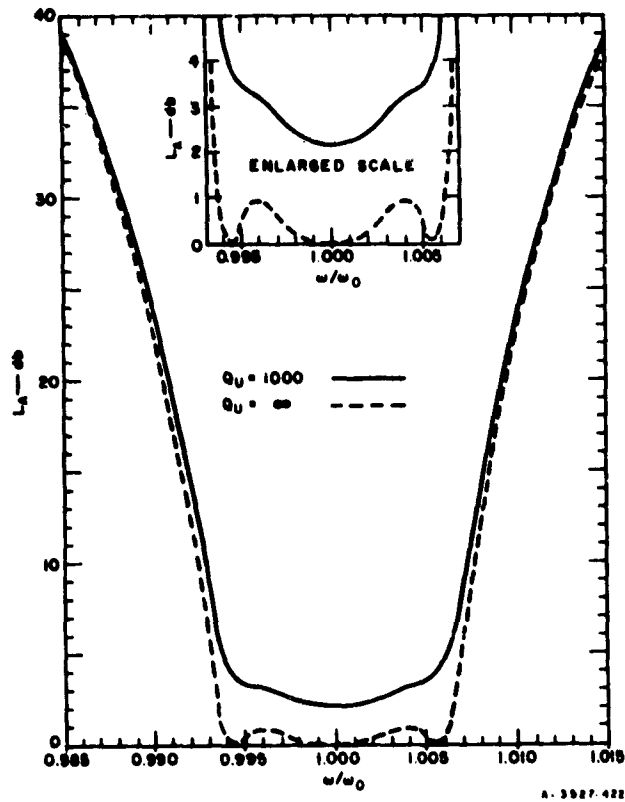
FIG. 11.07-3   RESPONSES WITH AND WITHOUT DISSIPATION
LOSS OF A 4-RESONATOR FILTER DESIGNED
FROM AN EQUAL-ELEMENT PROTOTYPE

676

The dashed line in Fig. 11.07-3 shows the attenuation of the filter when the resonators are lossless. The pass-band is seen to have ripples nearly 1 db in amplitude. Observe that when losses are included, the attenuation due to dissipation increases the loss at the band edges so much as to nearly obscure the ripples completely. This is typical of the effects of sizeable dissipation loss, regardless of the choice of low-pass prototype filter.

SEC. 11.08, DESIGN OF BAND-PASS IMPEDANCE-MATCHING NETWORKS USING THE METHODS OF CHAPTER 8

Very efficient impedance-matching networks can be designed for many applications by use of the filter-design techniques discussed in Chapter 8, along with the impedance-matching network low-pass prototypes discussed in Secs. 4.09 and 4.10. These procedures assume that the load to be matched can be approximated over the frequency band of interest by a simple R-L-C resonant circuit. This may seem like a serious restriction, but actually a very large number of microwave impedance-matching problems involve loads which approximate this situation satisfactorily over the frequency range for which a good impedance match is required.

The bandwidths for which the procedures described in this section will yield good impedance-matching network designs will depend partly on how closely the load to be matched resembles a simple R-L-C circuit within the frequency range of interest. However, since the procedures about to be described are based on the methods of Chapter 8, which involve approximations of a narrow-band sort, accurate results for bandwidths much over 20 percent can rarely be expected. Designs of 5 or 10 percent bandwidth which give nearly the theoretically optimum match for the given load and number of resonators should be relatively easy. The procedures described in Sec. 11.09, following, are recommended for the more wide-band cases since Sec. 11.09 is based on the methods of Chapter 10 which apply for very wide bandwidths as well as for narrow bandwidths.

Determination of the Load Parameters and the Low-Pass Prototype—
Before a satisfactory network to give a good impedance match over a prescribed frequency range can be designed, it is necessary to establish parameters that define the load. The following procedure is recommended:

677

(1) Make impedance measurements of the load across the desired frequency range for which a good impedance match is desired. Plot the resulting impedance data on a Smith chart, or in some other convenient form. Also plot the corresponding admittance vs. frequency characteristic. If the real part of the impedance is more nearly constant than the real part of the admittance, the load is best suited for approximate representation as a *series* R-L-C circuit. If the real part of the admittance is the most nearly constant over the frequency range of interest, the load is best suited to approximate representation as a *parallel* R-L-C circuit.

(2) If the real part of the impedance is the most constant, add a reactance element in *series* so as to bring the load to series resonance at f_0, the midband frequency of the frequency range over which a good impedance match is desired. If the real part of the admittance is the most nearly constant, add a reactance element in sh.. it with the load so as to bring the load to parallel resonance at f_0.

(3) Using the procedures in Sec. 11.02, determine Q_A, the Q of the resonated load. If the load is series-resonant, also determine R_A, the resistance of the load at resonance. If the load is parallel-resonant, determine G_A, the conductance of the load at resonance.

After the load circuit has been brought to resonance at f_0, and a measured value has been found for its Q, Q_A, and for its midband resistance R_A, or conductance G_A, the load is defined for the purposes of this design procedure.

With regard to the steps outlined above, several additional points should be noted. In many cases the nature of the load circuit will be well enough understood so that the impedance and admittance plots in Step 1 above will not be necessary. When adding a reactance element to bring the load to series or parallel resonance at f_0, the additional element should be as nearly lumped as possible, and it should be as close to the load as possible, if best performance is desired. Using a resonating element of a size that approaches a quarter-wavelength or more will *increase* the Q of the resonant load and decrease the quality of the impedance match that will be possible over the specified band. Using a lumped resonating discontinuity at an appreciable electrical distance from the load has a similar deleterious effect. However, in some practical situations where the resulting degradation in performance can be tolerated, sizeable matching elements or the locating of a resonating discontinuity at some distance from the load may be desirable as a matter of practical convenience.

678

In order to select an appropriate low-pass prototype for the band-pass matching network, the decrement

$$\delta \;=\; \frac{1}{wQ_A} \qquad\qquad (11.08\text{-}1)$$

must be computed where

$$w \;=\; \frac{f_2 - f_1}{f_0} \qquad\qquad (11.08\text{-}2)$$

$$f_0 \;=\; \frac{f_2 + f_1}{2} \qquad\qquad (11.08\text{-}3)$$

and where f_1 and f_2 are, respectively, the lower and upper edges of the frequency band over which a good match is desired. Knowing δ, the performance which is possible can be predicted as described in Secs. 4.09 and 4.10, and a suitable low-pass prototype can be determined as described in those sections.

It should be recalled that, for any load which has reactive elements as well as resistive elements in it, it is not possible to obtain a perfect match across a finite frequency band no matter how complicated an impedance-matching network is used (see Sec. 1.03). Thus, for any given load there are absolute restrictions on how good a match can be obtained across a given band of interest. Generally, adding one resonator (in addition to the resonator formed by the load) which calls for an $n = 2$ reactive element low-pass prototype circuit will give a very large improvement in performance. Going to a design worked out using an optimum $n = 3$ or $n = 4$ prototype will give still further improvements, but with rapidly diminishing returns for each increase in n. It would rarely be worthwhile to go to designs with n greater than 3 or 4; i.e., to use more than two or three resonators in addition to the resonator formed by the resonated load.

When designing waveguide impedance-matching networks, it will frequently be convenient to use reciprocal guide wavelength as a frequency variable, as was done in the design data discussed in Sec. 8.06. On that basis, the decrement becomes

$$\delta_\lambda = \cfrac{1}{w_\lambda\left(\cfrac{\lambda_{g0}}{\lambda_{ga} - \lambda_{gb}}\right)} = \cfrac{1}{w_\lambda Q_A \left(\cfrac{\lambda_0}{\lambda_{g0}}\right)^2} \qquad (11.08\text{-}4)$$

where

$$w_\lambda = \frac{\lambda_{g1} - \lambda_{g2}}{\lambda_{g0}} \qquad (11.08\text{-}5)$$

$$\lambda_{g0} = \frac{\lambda_{g1} + \lambda_{g2}}{2} \qquad (11.08\text{-}6)$$

where λ_{g1} and λ_{g2} are the guide wavelengths at the edges of the frequency band over which a good match is desired, λ_{g0} is the guide wavelength at midband, λ_{ga} and λ_{gb} are the guide wavelengths at the frequencies of the half-power points of the resonated load, λ_0 is the plane-wave wavelength at the midband frequency in the same medium of propagation as exists within the guide, and Q_A is the Q of the resonated load as determined by the methods in Sec. 11.02, or by other equivalent methods. Having a value for the decrement δ_λ, the low-pass prototype to be used is determined by use of the data in Secs. 4.09 and 4.10, using δ_λ in place of δ.

Adaptation of the Data in Chapter 8 for Impedance-Matching Network Design—The methods for band-pass filter design discussed in Chapter 8 are readily adapted for the design of impedance-matching networks. After the load has been resonated as described above, the load provides the first resonator of the filter. From that point on, the remainder of the filter (which comprises the actual impedance-matching network) can be of any of the forms discussed in Chapter 8. Figure 11.08-1 presents generalized information for the design of impedance-matching networks for series-resonated loads with the matching network consisting of series resonators coupled by K-inverters. This generalized information supplements that in Fig. 8.02-3, and it can be applied to the design of impedance-matching networks using a wide variety of resonator structures as discussed in Chapter 8. Figure 11.08-2 shows analogous data for the case of a parallel-resonant load with the matching network consisting of shunt resonators and J-inverters. These data supplement the data in Fig. 8.02-4.
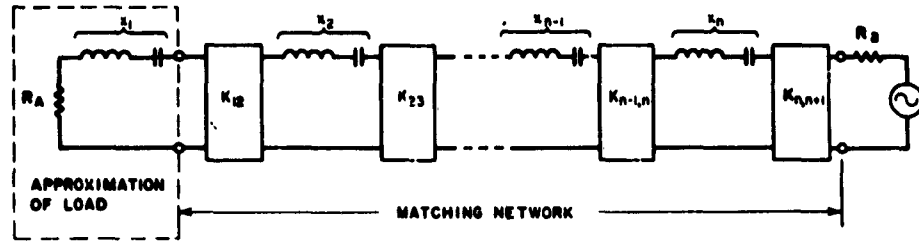
$$K_{12} = \frac{1}{\omega_1'} \sqrt{\frac{\omega R_A x_2}{g_1 g_2 \delta}} \cdot K_{k,k+1}\bigg|_{k=2\ \text{TO}\ n} = \frac{\omega}{\omega_1'} \sqrt{\frac{x_k x_{k+1}}{g_k g_{k+1}}} \cdot K_{n,n+1} = \sqrt{\frac{R_B x_n \omega}{g_n g_{n+1} \omega_1'}}$$

WHERE R_B AND THE RESONATOR SLOPE PARAMETERS $x_2, x_3, \cdots, x_n$ MAY BE CHOSEN ARBITRARILY.

A-3527-423

FIG. 11.08-1 COUPLED-RESONATOR MATCHING NETWORK FOR SERIES-RESONANT LOADS
This data supplements that in Fig. 8.02-3
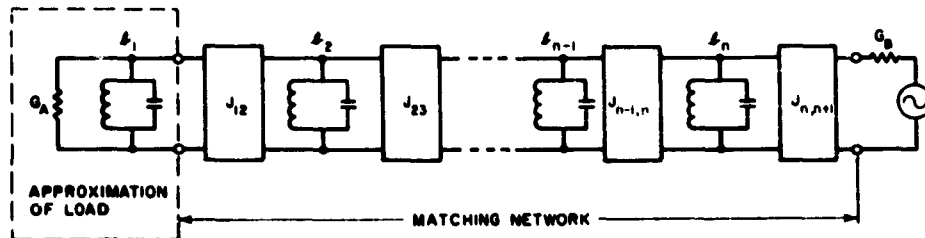
$$J_{12} = \frac{1}{\omega_1'} \sqrt{\frac{\omega G_A \ell_2}{g_1 g_2 \delta}} \cdot J_{k,k+1}\bigg|_{k=2\ \text{TO}\ n} = \frac{\omega}{\omega_1'} \sqrt{\frac{\ell_k \ell_{k+1}}{g_k g_{k+1}}} \cdot J_{n,n+1} = \sqrt{\frac{G_B \ell_n \omega}{g_n g_{n+1} \omega_1'}}$$

WHERE G_B AND THE RESONATOR SLOPE PARAMETERS $\ell_2, \ell_3, \cdots, \ell_n$ MAY BE CHOSEN ARBITRARILY

A-3527-424

FIG. 11.08-2 COUPLED-RESONATOR MATCHING NETWORK FOR SHUNT-RESONANT LOADS
This data supplements that in Fig. 8.02-4

681

To further make clear how the generalized information in Figs. 11.08-1 and 11.08-2 is used for the practical design of impedance-matching networks, the data given will be restated as they apply to several of the specific filter structures discussed in Chapter 8. Figure 11.08-3 shows how the data apply to the design of strip-line impedance-matching filters with $\lambda_0/2$ resonators of the form in Sec. 8.05. Note that in this case the load must exhibit shunt resonance, and Resonator 2 is capacitively coupled to the load. When the load has been resonated and an appropriate low-pass prototype has been established as discussed above, and using the equations for the $J_{k,k+1}/Y_0$ as given in Fig. 11.08-3, the remainder of the design of the circuit is as discussed in Sec. 8.05. The capacitive coupling B_{12} between Resonator 2 and the load will have a small detuning effect on the resonated load. As a result, it will tend to shift the resonant frequency of the load by about

$$\Delta f \ = \ \frac{-f_0 B_{12}}{2G_A Q_A} \ .$$
(11.08-7)

To compensate for this, the load should be retuned after the matching network is installed, or it should be pretuned to $f_0 + |\Delta f|$ before the matching network is installed.
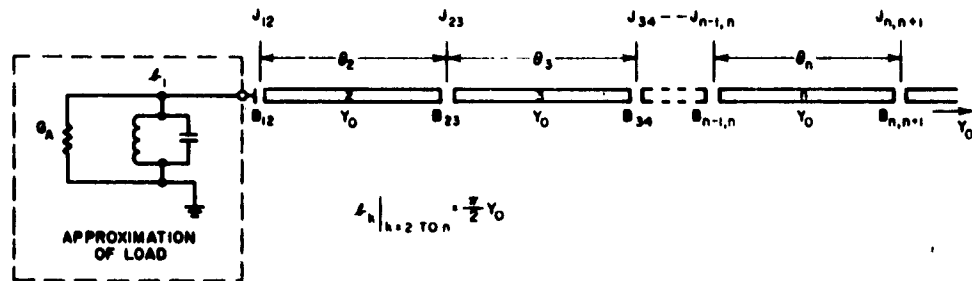
FIG. 11.08-3   SUPPLEMENTARY DATA FOR USE WITH THE MATERIAL IN SEC. 8.05
FOR DESIGN OF IMPEDANCE-MATCHING NETWORKS
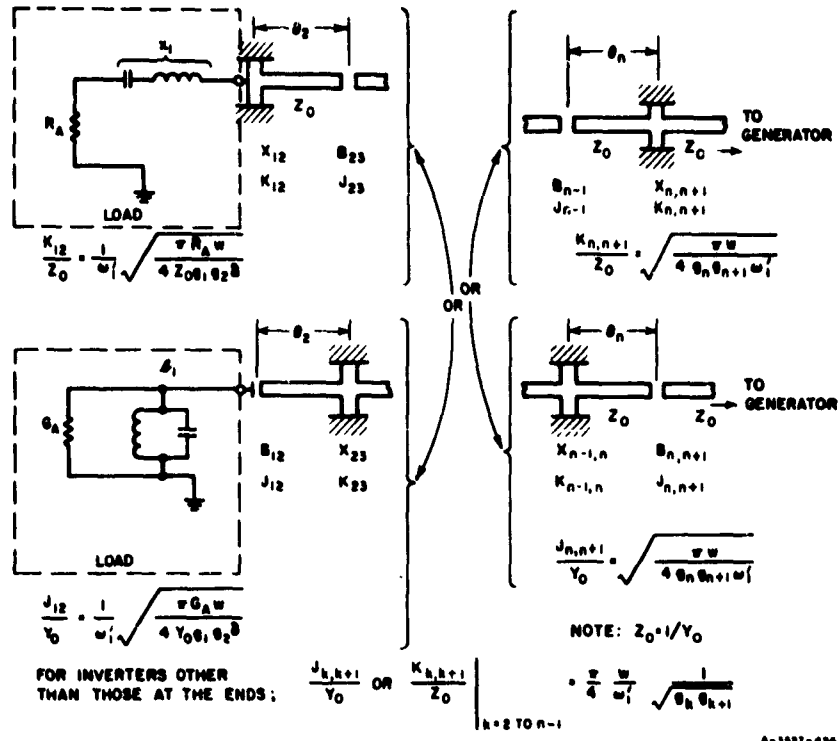
FIG. 11.08-4 SUPPLEMENTARY DESIGN DATA FOR USE WITH THE MATERIAL IN SEC. 8.08 FOR THE DESIGN OF IMPEDANCE-MATCHING NETWORKS

Figure 11.08-4 shows analogous data for design of impedance-matching networks whose resonators are in the quarter-wavelength, strip-line form discussed in Sec. 8.08. In this case the load may be either series- or shunt-resonated. If the load is series resonated, then it should be followed by a K-inverter consisting of a small shunt stub such as those discussed in Sec. 8.08. The shunt reactance X_{12} of this stub will have a small detuning effect on the load and will tend to shift its resonant frequency by about

$$\Delta f \;=\; \frac{-f_0 X_{12}}{2R_A Q_A} \tag{11.08-8}$$

This effect should be compensated for by retuning the load, or by precompensating the tuning of the load. If the load is parallel-resonated, then the load should be followed by a capacitive-gap J-inverter as is also shown in Fig. 11.08-4, and the detuning effect of the coupling susceptance

683

B_{12} is as given in Eq. (11.08-7). Figure 11.08-4 gives equations for the J- and K-inverters for design of the matching network, and the remainder of the design process is as described in Sec. 8.08.

Figure 11.08-5 presents data for the case where the matching network is to be a waveguide filter as discussed in Sec. 8.06. In this case the reference plane for the load must be referred to a point in the waveguide where the load will appear to be series-resonant. The load is coupled to the next resonator by a K-inverter consisting primarily of a shunt-inductive iris with shunt reactance X_{12}. This coupling reactance will tend to detune the load by an amount

$$\Delta f = \frac{-f_0 (X_{12}/Z_0)}{2(R_A/Z_0)Q_A} \qquad (11.08-9)$$

which can be compensated for either by retuning the load, or by moving the iris X_{12} slightly toward the load. Note that in Eq. (11.08-9) and in the equations in Fig. 11.08-5, the impedances are all normalized to the waveguide impedance, so that no difficulty arises from the ambiguity inherent in trying to define absolute values of waveguide impedance. Having computed the inverter parameters as given in Fig. 11.08-5, the
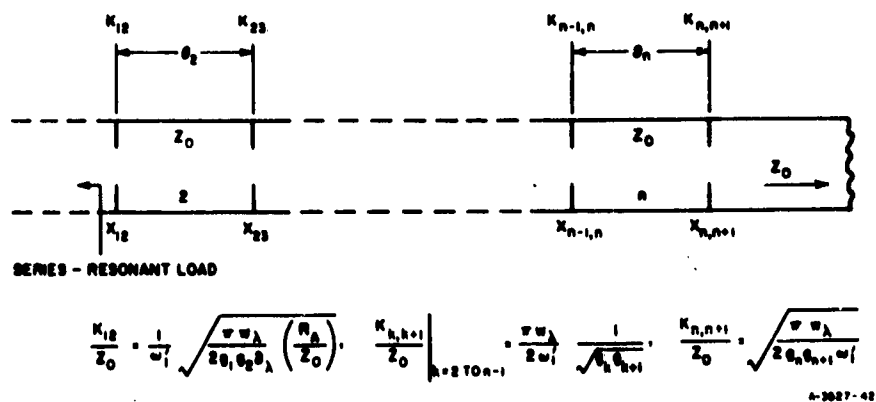
FIG. 11.08-5 SUPPLEMENTARY DATA FOR USE WITH THE MATERIAL IN
SEC. 8.06 FOR THE DESIGN OF WAVEGUIDE
IMPEDANCE-MATCHING NETWORKS

remainder of the design process is as described in Sec. 8.06. Of course, in this case, the decrement δ_λ for use in determining the low-pass prototype and for use in the equation for K_{12}/Z_0, is defined as in Eq. (11.08-4).

The equations in Figs. 11.08-3 to 11.08-5 were obtained by simply inserting the appropriate slope parameter values in the generalized equations in Figs. 11.08-1 and 11.08-2. In a similar fashion design equations can be obtained for a wide variety of impedance-matching structures. The best structure to use in a given situation may vary widely, depending on such considerations as the impedance level of the load as compared to that of the source, the allowable size, the fractional bandwidth required, etc. As mentioned above, the resonated load should be kept in as compact a form as possible if best results are desired. Also, for best results the inverter coupling to the load should be of nearly lumped-element form. A quarter-wavelength of line could be used in relatively narrow-band cases as an inverter for coupling to the load, but the performance achieved would not be as good as when a lumped- or nearly lumped-element coupling is used. This is because the quarter-wavelength line itself has selectivity effects which would add to those of the resonated load and thus make impedance matching over a specified band more difficult. However, in some relatively non-critical situations where the resulting depreciation in performance can be tolerated, a quarter-wavelength coupling to the load may be a desirable practical compromise.

Experimental Adjustment of Coupled-Resonator Impedance-Matching Networks—In cases where one resonator can be added to the circuit at a time, and where the couplings between resonators and their tunings are readily adjustable, while the resonator slope parameters α_2, α_3, ..., α_n or b_2, b_3,...., b_n are known, it may be convenient to determine the impedance-matching network design by a combination of theoretical and experimental procedures. Let us suppose that a load has been resonated in series as described above, and that its Q_A, its R_A, its decrement δ, and a desired $n = 2$ low-pass prototype have been determined. Assuming that the slope parameter α_2 for Resonator 2 is known, the inverter parameters K_{12} and K_{23} are then computed by use of Fig. 11.08-1, and it is desired to adjust the resonator couplings to achieve the couplings indicated by these inverter parameters.

685

Figure 11.08-6 illustrates a procedure for experimental adjustment of such a filter. At (a) is shown the resonated load connected directly to the desired driving generator. The VSWR between the generator and load is then V_1 at resonance as given in the figure. Next, the coupling reactance associated with the inverter K_{12} is added, and it is adjusted

$$Z_1\big|_{f_0} = R_A, \quad V_1 \text{ OR } \frac{1}{V_1} = \frac{R_B}{Z_1\big|_{f_0}} = \frac{R_B}{R_A}$$

(a)

$$Z_2\big|_{f_0} = \frac{K_{12}^2}{R_A}$$

$$V_2 \text{ OR } \frac{1}{V_2} = \frac{R_B}{Z_2\big|_{f_0}} = \frac{R_A R_B}{K_{12}^2}$$

(b)

$$Z_3\big|_{f_0} = \frac{K_{23}^2 R_A}{K_{12}^2}$$

$$V_3 \text{ OR } \frac{1}{V_3} = \frac{R_B}{Z_3\big|_{f_0}} = \frac{R_B K_{12}^2}{K_{23}^2 R_A}$$

(c)
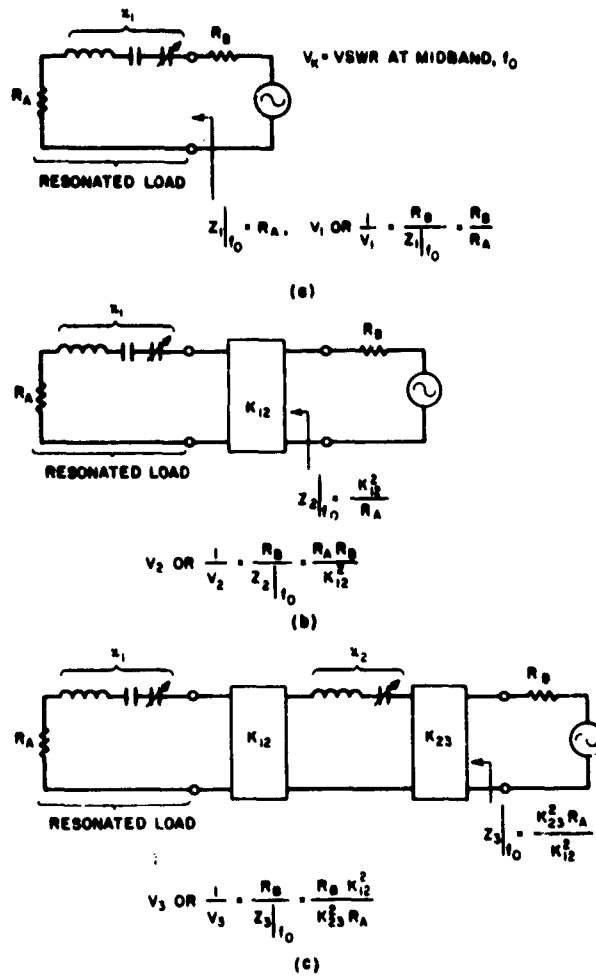
FIG. 11.08-6 PROCEDURE FOR EXPERIMENTAL
ADJUSTMENT OF AN IMPEDANCE
MATCHING NETWORK

686

until the VSWR at resonance is V_2, as indicated at (b) in the figure. Assuming that a slotted line is being used for the tests, the positions of the voltage minima must be checked to be sure that this V_2 corresponds to the desired $Z_2(\omega_0)$ and not its reciprocal (with respect to the slotted line impedance). Adding the coupling reactance associated with K_{12} will probably throw the load slightly off of the desired resonant frequency, so after the desired impedance is obtained at resonance, the load should be retuned. As long as V_2 is always measured at the frequency of resonance (no matter whether it is exactly the desired f_0 or not), the small correction required later in the load tuning should have negligible effect on the required coupling reactance.

Next, Resonator 2 along with the coupling reactance associated with the inverter K_{23} is added to the circuit as shown in Fig. 11.08-6(c). In this case, it is necessary both to bring Resonator 2 to the proper resonant frequency and to adjust the coupling reactance associated with K_{23} in order to achieve the desired impedance-matching effect. The tuning of Resonator 1 (i.e., the resonated load) can be assumed to be very nearly correct so that any mistuning evident in the VSWR characteristic of the circuit must be due mainly to mistuning of Resonator 2. If Resonator 2 is correctly tuned to f_0, the VSWR characteristic will have either a maximum or a minimum value at f_0, and the characteristic will be symmetrical about f_0 (except possibly for some distortion of the frequency scale as a result of the fact that the coupling between resonators varies with frequency). Thus, the tuning of Resonator 2, and the coupling associated with the inverter K_{23} should be adjusted until a VSWR characteristic symmetrical about f_0 is obtained with a VSWR at f_0 equal to the value V_3 corresponding to the impedance $Z_3|_{f_0}$, computed from the data at (c) in Fig. 11.08-6. Once again, the locations of the voltage minima on the slotted line should be checked to be sure that this V_3 corresponds to $Z_3|_{f_0}$ and not its reciprocal with respect to the slotted line impedance.

This would complete the adjustment of an $n = 2$ matching network. The same procedure can be applied to the adjustment of impedance-matching networks of any complexity by repetition of part of the same steps. Of course, if the resonators are in shunt, the same procedure applies, but the analysis is on the dual basis.

687

A Practical Example and Some Additional Experimental Techniques—A
practical example will now be considered. The circuit to be discussed
was adjusted by experimental procedures as described above, but some
additional techniques were involved that will also be explained. The
main difference was that only the Q of the load was known, and its
midband impedance was not known since all of the measurements on the
load were made through a coupling reactance of unknown value. As will
be seen, it was, nevertheless, still possible to carry out the required
adjustments.

Figure 11.08-7 shows the circuit under consideration. It is a
tunable up-converter in strip-line form.[5,6] A pumped, variable-capacitance
diode provides both gain and frequency conversion. This device has a
narrow-band, lower-sideband output circuit centered at 4037 Mc; hence,
the response of the over-all circuit is narrow band. However, by varying
the pump frequency from 4801 Mc to 5165 Mc the input frequency which
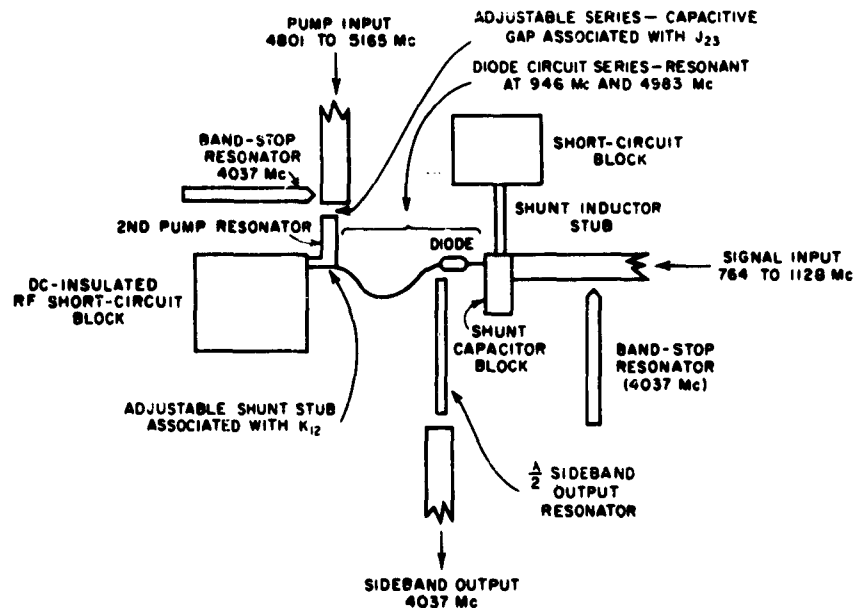
FIG. 11.08-7   SIMPLIFIED DRAWING OF A STRIP-TRANSMISSION-LINE
TUNABLE UP-CONVERTER

would be accepted and amplified varies from 764 to 1128 Mc. In order to achieve the desired performance, impedance-matching filters are required at both the signal input and pump input ports. Herein, we will review the steps that were taken to broadband the pump input channel.

When the pump circuit of this device was adjusted, the portions of the circuit that were electrically of most importance were the diode plus its 0.020-inch diameter, 207-ohm wire lead (which together consti-tuted the resonant load in this case), and the second pump resonator (see Fig. 11.08-7). The other portions of the circuit were greatly decoupled at the frequency range of interest. The second pump resonator was of the quarter-wavelength type in Fig. 11.08-4 having shunt-inductive coupling to the series-resonant diode circuit (which served as the first pump resonator), and having series-capacitance coupling to the pump input line. The second pump resonator shown in Fig. 11.08-7 had different cross-sectional proportions than the pump input line, but both were of 50 ohm impedance.

Figure 11.08-8 shows an approximate equivalent circuit for the pump channel of this device at frequencies around 5000 Mc. Though the load circuit (i.e., the diode circuit) is actually quite complex, it behaves like a simple series-resonant load in the frequency range of interest. The impedance inverter K_{12} and the admittance inverter J_{23} relate to coupling discontinuities as indicated in Fig. 11.08-7.[*] Note that in this circuit the pump power is all ultimately delivered to the diode parasitic loss resistor R_s. Since R_s is quite small compared to the reactances involved, the impedance-matching problem is relatively severe.

For the circuit in Fig. 11.08-7, the shunt stub associated with K_{12} was set to a length estimated to be about right when the device was first assembled. To adjust the circuit, the capacitive gap associated with J_{23} was closed so that there was, in effect, a 50-ohm line right up to the K_{12} discontinuity. (This was equivalent to removing the J_{23} box in Fig. 11.08-8 to leave a 50-ohm line right up to K_{12}.) Then with a slotted line connected to the pump input port of the device, VSWR tests were made to determine the Q, Q_A, of the

[*] Inverters K_{12} and J_{23} are approximately of the forms in Figs. 8.03-1(c) and 8.03-2(d), respectively. Note that though the second pump resonator is of the quarter-wavelength type, its physical length will be considerably less than a quarter wavelength due to the negative lengths of line associated with the inverters. See, for example Eq. (4) of Fig. 8.08-1.
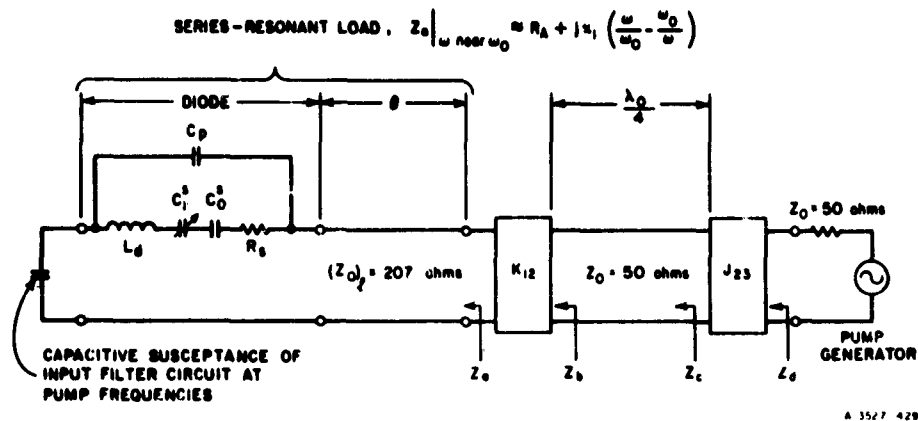
FIG. 11.08-8   APPROXIMATE EQUIVALENT CIRCUIT FOR THE PUMP INPUT
CHANNEL OF THE CIRCUIT IN FIG. 11.08-7 FOR FREQUENCIES
IN THE VICINITY OF 5000 Mc

diode-circuit at its pump-frequency resonance. Using the methods
described in Sec. 11.02 the Q_A of the pump circuit was found to be 77.
(Note that Q_A for the diode circuit corresponds to the unloaded Q as
measured by techniques of Sec. 11.02, and that this Q is independent
of the adjustment of the K_{12} shunt stub.)

The desired fractional bandwidth was specified to be w · 0.082,
so that the decrement of the load was

$$\delta \;=\; \frac{1}{wQ_A} \;=\; \frac{1}{0.082(77)} \;=\; 0.16 \quad .$$

According to Figs. 4.09-3 and 4.09-4, an n · 2 resonator design with
δ · 0.16 calls for a maximum transducer loss of 3.3 db with 0.84-db
ripple in the operating band. Since this was satisfactory for the
application under consideration, a larger value of n was not considered.
The corresponding optimum low-pass prototype element parameters were
then from Fig. 4.09-6 found to be g_0 · 1, g_1 · 6.30, g_2 · 0.157,
g_3 · 6.30, and ω_1' · 1.

690

By Fig. 11.08-4,

$$K_{12} = \frac{Z_0}{\omega_1'} \sqrt{\frac{\pi R_A w}{4 Z_0 g_1 g_2 \, \delta}} \qquad\qquad (11.08\text{-}10)$$

and

$$J_{23} = Y_0 \sqrt{\frac{\pi w}{4 g_2 g_3 \omega_1'}} \qquad\qquad , \qquad (11.08\text{-}11)$$

where $Y_0 = 1/Z_0$. All of the parameters needed to evaluate J_{23} were known, but K_{12} could not be evaluated because R_A was not known. (As previously mentioned, when Q_A was measured the K_{12} stub was set at some length estimated to be about right, but the length of the stub was not necessarily correct. It was not necessary to know K_{12} in order to determine Q_A by the methods of Sec. 11.02. However, the K_{12} parameter of the coupling stub would have to be known accurately in order to determine R_A.) This difficulty was bypassed by eliminating both K_{12} and R_A from the calculations in the following manner.

In Fig. 11.08-8, the impedance Z_b is at midband

$$Z_b\bigg|_{f_0} = \frac{K_{12}^2}{R_A} \qquad . \qquad\qquad (11.08\text{-}12)$$

Then from Eqs. (11.08-10) and (11.08-12)

$$Z_b\bigg|_{f_0} = \frac{Z_0 \pi w}{(\omega_1')^2 4 g_1 g_2 \delta} \qquad\qquad (11.08\text{-}13)$$

$$= \frac{50\pi(0.082)}{(1)^2 4(6.30)(0.157)(0.16)} = 20.4 \text{ ohms.}$$

Thus, with the J_{23} gap closed so as to give a 50-ohm line up to the K_{12} stub, the length of the K_{12} stub was adjusted so that the VSWR seen looking in the pump input port at resonance was

691

$$V_b = \frac{Z_0}{Z_b\Big|_{f_0}} \qquad\qquad (11.08\text{-}14)$$

$$= \frac{50}{20.4} = 2.45$$

while the vicinity of the K_{12} stub was a voltage minimum of the standing-wave pattern $vs.$ length.

Next the J_{23} gap in Fig. 11.08-7 was opened and adjusted so as to give a VSWR of $V_d = 6.30$ at midband. For each trial adjustment of the gap spacing, tuning screws near the capacitive-gap end of the second pump resonator were adjusted to give a VSWR response $vs.$ frequency which was approximately symmetrical about f_0. The $V_d = 6.30$ value can be computed as follows.

In Fig. 11.08-8 at midband

$$Z_c\Big|_{f_0} = \frac{Z_0^2}{Z_b\Big|_{f_0}} \ . \qquad\qquad (11.08\text{-}15)$$

Since J_{23} is an admittance inverter (Sec. 8.03)

$$Z_d\Big|_{f_0} = \frac{1}{Z_c\Big|_{f_0} J_{23}^2} = \frac{Z_b\Big|_{f_0}}{Z_0^2 J_{23}^2} \ . \qquad\qquad (11.08\text{-}16)$$

Then by Eqs. (11.08-11), (11.08-13), and (11.08-16),

$$Z_d\Big|_{f_0} = Z_0 g_0 g_3 \qquad\qquad (11.08\text{-}17)$$

$$= 50(1)(6.30) = 315 \text{ ohms.}$$

Thus, the VSWR seen on the 50-ohm pump input line at midband should be

$$Z_d = \frac{Z_d \big|_{f_0}}{Z_0} \qquad\qquad (11.08\text{-}18)$$

$$= \frac{315}{50} = 6.30$$

where the vicinity of the J_{23} gap should be a voltage maximum of the standing-wave pattern vs. length.

This completed the adjustment of the pump impedance-matching circuit, and the resulting transducer attenuation[*] characteristic as computed from measured VSWR is shown in Fig. 11.08-9. The measured fractional bandwidth is 0.0875 as compared to the 0.082 design objective, the 3.2-db peak pass-band loss compares favorably with the 3.3 db predicted value, while the pass-band ripple is around 0.4 db as compared with the 0.84-db predicted value. The measured performance is somewhat superior to the predicted performance because when the data in Fig. 11.08-9 was taken the lower-sideband output resor .or had been added to the circuit
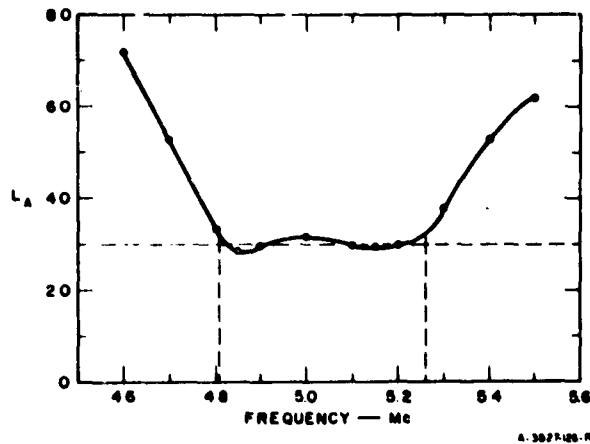
FIG. 11.08-9   TRANSDUCER ATTENUATION AT PUMP INPUT
PORT AS COMPUTED FROM MEASURED VSWR

---

[*] See Sec. 2.11 for a discussion of this term.

which caused the effective Q_A of the diode circuit to drop a little from the $Q_A = 77$ value which was originally obtained without the output resonator.[*]

It is interesting to consider just how much has been accomplished by the addition of the second pump resonator as a matching network. Let us again assume that $Q_A = 77$ and that the desired fractional band-width is $w = 0.082$ so that $\delta = 0.16$. If only the first pump resonator is used (i.e., just the resonant diode circuit along with the K_{12} adjustable coupling stub) and if the K_{12} coupling stub were adjusted so as to give a perfect match to the 50-ohm pump input line at midband, then *the reflection loss at the band edges would be about 10.9 db.* If the K_{12} coupling stub were adjusted in accordance with an optimum $n = 1$ design, as determined using the prototype data in Sec. 4.09, the loss at the band edges would be $(L_A)_{max} = 5.6$ db while the loss at midband would be $(L_A)_{min} = 3.3$ db. Adding an additional resonator to give an $n = 2$ design reduces the pass-band loss limits to $(L_A)_{max} = 3.3$ db and $(L_A)_{min} = 2.5$ db. An $n = 4$ design would give $(L_A)_{max} = 2.5$ db and $(L_A)_{min} = 2.3$ db, while an $n = \infty$ design would give $(L_A)_{max} = (L_A)_{min} = 2.0$ db. It is seen that going from an $n = 1$ to an $n = 2$ design gives a very large improvement, and that the incremental improvement for increasing values of n decreases very rapidly.

Other Forms of Coupled-Resonator Matching Networks—It would also be possible to construct a matching network in the form shown in Fig. 11.08-10, which has no inverter between the load and the adjacent matching-network resonator. This, however, is usually not very practical except in the cases of relatively wide-band matching networks. The slope parameter of Resonator 2 cannot be chosen arbitrarily in this case, and for narrow bandwidths b_2 will often become so large as to be difficult to realize with practical circuitry. The dual case where the first resonator of the matching network is in series would be especially difficult.

The design procedures in Sec. 11.09 can give designs which are more or less equivalent to that in Fig. 11.08-10, but a different point of view is used. As indicated above, such designs become most practical for relatively large bandwidths, say, around 30 percent or more.

---

[*] This drop in diode circuit Q was due to the shunt capacitance introduced by the output resonator causing the diode internal resistance to be somewhat more tightly coupled.
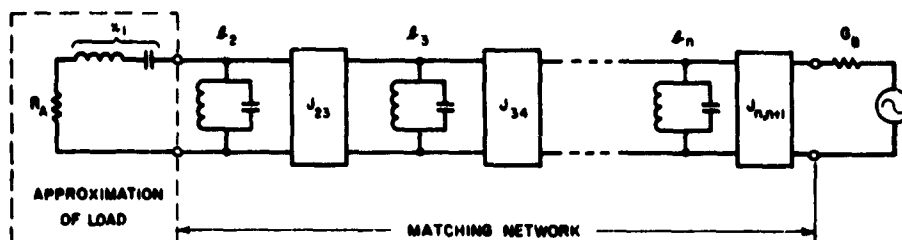
$$\ell_2 = \frac{\omega_1'\ \mathfrak{g}_2}{\omega \mathfrak{g}_0 R_A} \qquad J_{k,k+1}\Big|_{k=2 \text{ TO } n-1} = \frac{w}{\omega_1'}\sqrt{\frac{\ell_k\,\ell_{k+1}}{\mathfrak{g}_k\,\mathfrak{g}_{k+1}}} \qquad J_{n,n+1} = \sqrt{\frac{G_\theta\ \ell_n\, w}{\mathfrak{g}_n\ \mathfrak{g}_{n+1}\,\omega_1'}}$$

WHERE $\ell_3, \ell_4, \cdots, \ell_n$, AND G_θ MAY BE CHOSEN ARBITRARILY

A-3527-430

FIG. 11.08-10   AN ADDITIONAL GENERAL FORM OF COUPLED-RESONATOR-
FILTER IMPEDANCE-MATCHING NETWORK
The dual of this circuit applies when the load is shunt resonant

SEC. 11.09, DESIGN OF BAND-PASS IMPEDANCE-MATCHING NETWORKS BY THE METHODS OF CHAPTER 10

In this section, discussion of the design of impedance-matching networks will be continued so as to cover the design of matching net-works of relatively large bandwidths. The underlying fundamentals are much the same as those discussed in Sec. 11.08, but the procedures are modified to use the design point of view of Chapter 10.

In the methods of this section the load is first brought to series- or shunt-resonance at midband f_0, just as was discussed in Sec. 11.08. However, since relatively large bandwidths are involved in this case it may be desirable to use something other than the Q of the load as a basis for computing the load decrement δ. This is because the Q of the load will typically be relatively low for cases where a wide-band match is required, and also because it may be desirable to examine the impedance or admittance characteristics of the load more thoroughly than is implied by a Q measurement alone.

Figure 11.09-1 shows a suggested procedure for computing the required load parameters δ and R_A or G_A. The impedance or admittance characteristics of the resonated load are measured across the frequency band of interest, and then the required parameters are readily determined from the measured data as indicated in the figures. Note that the frequencies f_1 and f_2

695
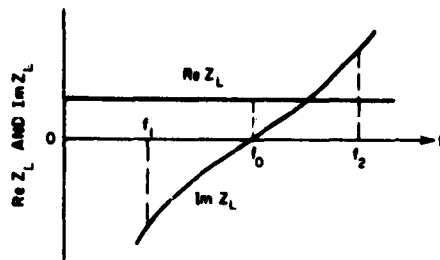
$$R_A = \operatorname{Re} Z_L \big|_{f=f_0} \qquad \delta = \frac{R_A}{|\operatorname{Im} Z_L|_{f=f_1, \text{OR} f_2}}$$

(a) CASE OF IDEALIZED SERIES-RESONATED LOAD Z_L
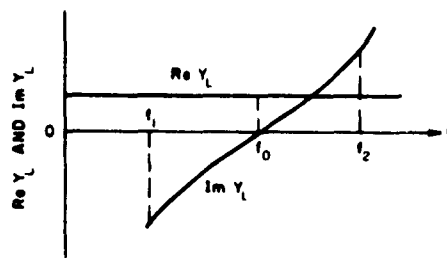
$$G_A = \operatorname{Re} Y_L \big|_{f=f_0} \qquad \delta = \frac{G_A}{|\operatorname{Im} Y_L|_{f=f_1, \text{OR} f_2}}$$

(b) CASE OF IDEALIZED SHUNT-RESONATED LOAD Y_L

A-3527-43

FIG. 11.09-1   DEFINITIONS OF LOAD
PARAMETERS IN A FORM
CONVENIENT FOR WIDE-
BAND MATCHING
Frequencies f_1 and f_2 are the
edges of the band for which an
impedance match is desired

indicated in the figures are
the edges of the frequency
band over which a good impedance
match is required. In the
figure the characteristics are
idealized in that the real
parts are constant with fre-
quency and the imaginary parts
have odd symmetry about f_0 so
that the magnitude of the
imaginary part of the impedance or
admittance is the same at f_1 as it is
at f_2. Note that on this basis
the decrement δ is simply the
ratio of the real part at f_0
to the magnitude of the imagin-
ary part at either f_1 or f_2.
In practical cases where the
load impedance or admittance
characteristic may deviate
appreciably from these ideal-
ized symmetrical characteristics,
average values should be taken
using the definitions in terms
of the idealized cases as a
guide. An example of a non-
idealized case will be
discussed later in this section.

After the parameters R_A
or G_A, and the decrement δ have
been determined for the load,
an appropriate low-pass prototype filter should be selected to have the
required δ value, as discussed in Sec. 4.09 and 4.10. The specified
value of R_A or G_A, the prototype filter parameters, the specified internal
resistance of the generator which is to drive the load, the specified
fractional bandwidth w, and the specified center frequency f_0, then
control the design of the matching network.

Figure 11.09-2 shows a form of impedance-matching network which can
be designed by the methods of Chapter 10. The load as shown is of a
form which would have an idealized symmetrical impedance characteristic
of the form in Fig. 11.09-1(a); however, as an example will soon show,
matching networks of the sort in the figure can be useful for consider-
ably more complex loads with impedance characteristics which deviate
considerably from the idealized symmetrical form. The matching network
in Fig. 11.09-2 could be constructed in strip-line form such as that in
the filter in Figs. 10.03-5(a), (b), and (c). Also, if desired, the
matching network could be converted into parallel-coupled strip-line
form. This could be accomplished by splitting each shunt stub Y_k
(except for Y_2 and Y_n) into two parallel stubs Y_k' and Y_k'' such that
$Y_k' + Y_k'' = Y_k$. Then the filter can be broken into open-wire-line sections
such as that on the right side of Fig. 5.09-2(a), which are exactly
equivalent to strip-line parallel-coupled sections such as that on the
left side of Fig. 5.09-2(a). The parallel-coupled line section admittances
are obtained by use of the relations in Fig. 5.09-2(a), and the line
dimensions can be obtained from the line admittances by use of the data
in Sec. 5.05. Whether the stub or parallel-coupled form is preferable
would depend mainly on what dimensions were practical. The stub form
would probably be convenient in most cases, though the parallel-coupled
form has additional adjustability since it would not be difficult to
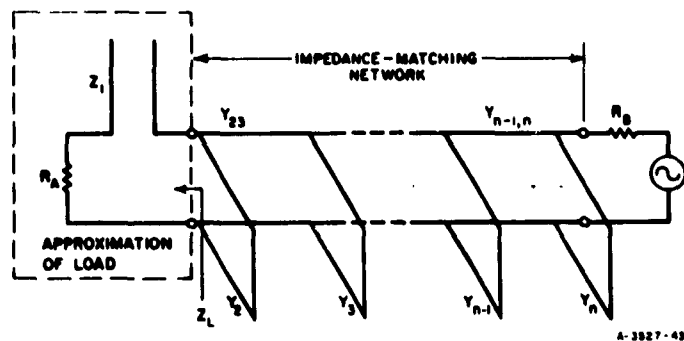
FIG. 11.09-2 IMPEDANCE-MATCHING NETWORK FORMED
FROM STUBS AND CONNECTING LINES
The series stub Z_1, the shunt stubs Y_k, and the
connecting lines $Y_{k,k+1}$ are all a quarter-
wavelength long at midband

697

provide for experimental adjustment of the spacing between the parallel-coupled elements. This would be equivalent to adjusting the line admittances $Y_{k,k+1}$ in Fig. 11.09-2. Experimental adjustment of these line admittances might be desirable in cases where the load impedance is quite complicated and deviates greatly from the idealized symmetrical case in Fig. 11.09-1(a), so that some cut-and-try procedures are desirable.

Table 11.09-1 presents design equations for impedance-matching networks of the form in Fig. 11.09-2. These design equations were derived in essentially the same way as were the design equations for the filters in Secs. 10.03 and 10.05. (The derivations of the design equations in Secs. 10.03 and 10.05 were discussed in Sec. 10.08.) The main difference is that the more general modified low-pass prototype in Fig. 11.09-3 was used for the equations in Table 11.09-1. Comparing this prototype with the one in Fig. 10.08-6, note that the prototype in Fig. 11.09-3 does not use a series coil on the right, and provision has been made so that the termination R_{n+1} on the right can be specified arbitrarily. A multiplying factor s has been included which is introduced so as to alter the impedance level as gradually as possible from one side of the prototype to the other, by making $C_{k+1} = sC_k$ for $k = 2$ to $n - 2$. The relations between the prototype and the stub filter in Fig. 11.09-2 are much the same as for the cases discussed in Sec. 10.08. The parameter d in Table 11.09-1 can be chosen $0 < d$ so as to adjust the admittance level within the filter. Typical convenient values are $d = 0.5$ to 1.

Figure 11.09-4 shows an impedance-matching network for use with a shunt-resonated load. This circuit is the dual of that in Fig. 11.09-2, except that the filter has been converted to parallel-coupled form by use of the relations in Fig. 5.09-2(b). Since series stubs are difficult to realize in a shielded construction, the parallel-coupled form of this filter will usually be the practical one to use. Table Table 11.09-2 presents design equations for this type of matching network.[*]

---

[*] These design equations were obtained from those in Table 11.09-1 by duality, which first gave a matching network consisting of series stubs and connecting lines. Then this circuit was converted to parallel-coupled form using the relations in Fig. 5.09-2(b).

Table 11.09-1

DESIGN EQUATIONS FOR IMPEDANCE-MATCHING NETWORKS OF THE FORM IN
FIG. 11.09-2 FOR SERIES-RESONATED LOADS

Determine the low-pass prototype parameters from the load decrement δ and the data in Secs. 4.09 and 4.10. The generator resistance R_B may be chosen arbitrarily, but R_A is a parameter of the load (see text). The following equations apply for $n \geq 3$.

Compute:

$$s = \sqrt[n-2]{\frac{R_A}{R_B}}$$

$$C_2 = g_2 \quad , \quad C_k \Big|_{\substack{k=3 \text{ to } n-1, \text{ if } n>3 \\ \text{(If } n=3 \text{ omit this equation.)}}} = 2d g_2 s^{k-2}$$

$$C_n \Big|_{n \geq 3} = g_0 g_n g_{n+1} \frac{R_A}{R_B}$$

where d may be chosen arbitrarily within limit $0 < d$ (see text).

$$C_2' = g_2 (1 - d) \quad , \quad C_2'' = d g_2$$

$$C_k' \Big|_{k=3 \text{ to } n} = C_{k-1}'' \quad , \quad C_k'' = C_k - C_k'$$

Letting

$$G_A = \frac{1}{R_A} \quad ,$$

$$\frac{J_{k,k+1}}{G_A} \Big|_{k=2 \text{ to } n-1} = \frac{1}{g_0} \sqrt{\frac{C_k C_{k+1}}{g_k g_{k+1}}}$$

$$N_{k,k+1} \Big|_{k=2 \text{ to } n-1} = \sqrt{\left(\frac{J_{k,k+1}}{G_A}\right)^2 + \left(\frac{C_k'' \tan \theta_1}{g_0}\right)^2}$$

where

$$\theta_1 = \frac{\pi}{2} \left(1 - \frac{w}{2}\right)$$

and $w = (f_2 - f_1)/f_0$ is the desired fractional bandwidth.

Table 11.09-1 *concluded*

The characteristic admittances of the shunt stubs are:

$$Y_2 = \frac{G_A}{g_0} a_1' C_2' \tan \theta_1 + G_A \left(N_{23} - \frac{J_{23}}{G_A} \right)$$

$$Y_k \Big|_{k=3 \text{ to } n-1, \text{ if } n > 3} = G_A \left(N_{k-1,k} + N_{k,k+1} - \frac{J_{k-1,k}}{G_A} - \frac{J_{k,k+1}}{G_A} \right)$$

$$Y_n \Big|_{n \geq 3} = \frac{G_A}{g_0} a_1' C_n'' \tan \theta_1 + G_A \left(N_{n-1,n} - \frac{J_{n-1,n}}{G_A} \right)$$

The characteristic admittances of the connecting lines are:

$$Y_{k,k+1} \Big|_{k=2 \text{ to } n-1} = G_A \left(\frac{J_{k,k+1}}{G_A} \right)$$
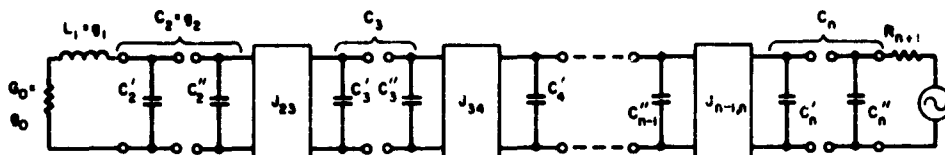
$$a = \sqrt[n-2]{\frac{1}{G_0 R_{n+1}}} \quad \text{WHERE } R_{n+1} \text{ IS ARBITRARY }, \ n \geq 3,$$

$$C_2 \cdot \theta_2, \ C_k \Big|_{k=3 \text{ TO } n-1} = 2 d \theta_2 \ a^{k-2}, \ C_n = \frac{\theta_n \theta_{n+1}}{R_{n+1}},$$

$$C_2' \cdot \theta_2 (1-d), \ C_2'' = d \theta_2, \ C_k' \Big|_{k=3 \text{ TO } n} = C_{k-1}'', \ C_k'' = C_k - C_k',$$

WHERE d MAY BE CHOSEN ARBITRARILY WITHIN LIMIT 0 < d.

$$J_{k,k+1} \Big|_{k=2 \text{ TO } n-1} = \sqrt{\frac{C_k C_{k+1}}{\theta_k \theta_{k+1}}}$$

A-3827-434

FIG. 11.09-3 MODIFIED LOW-PASS PROTOTYPE USED IN DERIVING
THE EQUATIONS IN TABLE 11.09-1

700
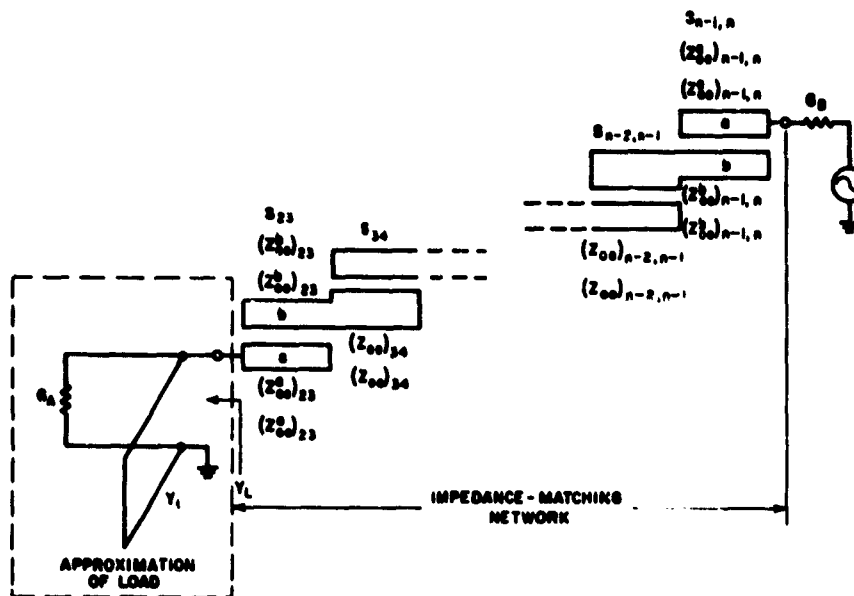
FIG. 11.09-4 IMPEDANCE-MATCHING NETWORK IN PARALLEL-COUPLED
FORM FOR MATCHING SHUNT-RESONATED LOAD
The stub Y_1 and the parallel-coupled sections $S_{k,k+1}$ are all a
quarter-wavelength long at midband

Let us now consider some examples of impedance-matching network
design. Figure 11.09-5 shows a lumped-element load network which has been
brought to resonance at f_0, and the figure also shows the resulting
computed impedance characteristic. Let us assume that a good match is
desired from $f_1/f_0 = 0.85$ to $f_2/f_0 = 1.15$, which calls for fractional
bandwidth of $w = 0.30$. From Figs. 11.09-1(a) and 11.09-5, $R_A = ReZ_L|_{f_0} =$
33.33 ohms. However, $|ImZ_L|_{f_1} = 110$ ohms, while $|ImZ_L|_{f_2} = 95$ ohms, so
there is some confusion about the calculation of δ. As a guess, an
in-between value of 100 ohms was used for some trial calculations so that*

$$\delta = \frac{33.33}{100} = 0.3 \quad .$$

Table 11.09-3 summarizes the parameters and resulting line admittances
for several $n = 3$ designs having different values of R_B or different
choices for the parameter d. Note that Designs 1 and 2 both use $R_B =$
100 ohms, but Design 1 uses $d = 1$ while Design 2 uses $d = 0.5$.

---

*A useful significant figure was inadvertently dropped in these calculations.

Table 11.09-2

DESIGN EQUATIONS FOR IMPEDANCE-MATCHING NETWORKS OF THE FORM IN
FIG. 11.09-4 FOR SHUNT-RESONATED LOADS

Determine the low-pass prototype parameters from the load decrement
δ and the data in Secs. 4.09 and 4.10. The generator conductance G_B may
be chosen arbitrarily, but G_A is a parameter of the load (see text). The
following equations cover cases where $n \geq 3$.

Compute:

$$\delta = \sqrt[n-2]{\frac{G_A}{G_B}}$$

$$L_2 = g_2 \quad , \quad L_k \Big|_{\substack{k=3 \text{ to } n-1, \text{ if } n>3 \\ (\text{If } n=3 \text{ omit this equation.})}} = 2 d g_2 \, s^{k-2}$$

$$L_n \Big|_{n \geq 3} = g_0 g_n g_{n+1} \frac{G_A}{G_B} \quad .$$

where d may be chosen arbitrarily within limit $0 < d$ (see text).

$$L_2' = g_2(1 - d) \quad , \quad L_2'' = d g_2$$

$$L_k' \Big|_{k=3 \text{ to } n} = L_{k-1}'' \quad , \quad L_k'' = L_k - L_k' \quad .$$

Letting

$$R_A = \frac{1}{G_A} \quad .$$

$$\frac{K_{k,k+1}}{R_A} \Big|_{k=2 \text{ to } n-1} = \frac{1}{\delta_0} \sqrt{\frac{L_k L_{k+1}}{g_k g_{k+1}}}$$

$$N_{k,k+1} \Big|_{k=2 \text{ to } n-1} = \sqrt{\left(\frac{K_{k,k+1}}{R_A}\right)^2 + \left(\frac{L_k'' \tan \theta_1}{\delta_0}\right)^2}$$

where

$$\theta_1 = \frac{\pi}{2}\left(1 - \frac{w}{2}\right)$$

and $w = (f_2 - f_1)/f_0$ is the desired fractional bandwidth.

Table 11.09-2 *concluded*

The even- and odd-mode impedances of the parallel-coupled lines are:

If $n = 3$

$$(Z_{oe}^a)_{23} = \frac{R_A \omega_1' L_2'}{\epsilon_0} \tan \theta_1 + R_A \left(N_{23} + \frac{K_{23}}{R_A} \right)$$

$$(Z_{oo}^a)_{23} = \frac{R_A \omega_1' L_2'}{\epsilon_0} \tan \theta_1 + R_A \left(N_{23} - \frac{K_{23}}{R_A} \right)$$

$$(Z_{oe}^b)_{23} = \frac{R_A \omega_1' L_3''}{\epsilon_0} \tan \theta_1 + R_A \left(N_{23} + \frac{K_{23}}{R_A} \right)$$

$$(Z_{oo}^b)_{23} = \frac{R_A \omega_1' L_3''}{\epsilon_0} \tan \theta_1 + R_A \left(N_{23} - \frac{K_{23}}{R_A} \right)$$

If $n \geq 4$,

$$(Z_{oe}^a)_{23} = \frac{R_A}{\epsilon_0} \omega_1' L_2' \tan \theta_1 + R_A \left(N_{23} + \frac{K_{23}}{R_A} \right)$$

$$(Z_{oo}^a)_{23} = \frac{R_A}{\epsilon_0} \omega_1' L_2' \tan \theta_1 + R_A \left(N_{23} - \frac{K_{23}}{R_A} \right)$$

$$(Z_{oe}^b)_{23} = R_A \left(N_{23} + \frac{K_{23}}{R_A} \right)$$

$$(Z_{oo}^b)_{23} = R_A \left(N_{23} - \frac{K_{23}}{R_A} \right)$$

$$(Z_{oe})_{h,h+1} \Big|_{\substack{h=3 \text{ to } n-2 \\ (\text{Omit if } n < 5)}} = R_A \left(N_{h,h+1} + \frac{K_{h,h+1}}{R_A} \right)$$

$$(Z_{oo})_{h,h+1} \Big|_{\substack{h=3 \text{ to } n-2 \\ (\text{Omit if } n < 5)}} = R_A \left(N_{h,h+1} - \frac{K_{h,h+1}}{R_A} \right)$$

$$(Z_{oe}^a)_{n-1,n} = \frac{R_A}{\epsilon_0} \omega_1' L_n'' \tan \theta_1 + R_A \left(N_{n-1,n} + \frac{K_{n-1,n}}{R_A} \right)$$

$$(Z_{oo}^a)_{n-1,n} = \frac{R_A}{\epsilon_0} \omega_1' L_n'' \tan \theta_1 + R_A \left(N_{n-1,n} - \frac{K_{n-1,n}}{R_A} \right)$$

$$(Z_{oe}^b)_{n-1,n} = R_A \left(N_{n-1,n} + \frac{K_{n-1,n}}{R_A} \right)$$

$$(Z_{oo}^b)_{n-1,n} = R_A \left(N_{n-1,n} - \frac{K_{n-1,n}}{R_A} \right)$$

FIG. 11.09-5 A HYPOTHETICAL LOAD AND ITS COMPUTED IMPEDANCE

Table 11.09-3

IMPEDANCE-MATCHING NETWORK DESIGNS 1 to 4 FOR THE LOAD IN FIG. 11.09-5

The impedance-matching network is of the form in Fig. 11.09-2

For all designs below: $w = 0.30$, $R_A = 33.33$ ohms, $\delta = 0.30$; and for
$n = 3$ Sec. 4.09 gives $g_0 = 1$, $g_1 = 3.30$, $g_2 = 0.52$, $g_3 = 2.10$, $g_4 = 0.40$
$\omega' = 1$, $(L_A)_{max} = 1.2$ db, and $(L_A)_{min} = 0.9$ db.

Design	d	R_B (ohms)	Y_2 (mhos)	Y_{23} (mhos)	Y_3 (mhos)
1	1.0	100	0.05494	0.01095	0.02495
2	0.5	100	0.05582	0.01095	0.02583
3	1.0	20	0.04495	0.02449	0.1549
4	1.0	500	0.06026	0.004899	0.002283

Within two significant figures the line admittances Y_2, Y_{23}, and Y_3
of the matching network are very nearly the same. This is to be
expected since the choice of d should, in theory, not affect the design
unless there are more than two resonators in the matching-network portion

784

of the circuit. (In this case, the matching-network portion has only
two resonators.)

Figure 11.09-6 shows the computed response of the load in Fig. 11.09-5
connected to matching-network Design 1 of Table 11.09-3. The dashed
curve is for the load as shown in Fig. 11.09-5 without any retuning.
Note that the attenuation (i.e., transducer attenuation[*]) curve tilts a
little to the right because of the disasymmetry of the reactance curve
of the load. The solid curve in Fig. 11.09-6 shows the result of
retuning the load by increasing the midband inductive reactance X_L from
340.3 ohms to 348.3 ohms. Note that the effect is to correct (actually
overcorrect) the tilt in the response. By Figs. 4.09-3 and 4.09-4 the
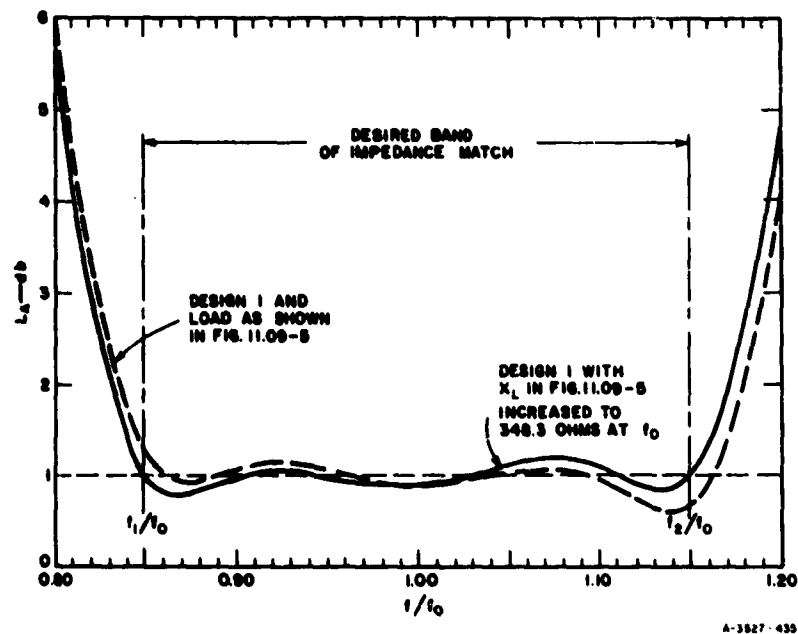
FIG. 11.09-6 TRANSDUCER ATTENUATION INTO THE LOAD IN
FIG. 11.09-5 USING MATCHING-NETWORK DESIGN 1

[*]See Sec. 2.11 for a discussion of this term.

peak pass-band attenuation into the load should be 1.2 db for this case, while the minimum pass-band attenuation should be about 0.9 db. As can be seen from Fig. 11.09-6, the pass-band ripple characteristic comes quite close to meeting these values.

Figure 11.09-7 shows the computed attenuation characteristics for the same retuned load as described above (i.e., with X_L = 348.3 ohms), but using matching-network Designs 3 and 4. Note that for Design 3 the generator resistance is R_g = 20 ohms, while for Design 4, R_g = 500 ohms. Thus, these two designs cover a range of choice of generator impedance of 25 to 1. As can be seen from the figure, the choice of R_g had no serious effect on the performance.

Figure 11.09-7 also shows the performance when no matching network is used but R_g is chosen to match the load impedance at resonance. Note
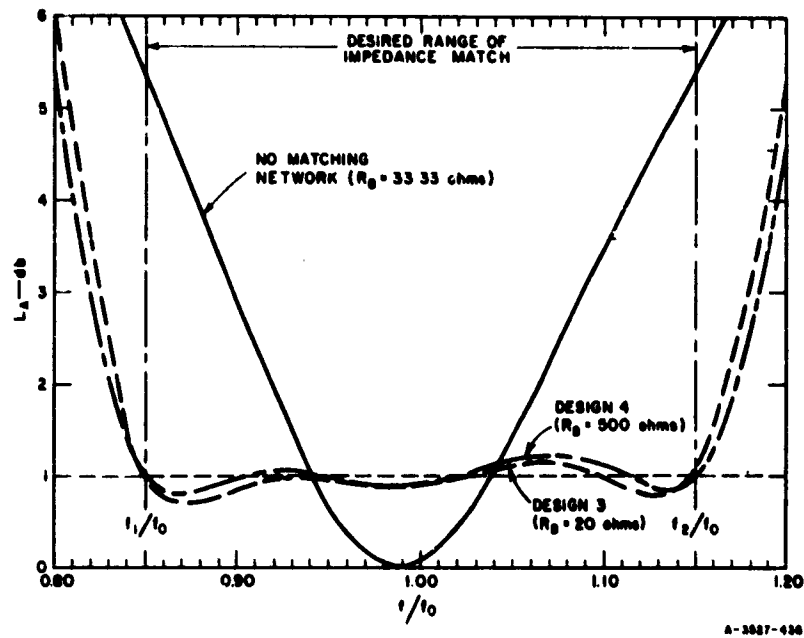
FIG. 11.09-7 TRANSDUCER ATTENUATION INTO THE LOAD IN
              FIG. 11.09-5 USING MATCHING-NETWORK DESIGNS 3
              AND 4, AND ALSO FOR CASE OF NO MATCHING-
              NETWORK
              In all cases shown the load is as in Fig. 11.09-5 except
              that X_L has been increased to X_L = 348.3 ohms at f_0

that the attenuation at the band edges in this case is 5.4 db as compared
with around 1.2-db maximum attenuation across the 30 percent band when
an $n = 3$ matching network is used. By Fig. 4.09-3, for a load with
$\delta = 0.30$, the best possible pass-band performance even with an infinite
number of impedance-matching resonators would have a pass-band attenuation
of 0.72 db.

Figure 11.09-8 shows another series-resonated load whose impedance
characteristic deviates quite markedly from the idealized symmetrical
characteristic in Fig. 11.09-1(a). Suppose that we wish to match over
a 40-percent band, ReZ_L varies over a 2 to 1 range in the band of
interest, while the reactance characteristic is also unsymmetrical. In
this case $R_A = ReZ_L\big|_{f_0} = 20$ ohms, while $|ImZ_L|\big|_{f_1} = 80$ ohms and
$|ImZ_L|\big|_{f_2} = 67$ ohms. Averaging these latter two values gives 73.5 ohms.
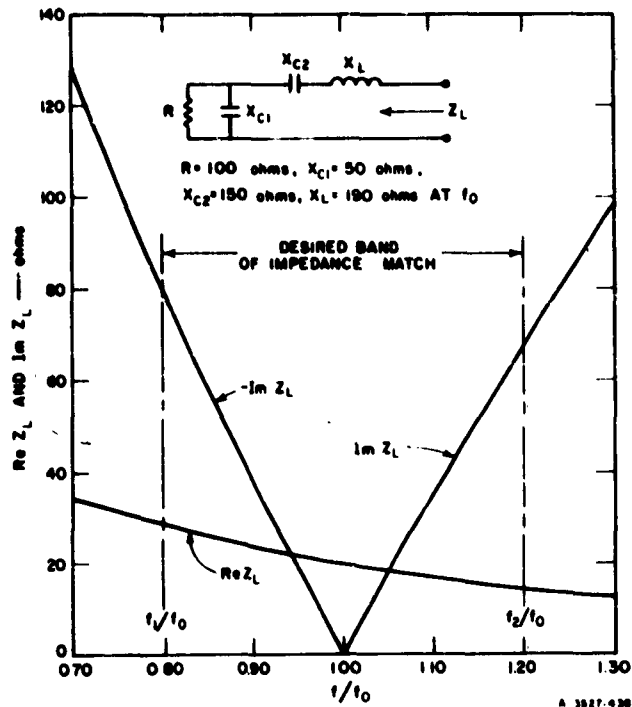
FIG. 11.09-8   A SERIES-RESONATED LOAD WHICH
DEVIATES MARKEDLY FROM THE
IDEALIZED CASE IN FIG. 11.09-1(a)

Thus, an estimated decrement value is

$$\delta = \frac{20}{73.5} = 0.272 \quad .$$

Table 11.09-4 summarizes the parameters of an $n = 3$ matching-network design for this load.

Table 11.09-4

IMPEDANCE-MATCHING NETWORK DESIGN 5 FOR THE LOAD IN FIG. 11.09-8

The impedance-matching network is of the form in Fig. 11.09-2

Design parameters: $w = 0.40$, $R_A = 20$ ohms, $\delta = 0.272$; and for $n = 3$ Sec. 4.09 gives $g_0 = 1.00$, $g_1 = 3.70$, $g_2 = 0.48$, $g_3 = 2.35$, $g_4 = 0.36$, $\omega_1' = 1$, $(L_A)_{max} = 1.4$ db, and $(L_A)_{min} = 1.07$ db.

Design	d	R_A (ohms)	Y_2 (mhos)	Y_{23} (mhos)	Y_3 (mhos)
5	1	100	0.06281	0.01342	0.01498

Figure 11.09-9 shows the computed transducer attenuation for the matching-network Design 5 in Table 11.09-4, used with the load in Fig. 11.09-8. The solid curve is for the original matching network with the stubs a quarter-wave-length long at frequency f_0. The dashed curve for Design 5 was computed with the Y_2 and Y_3 stubs lengthened by 2.5 percent in an effort to correct the skewedness of the response curve. As can be seen, this achieved the desired result but with a small loss in bandwidth. Note that the pass-band ripple maxima and minima are reasonably consistent with the $(L_A)_{max} = 1.4$ db and $(L_A)_{min} = 1.07$ db values predicted for $\delta = 0.272$ using Figs. 4.09-2 and 4.09-3. Figure 11.09-9 also shows the attenuation characteristic when no matching network is used but the generator resistance is chosen so as to give a match at resonance. Note that on this basis the attenuation is 5.9 db at the lower band edge and about 6.85 db at the upper band edge.

The above examples show that though the procedures for matching-network design based on the methods of Chapter 10 are approximate, they can give good results in close agreement with the theory. Also, the techniques described in this section are seen to be useful even if the load characteristics deviate appreciably from the idealized, symmetrical characteristics in Fig. 11.09-1. If the load impedance characteristics

708
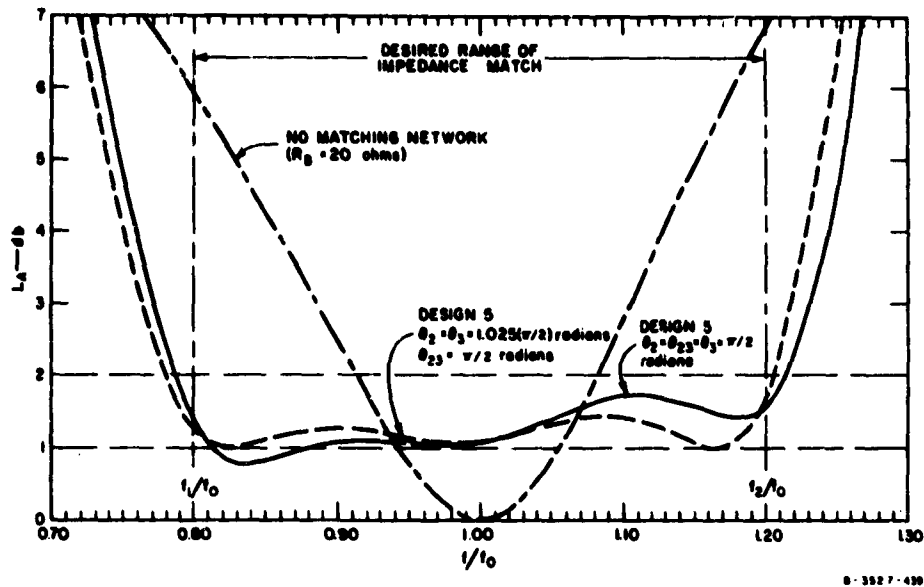
FIG. 11.09-9 TRANSDUCER ATTENUATION INTO THE LOAD IN FIG. 11.09-8
WITH AND WITHOUT MATCHING-NETWORK DESIGN 5
The parameters θ_2, θ_{23}, and θ_3 given are the electrical lengths of
the lines Y_2, Y_{23}, and Y_3 of the matching network at frequency f_0

are skewed, this can often be compensated for by minor tuning adjustments
on the load or on the resonant elements of the matching network.

In this section design data for only two specific types of wideband
matching networks have been given. Though most of the other structures
in Chapter 10 could also be used, the ones given in this section were
chosen as particularly useful examples. If desired, data for other
forms of matching networks can be obtained by the methods of Chapter 10
along with a modified low-pass prototype such as that in Fig. 11.09-3.
Other forms of networks may be desirable in special situations where
they might give more practical dimensions for the impedance levels and
space limitations involved.

SEC. 11.10, DESIGN OF WIDE-BAND COUPLING STRUCTURES
FOR NEGATIVE-RESISTANCE AMPLIFIERS

The same procedures as discussed in the preceding two sections
can also be used for the design of coupling networks for negative-
resistance devices. Consider, for example, the negative-resistance

amplifier shown in Fig. 11.10-1. The required negative resistance is
assumed to have been achieved by use of a device such as a tunnel diode
which has parasitic reactive elements in its equivalent circuit as well
as a negative resistance. A broad-banding network is then desirable in
order to compensate for the effects of these reactive elements so as
to give as good performance as possible over the required operating band.
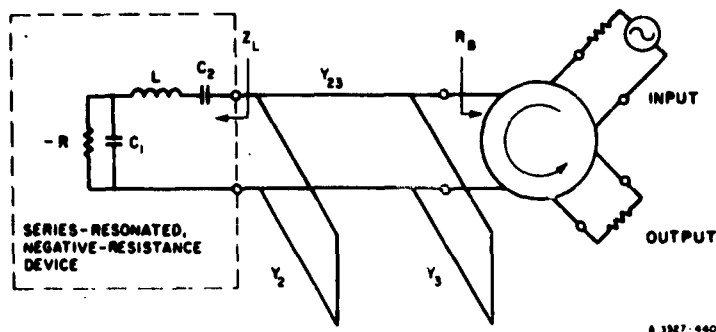
FIG. 11.10-1 EXAMPLE OF THE USE OF A FILTER STRUCTURE
FOR BROAD-BANDING A NEGATIVE-RESISTANCE
AMPLIFIER
The negative-resistance is assumed to have been
achieved using a device such as a tunnel diode which
has parasitic equivalent reactances as well as negative
resistance

In Sec. 1.04 it was explained that a negative resistance amplifier
with a prescribed response characteristic can be obtained by first
designing a related filter having the specified negative resistance
replaced by a positive resistance of the same magnitude. Then when a
circulator is placed at one end of the filter and the specified negative
resistance at the other, the desired gain characeristic can be obtained.
Section 4.11 along with Sec. 4.10 explained how to obtain element values
for a low-pass prototype so as to achieve a given gain characteristic
in a negative-resistance amplifier.

The following procedure is suggested for the design of coupling
networks for negative-resistance amplifiers of this sort:

(1) The negative-resistance device should be mounted as it will be
     in the finished amplifier including any voltage bias leads,
     etc. The negative-resistance device should be brought to
     resonance at the desired midband frequency f_0 by adding an
     additional reactive element.

710

(2) If the device is resonated in series, the impedance character-
istic of the device should be determined. If the device was
resonated in shunt, its admittance characteristic should be
determined.

(3) The real part of the impedance or admittance characteristic will
be negative. The real and imaginary part of the characteristic
should be plotted, but with the sign of the real part changed
to positive. (This corresponds to changing the negative
resistance in the equivalent circuit of the device to a positive
resistance.)

(4) The decrement δ of the plotted load characteristic for the
desired operating bandwidth should be determined as indicated
in Fig. 11.09-1 and the examples of Sec. 11.09. The parameter
R_A or G_A should also be obtained.

(5) The low-pass prototype for the coupling network is determined
as described in Sec. 4.11.[*]

(6) Using the specified R_A (or G_A) parameter of the load along
with the low-pass prototype parameters and the specified
resistance R_B (or conductance G_B) looking into the circulator,
the coupling network is designed in the same manner as the
matching networks discussed in Secs. 11.08 and 11.09.

The resonated negative-resistance device in the example in Fig. 11.10-1
has the same equivalent circuit as the load in Fig. 11.09-8, except
for the negative resistor. Plotting $-ReZ_L$ and ImZ_L for the resonated
negative-resistance device in Fig. 11.10-1 would give a characteristic
of the same general form as that in Fig. 11.09-8, and the determination
of the decrement δ would be done in the same manner as was described
with respect to that figure. The design of the coupling network would
follow the same procedures as that for Design 5 which was summarized
in Table 11.09-4, except for that the factors controlling the choice
of the low-pass prototype would be somewhat different. In the case of
Design 5 of Sec. 11.09 it was assumed desirable to minimize $(L_A)_{max}$, hence
the prototype element values were obtained from Fig. 4.09-7 which gives
element values which are optimized for that requirement. However, in
the case of a negative-resistance amplifier, a flat gain characteristic
may be a dominant requirement, and using the procedures of Secs. 4.10
and 4.11 a somewhat different prototype might be chosen.

---

[*]Note in Sec. 4.11 that for reasons of circuit stability as well as to obtain maximum bandwidth,
the prototype elements g_0 and g_1 (rather than g_n and g_{n+1}) must be associated with the
resonated negative-resistance device.

711

It is interesting to note what the gain of the circuit in Fig. 11.10-1 would be if the plots in Fig. 11.09-8 were its $-ReZ_L$ and ImZ_L load characteristics and if the matching network Design 5 of Table 11.09-4 were used as the coupling network. Referring to the slightly retuned response for Design 5 in Fig. 11.09-9, by use of the graph in Fig. 4.11-1, we see that the peak transducer gain in the pass band would be about 7 db [corresponding to $(L_A)_{min}$ of about 1 db], while the minimum gain in the pass band would be about 6 db [corresponding to $(L_A)_{max}$ of about 1.45 db]. For this specified negative-resistance device, if more gain were desired with the same pass-band-gain-variation tolerance, it would be necessary to go to a narrower bandwidth.

Additional discussions of negative-resistance amplifiers will be found in Ref. 8, and in numerous other references. The case of parametric amplifiers is similar in some respects, but is complicated by the manner in which the impedance seen at the idler frequency is reflected through the time-varying capacitance of the diode as an added impedance component seen at the input frequency.[9]

SEC. 11.11, BAND-PASS TIME-DELAY FILTERS

Although all of the information required for the design of band-pass time-delay filters has been presented previously, it appears desirable to review some of the band-pass delay-filter design procedures. Some general concepts related to time-delay filters were discussed in Sec. 1.05; element values and related data were given in Sec. 4.07 for low-pass prototype filters having maximally flat time delay, and in Sec. 4.08 the time-delay characteristics of filters with Tchebyscheff and maximally flat attenuation characteristics were compared with those of maximally flat time-delay networks. It was noted in Sec. 4.08 that for many cases a Tchebyscheff filter having small pass-band ripple (say 0.1 db or less) may make a more desirable type of time-delay network than will a maximally flat time-delay network. This is because although the maximally flat time-delay network has a more nearly constant time-delay characteristic, its attenuation may vary considerably over the range of interest. Thus, in cases where both the attenuation and delay characteristics are important, Tchebyscheff filters with small pass-band ripple may make an excellent compromise.

Let us suppose that a band-pass time-delay filter is desired to give 0.016 microsecond delay in an operating band from 1000 to 1100 Mc, and

712

that from the discussion in Sec. 4.08 it is decided to use a Tchebyscheff
low-pass prototype for the delay filter having 0.01-db pass-band ripple.
By Eq. (4.08-4) the midband time delay t_{d0} for the band-pass filter is

$$t_{d0} = \left(\frac{2\omega_1'}{\omega_2 - \omega_1}\right) t_{d0}' \quad \text{seconds} \quad (11.11\text{-}1)$$

where ω_1 and ω_2 are the radian band-edge frequencies of the band-pass
filter corresponding to the band-edge frequency ω_1' of the low-pass
prototype, and t_{d0}' is the time delay in seconds of the low-pass prototype
as $\omega' \to 0$.   For the problem at hand,

$$t_{d0}' = \left(\frac{\omega_2 - \omega_1}{2\omega_1'}\right) t_{d0} \quad \text{seconds} \quad (11.11\text{-}2)$$

$$= \frac{6.28(1100\text{-}1000)10^6}{2(1)} \quad (0.016 \times 10^{-6})$$

$$= 5.02 \text{ seconds,}$$

where $\omega_1' = 1$ is assumed for the low-pass prototype. By Eq. (4.08-2),

$$t_{d0}' = C_n \quad (11.11\text{-}3)$$

where by Fig. 4.13-2, for a Tchebyscheff filter with 0.01-db ripple,
and a band-edge frequency of $\omega_1' = 1$ radian/sec, for $n = 7$, $C_7 = 4.7$ seconds,
while for $n = 8$, $C_8 = 5.7$ seconds. Letting $n = 8$ so $t_{d0}' = C_8 = 5.7$ seconds,
the desired delay can be obtained by enlarging the bandwidth slightly
so that

$$\omega_2 - \omega_1 = \frac{2\omega_1' t_{d0}'}{t_{d0}} \quad (11.11\text{-}4)$$

$$= \frac{2(1)5.7}{0.016(10^{-6})} = 7.14 \times 10^8 \text{ rad/sec.}$$

$$f_2 - f_1 = \frac{7.14 \times 10^8}{6.28} = 113 \text{ Mc/sec.}$$

713

Thus, a band-pass filter designed from a 0.01-db-ripple, $n = 3$ Tchebyscheff prototype [whose element values are tabulated in Table 4.05-2(a)] so as to give a 113-Mc pass-band centered at 1050 Mc should have the desired midband time delay.*

When using Eq. (11.11-1), it should be realized that it is based on the assumption that the low-pass prototype phase characteristic maps linearly into the band-pass filter phase characteristic, so that the frequency mapping

$$\omega' = \frac{2\omega_1'}{w} \left(\frac{\omega - \omega_0}{\omega_0} \right) \tag{11.11-5}$$

where

$$w = \frac{\omega_2 - \omega_1}{\omega_0}$$

and

$$\omega_0 = \frac{\omega_2 + \omega_1}{2}$$

is valid. The mapping Eq. (11.11-5) is generally accurate for narrow-band designs (i.e., for designs with fractional bandwidths of, say, around $w = 0.05$ or less), and depending on the type of filter it may have satisfactory accuracy to quite large bandwidths. However, it should be realized that to the degree that the band-pass filter pass-band characteristics vs. frequency are not a linear mapping of the low-pass filter pass-band characteristics, the shapes of the low-pass and band-pass time-delay characteristics will differ since time delay is the derivative of the phase with respect to frequency.

Another factor that can alter the time-delay characteristic of the band-pass filter from that of its prototype is the dissipation loss. In general, the dissipation loss in a filter tends to cause the natural frequencies of vibration of a circuit to move toward the left side of the complex frequency plane away from the $j\omega$ axis (see Secs. 2.02 to 2.04). This will cause the phase and time-delay characteristics to be somewhat different than they would be if the filter circuit had no dissipation loss. For cases where the attenuation due to dissipation is not large (say a few tenths of a db or less), the alteration of the

---

* This assumes that the time delay due to the physical length of the microwave filter can be neglected, as is usually true.

714

time-delay characteristic due to this cause is probably small. The part of the response where attenuation will be most evident will be near the band edges, and there it should tend to smooth the time-delay characteristic, which should not be harmful.

REFERENCES

1. E. L. Ginzton, *Microwave Measurements*, pp. 417-424 (McGraw-Hill Book Company, Inc., New York City, 1957).

2. M. Dishal, "Alignment and Adjustment of Synchronously Tuned Multiple-Resonator-Circuit Filters," *Proc. IRE* 39, pp. 1448-1455 (November 1951).

3. S. B. Cohn and J. Shimizu, "Strip Transmission Lines and Components," Quarterly Progress Report 2, SRI Project 1114, Contract DA36-039 SC-63232, Stanford Research Institute, Menlo Park, California (May 1955).

4. S. B. Cohn, J. F. Cline, B. M. Schiffman, and P. M. Sherk, "Design Data for Antenna-Multicoupler Systems," Scientific Report 1, SRI Project 2183, Contract AF 19(604)-2247, Stanford Research Institute, Menlo Park, California (August 1957). Portions of this material are contained in the paper: J. F. Cline and B. M. Schiffman, "Tunable Passive Multi-couplers Employing Minimum-Loss Filters," *IRE Trans. PGMTT*-7, p. 121-127 (January 1959).

5. S. B. Cohn, "Dissipation Loss in Multiple-Coupled-Resonator Filters," *Proc. IRE* 47, pp. 1342-1348 (August 1959).

6. G. L. Matthaei, "Design Theory of Up-Converters for Use as Electronically Tunable Filters," *IRE Trans. PGMTT*-9, pp. 425-435 (September 1961).

7. G. L. Matthaei, "An Electronically Tunable Up-Converter," *Proc. IRE* 49, pp. 1703-1704 (November 1961).

8. E. S. Kuh and J. D. Patterson, "Design Theory of Optimum Negative-Resistance Amplifiers," *Proc. IRE* 49, pp. 1043-1050 (June 1961).

9. G. L. Matthaei, "A Study of the Optimum Design of Wide-Band Parametric Amplifiers and Up-Converters," *IRE Trans. PGMTT*-9, pp. 23-38 (January 1961).

10. J. J. Taub and B. F. Bogner, "Design of Three-Resonator Dissipative Band-Pass Filters Having Minimum Insertion Loss," *Proc. IRE* 45, pp. 681-687 (May 1957).

11. E. G. Fubini and E. A. Guillemin, "Minimum Insertion Loss Filters," *Proc. IRE* 47, pp. 37-41 (January 1959).

CHAPTER 12

BAND-STOP FILTERS

SEC. 12.01, INTRODUCTION

In most microwave systems the signal frequency has to be transmitted
and guided from one place to another with a minimum of attenuation, while
unwanted frequencies are strongly attenuated by band-pass filters which
pass the signal frequency with low attenuation. The common types of band-
pass filter provide adequate protection for most applications. However,
should some interfering frequency be particularly strong, special measures
may have to be taken to suppress it; or when a limited number of fre-
quencies are generated in a frequency generator system, high attenuation
may be needed only at certain frequencies. In such cases, a band-pass
filter, which discriminates against wide ranges of frequencies outside
the pass band, will not be as efficient as one or more band-stop filters
which discriminate against specific unwanted frequencies.

Figure 12.01-1 shows two types of band-stop filters to be discussed
in this chapter. Both of these filters are useful for situations where
relatively narrow stop bands are desired. The structure in Fig. 12.01-1(a)
is most suitable for designs having stop-band widths of, say, around
20 percent or less, while the same statement would also apply for the
structure in Fig. 12.01-1(b) if reciprocal guide wavelength (i.e., $1/\lambda_g$)
is used as the frequency variable. The structure in Fig. 12.01-1(a) can
be fabricated in either strip line or coaxial line, and it uses capaci-
tively coupled, band-stop resonator stubs which are spaced a quarter
wavelength apart at the stop-band center frequency. The waveguide filter
structure in Fig. 12.01-1(b) is similar in principle, but uses band-stop
resonator cavities which are coupled to the main waveguide by inductive
irises. In order to avoid interaction between the fringing fields at the
various resonator irises, the resonators are spaced three quarter guide
wavelengths apart.

Figure 12.01-2 shows another type of band-stop filter discussed in
this chapter. The structure shown is of strip-line form, though the
stubs are often most conveniently made from wire rods. This type of

(a)

(b)

A-3527-646

FIG. 12.01-1   STRIP-LINE AND WAVEGUIDE STRUCTURES FOR BAND-STOP FILTERS WITH NARROW STOP BANDS
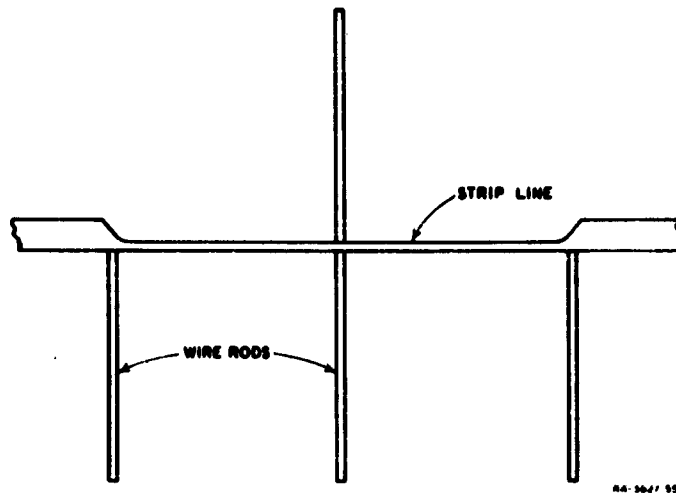
**FIG. 12.01-2 A BAND-STOP, STRIP-LINE FILTER STRUCTURE
HAVING A BROAD STOP BAND**

filter can be designed to give quite wide stop bands, with well controlled
Tchebyscheff or maximally flat pass bands, or pass bands of other shapes
between the stop bands. The stop bands are centered at frequencies where
the open-circuited stubs are a quarter-wavelength long or an odd multiple
of a quarter-wavelength long. The structure in Fig. 12.01-2 could in
principle also be used for filters having narrow stop bands; however, as
the stop-band width becomes narrower, the stub impedance required may
become very high. In order to avoid unreasonable impedances, the struc-
tures in Fig. 12.01-1 become preferable for narrow-stop-band or relatively
narrow-stop-band cases.

SEC. 12.02, LUMPED-ELEMENT BAND-STOP FILTERS FROM
            LOW-PASS PROTOTYPES

A low-pass filter prototype such as those discussed in Sec. 4.05 can
be transformed by suitable frequency transformations into either a band-
pass, a high-pass, or a band-stop filter. The transition from low-pass
to band-stop characteristic can be effected by the transformation

$$\frac{1}{\omega'} = \frac{1}{w\omega_1'}\left(\frac{\omega}{\omega_0} - \frac{\omega_0}{\omega}\right)$$

(12.02-1)

719

where ω' stands for the radian frequency of the low-pass prototype filter and ω for that of the band-stop filter. The remaining quantities in Eq. (12.02-1) are defined in Figs. 12.02-1 and 12.02-2.

It can be seen from Eq. (12.02-1) and Figs. 12.02-1 and 12.02-2 that the prototype- and band-stop-filter frequencies in Table 12.02-1 correspond.
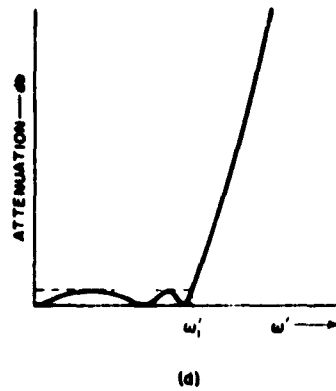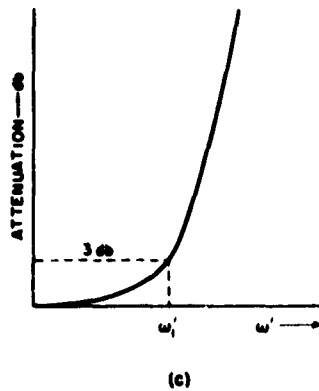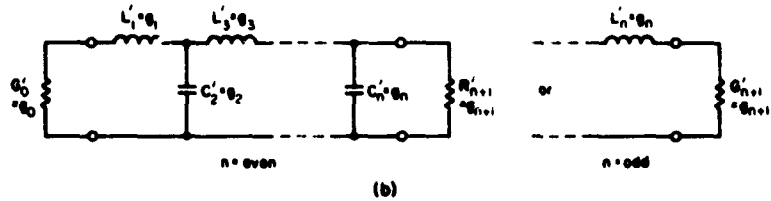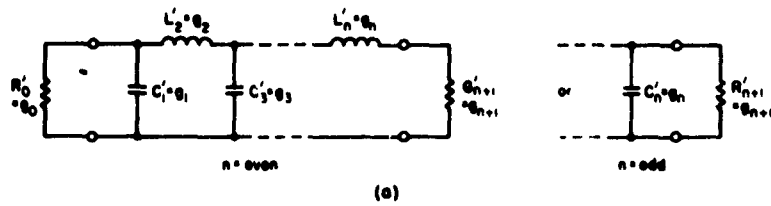
FIG. 12.02-1   LOW-PASS PROTOTYPE FILTER: (a) AND (b), FOUR BASIC CIRCUIT TYPES, DEFINING THE PARAMETERS g_0, g_1, ..., g_{n+1}; (c) AND (d), MAXIMALLY FLAT AND EQUI-RIPPLE CHARACTERISTICS, DEFINING THE BAND-EDGE ω'_1

720
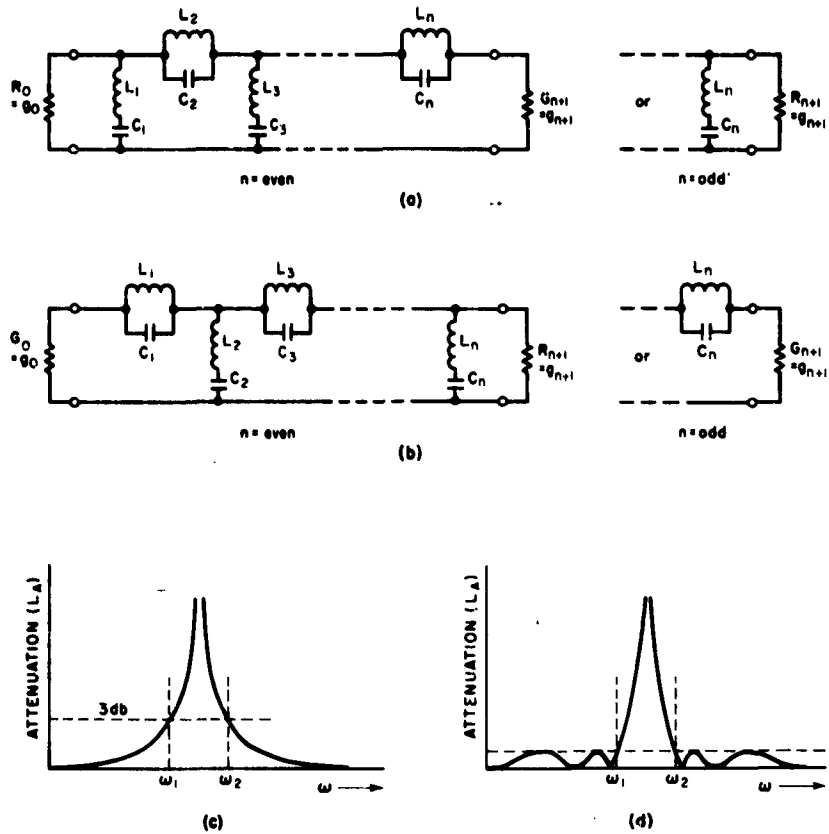
WHERE $\omega_0 = (\omega_1 \omega_2)^{1/2}$ and $w = \dfrac{\omega_2 - \omega_1}{\omega_0}$

FOR SHUNT BRANCHES, $x_i = \omega_0 L_i = \dfrac{1}{\omega_0 C_i} = \dfrac{1}{w \omega_i' g_i}$

FOR SERIES BRANCHES, $b_j = \omega_0 C_j = \dfrac{1}{\omega_0 L_j} = \dfrac{1}{w \omega_i' g_j}$

B-3527-227

FIG. 12.02-2 BAND-STOP FILTER: (a) AND (b), FOUR BASIC CIRCUIT TYPES DERIVABLE
FROM THEIR FOUR LOW-PASS COUNTERPARTS IN FIG. 12.02-1; (c) AND (d),
MAXIMALLY FLAT AND EQUI-RIPPLE CHARACTERISTICS DEFINING CENTER
FREQUENCY ω_0, AND FRACTIONAL BANDWIDTH w

721

Table 12.02-1

RELATION BETWEEN VARIOUS FREQUENCIES IN THE PROTOTYPE- AND BAND-STOP FILTER RESPONSES

ω'	ω
0	0 or ∞
ω'_1	$\omega_{1,2} = \omega_0\left[\left(1 + \frac{w^2}{4}\right)^{\frac{1}{2}} \mp \frac{w}{2}\right]$
	$= \omega_0\left(1 \mp \frac{w}{2}\right)$, when $w \ll 1$
∞	ω_0

To obtain the L_i and C_i in Fig. 12.02-2 in terms of the g_i in Fig. 12.02-1, it is simpler (but not essential) to derive Fig. 12.02-2(a) from Fig. 12.02-1(a) and Fig. 12.02-2(b), from Fig. 12.02-1(b) so that series impedances, go over to other series impedances, and shunt admittances to other shunt admittances. Multiplying both sides of Eq. (12.02-1) by $1/g_i$, one obtains the desired relation. For shunt branches, equating reactances,

$$\omega L_i - \frac{1}{\omega C_i} = \frac{1}{g_i \omega'} = \frac{1}{w\omega'_1 g_i}\left(\frac{\omega}{\omega_0} - \frac{\omega_0}{\omega}\right) \qquad (12.02\text{-}2)$$

which reduces to

$$\omega_0 L_i = \frac{1}{\omega_0 C_i} = \frac{1}{w\omega'_1 g_i} \qquad (12.02\text{-}3)$$

For series branches, equating susceptances,

$$\omega C_j - \frac{1}{\omega L_j} = \frac{1}{g_j \omega'} = \frac{1}{w\omega'_1 g_j}\left(\frac{\omega}{\omega_0} - \frac{\omega_0}{\omega}\right) \qquad (12.02\text{-}4)$$

which reduces to

$$\omega_0 C_j = \frac{1}{\omega_0 L_j} = \frac{1}{w\omega'_1 g_j} \qquad (12.02\text{-}5)$$

The *reactance slope parameter* $\propto$ of a resonator reactance $X = \omega L - 1/\omega C$ is

$$\propto = \frac{\omega_0}{2}\frac{dX}{d\omega}\Big|_{\omega=\omega_0} = \omega_0 L = \frac{1}{\omega_0 C} \qquad (12.02\text{-}6)$$

722

and similarly the *susceptance slope parameter* ℓ of a resonator susceptance $B = \omega C - 1/\omega L$ is

$$\ell = \left. \frac{\omega_0}{2} \frac{dB}{d\omega} \right|_{\omega = \omega_0} = \omega_0 C = \frac{1}{\omega_0 L} \quad . \quad\quad (12.02\text{-}7)$$

Now Eq. (12.02-3) for a shunt branch becomes

$$\alpha_i = \frac{1}{w \omega_1' g_i} \quad\quad (12.02\text{-}8)$$

and Eq. (12.02-5) for a series branch becomes

$$\ell_j = \frac{1}{w \omega_1' g_j} \quad . \quad\quad (12.02\text{-}9)$$

The circuits shown in Fig. 12.02-2 have the same impedance levels as the prototypes in Fig. 12.02-1. To change to another impedance level, every R and every L should be multiplied by the impedance scale factor while every G and every C should be divided by it.

SEC. 12.03, THE EFFECTS OF DISSIPATION LOSS ON BAND-STOP FILTER PERFORMANCE

The discussion in this section will be phrased in terms of the lumped-element band-stop filters in Sec. 12.02; however, this discussion also applies to the microwave-filter structures such as those in Figs. 12.01-1 and 12.02-2.

The solid lines in Fig. 12.03-1 show the attenuation characteristic of a typical band-stop filter of the forms in Fig. 12.02-2 for the situation where the resonators have no dissipation loss. However, in practical filters there will inevitably be dissipation loss, and the dashed lines in Fig. 12.03-1
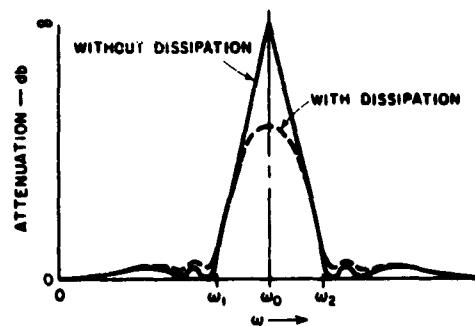
FIG. 12.03-1 THE EFFECTS OF DISSIPATION LOSS IN A BAND-STOP FILTER

723

illustrate its effects on filter performance. Note that the attenuation no longer goes to infin'ty at ω_0, but instead levels off at some finite value. Also note that near the edges of the pass bands of the filter there is an appreciable increase in the pass-band attenuation as a result of the dissipation. However, this increase in pass-band attenuation due to dissipation decreases rapidly as the frequency moves away from the stop band.

Figure 12.03-2 shows a filter of the type in Fig. 12.02-2 with resistors added to account for the dissipation loss of the resonators. If
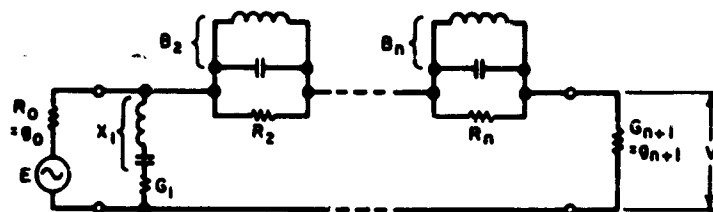
(1) ATTENUATION AT ω_0:

$$(L_A)_{\omega_0} = 20 \sum_{i=1}^{n} \log_{10} (g_i D_i) + 10 \log_{10} \left(\frac{g_0 g_{n+1}}{4} \right) \quad db$$

where $D_i = w\omega_1' Q_{ui}$

(2) RETURN LOSS AT ω_0:

$$10 \log_{10} \frac{1}{|\Gamma|^2} = \frac{17.37}{w\omega_1' g_0 g_1 Q_{u1}} \quad db$$

(3) DISSIPATION LOSS AT ω_1 AND ω_2:

$$\Delta L_A = 8.686 \frac{\omega_1'}{w} \left[\frac{g_1 g_0}{Q_{u1}} + \frac{g_2/g_0}{Q_{u2}} + \frac{g_3 g_0}{Q_{u3}} + \frac{g_4/g_0}{Q_{u4}} + \dots , \right.$$

$$\left. \dots + \frac{g_n/g_0}{Q_{un}} \right]_{\substack{for \\ n=even}} \quad or \quad \dots + \left. \frac{g_n g_0}{Q_{un}} \right]_{\substack{for \\ n=odd}} \quad db$$

RA-3627-233R

FIG. 12.03-2   A BAND-STOP FILTER WITH DISSIPATION, AND
FORMULAS FOR COMPUTING THE EFFECTS OF
THE DISSIPATION

724

the unloaded Q's of the resonators are $Q_{u1}, Q_{u2}, \ldots$, etc., then for the shunt branches of the circuit

$$G_b = \frac{Q_{ub}}{\alpha_b} \qquad (12.03\text{-}1)$$

where α_b is the reactance slope parameter of the resonator, while for the series branches of the circuit

$$R_b = \frac{Q_{ub}}{b_b} \qquad (12.03\text{-}2)$$

where b_b is the susceptance slope parameter of the resonator.

Figure 12.03-2 also presents a formula for computing the attenuation of the filter at the peak attenuation point ω_0. This formula was derived from the low-pass prototype circuit as discussed in Sec. 4.15. A formula is also given in Fig. 12.03-2 for the return loss at frequency ω_0. This is of interest if a band-stop filter is required to provide a short-circuit (or open-circuit) to an adjacent circuit at frequency ω_0. A formula is also given for estimating the increase in attenuation due to dissipation at the pass-band edge frequencies ω_1 and ω_2. This latter formula is based on several rather rough approximations which were discussed in Sec. 4.15. Though it is not highly accurate, this formula should be helpful in estimating the order of the dissipation loss at the pass-band edges. (It should give the ΔL_A in db at ω_1 and ω_2 within a factor of 2 or less.)

SEC. 12.04, AN APPROXIMATE DESIGN PROCEDURE FOR MICROWAVE FILTERS WITH VERY NARROW STOP BANDS

In this section a design approach for microwave filters with very narrow stop bands will be outlined. This approach is very simple and general in its application. However, in Sec. 12.09 will be found another approach which will give superior accuracy, especially if the stop-band width is appreciable. However, the design data there leads to designs which are somewhat more difficult to build because of transmission-line steps (which are not required when using the procedure of this section). Both design approaches are included for completeness.

To realize a band-stop filter in transmission line, it is more convenient to use only shunt branches, or only series branches. The circuit

725

of Fig. 12.02-2(a) can be converted into a circuit with only series-resonant shunt branches by means of impedance inverters (Sec. 4.12) which here are approximated by 90-degree line lengths, as shown in Fig. 12.04-1. The reactance slope parameters of this circuit in terms of the low-pass prototype parameters $g_0, g_1, \ldots, g_{n+1}$, and ω_1' are also given in Fig. 12.04-1. These formulas can be deduced with the help of Figs. 12.02-1 and 12.02-2, and the impedance-inverting property of quarter-wave lines.

In the circuit of Fig. 12.04-1(a), the output impedance and the input impedance have both been set equal to Z_0. In the case of maximally flat filters, or Tchebyscheff filters with n odd, the whole sequence of impedance inverters can be uniform, with the 90-degree lines all having impedances $Z_1 = Z_0$. However, for Tchebyscheff filters with n even, the low-pass prototype is not symmetrical, and the simplest way to obtain a symmetrical band-stop filter of the type shown in Fig. 12.0?-1(a) is to set the impedances of all the 90-degree lines equal to Z_1, which ceases to be equal to Z_0, and is given by

$$\left(\frac{Z_1}{Z_0}\right)^2 = \frac{1}{g_0 g_{n+1}} \qquad (12.04\text{-}1)$$

as stated in Fig. 12.04-1(a).

If the slope parameters determined by Fig. 12.04-1(a) are either too small or too large to realize conveniently, they may be adjusted up or down by controlling the impedances of the 90-degree lines. The formulas for the general case are given in Fig. 12.04-1(b). They reduce to the case of Fig. 12.04-1(a) when $Z_1 = Z_2 = \ldots = Z_{n-1}$. It should be noted that if the Z_i are chosen to be very unequal, then greater reflections will usually result somewhere in the pass band than would occur with a uniform impedance level $Z_i = Z_0$. This is because the 90-degree line sections between resonators are frequency-sensitive and approximate idealized inverters only over a limited frequency range. If the line sections in Fig. 12.04-1 were replaced by ideal inverters (Sec. 4.12) then the responses of the circuits in Fig. 12.04-1 would be identical to those of corresponding circuits of the form in Fig. 12.02-2 at all frequencies.

$$\frac{x_1}{Z_0} = \frac{1}{\omega_1' g_0 g_1 w}$$
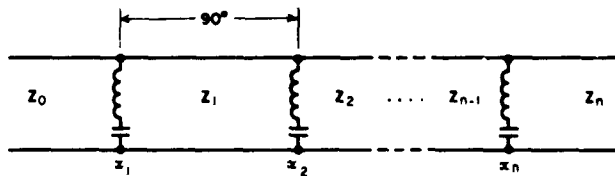
$$\left.\frac{x_i}{Z_0}\right|_{i=\text{even}} = \left(\frac{Z_1}{Z_0}\right)^2 \frac{g_0}{\omega_1' g_i w}$$

$$\left.\frac{x_i}{Z_0}\right|_{i=\text{odd}} = \frac{1}{\omega_1' g_0 g_i w}$$

$$\left(\frac{Z_1}{Z_0}\right)^2 = \frac{1}{g_0 g_{n+1}}$$

If $n =$ odd, $Z_1 = Z_0$

(a)

$$\frac{x_1}{Z_0} = \frac{1}{\omega_1' g_0 g_1 w}$$

$$\left.\frac{x_i}{Z_0}\right|_{i=\text{even}} = \left(\frac{Z_1 Z_3 \cdots Z_{i-1}}{Z_0 Z_2 \cdots Z_{i-2}}\right)^2 \frac{g_0}{\omega_1' g_i w}$$

$$\left.\frac{x_i}{Z_0}\right|_{\substack{i=\text{odd}\\i\neq 1}} = \left(\frac{Z_2 Z_4 \cdots Z_{i-1}}{Z_1 Z_3 \cdots Z_{i-2}}\right)^2 \frac{1}{\omega_1' g_0 g_i w}$$

If $n =$ even, $\dfrac{Z_0}{Z_n} = \left(\dfrac{Z_0 Z_2 \cdots Z_{n-2}}{Z_1 Z_3 \cdots Z_{n-1}}\right)^2 \dfrac{1}{g_0 g_{n+1}}$, or

If $n =$ odd, $\dfrac{Z_0}{Z_n} = \left(\dfrac{Z_1 Z_3 \cdots Z_{n-2}}{Z_2 Z_4 \cdots Z_{n-1}}\right)^2 \dfrac{g_0}{g_{n+1}}$

(b)

B-3527-226

FIG. 12.04-1 BAND-STOP FILTER WITH SHUNT BRANCHES AND QUARTER-WAVE COUPLINGS:
(a) EQUAL INVERTER IMPEDANCES, Z_1;
(b) GENERAL CASE OF UNEQUAL INVERTER IMPEDANCES

727

$$\frac{b_1}{Y_0} = \frac{1}{\omega_1' g_0 g_1 w}$$

$$\frac{b_i}{Y_0}\bigg|_{i=even} = \left(\frac{Y_1}{Y_0}\right)^2 \frac{g_0}{\omega_i' g_i w}$$

$$\frac{b_i}{Y_0}\bigg|_{i=odd} = \frac{1}{\omega_i' g_0 g_i w}$$

If $n = even$, $\left(\frac{Y_1}{Y_0}\right)^2 = \frac{1}{g_0 g_{n+1}}$

If $n = odd$, $Y_1 = Y_0$

(a)

$$\frac{b_1}{Y_0} = \frac{1}{\omega_1' g_0 g_1 w}$$

$$\frac{b_i}{Y_0}\bigg|_{i=even} = \left(\frac{Y_1 Y_3 \dots Y_{i-1}}{Y_0 Y_2 \dots Y_{i-2}}\right)^2 \frac{g_0}{\omega_i' g_i w}$$

$$\frac{b_i}{Y_0}\bigg|_{\substack{i=odd \\ i\neq 1}} = \left(\frac{Y_2 Y_4 \dots Y_{i-1}}{Y_1 Y_3 \dots Y_{i-2}}\right)^2 \frac{1}{\omega_i' g_0 g_i w}$$

If $n = even$, $\frac{Y_0}{Y_n} = \left(\frac{Y_0 Y_2 \dots Y_{n-2}}{Y_1 Y_3 \dots Y_{n-1}}\right)^2 \frac{1}{g_0 g_{n+1}}$, or

If $n = odd$, $\frac{Y_0}{Y_n} = \left(\frac{Y_1 Y_3 \dots Y_{n-2}}{Y_2 Y_4 \dots Y_{n-1}}\right)^2 \frac{g_0}{g_{n+1}}$

(b)

B-3527-229

FIG. 12.04-2   BAND-STOP FILTER WITH SERIES BRANCHES AND
QUARTER-WAVE COUPLINGS: (a) EQUAL INVERTER
ADMITTANCES, Y_1; (b) GENERAL CASE OF UNEQUAL
INVERTER ADMITTANCES

Figure 12.04-2 shows dual circuits to those in Fig. 12.04-1. The circuits in Fig. 12.04-2 use series-connected resonators which exhibit high reactance at resonance. The transmission properties of the filters in Fig. 12.04-2 are identical to those of Fig. 12.04-1.

We shall now consider the practical realization of resonators for microwave filters of the forms in Figs. 12.04-1 and 12.04-2.

SEC. 12.05, PRACTICAL REALIZATION OF BAND-STOP RESONATORS FOR NARROW-STOP-BAND FILTERS

The design procedures in Secs. 12.04 and 12.09 give the reactance-slope parameters x_i or susceptance-slope parameters b_i of the resonators of a narrow-stop-band filter and the impedances or admittances of the connecting lines. The practical design of microwave band-stop resonators so as to have prescribed slope parameters will now be considered.

In strip transmission line or coaxial line, the circuit of Fig. 12.04-1 may be realized by using non-contacting stubs, as shown in Fig. 12.01-1(a), with the gaps between the stubs and the main line forming the capacitances required in Fig. 12.04-1, and the stubs approximating the inductances. The stubs may be short-circuited and just under 90 degrees long, as shown in Fig. 12.01-1(a) and indicated in Fig. 12.05-1(a); or they may be open-circuited and just under 180 degrees long, as indicated in Fig. 12.05-1(b). Figures 12.05-1(c) and (d) show the corresponding dual cases. The inductively coupled resonator in Fig. 12.05-1(d) which is slightly less than a half wavelength long at resonance, is the type of resonator used in the waveguide band-stop filter in Fig. 12.01-1(b). The case of Fig. 12.05-1(a) will now be treated specifically, and then the cases of Figs. 12.05-1(b), (c), and (d) can be treated by extension of this first case.

The transmission lines will be supposed to be non-dispersive. (If waveguide or other dispersive line is used, replace normalized frequency ω/ω_0 by normalized reciprocal guide wavelength λ_{g0}/λ_g, where λ_g and λ_{g0} are the guide wavelengths at frequencies ω and ω_0, respectively.) Forcing the resonator reactance to be zero when $\omega = \omega_0$ and $\phi = \phi_0$ requires that

$$Z_b \tan \phi_0 = \frac{1}{\omega_0 C_b} \qquad (12.05-1)$$
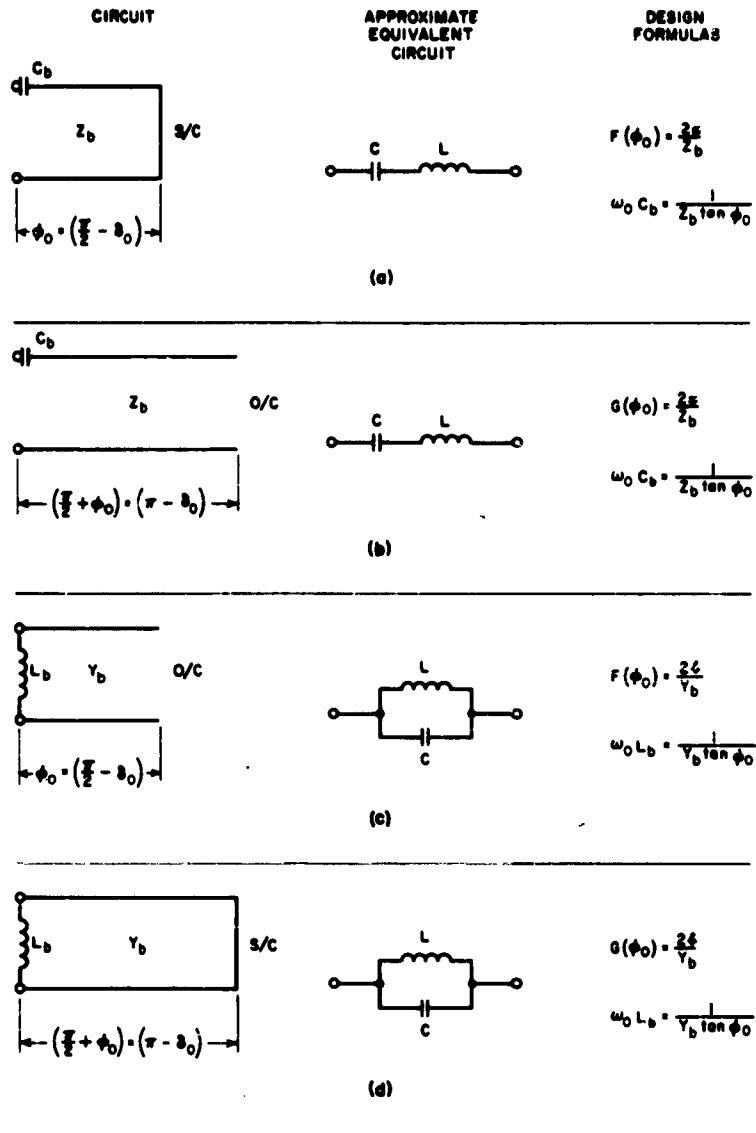
| CIRCUIT | APPROXIMATE EQUIVALENT CIRCUIT | DESIGN FORMULAS |

(a)

(b)

(c)

(d)

WHERE $F(\phi) = \phi \sec^2\phi + \tan\phi$ (TABLE 2)

$G(\phi) = 2F(\phi) + \frac{1}{2}(2\delta - \sin 2\delta)$

B-3527-23I

FIG. 12.05-1   REALIZATION OF RESONANT CIRCUITS IN TRANSMISSION LINE: (a) AND (b), SERIES RESONANT CIRCUIT, SUITABLE FOR STRIP OR COAXIAL LINE; (c) AND (d), SHUNT RESONANT CIRCUIT, SUITABLE FOR WAVEGUIDE

Since ϕ is proportional to ω,

$$\frac{d\phi}{\phi} = \frac{d\omega}{\omega} \quad , \qquad (12.05-2)$$

and the reactance slope parameter is

$$\alpha = \frac{\omega_0}{2} \frac{d}{d\omega} \left(Z_b \tan \phi - \frac{1}{\omega C} \right) \Bigg|_{\omega = \omega_0, \phi = \phi_0} \qquad (12.05-3)$$

$$= \frac{Z_b}{2} (\phi_0 \sec^2 \phi_0 + \tan \phi_0) = \frac{Z_b}{2} F(\phi_0) \qquad (12.05-4)$$

where the function $F(\psi)$ is defined by

$$F(\phi) = \phi \sec^2 \phi + \tan \phi \quad . \qquad (12.05-5)$$

This function can be determined numerically from Table 12.05-1.

To determine the three parameters C_b, Z_b, and ϕ_0, one of them may be selected arbitrarily, for instance Z_b. The slope parameter α or b is determined from Fig. 12.04-1 or 12.04-2, or from Sec. 12.09. For the circuit of Fig. 12.05-1(a), ϕ_0 is determined from the assumed value for Z_b by use of Eq. (12.05-4) and Table 12.05-1, and finally Eq. (12.05-1) yields C_b. These formulas and the ones corresponding to all four cases are summarized in Fig. 12.05-1.

For a given ϕ_0 and Z_b or Y_b, the slope parameter of the near-180-degree line is almost twice as great as the slope parameter of the near-90-degree line. More precisely, for the near-180-degree lines [Cases (b) and (d) in Fig. 12.05-1] one has to substitute

$$G(\phi) = \left(\frac{\pi}{2} + \phi \right) \sec^2 \phi + \tan \phi \qquad (12.05-6)$$

(ϕ in radians) for $F(\phi)$, which was used with the near-90-degree lines [Cases (a) and (c) in Fig. 12.05-1]. This can be written more conveniently as

$$G(\phi) = 2F(\phi) + \frac{2\delta - \sin 2\delta}{\pi} \qquad (12.05-7)$$

731

Table 12.05-1

TABLE OF $F(\phi) = \phi \sec^2 \phi + \tan \phi$

$\phi°$	$F(\phi)$	$\phi°$	$F(\phi)$	$\phi°$	$F(\phi)$	$\phi°$	$F(\phi)$	$\phi°$	$F(\phi)$	$\phi°$	$F(\phi)$
89.80	128907.01	83.80	134.59	77.80	35.03	71.80	15.88	65.80	9.05	59.00	5.54
89.60	32227.14	83.60	126.34	77.60	33.92	71.60	15.54	65.60	8.91	58.00	5.20
89.40	14324.32	83.40	118.82	77.40	32.86	71.40	15.22	65.40	8.77	57.00	4.89
89.20	8057.53	83.20	111.96	77.20	31.85	71.20	14.90	65.20	8.63	56.00	4.60
89.00	5157.05	83.00	105.68	77.00	30.88	71.00	14.59	65.00	8.49	55.00	4.34
88.80	3581.46	82.80	99.91	76.80	29.96	70.80	14.29	64.80	8.36	54.00	4.10
88.60	2631.38	82.60	94.60	76.60	29.09	70.60	14.00	64.60	8.23	53.00	3.88
88.40	2014.78	82.40	89.71	76.40	28.24	70.40	13.72	64.40	8.10	52.00	3.67
88.20	1592.03	82.20	85.19	76.20	27.44	70.20	13.45	64.20	7.98	51.00	3.48
88.00	1289.64	82.00	81.00	76.00	26.67	70.00	13.19	64.00	7.86	50.00	3.30
87.80	1065.91	81.80	77.11	75.80	25.93	69.80	12.93	63.80	7.74	49.00	3.13
87.60	895.73	81.60	73.50	75.60	25.22	69.60	12.68	63.60	7.62	48.00	2.98
87.40	763.30	81.40	70.14	75.40	24.55	69.40	12.44	63.40	7.51	47.00	2.83
87.20	658.21	81.20	67.01	75.20	23.89	69.20	12.21	63.20	7.40	46.00	2.69
87.00	573.44	81.00	64.08	75.00	23.27	69.00	11.98	63.00	7.29	45.00	2.57
86.80	504.05	80.80	61.34	74.80	22.67	68.80	11.76	62.80	7.19	44.00	2.44
86.60	446.55	80.60	58.77	74.60	22.09	68.60	11.54	62.60	7.08	43.00	2.33
86.40	398.36	80.40	56.36	74.40	21.53	68.40	11.33	62.40	6.98	42.00	2.22
86.20	357.58	80.20	54.10	74.20	21.00	68.20	11.13	62.20	6.88	41.00	2.12
86.00	322.76	80.00	51.97	74.00	20.48	68.00	10.93	62.00	6.79	40.00	2.02
85.80	292.79	79.80	49.97	73.80	19.99	67.80	10.73	61.80	6.69	39.00	1.93
85.60	266.82	79.60	48.08	73.60	19.51	67.60	10.55	61.60	6.60	38.00	1.84
85.40	244.16	79.40	46.29	73.40	19.05	67.40	10.36	61.40	6.51	37.00	1.76
85.20	224.27	79.20	44.61	73.20	18.60	67.20	10.18	61.20	6.42	36.00	1.68
85.00	206.73	79.00	43.01	73.00	18.17	67.00	10.01	61.00	6.33	35.00	1.61
84.80	191.16	78.80	41.50	72.80	17.76	66.80	9.84	60.80	6.24	34.00	1.53
84.60	177.29	78.60	40.07	72.60	17.36	66.60	9.68	60.60	6.16	33.00	1.46
84.40	164.89	78.40	38.71	72.40	16.97	66.40	9.51	60.40	6.08	32.00	1.40
84.20	153.74	78.20	37.42	72.20	16.59	66.20	9.36	60.20	6.00	31.00	1.33
84.00	143.69	78.00	36.19	72.00	16.23	66.00	9.20	60.00	5.92	30.00	1.27

Note:

$F(\phi) = (1/2)G(\phi)$

where

$$\delta \;=\; \frac{\pi}{2} - \phi \qquad\qquad (12.05\text{-}8)$$

is the amount by which the line length falls short of $\pi/2$ or π radians, respectively. The last term in Eq. (12.05-7), namely $(2\delta - \sin 2\delta)/\pi$, is usually very small, so that $G(\phi)$ is very nearly twice $F(\phi)$. For instance, when $\phi = \pi/3 = 60$ degrees, the error in $G(\phi)$ due to neglecting this term in Eq. (12.05-7) is less than ½ percent, while for $\phi = \pi/4 = 45$ degrees, the error is 3.4 percent. One may therefore still use Table 12.05-1 to solve for ϕ_0, looking up $F(\phi) = (1/2)G(\phi)$, and subse quently making a small correction if ϕ_0 is smaller than about 60 degrees.

SEC. 12.06, EXPERIMENTAL ADJUSTMENT OF THE COUPLINGS AND TUNING OF BAND-STOP RESONATORS

In constructing resonators of the forms in Fig. 12.05, usually the coupling capacitances C_k are realized by capacitive gaps, while the coupling inductances L_k usually apply to waveguide filters where the coupling inductance is achieved by an inductive iris. Since it is often difficult to compute the appropriate gap or iris size with as much ac- curacy as is desired, it is frequently convenient to experimentally adjust these couplings to their proper value. This is done most easily by testing one resonator at a time with the other resonators removed (in the case of a strip-line filter with capacitive gaps), or with the coupling irises of the other resonators covered with aluminum tape (in the case of a waveguide filter). Using this procedure the measured 3-db bandwidth for each resonator can be compared with a computed value, and the coupling altered until the computed value of 3-db bandwidth is obtained. Since in many cases the filter will be symmetrical, it will usually be only necessary to make this test on half of the resonators. Once the proper coupling gaps or iris sizes have been determined, they are simply duplicated for the other half of the filter.

The 3-db fractional bandwidths of the four types of resonators in Fig. 12.05-1 are given in Fig. 12.06-1. Case (a) in Fig. 12.06-1 may, for instance, be derived by noting that the insertion loss of a react- ance X in shunt with two resistances $R_a = R_1$ is 3 db when the reactance has the value $X = (1/2)R_1$. By Eq. (12.05-4)

R_0 FIG. 12.05-1(a) R_1

$$u = \frac{R_1}{Z_b} \frac{h(r)}{F(\phi_0)}$$

(a)

R_0 FIG. 12.05-1(b) R_1

$$u = \frac{R_1}{Z_b} \frac{h(r)}{G(\phi_0)}$$

(b)

FIG. 12.05-1(c)

G_0 G_1

$$u = \frac{G_1}{Y_b} \frac{h(r)}{F(\phi_0)}$$

(c)

FIG. 12.05-1(d)

G_0 G_1

$$u = \frac{G_1}{Y_b} \frac{h(r)}{G(\phi_0)}$$

(d)
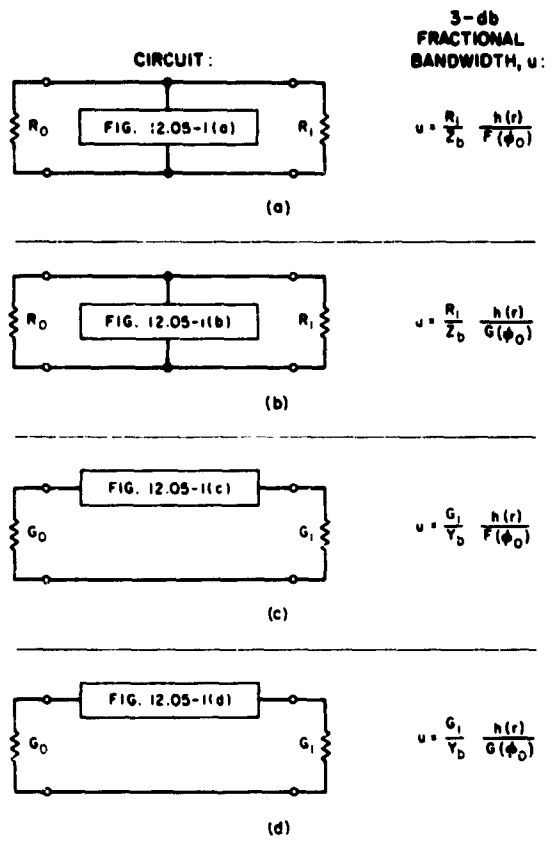
WHERE $h(r) = \dfrac{1}{\left[r - \left(\frac{r-1}{2} \right)^2 \right]^{1/2}}$

$r = R_1/R_0$ IN CASES (a) AND (b),

$r = G_1/G_0$ IN CASES (c) AND (d).

NOTE IF $R_1 = R_0$ OR $G_1 = G_0$, THEN $h(r) = 1$

B-3527-232R

FIG. 12.06-1   THREE-db FRACTIONAL BANDWIDTHS OF THE RESONATORS IN FIG. 12.05-1 PLACED ACROSS THE JUNCTION OF TWO TRANSMISSION LINES

$$\frac{Z_b}{2} F(\phi_0) \;=\; \alpha \;=\; -\frac{\omega_0}{2} \left.\frac{dX}{d\omega}\right|_{\omega=\omega_0} \quad . \qquad (12.06\text{-}1)$$

Since we are only considering small bandwidths, we may replace $2d\omega/\omega_0$ by the 3-db bandwidth, u, and dX by $(1/2)R_1$. Then

$$u \;=\; \frac{R_1}{Z_b} \frac{1}{F(\phi_0)} \quad . \qquad (12.06\text{-}2)$$

This equation would apply to the case of a resonator of the form in Fig. 12.05-1(a) connected across a uniform transmission line of characteristic impedance equal to $Z_0 = R_0 = R_1$ which is terminated at both ends in its characteristic impedance.

The equations in Fig. 12.06-1(a) and 12.06-1(b) were derived in a similar but more general fashion. Note that these equations provide for unequal loading at the left and right sides of the resonators. This is of interest for cases where the main transmission line may have impedance steps in it. In narrow-stop-band filters the loading resistances R_0 and R_1 can be estimated by computing the impedances seen looking left and right from the resonator in question with all other resonators removed. These impedances will be purely real at ω_0, but, of course, they will vary with frequency if impedance steps are present. However, in the case of narrow-stop-band filters, it should in most cases be permissible to regard these impedances as constant resistances across the range of interest. This is because the frequency band involved is small, and in practical situations any impedance steps involved will usually also be small. In many practical cases the main-line impedances will all be equal so that the factor $h(r)$ in Fig. 12.06-1 is equal to one.

The discussion above also applies to the dual cases in Fig. 12.06-1(c) and 12.06-1(d), where the equations are in terms of admittances instead of impedances. We may note in passing that if $r = R_1/R_0$ or G_1/G_0 is greater than $3 + 2\sqrt{2} = 5.8284$ or less than $3 - 2\sqrt{2} = 0.1716$, then the 3-db bandwidth does not exist, since the intrinsic mismatch of the junction causes a 3-db reflection loss and any reactance at the junction can only serve to increase it. A 10-db or similar bandwidth would then have to be used for the experimental adjustment. However, such cases are not likely to arise in practice and will not be considered further.

735

In the case of filters with narrow stop bands, the tuning of the resonators must be quite precise if the response is to be as specified. Tuning is easily accomplished using tuning screws located in a high-voltage region of each resonator. One resonator should be tuned at a time while the other resonators are detuned or decoupled by adding foreign bodies near the other resonators (in the case of a strip-line filter) or by covering the coupling irises of the other resonators with aluminum tape (in the case of waveguide filters). With the other resonators detuned or decoupled, a signal at the mid-stop-band frequency is fed through the main line of the filter, and then the resonator in question is tuned to give maximum attenuation of the signal (around 30 or 40 db in many practical cases). The main advantage in incapacitating the other resonators while any given resonator is being tuned is that this technique helps to keep the signal level sufficiently high so that a distinct minimum can be obse ed when each resonator is tuned. If more than one resonator is resonant at a time the signal level may become so low as to be undetectable.

SEC. 12.07, EXAMPLE OF A STRIP-LINE, NARROW-STOP-BAND FILTER DESIGN

Let us suppose that a filter is desired with the following specifications:

Frequency of infinite attenuation, f_0: 4.0 Gc

Pass-band ripple: 0.5 db

Fractional stop-band bandwidth to equal-ripple (0.5-db) points: $w = 0.05$

Minimum attenuation over 2-percent stop band: 20 db.

In order to estimate the number of resonators required, Eq. (12.02-1) is used in the form

$$\left| \frac{\omega'}{\omega_1'} \right| = \left| \frac{w}{\frac{\omega}{\omega_0} - \frac{\omega_0}{\omega}} \right| \qquad (12.07\text{-}1)$$

which with $w = 0.05$ and $\omega/\omega_0 = 1.01$ (corresponding to the prescribed upper 20-db point) yields $\left| \omega'/\omega_1' \right| = 2.5$. From Fig. 4.03-7, which applies to Tchebyscheff prototypes with 0.5-db ripple, we find that for $\left| \omega'/\omega_1' \right| = 2.5$

736

the attenuation is 12.5 db for $n = 2$ and 26 db for $n = 3$. Thus a design with $n = 3$ resonators will be required. Since the peak attenuation of this filter will surely be much greater than 20 db, the calculation of peak attenuation at ω_0 (discussed in Sec. 12.03) need not be made in order to fix the design. The design equations in Sec. 12.04 will be used in working out this example; however, the somewhat more accurate equations in Sec. 12.09 could also be used.

From Table 4.05-2(a), the low-pass prototype parameters for 0.5-db ripple and $n = 3$ are

$$g_0 = g_4 = 1.0$$

$$g_1 = g_3 = 1.5963 \qquad\qquad (12.07\text{-}2)$$

$$g_2 = 1.0967$$

and $\omega' = 1$. The filter takes the form shown in Fig. 12.01-1(a). From Fig. 12.04-1(a) with $Z_0 = Z_1$,

$$\left. \begin{array}{c} \dfrac{\alpha_1}{Z_0} = \dfrac{\alpha_3}{Z_0} = 12.528 \\[20pt] \dfrac{\alpha_2}{Z_0} = 18.232 \end{array} \right\} \qquad (12.07\text{-}3)$$

The physical embodiment of the filter is shown in Fig. 12.07-1.

The characteristic impedance of the main line, Z_0, was made 50 ohms, and the line consisted of a solid strip conductor 0.184 inch wide and 0.125 inch high, with a ground-plane spacing of 0.312 inch. The branch stubs were each made of square cross section, 0.125 inch by 0.125 inch, which gave the impedances $Z_{b1} = Z_{b2} = Z_{b3} = 59.4$ ohms (by Fig. 5.04-2). Therefore from Fig. 12.05-1(a),

and

$$\left. \begin{array}{c} F(\phi_{01}) = F(\phi_{03}) = \dfrac{2\alpha_1}{Z_0} \cdot \dfrac{Z_0}{Z_{b1}} = 21.1 \\[20pt] F(\phi_{02}) = \dfrac{2\alpha_2}{Z_0} \cdot \dfrac{Z_0}{Z_{b2}} = 30.7 \end{array} \right\} \qquad (12.07\text{-}4)$$
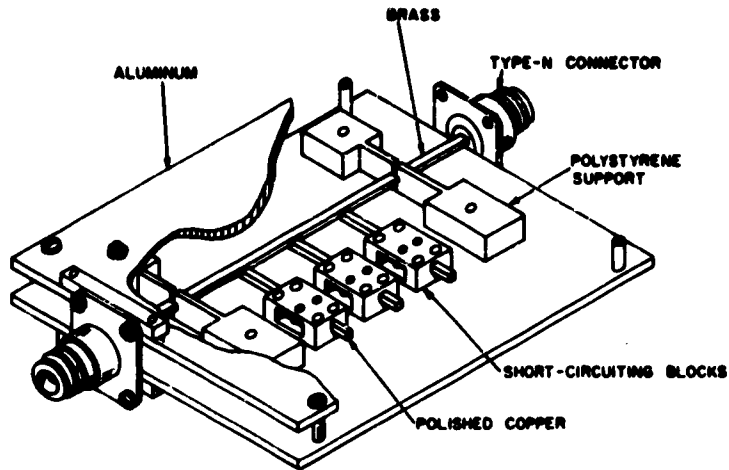
737

FIG. 12.07-1 A STRIP-LI.. BAND-STOP FILTER
WITH TH' RESONATORS

which can be solved by Table 12.05-1 to give

$$\left. \begin{array}{rcl} \phi_{01} = \phi_{03} = 74.2^\circ = 1.295 & \text{radians} \\ \phi_{02} = 77.0^\circ = 1.344 & \text{radians} \end{array} \right\} \quad (12.07\text{-}5)$$

Again from Fig. 12.05-1(a) we obtain

$$\left. \begin{array}{rcl} \omega_0 C_{b_1} = \omega_0 C_{b_3} = 0.004764 & \text{mho} \\ \omega_0 C_{b_2} = 0.003888 & \text{mho} \end{array} \right\} \quad (12.07\text{-}6)$$

which at 4.0 Gc yields

$$\left. \begin{array}{rcl} C_{b_1} = C_{b_3} = 0.1893 & \text{pf} \\ C_{b_2} = 0.1546 & \text{pf} \end{array} \right\} \quad (12.07\text{-}7)$$

738

With 0.125-by-0.125-inch stubs, such capacitances are obtained with a gap of the order of 0.031 inch, which is a quite suitable value, being small compared to a wavelength but still large enough to be achieved accurately without special measures such as using dielectric in the gap, which would increase the dissipation loss.

The length of the stubs is determined by Eq. (12.07-5) and the wavelength, which is 2.950 inches at 4.0 Gc. It was at first assumed that the reference plane was in the gap face opposite the main line. The capacitive gap of each stub was adjusted to give peak attenuation at 4.0 Gc and the 3-db bandwidth of the stop band of stubs 1 and 2 were then measured individually. The 3-db fractional bandwidths u_1 are given by Fig. 12.06-1(a):

$$\left. \begin{array}{l} u_1 = u_3 = \dfrac{Z_0}{Z_{b_1}} \dfrac{1}{F(\psi_{01})} = 0.040 \\[20pt] u_2 = \dfrac{Z_0}{Z_{b_2}} \dfrac{1}{F(\psi_{02})} = 0.0274 \end{array} \right\} \qquad (12.07\text{-}8)$$

At first, the measured bandwidths were slightly too narrow, showing the coupling to be too loose. The coupling gaps of the stubs were reduced until the required 3-db bandwidths were obtained. Then the lengths of the stubs were corrected to give the desired 4-Gc resonant frequency. The final dimensions were: outer stub lengths 0.605 inch, gaps 0.0305 inch; middle stub length 0.629 inch, gap 0.045 inch. The three stubs were then placed along the line as shown in Fig. 12.07-1. They are nominally 90 degrees apart between reference planes at 4.0 Gc, but the spacing is not critical, and they were simply placed a quarter-wavelength apart between centers (0.738 inch), and not further adjusted.

It is important that there should be no interaction, or mutual coupling, between stubs: with a ground-plane spacing of 0.312 inch, the attenuation of the TE_{10} mode (electric vector parallel to the ground planes) from stub to stub is more than 50 db at 4.0 Gc, which should be adequate; it is also necessary to maintain proper centering so as not to excite the parallel-plate mode.

The response of this filter was computed on a digital computer and is plotted in Fig. 12.07-2. The points shown are the measured results on the experimental filter. The circles represent the measured reflection loss of the filter, which may be compared with the computed curve, while the solid dots represent the total measured attenuation, including the effect of dissipation. The computed reflection loss reaches a ripple height of 0.7 db below, and 0.8 db above 4.0 Gc (instead of 0.5 db, which was called for by the low-pass prototype). The measured reflection loss reaches a peak of 1.2 db below, and 0.7 db above 4.0 Gc.

The somewhat oversize pass-band ripples in this filter are due mainly to the frequency sensitivity of the $\lambda_0/4$ coupling lines between resonators.
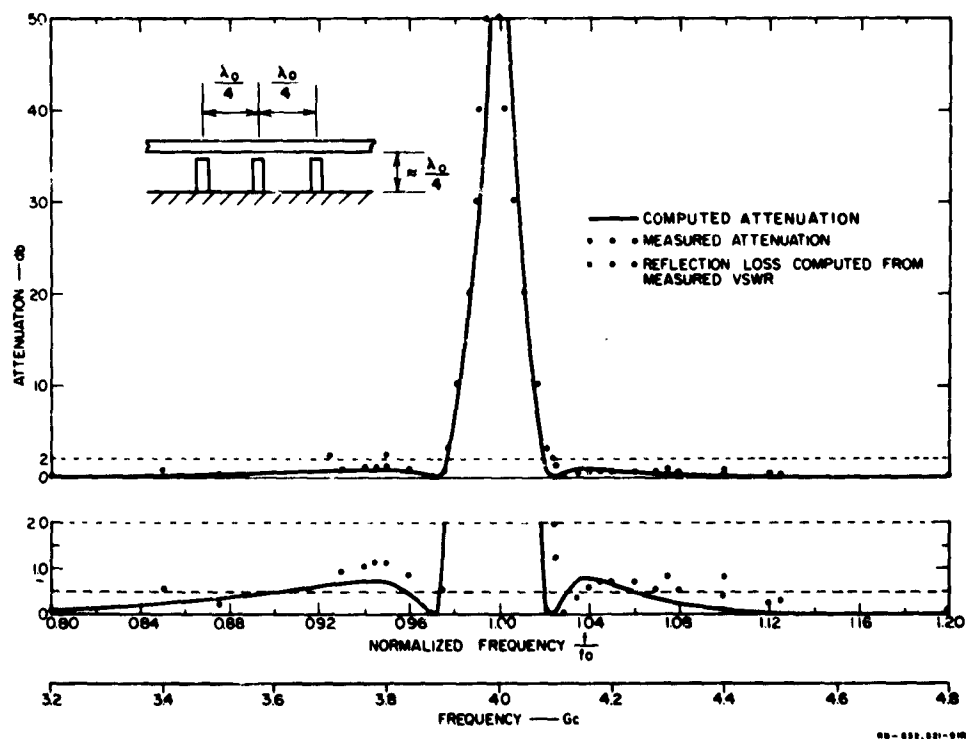
FIG. 12.07-2 COMPUTED AND MEASURED RESPONSE OF A STRIP-LINE BAND-STOP
FILTER WITH $\lambda_0/4$ SPACINGS BETWEEN RESONATORS

If the design method described in Sec. 12.09 is used, selectivity of the coupling lines can be taken into account in the design process so that the pass-band ripples should be very nearly as prescribed. A possible drawback of the procedure in Sec. 12.09 is that it necessarily calls for steps in the impedance level of the main transmission line. However, in the case of a strip-line filter, this should cause little difficulty. If this same filter design were to be obtained by the methods of Sec. 12.09, the main-line impedances and the resonator slope parameters would be obtained by the equations of that section. From that point on, the design procedure would be the same as described above.

The peak attenuation of the three-resonator filter was too great to measure, but the peak attenuation of each branch separately was measured. This gave 32 db for each of the two outer branches, and 28 db for the middle branch alone. Working back from the data in Fig. 12.03-2, this leads to unloaded Q values of 1000. The theoretical unloaded Q of such a pure all-copper line at this frequency is 2600. In this case the strip conductors of the resonators were made of polished copper and the ground planes were aluminum. Other losses were presumably introduced by the current concentrations caused by fringing fields at the gap, and by the short-circuit clamps. The value of $Q_u = 1000$ is consistent with experimental results generally obtained. The peak attenuation of all three branches together should by the first formula of Fig. 12.03-2 reach a value of 104 db, which, however, was beyond the measurement range of the available test equipment. There are, of course, additional stop bands at frequencies where the stubs are roughly an odd multiple of $\lambda_0/4$ long.

According to the formula for the dissipation loss ΔL_A in Fig. 12.03-2, the dissipation loss should be about 0.74 db at the equal-ripple band edges ω_1 and ω_2. The measurements indicated dissipation loss of roughly that size at the pass-band edges.

The bandwidth of the stop band to the 0.5-db points, both measured and computed, is very nearly 5.0 percent, the design goal. The attenuation over a 2-percent band exceeds 25.4 db by computation. (Compare the 20-db design specification, and the 25.8 db predicted for a three-branch filter.) The measured points in the stop band fall close to the computed curve, as can be seen from Fig. 12.07-2. For frequencies moving away from the stop-band edges into the pass bands, the dissipation loss will drop quite rapidly.

741

SEC. 12.08, NARROW-STOP-BAND WAVEGUIDE FILTER DESIGN
CONSIDERATIONS, AND AN EXAMPLE

A waveguide band-stop filter is most conveniently realized using resonators connected in series and spaced an odd multiple of a quarter wavelength apart along the waveguide. The equivalent circuit of such a filter is as shown in Fig. 12.04-2, while Fig. 12.01-1(b) shows a sketch of a waveguide realization of such a filter. It is seen that the resonators in Fig. 12.01-1(b) are spaced at intervals of three-quarters of a guide wavelength. It is believed that placing the reso-nators at one-quarter guide-wavelength intervals is not practical, because strong interaction results between the resonators by way of the fields about the coupling apertures. This interaction in an experimental band-stop filter, with quarter-guide-wavelength-spaced resonators, caused the stop-band response to have three peaks of high attenuation, with relatively low attenuation valleys in between, instead of the single high attenuation peak that is desired.

The appropriate normalized frequency variable to use with dispersive lines, as in a waveguide filter, is the normalized reciprocal guide wave-length, λ_{g0}/λ_{g}. Thus, a waveguide filter and a strip-line filter, each designed from the same low-pass prototype, can have identical responses if the waveguide filter response is plotted on a λ_{g0}/λ_{g} scale and the strip-line filter response on a ω/ω_0 scale. On this basis, the formula, which for the strip-line filter was

$$w = \frac{\omega_2 - \omega_1}{\omega_0} = \frac{\omega_2}{\omega_0} - \frac{\omega_1}{\omega_0} \quad \text{(TEM mode)} \qquad (12.08-1)$$

where ω_0, ω_1, and ω_2 are as defined in Fig. 12.02-2, is now replaced for a waveguide filter by

$$w_\lambda = \frac{\lambda_{g0}}{\lambda_{g2}} - \frac{\lambda_{g0}}{\lambda_{g1}} \quad \text{(waveguide)} \qquad (12.08-2)$$

where λ_{g0}, λ_{g1}, and λ_{g2} are analogously defined as the guide wavelengths at mid-stop-band, and at the lower and upper edges of the stop band, on a reciprocal guide-wavelength scale. If both responses are plotted on a frequency scale, however, the response of the waveguide filter derived

from the same prototype will be considerably narrower. For small stop-band bandwidths, the fractional width of the waveguide filter stop band on a frequency scale will be approximately $(\lambda_0/\lambda_{g0})^2$ times w_λ, which is the fractional bandwidth on a reciprocal guide-wavelength scale given by Eq. (12.08-2). (λ_0 is the free-space wavelength at the center of the stop band.) Thus in designing for a frequency fractional bandwidth w, the bandwidth w_λ in the formulas is set to be equal to $(\lambda_{g0}/\lambda_0)^2 w$ for the narrow bandwidths considered here.

In the waveguide filter each resonator formed from a waveguide of characteristic admittance Y_b, which has a length slightly less than one-half guide wavelength, is connected to the main waveguide of characteristic admittance Y_0 by means of a small elongated coupling iris. Each coupling iris has a length, l, which is less than one-half free-space wavelength, and can be represented to a good approximation as an inductance in series with the main waveguide. The equivalent circuit of the resonator and coupling iris combination is shown in Fig. 12.05-1(d).

The susceptance, B, of each coupling iris can be determined approximately in terms of the magnetic polarizability, M', of the iris. From Fig. 5.10-11 the expression is found to be

$$\frac{B}{Y_b} = -\frac{\lambda_g ab'}{4\pi M_1'} \tag{12.08-3}$$

where a and b' are as defined in Fig. 12.01-1(b). For irises cut in walls of infinitesimal thickness, t, having a length l which is much less than one-half free-space wavelength, the magnetic polarizability $M_1' = M_1$ is given in Fig. 5.10-4(a). In the usual situation when t is not infinitesimal and l is not much less than one-half free-space wavelength, one must use the magnetic polarizability M_1', which is related to M_1 by the approximate empirical relation

$$M_1' = \frac{M_1}{1 - \left(\frac{2l}{\lambda_0}\right)^2} \, 10^{-\left(\frac{1.36t}{l}\right)\sqrt{\left(1 - \frac{2l}{\lambda_0}\right)^2}} \tag{12.08-4}$$

where λ_0 is again the free-space wavelength at center frequency

corresponding to $\omega = \omega_0$, $\phi = \phi_0$, and $\lambda_g = \lambda_{g0}$. The resonant condition for each resonator becomes

$$Y_0 \tan \phi_0 = \frac{Y_b ab'}{4\pi M'_1} \lambda_{g0} \qquad (12.08\text{-}5)$$

where

$$\phi_0 = \frac{2\pi L}{\lambda_{g0}} - \frac{\pi}{2} \quad , \qquad (12.08\text{-}6)$$

and L is the length of the resonator.

The susceptance slope parameter, b, for each resonator as viewed from the main transmission line becomes

$$b = \frac{Y_b}{2} G(\phi) = Y_b F(\phi) \qquad (12.08\text{-}7)$$

where $F(\phi)$ is defined in Eq. (12.05-5) and $G(\phi)$ is defined in Eq. (12.05-7), and M'_1 has been assumed to be frequency invariant.

Example of a Waveguide Filter Design—As an example of the use of the above technique, we consider here the design of a 3-resonator waveguide band-stop filter using the same low-pass prototype circuit used for the strip-line filter described in Sec. 12.07. The filter has a design center frequency $f_0 = 10$ Gc and the resonators and main transmission line are fabricated from WR-90 waveguide. The fractional bandwidth of the strip-line filter was $w = 0.05$ on a frequency basis [Eq. (12.08-1)]. Here, we use $w_\lambda = 0.05$ on a reciprocal guide-wavelength basis [Eq. (12.08-2)]. The susceptance slope parameters for the two end resonators and the middle resonator can be determined from Fig. 12.04-2(a) with $Y_1 = Y_0$. They are, respectively,

$$\frac{b_1}{Y_0} = \frac{1}{\omega'_1 g_0 g_1 w_\lambda} = \frac{b_3}{Y_0} = 12.528$$

$$\qquad (12.08\text{-}8)$$

$$\frac{b_2}{Y_0} = \frac{g_0}{\omega'_1 g_2 w_\lambda} = 18.232$$

744

which correspond exactly to those previously computed for the strip-line filter. The stub characteristic admittances Y_b were chosen to be equal to Y_0. Therefore,

$$G(\phi_{01}) = G(\phi_{03}) = \frac{2b_1}{Y_0} = 25.056$$

$$(12.08\text{-}9)$$

$$G(\phi_{02}) = \frac{2b_2}{Y_0} = 36.464 \quad .$$

Referring to Table 12.05-1, we find

$$\phi_{01} + 90° = \phi_{03} + 90° = 159.5°$$

$$(12.08\text{-}10)$$

$$\phi_{02} + 90° = 163.0°$$

At a frequency of 10 Gc, λ_{g0} in WR-90 waveguide is 1.5631 inches. Therefore the lengths $L_1 = L_3$ of the two end resonators and length L_2 of the middle resonator are

$$L_1 = L_3 = 0.693 \quad \text{inch}$$

$$(12.08\text{-}11)$$

$$L_2 = 0.709 \quad \text{inch} \quad .$$

The magnetic polarizability, $(M_1')_1 = (M_1')_3$, of the irises in the end cavities, and the magnetic polarizability, $(M_1')_2$, of the iris in the middle cavity can be determined from Eq. (12.08-5) to be

$$(M_1')_1 = (M_1')_3 = 0.0167 \quad \text{inch}^3$$

$$(12.08\text{-}12)$$

$$(M_1')_2 = 0.0137 \quad \text{inch}^3 \quad .$$

It was decided to use elongated irises with round ends, as for the second curve from the top in Fig. 5.10-4(a). The iris sizes were determined by

first fixing the iris widths[*] as $w_1 = w_2 = w_3 = 0.125$ inch, and then computing successive approximations using Fig. 5.10-4(a) and Eq. (12.08-4). Since it was planned that the iris sizes would be checked experimentally as discussed in Sec. 12.06, the iris thickness t in Eq. (12.08-4) was assumed to be zero (which should cause the irises to come out slightly undersize). A suggested way for making these calculations is to convert Eq. (12.08-4) to the form

$$\left(M_1\right)_{k=1\,to\,3} = \left(M_1'\right)_k \left[1 - \left(\frac{2l_k}{\lambda_0}\right)^2\right] 10^{\left(\frac{1.36t}{l_k}\right)\sqrt{1-\left(\frac{2l_k}{\lambda_0}\right)^2}} \qquad (12.08\text{-}13)$$

Then using Fig. 5.10-4(a) and the desired polarizabilities $(M_1')_k$, preliminary values of the iris lengths l_k are obtained. Inserting these preliminary values of l_k in Eq. (12.08-13), compensated values $(M_1)_k$ for the polarizabilities are obtained which are then used with Fig. 5.10-4(a) to obtain compensated values for the iris lengths l_k. If desired, this procedure can be repeated in order to converge to greater mathematical accuracy; however, since Eq. (12.08-13) is in itself a rather rough approximation, the value of very high mathematical accuracy is rather doubtful.

By the above procedure, initial iris dimensions of $l_1 = l_3 = 0.430$ inch and $l_2 = 0.415$ inch for the iris lengths with $w_1 = w_2 = w_3 = 0.125$ inch were obtained. After tests made by measuring the 3-db bandwidth of Resonators 1 and 2 separately (by the methods discussed in Sec. 12.06), final values of $l_1 = l_3 = 0.481$ inch and $l_2 = 0.458$ inch for the iris lengths were obtained. The first version of this filter had $\lambda_0/4$ spacings between resonators, but this was found to be unsatisfactory due to interaction between the fringing fields around the irises of the various resonators (which resulted in considerable disruption of the stop-band performance). Thus a second version was constructed with $3\lambda_0/4$ spacings between resonators, and Fig. 12.08-1 shows the dimensions of this filter.

---

[*] The slot width w [Fig. 5.10-4(a)] is represented by the same symbol as the fractional bandwidth. This is the usual notation for both quantities. Since the slot calculation is only incidental in this context, it was felt to be less confusing to retain the w for slot width, than to change it.
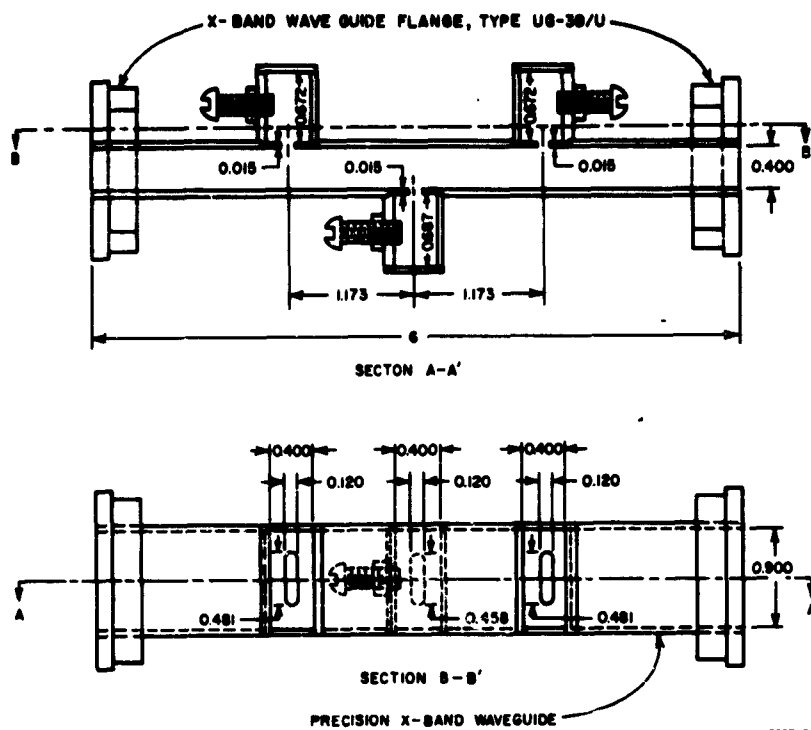
X-BAND WAVE GUIDE FLANGE, TYPE UG-38/U

0.015   0.015   0.015   0.400

1.173   1.173

SECTON A-A'

0.400   0.400   0.400
0.120   0.120   0.120

0.900

0.481   0.458   0.481

SECTION B-B'

PRECISION X-BAND WAVEGUIDE

A-3527-318

FIG. 12.08-1   DIMENSIONS OF A WAVEGUIDE BAND-STOP FILTER

The filter was tuned using the technique discussed in Sec. 12.06.
Figure 12.08-2 shows points from the resulting measured response of the
filter as compared with the theoretical response of this filter design
as determined using a digital computer. As can be seen from the figure,
the agreement is excellent.

Though the measured performance of this filter is in very good
agreement with its computed performance, it will be noted from Fig. 12.08-2
that the computed performance indicates pass-band ripples of about 1.2 db
instead of 0.5 db as was called for by the lumped-element prototype.
These oversize ripples have been found to be due to the frequency sensi-
tivity of the lines between resonators. If the $3\lambda_g/4$ coupling lines
between resonators were replaced by ideal impedance inverters the

Tchebyscheff ripples would be exactly 0.5 db. Computer calculations show that if $\lambda_0/4$ coupling lines are used, the ripples should peak at approximately 0.7 db. In Fig. 12.08-2 the 1.2-db ripple peaks are due to the still greater selectivity of the $3\lambda_0/4$ coupling lines used in this design. Use of the design procedure discussed in Sec. 12.09 would make it possible to take into account the selectivity of the coupling lines so that the ripples should come out very closely as prescribed.* However, the price that must be paid for this is that the
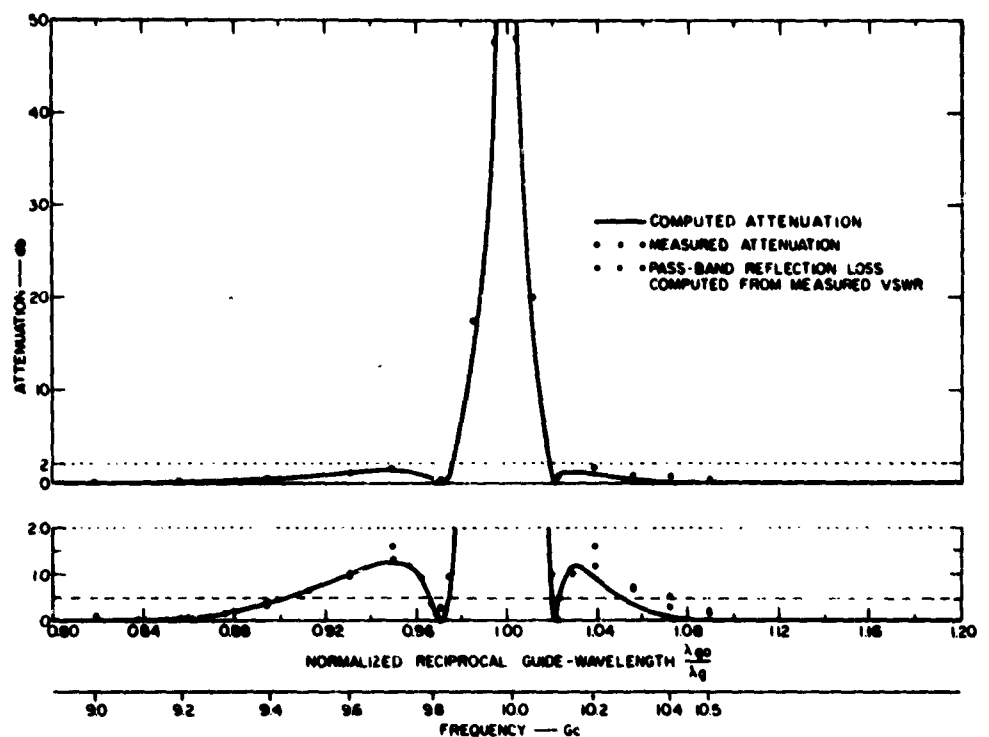
FIG. 12.08-2   COMPUTED AND MEASURED RESPONSE OF THE WAVEGUIDE BAND-STOP FILTER IN FIG. 12.08-1

* The design procedure described in Sec. 12.09 is exact if the filter is realized using only transmission lines and stubs. However, in the case of narrow-stop-band filters the stub impedances become unreasonable so that it is necessary to replace them with reactively coupled resonators. This substitution, of course, introduces an approximation.

procedure in Sec. 12.09 necessarily requires that there be steps in impedance along the main line of the filter. This introduces some added complication for manufacturing, but the difficulties introduced should not be great. Once the main line impedances and the resonator slope parameters are determined from the data in Sec. 12.09, the design process is the same as that described above.

SEC. 12.09, A DESIGN PROCEDURE WHICH IS ACCURATE FOR FILTERS WITH WIDE (AND NARROW) STOP-BAND WIDTHS*

In this section an exact design procedure will be discussed which is useful for the design of band-stop filters with either wide or narrow stop bands. The design equations given apply to filters with $\lambda_0/4$ stubs separated by connecting lines which are either $\lambda_0/4$ or $3\lambda_0/4$ long, where λ_0 is the wavelength at the mid-stop-band frequency. An example of this type of filter is shown in Fig. 12.01-2. In theory this type of filter can have any stop-band width; however, in practice the impedance of the stubs becomes unreasonable if the stop-band width is very narrow. In that case it would be desirable to replace the open-circuited stub reso- nators in the filter in Fig. 12.01-2 with capacitively coupled short- circuited stub resonators [as shown in Fig. 12.01-1(a)] having the same resonator slope parameters. This introduces some approximation into the design, but permits practical impedances. As has been mentioned previously, the main difference between a practical narrow-stop-band filter design obtained by the methods of this section and one obtained by the methods of Sec. 12.04 is that the method of this section calls for steps in transmission line, while usually none are necessary by the method of Sec. 12.04. However, the method of this section will give higher design accuracy even for narrow-stop-band cases where the ap- proximation mentioned above has been introduced.

The methods of this section permit exact design of filters of the form in Fig. 12.09-1(a) or their duals (which consist of $\lambda_0/4$ short- circuited stubs in series with $\lambda_0/4$ connecting lines). Filters of these types which have been designed by the methods of this section have attenuation characteristics which are related to the attenuation characteristics of low-pass prototype filters of the form in Figs. 12.02-1 by the mapping[†]

* The equations in this section and the examples in Sec. 12.10 were worked out by B. M. Schiffman.

† It can be shown that other methods of design[2,3] can lead to circuits of the form in Fig. 12.09-1(a) which have attenuation characteristics that are not mappings of the attenuation characteristics of low-pass pro- totypes of the form in Figs. 12.02-1(a), (b).
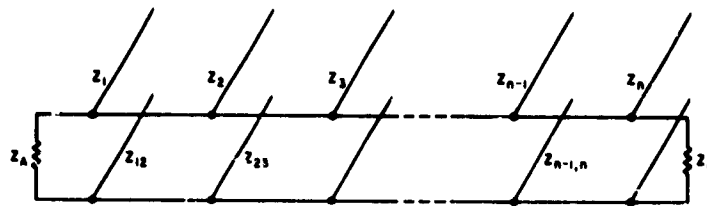
ALL STUBS AND CONNECTING LINES ARE $\lambda_0/4$ LONG

(a)
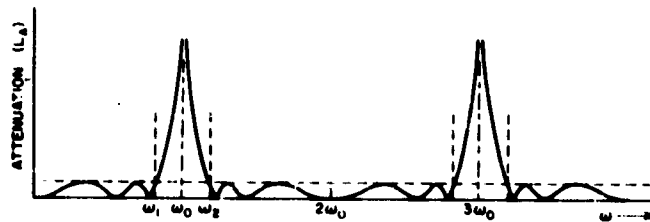
$\omega_0 = 1/2 \ (\omega_1 + \omega_2)$

$\lambda_0 = 2\pi v/\omega$

v = VELOCITY OF LIGHT IN MEDIUM

$a = \cot \ (\pi\omega_1/2\omega_0)$

$w = \dfrac{\omega_2 - \omega_1}{\omega_0}$

(b)

B-3627-363

FIG. 12.09-1   BANDSTOP FILTER: (a) n-STUB TRANSMISSION-LINE FILTER
DERIVED FROM n-ELEMENT LOW-PASS PROTOTYPE; (b) EQUI-
RIPPLE CHARACTERISTIC DEFINING CENTER FREQUENCY ω_0,
PARAMETER a, AND STOP BAND FRACTIONAL BANDWIDTH w

$$\omega' = \omega_1' a \ \tan\left(\frac{n}{2} \frac{\omega}{\omega_0}\right) \qquad (12.09\text{-}1)$$

where

$$a = \cot\left(\frac{n}{2} \frac{\omega_1}{\omega_0}\right) \qquad (12.09\text{-}2)$$

$$\omega_0 = \frac{\omega_1 + \omega_2}{2} \qquad (12.09\text{-}3)$$

ω' and ω_1' are frequency points in the low-pass filter response [such as
that in Fig. 12.02-1(d)], and ω, ω_0, ω_1, and ω_2 are frequency points in
the corresponding band-stop response in Fig. 12.09-1(b). Note that the
band-stop filter response in Fig. 12.09-1(b) has arithmetic symmetry,

750

and that the infinite attenuation point at ω_0 is repeated at frequencies
which are odd multiples of ω_0. At these frequencies the stubs in the
filter in Fig. 12.09-1(a) are an odd multiple of $\lambda_0/4$ long, so that they
short out the main line and cause infinite attenuation (theoretically).
In the dual case which uses series-connected stubs, the stubs present
open-circuits to the main line at these frequencies. Using the methods
of this section, if the low-pass prototype has, say, a Tchebyscheff re-
sponse with 0.1-db ripple, then the band-stop filter response should have
exactly 0.1-db Tchebyscheff ripple, with the entire response exactly as
predicted by the mapping Eqs. (12.09-1) to (12.09-3). (This statement,
of course, ignores problems such as junction effects which occur in the
practical construction of the filter.)

Table 12.09-1 presents design equations for filters of the form in
Fig. 12.09-1(a). After the designer has selected a low-pass prototype
filter (which gives him the parameters g_0, g_1, ..., g_{n+1}, and ω_1'); and
has specified ω_1, ω_2, and the source impedance Z_A; he can then compute
all of the line impedances. Table 12.09-1 treats filters of the form in
Fig. 12.09-1(a) having $n = 1$ up to $n = 5$ stubs. The same equations also
apply to the dual cases having short-circuited series stubs if all of the
impedances in the equations are replaced by corresponding admittances.
However, the case for which series stubs are of the most practical interest
is the case of waveguide band-stop filters, and as was noted in Sec. 12.08,
it will usually be desirable to use $3\lambda_0/4$ spacings between stubs for wave-
guide band-stop filters. Figure 12.09-2(a) shows a band-stop filter
with $3\lambda_0/4$ spacings between $\lambda_0/4$, short-circuited, series stubs, while
Fig. 12.09-2(b) shows the dual case having $\lambda_0/4$, open-circuited, shunt
stubs. Table 12.09-2 presents design equations for filters of the form
in Fig. 12.09-2(a) having $n = 2$ or $n = 3$ stubs.

As has previously been mentioned, the equations in Tables 12.09-1
and 12.09-2 are exact regardless of the stop-band width. However, in the
case of Table 12.09-1 and filter structures of the form in Fig. 12.09-1(a),
the impedances Z_j of the shunt stubs become so high as to be impractical,
in the case of narrow-stop-band designs. This difficulty can be gotten
around by replacing each open-circuited shunt stub, which has a resonator
reactance slope parameter of

$$x_j = \frac{\pi}{4} Z_j \qquad (12.09\text{-}4)$$

751

Table 12.09-1

EXACT EQUATIONS FOR BAND-STOP FILTERS
WITH $\lambda_0/4$ SPACING BETWEEN STUBS

The filter structure is as shown in Fig. 12.09-1(a). For the dual case
having short-circuited series stubs, replace all impedances in the equa-
tions below by corresponding admittances.

n = number of stubs

Z_A and Z_B = terminating impedances

Z_j ($j=1$ to n) = impedances of open-circuited shunt stubs

$Z_{j-1,j}$ ($j=2$ to n) = connecting line impedances

g_j = values of the elements of the low-pass prototype
network as defined in Fig. 12.02-1.

$\Lambda = \omega_1' a$

where

ω_1' = low-pass prototype cutoff frequency

and

a = bandwidth parameter defined in Eq. (12.09-2)

(In all cases the left terminating impedance Z_A is arbitrary).

Case of $n = 1$:

$$Z_1 = \frac{Z_A}{\Lambda g_0 g_1} \; ; \qquad\qquad Z_B = \frac{Z_A g_2}{g_0}$$

Case of $n = 2$:

$$Z_1 = Z_A \left(1 + \frac{1}{\Lambda g_0 g_1} \right) ; \qquad\qquad Z_{12} = Z_A \left(1 + \Lambda g_0 g_1 \right)$$

$$Z_2 = \frac{Z_A g_0}{\Lambda g_2} \; ; \qquad\qquad Z_B = Z_A g_0 g_3$$

Case of $n = 3$:

Z_1, Z_{12} and Z_2—same formulas as case $n = 2$

Table 12.09-1 concluded

$$Z_3 = \frac{Z_A \varepsilon_0}{\varepsilon_4}\left(1 + \frac{1}{\Lambda_{\varepsilon_3 \varepsilon_4}}\right) \quad ; \qquad\qquad Z_{23} = \frac{Z_A \varepsilon_0}{\varepsilon_4}(1 + \Lambda_{\varepsilon_3 \varepsilon_4})$$

$$Z_B = \frac{Z_A \varepsilon_0}{\varepsilon_4}$$

Case of n = 4:

$$Z_1 = Z_A\left(2 + \frac{1}{\Lambda_{\varepsilon_0 \varepsilon_1}}\right) \quad ; \qquad\qquad Z_{12} = Z_A\left(\frac{1 + 2\Lambda_{\varepsilon_0 \varepsilon_1}}{1 + \Lambda_{\varepsilon_0 \varepsilon_1}}\right)$$

$$Z_2 = Z_A\left(\frac{1}{1 + \Lambda_{\varepsilon_0 \varepsilon_1}} + \frac{\varepsilon_0}{\Lambda_{\varepsilon_2}(1 + \Lambda_{\varepsilon_0 \varepsilon_1})^2}\right) \quad ; \quad Z_{23} = \frac{Z_A}{\varepsilon_0}\left(\Lambda_{\varepsilon_2} + \frac{\varepsilon_0}{1 + \Lambda_{\varepsilon_0 \varepsilon_1}}\right)$$

$$Z_3 = \frac{Z_A}{\Lambda_{\varepsilon_0 \varepsilon_1}} \quad ; \qquad\qquad Z_{34} = \frac{Z_A}{\varepsilon_0 \varepsilon_5}(1 + \Lambda_{\varepsilon_4 \varepsilon_5})$$

$$Z_4 = \frac{Z_A}{\varepsilon_0 \varepsilon_5}\left(1 + \frac{1}{\Lambda_{\varepsilon_4 \varepsilon_5}}\right) \quad ; \qquad\qquad Z_B = \frac{Z_A}{\varepsilon_0 \varepsilon_5}$$

Case of n = 5:

Z_1, Z_{12}, Z_2, Z_{23}, Z_3—same formulas as case $n = 4$

$$Z_4 = \frac{Z_A}{\varepsilon_0}\left(\frac{1}{1 + \Lambda_{\varepsilon_5 \varepsilon_6}} + \frac{\varepsilon_6}{\Lambda_{\varepsilon_4}(1 + \varepsilon_4 \varepsilon_5)^2}\right) \quad ; \qquad Z_{34} = \frac{Z_A}{\varepsilon_0}\left(\Lambda_{\varepsilon_4} + \frac{\varepsilon_6}{1 + \Lambda_{\varepsilon_5 \varepsilon_6}}\right)$$

$$Z_5 = \frac{Z_A \varepsilon_6}{\varepsilon_0}\left(2 + \frac{1}{\Lambda_{\varepsilon_5 \varepsilon_6}}\right) \quad ; \qquad\qquad Z_{45} = \frac{Z_A \varepsilon_6}{\varepsilon_0}\left(\frac{1 + 2\Lambda_{\varepsilon_5 \varepsilon_6}}{1 + \Lambda_{\varepsilon_5 \varepsilon_6}}\right)$$

$$Z_B = \frac{Z_A \varepsilon_6}{\varepsilon_0}$$

(a)

(b)
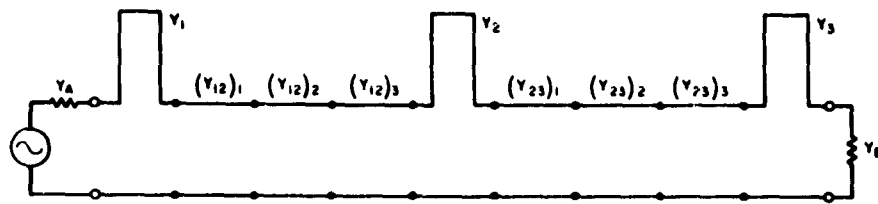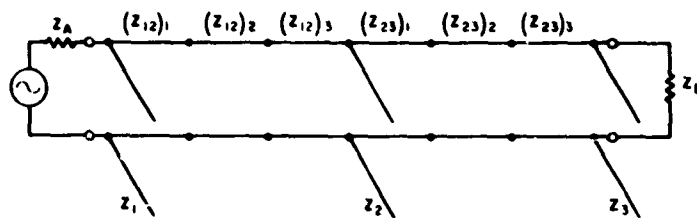
FIG. 12.09-2   BAND-STOP FILTERS WITH 3 $\lambda_0/4$ SPACING BETWEEN $\lambda_0/4$ STUBS

[see Fig. 5.08-1(d)], by a capacitively coupled short-circuited stub resonator as shown in Fig. 12.05-1(a), having the same resonator slope parameter. Then the design process becomes the same as that in the example of Sec. 12.07. The filter might take the strip-line form in Fig. 12.07-1, except that in this case the main line of the filter would have some steps in its dimensions since the connecting line impedances $Z_{j,j+1}$ are generally somewhat different from the terminating impedances. The computed performance of a filter design of this type obtained using the equations of this section is discussed in Sec. 12.10.

As previously mentioned, the case in Fig. 12.09-2(a) is of interest primarily for waveguide band-stop filters. Since the useful bandwidth of waveguides is itself rather limited, it is probable that band-stop filters with narrow stop-bands will be of most interest for the waveguide case. For narrow-stop-band designs the series-stub admittances Y_j will become so large as to make them difficult to construct (and especially difficult to

754

Table 12.09-2

EXACT EQUATIONS FOR BAND-STOP FILTERS WITH $3\lambda_0/4$ SPACING
BETWEEN STUBS OR RESONATOR IRISES

The filter structure is of the form in Fig. 12.09-2(a). For
the dual case in Fig. 12.09-2(b), replace all admittances in
the equations below with corresponding impedances.

n = number of stubs

Y_A, Y_B = terminating admittances

Y_j (j = 1 to n) = admittances of short-circuited
series stubs

$(Y_{j-1,j})_k$ = admittance of kth (k = 1, 2 or 3) con-
necting line from the left, between stubs
$j - 1$ and j

g_j = values of the elements of the low-pass prototype
network as defined in Fig. 12.02-1

Λ = $\omega_1' a$ where ω_1' = low-pass cutoff frequency and
a = bandwidth parameter defined in Eq. (12.09-2)

(In all cases the left terminating impedance is arbitrary)

Case of n - 2:

$$Y_1 = Y_A \left(1 + \frac{1}{\Lambda g_0 g_1}\right); \qquad (Y_{12})_1 = Y_A(1 + \Lambda g_0 g_1)$$

$$Y_2 = Y_A \frac{g_0}{\Lambda g_2}(1 + 2\Lambda g_2 g_3); \qquad (Y_{12})_2 = Y_A g_0 g_3 \left(\frac{1}{1 + \Lambda g_2 g_3}\right)$$

$$Y_B = Y_A g_0 g_3; \qquad (Y_{12})_3 = Y_A g_0 g_3 \left(\frac{1 + 2\Lambda g_2 g_3}{1 + \Lambda g_2 g_3}\right)$$

Case of n = 3:

$$Y_1 = Y_A \left(3 + \frac{1}{\Lambda g_0 g_1}\right) \qquad (Y_{12})_1 = Y_A \left(\frac{1 + 3\Lambda g_0 g_1}{1 + 2\Lambda g_0 g_1}\right)$$

$$(Y_{12})_2 = Y_A \left(\frac{1 + \Lambda g_0 g_1}{1 + 2\Lambda g_0 g_1}\right)$$

$$Y_2 = Y_A \frac{g_0}{\Lambda g_2} \qquad (Y_{12})_3 = Y_A(1 + \Lambda g_0 g_1)$$

$$(Y_{23})_1 = Y_A \frac{g_0}{g_4} (1 + \Lambda g_3 g_4)$$

$$Y_3 = Y_A \frac{g_0}{g_4}\left(3 + \frac{1}{\Lambda g_3 g_4}\right) \qquad (Y_{23})_2 = Y_A \frac{g_0}{g_4}\left(\frac{1 + \Lambda g_3 g_4}{1 + 2\Lambda g_3 g_4}\right)$$

$$Y_B = Y_A \frac{g_0}{g_4} \qquad (Y_{23})_3 = Y_A \frac{g_0}{g_4}\left(\frac{1 + 3\Lambda g_3 g_4}{1 + 2\Lambda g_3 g_4}\right)$$

construct with good unloaded Q's). Now the series stubs have a resonator susceptance slope parameter of

$$\text{\textit{f}}_j \;=\; \frac{\pi}{4}\,Y_j \tag{12.09-5}$$

and for narrow-stop band cases it is convenient to realize these resonator slope parameters using inductively coupled $\lambda_0/2$ short-circuited stub resonators of the form in Fig. 12.05-1(d). From this point on, the design process is the same as that in the example in Sec. 12.08. The completed filter might look like that in Fig. 12.08-1 except that the design equations of this section call for steps in the impedance along the main waveguide of the filter.

Derivation of the Design Equations in this Section—Exact methods for transmission line filter design such as the methods of Ozaki and Ishii[2,3] and of Jones[4] have existed for some time. However, though these methods are mathematically elegant, they are computationally so tedious that they have found little application in actual practice. The case described herein is an exception in that it is an exact method of design, yet is also very simple to use for the design of practical filters. The fundamental principle of this design method was first suggested by Ozaki and Ishii,[3] while the design equations in this section were worked out by B. M. Schiffman.[5]

The design procedure of this section hinges on Kuroda's identity.[2,3] This identity in transmission-line form is as shown in Fig. 12.09-3. Note that this identity says that a circuit consisting of an open-circuited shunt stub and a connecting line, which are both of the same length, has an exact equivalent circuit consisting of a short-circuited series stub with a connecting line at the opposite side.

Figure 12.09-4 traces out the way in which Kuroda's identity is used to relate a band-stop filter of the type in Fig. 12.09-1(a) to a low-pass prototype filter. Figure 12.09-4(a) shows a low-pass prototype filter for the case of $n = 3$ reactive elements. Applying the mapping Eq. (12.09-1) to the shunt susceptances and series reactances of this filter gives

$$\omega' C_j' \;=\; C_j' \omega_1' a\,\tan\!\left(\frac{\pi}{2}\,\frac{\omega}{\omega_0}\right) \tag{12.09-6}$$

$$Z_i' = \frac{Z_0^2 Y_1}{1 + Z_0 Y_1}$$

$$Z_0' = \frac{Z_0}{1 + Z_0 Y_1}$$

(a)

$$Y_i' = \frac{Z_1}{Z_0(Z_1 + Z_0)}$$

$$Z_0' = Z_0 + Z_1$$

(b)
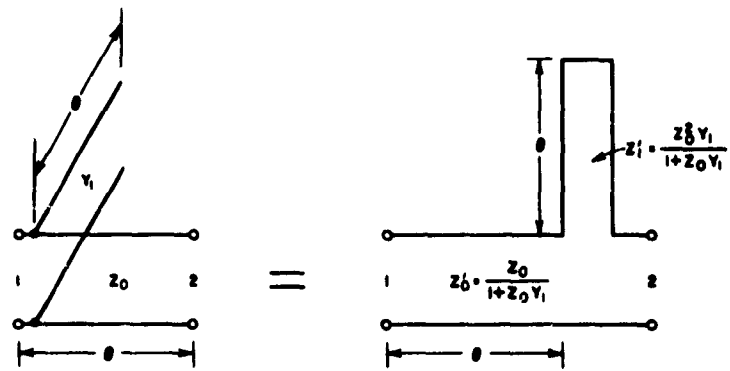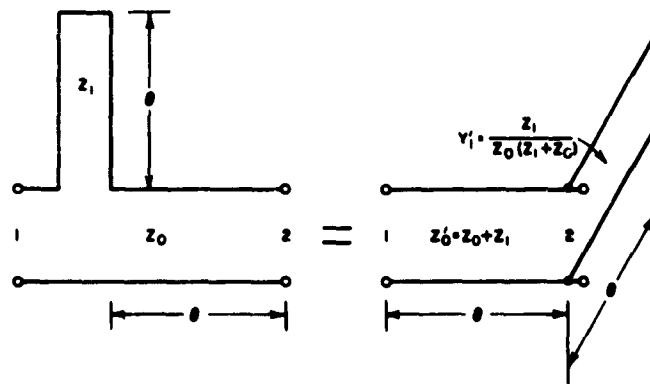
8-3627-575

FIG. 12.09-3   KURODA'S IDENTITY IN TRANSMISSION LINE FORM
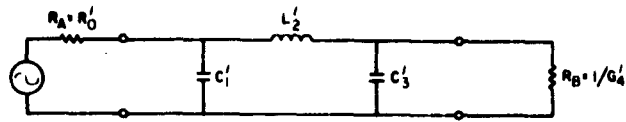
(a) PROTOTYPE
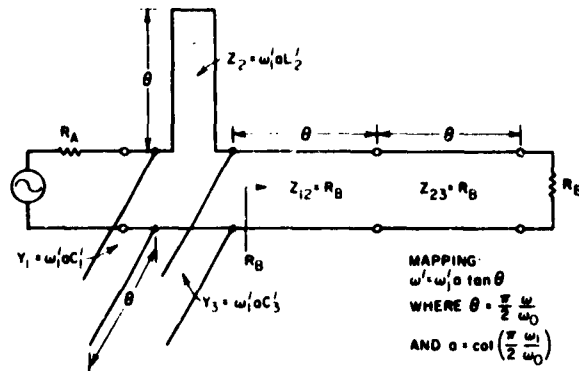
(b) MAPPED PROTOTYPE
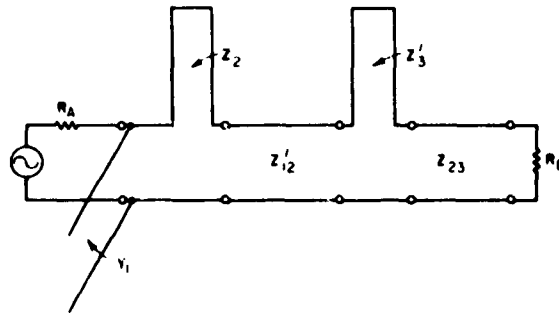
(c) AFTER APPLYING KURODA'S IDENTITY TO Y_3 AND Z_{12} IN PART (b)
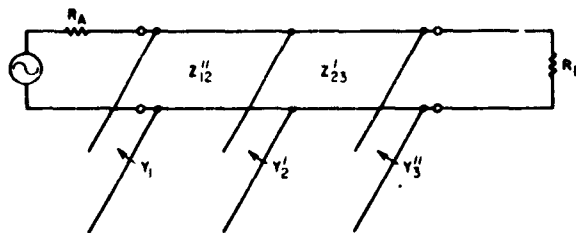
(d) AFTER APPLYING KURODA'S IDENTITY TO Z_2 AND Z_{12}' AND TO Z_3' AND Z_{23} IN PART (c)

FIG. 12.09-4   STAGES IN THE TRANSFORMATION OF A LOW-PASS PROTOTYPE
FILTER INTO A BAND-STOP TRANSMISSION-LINE FILTER

$$\omega' L'_j \; = \; L'_j \omega'_1 \; a \; \tan\left(\frac{\pi}{2}\frac{\omega}{\omega_0}\right) \quad . \qquad\qquad (12.09\text{-}7)$$

Note that the right side of Eq. (12.09-6) corresponds to the susceptance of an open-circuited stub having a characteristic admittance

$$Y_j \; = \; C'_j \omega'_1 a \quad , \qquad\qquad (12.09\text{-}8)$$

the stub being $\lambda_0/4$ long at ω_0. Similarly, the right side of Eq. (12.09-7) corresponds to the reactance of a short-circuited stub of characteristic impedance

$$Z_j \; = \; L'_j \omega'_1 a \quad , \qquad\qquad (12.09\text{-}9)$$

the stub being $\lambda_0/4$ long at frequency ω_0. Thus, the shunt capacitors in the low-pass prototype become open-circuited shunt stubs in the mapped filter, while the series inductance in the prototype becomes a short-circuited series stub in the mapped filter.

Note that in the mapped filter in Fig. 12.09-4(b), the terminations seen by the reactive part of the filter are still R_A on the left and R_B on the right. However, on the right, two additional line sections of impedance $Z_{12} = Z_{23} = R_B$ have been added. Since their characteristic impedance matches that of the termination, they have no effect on the attenuation characteristic of the circuit, their only effect on the response being to give some added phase shift. The circuit in Fig. 12.09-4(b) then has a response which is the desired exact mapping of the low-pass prototype response. The only trouble with the filter in Fig. 12.09-4(b) is that it contains a series stub which is difficult to construct in a shielded TEM-mode microwave structure.

The series stub in Fig. 12.09-4(b) can be eliminated by application of Kuroda's identity (Fig. 12.09-3). Applying Kuroda's identity to stub Y_3 and line Z_{12} in Fig. 12.09-4(b) gives the circuit in Fig. 12.09-4(c). Then applying Kuroda's identity simultaneously to stub Z_2 and line Z'_{12}, and to stub Z'_3 and line Z_{23} in Fig. 12.09-4(c) gives the circuit in Fig. 12.09-4(d). Note that the circuit in Fig. 12.09-4(d) has exactly the same input impedance and over-all transmission properties as the circuit in Fig. 12.09-4(b), while the circuit in Fig. 12.09-4(d) has no series stubs.

759

The equations in Tables 12.09-1 and 12.09-2 were derived by use of repeated applications of the procedures described above. For reasons of convenience, the equations in the tables use a somewhat different notation than does the example in Fig. 12.09-4; however, the principles used are the same. The equations in the tables in this section also provide for a shift in impedance level from that of the low-pass prototype.

SEC. 12.10, SOME EXAMPLES ILLUSTRATING THE PERFORMANCE OBTAINABLE USING THE EQUATIONS IN SEC. 12.09

In this section both a wide-stop-band filter example and a narrow-stop-band filter example will be discussed, both being designed by the methods of Sec. 12.09. In the case of the narrow-stop-band design, the high-impedance shunt stubs will be replaced by capacitively coupled stubs of moderate impedance, as was discussed in the preceding section.

A Wide-Stop-Band Example—Let us assume that a design is desired having 0.1-db pass-band Tchebyscheff ripple with the band edges at $f_1 = 1.12$ Gc and $f_2 = 2.08$ Gc. This puts the stop-band center at $f_0 = (f_1 + f_2)/2 = 1.60$ Gc. Let us further suppose that at least 30-db attenuation is required at the frequencies $f = 1.600 \pm 0.115$ Gc. Now $\omega_1/\omega_0 = f_1/f_0 = 1.12/1.60 = 0.70$; while at the lower 30-db point, $\omega/\omega_0 = f/f_0 = (1.600-0.115)/1.500 = 0.9283$. By Eq. (12.09-2), $a = 0.5095$; and by Eq. (12.09-1), the low-pass prototype should have at least 30-db attenuation for $\omega'/\omega_1' = 4.5$. By Fig. 4.03-5 we find that an $n = 3$ prototype will have 34.5-db attenuation for $\omega'/\omega_1' = 4.5$, while an $n = 2$ design will have only 15.5-db attenuation. Hence, an $n = 3$ design must be used.

From Table 4.05-2(a) the low-pass prototype parameters $g_0 = 1$, $g_1 = 1.0315$, $g_2 = 1.1474$, $g_3 = 1.0315$, $g_4 = 1.0000$, and $\omega_1' = 1$ were obtained. Using Table 12.09-1 with $Z_A = 50$ ohms, the line impedances were then computed to be $Z_1 = Z_3 = 145.1$ ohms, $Z_{12} = Z_{23} = 76.3$ ohms, $Z_2 = 85.5$ ohms, and $Z_B = 50$ ohms. The filter was constructed in strip-line form, and its dimensions are shown in Fig. 12.10-1. Note that the $Z_2 = 85.5$-ohm stub has been realized as two 176-ohm stubs in parallel. This was done so that narrower stubs could be used which should have less junction effect.*

FIG. 12.10-1   A STRIP-LINE, WIDE-STOP-BAND FILTER

The stubs in this case are realized using round wire supported by Polyfoam.
The dimensions of the round wires were determined by use of the approximate
formula

$$d = \frac{4b}{\pi \ antilog_{10}\left(\frac{\sqrt{\epsilon_r}\,Z}{138}\right)} \qquad (12.10-1)$$

where d is the rod diameter, b is the ground plane spacing, ϵ_r is the
relative dielectric constant, and Z is the desired line impedance.

Figure 12.10-2 shows the measured and computed performance of the
filter in Fig. 12.10-1. Note that the computed performance is in perfect
agreement with the specifications, as it should be. The measured per-
formance of the filter is also in excellent agreement with the specifica-
tions, except that the filter is tuned slightly high. This could have
been corrected by the addition of tuning screws.

A Narrow-Stop-Band Filter Example—Figure 12.10-3(a) shows another
3-stub band-stop filter design worked out using Table 12.09-1 and the same
low-pass prototype as was used for the design described above. However,
in this case the pass-band edges were defined so as to give a stop-band

761
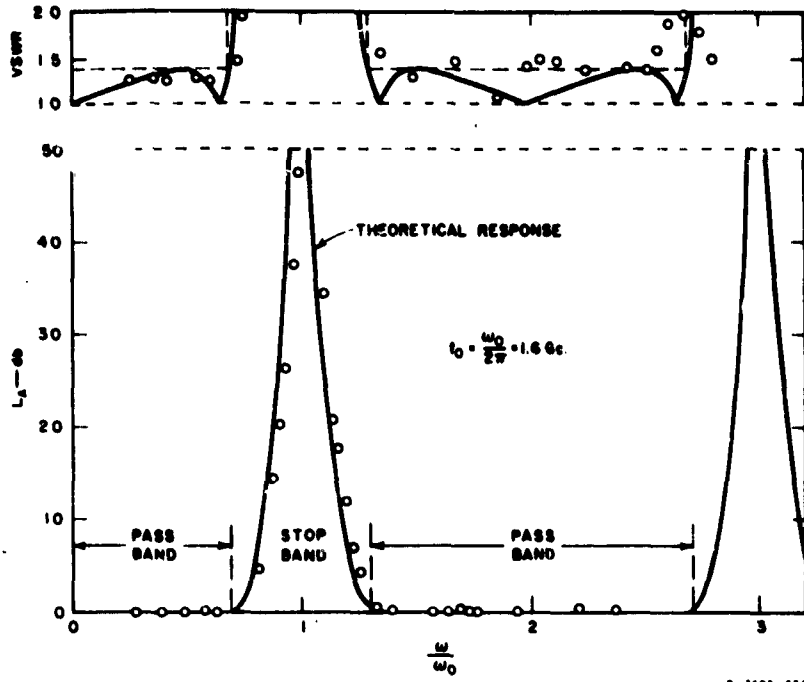
FIG. 12.10-2 COMPUTED AND MEASURED PERFORMANCE OF THE
WIDE-STOP-BAND FILTER IN FIG. 12.10-1
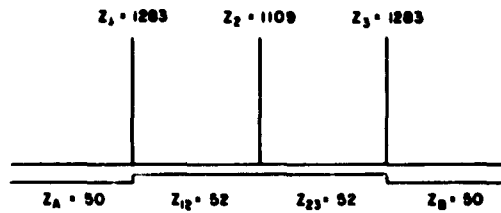
(a)
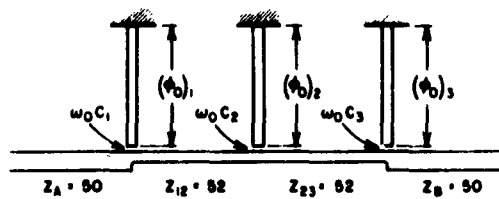
ALL STUBS HAVE $Z_1' = 151.5$ ohms

$\omega_0 C_1 = \omega_0 C_3 = 0.00239$ mho, $\omega_0 C_2 = 0.00259$ mho

$(\phi_0)_1 = (\phi_0)_3 = 70.1°$, $(\phi_0)_2 = 68.7°$

(b)

FIG. 12.10-3 NARROW-STOP-BAND FILTERS

762

fractional bandwidth of $w = 0.05$ as measured to the equal-ripple pass-band edges. As can be seen from the figure, in this case the line impedances $Z_{12} = Z_{23}$ are very nearly the same as the terminating impedances; however, the stub impedances are in excess of 1,000 ohms. To eliminate these impractical stub impedances, the open-circuited stub resonators were replaced by capacitively coupled short-circuited stub resonators as described in Sec. 12.09. The stub impedances were arbitrarily set at 151.5 ohms, but probably a lower impedance would have been a better choice from the standpoint of obtaining maximum resonator unloaded Q's. Figure 12.10-3(b) shows the design using capacitively coupled resonators.

Figure 12.10-4 shows the computed responses of these two designs. Note that the exact design [in Fig. 12.10-3(a)] has the desired 0.1-db pass-band ripple as specified. Though the approximate design with capacitively coupled stubs deviates a little from the specifications, it comes very close to the response over the frequency range shown. However, as can be seen from Fig. 12.10-5, which shows the same responses with enlarged scale over a larger frequency range, at higher frequencies the response of the approximate design deviates a good deal from that of the exact design. This is due to the variation of the coupling susceptances with frequency. Though either the method of Sec. 12.04 or the method of Sec. 12.09 will involve some error, narrow-band designs worked out by starting with the equations in Sec. 12.09 can be expected to give more accurate results.
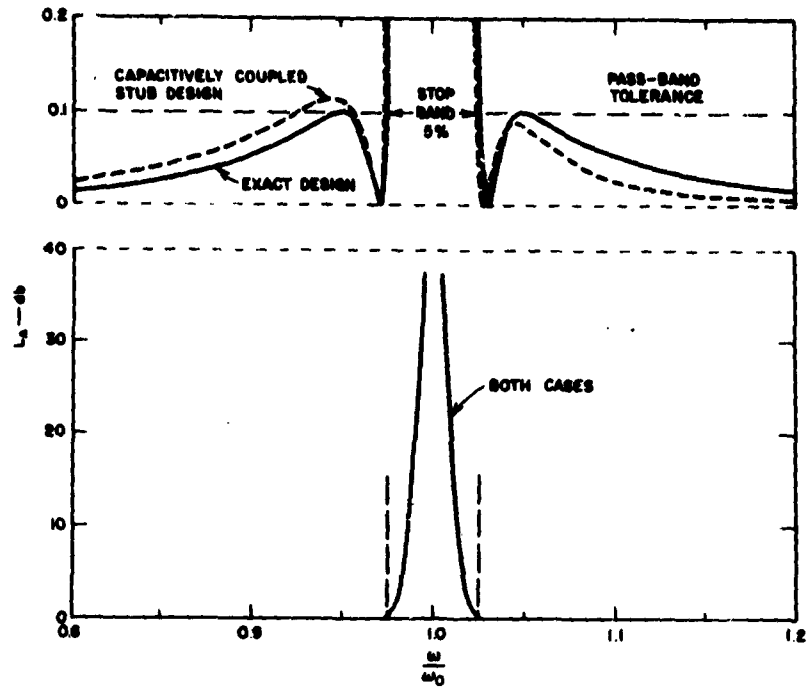
FIG. 12.10-4 COMPUTED RESPONSE OF THE FILTERS IN FIG. 12.10-3
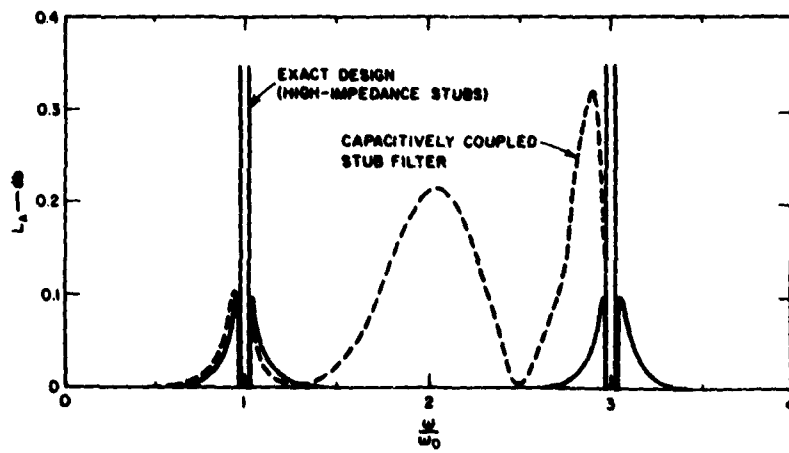
FIG. 12.10-5 THE RESPONSES IN FIG. 12.10-4 WITH AN ENLARGED SCALE

REFERENCES

1. Leo Young, G. L. Matthaei, and E. M. T. Jones, "Microwave Bandstop Filters with Narrow Stop Bands," *IRE Trans.*, *PGMTT*-10, pp. 416-427 (November 1962).

2. H. Ozaki and J. Ishii, "Synthesis of Transmission-Line Networks and Design of UHF Filters," *IRE Trans.*, *PGCT*-2, pp. 325-336 (December 1955).

3. H. Ozaki and J. Ishii, "Synthesis of a Class of Strip-Line Filters," *IRE Trans.*, *PGCT*-5, pp. 104-109 (June 1958).

4. E. M. T. Jones, "Synthesis of Wide-Band Microwave Filters to Have Prescribed Insertion Loss," *IRE Convention Record*, 1956 National Convention, Part 5, pp. 119-128.

5. B. M. Schiffman, P. S. Carter, Jr., and G. L. Matthaei, "Microwave Filters and Coupling Structures," Quarterly Progress Report 7, Sec. II, SRI Project 3527, Contract DA 36-039 SC-87398, Stanford Research Institute, Menlo Park, California (October 1962).

765

TEM-MODE, COUPLED-TRANSMISSION-LINE DIRECTIONAL COUPLERS, AND BRANCH-LINE DIRECTIONAL COUPLERS

SEC. 13.01, INTRODUCTION

Though there are many possible kinds of directional couplers, the discussion in this book will be confined to only two types. They are TEM-mode couplers consisting of parallel, coupled transmission lines[1-7] (Secs. 13.01 to 13.08), and branch-line couplers which may be of either TEM-mode or waveguide form[8-11] (Secs. 13.09 to 13.14). TEM-mode, coupled-transmission-line couplers are included because they relate very closely to some of the directional filters discussed in Chapter 14, they are a very widely used form of coupler, and they are a type of coupler of which the authors have special knowledge. The branch-line couplers are included because, as is discussed in Chapter 15, they are useful as part of high-power filter systems, and because they also are a form of coupler of which the authors happen to have special knowledge in connection with high-power filter work. No effort will be made to treat the numerous other useful forms of couplers which appear at this time to be less closely related to the topics in this book.

Figure 13.01-1 illustrates schematically a quarter-wavelength coupler and a three-quarter-wavelength coupler, together with their frequency responses. These couplers, like all couplers analyzed in this chapter, have end-to-end symmetry. The coupled signal travels in the direction opposite to that of the input signal and therefore these couplers are often referred to as "backward couplers." The electrical length, θ, of each coupled section in the two couplers is 90 degrees at midband. The variation of coupling with frequency in the single-section, quarter-wavelength coupler is approximately sinusoidal. The coupling variation with frequency is much less in the 3-section coupler, which is formed by cascading three, quarter-wavelength couplers. It can be made to be maximally-flat or equal-ripple by adjusting the couplings of the three individual couplers. Even greater bandwidths can be obtained by cascading more than three couplers.
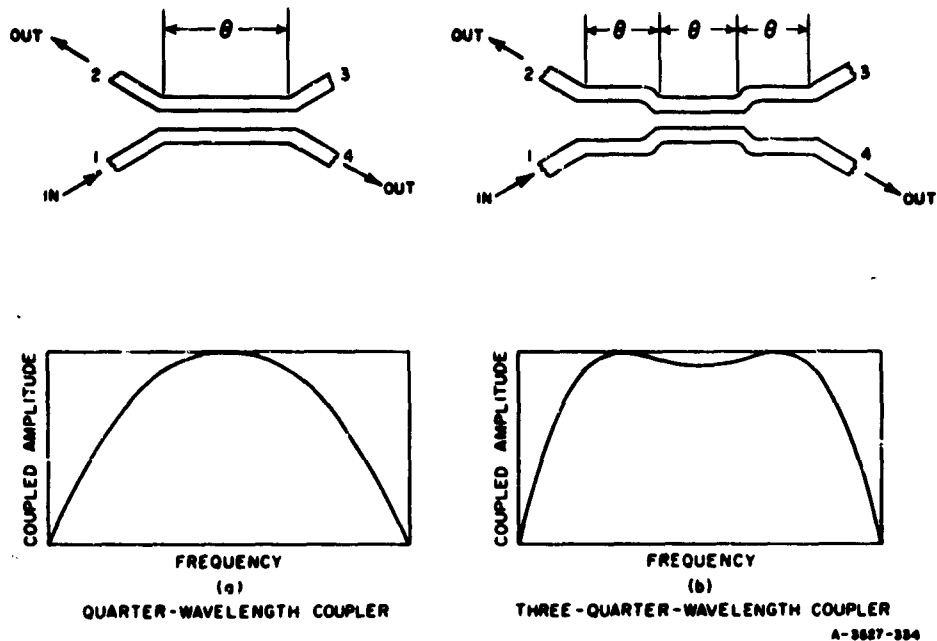
FIG. 13.01-1   SKETCH SHOWING TYPICAL CONFIGURATIONS AND FREQUENCY
RESPONSES FOR TEM-MODE, COUPLED-TRANSMISSION-LINE
DIRECTIONAL COUPLERS OF ONE AND THREE SECTIONS

A variety of physical configurations for the coupled TEM lines can
be used in these couplers, as is illustrated in Fig. 13.01-2. The con-
figurations (a), (b) and (c) are most suitable for couplers having weak
coupling such as 20 db, 30 db, etc.   The configurations (d), (e), (f),
(g) and (h) are most suitable for couplers having tight coupling such as
3 db.   Intermediate values of coupling can usually most easily be obtained
with configurations (d), (e), (f), and (g), although configuration (a) is
often useful.   Configuration (e) has a disadvantage in that the individual
lines are unsymmetrically located with respect to the ground planes; hence
the connections at the ends tend to excite ground-plane modes.   This can
be prevented, however, if the structure is closed in at the sides so that
only the desired TEM modes can propagate.   Configuration (f) avoids this
difficulty by making one of the lines double, while the other line inter-
leaves the double line in order to give tight coupling.   In this manner
the structure is made to be electrically balanced with respect to the

768

ground planes, and ground-plane modes will not be excited. Configuration
(h) uses conductors A and B of circular cross section, surrounded by a
conductor C. The electrical potential of C is floating with respect to
the potentials of the ground planes D and of conductors A and B. The ad-
dition of the floating shield C has the effect of greatly increasing the
coupling between lines A and B.

The actual configuration to use in a particular application depends
on a number of factors. However, configuration (a) is most frequently
used for weak coupling while configuration (e) is often used for tight
coupling. Both of these configurations can be fabricated by printed-
circuit techniques. Configuration (c), utilizing round conductors, is
particularly good for weak-coupling, high-power applications. When con-
figuration (e) is fabricated using thick strips with rounded edges, it is

(a)

(b)

(c)
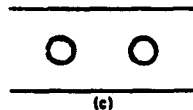
WEAK COUPLING CONFIGURATIONS

(d)

(e)

(f)

(g)

(h)
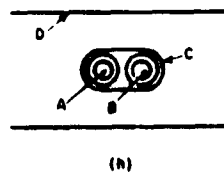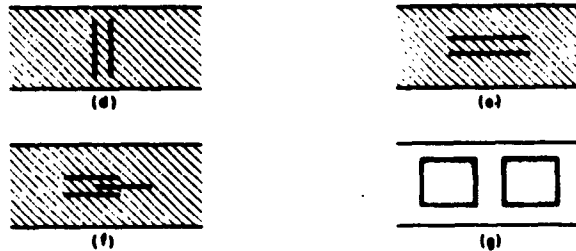
TIGHT COUPLING CONFIGURATIONS

DIELECTRIC

CONDUCTOR

FIG. 13.01-2 CROSS SECTIONS OF TYPICAL TEM-MODE,
COUPLED-TRANSMISSION-LINES

769

suitable for strong-coupling, high-power applications. Reference to the detailed designs presented in Secs. 13.05 and 13.06 may also help the reader decide on the most appropriate configuration for his particular application.

It is essential for the operation of these couplers that the cross section be uniformly filled with air or some other low-loss dielectric material. Configurations (c) and (g) have enough rigidity so that they can be air-filled. With the other configurations it is usually necessary to use a rigid, low-loss dielectric material for mechanical support.

SEC. 13.02, DESIGN RELATIONS FOR TEM-MODE, COUPLED-TRANSMISSION-LINE DIRECTIONAL COUPLERS OF ONE SECTION

TEM-mode coupled-transmission-line directional couplers theoretically are perfectly matched and have infinite directivity at all frequencies. When a wave of voltage amplitude E is incident upon Port 1 of a quarter-wavelength coupler (Fig. 13.01-1), the voltage at Port 2 is given by

$$\frac{E_2}{E} = \frac{jc \sin \theta}{\sqrt{1 - c^2} \cos \theta + j \sin \theta}$$

(13.02-1)

while the voltage at Port 4 is given by

$$\frac{E_4}{E} = \frac{\sqrt{1 - c^2}}{\sqrt{1 - c^2} \cos \theta + j \sin \theta}$$

(13.02-2)

where c is the *coupling factor*, which is the midband value of $|E_2/E|$.

Since the phases of E_2 and E_4 are usually of little interest, Eqs. (13.02-1) and (13.02-2) can be reduced to

$$\left|\frac{E_2}{E}\right|^2 = \frac{c^2 \sin^2 \theta}{1 - c^2 \cos^2 \theta}$$

(13.02-1a)

and

$$\left|\frac{E_4}{E}\right|^2 = \frac{1 - c^2}{1 - c^2 \cos^2 \theta}$$

(13.02-2a)

770

For small values of c, Eq. (13.02-1) predicts that E_3/E varies as $\sin \theta$. For large values of c the coupling variation with frequency is as shown in Fig. 13.02-1. The voltage at Port 3 is zero. (These results are proved in Sec. 13.07.)

The electrical length, θ, of the coupled lines is related to the physical length l by means of the relation $\theta = 2\pi l / \lambda$, where λ is the wavelength in the medium surrounding the coupled lines. The midband voltage coupling factor c is

$$c = \frac{Z_{oe}/Z_{oo} - 1}{Z_{oe}/Z_{oo} + 1} \qquad (13.02\text{-}3)$$

where Z_{oe} and Z_{oo} are the even- and odd-mode impedances discussed below. In order that the coupler be perfectly matched to its terminating transmission line of characteristic impedance Z_0, it is necessary that

$$Z_0 = \sqrt{Z_{oe} Z_{oo}} \qquad (13.02\text{-}4)$$

The even-mode impedance Z_{oe} is the characteristic impedance of a single coupled line to ground when equal currents are flowing in the two lines, while the odd-mode impedance Z_{oo} is the characteristic impedance of a single line to ground when equal and opposite currents are flowing in the two lines. Values of Z_{oe} and Z_{oo} for a number of cross sections are presented in Sec. 5.05.

Equations (13.02-3) and (13.02-4) can be rearranged to give the convenient design relations

$$Z_{oe} = Z_0 \sqrt{\frac{1 + c}{1 - c}} \qquad (13.02\text{-}5)$$

and

$$Z_{oo} = Z_0 \sqrt{\frac{1 - c}{1 + c}} \qquad (13.02\text{-}6)$$

The physical dimensions necessary to give the required even- and odd-mode impedances Z_{oe} and Z_{oo} can then be obtained from Sec. 5.05.
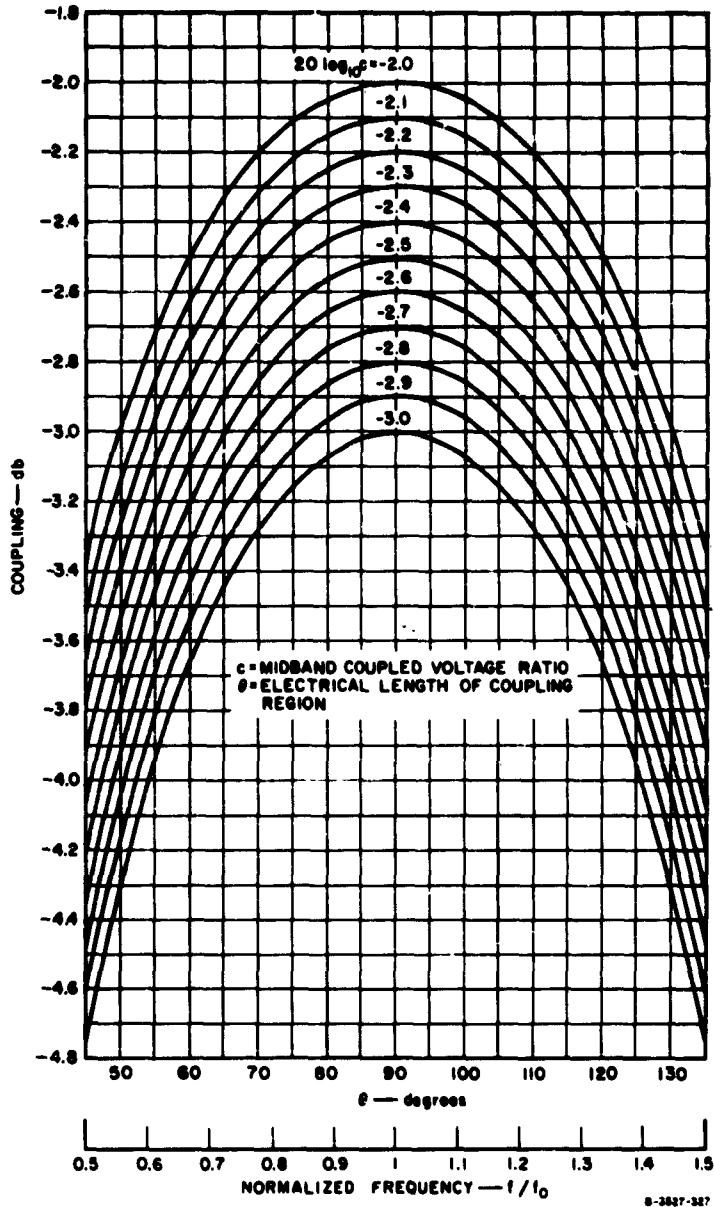
FIG. 13.02-1 COUPLING AS A FUNCTION OF FREQUENCY FOR
TEM-MODE, COUPLED-TRANSMISSION-LINE
DIRECTIONAL COUPLERS OF ONE SECTION,
HAVING TIGHT COUPLING

772

SEC. 13.03, DESIGN RELATIONS FOR TEM-MODE, COUPLED-TRANSMISSION-LINE DIRECTIONAL COUPLERS OF THREE SECTIONS

The analysis of TEM-mode couplers of more than one section soon leads to long and complicated expressions. The problem simplifies somewhat when one recognizes that the TEM-mode coupler is analytically similar to the quarter-wave transformer. That is to say, the even and odd modes of operation are duals of each other (impedance in one corresponds to admittance in the other, and vice versa), and the mathematics of each mode then reduces to the analysis of cascaded transmission-line sections, each of which is one-quarter wavelength long at center frequency. There is, however, one major difference between the desired performance of the TEM-mode coupler and that of the quarter-wave transformer of Chapter 6: Whereas the quarter-wave transformer is required to have *low* reflection in the operating band, the "quarter-wave filter"* on which the TEM coupler is based is required to have a sizeable specified and nearly constant reflection coefficient across the band of operation. Thus the transducer loss functions are not the same, and the numerical data in Chapter 6 then do not apply to TEM-mode directional couplers. A new analysis has to be undertaken for the quarter-wave filter prototype. Figure 13.03-1(a) shows a three-section coupler and Fig. 13.03-1(b) shows a quarter-wave-filter prototype from which it can be designed.

The results of an analysis of a symmetrical three-section coupler (Fig. 13.03-1) will be given without proof in this section. It will be followed in Sec. 13.04 with a first-order formula for a symmetrical coupler of any (odd) number of sections, and some particular solutions for five-section couplers.

Since this type of coupler has matched resistive impedances at all of its ports, $|E/E_4|^2$ corresponds to the transducer loss ratio. For three-section couplers it is given by a polynomial in $\cos^2 \theta$ (compare with Sec. 6.02),

$$\left| \frac{E}{E_4} \right|^2 = A_0 + A_1 \cos^2 \theta + A_2 \cos^4 \theta + A_3 \cos^6 \theta \qquad (13.03\text{-}1)$$

---

*The term "quarter-wave filter" is introduced to distinguish the resulting physically symmetrical structures from quarter-wave impedance transformers with a monotone sequence of steps, as in Chapter 6.

773

COUPLING
FACTORS: c_1 c_2 c_1

WHERE $|E|^2 = |E_2|^2 + |E_4|^2$

(a) TEM-MODE COUPLER

JUNCTION
VSWR'S: V_1 V_2 V_2 V_1

LINE
IMPEDANCES.   1 Z_1 Z_2 Z_1 1
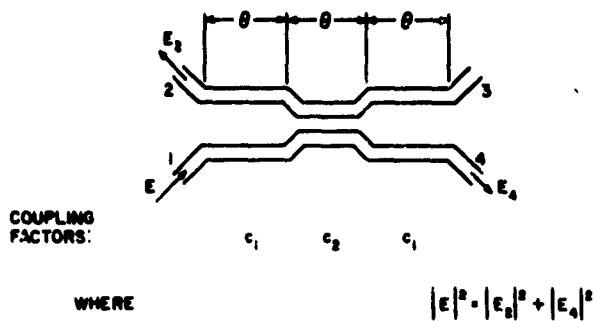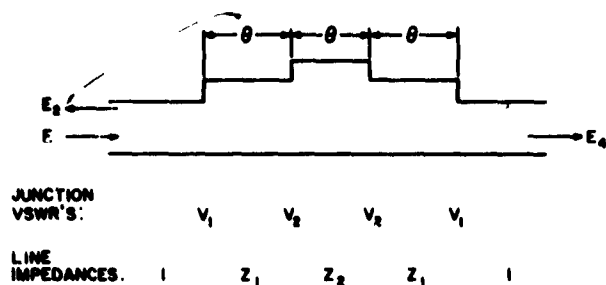
(b) PROTOTYPE QUARTER-WAVE FILTER

SOURCE: Proc. IEE (see Ref. 24 by L. Young)

FIG. 13.03-1   THREE-SECTION TEM-COUPLER AND
               QUARTER-WAVE FILTER PROTOTYPE

where A_0, A_1, A_2, and A_4 are functions of the end- and middle-section
coupling factors c_1 and c_2. The A's are given by

$$A_0 = L_0^2 \tag{13.03-2}$$

$$A_1 = (L_2 - 1)^2 - L_0^2 - L_0 L_1 L_2 \tag{13.03-3}$$

$$A_2 = \left(\frac{L_1 L_2}{2}\right)^2 + L_0 L_1 L_2 - 2L_2(L_2 - 1) \tag{13.03-4}$$

$$A_3 = L_2^2 - \left(\frac{L_1 L_2}{2}\right)^2 \tag{13.03-5}$$

774

in which

$$L_0 = \frac{1 + c_1^2 - 2c_1 c_2}{(1 - c_1^2)\sqrt{1 - c_2^2}}$$

$$L_1 = \frac{2}{\sqrt{1 - c_1^2}}$$

$$L_2 = 2 + \frac{2(1 - c_1 c_2)}{\sqrt{(1 - c_1^2)(1 - c_2^2)}}$$

(13.03-6)

The coupling voltage E_2 is then found (from conservation of energy) to be related to E and E_4 by

$$\left|\frac{E_2}{E}\right|^2 = 1 - \left|\frac{E_4}{E}\right|^2 \quad .$$

(13.03-7)

Design Formulas—Since the three-section coupler shown in Fig. 13.03-1 is symmetrical, one has to determine two even-mode and two odd-mode impedances, so that its physical dimensions can be determined from Sec. 5.05. The even- and odd-mode impedances $(Z_{oe})_1$, $(Z_{oo})_1$, $(Z_{oe})_2$, and $(Z_{oo})_2$ are related to the coupling factors c_1 and c_2 by

$$(Z_{oe})_i = Z_0 \sqrt{\frac{1 + c_i}{1 - c_i}} \qquad (i = 1,2)$$

(13.03-8)

and

$$(Z_{oo})_i = Z_0 \sqrt{\frac{1 - c_i}{1 + c_i}} \qquad (i = 1,2) \quad .$$

(13.03-9)

Design formulas for c_1 and c_2 will now be stated, and their derivation will be indicated afterwards. The midband over-all coupling is denoted by c_0, which is the value of $|E_2/E|$ at midband. The coupler performance is usually specified by the midband coupling c_0 and one other parameter which determines the shape of the coupling response against frequency, for instance whether it is to be maximally flat or to have a

775

specified ripple. This parameter is here denoted by V_1 and is determined from Figs. 13.03-2 and 13.03-3 as will be explained below. The design procedure for a three-section coupler (Fig. 13.03-1) is then as follows:

1. Determine the midband coupling, c_0. For instance, for a three-section 3-db coupler with 0.3-db ripple, $10 \log_{10} (c_0^2) = 3.3$ db.

2. Then determine $V_{1,MF}$ from Fig. 13.03-2. For a maximally flat coupler, $V_1 = V_{1,MF}$. For an equal-ripple coupler, determine V_1 from Fig. 13.03-3. Use the 10-db curve for all couplers with coupling weaker than 10 db.

   If the ripple is specified (for instance, if the coupling is to lie between 2.7 and 3.3 db, the ripple is 0.3 db), then the lower curves in Fig. 13.03-3 are used. If the fractional bandwidth w is specified, the upper curves in Fig. 13.03-3 are used. (The fractional bandwidth w is here defined, as usual, by

$$ w = \frac{f_2 - f_1}{f_0} = 2\left(\frac{f_2 - f_1}{f_2 + f_1}\right) , \qquad (13.03\text{-}10) $$

   where f_1 and f_2 are the band-edge frequencies of the equal-ripple pass band. Either the ripple or the bandwidth may be specified, and they are related as shown in Fig. 13.03-4.*

3. Determine R from

$$ R = \frac{1 + c_0}{1 - c_0} \qquad (13.03\text{-}11) $$

   where c_0 is the coupling factor. [The midband coupling in decibels is $10 \log_{10}(c_0^2)$ db.]

4. Determine V_2 from

$$ V_2 = V_1\sqrt{R} . \qquad (13.03\text{-}12) $$

5. Determine Z_1 and Z_2 from

$$ Z_1 = V_1 , \quad Z_2 = V_1 V_2 \qquad (13.03\text{-}13) $$

6. Finally, determine c_1 and c_2 from

$$ c_1 = \frac{Z_1^2 - 1}{Z_1^2 + 1} \quad \text{and} \quad c_2 = \frac{Z_2^2 - 1}{Z_2^2 + 1} . \qquad (13.03\text{-}14) $$

---

* There is a slight inconsistency in these curves owing to a lack of more complete numerical data. The 10-db curve refers to 10 db at center frequency; the 3-db curve refers to 3-db average over the band.

776
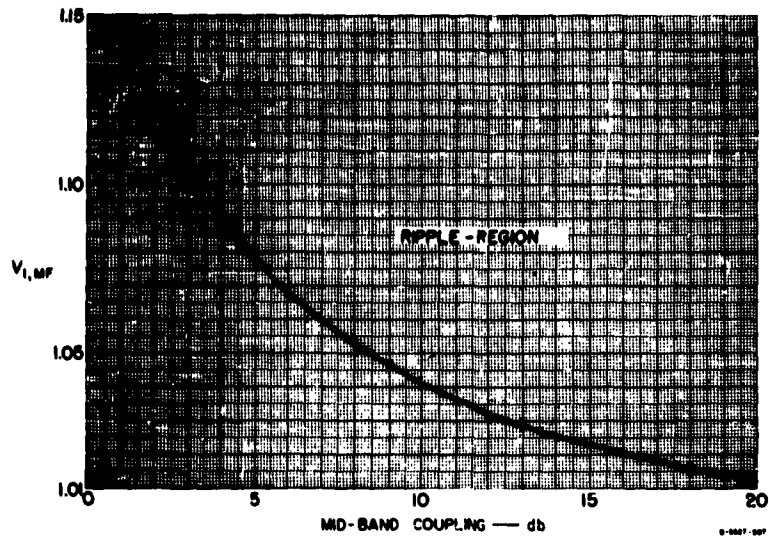
FIG. 13.03-2 $V_1 = V_{1,MF}$ OF MAXIMALLY FLAT, THREE-SECTION,
TEM-MODE COUPLER AS A FUNCTION OF MIDBAND COUPLING
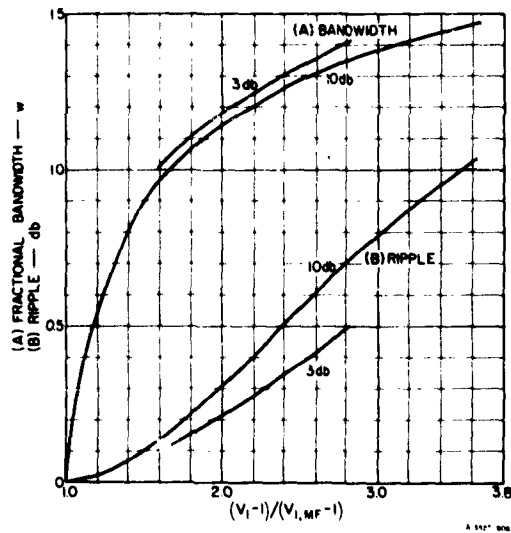
FIG. 13.03-3   FRACTIONAL BANDWIDTH AND RIPPLE AS V_1 IS INCREASED,
FOR 3-db AND 10-db, THREE-SECTION TEM-MODE COUPLERS

777

The $(Z_{oo})_i$ and $(Z_{oe})_i$ are then given by Eqs. (13.03-8) and (13.09-9) and the physical dimensions can be obtained from Sec. 5.05, as already pointed out.
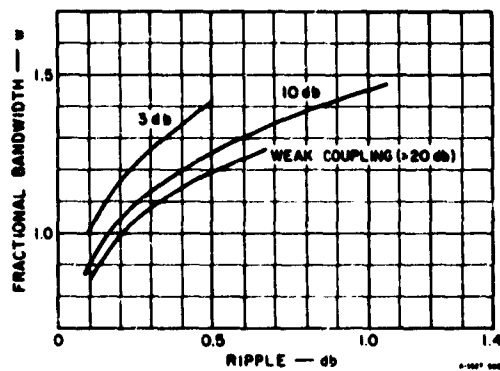
FIG. 13.03-4   FRACTIONAL BANDWIDTH AS A
FUNCTION OF RIPPLE FOR
THREE-SECTION TEM-MODE
COUPLERS WITH 3-db, 10-db,
AND WEAK COUPLING FACTORS

Quarter-Wave Filter Parameters—The parameters V_i, V_2, Z_1, Z_2, and R just introduced have meaning in terms of the quarter-wave filter proto- type circuit, which will be explained more fully in Sec. 13.08. The essence of this design concept is that the backward-coupled wave of the TEM-mode coupler (E_2 in Fig. 13.03-2) corresponds analytically to the reflected wave of the quarter-wave filter, as indicated in Fig. 13.03-1(a) and (b). One therefore has to synthesize only a two-port (instead of a four-port), making its reflected wave behave as one would want the coupling to be. The V_i are the step-VSWR's, and the Z_i are the normalized impedances [Fig. 13.03-1(b)] which are turned into the $(Z_{oo})_i$ and $(Z_{oe})_i$ by means of Eqs. (13.03-8) through (13.03-14). Equation (13.03-6) also simplifies to

$$L_0 = \frac{1}{2}\left(\frac{V_1}{V_2} + \frac{V_2}{V_1}\right)$$

$$L_1 = V_1 + \frac{1}{V_1}$$

$$L_2 = V_2 + 2 + \frac{1}{V_2} \ . \qquad (13.03\text{-}15)$$

The parameter R corresponds to the midband VSWR of the quarter-wave filter, and c_0 is its midband reflection coefficient. Furthermore, at midband its section lengths are $\theta = \pi/2$, and the reflected and transmitted powers are then given by

$$\left|\frac{E_2}{E}\right|^2 = c_0^2 = \left(\frac{R-1}{R+1}\right)^2 \qquad (13.03\text{-}16)$$

and

$$\left|\frac{E_4}{E}\right|^2 = \frac{1}{A_0} = \frac{1}{L_0^2} = \frac{4R}{(R+1)^2} \ . \qquad (13.03\text{-}17)$$

Maximally Flat Coupling—To obtain a maximally flat response at $\theta = \pi/2$, we may specify

$$A_1 = 0 \qquad (13.03\text{-}18)$$

in Eq. (13.03-1). Eliminating V_2 leaves a quartic equation in V_1:

$$\left(V_1\sqrt{R} + 1 + \frac{1}{V_1\sqrt{R}}\right)^2 - \frac{R+1}{2\sqrt{R}}\left(2V_1 + \frac{2}{V_1} + V_1^2\sqrt{R} + \frac{1}{V_1^2\sqrt{R}}\right) = \frac{3(R+1)^2}{4R} \ . \quad (13.03\text{-}19)$$

The solution of this equation is graphed in Fig. 13.03-2 where $V_1 = V_{1,MF}$ is plotted against the midband coupling in decibels. Selecting $V_1 = V_{1,MF}$ from Fig. 13.03-2 or Eq. (13.03-19) will give a maximally flat response. (It turns out that when A_1 is thus made to vanish, A_2 is not equal to zero. To obtain a flatter response with both A_1 and A_2 equal to zero, the coupler or filter cannot be symmetrical between ends.)

779

When the midband coupling is maintained constant while V_1 is increased above the curve in Fig. 13.03-2, the coupling-versus-frequency characteristic turns from maximally flat to equal-ripple. The ripple region for V_1 is indicated in Fig. 13.03-2.

10-db Couplers—A maximally flat, 10-db coupler has the quarter-wave filter parameters $V_1 = Z_1 = 1.041$, $V_2 = Z_2/Z_1 = 1.446$ (so $Z_2 = 1.505$), and hence $c_1 = 0.0403$, $c_2 = 0.388$. As V_1 is increased, the coupling response develops ripples, as can be seen from Fig. 13.03-5 which shows six curves of coupling against frequency for $V_1 = 1.04$, 1.06, 1.08, 1.10, 1.12, and 1.14. The coupling is symmetrical about the center frequency in Fig. 13.03-5, and is therefore plotted only for frequencies above midband. The midband coupling has been maintained at 10 db by satisfying Eq. (13.03-12) with $R = 1.926$. [This R is obtained from Eq. (13.03-11) with $c_0 = 0.3162$, corresponding to 10-db coupling.] For any given V_1, the parameters c_1 and c_2, and the even- and odd-mode impedances, $(Z_{oe})_i$ and $(Z_{oo})_i$, can be derived from Eqs. (13.03-8) through (13.03-14).
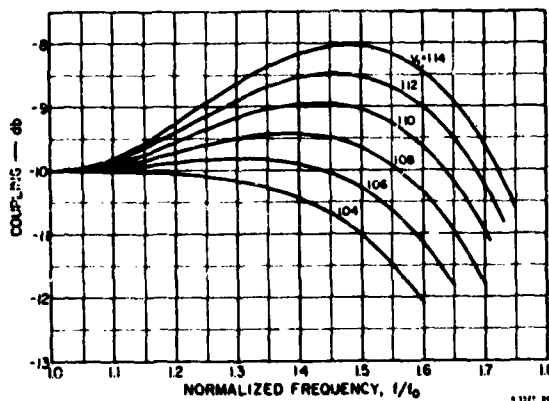
FIG. 13.03-5   COUPLING AS A FUNCTION OF
              FREQUENCY FOR SIX THREE-
              SECTION TEM-MODE COUPLERS
              HAVING 10-db MIDBAND COUPLING

3-db Couplers[1,5]—Similar curves for 3-db couplers are reproduced in Fig. 13.03-6, except that here the *average* coupling is maintained constant at 3 db. (In Fig. 13.03-5 the *midband* coupling was maintained constant at 10 db.) The five curves shown in Fig. 13.03-6 have coupling ripples of 0.1, 0.2, 0.3, 0.4, and 0.5 db, respectively, and their coupling factors are given in Table 13.03-1.
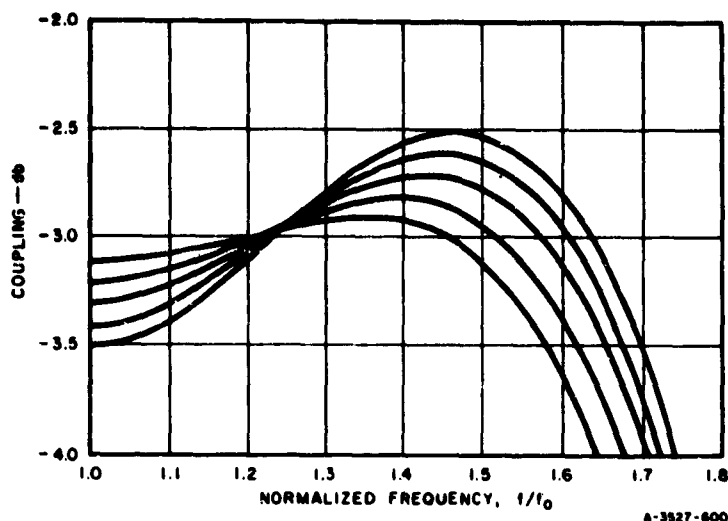
FIG. 13.03-6   COUPLING AS A FUNCTION OF FREQUENCY FOR
FIVE THREE-SECTION TEM-MODE COUPLERS
HAVING 3-db AVERAGE COUPLING

0-db Coupling—It can be shown for
the maximally flat, three-section coupler
that in the limit as R tends to infinity,
and as the coupling ratio therefore tends
to unity (0-db), V_1 tends ultimately to
$\sqrt{3/2}$. (V_2 tends to infinity.) Thus V_1
for the maximally flat three-section
coupler never exceeds $\sqrt{3/2} = 1.224745$,
or equivalently, c_1 never exceeds 0.2.
(Of course it is not possible to ever
attain 0-db coupling, just as it is
impossible to ever attain complete reflec-
tion in a stepped-impedance filter.)

Table 13.03-1

DESIGN PARAMETERS FOR
THREE-SECTION, 3-db,
TEM-MODE COUPLERS

db RIPPLE	c_1	c_2	c_0
±0.1 db	0.15505	0.8273	0.6998
±0.2 db	0.18367	0.8405	0.6918
±0.3 db	0.21104	0.85241	0.6839
±0.4 db	0.23371	0.86119	0.6760
±0.5 db	0.25373	0.86838	0.6683

SEC. 13.04, RELATIONS FOR TEM-MODE COUPLED-TRANSMISSION-LINE
DIRECTIONAL COUPLERS OF FIVE AND MORE SECTIONS

First-Order Design Theory—It is not difficult to show that for weak
couplings the amplitude coupling ratio, $c(\theta)$, of an n-section coupler as

a function of θ, is

$$\left|\frac{E_2}{E}\right| = c_1 \sin n\theta + (c_2 - c_1) \sin (n-2)\theta + \ldots$$

$$+ (c_i - c_{i-1}) \sin (n - 2i + 2)\theta + \ldots$$

$$+ (c_{[(n+1)/2]} - c_{[(n-1)/2]}) \sin \theta \qquad (13.04\text{-}1)$$

in the notation of Fig. 13.04-1. If, for example, it is required to obtain maximally flat coupling, then the c_i must satisfy a set of $(n-1)/2$ linear equations

$$\left.\left[\frac{d^p c_{-})}{d\theta^p}\right]\right|_{\theta=\pi/2} = 0 \qquad\qquad \Bigg\}$$

$$\text{for } p = 2, 4, 6, \ldots, n-1 \qquad\qquad (13.04\text{-}2)$$

in addition to one equation, determining the center-frequency coupling. The solutions of the system of equations (13.04-2) for $n = 3$ and $n = 5$ can be shown to be,

$$\text{for } n = 3, \quad c_2 = 10 c_1 ; \qquad c_0 = c_2 - 2c_1 = 8c_1 \qquad (13.04\text{-}3)$$
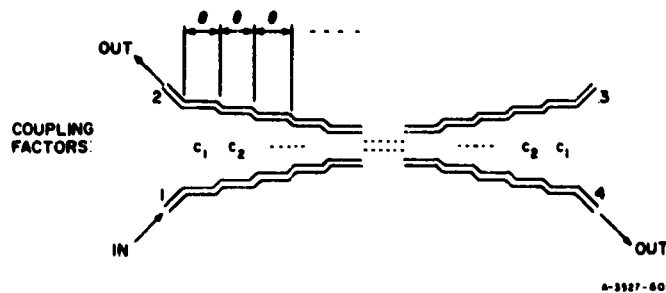
SOURCE: Proc. IEE (see Ref. 24 by L. Young)

FIG. 13.04-1   TEM-MODE COUPLER OF n SECTIONS

and for $n = 5$,

$$\frac{c_3}{536} = \frac{c_2}{84} = \frac{c_1}{9}$$

$$c_c = c_3 - 2c_2 + 2c_1 = 386 c_1 / 9$$

$$(13.04-4)$$

It can also be shown that Eq. (13.03-19) for the maximally flat, three-section coupler reduces in the first-order approximation to

$$V_1 = \frac{7 + \sqrt{R}}{8} \quad . \qquad (13.04-5)$$

Solutions for Five-Section Couplers—As was the case with the three-section coupler in Sec. 13.03, the solution of the five-section coupler is most easily expressed in terms of the normalized quarter-wave filter impedances Z_1, Z_2, and Z_3, which are again related to the coupling factors c_i (Fig. 13.04-1) by

$$Z_i^2 = \frac{1 + c_i}{1 - c_i} \quad , \quad \text{or} \quad c_i = \frac{Z_i^2 - 1}{Z_i^2 + 1}$$

$$(i = 1, 2, 3) \qquad (13.04-6)$$

corresponding to Eq. (13.03-14) for the three-section coupler. Again the $(Z_{oe})_i$ and $(Z_{oo})_i$ are obtained as in Eqs. (13.03-8) and (13.03-9), but with $i = 1, 2, 3$.

The first-order solution in Eq. (13.04-4) for maximally flat coupling must become less accurate as the c_i approach unity, since they can never exceed unity. Equation (13.04-4) becomes more accurate for appreciable couplings if we substitute $\log Z_i$ for c_i. [Compare the similarly expedient substitution used in Eq. (6.06-11) in the first-order theory of quarter-wave transformers.] Then for maximally flat couplers, to a good approximation,

$$\frac{\log Z_3}{536} = \frac{\log Z_2}{84} = \frac{\log Z_1}{9} \quad . \qquad (13.04\text{-}7)$$

The Z_1, Z_2, and Z_3 are completely determined when the midband coupling factor c_0 is also specified, from the formula

$$\log Z_3 - 2 \log Z_2 + 2 \log Z_1 = \frac{1}{2} \log \left(\frac{1 + c_0}{1 - c_0} \right) \qquad (13.04\text{-}8)$$

(which is a special case of the more general formulas for n-section couplers given later in Sec. 13.08). The first-order equations, Eqs. (13.04-7) and (13.04-8), for maximally flat coupling have been found to hold very well for coupling as tight as 10-db $(c_0^2 = 0.1)$. The coupling becomes weaker as the frequency deviates from midband. The following fractional bandwidths are obtained for various coupling deviations from the midband c_0 (when c_0 corresponds to 10-db coupling or less): $w = 0.82$ for 0.1 db deviation; $w = 1.01$ for 0.25 db deviation; $ = 1.13$ for 0.5 db deviation; $w = 1.32$ for 1.0 db deviation; and $w = \text{`} 1$ for 2.0 db deviation.

The first-order relation in Eqs. (13.04-7) and (13.04-8) for maximally flat coupling were even solved for a 3-db coupler $(c_0^2 = 0.5)$ with the following results. The solution is easily found to be

$$\left.
\begin{aligned}
Z_1 &= 1.0207 \\[8pt]
Z_2 &= 1.2114 \\[8pt]
Z_3 &= 3.4004 \quad .
\end{aligned}
\right\} \qquad (13.04\text{-}9)$$

As the frequency departs from midband, the coupling at first becomes stronger, going from 3.01 db to 2.97 db, and then becomes weaker. It is 3.11 db at the edges of a 103-percent band ($w = 1.03$), and 3.51 db at the edges of a 124-percent band ($w = 1.24$).

An exact solution for a particular 3-db coupler has been given by Cohn and Koontz.[12] They found by trial-and-error that with

$$Z_1 = 1.098$$

$$Z_2 = 1.417$$

$$Z_3 = 4.130$$

an equal-ripple characteristic (with three ripples) was obtained, the coupling being 3.01 ± 0.163 db over a fractional bandwidth of $w = 1.41$. (The midband coupling is 2.847 db.)

In all cases the coupler is determined by the Z_i, which give the c_i from Eq. (13.04-6), and the $(Z_{oe})_i$ and $(Z_{oo})_i$ from Eqs. (13.03-8) and (13.03-9), the physical dimensions then being obtained from Sec. 5.05.

SEC. 13.05, TYPICAL DESIGNS FOR TEM-MODE, COUPLED-TRANSMISSION-LINE DIRECTIONAL COUPLERS OF ONE SECTION WITH APPROXIMATELY 3 db AVERAGE COUPLING

Figure 13.05-1 shows what has proved to be a very popular method of construction for a completely shielded quarter-wavelength coupler having tight coupling.[6] In this structure the individual lines are not symmetrically located with respect to the upper and lower ground planes; hence there is a tendency for the connections at the ends to excite ground-plane modes. However, if the structure is completely closed in at the sides as shown in Fig. 13.05-1, such modes are cut off, and no difficulty should be encountered. The coupler illustrated was designed to have 2.9 db midband coupling at Port 2. The actual measured coupling, directivity and VSWR of the coupler is also shown in the figure. The excellent values shown were obtained without recourse to any special matching techniques since the center frequency was only 225 Mc. For operation at frequencies on the order of 1000 Mc and higher it is usually necessary to place capacitive tuning screws at either end of the coupled lines. These compensate the discontinuities there, and allow satisfactory values of directivity and VSWR to be achieved. The coupling response is usually little affected by these matching devices.

The procedure used to design this coupler which uses 0.002-inch-thick copper strips supported by polystyrene dielectric having a relative dielectric constant $\epsilon_r = 2.56$ is as follows. The midband coupling is 2.9 db, so $c = 0.716$. The terminating impedance Z_0 is equal to 50 ohms, and therefore Eqs. (13.02-5) and (13.02-6) yield $\sqrt{\epsilon_r} \, Z_{oe} = 197$ ohms and $\sqrt{\epsilon_r} \, Z_{oo} = 32.5$ ohms. The spacing between the strips was chosen to be
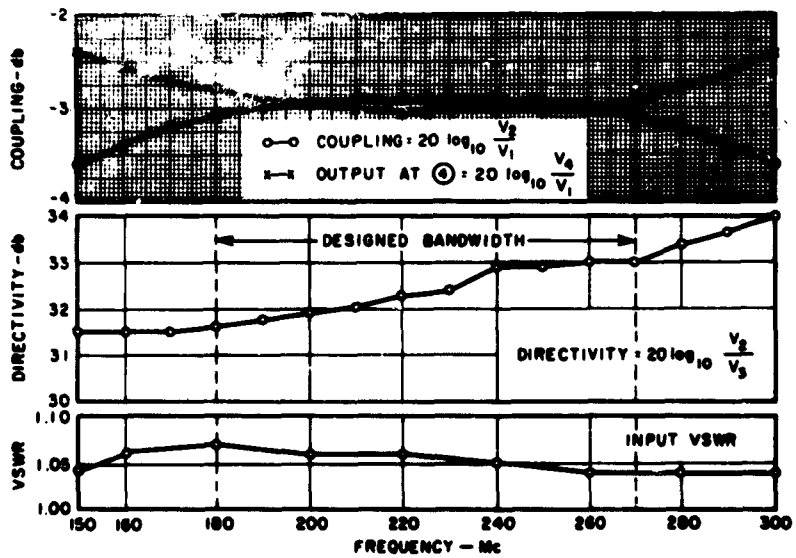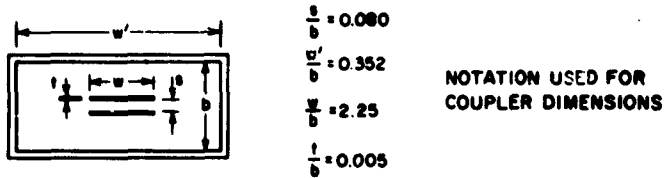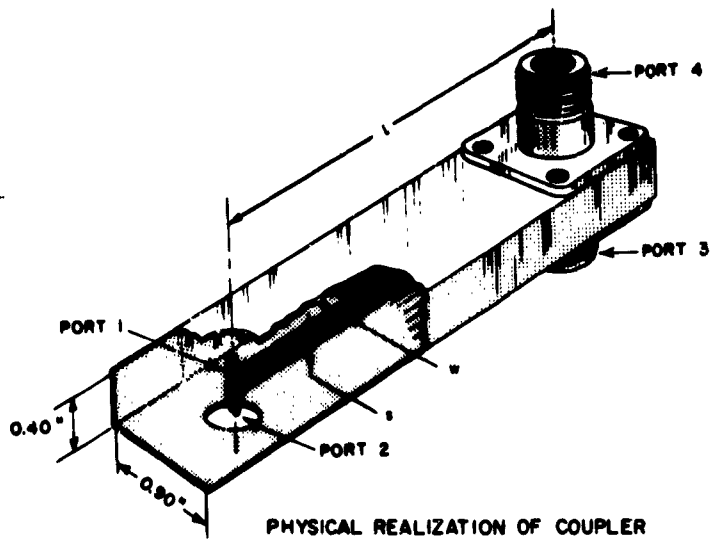
PHYSICAL REALIZATION OF COUPLER

$\frac{s}{b} = 0.080$

$\frac{w'}{b} = 0.352$

$\frac{w}{b} = 2.25$

$\frac{t}{b} = 0.005$

NOTATION USED FOR
COUPLER DIMENSIONS

MEASURED PERFORMANCE

A-3867-336

FIG. 13.05-1   CONSTRUCTION DETAILS AND MEASURED PERFORMANCE
OF A PRINTED-CIRCUIT, 3-db COUPLER

786

0.032 inch so that with $b = 0.400$ inch in Fig. 13.05-1, $s/b = 0.08$, and $t/b = 0.005$. The value of w/b is then determined from either Eq. (5.05-16) or Eq. (5.05-17), using the values of $C'_{fe}/\epsilon = 0.545$ or $C'_{fo}/\epsilon = 1.21$ determined from Fig. 5.05-4. In using Eq. (5.05-16) one should use the value $(s + 2t)/b = 0.09$ for s/b in that formula, which assumes $t/b = 0$, since it is the fields external to the strips that are significant in determining Z_{oe}. One finds that $w/b = 0.373$. Using Eq. (5.05-17) with $s/b = 0.08$, since the fields between the strips are of most significance in determining Z_{oo}, one finds $w/b = 0.337$. The fact that different values of w/b are obtained using these two formulas is a reflection of the fact that they are only approximately correct.

The actual value of w/b used in this coupler was 0.352, which lies between these two theoretical values. It was computed by an approximate technique before Eqs. (5.05-16) and (5.05-17) were available. The spacing $(w' - w)/2$ between the edges of the strips and the side walls of the metal case is great enough so that it does not have any appreciable effect on the even- and odd-mode impedances of the strips.

Another useful type of printed-circuit configuration[13] for tight coupling is illustrated in Fig. 13.05-2. The measured response of a coupler constructed with these dimensions is shown in Fig. 13.05-3. This coupler was designed to operate at a 50-ohm impedance level and to have 2.8-db coupling at midband. However, the absorption in the dielectric material having relative dielectric constant $\epsilon_r = 2.77$ was sufficient to reduce the transmission by 0.2 db.

The dimensions of the strips are determined as follows. Equations (13.02-5) and (13.02-6) multiplied by $\sqrt{\epsilon_r}$ yield $\sqrt{\epsilon_r} \, Z_{oe} = 205$ ohms and $\sqrt{\epsilon_r} \, Z_{oo} = 32.8$ ohms. A value of $\Delta C/\epsilon = 4.82$ is then determined from Eq. (5.05-20). Next, a value of $g/b = 0.096$ was chosen and $d/g = 0.445$ read from Fig. 5.05-5. Figure 5.05-6 and Fig. 5.05-7 then yield $C'_{ca}/\epsilon = 0.55$ and $C'_{ee}/\epsilon = 0.115$, respectively. Using these values and the value of $C_{ee}/\epsilon = 1.81$ determined from Eq. (5.05-21) one finds an initial value of $c/b = 0.108$. Figure 5.05-8 yields $C'_{se}/\epsilon = -0.105$, and Eq. (5.05-22a) yields $a/b = 0.284$. Since the strip width c is narrow enough compared to b so that the fringing fields at either edge interact and decrease its total strip capacitance, it is necessary to increase the value of c as given in Eq. (5.05-22c), yielding the final values of $c/b = 1.42$.

787

NOTATION USED FOR COUPLER DIMENSIONS

DIMENSIONS OF COUPLED STRIPS
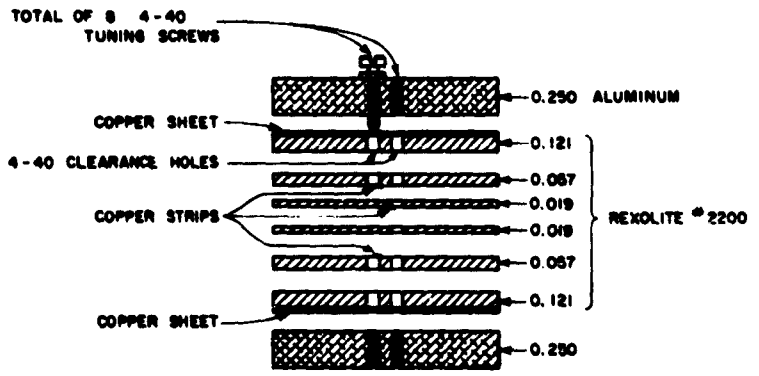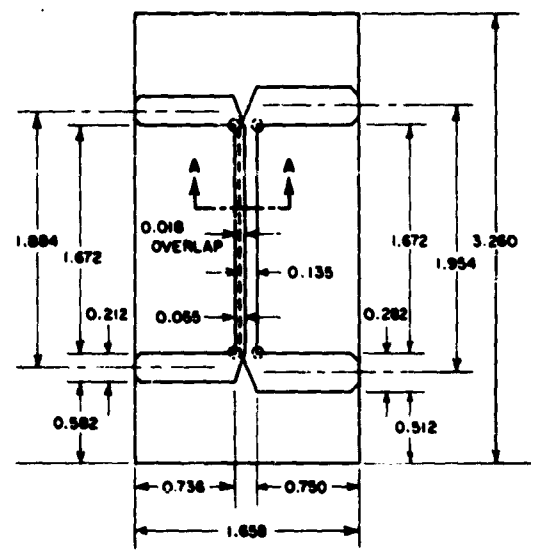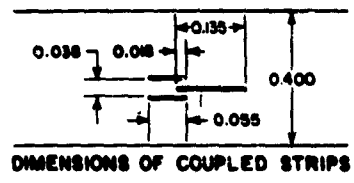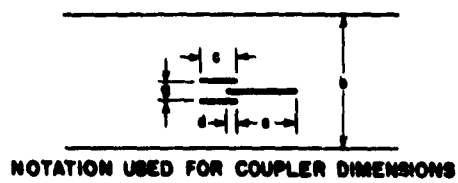
EXPLODED VIEW OF SECTION A-A

A-3887-336

FIG. 13.05-2 DETAILS OF CONSTRUCTION OF 1000-Mc, 3-db COUPLED-TRANSMISSION-LINE
DIRECTIONAL COUPLIER USING INTERLEAVED STRIPS

FIG. 13.05-3 MEASURED PERFORMANCE OF 1000-Mc, 3-db BACKWARD COUPLER USING INTERLEAVED STRIPS

The method of construction used for this coupler is clearly indicated in Fig. 13.05-2. The series inductive discontinuities introduced by the mitered corners at each port of the coupler were compensated by means of the capacitive screws shown in the figure. These screws were introduced in a symmetric fashion about the midplane of the coupler to prevent unwanted excitation of the parallel-plate TEM mode. This method of compensating the coupler was found to be much more effective than adding capacitive tabs directly to the strips themselves.

789

A directional coupler having tight coupling can also be constructed
using thick strips[14] of the type illustrated in Fig. 13.05-4. The strips
in this method of construction are thick
enough so that they have a substantial
amount of mechanical rigidity. Hence,
they may be supported at discrete points
by means of low-reflection dielectric
spacers, similar to those used to support
the center conductors of coaxial lines.
In some cases they may be simply held in
place by means of the connectors at each
of the four ports. Capacitive tuning
screws are usually necessary at each port
of this type of coupler to compensate
the inevitable discontinuities.

A-3827-330

FIG. 13.05-4 NOTATION FOR 3-db
COUPLER USING
THICK COUPLED
STRIPS

As an example of the method of choosing the dimensions of the
coupled strips for such a coupler the theoretical design of a quarter-
wavelength coupler having 2.7 db midband coupling and operating at a
50-ohm impedance level will now be considered. (The coupling over an
octave bandwidth will then be 3.0 ± 0.3 db.) Reference to Eqs. (13.02-5)
and (13.02-6) shows that Z_{oe} = 127.8 ohms and Z_{oo} = 19.6 ohms, and
Eq. (5.05-20) yields the value of $\Delta C/\epsilon$ = 8.13. The thickness of the
strips is then arbitrarily set so that t/b = 0.1. Figure 5.05-9 then
yields the values of s/b = 0.015 and C'_{fe}/ϵ = 0.578. From Fig. 5.05-10(b)
one finds C'_f/ϵ = 1.2, and from Eq. (5.05-18), C_{oe}/ϵ = 2.95. Then, using
Eq. (5.05-23), one finds w/b = 0.396.

In order to minimize discontinuity effects it is usually best to
choose $b \leq 0.1\lambda$, where λ is the wavelength in the dielectric material
filling the cross section. The length of the coupled strips is of
course 0.25λ at midband.

An interesting structure due to Cohn[7*] which is suitable for strong coupling
was indicated in Fig. 13.01-2(h); a completely shielded version is
shown in Figs. 13.05-5 and 13.05-6. Two coaxial transmission lines
are placed side-by-side. Their inner conductors A and B are entirely
separate, but their outer conductors touch and become the conductor C
in Fig. 13.05-5. The double-barreled conductor C is made one-quarter
wavelength long and its potential "floats" between that of the two
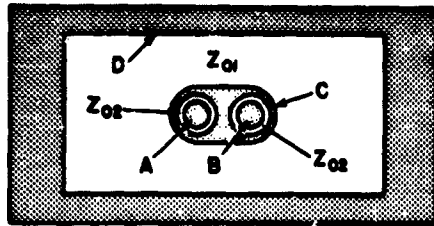
A-3527-602

FIG. 13.05-5   RE-ENTRANT COUPLED
                CROSS SECTION

conductors A and B, and that of the metal case D. The conductor C is held in position by dielectric supports (not shown in the figures). The conductor A in Fig. 13.05-5 connects Ports 3 and 4 in Fig. 13.05-6, while conductor B connects Ports 1 and 2. The characteristic impedance of C within D is denoted by Z_{01} (Fig. 13.05-5), and the two concentric lines within C each have characteristic impedance Z_{02}. The analysis is again carried out in terms of an even and an odd mode. For the odd mode, A and B are at equal and opposite potentials, and C is at ground potential. Therefore

$$Z_{oo} = Z_{02} \qquad\qquad (13.05\text{-}1)$$

For the even mode, each inner coaxial line (A or B to C) is in series with half the outer line (C to D), because the floating conductor C passes the currents flowing from its inner surface onto its outer surface which is therefore in series with it. This leads to[7]

$$Z_{oe} = Z_{02} + 2Z_{01} \qquad . \qquad (13.05\text{-}2)$$

The coupling is then determined as before from Eqs. (13.02-4) through (13.02-6).

For example, it was shown above that for a 2.7 db coupler with $Z_0 = 50$ ohms, one requires $Z_{oe} = 127.8$ ohms and $Z_{oo} = 19.6$ ohms.
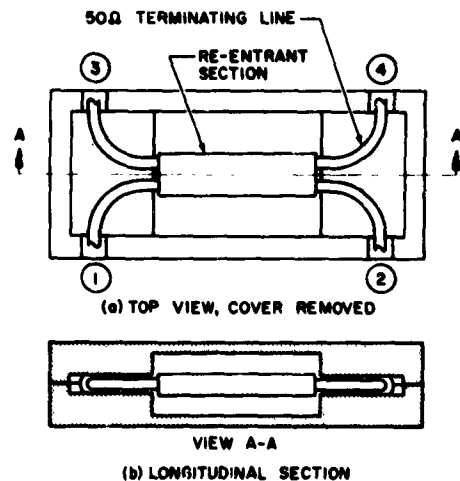
(a) TOP VIEW, COVER REMOVED

VIEW A-A

(b) LONGITUDINAL SECTION

A-3527-603

FIG. 13.05-6   VIEWS OF THE RE-ENTRANT
                DIRECTIONAL COUPLER

791

Solving for Z_{01} and Z_{02} from Eqs. (13.05-1) and (13.05-2),

$$Z_{01} = 54.1 \text{ ohms} , \quad Z_{02} = 19.6 \text{ ohms} .$$

In an experimental model[7], two tubes of 0.250-inch outside diameter were soldered together to form C, and the space between the tubes was filled with solder. The tube wall thickness was 0.022 inch, leaving an inner diameter of 0.206 inch. The inner conductors A and B were of diameter 0.149 inch to yield an impedance of $Z_{02} = 19.6$ ohms. The impedance Z_{01} of the outer line was obtained from data such as that in Fig. 5.04-2 for a rectangular inner conductor, by taking $t = 0.250$ inch; the effective width w was determined by equating cross-sectional areas. Then $w = (1 + \pi/4)t = 1.786t$. From Fig. 5.04-2 the plate-to-plate spacing is then $b = 0.746$ inch.

The impedance of the four lines emerging from the coupler is to be 50 ohms. (This applied to the region in which the inner conductors are curved 90-degrees toward the four ports in Fig. 13.05-6.) The dimensions for this "slab-line" region (circular inner conductor between ground planes) were chosen to be: diameter of inner conductor = 0.125 inch, plate-to-plate spacing $b = 0.228$ inch. (This gives a 50-ohm line.[7]) Since this plate-to-plate spacing (0.228 inch), is less than the height of the double-barreled conductor C (0.250 inch), a small gap has to be allowed between the step in b from 0.746 inch to 0.228 inch and the re-entrant section. This is clearly shown in Fig. 13.05-6. A gap of 0.050 inch was allowed.

Directivities better than 29 db over an octave bandwidth were reported for two experimental couplers, one centered at 500 megacycles and one at 1500 megacycles.[7] A three-section coupler was also built, with only the middle section re-entrant, the two outer sections being of the type shown in Fig. 13.01-2(a).[7]

SEC. 13.06, TYPICAL DESIGNS FOR TEM-MODE, COUPLED-TRANSMISSION-LINE DIRECTIONAL COUPLERS OF ONE SECTION AND WITH WEAK COUPLING

This section describes the theoretical design of TEM-mode couplers operating at a 50-ohm impedance level and having 20-db coupling at midband. Each coupler has a length $\ell = 0.25\lambda$ at midband, where λ is

the wavelength in the dielectric
surrounding the coupled lines. In
order to minimize discontinuity
effects, the spacing b between
ground planes in these couplers
should be no more than a tenth of
a wavelength at the highest operat-
ing frequency.

Figure 13.06-1 illustrates the
cross section of the first coupler
to be considered. The coupled strips
usually have a negligible thickness,
t, and are assumed to be supported by means of a dielectric of relative
dielectric constant $\epsilon_r = 2.56$ completely filling the cross section.
Values of $\sqrt{\epsilon_r}\, Z_{oe} = 88.5$ ohms and $\sqrt{\epsilon_r}\, Z_{oo} = 72.3$ ohms are obtained
using Eqs. (13.02-5) and (13.02-6). Then using Fig. 5.05-3(a) one finds
$s/b = 0.32$ and using Fig. 5.05-3(b) one finds $w/b = 0.715$.

The cross section of the second type of coupler to be considered
is illustrated in Fig. 13.06-2. The thickness, t, of these coupled
strips will be assumed to be negligible as well as the thickness of the
slot of width d. The length of this slot is of course a quarter wave-
length at midband. The dielectric material supporting these strips has
$\epsilon_r = 2.56$. Equations (13.02-5) and (13.02-6) yield $\sqrt{\epsilon_r}\, Z_{oe} = 88.5$ ohms
and $\sqrt{\epsilon_r}\, Z_{oo} = 72.3$ ohms. The value of $\sqrt{\epsilon_r}\, Z_{oo}$ is equal to $\sqrt{\epsilon_r}\, Z_0$, the
characteristic impedance of an uncoupled line, and therefore the value
of $w/b = 0.86$ can be obtained from Fig. 5.04-1. Then by the use of
Eqs. (5.05-7) through (5.05-10) one finds $d/b = 1.05$.

The third type of coupler to be considered is shown in cross section
in Fig. 13.06-3. In this type of coupler the conductors do not need
to be surrounded with dielectric for support. In addition, the round
conductors make this type of coupler ideal for high-power applications.
Using Eqs. (13.02-5) and (13.02-6) we find $Z_{oe} = 55.3$ ohms and $Z_{oo} = $
45.2 ohms. Then from Eq. (5.05-11) one finds $s/b = 1.01$ and from
Eq. (5.05-12) one finds $d/b - 0.59$.

A-3627-329

FIG. 13.06-1 NOTATION FOR 20-db
COUPLER USING EDGE-
COUPLED FLAT STRIPS
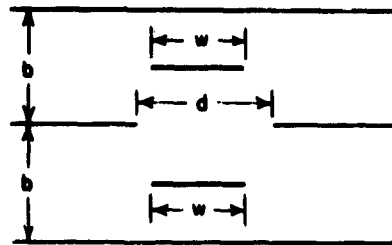
A-3527-328

A-3527-331

FIG. 13.06-2 NOTATION FOR 20-db
COUPLER USING
SLOT-COUPLED
FLAT STRIPS
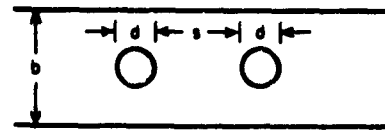
FIG. 13.06-3 NOTATION FOR 20-db
COUPLER USING
ROUND CONDUCTORS

SEC. 13.07, DERIVATION OF DESIGN FORMULAS FOR TEM-MODE, COUPLED-TRANSMISSION-LINE COUPLERS OF ONE SECTION

The basic coupled-transmission-line directional coupler is shown schematically at the top of Fig. 13.07-1 with resistance terminations Z_0 at each port. It is excited with a voltage $2E$ in series with Port 1. At the bottom of Fig. 13.07-1 the same directional coupler is shown in two different states of excitation. In the odd excitation, out-of-phase voltages are applied in series with Ports 1 and 2 while the even excitation applies in-phase voltages in series with these ports. Through the principle of superposition it may be seen that the behavior of the directional coupler with voltage $2E$ applied in series with Port 1 can be obtained from its behavior with even- and odd-voltage excitations.

Symmetry considerations show that a vertical electric wall may be placed between the strips of the coupler when it is excited with voltages having odd symmetry, and a vertical magnetic wall may be inserted between the strips when it is excited with voltages having even symmetry. The characteristic impedance of one of these strips in the presence of an electric wall is Z_{oo}, while the characteristic impedance of a strip in presence of a magnetic wall is Z_{oe}.

In order for the directional coupler to be perfectly matched at all frequencies it is necessary that the input impedance Z_{in} be equal to Z_0. Applying the principle of superposition, one sees that the input impedance of the directional coupler terminated in Z_0 can be written as
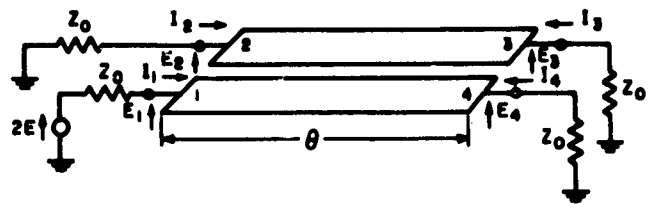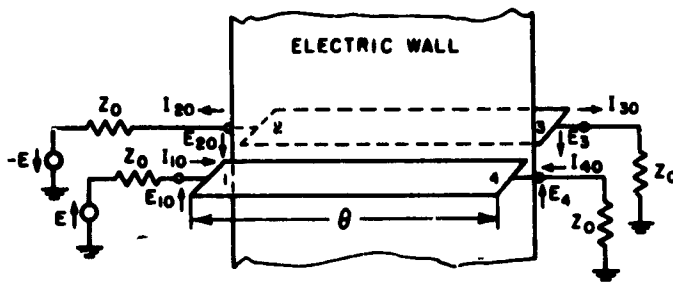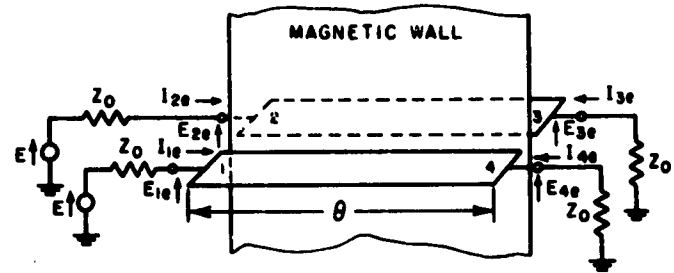
FIG. 13.07-1 COUPLED-STRIP DIRECTIONAL COUPLER
WITH EVEN AND ODD EXCITATION

$$Z_{in} = \frac{E_{1o} + E_{1e}}{I_{1o} + I_{1e}} = \frac{\dfrac{Z_{1o}}{Z_0 + Z_{1o}} + \dfrac{Z_{1e}}{Z_0 + Z_{1e}}}{\dfrac{1}{Z_0 + Z_{1o}} + \dfrac{1}{Z_0 + Z_{1e}}} \qquad (13.07\text{-}1)$$

where

$$Z_{1o} = Z_{oo} \frac{Z_0 + jZ_{oo} \tan \theta}{Z_{oo} + jZ_0 \tan \theta} \qquad (13.07\text{-}2)$$

and

$$Z_{1e} = Z_{oe} \frac{Z_0 + jZ_{oe} \tan \theta}{Z_{oe} + jZ_0 \tan \theta} \qquad . \qquad (13.07\text{-}3)$$

When Eq. (13.07-2) and Eq. (13.07-3) are substituted into Eq. (13.07-1) it is found that $Z_{in} = Z_0$ when

$$Z_0 = \sqrt{Z_{oo} Z_{oe}} \qquad , \qquad (13.07\text{-}4)$$

for all values of θ.

Under the condition that $Z_0 = \sqrt{Z_{oe} Z_{oo}}$, the voltage appearing at Port 1 of the coupler is $E_1 = E$. The voltages $E_{2e} = E_{1e}$ and $E_{3e} = E_{4e}$ may be determined from the straightforward analysis of a transmission line of length θ, and characteristic impedance Z_{oe} terminated at either end by an impedance $\sqrt{Z_{oe} Z_{oo}}$ and fed by a voltage E. Likewise the normal-mode voltages $E_{2o} = -E_{1o}$ and $E_{3o} = -E_{4o}$ may be determined from a similar analysis of a transmission line of length θ and characteristic impedance Z_{oo} terminated by $\sqrt{Z_{oe} Z_{oo}}$. The results of this analysis show that

$$\frac{E_2}{E} = \frac{E_{2e} - E_{2o}}{E} = j \frac{\sin \theta \left(\sqrt{\dfrac{Z_{oe}}{Z_{oo}}} - \sqrt{\dfrac{Z_{oo}}{Z_{oe}}} \right)}{2 \cos \theta + j \sin \theta \left(\sqrt{\dfrac{Z_{oe}}{Z_{oo}}} + \sqrt{\dfrac{Z_{oo}}{Z_{oe}}} \right)} \qquad (13.07\text{-}5)$$

$$= \frac{jc \sin \theta}{\sqrt{1 - c^2} \cos \theta + j \sin \theta} \tag{13.07-6}$$

$$E_3 = E_{3_e} - E_{3_o} = 0 \tag{13.07-7}$$

$$\frac{E_4}{E} = \frac{E_{4_e} - E_{4_o}}{E} = \frac{2}{2 \cos \theta + j \sin \theta \left(\sqrt{\frac{Z_{o_e}}{Z_{o_o}}} + \sqrt{\frac{Z_{o_o}}{Z_{o_e}}} \right)} \tag{13.07-8}$$

$$= \frac{\sqrt{1 - c^2}}{\sqrt{1 - c^2} \cos \theta + j \sin \theta} \tag{13.07-9}$$

The maximum coupled voltage E_2 occurs when the coupler is a quarter-wavelength long (i.e., $\theta = 90°$). Therefore, from Eq. (13.07-5) a maximum coupling factor c may be defined as in Eq. (13.02-3). With this substitution, the voltage at Port 2 can be written as Eq. (13.02-1) while the voltage at Port 4 can be written as Eq. (13.02-2). The maximum coupling occurs at center frequency ($\theta = \pi/2$) and is given by (Eq. (13.02-3).

SEC. 13.08, QUARTER-WAVE FILTER PROTOTYPE CIRCUITS FOR TEM-MODE, COUPLED-TRANSMISSION-LINE DIRECTIONAL COUPLERS

A single-section, quarter-wave filter prototype circuit is shown in Fig. 13.08-1. It consists of two impedance steps (one up and one down), separated by an electrical distance θ. All characteristic impedances are normalized with respect to the characteristic impedances of the two terminating lines, which are taken as unity. The wave amplitudes a_1, b_1, and a_2 (Fig. 13.08-1) are defined in terms of the power flow,[16] i.e. $|a_1|^2$ and $|a_2|^2$ represent power carried forward, while $|b_1|^2$ represents reflected power. With the notation of Fig. 13.08-1 it can be shown[16] that

$$\frac{b_1}{a_1} = \frac{\Gamma(1 - e^{-2j\theta})}{1 - \Gamma^2 e^{-2j\theta}} \tag{13.08-1}$$

or equivalently,
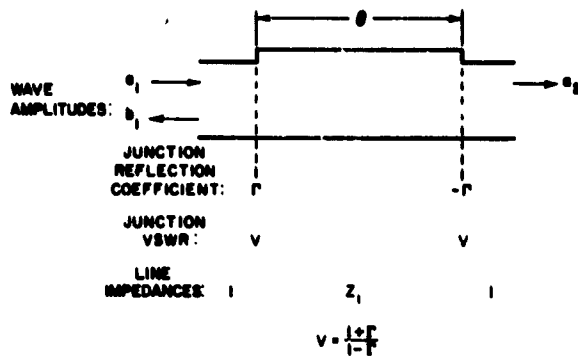
FIG. 13.08-1 QUARTER-WAVE FILTER PROTOTYPE
FOR SINGLE-SECTION TEM-MODE
COUPLER

$$\frac{b_1}{a_1} = \frac{\left(\dfrac{2\Gamma}{1 + \Gamma^2}\right) j \sin \theta}{\left(\dfrac{1 - \Gamma^2}{1 + \Gamma^2}\right) \cos \theta + j \sin \theta} \qquad , \qquad (13.08-2)$$

and

$$\frac{a_2}{a_1} = \frac{(1 - \Gamma^2)e^{-j\theta}}{1 - \Gamma^2 e^{-2j\theta}} \qquad (13.08-3)$$

$$= \frac{\left(\dfrac{1 - \Gamma^2}{1 + \Gamma^2}\right)}{\left(\dfrac{1 - \Gamma^2}{1 + \Gamma^2}\right) \cos \theta + j \sin \theta} \qquad . \qquad (13.08-4)$$

Equations (13.07-6) and (13.07-9) with Eqs. (13.08-2) and (13.08-4) now
show that b_1/a_1 corresponds to E_2/E, and a_2/a_1 corresponds to E_4/E,
and that these equations are mathematically equivalent when we set

$$c = \frac{2\Gamma}{1 + \Gamma^2} = \frac{Z_1^2 - 1}{Z_1^2 + 1} \qquad (13.08-5)$$

798

when Z_1 is chosen greater than unity.   Conversely

$$\Gamma = \frac{1 - \sqrt{1 - c^2}}{c} \tag{13.08-6}$$

It follows that quarter-wave, coupled TEM-mode directional couplers can be solved as quarter-wave filters as discussed at the beginning of Sec. 13.03.   It can be shown that for the single-section coupler of Fig. 13.01-1(a), [compare Eqs. (6.02-5) and (6.02-6)]

$$\left|\frac{E}{E_4}\right|^2 = 1 + \frac{(R - 1)^2}{4R} \sin^2 \theta \tag{13.08-7}$$

where

$$R = Z_1^2 = \frac{1 + c}{1 - c} \tag{13.08-8}$$

is the VSWR of the prototype filter (Fig. 13.08-1) at center frequency ($\theta = \pi/2$).   The over-all power coupling ratio is then

$$\left.\begin{array}{l} \left|\dfrac{E_2}{E}\right|^2 = 1 - \left|\dfrac{E_4}{E}\right|^2 \\[3em] \qquad = \dfrac{\dfrac{(R - 1)^2}{4R} \sin^2 \theta}{1 + \dfrac{(R - 1)^2}{4R} \sin^2 \theta} \\[3em] \qquad = \dfrac{c^2 \sin^2 \theta}{1 - c^2 \cos^2 \theta} \ . \end{array}\right\} \tag{13.08-9}$$

Table 13.08-1 summarizes the principal formulas for TEM-mode couplers (with and without end-to-end symmetry) in terms of the parameters of the prototype quarter-wave filter.

Table 13.08-1

GENERAL FORMULAS FOR THE DESIGN OF TEM-MODE COUPLED-TRANSMISSION-
LINE DIRECTIONAL COUPLERS FROM THE QUARTER-WAVE FILTER PROTOTYPE

The midband VSWR R of the quarter-wave filter is related to the over-all
coupling factor c_0 of the coupler by

$$R = \frac{1 + c_0}{1 - c_0} \quad \text{or} \quad c_0 = \frac{R - 1}{R + 1}$$

The midband VSWR R of the quarter-wave filter is

$$R = \left(\frac{Z_1 Z_3 Z_5 \cdots}{Z_2 Z_4 Z_6 \cdots}\right)^{\pm 2} > 1$$

where the Z_i are the normalized impedances of the quarter-wave filter prototype
sections.

The coupling factors c_i of the several coupler sections are related to the
normalized impedances Z_i of the quarter-wave filter prototype sections by

$$Z_i^2 = \frac{1 + c_i}{1 - c_i} \quad , \quad c_i = \frac{Z_i^2 - 1}{Z_i^2 + 1} \quad .$$

The even-mode and odd-mode impedances, $(Z_{oe})_i$ and $(Z_{oo})_i$, of the coupler
sections are given by

$$(Z_{oe})_i = Z_0 \sqrt{\frac{1 + c_i}{1 - c_i}}$$

$$(Z_{oo})_i = Z_0 \sqrt{\frac{1 - c_i}{1 + c_i}} \quad .$$

Certain simplifications result for couplers with end-to-end symmetry. In that case n
is odd, and

$$c_i = c_{n+1-i}$$

$$Z_i = Z_{n+1-i}$$

$$V_i = V_{n+2-i} = \text{VSWR of } i\text{th step in prototype}$$

and

$$R = \left(V_1 V_3 V_5 \cdots V_n\right)^2$$

$$= \left(V_2 V_4 V_6 \cdots V_{n+1}\right)^2$$

Figure 13.03-1 showed a symmetrical TEM-mode coupler of three sections together with its quarter-wave filter prototype, and the associated notation. Notice that the filter has end-to-end symmetry, unlike the transformers in Chapter 6. This prototype filter is not matched at center frequency, as zero reflection in the prototype corresponds to zero coupling in the corresponding directional coupler. The TEM-mode coupled-transmission-line directional coupler performs exactly as a quarter-wave filter in which the forward and backward waves have been separated and have become two traveling waves (in opposite directions) on two parallel transmission lines, the over-all reflection coefficient of the prototype becoming the over-all coupling factor of the coupler. This is indicated in Fig. 13.03-1.

No quarter-wave filter prototype solutions for couplers with seven or more sections have been obtained to date. The equal-ripple characteristics desired of three-, five-, and seven-section symmetrical couplers (and prototypes) are summarized in Fig. 13.08-2. Solutions for the three-section coupler were presented in Sec. 13.03, and for the five-section coupler in Sec. 13.04.

Phase Relation Between Outputs—For a symmetrical coupler the two outputs E_2 and E_4 (shown for a three-section coupler in Fig. 13.03-1) are in quadrature at all frequencies (i.e., differ by 90 degrees when measured at the extremities of the coupler). This result follows at once from the quarter-wave filter analogy, since for any symmetrical dissipation-free 2-port, the reflected and transmitted wave amplitudes are orthogonal.[17]

SEC. 13.09, CONSIDERATIONS AND GENERAL FORMULAS FOR
BRANCH-LINE COUPLERS

Branch-line couplers are directional couplers consisting of two parallel transmission lines coupled through a number of branch lines (Fig. 13.09-1). The lengths of the branch lines and their spacings are all one-quarter guide wavelength at center frequency, as shown in Fig. 13.09-1. The characteristic impedances of the two parallel main lines may be changed from section to section, and the branch impedances may be adjusted also to improve the electrical performance.

Figure 13.09-1 could represent the cross section of the inner conductor of a coaxial line, or the printed center conductor of a strip
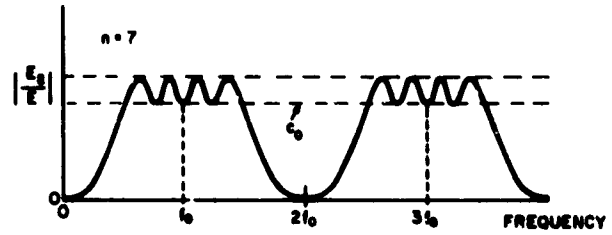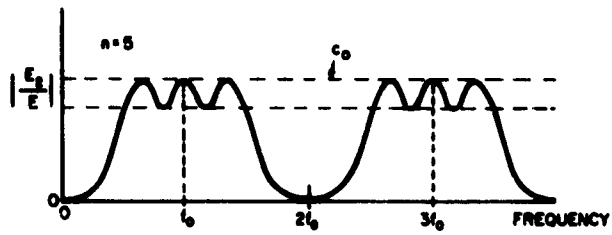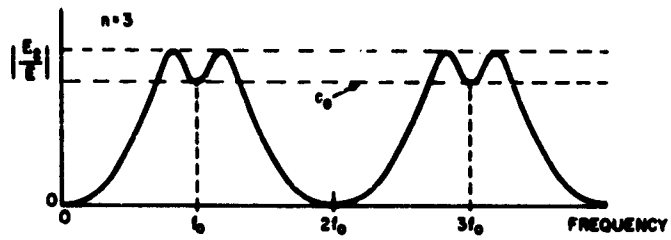
A-3687-006

SOURCE: Proc. IEE (see Ref. 24 by L. Young)

FIG. 13.08-2 DESIRED COUPLING CHARACTERISTICS OF
THREE-, FIVE-, AND SEVEN-SECTION
TEM-MODE SYMMETRICAL COUPLERS
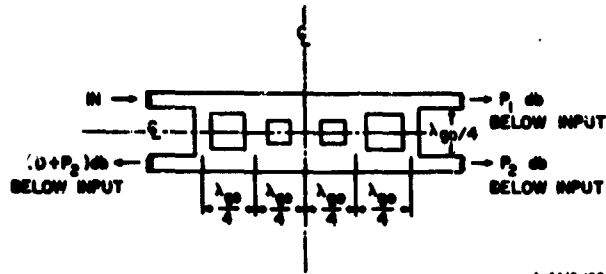
FIG. 13.09-1   BRANCH-LINE COUPLER SCHEMATIC

transmission line, or the E-plane cross section of a waveguide
(Sec. 13.14). The output at the in-line termination is denoted by P_1 db
(below the input), the coupling is P_2 db, and the directivity is
D db (see Fig. 13.09-1).

The branches may be in shunt with the main line (as in coaxial and
strip transmission line) or in series with it (as in waveguide). For
shunt junctions it is more convenient to use admittances, and for series
junctions it is more convenient to use impedances. The term "immittance"
will be used to denote either (shunt) admittances or (series) impedances.
The notation giving the characteristic immittances is depicted in
Fig. 13.09-2. The coupler is supposed to have end-to-end symmetry, so
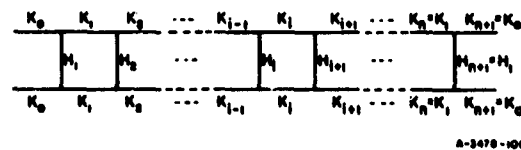
that $H_{n+1} = H_1$, etc., and $K_1 = K_n$, etc. It will be convenient
to normalize with respect to the
terminating immittances $K_0 = K_{n+1} = 1$ throughout this chapter.

FIG. 13.09-2   BRANCH-LINE COUPLER
NOTATION

All the junctions will be
assumed to be ideal shunt or
series junctions in the design
procedure, and each line length
between junctions will be assumed
to vary as a line one-quarter
guide wavelength along at the center frequency. The effect of the
junction reference planes (Sec. 13.14) is included only in calculating
the final physical dimensions; the effect of junction discontinuity

803

reactances is often not large, and in many cases can be compensated using the data in Sec. 5.07 and in Refs. 18, 19, and 20, as will be discussed in an example in Sec. 13.14. The appearance of branch-line couplers (Sec. 13.11) in rectangular wave-guide frequently works out as indicated in Fig. 13.09-1 (see Sec. 13.14), where the two outer walls (top and bottom of Fig. 13.09-1) have been shown as straight lines. However, this result should not necessarily be assumed to hold in all cases.

Even- and Odd-Mode Analysis—Branch-line couplers may be analyzed in terms of an even mode (two in-phase inputs) and an odd mode (two out-of-phase inputs) which are then superposed, adding at one port and cancelling at the other, thus yielding only one actual input. This is summarized in Fig. 13.09-3. For shunt-connected branches the two inputs of the odd mode produce zero voltage across the center of all the branches, and thus a short-circuit may be placed there; the two halves may therefore be "separated", each half consisting of a transmission line with 45-degree shorted stubs at 90-degree spacings. Meanwhile the even mode similarly yields 45-degree open-circuited stubs (Fig. 13.09-3). The 45-degree short-circuited stubs, and the 45-degree open-circuited stubs produce equal and opposite phase shifts $\pm\theta$ at center frequency in the even- and odd-mode inputs. For a matched coupler with perfect directivity the two outputs are then $\cos^2\theta$ and $\sin^2\theta$ in power, when the input power (sum of even and odd modes) is unity. For the case of series-connected stubs, the same reasoning applies, only the roles of the even and odd modes are reversed. For a fuller explanation, the references should be consulted.[8-11]

Cascaded Matched Directional Couplers—When matched couplers are cascaded, as shown in Fig. 13.09-4, they act as a single directional coupler, and the over-all couplings of the combination, $P_{1,\text{com}}$ and $P_{2,\text{com}}$ are readily calculated from the individual couplings $P_{1,i}$ db and $P_{2,i}$ db by the following formula:

$$P_{1,\text{com}} = 20 \log_{10}\left[\cos\left(\sum_{i=1}^{N}\theta_i\right)\right] \qquad \text{db} \qquad (13.09\text{-}1)$$
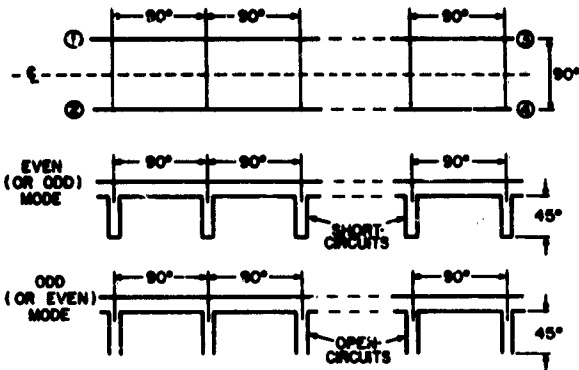
PORT	1	2	3	4
EVEN MODE	↑	↑	λ_θ	λ_θ
ODD MODE	↑	↓	θ	θ
SUM	↑	ZERO	↓	→
AMPLITUDE	1	0	$\cos\theta$	$\sin\theta$
POWER	1	0	$\cos^2\theta$	$\sin^2\theta$

B-3478-102

FIG. 13.09-3 SUMMARY OF EVEN- AND ODD-MODE
ANALYSIS
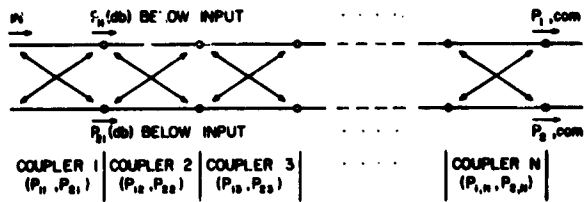
A-3478-103

FIG. 13.09-4 SEVERAL MATCHED DIRECTIONAL
COUPLERS IN CASCADE

Table 13.09-1

MIDBAND FORMULAS FOR BRANCH-LINE COUPLERS UP TO SIX BRANCHES

	2-BRANCHES	3-BRANCHES	4-BRANCHES	5-BRANCHES	6 BRANCHES
Condition for Perfect Match and Directivity	$K_1^2 = 1 - H_1^2$	$H_2 = \dfrac{2H_1 K_1^2}{1 + H_1^2}$	$K_2^2 = H_2^2 + \dfrac{K_1^2(K_1^2 - 2H_1 H_2)}{1 + H_1^2}$	$\dfrac{H_3}{K_2^2} = \dfrac{2(H_2 + H_1^2 H_2 - H_1 K_1^2)}{K_1^4 + H_2^2(1 + H_1^2) - 2H_1 H_2 K_1^2}$	(see original)
$\dfrac{E_2}{E_1} = \text{antilog}\left(\dfrac{P_1 - P_2}{20}\right)$ (P_1 and P_2 positive)	$\dfrac{2H_1}{1 - H_1^2 + K_1^2}$	$\dfrac{2H_1(K_1^2 + H_2(1 - H_1^2)}{2(K_1^2 - H_1 H_2)}$	$\dfrac{2H_1(K_1^2 - H_1 H_2^2 + H_2 K_1^2)}{K_1^4 + (1 - H_1^2)(K_1^2 - H_2^2) - 2H_1 H_2 K_1^2}$	(see original)	(see original)
Conditions for 3-db Directional Coupler	$H_1 = 1$ $K_1 = \sqrt{2}$	$H_1 = \sqrt{2} - 1$ $K_1^2 = H_2\sqrt{2}$	$H_2 = \dfrac{K_1^2(1 - H_1)}{1 + 2H_1 - H_1^2}$ $H_2^2 = \dfrac{2H_2^2}{(1 - H_1)^2}$, $K_2 = \dfrac{H_2\sqrt{2}}{1 - H_1}$ if $H_1 < 1$	$\dfrac{K_1^2}{1 + H_1} = \dfrac{H_2(2K_2^2 - H_2 H_3)}{K_2^2 - H_2 H_3}$ $\dfrac{K_1^4}{1 - 2H_1 - H_1^2} = \dfrac{H_2(2K_2^2 - H_2 H_3)}{H_3}$	$\dfrac{K_1^2(1 - H_1)}{1 + 2H_1 - H_1^2} = H_2 + \dfrac{H_3 K_1^2}{K_2^2 - H_3^2}$ $\dfrac{K_1^2}{1 - H_1} = \dfrac{(K_2^2 - H_2 H_3 - H_2 K_3)(K_2^2 - H_2 H_3 + H_3 K_3)}{H_2(K_2^2 - H_3^2) + H_3 K_3^2}$
Conditions for 6-db Directional Coupler	not possible ($H_1, K_1 \to \infty$)	$H_1 = 1$ $H_2 = K_1^2$	$K_2 = H_2$ $H_2 = \dfrac{K_1^2}{2H_1}$	$\dfrac{K_1^2}{H_1} = \dfrac{H_2(2K_2^2 - H_2 H_3)}{K_2^2 - H_2 H_3}$ $\dfrac{K_1^4}{1 - H_1^2} = \dfrac{H_2(2K_2^2 - H_2 H_3)}{H_3}$	$H_3 = \dfrac{H_3 K_1^2}{K_1^2 - 2H_1 H_2}$ for $K_1^2 > 2H_1 H_2$ $K_2^2 = H_2(K_3 + H_3)$, $K_2 > H_2 H_3$

SOURCE: *Proc. Nat. Electronics Conf.* (see Ref. 10 by Leo Young).

$$P_{2,\text{com}} = 20 \log_{10} \left[\sin\left(\sum_{i=1}^{N} \theta_i \right) \right] \qquad \text{db} \qquad (13.09\text{-}2)$$

where

$$\theta_i = \cos^{-1} \left[\text{antilog} \left(\frac{P_{1,i}}{20} \right) \right] \qquad (13.09\text{-}3)$$

$$= \sin^{-1} \left[\text{antilog} \left(\frac{P_{2,i}}{20} \right) \right] \qquad (13.09\text{-}4)$$

For instance, a phase shift of $\theta = 30$ degrees yields a 6-db coupler, and a phase shift of $\theta = 90$ degrees yields a 0-db coupler; therefore, a cascade of three matched 6-db couplers results in a 0-db coupler.

Midband Formulas.—There are certain relations which ensure perfect match and perfect directivity at center frequency. Furthermore, at center frequency the ratio of the two output voltages $E_1 \propto$ antilog $(-P_1/20)$ and $E_2 \propto$ antilog $(-P_2/20)$ can be written down fairly simply in terms of the H_i and K_i in Fig. 13.09-2. Table 13.09-1 gives these formulas for up to six branches. Also given are simpler formulas which determine the conditions for 3-db and 0-db coupling, together with perfect match and perfect directivity, at center frequency.

SEC. 13.10, PERIODIC BRANCH-LINE COUPLERS

Additional restrictions may be placed on the immittances of symmetrical couplers (Fig. 13.09-2). In particular when

$$\left. \begin{array}{l} K_i = K_0 , \quad i = 1,2,\ldots, n+1, \\[2ex] H_i = H_2 , \quad 2 \le i \le n, \end{array} \right\} \qquad (13.10\text{-}1)$$

and further, when $H_1 = H_{n+1}$ is chosen to give a perfect input match at center frequency, then such couplers will herein be called *periodic*. Thus the through-lines are uniform, and all the interior branches are the same. Such couplers have been analyzed by Reed and Wheeler.[8,9] Let the power coupling ratio at center frequency be denoted by

$$c_0^2 = \text{antilog}\left(-\frac{P_2}{10}\right) \qquad (13.10\text{-}2)$$

where P_2 is in decibels and was defined in Fig. 13.09-1. (For example, for a 6-db coupler, $c_0^2 = \frac{1}{4}$.) The solution of periodic couplers involves the Tchebyscheff polynomials $S_n(x)$, which have been tabulated numerically,[21] and which are defined by

$$\left.\begin{aligned}
S_0(x) &= 1 \\
S_1(x) &= x \\
S_2(x) &= x^2 - 1 \\
S_3(x) &= x^3 - 2x \\
S_4(x) &= x^4 - 3x^2 + 1 \\
S_5(x) &= x^5 - 4x^3 + 3 \\
S_6(x) &= x^6 - 5x^4 + 6x^2 - 1 \\
S_n(x) &= xS_{n-1}(x) - S_{n-2}(x)
\end{aligned}\right\} \qquad (13.10\text{-}3)$$

The immittances H_1 and H_2 of a periodic coupler then have to satisfy[9]

$$S_{n-1}(-H_2) = \left\{\begin{aligned}
&\sqrt{1 - c_0^2}\,, &&\text{when } n = \text{odd} \\
&\text{or } c_0\,, &&\text{when } n = \text{even}
\end{aligned}\right\} \qquad (13.10\text{-}4)$$

and

$$H_1 = \left| \frac{\left|\sqrt{1 - S_{n-1}^2(-H_2)}\right| - |S_{n-2}(-H_2)|}{S_{n-1}(-H_2)} \right| \qquad (13.10\text{-}5)$$

Table 13.10-1[9] gives solutions for some 0-db, 3-db, and 10-db couplers.

The performances of four different 3-db periodic couplers given by Table 13.10-1 are summarized in Tables 13.10-2 and 13.10-3. The maximum VSWR over three specified fractional bandwidths

$$w_b = 2\left(\frac{\lambda_{g1} - \lambda_{g2}}{\lambda_{g1} + \lambda_{g2}}\right) \qquad (13.10\text{-}6)$$

EXAMPLES OF 0-, 3-, AND 10-db PERIODIC COUPLERS

Number of Sections (n)	0-db Coupler		3-db Coupler		10-db Coupler	
	N_1	N_2	N_1	N_2	N_1	N_2
2	1.000	1.000	0.4141	0.7071	0.162	0.3162
3	0.500	1.000	0.2346	0.5412	0.0945	0.2265
4	0.618	0.618	0.2088	0.3810	0.0811	0.1602
5	0.309	0.618	0.1464	0.3179	0.0592	0.1312
6	0.445	0.445	0.1374	0.2585		
7	0.2225	0.445	0.1064	0.2257		
8	0.3473	0.3473	0.1022	0.1948		
9	0.1736	0.3473	0.0837	0.1752		
10	0.2846	0.2846				
11	0.1423	0.2846				
12	0.2410	0.2410				
13	0.1205	0.2410	0.0587	0.1210		

SOURCE: *IRE Trans. PGMTT* (see Ref. 9 by J. Reed)

Table 13.10-2

MAXIMUM VSWR OF SEVERAL 3-db PERIODIC COUPLERS OVER STATED BANDWIDTHS

FRACTIONAL BANDWIDTH w_b	COUPLERS			
	Four-branch	Five-branch	Six-branch	Eight-branch
0.16	1.02	1.05	1.02	1.01
0.28	1.08	1.10	1.05	1.04
0.48	1.32	1.12	1.15	1.07

SOURCE: Tech. Note 3, Contract AF30(602)-2392, SRI (see Ref. 22 by Leo Young)

Table 13.10-3

COUPLING UNBALANCE (db) OF SEVERAL 3-db PERIODIC COUPLERS OVER STATED BANDWIDTHS

FRACTIONAL BANDWIDTH w_b	COUPLERS			
	Four-branch	Five-branch	Six branch	Eight-branch
0.16	0.20	0.18	0.16	0.14
0.28	0.67	0.51	0.49	0.43
0.48	2.3	1.6	1.5	1.4

SOURCE: Tech. Note 3, Contract AF30(602)-2392, SRI (see Ref. 22 by Leo Young)

is shown in Table 13.10-2, where λ_{g1} is the longest guide wavelength, and λ_{g2} is the shortest guide wavelength over the band under consideration. The guide wavelength at band-center is given by

$$\lambda_{g0} = \left(\frac{2\lambda_{g1}\lambda_{g2}}{\lambda_{g1} + \lambda_{g2}} \right) \qquad . \qquad (13.10\text{-}7)$$

The coupling P_2 becomes stronger, and the coupling P_1 becomes weaker, than 3 db at about the same rate, as the frequency changes from band-center. The total variation $|\Delta P_1| + |\Delta P_2|$, referred to as the "coupling unbalance," is shown in Table 13.10-3 for the same 3-db couplers.

The performances of five different 0-db periodic couplers given by Table 13.10-1 are summarized in Tables 13.10-4 and 13.10-5 over the same

Table 13.10-4

MAXIMUM VSWR OF SEVERAL 0-db PERIODIC COUPLERS
OVER STATED BANDWIDTHS

FRACTIONAL BANDWIDTH w_b	COUPLERS				
	Six-branch	Eight-branch	Ten-branch	Twelve-branch	Fourteen-branch
0.16	1.10	1.06	1.04	1.03	1.02
0.28	1.19	1.09	1.05	1.03	1.02
0.46	1.21	1.10	1.12	1.09	1.05

SOURCE: Tech. Note 3, Contract AF30(602)-2392, SRI (see Ref. 22 by Leo Young)

Table 13.10-5

MAXIMUM INSERTION LOSS (db) OF SEVERAL 0-db PERIODIC COUPLERS
OVER STATED BANDWIDTHS

FRACTIONAL BANDWIDTH w_b	COUPLERS						
	Three-branch	Four-branch	Six-branch	Eight-branch	Ten-branch	Twelve-branch	Fourteen-branch
0.16	0.7	0.1	0.02	0.01	0.006	0.004	0.003
0.28	2.0	0.7	0.11	0.04	0.02	0.013	0.011
0.48	3.1	1.9	0.33	0.22	0.19	0.15	0.113

SOURCE: Tech. Note 3, Contract AF30(602)-2392, SRI (see Ref. 22 by Leo Young)

three specified fractional bandwidths. More detailed characteristics of some of these and other couplers are given in Refs. 9 and 22. Only couplers with an even number of branches (n odd) are given in

810

Tables 13.10-4 and 13.10-5; the performance of couplers with an odd number of branches (n even) is not as good. This is probably due to the fact that all the branches have the same immittances, including the two end ones, when the number of branches is odd, and thus there is no end-matching effect. For instance, a twelve-branch, 0-db periodic coupler gives better electrical performance than a thirteen-branch 0-db periodic coupler.[22]

SEC. 13.11, THE CHARACTERISTICS AND PERFORMANCE OF SYNCHRONOUS BRANCH-LINE COUPLERS

The *synchronous tuning condition* as it applies to transmission-line filters was formally defined toward the end of Sec. 6.01. Now recall that the even- and odd-mode analysis reduces a branch-guide coupler to two transmission-line filters, as indicated in Fig. 13.09-3. When the through-line impedance is uniform, neither of these two filters is synchronously tuned, since the reflections from any two finite reactances spaced one-quarter wavelength apart are not phased for maximum cancellation. They can be so phased, however, by adjusting the through-line impedances, and it turns out that both the even- and the odd-mode "filters" (Fig. 13.09-3) then become synchronously-tuned with the same choice of through-line impedances.[11] A quarter-wave transformer (Chapter 6) can then be used as a prototype circuit, resulting in a clearly marked pass band, in which the VSWR and directivity are nearly optimized. To meet a specified electrical performance over a given bandwidth, fewer branches will then be required with such optimized couplers than with periodic couplers (Sec. 13.10); from numerical examples, it appears that generally about half as many branches[22] will do. On the other hand, some of these branches will be wider than any in the corresponding periodic design, and so may depart more from ideal junction behavior. Such factors should be taken into account before deciding on the type of coupler. The chief advantages of synchronous couplers over periodic couplers are that they are more compact (for a specified performance), since there are fewer branches, and that the performance can be predicted fairly accurately.

The first step in designing a synchronous coupler with a specified center frequency coupling $P_{2,0}$ decibels and a specified fractional bandwidth w_b over which the performance is to be optimum, is to determine the output-to-input impedance ratio R and the fractional bandwidth w_q of the quarter-wave transformer prototype. They are generally obtained closely enough by the approximate relations

811

$$P_{2,0} = 20 \log_{10}\left(\frac{R+1}{R-1}\right) \qquad db \qquad (13.11\text{-}1)$$

and

$$w_b = 0.6 w_q \qquad (13.11\text{-}2)$$

Equation (13.11-1) is plotted in Fig. 13.11-1. It is exact for couplers which are perfectly matched at center frequency (such as all couplers with even n, and any maximally flat couplers). It is accurate enough for nearly all practical cases, but overestimates the numerical value of $P_{2,0}$ in proportion to the reflection loss. (An exact formula, necessary only when the center-frequency VSWR is high, is given in Ref. 11). Notice that 0-db coupling would require $R \rightarrow \infty$, and can, therefore, not be realized in a single synchronous design. However, two synchronous 3-db couplers, or three synchronous 6-db couplers, etc., can be cascaded to give a 0-db coupler.

Equation (13.11-2) is less accurate, the numerical factor generally lying between 0.5 and 0.7. A more accurate determination can be made from Fig. 13.11-2 after the number of branches has been selected. In this figure are plotted the best estimates of the bandwidth contraction factor

$$\beta = w_b/w_q \qquad (13.11\text{-}3)$$

FIG. 13.11-1   PLOT OF CENTER-FREQUENCY COUPLING $P_{2,0}$ vs. IMPEDANCE-RATIO PARAMETER R FOR A MATCHED BRANCH-LINE COUPLER
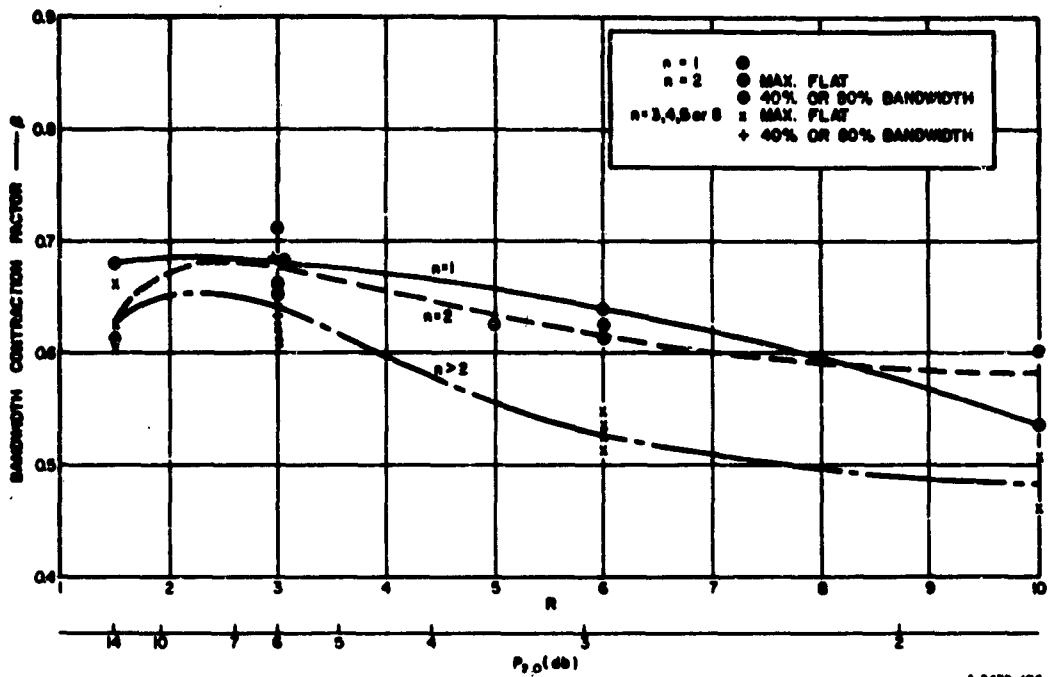
FIG. 13.11-2   BEST ESTIMATES FOR BANDWIDTH CONTRACTION FACTOR β
BASED ON 27 INDIVIDUAL SOLUTIONS

against R, or $P_{2,0}$ and with n as a parameter, based on a large number of numerical solutions.[11]

Having determined R and w_q from the specified coupling $P_{2,0}$ and the coupler fractional bandwidth w_b, the only remaining independent parameter is the number of sections, n, or number of branches, $n + 1$ (Fig. 13.09-2). For a given R and w_q, the ripple VSWR V_r of the transformer decreases with increasing n, and is readily determined from Sec. 6.02. The maximum pass-band VSWR of the coupler, V_{max}, and its minimum directivity D_{min}, may then be obtained to a good approximation by

$$V_{max} \;=\; 1 + \frac{V_r - 1}{\text{antilog } (P_2/20)} \qquad\qquad (13.11\text{-}4)$$

$$D_{\text{min}} = -20 \log_{10} \left[\frac{V_r - 1}{2 \ \text{antilog} \ (P_1/20)} \right] - P_2 \quad \text{db} \quad . \quad (13.11-5)$$

(The directivity D is defined as the ratio of power out of the "decoupled" arm to power out of the coupled arm. See Fig. 13.09-1.) Exact formulas (necessary only for large V_r) are given in Ref. 11. The number of sections n must be made large enough to meet the desired performance.

The frequency variation of the input VSWR V, the directivity D (db) and the two couplings (the in-line coupling P_1 and the cross-over coupling P_2, both in db), are plotted in Figs. 13.11-3, 4 and 5 for couplers based on *maximally flat* quarter-wave transformer prototypes for $n = 1$, 2, 4, and 8, and for $R = 1.5$, 3 and 6, corresponding to
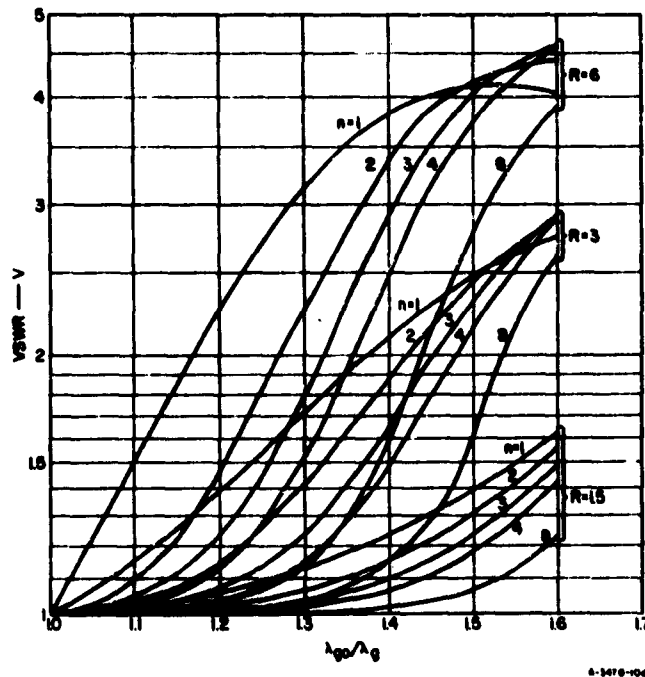
FIG. 13.11-3   VSWR CHARACTERISTICS OF SOME
                MAXIMALLY FLAT, BRANCH-LINE COUPLERS
                Immittances of these couplers are given in
                Tables 13.12-1 and 13.12-2
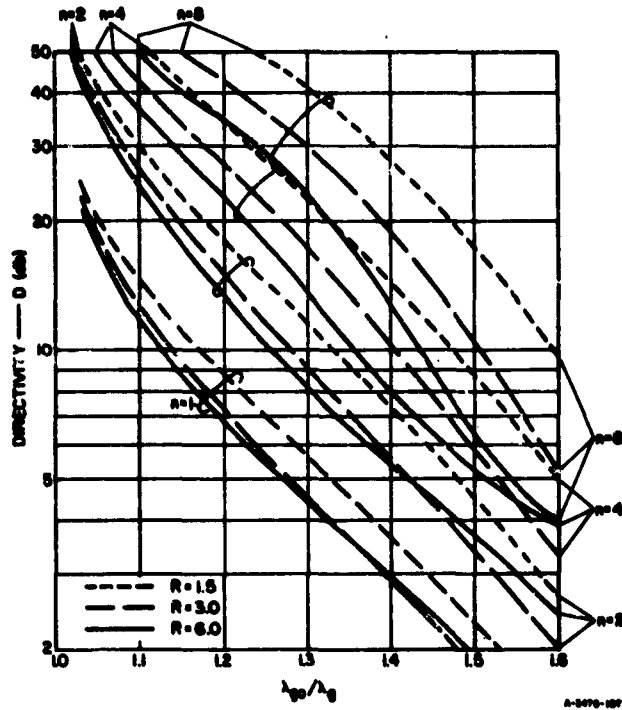
FIG. 13.11-4 DIRECTIVITY CHARACTERISTICS OF SOME
MAXIMALLY FLAT, BRANCH-LINE COUPLERS
Immittances of these couplers are given in
Tables 13.12-1 and 13.12-2
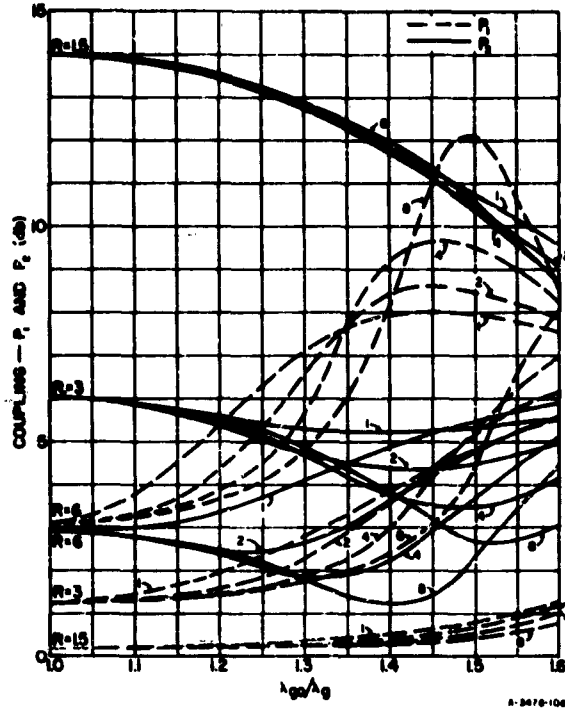
FIG. 13.11-5 COUPLING CHARACTERISTICS OF
SOME MAXIMALLY FLAT, BRANCH-
LINE COUPLERS
Immittances of these couplers are
given in Tables 13.12-1 and 13.12-2

couplings $P_{2,0}$ of approximately 14, 6, and 3 db. The graphs are plotted against the quantity (λ_{g0}/λ_g), where λ_g is the guide wavelength, and λ_{g0} is its value at band-center. The response is symmetrical about $(\lambda_{g0}/\lambda_g) = 1$, so that Figs. 13.11-3, 4, and 5 actually cover the range from 0.4 to 1.6, although only the portion from 1.0 to 1.6 is shown. For non-dispersive (TEM mode) lines, the guide wavelength λ_g reduces to the free-space wavelength λ, and then λ_{g0}/λ_g reduces to $\lambda_0/\lambda = f/f_0$, where f is the frequency, and f_0 is its value at band-center (also called the center frequency).

It can be seen from Fig. 13.11-5 that the coupling P_2 generally becomes stronger (P_2 measured in decibels decreases) on either side of center frequency (the curves are symmetrical about $\lambda_{g0}/\lambda_g = 1$), and correspondingly P_1 becomes weaker (P_1 measured in decibels increases).

The frequency variations of P_1 and P_2 for couplers based on Tchebyscheff transformer prototypes have been found to be very similar to the curves shown in Fig. 13.11-5 for couplers based on maximally flat transformer prototypes.

SEC. 13.12, TABLES OF IMMITTANCES OF SYNCHRONOUS BRANCH-LINE COUPLERS

It was shown in Sec.13.11 how to determine the quarter-wave transformer prototype parameters R, w_q, and the number of sections n (corresponding to $n + 1$ branches). The computation of the coupler immittances H_i and K_i (Fig. 13.09-2) is quite tedious, and will not be treated here. The design process is simplified by the use of a special chart,[11] which can handle any transformer impedances. In practice, it is likely that maximally flat and Tchebyscheff transformers (Chapter 6) will usually be taken for prototypes; the immittances H_i and K_i derived from such transformers were computed on a digital computer[2] and are tabulated in Tables 13.12-1 to 13.12-8. Most cases of practical interest can be obtained from these tables by interpolation.

Table 13.12-1

BRANCH-LINE COUPLER IMMITTANCES FOR $n = 1$ SECTION (TWO BRANCHES)

$n = 1$		
R	K_1	H_0
1.25	1.006	0.1119
1.50	1.021	0.2040
2.00	1.061	0.3535
2.50	1.108	0.4732
3.00	1.155	0.5775
4.00	1.250	0.7500
5.00	1.341	0.894
6.00	1.429	1.021
8.00	1.592	1.238
10.00	1.739	1.423

SOURCE: *IRE Trans. PGMTT* (see Ref. 11 by Lee Young)

Table 13.12-2

IMMITTANCES OF MAXIMALLY FLAT BRANCH-LINE COUPLERS FOR n = 2 TO 8 SECTIONS (THREE TO NINE BRANCHES)

n	K_1	K_2	K_3	K_4	H_1	H_2	H_3	H_4	H_5
n = 2									
1.50	1.0153				0.1010	0.2052			
2.00	1.04.9				0.1715	0.3639			
2.50	1.0783				0.2251	0.4983			
3.00	1.1124				0.2679	0.6188			
4.00	1.1785				0.3333	0.8333			
5.00	1.2399				0.3819	1.0249			
6.00	1.2965				0.4202	1.2008			
8.00	1.3978				0.4775	1.5196			
10.00	1.4861				0.5194	1.8070			
n = 3									
1.50	1.0089	1.0206			0.0501	0.1539			
2.00	1.0258	1.0606			0.0840	0.2694			
2.50	1.0446	1.1067			0.1086	0.3656			
3.00	1.0634	1.1546			0.1274	0.4498			
4.00	1.0988	1.2499			0.1542	0.5957			
5.00	1.1307	1.3416			0.1732	0.7220			
6.00	1.1594	1.4288			0.1854	0.8351			
8.00	1.2087	1.5909			0.2029	1.0344			
10.00	1.2501	1.7392			0.2138	1.2091			
n = 4									
1.50	1.0047	1.0176			0.0249	0.1017	0.1548		
2.00	1.0137	1.0517			0.0415	0.1750	0.2738		
2.50	1.0235	1.0907			0.0533	0.2331	0.3758		
3.00	1.0333	1.1307			0.0620	0.2814	0.4676		
4.00	1.0514	1.2093			0.0740	0.3596	0.6326		
5.00	1.0675	1.2835			0.0817	0.4220	0.7811		
6.00	1.0816	1.3530			0.0870	0.4743	0.9185		
8.00	1.1057	1.4795			0.0935	0.5589	1.1698		
10.00	1.1256	1.5924			0.0971	0.6265	1.3986		
n = 5									
1.50	1.0024	1.0124	1.0206		0.0124	0.0630	0.1285		
2.00	1.0070	1.0363	1.0606		0.0206	0.1069	0.2259		
2.50	1.0121	1.0630	1.1067		0.0264	0.1400	0.3070		
3.00	1.0170	1.0902	1.1546		0.0306	0.1662	0.3804		
4.00	1.0262	1.1421	1.2499		0.0363	0.2058	0.5078		
5.00	1.0342	1.1899	1.3416		0.0398	0.2348	0.6196		
6.00	1.0413	1.2335	1.4288		0.0422	0.2573	0.7210		
8.00	1.0532	1.3106	1.5909		0.0450	0.2904	0.9019		
10.00	1.0630	1.3769	1.7392		0.0464	0.3140	1.0625		
n = 6									
1.50	1.0012	1.0079	1.0185		0.0062	0.0376	0.0957	0.1290	
2.00	1.0035	1.0230	1.0544		0.0103	0.0631	0.1658	0.2284	
2.50	1.0061	1.0397	1.0956		0.0131	0.0817	0.2225	0.3138	
3.00	1.0086	1.0564	1.1380		0.0152	0.0959	0.2707	0.3908	
4.00	1.0132	1.0878	1.2216		0.0180	0.1162	0.3509	0.5295	
5.00	1.0172	1.1161	1.3010		0.0197	0.1301	0.4170	0.6549	
6.00	1.0208	1.1414	1.3758		0.0208	0.1402	0.4738	0.7712	
8.00	1.0268	1.1852	1.5128		0.0221	0.1539	0.5689	0.9846	
10.00	1.0317	1.2220	1.6361		0.0228	0.1626	0.6477	1.1796	
n = 7									
1.50	1.0006	1.0047	1.0143	1.0206	0.0031	0.0218	0.0665	0.1126	
2.00	1.0018	1.0137	1.0419	1.0606	0.0051	0.0364	0.1135	0.1983	
2.50	1.0030	1.0236	1.0731	1.1067	0.0065	0.0468	0.1499	0.2709	
3.00	1.0043	1.0334	1.1048	1.1546	0.0076	0.0546	0.1795	0.3355	
4.00	1.0066	1.0516	1.1662	1.2499	0.0089	0.0653	0.2258	0.4497	
5.00	1.0086	1.0678	1.2233	1.3416	0.0098	0.0724	0.2612	0.5509	
6.00	1.0104	1.0822	1.2759	1.4288	0.0103	0.0772	0.2898	0.6431	
8.00	1.0134	1.1067	1.3699	1.5909	0.0110	0.0834	0.3339	0.8090	
10.00	1.0159	1.1270	1.4520	1.7392	0.0113	0.0869	0.3672	0.9574	
n = 8									
1.50	1.0003	1.0027	1.0101	1.0190	0.0015	0.0124	0.0440	0.0895	0.1129
2.00	1.0009	1.0079	1.0293	1.0559	0.0025	0.0207	0.0743	0.1558	0.2000
2.50	1.0015	1.0135	1.0508	1.0982	0.0032	0.0265	0.0969	0.2100	0.2748
3.00	1.0021	1.0191	1.0724	1.1419	0.0037	0.0308	0.1146	0.2567	0.3425
4.00	1.0033	1.0295	1.1134	1.2282	0.0044	0.0366	0.1408	0.3357	0.4644
5.00	1.0043	1.0386	1.1508	1.3104	0.0049	0.0402	0.1595	0.4021	0.5749
6.00	1.0052	1.0467	1.1846	1.3881	0.0051	0.0427	0.1737	0.4601	0.6775
8.00	1.0067	1.0603	1.2436	1.5308	0.0055	0.0457	0.1939	0.5591	0.8661
10.00	1.0080	1.0715	1.2940	1.6598	0.0056	0.0474	0.2078	0.6426	1.0388

Table 13.12-3

IMMITTANCES OF BRANCH-LINE COUPLERS FOR n = 2, 3, AND 4 SECTIONS
(THREE, FOUR, AND FIVE BRANCHES) WHEN w_q = 0.20

R	K_1	K_2	H_1	H_2	H_3
n = 2					
1.50	1.0155		0.1022	0.2036	
2.00	1.0453		0.1738	0.3594	
2.50	1.0790		0.2282	0.4922	
3.00	1.1135		0.2717	0.6111	
4.00	1.1803		0.3385	0.8229	
5.00	1.2425		0.3883	1.0121	
6.00	1.3000		0.4276	1.1859	
8.00	1.4029		0.4870	1.5007	
10.00	1.4929		0.5307	1.7845	
n = 3					
1.50	1.0090	1.0206	0.0511	0.1530	
2.00	1.0262	1.0606	0.0856	0.2678	
2.50	1.0454	1.1067	0.1108	0.3634	
3.00	1.0645	1.1546	0.1300	0.4473	
4.00	1.1006	1.2499	0.1574	0.5925	
5.00	1.1331	1.3416	0.1761	0.7182	
6.00	1.1624	1.4288	0.1897	0.8309	
8.00	1.2129	1.5909	0.2078	1.0295	
10.00	1.2554	1.7392	0.2193	1.2036	
n = 4					
1.50	1.0048	1.0177	0.0256	0.1017	0.1535
2.00	1.0140	1.0519	0.0426	0.1751	0.2715
2.50	1.0241	1.0909	0.0547	0.2332	0.3727
3.00	1.0341	1.1311	0.0636	0.2817	0.4638
4.00	1.0527	1.2099	0.0760	0.3602	0.6274
5.00	1.0692	1.2844	0.0839	0.4230	0.7747
6.00	1.0837	1.3543	0.0894	0.4756	0.9110
8.00	1.1085	1.4814	0.0962	0.5610	1.1603
10.00	1.1290	1.5949	0.1000	0.6293	1.3872

SOURCE: Tech. Note 3, Contract AF30(602)-2392,
SRI (see Ref. 22 by Leo Young)

Table 13.12-4

IMMITTANCES OF BRANCH-LINE COUPLERS FOR n = 2, 3, AND 4 SECTIONS
(THREE, FOUR, AND FIVE BRANCHES) WHEN w_q = 0.40

R	K_1	K_2	H_1	H_2	H_3
n = 2					
1.50	1.0159		0.1061	0.1958	
2.00	1.0464		0.1807	0.3456	
2.50	1.0811		0.2376	0.4733	
3.00	1.1166		0.2835	0.5876	
4.00	1.1857		0.3543	0.7913	
5.00	1.2503		0.4078	0.9731	
6.00	1.3102		0.4506	1.1400	
8.00	1.4181		0.5162	1.4424	
10.00	1.5132		0.5655	1.7148	
n = 3					
1.50	1.0095	1.0206	0.0540	0.1500	
2.00	1.0275	1.0606	0.0907	0.2627	
2.50	1.0477	1.1067	0.1176	0.3567	
3.00	1.0679	1.1546	0.1381	0.4391	
4.00	1.1061	1.2499	0.1678	0.5821	
5.00	1.1407	1.3416	0.1882	0.7062	
6.00	1.1719	1.4288	0.2031	0.8174	
8.00	1.2260	1.5909	0.2235	1.0139	
10.00	1.2718	1.7392	0.2367	1.1862	
n = 4					
1.50	1.0052	1.0178	0.0276	0.1016	0.1497
2.00	1.0150	1.0523	0.0459	0.1751	0.2647
2.50	1.0259	1.0917	0.0590	0.2335	0.3634
3.00	1.0367	1.1323	0.0688	0.2823	0.4522
4.00	1.0567	1.2119	0.0823	0.3617	0.6117
5.00	1.0745	1.2873	0.0911	0.4255	0.7554
6.00	1.0904	1.3580	0.0972	0.4791	0.8884
8.00	1.1173	1.4869	0.1048	0.5667	1.1315
10.00	1.1397	1.6023	0.1093	0.6373	1.3528

Table 13.i2-5

IMMITTANCES OF BRANCH-LINE COUPLERS FOR $n = 2$, 3, AND 4 SECTIONS
(THREE, FOUR, AND FIVE BRANCHES) WHEN $w_q = 0.60$

R	K_1	X_2	H_1	H_2	H_3
			$n = 2$		
1.50	1.0165		0.1128	0.1824	
2.00	1.0483		0.1925	0.3220	
2.50	1.0846		0.2539	0.4408	
3.00	1.1218		0.3037	0.5471	
4.00	1.1945		0.3818	0.7363	
5.00	1.2630		0.4418	0.9051	
6.00	1.3269		0.4906	1.0598	
8.00	1.4430		0.5674	1.3398	
10.00	1.5464		0.6271	1.5917	
			$n = 3$		
1.50	1.0103	1.0206	0.0594	0.1446	
2.00	1.0299	1.0606	0.1000	0.2535	
2.50	1.0518	1.1067	0.1299	0.3444	
3.00	1.0739	1.1546	0.1530	0.4243	
4.00	1.1159	1.2499	0.1867	0.5632	
5.00	1.1542	1.3416	0.2104	0.6839	
6.00	1.1889	1.4288	0.2281	0.7925	
8.00	1.2497	1.5909	0.2529	0.9845	
10.00	1.3018	1.7392	0.2696	1.1533	
			$n = 4$		
1.50	1.0058	1.0181	0.0313	0.1012	0.1432
2.00	1.0169	1.0530	0.0522	0.1746	0.2533
2.50	1.0292	1.0930	0.0672	0.2332	0.3476
3.00	1.0413	1.1342	0.0785	0.2824	0.4327
4.00	1.0642	1.2152	0.0942	0.3630	0.5853
5.00	1.0845	1.2920	0.1046	0.4283	0.7228
6.00	1.1027	1.3641	0.1119	0.4836	0.8500
8.00	1.1339	1.4960	0.1214	0.5746	1.0826
10.00	1.1600	1.6143	0.1271	0.6486	1.2944

SOURCE: Tech. Note 3, Contract AF30(602)-2392,
SRI (see Ref. 22 by Leo Young)

Table 13.12-6

IMMITTANCES OF BRANCH-LINE COUPLERS FOR n = 2, 3, AND 4 SECTIONS
(THREE, FOUR, AND FIVE BRANCHES) WHEN w_q = 0.80

R	K_1	K_2	H_1	H_2	H_3
			n = 2		
1.50	1.0173		0.1225	0.1630	
2.00	1.0508		0.2097	0.2875	
2.50	1.0891		0.2776	0.3933	
3.00	1.1286		0.3333	0.4879	
4.00	1.2062		0.4221	0.6557	
5.00	1.2798		0.4919	0.8049	
6.00	1.3491		0.5499	0.9413	
8.00	1.4760		0.6437	1.1872	
10.00	1.5905		0.7192	1.4075	
			n = 3		
1.50	1.0114	1.0206	0.0679	0.1361	
2.00	1.0334	1.0606	0.1147	0.2388	
2.50	1.0580	1.1067	0.1495	0.3247	
3.00	1.0830	1.1546	0.1768	0.4004	
4.00	1.1309	1.2499	0.2175	0.5324	
5.00	1.1749	1.3416	0.2468	0.6476	
6.00	1.2153	1.4288	0.2692	0.7513	
8.00	1.2870	1.5909	0.3020	0.9353	
10.00	1.3491	1.7392	0.3254	1.0975	
			n = 4		
1.50	1.0069	1.0184	0.0374	1.0097	0.1339
2.00	1.0199	1.0540	0.0626	0.1724	0.2368
2.50	1.0344	1.0947	0.0808	0.2309	0.3251
3.00	1.0489	1.1368	9.0947	0.2803	0.4045
4.00	1.0763	1.2196	0.1143	0.3620	0.5472
5.00	1.1009	1.2983	0.1276	0.4288	0.6757
6.00	1.1230	1.3725	0.1372	0.4860	0.7946
8.00	1.1614	1.5083	0.1501	0.5813	1.0119
10.00	1.1939	1.6306	0.1582	0.6598	1.2097

Table 13.12-7

IMMITTANCES OF BRANCH-LINE COUPLERS FOR n = 2, 3, AND 4 SECTIONS
(THREE, FOUR, AND FIVE BRANCHES) WHEN w_q = 1.00

R	K_1	K_2	H_1	H_2	H_3
			n = 2		
1.50	1.0183		0.1354	0.1373	
2.00	1.0537		0.2326	0.2418	
2.50	1.0944		0.3091	0.3303	
3.00	1.1364		0.3728	0.4090	
4.00	1.2195		0.4759	0.5480	
5.00	1.2990		0.5590	0.6708	
6.00	1.3742		0.6294	0.7824	
8.00	1.5133		0.7463	0.9821	
10.00	1.6397		0.8432	1.1595	
			n = 3		
1.50	1.0131	1.0206	0.0807	0.1233	
2.00	1.0383	1.0606	0.1369	0.2165	
2.50	1.0668	1.1067	0.1795	0.2948	
3.00	1.0958	1.1546	0.2134	0.3639	
4.00	1.1521	1.2499	0.2652	0.4847	
5.00	1.2047	1.3416	0.3039	0.5904	
6.00	1.2534	1.4288	0.3347	0.6859	
8.00	1.3412	1.5909	0.3817	0.8556	
10.00	1.4189	1.7392	0.4173	1.0057	
			n = 4		
1.50	1.0084	1.0188	0.0472	0.0961	0.1214
2.00	1.0246	1.0552	0.0794	0.1667	0.2147
2.50	1.0426	1.0969	0.1030	0.2240	0.2946
3.00	1.0607	1.1400	0.1211	0.2728	0.3665
4.00	1.0952	1.2251	0.1476	0.3545	0.4956
5.00	1.1267	1.3062	0.1661	0.4223	0.6118
6.00	1.1554	1.3828	0.1799	0.5803	0.7191
8.00	1.2057	1.5237	0.1994	0.5802	0.9152
10.00	1.2490	1.6510	0.2127	0.6635	1.0935

Table 13.12-8

IMMITTANCES OF BRANCH-LINE COUPLERS FOR $n = 2$, 3, AND 4 SECTIONS (THREE, FOUR, AND FIVE BRANCHES) WHEN $w_q = 1.20$

R	K_1	K_2	H_1	H_2	H_3
			$n = 2$		
1.50	1.0192		0.1513	0.1056	
2.00	1.0565		0.2607	0.1855	
2.50	1.0995		0.3479	0.2527	
3.00	1.1441		0.4212	0.3121	
4.00	1.2325		0.5419	0.4160	
5.00	1.3174		0.6410	0.5067	
6.00	1.3982		0.7263	0.5884	
8.00	1.5481		0.8708	0.7331	
10.00	1.6852		0.9929	0.8601	
			$n = 3$		
1.50	1.0152	1.0206	0.0994	0.1046	
2.00	1.0445	1.0606	0.1696	0.1838	
2.50	1.0780	1.1067	0.2238	0.2504	
3.00	1.1125	1.1546	0.2680	0.3092	
4.00	1.1800	1.2499	0.3376	0.4123	
5.00	1.2439	1.3416	0.3918	0.5025	
6.00	1.3040	1.4288	0.4364	0.5841	
8.00	1.4140	1.5909	0.5082	0.7291	
10.00	1.5133	1.7392	0.5657	0.8572	
			$n = 4$		
1.50	1.0108	1.0192	0.0631	0.0886	0.1047
2.00	1.0315	1.0566	0.1066	0.1542	0.1851
2.50	1.0548	1.0994	0.1393	0.2080	0.2539
3.00	1.0785	1.1438	0.1650	0.2544	0.3157
4.00	1.1243	1.2316	0.2037	0.3331	0.4263
5.00	1.1667	1.3156	0.2320	0.3995	0.5256
6.00	1.2059	1.3951	0.2541	0.4578	0.6171
8.00	1.2761	1.5419	0.2873	0.5581	0.7837
10.00	1.3381	1.6753	0.3119	0.6437	0.9345

SOURCE: Tech. Note 3, Contract AF30(602)-2392, SRI (see Ref. 22 by Leo Young)

The notation for the immittances H_i and K_i is shown in Fig. 13.09-2. For a coupler with series T-junctions, H_i and K_i are both characteristic impedances (e.g. for E-plane junctions in waveguide); for a coupler with shunt T-junctions, H_i and K_i are both characteristic admittances (e.g., for coaxial or strip transmission lines).

SEC. 13.13, EXAMPLES ILLUSTRATING THE DESIGN AND PERFORMANCE OF SYNCHRONOUS BRANCH-LINE COUPLERS

Example—A 3-db coupler is to have an input VSWR of less than 1.10 and a directivity in excess of 20 db over a 24-percent fractional bandwidth.

From Fig. 13.11-1, when $P_{2,0} = 3$ db, then by Eq. (13.11-1), $R = 5.84$. Try a two-branch coupler first, corresponding to a single-section, quarter-wave transformer prototype ($n = 1$). From Fig. 13.11-2, $\beta = 0.64$ for $n = 1$, so that the prototype fractional bandwidth must be $w_b/\beta = 24/0.64$ percent, or nearly 40 percent by Eq. (13.11-3). The maximum VSWR of a single-section quarter-wave transformer of $R = 6$, and $w_q = 0.40$, is 1.86, from Table 6.02-2. It follows from Eq. (13.11-4) that V_{max} of the coupler would then be considerably greater than the 1.10 specified.

Try a three-branch coupler next, corresponding to a two-section, quarter-wave transformer ($n = 2$). From Fig. 13.11-2, $\beta = 0.62$ for $n = 2$, so that the prototype fractional bandwidth must be $24/0.62$ percent, or almost 40 percent. Now the maximum VSWR of a two-section quarter-wave transformer of $R = 6$, $w_q = 0.40$, is 1.11 from Table 6.02-2. For a 3-db coupler, Eq. (13.11-4) yields $V_{max} = 1 + 0.11/1.414 = 1.08$, which is below the 1.10 specified. The directivity from Eq. (13.11-5) will be better than $-20 \log_{10} (0.04) - P_2 = 25$ db, which exceeds the 20 db specified.

Thus the prototype quarter-wave transformer will in this case have two sections ($n = 2$), $R = 5.84$, and bandwidth $w_q = 0.40$. The corresponding branch-guide coupler design can be obtained by interpolation from Table 13.12-4.

If we may use Fig. 13.11-5 as a guide, then over the 24-percent band specified, this three-branch, 3-db coupler would be expected to change each of its couplings, P_1 and P_2, by a little under 0.3 db. Thus if

the coupler were designed to have 3-db coupling at center frequency (corre-
sponding to $R = 5.84$ picked before), then P_2 would go to 2.7 db and P_1 to
3.3 db at the 24-percent band edges. If the specification required both P_1
and P_2 to be maintained to within ±0.15 db of 3 db over the 24-percent band,
or generally to optimize the balance over the band as a whole, then the coupler
would be designed with $P_{2,0} = 3.15$ db, corresponding to $R = 5.7$, by
Fig. 13.11-1 or Eq. (13.11-1). With this choice, and from Table 13.12-4,

$$K_0 = 1 \quad , \quad K_1 = 1.2902 \quad , \quad H_1 = 0.4363 \quad , \quad H_2 = 1.0844 \quad .$$

The performance of this coupler was analyzed by computer and is reproduced
in Fig. 13.13-1. It is found to conform very closely to the specifications.
(Again, this is plotted only for one side of band-center, since the response
is symmetrical as plotted.) From Fig. 13.13-1, the analyzed performance
over the 24-percent bandwidth is: maximum VSWR, 1.07 (1.08 was predicted);
minimum directivity, 26 db (25 db was predicted), couplings P_1 and P_2
both within ±0.2 db of 3 db (±0.15 db was predicted).

   Comparison of Synchronous and Periodic Couplers—The maximum VSWR
and the coupling unbalance of several 3-db periodic couplers was given in
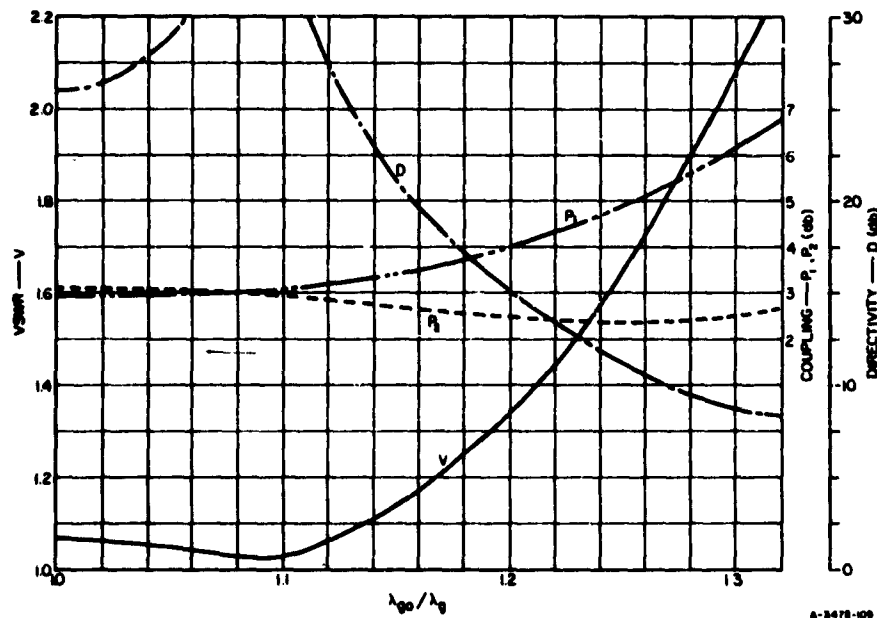
FIG. 13.13-1   COMPUTED PERFORMANCE OF A THREE-BRANCH (n = 2) COUPLER

Tables 13.10-2 and 13.10-3 for three particular bandwidths w_b. None of the periodic couplers could be designed for any particular bandwidth, and the performance of any one coupler simply degenerates slowly as its operating bandwidth is increased. (For instance, the VSWR ripples keep getting bigger.) To improve the performance over any particular bandwidth one can increase the number of branches (but avoid an increase from an even to an odd number of branches).

By contrast, synchronous couplers have a clearly defined pass band over which at least their VSWR an! directivity is optimized. Three different four-branch synchronous couplers were obtained from the tables in Sec. 13.12. Each has $n = 3$ and $R = 5.5$, and their several transformer prototype bandwidths are $w_q = 0.40$ (Case 1), $w_q = 0.60$ (Case 2), and $w_q = 0.80$ (Case 3). These three couplers give about optimum performance over bandwidths of $w_b = 0.16$, $w_b = 0.28$ and $w_b = 0.48$, respectively, corresponding to the bandwidths in Tables 13.10-2 and 13.10-3. The maximum VSWR and coupling unbalance over their respective pass bands is shown in Table 13.13-1. A comparison with Tables 13.10-2 and 13.10-3 shows that the VSWR of the four-branch synchronous couplers is as good as (or better than) that of the eight-branch periodic coupler. There is also a slight improvement in the coupling unbalance over the four-branch periodic coupler.

SEC. 13.14, DESIGN OF AN EXPERIMENTAL BRANCH-LINE COUPLER IN WAVEGUIDE

The design of a 6-db coupler in waveguide will now be discussed. A prototype transformer having $n = 4$ (five branches), $R = 3$ and $w_q = 0.40$ was selected. At that time[11] the tables in Sec. 13.12 were not available and the following immittances were calculated by charts;[11] the more exact values from Table 13.12-4 (not used in the construction) are shown in parentheses:

$$\left.\begin{array}{ll} K_0 = 1.0 \ (1.0) & H_1 = 0.070 \ (0.0688) \\ K_1 = 1.036 \ (1.0367) & H_2 = 0.274 \ (0.2823) \\ K_2 = 1.127 \ (1.1323) & H_3 = 0.450 \ (0.4522) \end{array}\right\} \quad (13.14-1)$$

It was verified by analysis on a digital computer that the immittances from the tables (in parentheses) would give a slightly improved coupler; the improvement was, however, not large enough to warrant the expense of building a new model. It was also demonstrated[11,22] that the performance of this

827
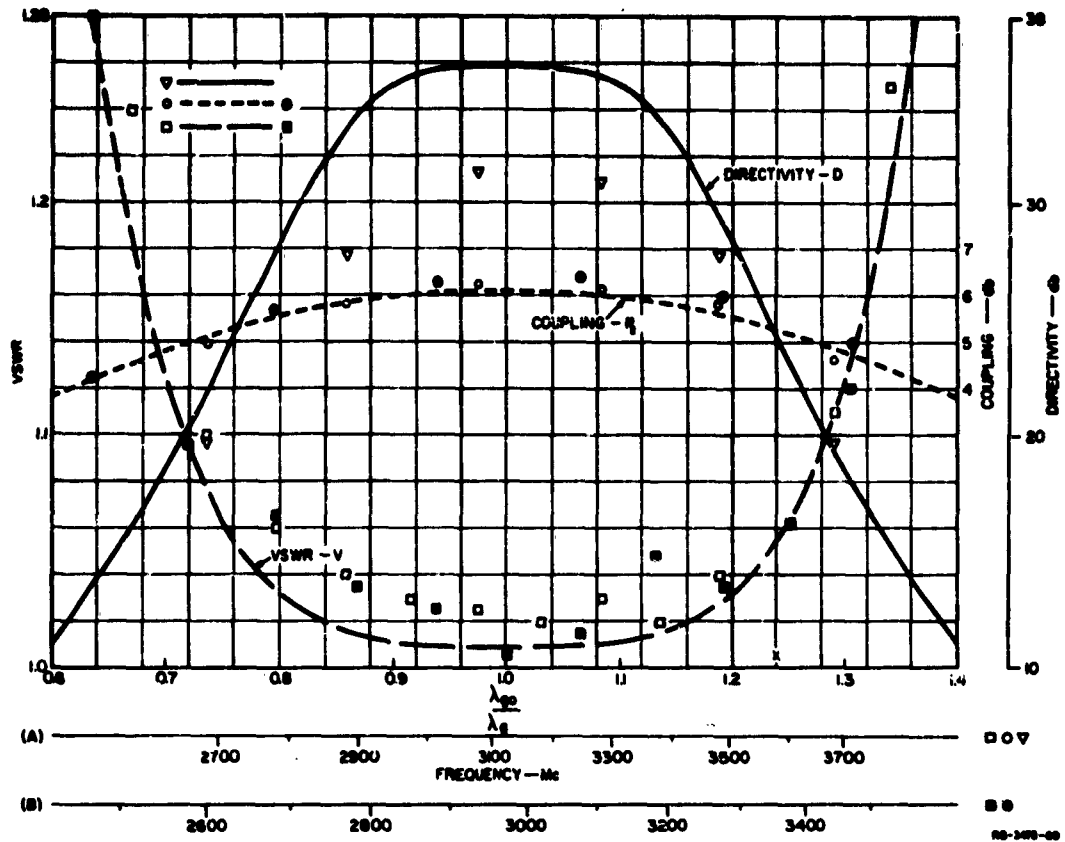
FIG. 13.14-1 PERFORMANCE OF FIVE-BRANCH (n = 4) COUPLER
Lines are computed; points are measured on experimental
models shown in Figs. 13.14-3, 13.14-4, and 13.14-5

coupler could be predicted accurately. The details of the calculation are
similar to the example in Sec. 13.13, and are not reproduced here.

The computed performance of this coupler is shown in Fig. 13.14-1. The ex-
perimental points are plotted in the same figure, and will be explained below.

Construction and Experimental Performance — The coupler was to be con-
structed in S-band, with rectangular waveguide outputs of 2.840 inches by
1.420 inches. The center frequency was to be 2975 Mc. (Therefore, λ_{g0} = 5.54 inches.)

Since waveguide T-junctions are series junctions, the immittances
K_i and H_i are impedances; however, since waveguide T-junctions are not

828

perfect series junctions, they can be represented by an equivalent cir-
cuit such as is shown in Fig. 13.14-2. (This is the same circuit es
Fig. 6.1-2 on p. 338 of Ref. 20.) At any T-junction of the coupler,
K_{i-1} and K_i are generally not equal, although they differ only slightly,
so that K_{av} in Fig. 13.14-2(a) was set equal to their arithmetic mean
$(K_{i-1} + K_i)/2$. Similarly the wave-guide height substituted into the
graphs of Ref. 20 to obtain the T-junction properties was $b_{av} = (b_{i-1} +$
$b_i)/2$, and the junction was treated as if it were symmetrical [see
Fig. 13.14-2(a)].

The waveguide heights (their b-dimensions) were first taken as pro-
portional to the respective K or H values (Eq. 13.14-1); they were fixed
by the b-dimensions of the four ports, which were each equal to $b_0 =$
1.420 inches. This determined the b-dimensions in the through-guides
without further adjustments, but the b-dimensions of the branch guides
had to be further increased to allow for the transformer factor denoted
by n^2 in Ref. 20 (no connec-
tion with the number of sec-
tions, n). This factor was
found from Table 6.1-10 on
p. 346 in Ref. 20, and the
branch b-dimensions, were in-
creased by a factor $1/n^2$.
Since this changed the junc-
tion dimensions, the quantity
n^2 had to be worked out again,
and more times if necessary
(usually this is not neces-
sary) until each product of
n^2 and the branch guide
b-dimension was proportional
to the appropriate impedance H.
Finally, the reference plane
positions, d and d', of each
junction were determined[20]
(Fig. 13.14-2).
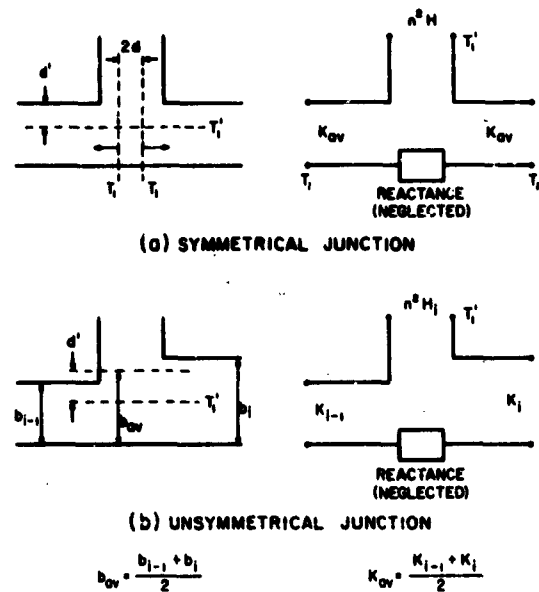
(o) SYMMETRICAL JUNCTION

(b) UNSYMMETRICAL JUNCTION

$$b_{av} = \frac{b_{i-1} + b_i}{2} \qquad K_{av} = \frac{K_{i-1} + K_i}{2}$$

A-3478-HO

FIG. 13.14-2 EQUIVALENT CIRCUITS OF
T-JUNCTIONS

The dimensions of this coupler were calculated, using the impedances of Eq. (13.14-1) and the T-junction equivalent circuits in Ref. 20. (The series reactances were included in several of the earlier computations analyzing the coupler performance. Their presence was found to affect the performance only slightly, and has been ignored in all later computations.)

The coupler E-plane cross section might be expected to require stepped top and bottom walls (Fig. 13.09-1) to obtain the changes in impedance K_i called for in Eq. (13.14-1). However, the reference planes (T_1' in Fig. 13.14-2) move in such a manner that the branches have to be shortened more where the impedances K are larger, with the result that the top and bottom walls (Fig. 13.09-1) come out almost straight. In order to obtain straight top and bottom walls as shown in Fig. 13.09-1, and yet maintain the correct impedances K_i, branch lengths some of which differ slightly from the lengths calculated[20] have to be accepted.

The dimensions so calculated are shown in Fig. 13.14-3. The coupler was constructed in two halves as shown in Fig. 13.14-4. Three jig-plates of aluminum were used to make a U-shaped channel, in which six aluminum blocks were placed and bolted down to form the waveguide channels. The end blocks contain transformers from the waveguide height of 1.420 inches

CHANNEL DEPTH = 1.420

A-3478-M
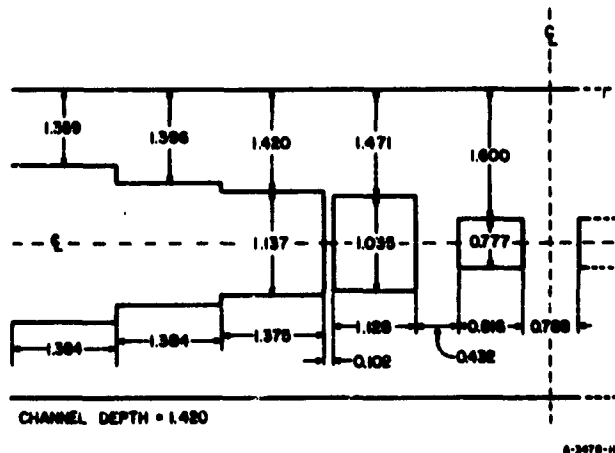
FIG. 13.14-3   DIMENSIONS OF FIRST S-BAND, FIVE-BRANCH, 6-db COUPLER
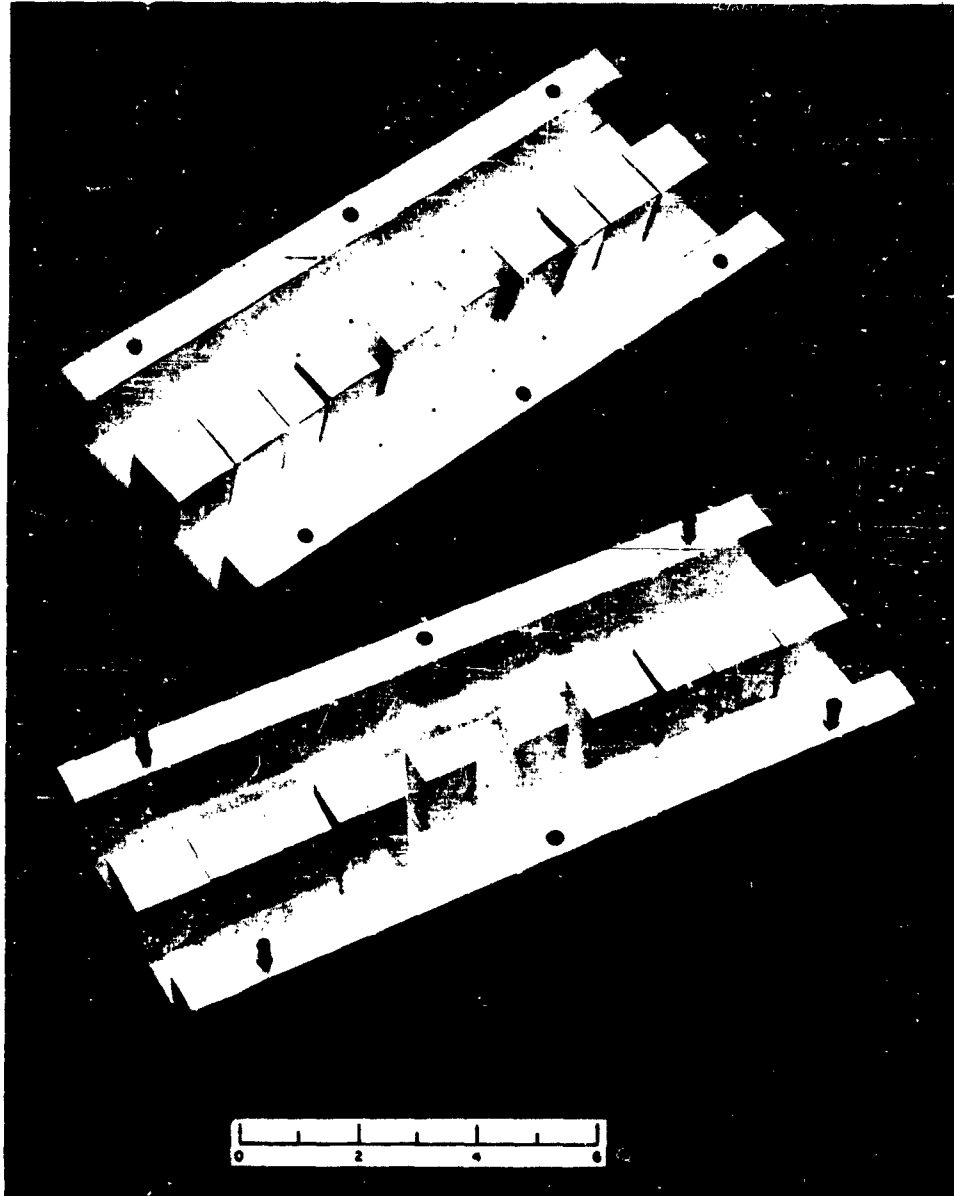
FIG. 13.14-4   EXPLODED VIEW OF S-BAND, EXPERIMENTAL FIVE-BRANCH, 6-db COUPLER

to 1.340 inches, so that standard WR-284 waveguide test equipment could
be connected. The depth of all the channels is half of 2.840 inches,
or 1.420 inches. The two pieces shown in Fig. 13.14-4 were finally
superimposed and bolted together to form the 6-db coupler.

The measured performance of the completed coupler is shown by the
light points in Fig. 13.14-1, which go with the frequency scale (A) near
the bottom of Fig. 13.14-1. Plotted on a λ_{g0}/λ_g scale, the points
fit the computed curves very closely; however, the center frequency is
3125 Mc instead of the design value of 2975 Mc. This discrepancy is
thought to result from the relatively large b-dimensions which, for
instance, make the length of an outline edge on the two center squares
in Fig. 13.14-3 only about one-seventh wavelength. Thus, non-propagating
higher-order modes could be set up, giving rise to interaction effects
at such close spacings.

All branch lengths and spacings, nominally one-quarter wavelength,
were then scaled in the ratio of the guide wavelengths to reduce the
center frequency from 3125 to 2975 Mc, and the coupler was tested again.
Its center frequency moved down as expected, but the coupling there
became stronger, going from 6.1 to 5.8 db. Since the coupling becomes
stronger still at off-center frequencies, it was decided to reduce the
branch heights to weaken the coupling by 0.5 db at center frequency,
changing the 5.8 db to 6.3 db coupling. The new dimensions calculated
are shown in Fig. 13.14-5. The measured results are shown by the black
points in Fig. 13.14-1 which go with the frequency scale (B) at the
bottom of Fig. 13.14-1. It is seen that this coupler gives the desired
center frequency, and its performance closely follows the computed curves.

Power-Handling Capacity—All edges orthogonal to the electric field
of the TE_{10} mode were then rounded off to increase the power-handling
capacity. The edges of the eight rectangular blocks were rounded to a
radius of one-eighth inch; the edges of the four outside blocks, on the
faces defining the outside edges of the narrowest branches, were rounded
to a radius of one-sixteenth inch. These radii were estimated from
Fig. 15.02-5 to reduce the field strength at the edges to less than
double the field strength in the waveguides.[23] Any further rounding
would have helped very little. The performance of the coupler with
rounded edges was measured, and found to reproduce the performance shown
in Fig. 13.14-1 to within experimental accuracy.

832

(ROUNDED CORNERS NOT SHOWN:
SEE TEXT)

CHANNEL DEPTH=1.420

RA-3470-57
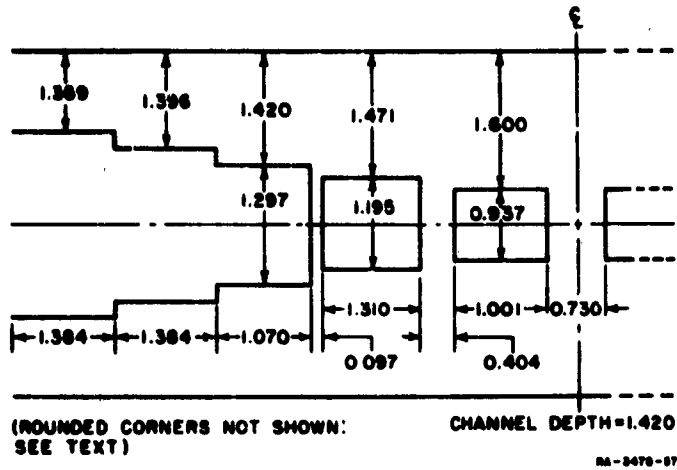
FIG. 13.14-5 DIMENSIONS OF S-BAND, FIVE-BRANCH,
6-db COUPLER AFTER MODIFICATIONS

It was estimated[22] that this coupler should handle about 39-percent
of the peak power handled by the waveguide. This is chiefly determined
by the radii of the T-junction corners. In WR-284 waveguide, this
corresponds roughly to 1.0 megawatt. The coupler was tested[11] at high
power using a 3.8-microsecond pulse at 60 pps, at a frequency of 2857 Mc.
With air at atmospheric pressure, no arcing was observed with 1 megawatt
peak power.

REFERENCES

1. S. B. Cohn, J. K. Shimizu, E. M. T. Jones and P. M. Sherk, "Strip Transmission Lines and Components," Final Report, Contract DA 36-039 SC-63232, Stanford Research Institute, Menlo Park, California (February 1957).

2. B. M. Oliver, "Directional Electromagnetic Couplers," *Proc. IRE* 42, pp. 1686-1692 (November 1954).

3. W. L. Firestone, "Analysis of Transmission Line Directional Couplers," *Proc. IRE* 42, pp. 1529-1538 (October 1954).

4. E. M. T. Jones and J. T. Bolljahn, "Coupled-Strip-Transmission Line Filters and Directional Couplers," *IRE Trans. PGMTT*-4, pp. 75-81 (April 1956).

5. J. K. Shimizu and E. M. T. Jones, "Coupled-Transmission Line Directional Couplers," *IRE Trans. PGMTT*-6, pp. 403-410 (October 1958).

6. J. K. Shimizu, "A Strip-Line 3 db Directional Coupler," Scientific Report 1, Contract AF 19(604)-1571, Stanford Research Institute, Menlo Park, California (June 1957).

7. S. B. Cohn and S. L. Wehn, "Microwave Hybrid Coupler Study Program," Second Quarterly Progress Report, Contract DA 36-2395c-87435, Rantec Corporation, Calabasas, California (November 1961).

8. J. Reed and G. Wheeler, "A Method of Analysis of Symmetrical Four-Port Networks," *IRE Trans. PGMTT*-4, pp. 246-252 (October 1956).

9. J. Reed, "The Multiple Branch Waveguide Coupler," *IRE Trans. PGMTT*-6, pp. 398-403 (October 1958).

10. Leo Young, "Branch Guide Directional Couplers," *Proc. Nat. Electronics Conf.*, Vol. 12, pp. 723-732 (1956).

11. Leo Young, "Synchronous Branch Guide Directional Couplers for Low and High Power Applications," *IRE Trans. PGMTT*-10, pp. 459-475 (November 1962).

12. S. B. Cohn and R. H. Koontz, "Microwave Hybrid Coupler Study Program," Third Quarterly Progress Report, Contract DA 36-239-SC-87435, Rantec Corporation, Calabasas, California (February 1962).

13. W. J. Getsinger, "A Coupled Strip-Line Configuration Using Printed-Circuit Construction that Allows Very Close Coupling," *IRE Trans. PGMTT*-9, pp. 535-544 (November 1961).

14. W. J. Getsinger, "Coupled Rectangular Bars Between Parallel Plates," *IRE Trans. PGMTT*-10, pp. 65-72 (January 1962).

15. A. L. Fel'dshtein, "Synthesis of Stepped Directional Couplers," *Radiotekhnika i Elektronika*, Vol. 6, No. 2, pp. 234-240 (February 1961); English translation, Pergamon Press, pp. 75-85 (1961).

16. Leo Young, "Analysis of a Transmission Cavity Wavemeter," *IRE Trans. PGMTT*-8, pp. 436-439 (July 1960). [The exponent in the numerator of Eq. (20) should be $-J\theta$ and not $-2 J\theta$].

17. Leo Young, "A Theorem on Lossless Symmetrical Networks," *IRE Trans. PGCT*-7, p. 75 (March 1960).

18. S. B. Cohn, W. J. Getsinger, E. M. T. Jones, B. M. Schiffman, J. K. Shimizu, "Design Criteria for Microwave Filters and Coupling Structures," Tech. Report 3, Contract DA 36-039 SC-74862, Stanford Research Institute, Menlo Park, California (August 1958).

19. A. G. Franco and A. A. Oliner, "Symmetric Strip Transmission Line Tee Junction," *IRE Trans. PGMTT*-10, pp. 118-124 (March 1962).

20. N. Marcuvitz, *Waveguide Handbook*, pp. 336-350, MIT Rad. Lab. Series, Vol. 10 (McGraw-Hill Book Co., Inc., New York, N. Y. 1951).

21. "Tables of Chebyshev Polynomials $S_n(x)$ and $C_n(x)$," National Bureau of Standards Applied Mathematics Series No. 9, United States Government Printing Office, Washington 25, D. C. (1952).

22. Leo Young, "The Design of Branch Guide Directional Couplers for Low and High Power Applications," Tech. Note 3, Contract AF 30(602)-2392, Stanford Research Institute, Menlo Park, California. RADC-TDR-62-130 (February 1962).

23. S. B. Cohn, "Rounded Corners in Microwave High-Power Filters and Other Components," *IRE Trans. PGMTT*-9, pp. 389-397 (September 1961).

24. Leo Young, "The Analytical Equivalence of TEM-Mode Directional Couplers and Transmission-Line Stepped-Impedance Filters," *Proc. IEE*, 110, pp. 275-281 (February 1963).

of Fig. 14.01-1(c) is typical of a multi-resonator directional
filter.

The midband insertion loss, between the ports having the band-
pass frequency response, of an actual directional filter employing
resonators with a finite unloaded Q is the same as that of a two-port
band-pass filter having the same frequency response and utilizing
resonators with the same unloaded Q. The midband insertion loss can
be computed by the methods given in Secs. 4.13 and 11.06.

Figure 14.01-2 gives an example of the use of directional
filters. In the case of Filters a, b, and d, the isolated port is
not used. However, in the case of Filter c, it is used to permit
f_c and f_d to appear at a common port. Because the directional filter
is a reciprocal device, Fig. 14.01-2 can also be used as an example of
a frequency combining device if all the arrows are reversed. Count-
less other interconnections of directional filters are feasible to
meet specific requirements.
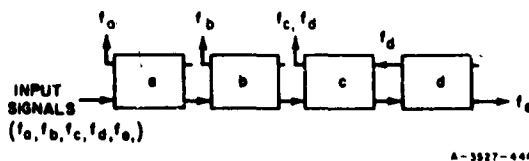
FIG. 14.01-2   EXAMPLE OF DIRECTIONAL-FILTER
              APPLICATION TO CHANNEL
              SEPARATION

A variety of directional filters have been devised, although only
a limited number have found wide application. The most useful types
are discussed in detail in this chapter and are illustrated in
Fig. 14.01-3.

The directional filter shown in Fig. 14.01-3(a) utilizes two
rectangular waveguides operating in the dominant TE_{10} mode connected
by means of cylindrical direct-coupled cavity resonators operating in
the circularly polarized TE_{11} mode. Any number of circularly polarized
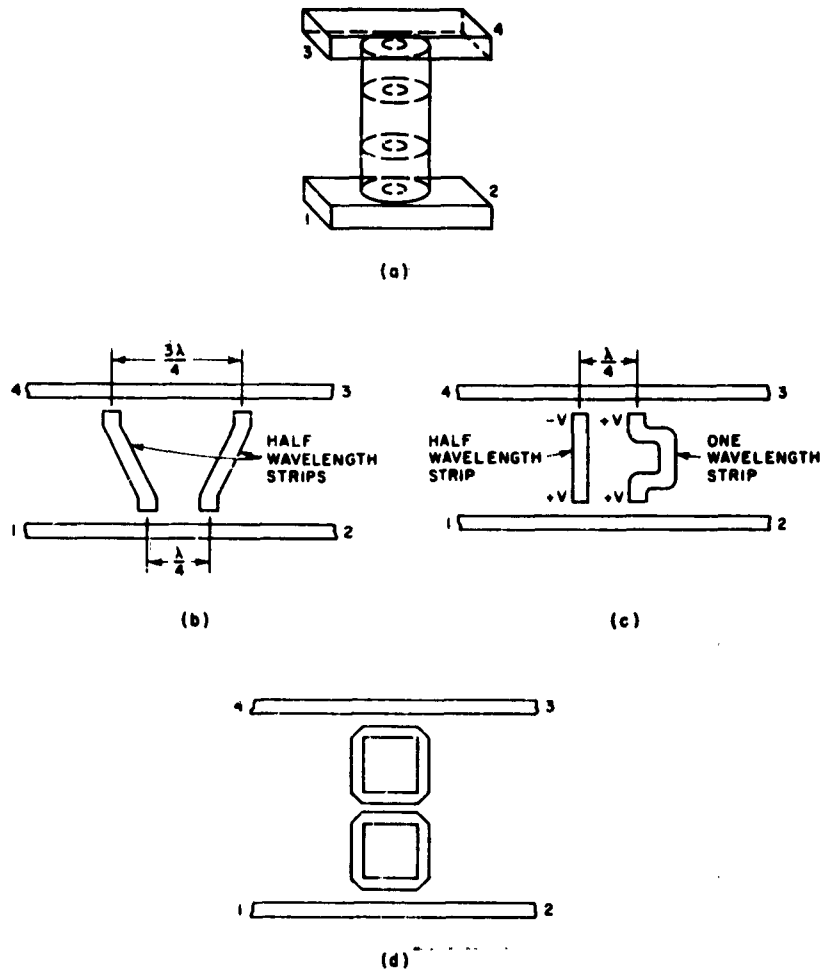
(a)

(b)

(c)

(d)

B-3527-447

FIG. 14.01-3   TYPES OF DIRECTIONAL FILTERS DISCUSSED
IN THIS CHAPTER

TE_{11} resonators can be used in this directional filter to obtain increased
off-channel rejection. The pass band of this type of filter is typically
only a fraction of one percent wide. However, by using special coupling
apertures between the rectangular waveguides. bandwidths on the order of
3 percent can be obtained for single cavity filters and bandwidths of
about 2 percent can be obtained for multi-cavity filters. The high-Q

837

cavities used in this type of filter permit relatively low-loss performance for a given pass-band width.

The two forms of strip-line directional filters shown in Fig. 14.01-3(b) and -3(c) have essentially the same frequency response. The resonators in these directional filters cannot be cascaded to obtain increased off-channel rejection as could those in the previously described waveguide directional filter.[3] Therefore, this type of directional filter is suitable for use when only a single-resonator band-pass frequency response is required between Ports 1 and 4. Pass-band widths of several percent are easily obtained with this type of directional filter.

The strip-line directional filter shown in Fig. 14.01-3(d) utilizes traveling-wave ring resonators which are typically one wavelength in mean circumference at midband. They are coupled to one another, and to the terminating strip lines, by means of quarter-wavelength directional couplers of the type discussed in Chapter 13. As in the case of the waveguide directional filter, any number of traveling-wave ring resonators can be utilized to obtain increased off-channel rejection between Ports 1 and 4. Pass-band widths on the order of 10 percent or more can in principle be obtained with this type of directional filter because it is possible to tightly couple the traveling-wave rings to the terminating lines and to each other. However, in practice, these devices are usually designed for more modest bandwidths up to only a few percent. Strip-line construction for directional filters, of course, has an advantage of ease of manufacture. However, the resonator Q's are lower so that the losses will be greater for a given pass-band width than if cavities are used.

This latter type of directional filter could also be realized in waveguides using any of a variety of waveguide couplers to connect a waveguide ring to the external waveguide, but it appears that this form of filter has not been used in practice. A closely related form of waveguide traveling-wave ring structure which has been used extensively as a power multiplier is shown in Fig. 14.01-4. This structure is formed from a single-resonator traveling-wave ring directional filter in which the output waveguide has been removed. When the ring, which typically has a length of several guide wavelengths, is resonant, most of the power entering Port 1 is delivered to the large amplitude traveling wave within the ring, while the remainder is delivered to the load. The average power level of the wave circulating within the ring can be made quite high. As an example of
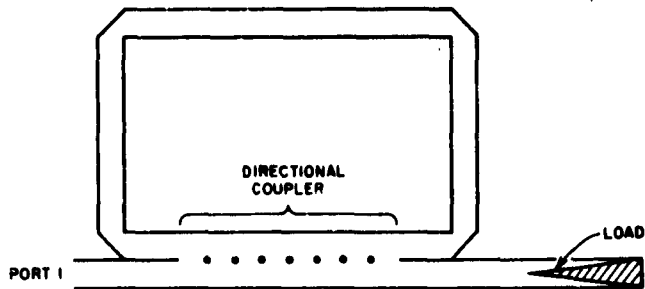
A-3527-448

FIG. 14.01-4 WAVEGUIDE TRAVELING-WAVE-RING
POWER MULTIPLIER

the power multiplication that can be obtained it is found that if the at-
tenuation of a wave traveling once around the ring is 0.2 db and the directional
coupler has a coupling of -16 db, the average power level of the wave circulating
within the ring is 20 times the input power. Thus, microwave devices such as
waveguide windows which absorb little power but must be able to operate with high
power passing through them, can be tested by inserting them in the ring circuit—
while the ring circuit itself is excited by a relatively low-power source.

Another circuit which operates as a directional filter is discussed in
Sec. 16.02. This circuit uses two hybrid junctions and two conventional
filters to obtain a directional filter type of operation.

SEC. 14.02, WAVEGUIDE DIRECTIONAL
FILTERS

This section presents design informa-
tion and measured performance for the type
of waveguide directional filter illustrated
in Fig. 14.02-1. This filter utilizes two
rectangular waveguides operating in the
TE_{10} mode connected by means of cylindrical,
direct-coupled cavity resonators operating
in the circularly polarized TE_{11} mode.
Coupling between the cavities is obtained
by means of circular apertures, while
coupling between the cavities and the ex
ternal waveguide is obtained either by
means of the circular apertures shown or by
other types of apertures described later
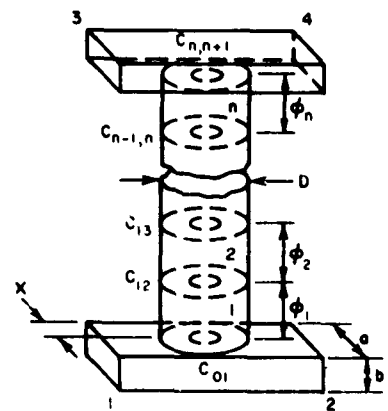
A-3527-449

FIG. 14.02-1 A WAVEGUIDE
DIRECTIONAL
FILTER HAVING
n RESONATORS

839

At the midband frequency a signal incident on Port 1 excites circularly polarized TE_{11} modes in the various cavities. The circularly polarized wave in the nth cavity then excites a TE_{10} mode in the external waveguide traveling toward Port 4. No power is transmitted to Port 3. The frequency response at Port 4 is equivalent to that of a band-pass filter, while the response at Port 2 is complementary and equivalent to that of a band-reject filter.

The shape of the attenuation response for transmission between Port 1 and Port 4 is governed by the number of resonant cavities in the directional filter. In fact, any shape of band-pass frequency response, such as those shown at the right in Fig. 14.02-2, that can be obtained with an n-cavity band-pass waveguide filter (Sec. 8.06) can also be obtained with this type of n-cavity directional filter. The width of the pass-band response at Port 4 is typically only a fraction of a percent. However, as explained later the width of the pass band can be increased to several percent by using specially shaped coupling apertures between the rectangular waveguides and the cylindrical cavities.

Table 14.02-1 is a design chart for the waveguide directional filter shown in Fig. 14.02-1. In this chart the design parameters for waveguide

(a) MAXIMALLY FLAT RESPONSES

(b) TCHEBYCHEFF RESPONSES
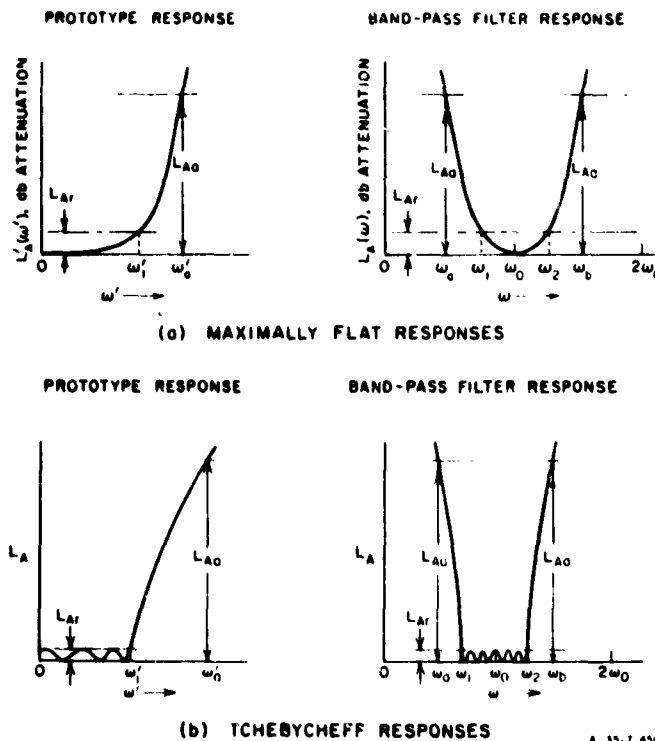
FIG. 14.02-2 SOME LOW-PASS PROTOTYPE RESPONSES AND CORRE-SPONDING BAND-PASS FILTER RESPONSES

Table 14.02-1
DESIGN EQUATIONS FOR CIRCULAR-WAVEGUIDE DIRECTIONAL FILTERS

The parameters g_0, g_1, ... , g_{n+1} are as defined in Sec. 4.04, while ω_1', ω_0, ω_1, and ω_2 are as defined in Fig. 14.02-2.

$$(Q_e)_A = \frac{g_0 g_1 \omega_1'}{w} = \text{external } Q \tag{1}$$

$$k_{i,i+1}\Big|_{i=1 \text{ to } n} = \frac{w}{\omega_1' \sqrt{g_i g_{i+1}}} = \begin{array}{l}\text{coupling}\\\text{coefficient}\end{array} \tag{2}$$

$$(Q_e)_B = \frac{\omega_1' g_n g_{n+1}}{w} = \text{external } Q \tag{3}$$

where

$$w = \frac{\omega_1 - \omega_1}{\omega_0} \quad \text{and} \quad \omega_0 \approx \frac{\omega_1 + \omega_2}{2} \tag{4}$$

$$c_{01} = 1\Big/\sqrt{\frac{(Q_e)_A}{2\pi p}\left(\frac{\lambda_0}{\lambda_{g0}'}\right)^2 + \frac{1}{2}} \tag{5}$$

$$c_{i,i+1}\Big|_{i=1 \text{ to } n-1} = p\pi k_{i,i+1}\left(\frac{\lambda_{g0}'}{\lambda_0}\right)^2 \tag{6}$$

$$c_{n,n+1} = 1\Big/\sqrt{\frac{(Q_e)_B}{2\pi p}\left(\frac{\lambda_0}{\lambda_{g0}'}\right)^2 + \frac{1}{2}} \tag{7}$$

where $(c_{i,i+1})^2$ is the power coupling factor, and where p is the number of half-wavelengths in the resonators.

To determine aperture sizes first compute the polarizabilities (the equations given are most accurate for very small apertures):

$$M_{i,i+1}\Big|_{i=0 \text{ and } n} = \sqrt{\frac{3a^3 bD^2 \lambda_{g0}'(c_{i,i+1})^2}{32\pi^2 \lambda_{g0} \cos^2\left(\frac{\pi x}{a}\right)}} \tag{8}$$

$$M_{i,i+1}\Big|_{i=1 \text{ to } n-1} = \frac{3c_{i,i+1} D^2 \lambda_{g0}'}{32\pi} \tag{9}$$

841

Table 14.02-1 *concluded*

where a, b, and D are defined in Fig. 14.02-1, and

$$x = \frac{a}{\pi} \cot^{-1} \frac{2a}{\lambda_{g0}} = \begin{array}{l} \text{distance of a small aperture} \\ \text{from side of waveguide} \end{array} \quad (10)$$

$$\lambda'_{g0} = \frac{\lambda_0}{\sqrt{1 - \left(\frac{\lambda_0}{1.706D}\right)^2}} = \begin{array}{l} \text{guide wavelength in cy-} \\ \text{lindrical waveguide of} \\ \text{diameter } D \text{ at frequency } \omega_0 \end{array} \quad (11)$$

$$\lambda_{g0} = \frac{\lambda_0}{\sqrt{1 - \left(\frac{\lambda_0}{2a}\right)^2}} = \begin{array}{l} \text{guide wavelength in rectan-} \\ \text{gular waveguide of width } a \text{ at} \\ \text{frequency } \omega_0 \end{array} \quad (12)$$

λ_0 = wavelength of a plane wave at frequency ω_0 .

For small circular apertures, the required hole diameters are approximately

$$d_{i,i+1}\Big|_{i=0 \text{ to } n} = \sqrt[3]{6M_{i,i+1}} \quad (13)$$

Approximate corrections for aperture thickness t and size can be obtained by computing compensated polarizabilities

$$(M_{i,i+1})_c = M_{i,i+1}\left[1 - \left(\frac{1.7d_{i,i+1}}{\lambda_0}\right)^2\right] 10^{\frac{1.6t}{d_{i,i+1}}\sqrt{1-\left(\frac{1.7d_{i,i+1}}{\lambda_0}\right)^2}} \quad (14)$$

and then recomputing the $d_{i,i+1}$ using Eq. (13) and the $(M_{i,i+1})_c$.

$$\phi_i = \pi p - \frac{1}{2}\left[\tan^{-1}\frac{2X_{i-1,i}}{Z'_0} + \tan^{-1}\frac{2X_{i,i+1}}{Z'_0}\right] \quad \text{radians}$$

$$= \text{electrical distance between irises} \quad (15)$$

where

$$\frac{X_{i,i+1}}{Z'_0} = \frac{16M_{i,i+1}}{0.955D^2\lambda'_{g0}}$$

$$= \text{normalized shunt reactance of iris}$$

A suggested low-pass to band-pass mapping (Sec. 8.04) is

$$\frac{\omega'}{\omega'_1} = \frac{2}{w}\left(\frac{\omega - \omega_0}{\omega_0}\right) \quad (16)$$

directional filters are specified in terms of the band-pass frequency response at Port 4. This band-pass response is related in turn to the coupling coefficients $k_{i,i+1}$ and external Q's, $(Q_e)_A$ and $(Q_e)_B$, of a two-port band-pass filter having an identical frequency response. It is also related to the response of a low-pass prototype filter having element values g_0, g_1, g_2, ..., g_{n+1}. As discussed in Secs. 4.13 and 11.06, the increase in midband attenuation $(\Delta L_A)_0$ at Port 4 due to dissipation in the circuit can be computed from the prototype element values and the Q's of the resonators.

The quantity c in this chart is the square root of a power coupling factor. It is related to the square of the magnitude of a scattering coefficient (Sec. 2.12) as defined in Figs. 5.10-7 and 5.10-10. For example, the power coupling factor $(c_{i,i+1})^2$ between the cavities i and $i + 1$ is defined as follows. Let cavity $i + 1$ be extended in length and a matched load* inserted inside. Let cavity i be cut in two and power fed to iris i, $i+1$ from a linearly or circularly polarized matched generator.* Then the ratio of the power delivered to the load to that available from the generator is $(c_{i,i+1})^2$, which is the same as $|S_{12}|^2$ in Fig. 5.10-7.

The power coupling factors $(c_{01})^2$ and $(c_{n,n+1})^2$ are defined in a similar way. Again we assume that cavity number 1 is extended and a matched load* inserted inside. Likewise, a matched load* is placed at Port 2 and a matched generator* is placed at Port 1. The ratio of the total power in the circularly polarized wave delivered to the load in the cylindrical guide to that available from the generator is $(c_{01})^2$, which in Fig. 5.10-10 is $|S_{14}|^2 + |S_{13}|^2$, where for the case of circular polarization $|S_{14}| = |S_{13}|$.

In practically all cases, the length of the cavities is approximately one-half guide wavelength, $\lambda'_{g0}/2$, at midband. However, the cavities can in principle be designed to be approximately an integral number p of half guide-wavelengths long. The exact electrical length ϕ_i of the cavities, which is given in the chart, is reduced somewhat from the value of 180 p degrees because of the stored magnetic energy in the coupling apertures.

In order that a pure circularly polarized wave be induced in the cylindrical cavities, it is necessary, when using circular coupling apertures between the end cavities and the rectangular waveguides, to offset the axis of the cavities a distance x from the side of the rectangular guide as given in Table 14.02-1. In this case a perfectly circularly

---

* "Matched" as used here refers to matching the guide impedance.

larized wave is induced only at the design center frequency, although
e wave is nearly circularly polarized over the range of pass-band fre-
encies. A type of coupling arrangement using three slots that produces
essentially circularly polarized wave in the cavities[8] over a much
der frequency interval is shown in Fig. 14.02-3. In this arrangement
axis of the cylindrical cavities coincides with the axis of the
tangular guides.

Waveguide directional filters having larger bandwidths can be ob-
ined by using large coupling apertures of the types shown in Fig. 14.02-4.
e dimensions of these apertures are too large to be computed very ac-
rately using the small-aperture coupling data presented in Chapter 5.
wever, in the case of the two-slot configuration in Fig. 14.02-4(b)
ethe's theory can be used to obtain a first approximation for the coupling
lots, and then corrections can be made after experimental tests. If M_1
is the magnetic polarizability of the transverse slot in the transverse
direction while M_2 is the magnetic polarizability of the longitudinal slot
in the longitudinal direction, then according to Bethe's small aperture
theory

$$M_2 = \frac{R c k_c r_2}{4\pi\sqrt{2}\left(\sin\frac{\pi x_2}{a}\right) J_1(k_c r_2)}\sqrt{\frac{3a^3 b\lambda_s'}{\lambda_s}} \qquad (14.02\text{-}1)$$

and

$$M_1 = \frac{M_2\lambda_s \sin\left(\frac{\pi x_2}{a}\right)\dfrac{J_1(k_c r_2)}{k_c r_2}}{2a\cos\left(\frac{\pi x_1}{a}\right)\left[J_0(k_c r_1) - \dfrac{J_1(k_c r_1)}{k_c r_1}\right]} \qquad (14.02\text{-}2)$$

where

λ_s = guide wavelength in rectangular guide

λ_s' = guide wavelength in circular guide

a = width of rectangular guide

b = height of rectangular guide

R, r_1, r_2, x_1, and x_2

A-3527-451
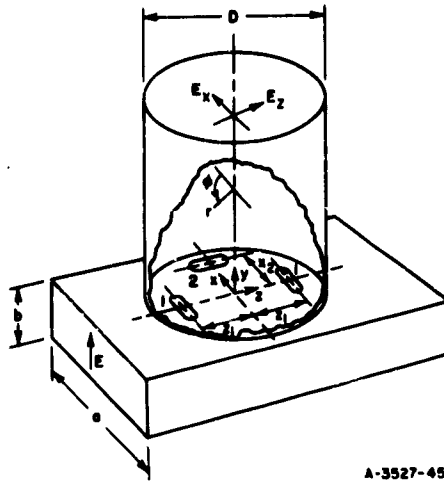
Assuming small apertures, the condition for circular polarization is

$$\frac{M_2}{M_1} = \frac{4x_2 a J_1(\alpha z_1)\ \cos\ (360 z_1/\lambda_{g0})}{\xi z_1 \lambda_{g0} J_1(\alpha x_2)\ \sin\ (180 x_2/a)}$$

M_1 = magnetic polarizability of each transverse slot
[Fig. 5.10-4(a)]

M_2 = magnetic polarizability of the longitudinal slot
[Fig. 5.10-4(a)]

λ_{g0} = guide wavelength in rectangular guide at midband frequency

α = $2\pi/1.705D$

ξ = tolerance factor: when $\xi = 1.02$ the axial ratio in the circular guide is less than 1.02 from $\lambda_g = 8.82 z_1$ to $6.28 z_1$. The design center value of λ_{g0} in this case is $7.30 z_1$.

Under this condition

$$c^2 = \frac{128\pi^2 \lambda_{g0} M_2^2\ \sin^2\ (180 x_2/a)\ [J_1(\alpha x_2)]^2}{3a^3 b D^2 \lambda'_{g0} \alpha^2 x_2^2}$$

λ'_{g0} = guide wavelength in circularly polarized cavity at midband

SOURCE: *Proc. IRE* (see Ref. 8 by S. B. Cohn)

FIG. 14.02-3 APPROXIMATE DESIGN EQUATIONS FOR A BROADBAND,
CIRCULAR-POLARIZATION COUPLER
The axial ratio is the ratio of the field strengths E_x and E_z
at right angles to each other

845

(a) RECTANGULAR – APERTURE COUPLER   (b) TWO – SLOT COUPLER

(c) LARGE CIRCULAR HOLE COUPLER
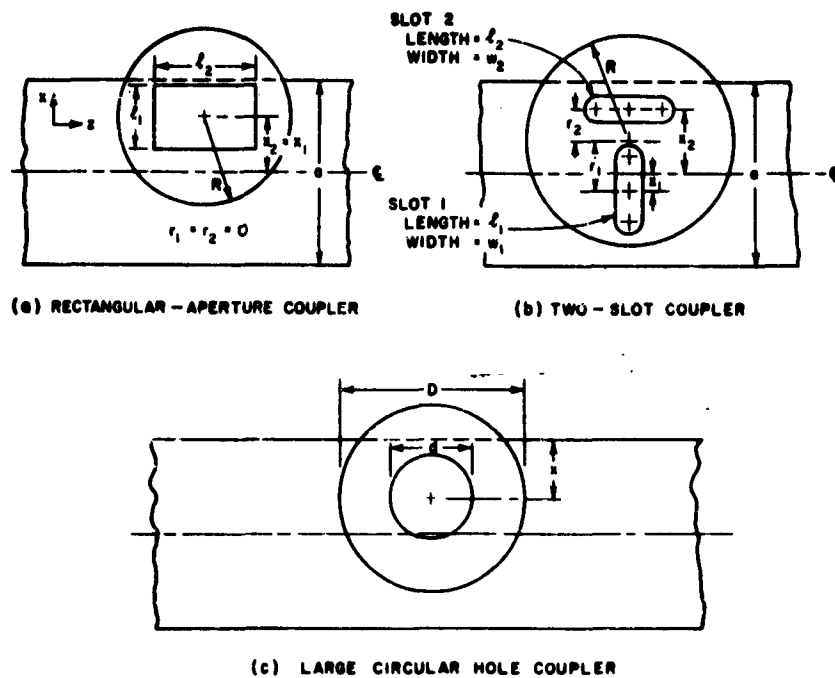
FIG. 14.02-4   APERTURE CONFIGURATIONS HAVING LARGE COUPLING
FACTORS

are distances as indicated in Fig. 14.02-4(b), $k_c = 1.84/R$, and c is the square root of the power coupling factor and is equal to c_{01} or $c_{n,n+1}$ obtained from Eq. (5) or Eq. (7) of Table 14.02-1. The trial dimensions of the slots can be obtained from Fig. 5.10-4(a) along with the thickness and size correction given by Eq. (5.10-6). Cut and try refinement of the slot dimensions can then be achieved using experimental techniques described later in this section.

Table 14.02-2 shows the final dimensions and measured performance for several aperture designs of the types in Fig. 14.02-4. These designs all have relatively tight coupling, but that of the two-slot configurations is decidedly the tightest. The *axial ratio* referred to in these data is the ratio of field strengths at right angles to each other in a plane perpendicular to the axis of the circular guide. For perfect circular polarization the axial ratio is one. Figure 14.02-5 shows the measured power coupling and axial ratio as a function of frequency for the two-slot configuration whose dimensions are given in the column on the far right in Table 14.02-2.

846

Table 14.02-2

TYPICAL COUPLING PROPERTIES OF LARGE APERTURES FOR
WAVEGUIDE DIRECTIONAL FILTERS AT f = 9780 Mc

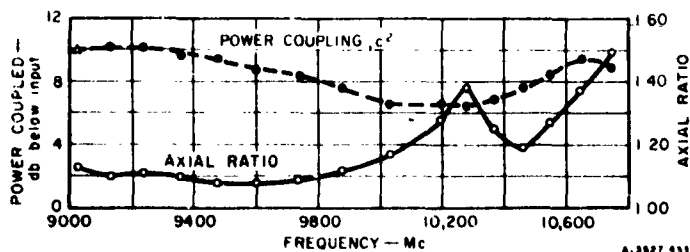|	CIRCULAR HOLE [Fig. 14.02-4(c)]	RECTANGULAR APERTURE [Fig. 14.02-4(a)]	TWO-SLOT COUPLER [Fig. 14.02-4(b)]	TWO-SLOT COUPLER [Fig. 14.02-4(b)]
Dimensions (inches)	d = 0.440 x = 0.207 from side wall $r_1 = r_2 = 0$ D = 1.114	l_1 = 0.442 l_2 = 0.450 $x_1 = x_2$ = 0.229 from center line $r_1 = r_2 = 0$ R = 0.554	l_1 = 0.461 w_1 = 0.136 l_2 = 0.518 w_2 = 0.142 x_1 = 0 x_2 = 0.320 r_1 = 0.243 r_2 = 0.077 R = 0.554	l_1 = 0.510 w_1 = 0.136 l_2 = 0.565 w_2 = 0.142 x_1 = 0 x_2 = 0.320 r_1 = 0.243 r_2 = 0.077 R = 0.554
Aperture Thickness (t) (inches)	0.023	0.025	0.025	0.025
Axial Ratio	1.03	1.04	1.04	1.10
Total Coupling Factor (db) $10 \log_{10} c^2$	-17.3	-12.8	-8.8	-8.2
VSWR in Rectangular Waveguide	1.05	1.08	1.25	1.23
$(Q_e)_A$ =	556	194	73.5	63.5

FIG. 14.02-5 POWER COUPLING AND AXIAL RATIO OF A PAIR
OF SLOTS HAVING LARGE COUPLING FACTORS
The slot dimensions are shown in the column at the
far right in Table 14.02-2

847
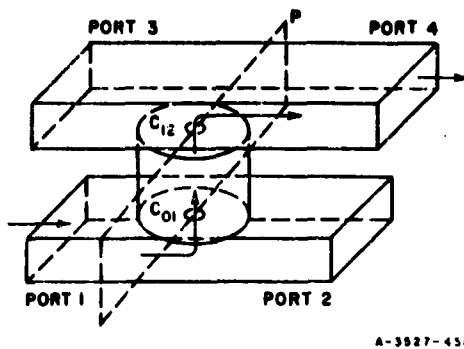
FIG. 14.02-6 SINGLE-CAVITY WAVEGUIDE
DIRECTIONAL FILTER

A single-cavity X-band wave-
guide directional filter of the
type in Fig. 14.02-6 is photographed
in assembled and disassembled form
in Fig. 14.02-7. In this filter the
cylindrical cavity (which was made
of brass) was split along its mid-
plane—a position of minimum longi-
tudinal wall current—so that the
unloaded Q of the cavity was not
appreciably degraded by the joint.
The two halves of the experimental
filter were held together by a
C-clamp; however, they could also
be easily soldered together. The capacitive tuning screws shown in the
picture were adjusted so that the two spacially orthogonal TE_{11} modes
that can exist in the cavity resonated at the same frequency. The neces-
sity for this tuning procedure can be made plausible if one remembers
that the circularly polarized mode induced in the cavity can be resolved
into spacially orthogonal TE_{11} modes excited in time quadrature.

In this filter the terminating guides have inside dimensions
$a = 0.900$ inch and $b = 0.400$ inch while the coupling apertures have a
thickness $t = 0.020$ inch. The cavity diameter $D = 1.114$ inch, the coupling
hole diameters $d = 0.414$ inch and the cavity height $h = 0.716$ inch. The
axis of the cylindrical cavities was offset a distance $x = 0.207$ inch from
the sidewall of the rectangular waveguides. The measured performance of
this single cavity waveguide directional filter is shown in Fig. 14.02-8.
The measured loaded Q, Q'_L, of this cavity loaded at both ends was 249 and
the midband attenuation $(L_A)_0 = 0.72$ db or $(P_{avail}/P_{out}) = 1.19$. Using the
relation

$$Q'_e = Q'_L \sqrt{\frac{P_{avail}}{P_{out}}} = \frac{Q_e}{2} \qquad (14.02\text{-}3)$$

which applies for single-cavity directional filters as well as single-
cavity two-port filters, we find that the external Q, Q'_e, of the cavity

348
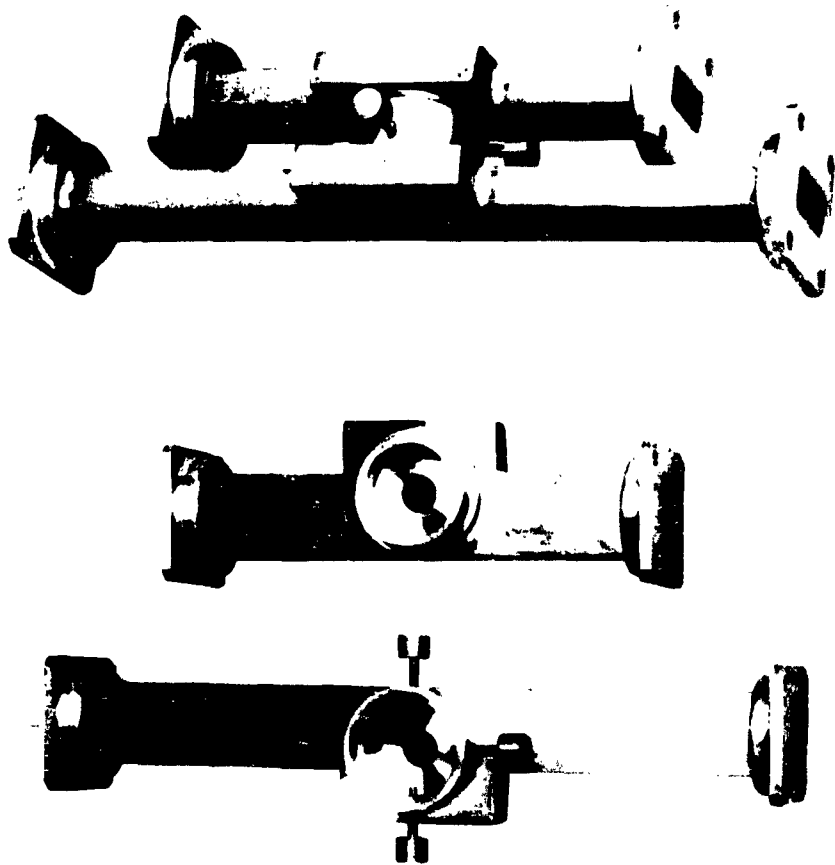
FIG. 14.02-7 VIEWS OF THE SINGLE-CAVITY WAVEGUIDE DIRECTIONAL FILTER
ASSEMBLED AND DISASSEMBLED
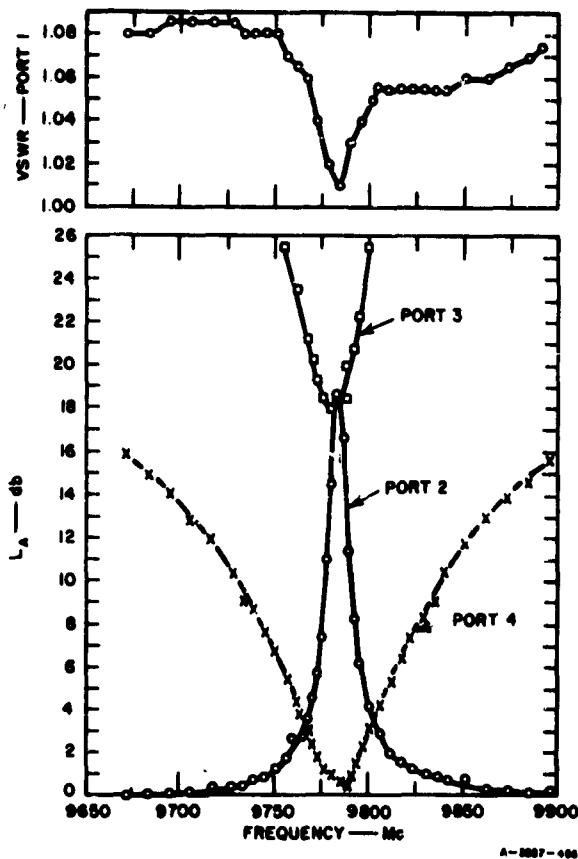
FIG. 14.02-8 EXPERIMENTAL RESULTS FOR THE
SINGLE-CAVITY WAVEGUIDE
DIRECTIONAL FILTER

loaded at both ends is 271. Therefore, the external Q, Q_e, of the cavity
loaded at one end as given in Table 14.02-1 is 542. Again using the
relation that

$$\frac{1}{Q'_L} = \frac{1}{Q_e} + \frac{1}{Q_a}$$

(14.02-4)

the unloaded Q, Q_a, of the cavity is 3030. This value would be approxi-
mately doubled if the cavity had been made of copper or if it were silver-
plated.

The value of the coupling factor $(c_{01})^2$ computed from the measured value $Q_e = (Q_e)_A = 542$, using Eq. (5) in Table 14.02-1, is $(c_{01})^2 = 0.0195$, or -17.1 db. Using $d_{01} = 0.414$ inch and solving for $(c_{01})^2$ using Eqs. (13) and (8) of Table 14.02-1 gives $(c_{01})^2 = -16.6$ db, which is in unexpectedly good agreement with the value obtained from (Q_e), considering that the hole is quite large and is close to the side wall. Technically, both a large-aperture correction and a thickness correction as in Eq. (14) of Table 14.02-1 should also be applied, but these corrections are very rough approximations and are in this case made to be quite uncertain due to the close proximity of the side wall. In such cases, experimental checking of the apertures is desirable. (This was done in the case of this design by experimentally determining Q_e.)

A two-cavity waveguide directional filter of the type illustrated in Fig. 14.02-9 was also constructed by modifying the single-cavity filter described above. The modification was accomplished by inserting a length of cylindrical guide contain-ing a coupling iris at its midplane, between the two halves of the original filter. The diameter d_{12} of the cen-tral iris in this filter was progressively enlarged to ob-tain first an undercoupled response, then a critically coupled response and finally an overcoupled response. The measured response of these filters when critically coupled, and overcoupled is shown in Figs. 14.02-10(a) and 14.02-10(b), respectively. A

FIG. 14.02-9 A TWO-CAVITY WAVEGUIDE DIRECTIONAL FILTER

tabular summary of the filter dimensions and performance is presented in Table 14.02-3.

The experimentally determined central-iris diameter, $d_{12} = 0.190$ inch, for critical coupling agreed reasonably well with the $d_{12} = 0.178$ inch value computed using the formulas in Table 14.02-1 and the correction in Eq. (5.10-6). The measured midband attenuation $(\Delta L_A)_0$ due to dissipation in the two-cavity directional filter also agreed well with that calculated

851

FIG. 14.02-10(a) MEASURED PERFORMANCE OF A
CRITICALLY COUPLED TWO-
CAVITY WAVEGUIDE DIRECTIONAL
FILTER

from Eq. (4.13-11). For example, consider the critically coupled or
maximally flat case having the low-pass prototype elements g_0 = 1,
g_1 = g_2 = 1.414, g_3 = 1, and 3-db point ω_1' = 1, w = 0.00317, and the
measured unloaded Q, Q_u = 3030, as determined from measurements on the
single-cavity filter, then the dissipation factor (Sec. 4.13) is
d = ω_1'/wQ_u = 0.0104. Equation (4.13-11) yields a value of $(\Delta L_A)_0$ =
1.28 db as compared with the measured midband loss of 1.25 db. Nearly
all of this loss was due to dissipation since the midband VSWR was
very low.

Four tuning screws were used in each of the cavities for tuning
purposes. The technique used to adjust these tuning screws is described

852
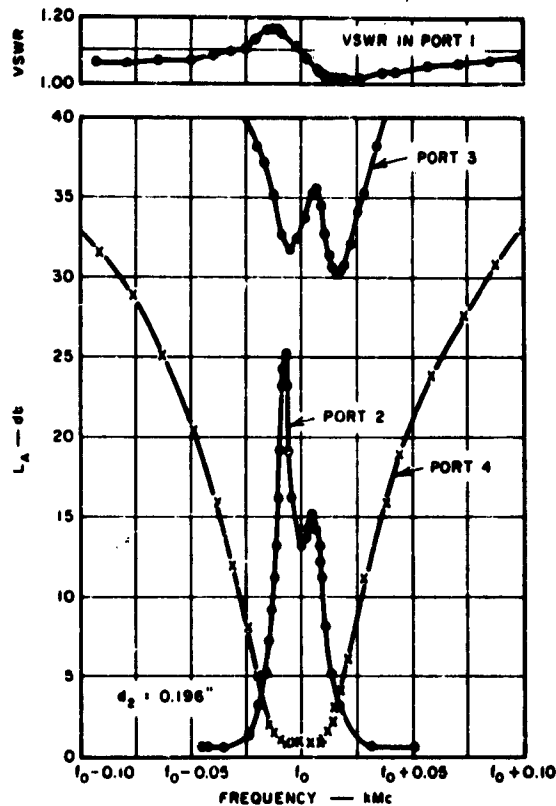
FIG. 14.02-10(b) MEASURED PERFORMANCE OF A
SLIGHTLY OVER-COUPLED TWO-
CAVITY WAVEGUIDE DIRECTIONAL
FILTER

below. Tuning of waveguide single-cavity directional filters can be
accomplished in a straightforward manner. The proper procedure is to
place matched detectors at Port 4 and Port 2, a matched load at Port 3
and a generator at Port 1. Then one adjusts the four equally spaced
tuning screws for maximum signal at Port 4 and minimum signal at Port 2.

In multiple-cavity filters this simple technique is difficult to
apply and it is better to use another technique. One such technique con-
sists of tuning each cavity separately using the apparatus illustrated in
Fig. 14.02-11. In this apparatus a linearly polarized signal is fed into
the cylindrical cavity through a rectangular- to cylindrical-waveguide

853

Table 14.02-3

DIMENSIONS AND SUMMARY OF THE MEASURED PERFORMANCE
OF A TWO-CAVITY WAVEGUIDE DIRECTIONAL FILTER

	UNDER- COUPLED	CRITICALLY COUPLED*	OVER- COUPLED[†]
Resonant frequency, f_0	9775 Mc	9774 Mc	9774 Mc
Fractional 3 db bandwidth	0.00256	0.00317	0.00338
Insertion loss (at f_0)[§]	0.90 db	1.25 db	0.95 db
VSWR at f_0	--	1.10	1.04
Maximum VSWR (off resonance)	--	1.14	1.17
Diameter d_{12} of central iris	0.179 in.	0.190 in.	0.196 in.
Thickness t_{12} of central iris	0.025 in.	0.025 in.	0.025 in.
Diameter $d_{01} = d_{23}$ of end irises	0.414 in.	0.414 in.	0.414 in.
Thickness $t_{01} = t_{23}$ of end irises	0.023 in.	0.023 in.	0.023 in.
Inside diameter of each cavity, D	1.114 in.	1.114 in.	1.114 in.
Height of each cavity, h	0.770 in.	0.770 in.	0.770 in.
Displacement of cylindrical guide axis from side wall of the rectangular guide	0.207 in.	0.207 in.	0.207 in.
Height of rectangular guide	0.400 in.	0.400 in.	0.400 in.
Width of rectangular guide	0.900 in.	0.900 in.	0.900 in.

* Shown in Fig. 14.02-10(a)

[†] Shown in Fig. 14.02-10(b)

[§] The inside surfaces of the cavities were machined brass. By
polishing and plating the inside surfaces it is believed that
midband insertion losses of 0.5 db could easily be obtained.
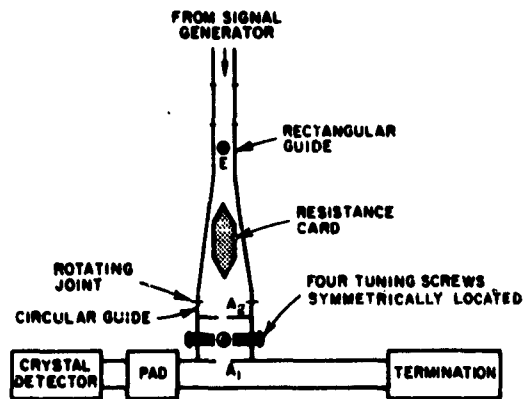
FIG. 14.02-11 SCHEMATIC DIAGRAM OF SETUP
FOR PRETUNING CAVITIES OF
THE TWO-CAVITY DIRECTIONAL
FILTER

transition, past a rotating joint. A resistance card within the transi-
tion serves the purpose of damping out any cross-polarized wave that
might be reflected from the cavity. When the electric field in the
exciting guide is oriented as shown, the two tuning screws parallel to
the electric field are adjusted for maximum signal in the detector.
Next the exciting guide is rotated by 90 degrees and the other pair of
screws is adjusted for maximum signal in the detector. Since the pairs
of tuning screws do not furnish completely independent adjustment, this
process is repeated until the signal at the detector is independent of
the polarization orientation of the exciting wave. The measured perform-
ance shown in Fig. 14.02-10 was obtained by pretuning the cavities in
this fashion, and without further adjustment of the assembled filter.

Another technique for tuning a multicavity filter of this sort is
to use the setup in Fig. 14.02-11 to feed a linearly polarized signal
through all the cavities simultaneously. In this case a slotted line is
inserted in the rectangular guide at the top and the cavities may be
tuned for each of the two orthogonal linear polarizations by observing
the quarter-wavelength shift of the voltage minimum in the input wave-
guide as successive cavi-
ties are brought to reso-
nance. This procedure is
the same as that described
in Sec. 11.05 for tuning
direct-coupled cavity fil-
ters. Alternatively, if
one has a sweep signal
source available, it may
be possible to tune the
cavities by simply maxi-
mizing the signal at the
detector in the rectangu-
lar waveguide for the two
orthogonal linear polari-
zations.

FIG. 14.02-12   SCHEMATIC DIAGRAM OF SETUP FOR
MEASURING THE PERFORMANCE OF
APERTURES HAVING LARGE
COUPLING FACTORS

The technique for
measuring the coupling and axial ratio of the wave excited by the large
apertures of Fig. 14.02-4 is illustrated in Fig. 14.02-12. The power
coupling factor c^2 is equal to the sum of the power received by the

detector in the position shown and that received when it is rotated
90 degrees, divided by the available power from the generator. The
axial ratio is the square root of the ratio of the maximum to the minimum
power received by the detector as it is rotated.

SEC. 14.03, STRIP TRANSMISSION LINE DIRECTIONAL FILTERS USING HALF- OR FULL-WAVELENGTH STRIPS

A form of strip-transmission-line directional filter that has proved
to be very useful is illustrated in Fig. 14.03-1 together with pertinent
design information. It might seem that the resonators in this type of
filter could be cascaded as shown in Fig. 14.03-2 to obtain a directional
filter having a multiple resonator response, but this is not the case.[3]

$$\frac{1}{Q} = \frac{\omega_2 - \omega_1}{\omega_0} = \frac{2\omega_0^2 C^2 Z Z_0}{\pi} = \frac{1}{\left(\begin{array}{c} Q \text{ OF DISSIPATIONLESS CIRCUIT} \\ \text{LOADED AT PORTS I AND 4} \end{array}\right)}$$

$$2\phi = \pi - 2\omega_0 C Z_0 \quad \text{RADIANS}$$

$$2\phi_1 = 2\pi - 2\sqrt{T} \omega_0 C Z_0 \quad \text{RADIANS}$$

FIG. 14.03-1   DESIGN INFORMATION FOR HALF-WAVELENGTH-STRIP AND ONE-WAVELENGTH-STRIP DIRECTIONAL FILTERS

Therefore, this type of directional filter is suitable to use only when a single resonator band-pass frequency response is desired between Port 1 and Port 4.

The action of the filters in Fig. 14.03-1 can be understood by invoking the principle of superposition. Excitation of Port 1 with a wave of amplitude V is equivalent to excitation of Port 1 and Port 4 at the reference planes T_1 and T_4 with waves both of amplitude $+V/2$ (even-mode case), and excitation of Ports 1 and 4 at the same reference planes with waves of amplitude $+V/2$ and $-V/2$, respectively (odd-mode case). Even-mode excitation of Ports 1 and 4 at the center frequency causes only the right-hand strip to resonate, which reflects waves having amplitude $+V/2$ at Port 1 and Port 4. On the other hand, odd-mode excitation causes only the left-hand strip to resonate, re-flecting waves having ampli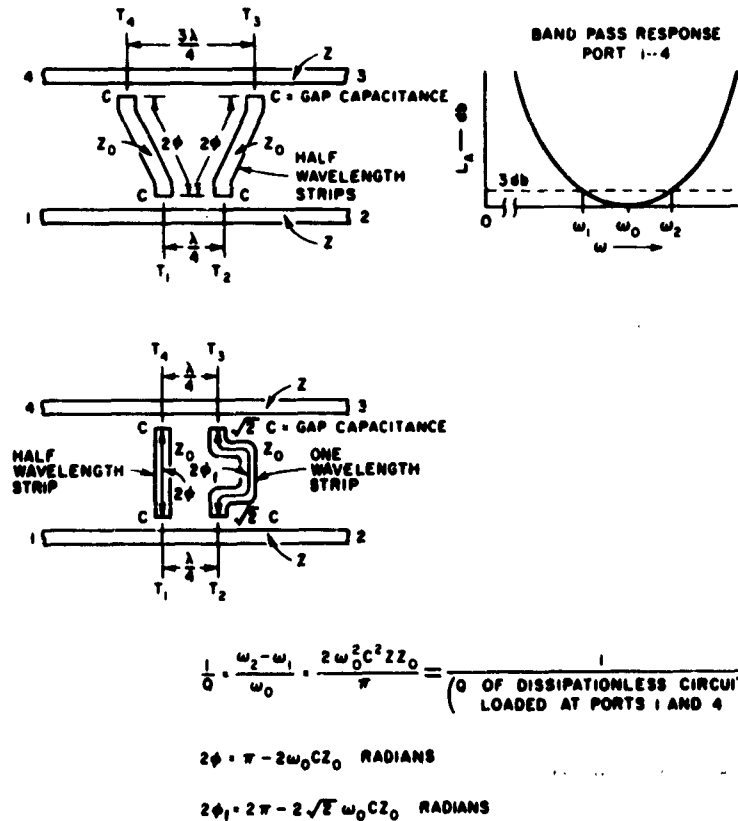tude $-V/2$ at Port 1 and $+V/2$ at Port 4. There-fore, at the resonant frequency of the strips the amplitude of the reflected wave at Port 4 is V while that at Port 1 is zero. Or, in other words, at the center frequency a signal inci-dent on Port 1 is ideally completely transferred to Port 4. At frequen-cies off resonance a signal incident at Port 1 passes through unattenu-ated to Port 2.
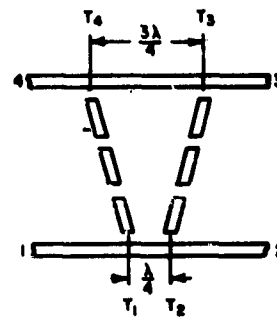
FIG. 14.03-2 EXAMPLE OF A MULTI-RESONATOR STRUCTURE THAT DOES NOT HAVE DIRECTIONAL FILTER PROPERTIES

The reason multiple-strip-resonator structures of the type shown in Fig. 14.03-2 cannot be used as directional filters can also be qualita-tively understood by applying the principle of superposition. It can be seen that when either odd-mode waves or even-mode waves are incident on Ports 1 and 4, some of the resonators in both the left- and right-hand string of resonators will be excited. Therefore, the necessary destruc-tive interference between the even- and odd-mode reflected waves at Port 1 and the necessary constructive interference between even- and odd-mode reflected waves at Port 4 is not obtained and directional filter action does not result. On the other hand, Wanselow and Tuttle[9] have

reported that marginal directional-filter performance is obtained using multiple-resonator structures of the type shown in Fig. 14.03-2. The explanation of this apparent paradox appears to be that Wanselow and Tuttle placed a short-circuit at Port 3, presumably at reference plane T_3, thus reducing it to a three-port device. Under these conditions when a signal is incident at Port 1 the right-hand chain of resonators would reflect a relatively high shunt impedance at Port 1 while the short-circuit at reference plane T_3 would reflect a shunt open-circuit at reference plane T_4. Therefore, the transmission characteristic between Port 1 and Port 4 roughly approximates that of the multi-resonator chain at the left of the structure in Fig. 14.03-2.

The dimensions of the TEM lines having the characteristic impedances Z and Z_e shown in Fig. 14.03-1 can be determined from Figs. 5.04-1 or 5.04-2. The gap spacing at the ends of the resonators necessary to realize the coupling capacitances C can be determined approximately from Fig. 5.05-9 by making use of the relation that C is approximately equal to ΔC times the width of the resonator strip.

(a)

(b)

A-1027-464
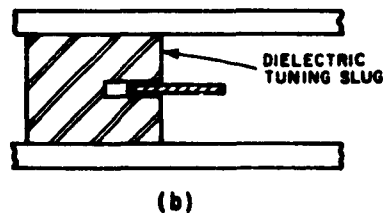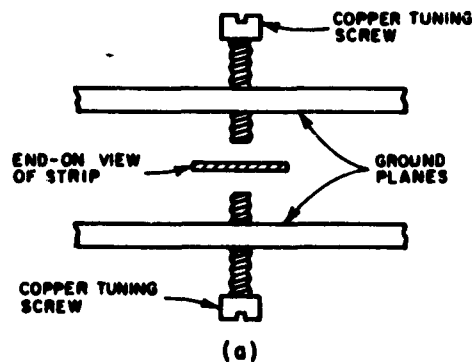
FIG. 14.03-3 METHODS OF TUNING A
STRIP-LINE DIRECTIONAL
FILTER

In order to tune the two resonators in the directional filter to the same frequency, copper tuning screws or dielectric tuning slugs of the types shown in cross section in Fig. 14.03-3 may be employed. For maximum effectiveness these tuners should be used near either end of a resonator where the electric field is high. In addition, if copper tuning screws are used they should be inserted asymmetrically from either ground plane so that the parallel plate TEM mode is not excited.

The measured response of a typical strip-line directional filter of this type is shown in Fig. 14.03-4.
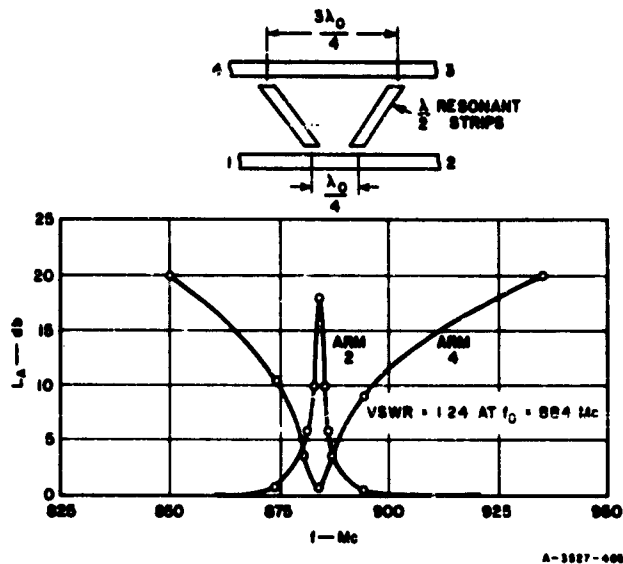
FIG. 14.03-4   RESPONSE OF STRIP-LINE HALF-
WAVELENGTH-RESONATOR
DIRECTIONAL FILTER

SEC. 14.04, TRAVELING-WAVE-LOOP DIRECTIONAL FILTER

A type of strip-transmission-line directional filter that can be
made with multiple resonators to obtain increased off-channel rejection
is illustrated in Fig. 14.04-1. The resonators in this directional
filter are traveling-wave loops whose mean circumference is a multiple
of 360 degrees at the midband frequency. Coupling between the loops is
obtained by the use of quarter-wavelength directional couplers of the
type described in Chapter 13. At the midband frequency a signal incident
on Port 1 excites clockwise traveling waves in each of the loops. The
traveling wave in the nth loop excites a signal at Port 4. At frequencies
well removed from the resonant frequency of the loops a signal incident on
Port 1 is transferred to Port 2.

The design chart in Table 14.04-1 summarizes the design of traveling-
wave-loop filters from low-pass prototypes so as to give a desired band-
pass response between Ports 1 and 4. The voltage coupling factors $c_{i,i+1}$
are the midband voltage couplings of the strip-line directional couplers

859
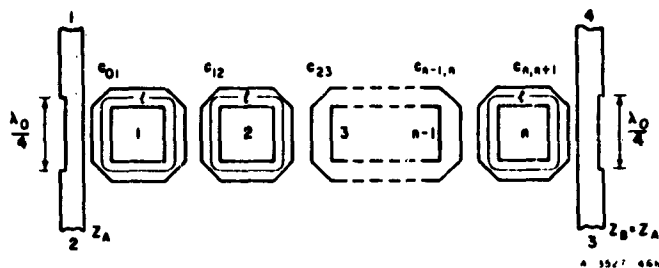
FIG. 14.04-1   A TRAVELING-WAVE-LOOP DIRECTIONAL
FILTER HAVING n RESONATORS

as defined in Eq. (13.02-2), while the coupling coefficients $k_{i,i+1}$ are
the resonator coupling coefficients in Fig. 8.02-3. It would also be
possible to build this type of traveling-wave-loop directional filter in
waveguide form. In this case the design parameters in Table 14.04-1 must
be modified by inclusion of the factor $(\lambda'_{g0}/\lambda_0)^2$ in exactly the same
fashion as is done in Table 14.02-1.

The layout of two, single-loop, directional filters, one of which is
tuned to 1024 Mc and the other of which is tuned to 1083 Mc, is shown in
Fig. 14.04-2. The measured performance of the device is shown in
Fig. 14.04-3. The filter having a center frequency of 1024 Mc was de-
signed to have a 3 db bandwidth of 8.2 Mc [Q_e = 250 and $(c_{01})^2$ = $(c_{12})^2$ =
0.0251] while the other filter was designed to have a 3 db bandwidth of
6.9 Mc [Q_e = 314 and $(c_{01})^2$ = $(c_{12})^2$ = 0.020].

The length of the ring resonators along the coupled transmission
lines was made to be a quarter wavelength measured in the dielectric at
the midband frequency in each case. The length of each of the other two
sides of the resonator plus the equivalent length of the two matched,
mitered corners, was also made approximately a quarter wavelength,
measured in the dielectric at midband. Data on the equivalent length of
matched mitered corners is presented in Fig. 5.07-4, although the design
under discussion was made before these data were available.

Table 14.04-1

DESIGN EQUATIONS FOR TRAVELING WAVE-LOOP DIRECTIONAL
FILTERS AS SHOWN IN FIG. 14.04-1

The parameters g_0, g_1, ..., g_{n+1} are as defined in Sec. 4.04,
and ω_1', ω_0, ω_1, and ω_2 are as defined in Fig. 14.02-2.

$$(Q_e)_A = \frac{g_0 g_1 \omega_1'}{w} = \text{external } Q \qquad (1)$$

$$k_{i,i+1}\Big|_{i=1 \text{ to } n-1} = \frac{w}{\omega_1'\sqrt{g_i g_{i+1}}} = \begin{array}{l}\text{coupling}\\\text{coefficient}\end{array} \qquad (2)$$

$$(Q_e)_B = \frac{\omega_1' g_n g_{n+1}}{w} = \text{external } Q \qquad (3)$$

where

$$w = \frac{\omega_2 - \omega_1}{\omega_0} \quad \text{and} \quad \omega_0 = \frac{\omega_1 + \omega_2}{2} \qquad (4)$$

$$c_{01} = 1\Big/\sqrt{\frac{(Q_e)_A}{2\pi m} + \frac{1}{2}} \qquad (5)$$

$$c_{i,i+1}\Big|_{i=1 \text{ to } n-1} = m \pi k_{i,i+1} \qquad (6)$$

$$c_{n,n+1} = 1\Big/\sqrt{\frac{(Q_e)_B}{2\pi m} + \frac{1}{2}} \qquad (7)$$

where the $c_{i,i+1}$ are *voltage* coupling factors, and m is the
number of full wavelengths in the resonator loops at resonance.

The odd- and even-mode impedances of the directional-coupler
sections are

$$(Z_{oe})_{i,i+1}\Big|_{i=0 \text{ to } n} = Z_0\sqrt{\frac{1 + c_{i,i+1}}{1 - c_{i,i+1}}} \qquad (8)$$

$$(Z_{oo})_{i,i+1}\Big|_{i=0 \text{ to } n} = Z_0\sqrt{\frac{1 - c_{i,i+1}}{1 + c_{i,i+1}}} \qquad (9)$$

The directional-coupler sections are a quarter-wavelength
long at ω_0.

A suggested low-pass to band-pass mapping (Sec. 8.04) is

$$\frac{\omega'}{\omega_1'} = \frac{2}{w}\left(\frac{\omega - \omega_0}{\omega_0}\right) \qquad (10)$$
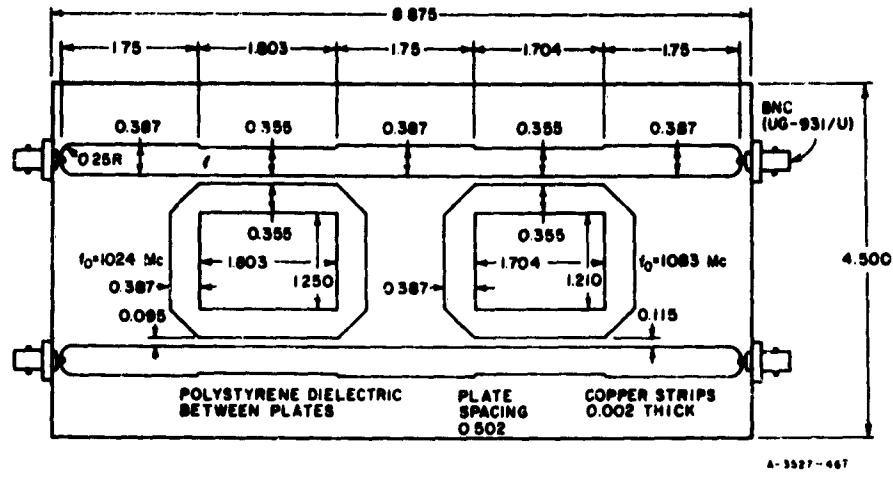
FIG. 14.04-2 LAYOUT OF A DUAL-LOOP DIRECTIONAL FILTER CIRCUIT

FIG. 14.04-3 MEASURED RESPONSE OF DUAL-LOOP
DIRECTIONAL FILTER CIRCUIT

The region of each loop that is coupled to the terminating lines is designed according to the formulas in Chapter 13 as a matched, 50-ohm directional coupler having the coupling specified above. The necessary even- and odd-mode impedances Z_{oe} and Z_{oo} are determined from Eqs. (13.02-5) and (13.02-6) or Eqs. (8) and (9) of Table 14.04-1. The widths of the strips necessary to realize these impedances are determined from Fig. 5.05-3 in the case of typical printed-circuit construction. The width of the strips forming the remainder of the loops is a value appropriate for a 50-ohm transmission line as determined from Fig. 5.04-1 or 5.04-2. Thus theoretically, a 50-ohm impedance level is preserved throughout the complete circumference of the loop.

In practice, it is found to be difficult to design the loops accurately enough so that there are no reflections on the loops and some sort of tuning is required if a single traveling-wave is to be established on each loop. Even a quite small discontinuity in any loop will generate a wave of substantial magnitude traveling in a direction opposite to that of the desired wave since it is repeatedly excited by the wave traveling in the desired direction. One method of tuning the loops that has been found to be appropriate when large quantities of directional filters are required consists of empirically adjusting the width of the loops and the width of the corners on a prototype model, and then mass-producing this design. Another effective technique for tuning each loop is to use four pairs of tuning screws, of the type shown in Fig. 14.03-3(a), placed at quarter-wavelength intervals around the perimeter as shown in Fig. 14.04-4.

FIG. 14.04-4 SKETCH ILLUSTRATING THE
PLACEMENT OF TUNING SCREWS
IN A TRAVELING-WAVE-LOOP
DIRECTIONAL FILTER

In practice it has been found that, for the filters shown in Fig. 14.04-2, size 4-40 screws can be used to tune the loops over ∩ 6-percent frequency band.

Proper adjustment of the tuning screws for a single-resonator traveling-wave-loop directional filter can be accomplished by observing the response of matched detectors at Port 2 and Port 4 when a matched load is placed at Port 3 and a signal source is placed at Port 1. If a sweeping signal source is available to feed Port 1 this same procedure can be used to tune two- and three-resonator traveling-wave-loop directional filters.

SEC. 14.05, TRAVELING-WAVE RING RESONATOR

The traveling-wave ring resonator of the type illustrated in Fig. 14.05-1 which is closely related to the traveling-wave loop directional filters has found wide acceptance as a passive power multiplying device, for use in testing components that must carry high power. This device which is usually constructed in waveguide can be thought of as being formed by removing the output coupler from a single-loop waveguide directional filter. The traveling-wave ring is usually several wavelengths long to allow the insertion of test pieces within the ring. By adjusting the variable phase shifter and variable impedance matching transformer shown in Fig. 14.05-1 a pure traveling wave can be excited in the ring even though the component under test is slightly mismatched.
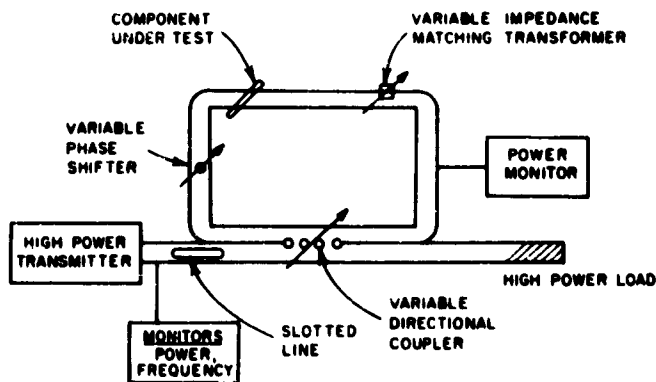
SOURCE: *IRE Trans. PGMTT* (see Ref. 4 by K. Tomiyasu)

FIG. 14.05-1   A RESONANT RING CIRCUIT

Most of the power delivered by the generator is used to set up a high-amplitude traveling wave within the ring and only a small amount of it is delivered to the load. The expression for the multiplication or power gain, of the wave within the loop is given by

$$\text{Power Gain} = \left[\frac{c}{1 - 10^{-\alpha/2 0} \sqrt{1 - c^2}} \right]^2 \qquad (14.05\text{-}1)$$

where

    c = voltage coupling factor of the directional coupler

    α = one-way attenuation around the ring measured in db.

Equation (14.05-1) has been plotted in two different ways in Figs. 14.05-2(a), (b) to facilitate the determination of the power gain in the traveling-wave

FIG. 14.05-2(a)   RESONANT RING CHARACTERISTICS WITH POWER GAIN AS A PARAMETER

FIG. 14.05-2(b)   RESONANT RING POWER GAIN WITH COUPLING
FACTOR IN db AS A PARAMETER

ring. It is seen that substantial power gains can be obtained even for
relatively larger values of the one-way ring attenuation, α.

SEC. 14.06, DERIVATION OF FORMULAS FOR WAVEGUIDE DIRECTIONAL FILTERS

The detailed performance of the waveguide directional filters de-
scribed in Sec. 14.02, the traveling-wave loop directional filters
described in Sec. 14.04, and the traveling-wave ring resonator can be
most easily understood by considering the behavior of the multiply-
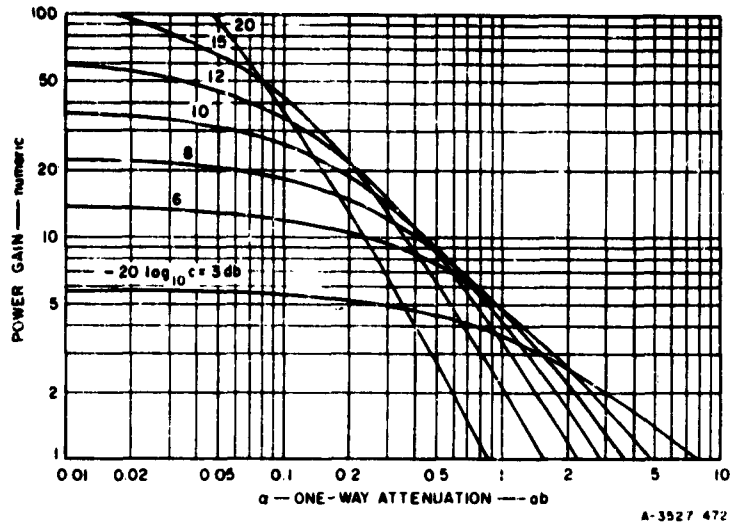reflected waves within the resonators. This section presents such an
analysis for the waveguide directional filter. Consider first the single-
cavity waveguide directional filter of the type shown in Fig. 14.02-6 and
assume that the following conditions are satisfied:

(1)   The coupling apertures excite a pure circularly polarized
TE_{11} wave in the circular waveguide and introduce no re-
flection in the rectangular waveguide.

(2)   The cavity is perfectly symmetrical about its axis, so
that the two orthogonal linearly polarized modes in the
cavity resonate at the same frequency.

866

(3) Each port of the filter is terminated in its character-
    istic impedance.

The reference plane, P, is chosen to be perpendicular to the axes
of the rectangular waveguides at the center points of the coupling aper-
tures. With a wave of unit amplitude incident on Port 1, the amplitudes
in the four ports of the filter at the instant just after the wave coupled
into the cavity has been reflected for the first time by the upper end
wall are as follows:

Port 1 E_1 = 1   Port 3 E_3 = 0

                                                              (14.06-1)

Port 2 E_2 = $-\sqrt{1 - c_1^2}$ Port 4 E_4 = $c_1 c_2 e^{-\alpha h - j\theta}$

where $(c_{01})^2$, which will be replaced here by c_1^2, is the power coupling
factor (as defined in Table 14.02-1) of the lower aperture, and $c_2^2 = (c_{12})^2$
is that of the upper aperture, h is the axial height of the cavity, α is
the attenuation constant in nepers per unit length in the circular wave-
guide, and θ is the electrical length in radians of the cavity plus the
phase shifts introduced by the apertures.

In the neighborhood of resonance, and in the case of narrow bandwidth,

$$\theta = p\pi \frac{\lambda'_{s0}}{\lambda'_s} - \pi$$ (14.06-2)

where

λ'_{s0} is the value of λ'_s at resonance, and

p is the number of half-wave field variations along
     the axis of the cavity.

Because of multiple reflections between the end walls of the cavity, the
steady-state wave amplitude in Port 4 is composed of an infinite summation
of components, as follows:

$$E_4 = c_1 c_2 e^{-(\alpha h + j\theta)} + c_1 c_2 (1 - c_1^2)^{\frac{1}{2}} (1 - c_2^2)^{\frac{1}{2}} \rho_0^2 e^{-3(\alpha h + j\theta)} + \ldots$$

$$\ldots$$

$$+ c_1 c_2 (1 - c_1^2)^{\frac{p-1}{2}} (1 - c_2^2)^{\frac{p-1}{2}} \rho_0^{2(p-1)} e^{-(2p-1)(\alpha h + j\theta)} + \ldots$$

                                                              (14.06-3)

where ρ_0 is the factor by which the reflected wave amplitude at an end wall is reduced because of dissipation loss on that wall. ρ_0 is approximately equal to the magnitude of the voltage reflection coefficient of the end wall in the absence of the aperture. Therefore,

$$\rho_0 = \left| \frac{Z_s - Z_0}{Z_s + Z_0} \right| = \left| \frac{R_s + jR_s - Z_0}{R_s + jR_s + Z_0} \right| \qquad (14.06\text{-}4)$$

where

    Z_s is the surface impedance of the end wall in ohms per square,

    R_s is the surface resistivity of the end wall in ohms per square, and

    $Z_0 = 377\lambda'_g/\lambda$ is the wave impedance of the circular waveguide in ohms per square.

Since $R_s \ll Z_0$, ρ_0 may be approximated by

$$\rho_0 = 1 - \frac{R_s \lambda}{60\pi\lambda'_g} \qquad . \qquad (14.06\text{-}5)$$

The amplitude E_4 may be expressed in closed form, as follows:

$$E_4 = \frac{c_1 c_2 e^{-(ah+j\theta)}}{1 - (1 - c_1^2)^{1/2}(1 - c_2^2)^{1/2}\rho_0^2 e^{-2(ah+j\theta)}} \qquad . \qquad (14.06\text{-}6)$$

In a similar manner, a formula for E_2 may be obtained:

$$\begin{aligned}
E_2 &= (1 - c_1^2)^{1/2} - c_1^2(1 - c_2^2)^{1/2}\rho_0 e^{-2(ah+j\theta)} \\[2mm]
&\quad - c_1^2(1 - c_2^2)(1 - c_1^2)^{1/2}\rho_0^3 e^{-4(ah+j\theta)} \\[2mm]
&\quad - c_1^2(1 - c_2^2)^{3/2}(1 - c_1^2)\rho_0^5 e^{-6(ah+j\theta)} - \cdots \\[2mm]
&= (1 - c_1^2)^{1/2} - \frac{c_1^2(1 - c_2^2)^{1/2}\rho_0 e^{-2(ah+j\theta)}}{1 - (1 - c_1^2)^{1/2}(1 - c_2^2)^{1/2}\rho_0^2 e^{-2(ah+j\theta)}} \qquad (14.06\text{-}7)
\end{aligned}$$

or

$$E_2 = \frac{(1 - c_1^2)^{\frac{1}{2}} - (1 - c_2^2)^{\frac{1}{2}}[\rho_0^2 - c_1^2\rho_0(\rho_0 - 1)]e^{-2(\alpha h + j\theta)}}{1 - (1 - c_1^2)^{\frac{1}{2}}(1 - c_2^2)^{\frac{1}{2}}\rho_0^2 e^{-2(\alpha h + j\theta)}}. \quad (14.06\text{-}8)$$

At resonance $\theta = (p - 1)\pi$, so that

$$e^{-2(\alpha h + j\theta)} = e^{-2\alpha h} \quad , \quad (14.06\text{-}9)$$

Also, in the usual case of light coupling, $c_1^2\rho_0(\rho_0 - 1) <<< \rho_0^2$. Therefore, the condition for a perfect null on Port 2 at resonance is

$$\frac{e^{4\alpha h}}{\rho_0^4} = \frac{(1 - c_2^2)}{(1 - c_1^2)} \quad . \quad (14.06\text{-}10)$$

In the usual design problem cavity losses are sufficiently low that c_1^2 and c_2^2 determined from Eq. (14.06-9) will be almost equal. In that case if one makes the couplings equal, a deep, although imperfect, rejection on Port 2 will generally be obtained. A formula for the loaded Q, Q_L', of the cavity loaded at both ends, will now be derived for $c_1^2 = c_2^2 = c^2$.

Q_L' is defined as $f_0/2(f_0 - f_1)$ where f_1 is the frequency at which the transmitted power has fallen to one half of the value it has at the center frequency, f_0. It is necessary, therefore, to find the angle θ_1 corresponding to the frequency f_1. The first step is to form

$$|E_4 E_4^*| = \frac{1}{2} = \frac{c^4 e^{-2\alpha h} e^{j\theta_1} e^{-j\theta_1}}{|1 - (1 - c^2)\rho_0^2 e^{-2\alpha h}(\cos 2\theta_1 - j \sin 2\theta_1)|^2} \quad .$$

$$(14.06\text{-}11)$$

This yields

$$\cos 2\theta_1 = 1 - \frac{[1 - (1 - c^2)\rho_0^2 e^{-2\alpha h}]^2}{2(1 - c^2)\rho_0^2 e^{-2\alpha h}} \quad . \quad (14.06\text{-}12)$$

869

At resonance, $\theta = \theta_0 = (p-1)\pi$ and therefore, in the case of narrow bandwidth, $\cos 2\theta_1$ may be replaced by $\cos 2(\delta\theta)_1$, where $(\delta\theta)_1 = \theta_0 - \theta_1$, and hence

$$\cos 2\theta_1 = 1 - \frac{[2(\delta\theta)_1]^2}{2} + \ldots \qquad (14.06\text{-}13)$$

Thus

$$(\delta\theta)_1 = \frac{1 - (1 - c^2)\rho_0^2 e^{-2a\hbar}}{2(1 - c^2)^{\frac{1}{2}}\rho_0 e^{-a\hbar}} \qquad (14.06\text{-}14)$$

Next a relationship between $(\delta\theta)_1$ and $(\delta f)_1 = f_0 - f_1$ is needed. With the aid of the well-known formula for guide wavelength in terms of frequency, we obtain

$$\delta\theta = \frac{-p\pi\lambda'_{s0}}{(\lambda'_s)^2}\,\delta\lambda'_s = -p\pi\frac{\delta\lambda'_s}{\lambda'_s} = p\pi\frac{\delta f}{f}\left(\frac{\lambda'_s}{\lambda}\right)^2 \qquad (14.06\text{-}15)$$

Now we make use of the definition of Q'_L given above to obtain

$$Q'_L = \frac{p\pi(1 - c^2)^{\frac{1}{2}}\rho_0 e^{-a\hbar}}{1 - (1 - c^2)\rho_0^2 e^{-2a\hbar}}\cdot\left(\frac{\lambda'_s}{\lambda}\right)^2 \qquad (14.06\text{-}16)$$

This is the complete doubly loaded Q of the cavity including the effects of internal losses and external loading. If internal losses are negligible compared to external loading, Q'_L becomes equal to the doubly loaded external Q, Q'_e as follows

$$Q'_e = \frac{p\pi(1 - c^2)^{\frac{1}{2}}}{c^2}\cdot\left(\frac{\lambda'_s}{\lambda}\right)^2 = p\pi\left(\frac{\lambda'_s}{\lambda}\right)^2\left(\frac{1}{c^2} - \frac{1}{2}\right). \qquad (14.06\text{-}17)$$

However, in most cases one can replace the numerator factor $(1 - c^2)^{\frac{1}{2}}$ by unity. If c_1 and c_2 are slightly unequal, the formulas for Q will hold sufficiently closely with $c^2 = c_1 c_2$. The external Q, Q_e, of the end resonator of a multiple cavity directional filter which is externally loaded at only one end as defined in Table 14.02-1 is $2Q'_e$.

Since $E_1 = 1$, the relative power transmitted out of Port 4 at resonance is simply $|t|^2 = E_4^2$ with $\theta = 0$. Therefore

$$|t|^2 = \frac{c_1^2 c_2^2 e^{-2\alpha h}}{[1 - (1 - c_1^2)^{1/2}(1 - c_2^2)^{1/2}\rho_0^2 e^{-2\alpha h}]^2} \qquad (14.06\text{-}18)$$

or, if $c_1 = c_2 = c$,

$$|t|^2 = \frac{c^4 e^{-2\alpha h}}{[1 - (1 - c^2)\rho_0^2 e^{-2\alpha h}]^2} \qquad (14.06\text{-}19)$$

The attenuation in db is $10 \log_{10}(1/|t|^2)$, or

$$L_A = 20 \log_{10}\left[\frac{1 - (1 - c^2)\rho_0^2 e^{-2\alpha h}}{c^2 e^{-\alpha h}}\right] \quad \text{db} \quad . \quad (14.06\text{-}20)$$

If Eq. (14.06-17) is combined with Eqs. (14.06-14) and (14.06-15) we obtain $Q_e' = Q_L'/(\rho_0|t|)$. However, ρ_0 is of the order of 0.9999, and hence we may relate the external Q and complete loaded Q by the following simple expression:

$$Q_e' = \frac{Q_L'}{|t|} \quad . \quad (14.06\text{-}21)$$

It may also be shown that, in the case of high Q and narrow bandwidth, the above equations reduce to the following relationship between Q_L', Q_e', and the unloaded Q, Q_u, of the cavity:

$$\frac{1}{Q_L'} = \frac{1}{Q_u} + \frac{1}{Q_e'} \quad . \quad (14.06\text{-}22)$$

This is the same well-known expression that applies to a simple two-port filter consisting of a single resonator. The formula for unloaded Q in terms of the waveguide-cavity parameters is

$$Q_a = \cfrac{1}{\cfrac{\alpha \lambda^2}{\pi \lambda_g'} + \cfrac{R_s}{30\pi^2 p}\left(\cfrac{\lambda}{\lambda_g'}\right)^3} \qquad (14.06\text{-}23)$$

The value of the power coupling factors $(c_{01})^2$ and $(c_{n,n+1})^2$ for the end apertures in Fig. 14.02-1 in terms of the low-pass prototype elements are obtained by combining Eq. (14.06-17) with either Eq. (6) or Eq. (7) in Fig. 8.02-3, using the approximation $\sqrt{1 - (c_{01})^2}/c^2 \approx (1/c^2) - 1/2$.

For multiple-resonator directional filters the values $c_{i,i+1}$ for the internal apertures in Fig. 14.02-1 in terms of the low-pass prototype elements are obtained by using the relation

$$c_{i,i+1} = \left| \frac{2Y_0'}{B_{i,i+1}} \right| \qquad (14.06\text{-}24)$$

in conjunction with Eqs. (2) and (4) in Fig. 8.06-1. The coefficient of coupling $k_{i,i+1}$ is then obtained by the use of Eq. (8) in Fig. 8.02-3.

SEC. 14.07, DERIVATION OF FORMULAS FOR TRAVELING-WAVE LOOP DIRECTIONAL FILTERS AND THE TRAVELING-WAVE RING RESONATOR

An analysis similar to that presented in Sec. 14.06 can be carried through for traveling-wave loop directional filters. By particularizing the analysis the power gain for the traveling-wave ring resonator can also be obtained. This analysis is restricted to the case of TEM-mode propagation on the loop, although the results can be modified to apply to the case where the loop is a dispersive transmission line as explained below and in Sec. 14.04.

It is further assumed in this analysis that: (1) all transmission lines have the same characteristic impedance, Z_A, (2) all directional couplers are designed to be perfectly matched if terminated in Z_A, and they have infinite directivity, and (3) no points of reflection exist in the loop and therefore a pure traveling wave exists. A schematic diagram of the filter is given in Fig. 14.07-1. The phases of the voltages shown at the terminals of the directional couplers are, for convenience, referred to the midplanes of the directional couplers. The amplitudes

shown, however. apply at the terminals
of the couplers. The total length of
the loop at resonance, including the
lengths of the coupling regions, is
$l = m\lambda_0$, where m is an integer and λ_0
is the plane-wave wavelength at the
resonant frequency. In Fig. 14.07-1
it is seen that the following voltages
are excited during the first traversal
of the loop by the traveling wave.
For simplicity, we will again replace
c_{01} by c_1 and c_{12} by c_2:

$$E_1 = 1 \ \angle 0 \qquad (14.07\text{-}1)$$

$$E_2 = (1 - c_1^2)^{1/2} \ \angle 0 \qquad (14.07\text{-}2)$$

**FIG. 14.07-1 SCHEMATIC DIAGRAM
OF TRAVELING-WAVE-
LOOP DIRECTIONAL
FILTER**

$$E_3 = 0 \qquad (14.07\text{-}3)$$

$$E_4 = c_1 c_2 e^{-\frac{\alpha l}{2}} \ \angle 0 \qquad (14.07\text{-}4)$$

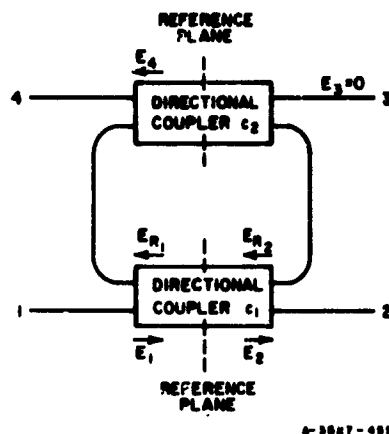$$E_{R_1} = c_1 \ \angle +90 \qquad (14.07\text{-}5)$$

$$E_{R_2} = c_1 (1 - c_2^2)^{1/2} e^{-\alpha l} \ \angle +90 \qquad (14.07\text{-}6)$$

where c_1 and c_2 are the voltage coupling factors of the directional
couplers, and α is the attenuation in nepers per unit length of the loop
transmission line.

For the mth traversal of the loop, the voltages may be written in
terms of E_{R_2} as follows:

$$E_2 = (1 - c_1^2)^{1/2} - c_1 E_{R_2} \ \angle 0 \qquad (14.07\text{-}7)$$

$$E_3 = 0 \qquad (14.07\text{-}8)$$

$$E_4 = \frac{c_2 e^{\frac{\alpha l}{2}}}{(1 - c_2^2)^{\frac{1}{2}}} E_{R_2} \quad \angle 0 \qquad (14.07\text{-}9)$$

$$E_{R_1} = \frac{e^{\alpha l}}{(1 - c_2^2)^{\frac{1}{2}}} E_{R_2} \quad \angle +90 \qquad (14.07\text{-}10)$$

where

$$E_{R_2} = c_1(1 - c_2^2)^{\frac{1}{2}} e^{-\alpha l}[1 + \sum_{j=1}^{j=n}(1 - c_1^2)^{j/2}(1 - c_2^2)^{j/2} e^{-j\alpha l}] \quad \angle +90 \quad .$$

$$(14.07\text{-}11)$$

Letting $n \to \infty$ and summing this expression in closed form, we obtain

$$E_{R_2} = \frac{c_1(1 - c_2^2)^{\frac{1}{2}} e^{-\alpha l}}{1 - (1 - c_1^2)^{\frac{1}{2}}(1 - c_2^2)^{\frac{1}{2}} e^{-\alpha l}} \quad \angle +90 \quad . \qquad (14.07\text{-}12)$$

The condition for perfect rejection between Ports 1 and 2 may be obtained by setting $E_2 = 0$, which yields

$$e^{2\alpha l} = \frac{1 - c_2^2}{1 - c_1^2} \qquad (14.07\text{-}13)$$

For perfect rejection, Eq. (14.07-13) requires $c_2 < c_1$ if $\alpha > 0$.

The doubly loaded Q of the filter may be calculated assuming $c_1 = c_2 = c$. At resonance the output voltage is

$$E_4 = \frac{c^2 e^{-\frac{\alpha l}{2}}}{1 - (1 - c^2)e^{-\alpha l}} \qquad (14.07\text{-}14)$$

At a different frequency which corresponds to an electrical length around the loop equal to $2\pi n + \theta$, the output voltage is

$$E_4 = \frac{c^2 e^{-(\alpha l + j\theta)/2}}{1 - (1 - c^2)e^{-(\alpha l + j\theta)}} \quad . \qquad (14.07\text{-}15)$$

Defining $Q'_L = f_L/2(f_0 - f_1) = m\pi/\theta_1$, where f_1 and θ_1 are values at the half-power point, we have from Eqs. (14.07-14) and (14.07-15),

$$E_4 = \left| \frac{c^2 e^{-(\alpha l + j\theta_1)/2}}{1 - (1 - c^2)e^{-(\alpha l + j\theta_1)}} \right| = \frac{\sqrt{2}}{2} \frac{c^2 e^{\frac{\alpha l}{2}}}{[1 - (1 - c^2)e^{-\alpha l}]} \quad . \qquad (14.07\text{-}16)$$

Taking absolute magnitudes of each side and simplifying, we may solve for θ_1 in terms of c and αl:

$$\cos \theta_1 = 1 - \frac{[1 - (1 - c^2)e^{-\alpha l}]^2}{2(1 - c^2)e^{-\alpha l}} \quad . \qquad (14.07\text{-}17)$$

If θ_1 is small, we may replace $\cos \theta_1$ by $1 - \theta_1^2/2$ which yields

$$\theta_1 = \frac{1 - (1 - c^2)e^{-\alpha l}}{(1 - c^2)^{\frac{1}{2}}e^{-\frac{\alpha l}{2}}} \quad . \qquad (14.07\text{-}18)$$

The doubly loaded Q of this filter* is

$$Q'_L = \frac{m\pi(1 - c^2)^{\frac{1}{2}}e^{-\frac{\alpha l}{2}}}{1 - (1 - c^2)e^{-\alpha l}} \quad . \qquad (14.07\text{-}19)$$

It should be noted that this expression gives the true loaded Q of the resonator as it would be measured, and takes account of the external loading due to both couplers combined with the losses in the transmission line of the loop.

The attenuation at resonance is given by $20 \log_{10} E_1/E_4$, and since $E_1 = 1$ we have

_____

* When a waveguide loop is used in the filter, Q'_L as given in Eq. (14.07-19) must be multiplied by $(\lambda_g/\lambda)^2$ where λ_g is the guide wavelength and λ is the free-space wavelength. Equation (14.07-20) for attenuation applies without change to the waveguide case.

$$L_A = 20 \log_{10} \frac{1 - (1 - c^2)e^{-\alpha l}}{c^2 e^{-\frac{\alpha l}{2}}} \quad . \qquad (14.07\text{-}20)$$

Equations (14.07-19) and (14.07-20) were derived assuming equal characteristic impedances of the transmission lines and assuming c to be the voltage coupling, but they apply correctly to unequal impedances of the ring and input and output Ports if c^2 is defined as the power coupling factor of the directional couplers.

The design equations in Table 14.04-1 are derived from the above analysis in exactly the same manner as the design equations in Table 14.02-1 for the waveguide directional filter were derived from the analysis in Sec. 14.06.

The traveling-wave ring resonator power gain is numerically equal to $|E_{R_1}|^2$ when $c_2 = 0$. The value of power gain given in Eq. (14.05-1) is obtained when $\frac{E}{E}$ (14.07-10) is evaluated for this condition.

SEC. 14.08. DERIVATION OF FORMULAS FOR STRIP-TRANSMISSION-LINE DIRECTIONAL FILTERS USING HALF-WAVELENGTH AND ONE-WAVELENGTH STRIPS

The strip transmission line directional filters using half-wavelength and one-wavelength strips are most easily analyzed by considering the even- and odd-mode excitation of Ports 1 and 4 as described in Sec. 14.03. The present analysis will assume that the electrical spacing between resonators is constant over the pass band of the filter, which is essentially correct for the usual narrow-band directional filters.

Referring to Fig. 14.03-1, when an even mode wave is incident on Ports 1 and 4 at the reference planes T_1 and T_4 shown in the figure, the wave will pass by the left-hand resonator but will be reflected at reference planes T_3 and T_2, since it excites only the right-hand strip in a resonant mode. Similarly, when an odd mode wave is incident on Ports 1 and 4, it will be reflected at reference planes T_1 and T_4, since it excites only the left-hand strip in a resonant mode. The voltage reflection coefficient Γ in each case at the appropriate reference planes will be the same and can be written as

$$\Gamma = \frac{1}{1 + j\frac{2X}{Z}} \quad . \qquad (14.08\text{-}1)$$

876

In this equation Z is the characteristic impedance of the main transmission lines and X is the shunt reactance introduced by a half-wavelength strip resonator with its midpoint grounded, or a full-wavelength resonator with its midpoint open-circuited. The shunt reactance presented by the half-wavelength strip is

$$ X \;=\; -\frac{1}{\omega C} + Z_0 \, \tan \phi \qquad\qquad (14.08\text{-}2) $$

where C is the capacitance of the gap at either end of the half-wavelength strip and 2ϕ is its electrical length. The shunt reactance presented by the one-wavelength strip is

$$ X_f \;=\; -\frac{1}{\omega C_f} - Z_0 \, \cot \phi_f \qquad\qquad (14.08\text{-}3) $$

where C_f is the capacitance at either end of the one-wavelength strip and $2\phi_f$ is its electrical length. In order that the half-wavelength and the one-wavelength resonators have the same frequency response it is necessary that $X_f = X$ over the pass band: or stated another way, the reactance slope parameter α must be the same for the two resonators. Since $\phi_f = 2\phi$ it can be shown that this condition obtains when $C_f = \sqrt{2}\, C$.

Because the even- and odd-mode reflected waves add at Port 4, and cancel at Port 1, the attenuation L_A, between Port 1 and Port 4, can be written either as

$$ L_A \;=\; 10 \, \log_{10} \frac{1}{|\Gamma|^2} \;=\; 10 \, \log_{10} \left[1 + 4\!\left(\frac{Z_0}{Z} \tan \phi - \frac{1}{\omega C Z}\right)^{\!2} \right] \quad \text{db} $$

$$ (14.08\text{-}4) $$

using the parameters for the half-wavelength strip or as

$$ L_A \;=\; 10 \, \log_{10} \left[1 + 4\!\left(\frac{Z_0}{Z} \cot \phi_f + \frac{1}{\sqrt{2}\,\omega C Z}\right)^{\!2} \right] \quad \text{db} \quad (14.08\text{-}5) $$

using the parameters for the one-wavelength strip. Equation (14.08-4) shows that the electrical length ϕ_0 of the half-wavelength strip at midband is given by

$$\tan \phi_0 = \frac{1}{\omega C} . \qquad (14.08\text{-}6)$$

Similarly, the electrical length ϕ_{0f} of the one-wavelength strip at mid-band is given by

$$\cot \phi_{0f} = -\frac{1}{\sqrt{2}\omega C Z_0} . \qquad (14.08\text{-}7)$$

The bandwidth of either directional filter will now be computed using the parameters of the half-wavelength strip. Inspection of Eq. (14.08-4) shows that the attenuation increases to 3 db when

$$\left| \frac{Z_0}{Z} \tan \phi - \frac{1}{\omega C Z} \right| = \frac{1}{2} . \qquad (14.08\text{-}8)$$

For narrow bandwidth and infinite unloaded Q, the doubly loaded external Q, Q'_e is determined from Eq. (14.08-5), using Taylor series expansion techniques similar to those used in deriving Eqs. (14.06-17) and (14.07-19), to be

$$Q'_e = \frac{f_0}{(\Delta f)_{3db}} = \frac{\pi}{2} \frac{Z_0}{Z} \frac{1}{(\omega_0 C Z_0)^2} . \qquad (14.06\text{-}9)$$

REFERENCES

1. S. B. Cohn and F. S. Coale, "Directional Channel Separation Filters," *Proc. IRE* 44, pp. 1018-1024 (August 1956).

2. F. S. Coale, "A Traveling-Wave Directional Filter," *IRE Trans. MTT*-4, pp. 256-260 (October 1956).

3. R. L. Sleven, P. E. Dorato, "Strip Transmission Line Directional Filter," paper presented at Institute of Radio Engineers PGMTT National Symposium 9-11 May 1960, San Diego, California.

4. K. Tomiyasu, "Attenuation in a Resonant Ring Circuit," *IRE Trans. MTT*-8, pp. 253-254 (March 1960).

5. L. Young, "A Hybrid-Ring Method of Simulating Higher Powers than Are Available in Waveguide," *Proc. IEE* (London) Vol. 101, Part III, pp. 189-190 (May 1954).

6. L. J. Milosevic and R. Vautey, "Traveling-Wave Resonator," *IRE Trans. MTT*-6, pp. 126-143 (April 1958).

7. S. J. Miller, "The Traveling Wave Resonator and High-Power Microwave Testing," *The Microwave Journal*, pp. 50-58 (September 1960).

8. S. B. Cohn, "Impedance Measurements by Means of a Broadband Circular Polarization Coupler," *Proc. IRE* 42, pp. 1554-1558 (October 1954).

9. R. D. Wanselow and L. P. Tuttle, Jr., "Practical Design of Strip-Transmission Line Half-Wavelength Resonator Directional Filters," *IRE Trans. MTT*-7, No. 1, pp. 168-173 (January 1959).

HIGH-POWER FILTERS

SEC. 15.01, INTRODUCTION AND GENERAL CONSIDERATIONS

High-power microwave radar transmitters radiate an appreciable amount of spurious output power—that is, frequency components other than the carrier frequency and the normal sideband modulation components.[1-21] At the outputs of these transmitters it is necessary to use high-power filters, that will pass the carrier frequency and normal modulation components but will suppress the spurious emissions, and thus keep them from causing interference in neighboring equipments.

Another application of high-power filters is to systems in which two (or more) transmitters operating at different frequencies are required to be connected to a single antenna. This is analogous to the more common diplexing (or multiplexing) with several receivers connected to a single antenna, with the additional requirement of high power-handling capacity (either high pulse power, or high average power, or both).

This section presents the design considerations for high-power filters and illustrates the manner in which various types of filters can be utilized to achieve specified objectives. Later sections in the chapter present more detailed information on the most common types of high-power filters.

Transmitter Spurious Emissions—Common types of high-power microwave transmitters in use at the present time are the magnetron oscillator, the klystron amplifier and the traveling-wave-tube amplifier. Each of these tubes produces an appreciable amount of power at frequencies which are harmonics of the fundamental frequency. In addition, the magnetron often emits so-called moding frequencies near the carrier frequency as is illustrated in Fig. 15.01-1, which are produced when the magnetron oscillates weakly in modes other than the desired mode. Figure 15.01-1 shows that the spurious harmonic power from the magnetron decreases as the harmonic frequency increases but that the power at even harmonics tends to be lower than that from adjacent odd harmonics. The spurious harmonic power from
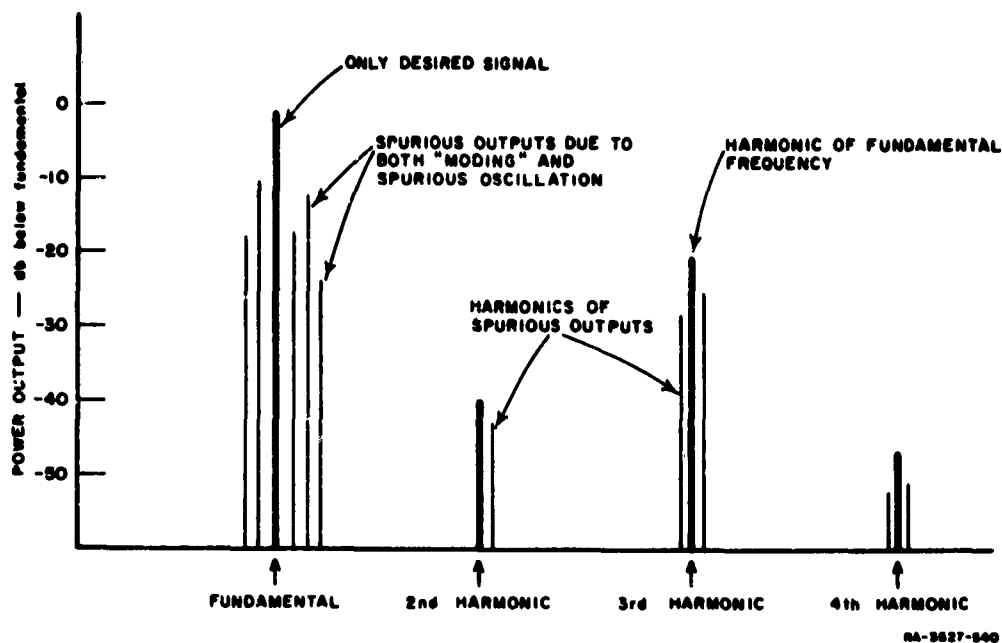
FIG. 15.01-1 TYPICAL FREQUENCY SPECTRUM OF SIGNALS GENERATED
BY A MAGNETRON OSCILLATOR
Note: Fine structure representing the cross modulation product for
each of the above lines is not shown.

klystron and traveling-wave tube amplifiers usually decreases monotonically
as the order of the harmonic increases. The harmonic power output from a
klystron transmitter is shown in Fig. 15.01-2. These particular data[20] were
taken on a CW klystron amplifier, but appear to be representative of pulsed
tubes also. Here the klystron was first set up without regard to harmonic
output (as it would be normally) and the harmonic output was measured
(Lines A, Fig. 15.01-2). Then various electrode voltages were adjusted and
the drive power reduced by 3 db to minimize the second harmonic, without
changing the fundamental power output, and the harmonic output was measured
again (Lines B, Fig. 15.01-2). There is a considerable improvement (at
least 13 db, and up to 24 db), showing that much "filtering" can be per-
formed by appropriate adjustments on the transmitter alone.

The relative harmonic power levels from a high-power traveling-wave
tube may be as much as 20 db greater than those from a klystron. Several
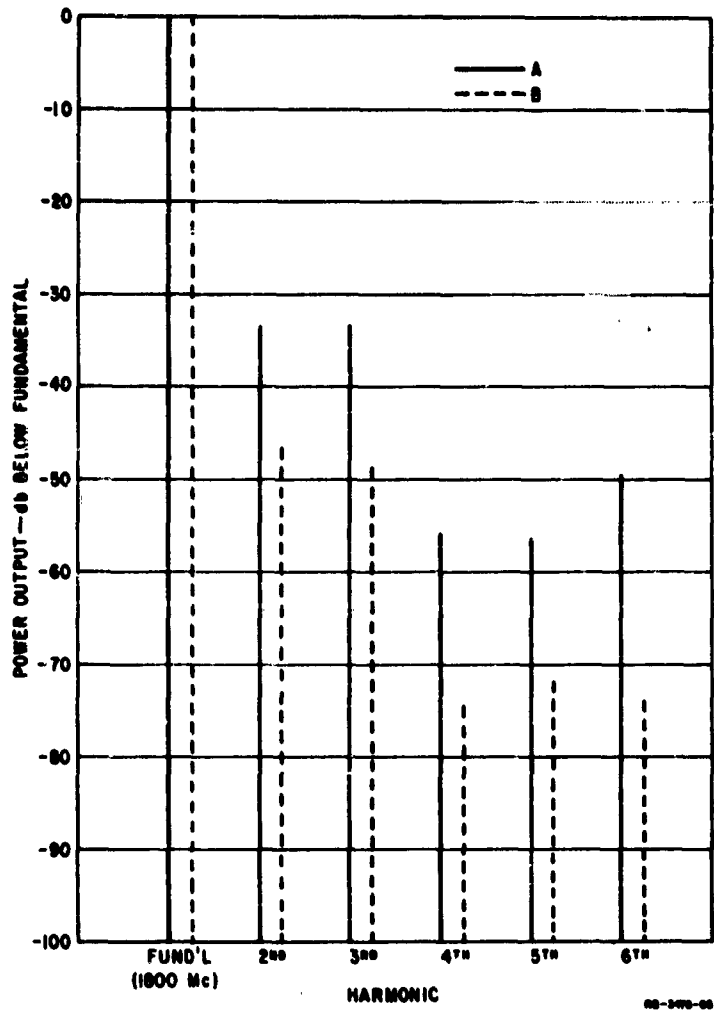
FIG. 15.01-2   FREQUENCY SPECTRUM OF A KLYSTRON AMPLIFIER
OUTPUT; (A) AND (B) BEFORE AND AFTER TUBE
ADJUSTMENT TO MINIMIZE HARMONIC OUTPUT
WITH CONSTANT FUNDAMENTAL OUTPUT

other types of spurious emissions from high-power tubes can occur and they have been summarized by Tomiyasu.[21]

Filters for Suppressing the Spurious Emissions—Filters for this purpose should ideally have a low-attenuation pass band just wide enough to pass the carrier frequency and its modulation components, and they should have a stop band that extends upward over many octaves to suppress the harmonic frequencies. Furthermore, it is always desirable and often mandatory to preclude the possibility of having resonances at the spurious frequencies occur in the transmission line between the high-power source and the filter. The prevention of such resonances is important if breakdown problems are to be minimized and optimum operation of the tube is to be assured. It is usually impossible to obtain all these characteristics simultaneously with a single filter, and therefore various combinations of filters and auxiliary structures of the type described below are required.

Figure 15.01-3 is a schematic diagram of the most common filter combinations for high-power applications. Filter combination (a) utilizes two reflective band-pass filters and two 3-db hybrids. In the pass band, power is transferred unattenuated from input to output. However in the stop band, power is reflected from the filters. Over the operating frequency band of the hybrids, most of this reflected power is dissipated in the load on the left and a good match is presented to the transmitter. (The termination at the upper right would ideally receive no power; it is included to absorb any stray power due to mismatch of the output load, etc.) At frequencies outside the operating band of the hybrids, an appreciable mismatch may exist at the transmitter.

Filter combination (b) uses a reflective low-pass filter, a 3-db hybrid and resistively terminated tapered waveguides which function as high-pass filters.[22] The pass band of this combination occurs when the low-pass filter is operating in its pass band and the high-pass filters are operating in their stop band and reflect all the power incident on them. As frequency is increased, the attenuation of the combination increases because the high-pass filters begin to propagate and most of the power incident on them is dissipated in the matched loads. However, not all of the unwanted power is so absorbed, since some modes which propagate in the regular waveguide will be cutoff in the tapered guides. Any reflected power in the stop band is also attenuated by the low-pass filter. A relatively good match is obtained over the operating band of the 3-db
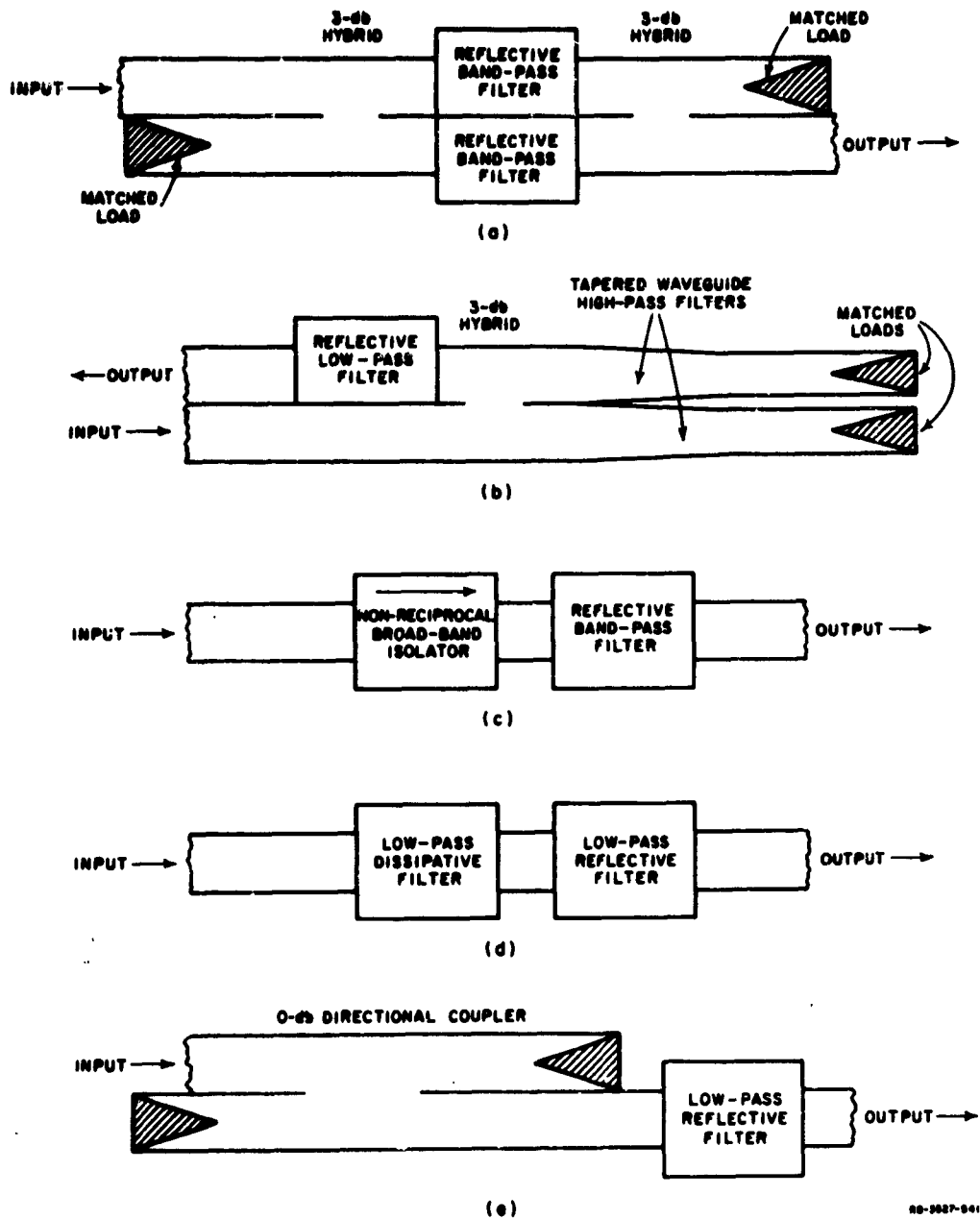
FIG. 15.01-3 COMMON FILTER AND COUPLER COMBINATIONS USEFUL IN SUPPRESSING
SPURIOUS EMISSIONS FROM HIGH-POWER TRANSMITTERS

hybrids, even though outside their operating band an appreciable mismatch may exist. Branch-guide directional couplers of the type described in Chapter 13 are quite suitable for use in the circuits shown in Fig. 15.01.3(a) and 15.01-3(b), as are short-slot hybrids[23] in which the coupling aperture is in the side wall.

The filter combination in Fig. 15.01-3(c) employs a non-reciprocal broadband high-power isolator[24] in conjunction with a reflective band-pass filter. The bandwidth of the isolator would be ideally much greater than the pass-band width of the reflective filter. Thus, a good match would be presented to the transmitter over the operating bandwidth of the isolator. The operating bandwidth of presently available isolators is not great enough for applications where higher harmonics must be absorbed, although isolators can be used to absorb the spurious emissions near the fundamental frequency.

The filter combination in Fig. 15.01-3(d) cascades a low-pass reflective filter and a low-pass dissipative filter (i.e., a filter that attenuates by absorbing power incident upon it and which is typically quite well matched both in its pass band and in its stop band). In the pass band, both of these filters have low attenuation. The dissipative filter will typically have relatively high attenuation at the second and third harmonic frequencies and less attenuation at the lower frequencies. If the reflective filter is of the waffle-iron type described in Sec. 15.05, its high-attenuation stop band may extend from the second harmonic up through the tenth harmonic of the fundamental frequency. In this case, the combination shown would be designed so that the waffle-iron filter provides most of the attenuation and the dissipative filter acts primarily as a pad, thus presenting a good match to the transmitter at the harmonic frequencies. For applications where large attenuation at harmonics above the third is not required, the reflective filter shown in Fig. 15.01-3(d) may be omitted and the length of the dissipative filter may be increased to provide the necessary attenuation at the second and third harmonic frequencies.

The filter combination in Fig. 15.01-3(e) replaces the low-pass dissipative filter in Fig. 15.01-3(d) by a coupler which, in the fundamental band, is directional with 0-db coupling, and whose geometry is such that power at the second harmonic and higher frequencies goes mostly straight through into the dummy load, instead of to the reflective filter at the

output. Transvar couplers, branch-guide couplers[23,25] (Chapter 13), and side-wall and top-wall short-slot hybrids have been tried in the circuit of Fig. 15.01-3(e). Branch-guide couplers have the advantage that filters can be built into the branches to improve the separation between the fundamental and the harmonic frequencies. Experiments indicate that two 3-db side-wall short-slot couplers cascaded to form a 0-db coupler give relatively good performance in the circuit in Fig. 15.01-3(e), be-sides being compact and relatively inexpensive.[23]

A dissipative filter may also be placed between the transmitter and the filter combinations in Figs. 15.01-3(a) and 15.01-3(b) to improve the match presented to the transmitter at frequencies outside the operating band of the hybrids.

Placement of Filter—A filter to suppress harmonic frequencies should be placed near the output of the system past the last nonlinear circuit element. For instance there is some evidence that TR-switches generate substantial amounts of harmonics, so that it is preferable to put the spurious-frequency-suppression filter between the duplexer and the antenna, rather than immediately after the transmitter and before the duplexer.

SEC. 15. 02, POWER-HANDLING CAPACITY OF VARIOUS TRANSMISSION-LINES

The power-handling capacity of transmission lines propagating pulsed signals having short duration (less than about 5 microseconds) and having a low average power level, but a high pulse-power level, is usually limited by breakdown due to ionization of the gas that fills the guide. Under these conditions there is no appreciable heating of the waveguide. The voltage gradient at which such a breakdown occurs in air is approxi-mately 29 kv/cm per atmosphere when the distance between electrodes is much greater than the oscillation distance of free electrons, which in turn is much greater than the mean free path of the electrons. These con-ditions are satisfied for the common air-filled waveguides and coaxial lines operating over the frequency range from 1 to 100 Gc and at pressures from 0.1 to 10 atmospheres. The breakdown which occurs under these cir-cumstances is an electrode-less discharge, since most of the free electrons execute many cycles of oscillation before reaching an electrode. Gould[26] and others[27] have made extensive studies of gaseous breakdown phenomena and

the interested reader should consult their publications for more detailed information. Hart, et al.,[28,29] have also measured the pulse-power capacity of a variety of waveguide components.

The other condition that is necessary for the initiation of discharge is the presence of a free electron. Such an electron will always be supplied eventually by cosmic ray bombardment or natural radioactivity. However, it is usually found expedient when making voltage breakdown measurements to supply electrons from a radioactive source such as cobalt-60. Such a source might typically have a strength of 100 milli-curies (i.e., emit 3.7×10^9 electrons per second).

A minimum value of the breakdown field strength occurs at a pressure where the radio frequency is equal to the gas collision frequency. For air at microwave frequencies, this pressure varies linearly from a pressure of approximately 1 mm of mercury at 1 Gc to approximately 10 mm of mercury at 10 Gc. At lower pressures, the breakdown field strength increases rapidly. At pressures on the order of 10^{-6} mm of mercury, corresponding to a good vacuum, breakdown is no longer due to ionization of the remaining gas molecules, but to other mechanisms. The exact mechanism of breakdown at high vacuum is not completely understood; however, it seems likely that the most important process that occurs is field emission whereby electrons are pulled loose from metal surfaces by electric fields having strengths of megavolts per cm.[30] Such field strengths can arise from minute irregularities on the surface even when the average field strength over the surface is much lower. Thus, it is very important in evacuated[31] high-power filters and transmission lines that the inside surfaces be quite smooth. For smooth surfaces a breakdown dc-field strength of 350 kv/cm is often used as a design value in high-power tubes and it seems that this is a reasonable value to use for microwave breakdown field strengths in a high vacuum until more data on this subject become available.

Another phenomenon, which under ordinary circumstances will not appreciably reduce the power transmitted through an evacuated high-power transmission line or filter, is called *multipactor*. This is a resonant secondary-emission phenomenon which occurs when an electron under the action of an electric field has a transit time between opposite electrodes equal to one-half the period of an RF cycle. It typically occurs at RF voltages of the order of 1000 volts. This phenomenon has recently been utilized to make TR-switches.[32]

Figure 15.02-1 gives the pulse-power capacity[33] of a variety of
standard rectangular waveguides over their normal frequency bands when
filled with air at atmospheric pressure, which can be computed from
Eq. (5.06-14) on the assumption that the peak electric field for break-
down is 29 kv/cm. The various waveguides are given their RETMA or EIA
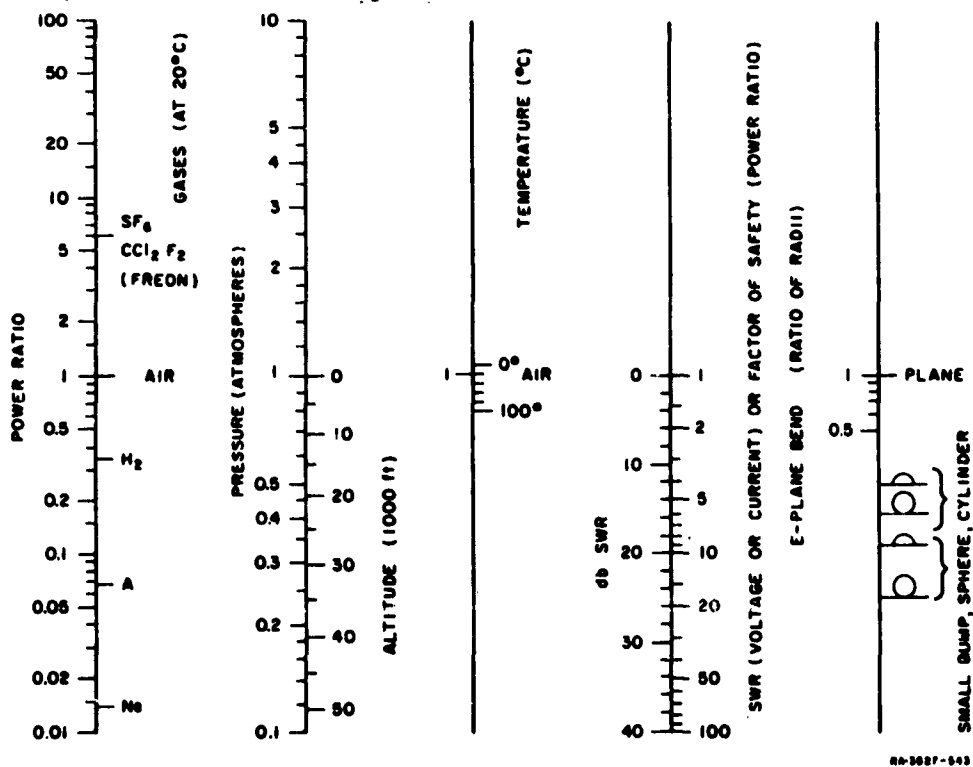designation (which is the width of the waveguide, to three significant
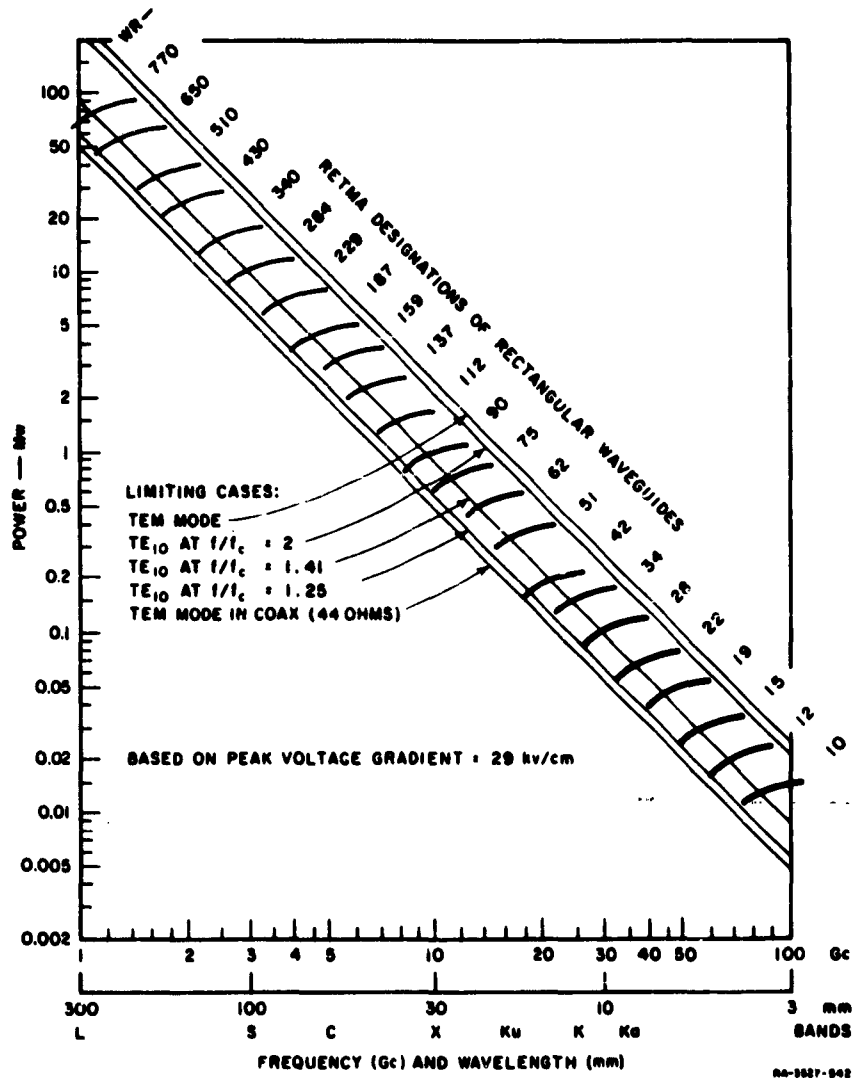
SOURCE: Wheeler Monographs (See Ref. 33 by H. A. Wheeler)

FIG. 15.02-1 CHART OF PULSE-POWER CAPACITY OF WAVEGUIDES

digits, measured in inches and multiplied by 100). Also shown is the
pulse-power capacity of a 44-ohm coaxial line [which can be computed
from Eq. (5.03-7)], for the case of a line having a mean circumference
of one wavelength (outer diameter of 0.430 wavelength and inner diameter
of 0.206 wavelength). This is the coaxial line with maximum pulse-power
capacity[34] when only the dominant TEM mode is to be allowed to propagate.
The highest line on the chart is computed for a hypothetical parallel-
strip waveguide propagating a TEM mode having a width and height equal
to one-half wavelength. This is the largest size guide that will support
the TEM mode to the exclusion of higher modes.

The chart in Fig. 15.02-2 (which looks like a nomogram but is not)
gives a series of power-adjusting factors[35] for waveguides and coaxial

FIG. 15.02-2   CHART OF FACTORS FOR ADJUSTING POWER CAPACITY ESTIMATES
The scale of the ordinates is the same as that in Fig. 15.02-1

lines in the frequency range of 1-100 Gc. These factors are plotted on the same logarithmic scale as that used in Fig. 15.02-1. Therefore, the scale reading on the chart of Fig. 15.02-1 can be adjusted by the distance from the center on one or more of the scales in Fig. 15.02-2, in a manner similar to multiplication on a slide rule. The reference condition for each scale is noted at the-center. The standard conditions are air, 20°C, one atmosphere (zero altitude), pure traveling wave (unity VSWR or 0-db VSWR), straight, smooth waveguide (no bend, no bump).

As an example of the use of these charts, we will determine the amount of power that can be delivered to a load through a WR90 waveguide at 10 Gc for a specified set of conditions. We assume that the waveguide is filled with air at 20°C, and is operating at 5,000 feet altitude. A VSWR of 3 db exists on the line, the factor of safety is two, and all other conditions are normal. From Fig. 15 02-1, we find that the pulse power capacity of the guide is 1 Mw, the power ratio for operation at 5,000 feet is 0.7, the power ratio for the 3 db VSWR is 0.7 and the power ratio for the specified factor of safety is 0.5. Therefore, the pulse-power capacity becomes 1 Mw $\times$ 0.7 $\times$ 0.7 $\times$ 0.5 = 0.25 Mw.

Cohn[35] has computed the static electric field for two-dimensional rounded-corner geometries. These results may be applied to actual filter structures with sufficient accuracy for practical purposes if the following two conditions are satisfied: (1) the rounded-corner geometry of the high-power filter may be considered to be composed of infinite cylindrical surfaces, and (2) the essential portions of the rounded corners are small in terms of wavelength so that the field distributions in these regions approximate the static field distributions.

Cohn's results[35] are presented in terms of E_{max}/E_0, where E_{max} is the maximum electric field at a rounded corner and E_0 is the reference electric field at some position well removed from the rounded corner. Since the pulse-power capacity of the filter is proportional to the square of the electric field, the adjusting factor for filters with rounded corners is $(E_0/E_{max})^2$. Two types of two-dimensional curved boundaries are considered: (1) the optimum boundary shape which yields constant electric field over the curved surface, and (2) an approximately circular cross-section shape which would be used in most practical filter structures. A curve for a three-dimensional spherical-corner geometry will be given in Sec. 15.05.

One type of curved boundary that arises in high-power filters is illustrated in Fig. 15.02-3; it consists of an array of 180-degree corners. The shapes of these corners are adjusted for constant electric field strength along their curved portions. Curves giving the shapes of these corners in more detail are presented in Fig. 15.02-4. The constant electric-field strength E_{max} along the curved boundaries turns out to be very simply related to the uniform field E_0 well below the array as follows:

$$\frac{E_{max}}{E_0} = \sqrt{\frac{l}{t}} \quad . \tag{15.02-1}$$

On the straight vertical boundaries the electric field drops off very rapidly.

Another type of rounded corner configuration often encountered is the rounded corner near an electric wall. The ratio E_{max}/E_0 for this type of corner is shown in Fig. 15.02-5 both for the optimum- or uniform-field-strength corner and the approximately circular corner. Also shown is the defining radius for the uniform-field-strength corner. It is seen that the E_{max}/E_0 for the approximately circular boundary is not very much greater than for the uniform-field-strength boundary. Since the uniform-field-strength boundary is much harder to machine, the circular boundary would probably be used in most applications.

An abrupt change in height of a waveguide (case of radius $r = 0$), or in diameter of a coaxial line (cases of $r = 0$), has an equivalent circuit consisting simply of a shunt capacitive susceptance $B|_{r=0}$ at reference planes corresponding with the step itself. Graphical data for such a waveguide discontinuity are given in Fig. 5.07-11, while the equivalent discontinuity capacitance in a coaxial line is given in Fig. 5.07-2. A rounded corner of the type shown in Fig. 15.02-5 will have the shunt susceptance of a sharp corner reduced by the amount ΔB. The value of ΔB for a rounded corner in waveguide is plotted in Fig. 15.02-6. Thus, the total susceptance B of the rounded corner is
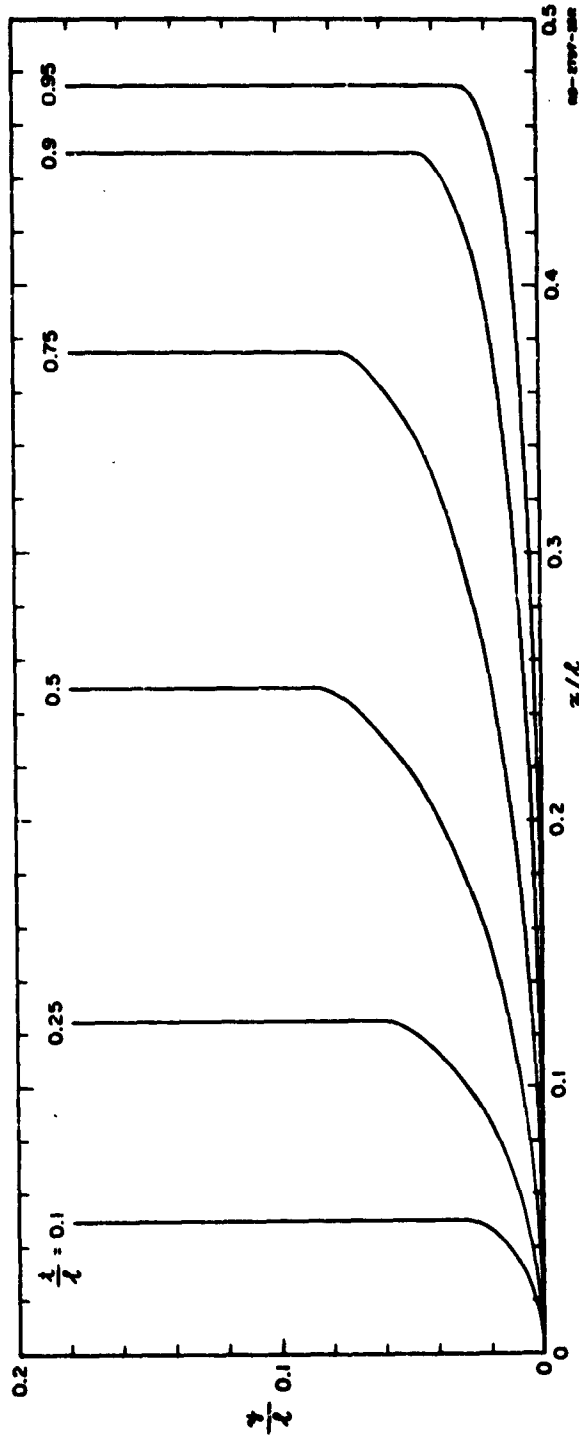
$$B = B|_{r=0} + \Delta B \quad . \tag{15.02-2}$$

Note that ΔB is a negative number. Rounding the corner also results in an increase in stored magnetic energy. This may be taken into account by

$\frac{t}{\ell} \cdot 0.25$

$\frac{t}{\ell} \cdot 0.5$

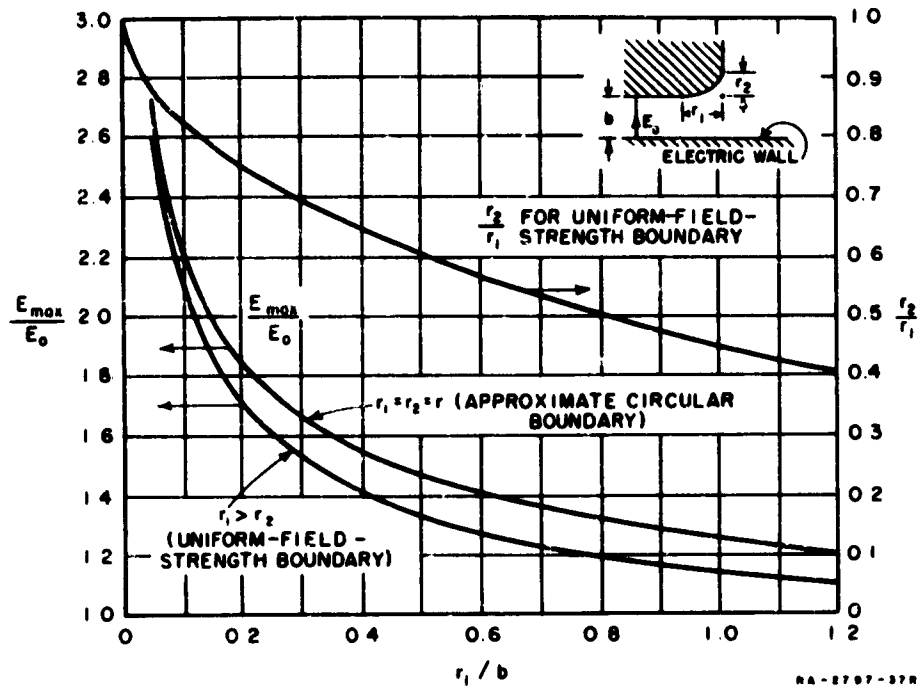$\frac{t}{\ell} \cdot 0.9$

RC-2797-24R
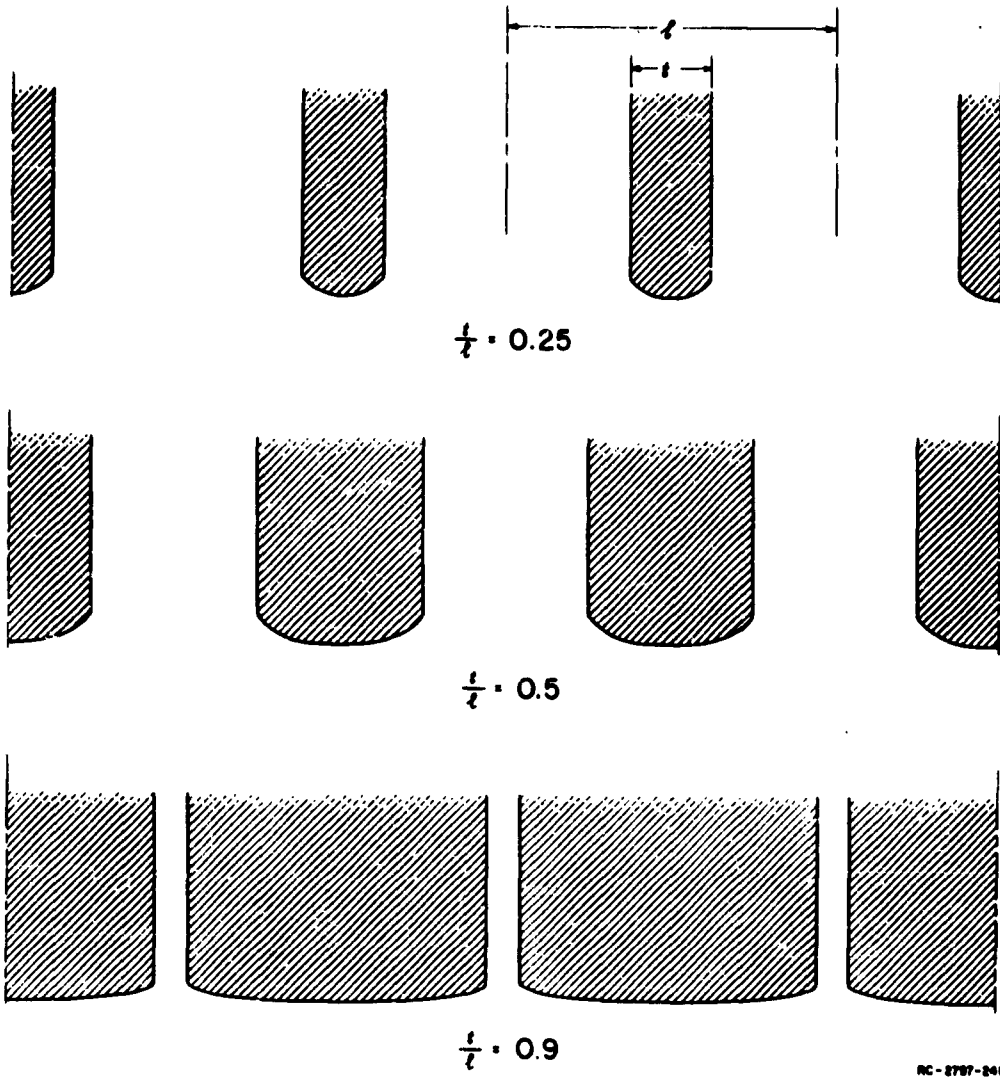
SOURCE: *IRE Trans. PGMTT* (See Ref. 35 by S. B. Cohn)

FIG. 15.02-3   ARRAYS OF ROUNDED 180-DEGREE CORNERS SHAPED FOR CONSTANT
ELECTRIC FIELD
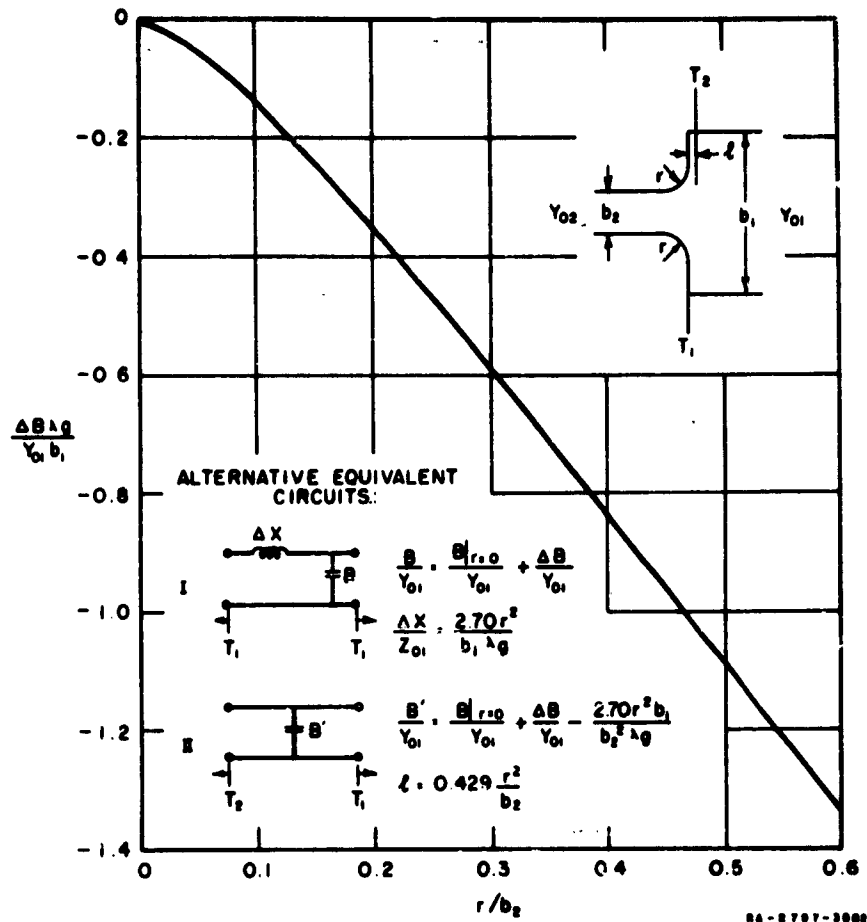The shapes of the curved surfaces are given in Fig. 15.02-4

893

SOURCE: *IRE Trans. PGMTT* (See Ref. 35 by S. B. Cohn)

FIG. 15.02-4   SHAPES OF ROUNDED 180-DEGREE CORNERS FOR VARIOUS VALUES OF t/l

FIG. 15.02-5   PLOT OF E_{max}/E_0 FOR ROUNDED 90-DEGREE CORNER NEAR AN
ELECTRIC WALL; ALSO, r_2/r_1 FOR A UNIFORM-FIELD-STRENGTH
BOUNDARY

FIG. 15.02-6   CAPACITIVE SUSCEPTANCE CORRECTION AND EQUIVALENT
CIRCUITS FOR ROUNDED STEP IN WAVEGUIDE

adding a series-inductive element in the equivalent circuit at the
reference plane of the step, or by a shift of one of the reference
planes and modification of B.   These alternative equivalent circuits
are shown in Fig. 15.02-6.   Values of ΔB shown are accurate for
$r \leq (b_1 - b_2)/4$, and for $X/Z_{02} < 0.3$, where $Z_{02} = 1/Y_{02}$.   The final type
of rounded-corner geometry considered is the rounded corner near a
magnetic wall.   A graph giving the field strengths and defining radii
for the uniform field strength boundary is given in Fig. 15.02-7.   Com-
paring this figure with Fig. 15.02-5, it is seen that the field

strengths near the magnetic wall are slightly higher than those near
the electric wall.

The average power rating of transmission lines is determined by
the permissible temperature rise in their walls.[36,37] Curves giving the
average power rating for copper waveguide for various conductor temper-
ature rises are given in Fig. 15.02-8. In deriving these curves, it was
assumed that the heat is transferred from the waveguide only by thermal
convection and thermal radiation, and that the emissivity of the wave-
guide walls is 0.3. An additional assumption is that the dissipation of
power per unit area in the walls is uniform for all walls. When the
ambient temperature is different from the assumed reference of 40°C the
curves of Fig. 15.02-9 can be used to determine the correction factor F
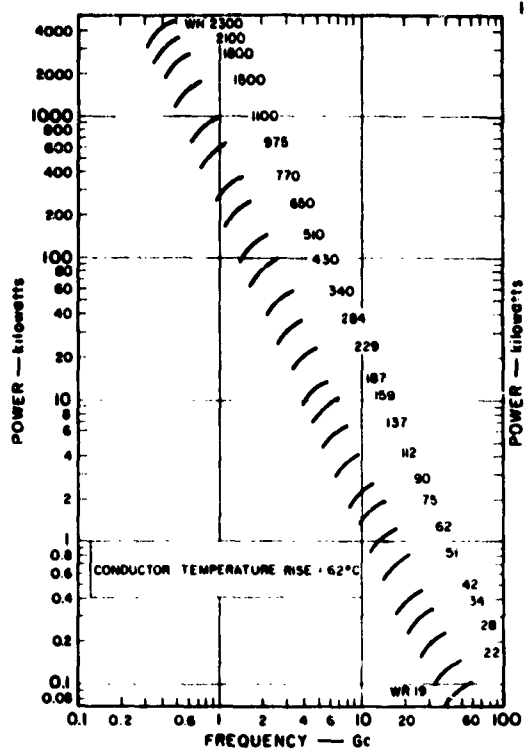for the average power rating.
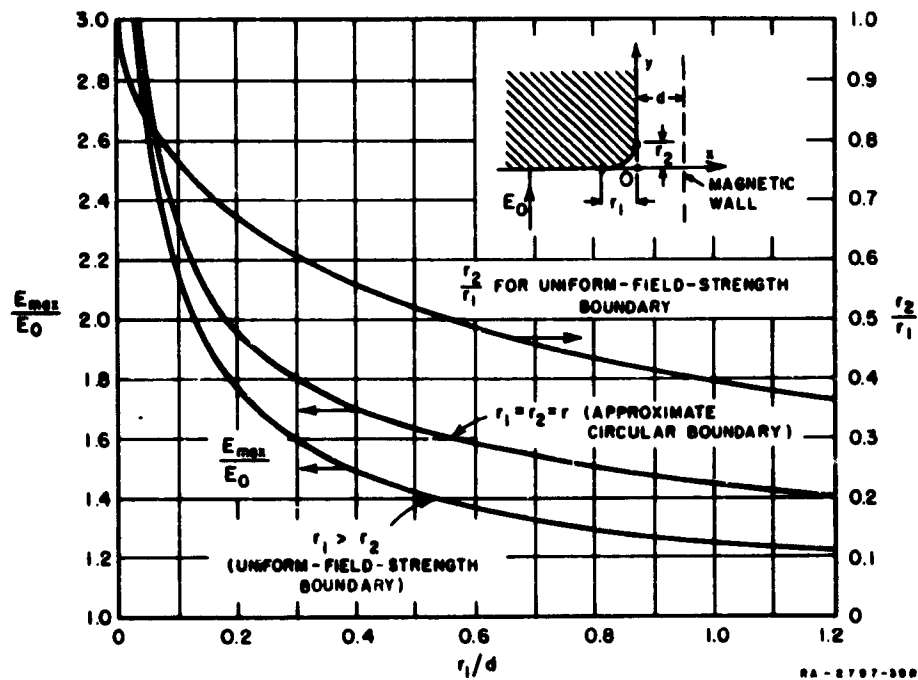
FIG. 15.02-7   PLOT OF E_{max}/E_0 FOR ROUNDED 90-DEGREE CORNER NEAR
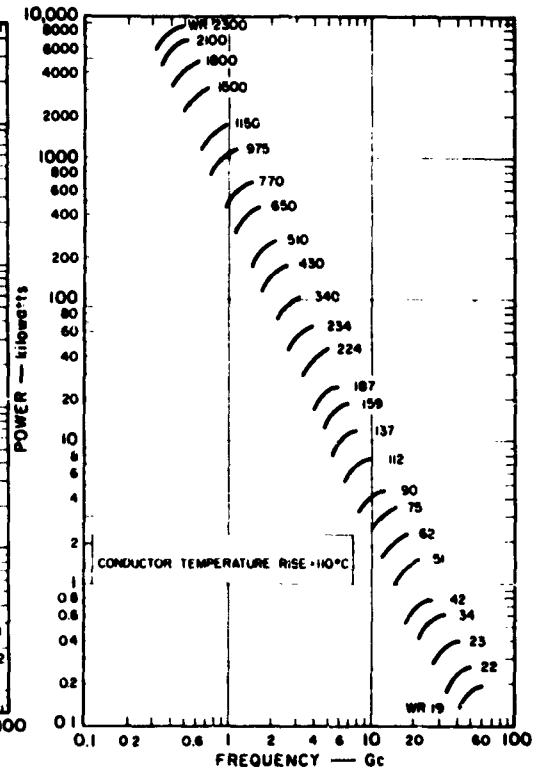A MAGNETIC WALL; ALSO, r_2/r_1 FOR A UNIFORM-FIELD-
STRENGTH BOUNDARY
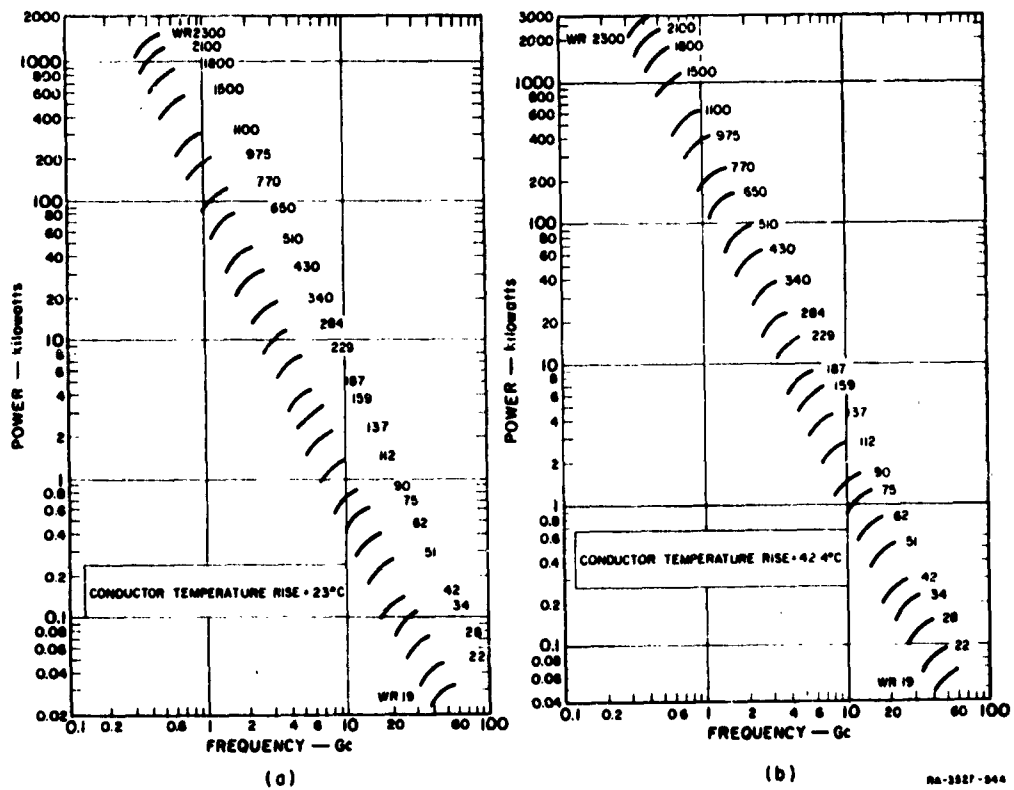
FIG. 15.02-8   THEORETICAL CURVES OF THE AVERAGE POWER RATING FOR COPPER
RECTANGULAR WAVEGUIDE OPERATING IN THE TE_{10} MODE WITH UNITY
VSWR AT AN AMBIENT TEMPERATURE OF 40°C, FOR VARIOUS TEMPERATURE
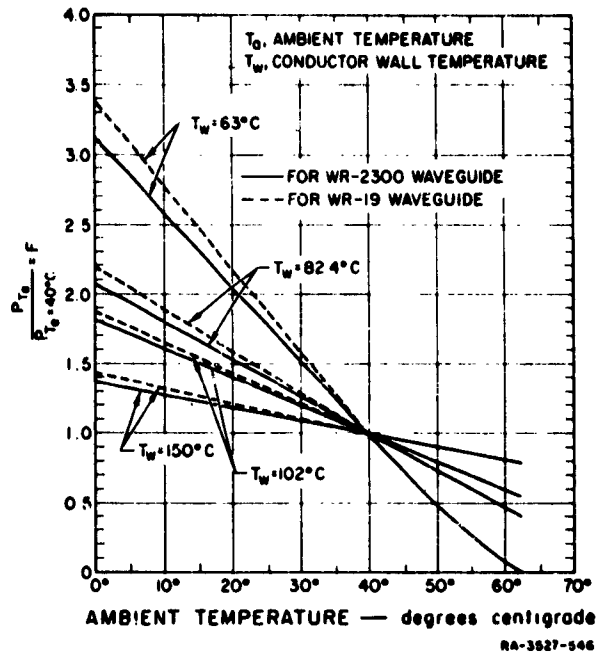RISES (THE WAVEGUIDES ARE LISTED BY THEIR RETMA DESIGNATION)

FIG. 15.02-8   Concluded

FIG. 15.02-9 CORRECTION FACTOR CURVE FOR
AVERAGE POWER RATING OF
RECTANGULAR WAVEGUIDE FOR
VARIOUS AMBIENT TEMPERATURES
AND CONDUCTOR WALL TEMPERATURES

Standing waves in the waveguide reduce the average power rating of waveguides for a given permissible temperature rise because they produce local hot spots along the wall.

The heat conductivity of the copper waveguides is sufficiently great that an appreciable amount of heat flows axially from these hot spots, thus reducing their temperature. The derating factor that must be applied to waveguide for various values of VSWR is shown in Fig. 15.02-10 and Fig. 15.02-11 for both a copper waveguide and a hypothetical waveguide in which there is no axial heat transfer. The curves in Fig. 15.02-10 apply to the case where the amount of power delivered to the load is a constant while those in Fig. 15.02-11 apply when the amount of power incident on the waveguide is constant.
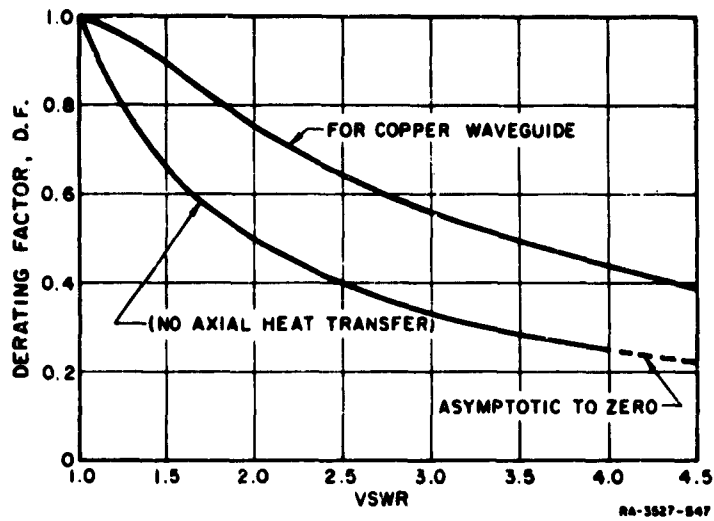
FIG. 15.02-10 POWER DERATING FACTOR DUE TO VSWR FOR THE
CONDITION THAT A CONSTANT POWER IS TO BE
DELIVERED TO THE LOAD
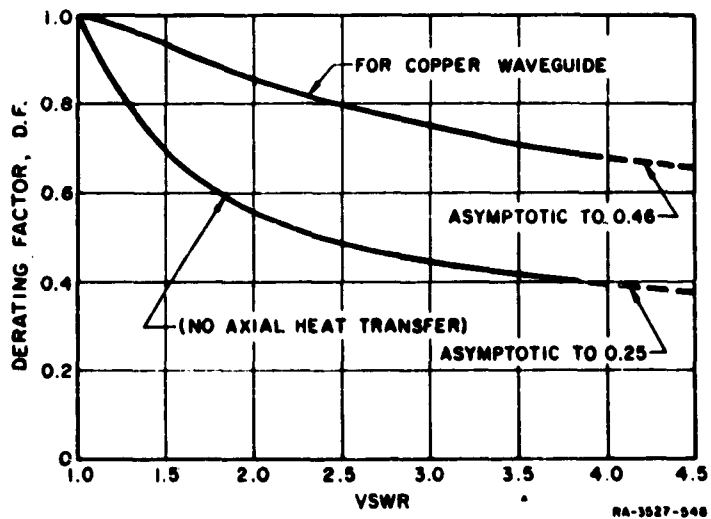
FIG. 15.02-11 POWER DERATING FACTOR DUE TO VSWR FOR THE
CONDITION THAT A CONSTANT POWER IS INCIDENT
ON THE WAVEGUIDE

901

Directional Couplers—Directional couplers are shown in several of the circuits in Fig. 15.01-3. Not much is known about the power-handling capacity of short-slot couplers. Estimates* for the 3-db side-wall coupler range from full line power down to one-third line power. The 3-db top-wall coupler is less well-suited for handling high power and will break down at about one-quarter full line power.

The power-handling capacity of branch-line couplers is approximately independent of the coupling ratio and the branch-to-through-guide impedance ratios. In waveguide it is determined largely by the radii of the corners at the T-junctions, and can be estimated from Fig. 15.02-5. The power-handling capacity can readily be made equal to 40 percent of line power as in the example in Sec. 13.14, and could probably be increased to 60 or 70 percent by doubling the corner radius used in that example.

SEC. 15.03, THEORETICAL PULSE-POWER CAPACITY OF DIRECT-COUPLED-RESONATOR FILTERS

This section will discuss the pulse-power capacity of band-pass filters of the type shown in Fig. 15.03-1(a) having a frequency response such as the band-pass response in Fig. 15.03-1(b). The design information will be presented primarily for narrow-band filters in terms of the element values g_k of the low-pass prototype filter shown in Fig. 15.03-1(c). The cavities constituting the filter can be fabricated from transmission lines having any cross-sectional shape, and the terminating transmission lines can have the same, or a different cross section.

The pulse-power capacity is limited by voltage breakdown at the positions of high electric field within the filter. When the usual inductive coupling apertures are used between the cavities, the peak electric fields do not occur in the apertures but rather within the cavities themselves as indicated schematically in Fig. 15.03-1(a).

Pulse-Power Capacity at Midband of Narrow-Band Filters—Power handling may become a severe problem in narrow-band filters. Most narrow-band filter designs are based on a low-pass prototype circuit (Chapter 4), and they are usually well-matched at midband. We shall therefore first restrict ourselves to narrow-band filters which are reflectionless at midband. An exact general formula will be given later [Eq. (15.03-4)].

---

*
Private communication from H. J. Riblet to L. Young (July 9, 1962). (Note added in proof: A recent measurement by SRI, in a direct comparison with uniform waveguide, gives about 70-percent of line power for the side-wall coupler, and about 40-percent for the top-wall coupler.)
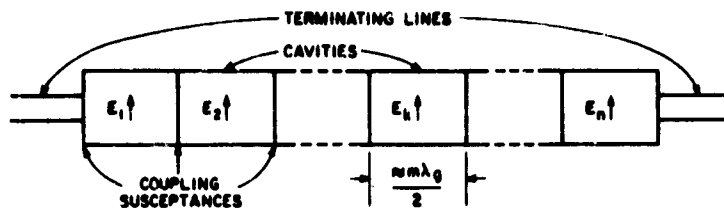
(a) WAVEGUIDE BAND-PASS FILTER
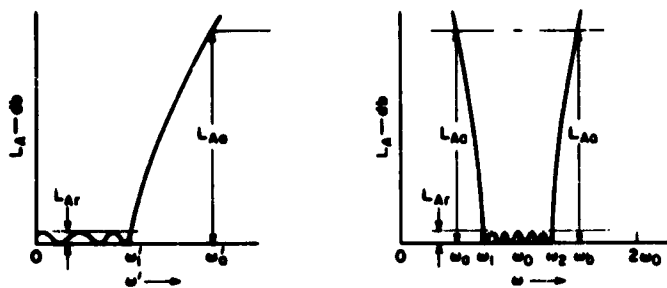
(b) LOW-PASS PROTOTYPE RESPONSE AND CORRESPONDING
BAND-PASS FILTER RESPONSE

(c) LOW-PASS PROTOTYPE FILTER

FIG. 15.03-1 WAVEGUIDE BAND-PASS FILTER AND EQUIVALENT LOW-PASS PROTOTYPE

We will define P_{qk} as the pulse power (*i.e.*, the power level during a short pulse) that could be transmitted through an n-cavity filter at the onset of voltage breakdown in Cavity k. Then it will be shown at the end of this section (an independent proof is also given in Ref. 38) that at the midband frequency f_0,

$$(P_{qk})_0 \quad = \quad \frac{P'_{qk} \pi m w}{2 g_k \omega'_1} \left(\frac{\lambda_{g0}}{\lambda_0}\right)^2 \qquad (15.03\text{-}1)$$

where P'_{qk} is the pulse-power capacity of a matched waveguide having the same cross section as the cavity, $(P_{qk})_0$ is P_{qk} for $f = f_0$, λ_{g0} is the guide wavelength in the cavity at f_0, λ_0 is the free-space wavelength at f_0, m is the length of the cavity measured in half guide wavelengths, the fractional bandwidth is $w = (\omega_2 - \omega_1)/\omega_0$, and g_k is the corresponding element in the equivalent low-pass prototype circuit, *having element values normalized so that* $g_0 = 1$. Because the values of g_k are not necessarily the same for each element in the low-pass prototype, the pulse-power capacity of the over-all filter is limited by voltage break-down in the cavity associated with the largest value of g_k. When all the elements in the low-pass prototype are equal, the midband pulse-power capacity of the filter is maximized for a given off-channel selectivity. Use of the equal-element low-pass prototype also results in approximately the minimum midband dissipation loss $(\Delta L_A)_0$, for given resonator Q's and off-channel rejection, as discussed in Sec. 11.07 and Sec. 6.14.
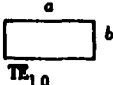
Table 15.03-1 gives formulas for the pulse-power ratings P'_q of some common transmission lines. The midband pulse-power ratings $(P_{qk})_0$ of the cavity resonators constructed from them as computed from Eq. (15.03-1) are also presented. As is pointed out later in this section, the power capacity near band edge is less than that at midband. Table 15.03-1 gives all dimensions in centimeters, frequencies in gigacycles and powers in megawatts. The components are assumed to be filled with air at atmospheric pressure so that the peak voltage gradient is taken as 29 kv/cm. The factor $\lambda_g/\{\lambda[1 - (\lambda/\lambda_g)^2]\}$ which occurs in the right-hand column of Table 15.03-1 is a dimensionless function of the wavelength-to-cutoff wavelength ratio, and will generally lie between 3 and 4.

The midband pulse-power capacity $(P_{qk})_0$ of the air-filled cavities operating at atmospheric pressure is also plotted for convenience in

Table 15.03-1

PULSE-POWER RATING OF SOME COMMON TRANSMISSION LINES AND CAVITY RESONATORS CONSTRUCTED FROM THEM

(Based on a Peak Voltage Gradient of 29 kv/cm)

Note: Dimensions and wavelengths are in cm. w = fractional bandwidth = $(\omega_2 - \omega_1)/\omega_0$
Frequencies f, and f_c are in gigacycles. $= (f_2 - f_1)/f_0$.
P'_q and $(P_{qk})_0$ are in megawatts. n = number of half-wavelengths in resonators.
f_c = cutoff frequency of guide. g_k, and ω'_1 are defined in Fig. 15.03-1,
where the g_k are assumed to be normalized
so that $g_0 = 1$.

	P'_q, PULSE-POWER CAPACITY OF A MATCHED LINE	λ_c, CUTOFF WAVELENGTH	$(P_{qk})_0$, MIDBAND PULSE-POWER CAPACITY OF AN n-SECTION FILTER AT THE ONSET OF BREAKDOWN IN CAVITY k
TE_{10}	$0.14 \times \dfrac{\lambda}{\lambda_g} \lambda_c^2 \dfrac{b}{a}$ TE_{10} mode	$2a$	$198 \dfrac{nbw}{a g_k \omega'_1 f^2} \cdot \dfrac{\lambda_g}{\lambda\left[1 - \left(\frac{\lambda}{\lambda_g}\right)^2\right]}$
TE_{11}	$0.144 \times \dfrac{\lambda}{\lambda_g} \lambda_c^2$ TE_{11} mode	$3.415a$	$204 \dfrac{nw}{g_k \omega'_1 f^2} \cdot \dfrac{\lambda_g}{\lambda\left[1 - \left(\frac{\lambda}{\lambda_g}\right)^2\right]}$
TE_{01}	$0.625 \times \dfrac{\lambda}{\lambda_g} \lambda_c^2$ TE_{01} mode	$1.64a$	$886 \dfrac{nw}{g_k \omega'_1 f^2} \cdot \dfrac{\lambda_g}{\lambda\left[1 - \left(\frac{\lambda}{\lambda_g}\right)^2\right]}$
TEM $Z_0 = 30$ ohms	$1.29\, b^2$ TEM mode	None	$2.03 \dfrac{nwb^2}{g_k \omega'_1}$
TEM $Z_0 = 50$ ohms	$1.105\, b^2$ TEM mode	None	$1.74 \dfrac{nwb^2}{g_k \omega'_1}$
TEM $Z_0 = 44.4$ ohms	$0.055\, \lambda_c^2$ Maximum pulse-power rating when operating at cutoff wavelength λ_c of first higher order TE mode	$\lambda_c = \dfrac{30}{f_c} \approx \pi(a + b)$ (Cutoff wavelength of first higher order TE mode)	$77.8 \dfrac{nw}{g_k \omega'_1 f_c^2} = 1.87 \dfrac{nwb^2}{g_k \omega'_1}$

905

Fig. 15.03-2. In this figure frequencies are in gigacycles and powers in megawatts. If the cavities are filled with some other gas, or are operated at a different pressure the power adjusting factors in Fig. 15.02-2 may be employed in conjunction with Fig. 15.03-2 to determine the midband power capacity of the filter.

Pulse-Power Capacity of Narrow-Band Filters as a Function of Frequency—The peak electric fields in the various cavities of a band-pass filter vary with frequency. A particularly simple way to calculate this variation in narrow-band filters is to make use of the fact that the peak electric fields in the cavities are proportional to the voltages across the capacitances and the currents through the inductances in the low-pass prototype.[39]

Figure 15.03-3 is a plot of the square of the normalized peak electric fields in the cavities of a three-cavity filter, whose low-pass prototype has element values g_0, g_1, g_2, g_3, and g_4 all equal to unity. The curves are plotted against the angular frequency variable ω' of the low-pass prototype. Also included for reference is the insertion-loss characteristic of the low-pass prototype. The analytic expressions for the square of the normalized peak electric fields in the three cavities are

$$\left. \begin{aligned} E_1^2 &= \frac{1 - \omega'^2 + \omega'^4}{P_{avail}/P_{out}} \\[2mm] E_2^2 &= \frac{1 + \omega'^2}{P_{avail}/P_{out}} \\[2mm] E_3^2 &= \frac{1}{P_{avail}/P_{out}} \end{aligned} \right\} \tag{15.03-2}$$

The transducer loss ratio P_{avail}/P_{out} is given by

$$\frac{P_{avail}}{P_{out}} = 1 + \frac{\omega'^2(1 - \omega'^2)^2}{4} \tag{15.03-3}$$

Reference to Fig. 15.03-3 shows that the square of the normalized peak electric field in Cavity 2 for $\omega' = 1.24$ rises to 2.25 times the midband value. Therefore, the pulse-power capacity of this filter is only 0.445 times the midband value of P_{q2} determined from Fig. 15.03-2.
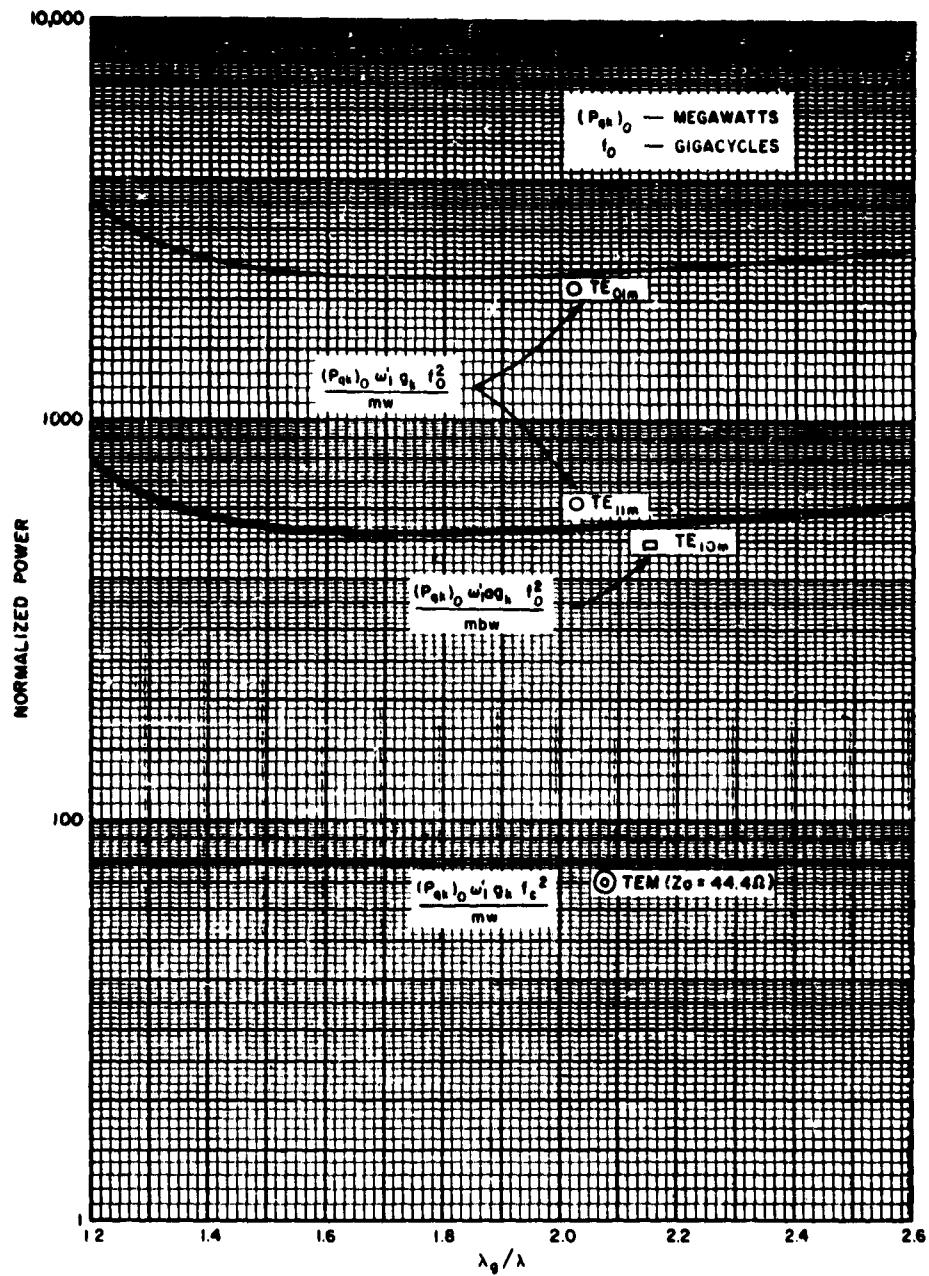
FIG. 15.03-2 MIDBAND PULSE-POWER CAPACITY $(P_{qk})_0$ OF AN n-CAVITY FILTER
AT THE ONSET OF BREAKDOWN IN CAVITY k (BASED ON PEAK
VOLTAGE GRADIENT OF 29 kv/cm)
See Table 15.03-1 for definitions of parameters
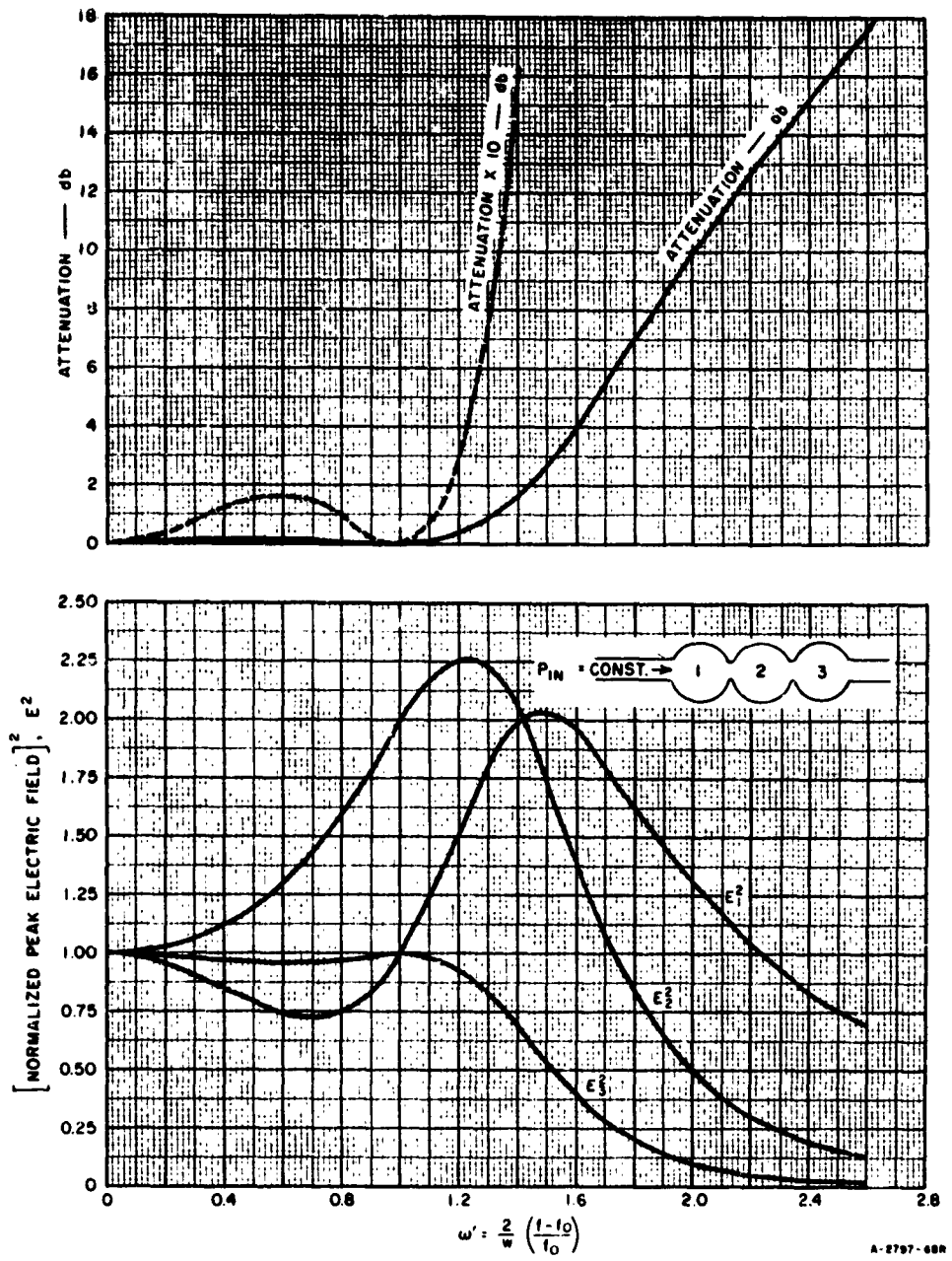
SOURCE: Technical Note 2, Contract AF 30(602)-1998 SRI
(See Ref. 38 by E. M. T. Jones)

FIG. 15.03-3   THE SQUARE OF THE PEAK ELECTRIC FIELD AS A FUNCTION OF
FREQUENCY IN A THREE-CAVITY FILTER HAVING AN EQUAL-
ELEMENT LOW-PASS PROTOTYPE

908

Filters of Arbitrary Bandwidth—It is possible to determine exactly the peak electric fields in transmission-line resonators of band-pass filters having arbitrary bandwidth, both at midband and at any other frequency.[40] One computes the internal voltage standing-wave ratios S_k (Sec. 6.14) seen looking toward the load in each cavity. Then one computes the ratio P'_{qk}/P_{qk} in each cavity from the relation

$$\frac{P'_{qk}}{P_{qk}} = S_k \qquad (15.03\text{-}4)$$

where P'_{qk} is again the power rating of a matched waveguide with the same cross section as cavity resonator k. The equivalent power ratio (E.P.R.) is defined as the ratio of P'_{qk} to the maximum incident (or available) power which can be handled without breakdown,

$$\text{E.P.R.} = \frac{P'_{qk}}{P_{qk}} (1 - |\rho_0|^2) = S_k(1 - |\rho_0|^2) \qquad (15.03\text{-}5)$$

since the power, P_{qk}, transmitted to the load, is the incident power times $(1 - |\rho_0|^2)$, ρ_0 being the input reflection coefficient.

The midband values of the internal VSWR's S_k are easily determined for synchronous filters as in Sec. 6.14, and the same S_k then give the pulse-power handling capacity directly from Eq. (15.03-4) or (15.03-5).

Figure 15.03-4 shows the equivalent power ratio (E.P.R.) calculated from Eq. (15.03-5) for a six-cavity shunt-inductively-coupled (or series-capacitively-coupled) filter (such as that in Fig. 8.06-1) in which the transmission lines terminating the filter have the same cross section as the cavities. This filter was designed in Sec. 9.04 to have a 10-percent fractional bandwidth, measured on a reciprocal guide wavelength basis, with a 0.01-db attenuation ripple in the pass band. In this filter, Cavity 1 is nearest the generator while Cavity 6 is nearest the load.

Connection with Group Delay and Dissipation Loss—The universal delay curves, Figs. 6.15-1 through 6.15-10 may be used to obtain an estimate of the frequency variation of the power-handling capacity of filters satisfying Eq. (6.09-1), which includes most filters up to about 20-percent bandwidth. It is supposed that the midband power-handling capacity has
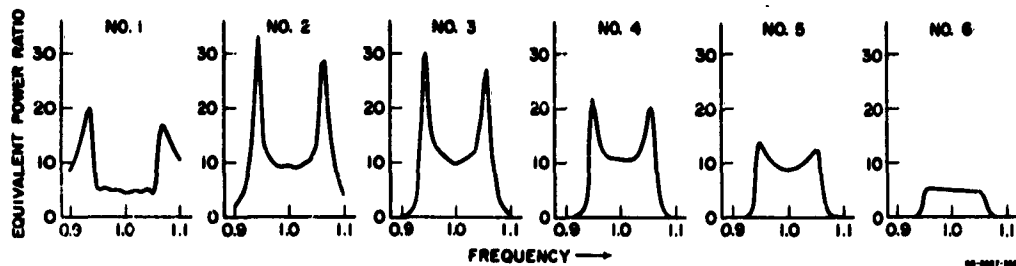
FIG. 15.03-4 EQUIVALENT POWER RATIO IN THE SIX CAVITIES OF THE FILTER
DESIGNED IN SECTION 9.04 TO HAVE A 10 PERCENT BANDWIDTH
WITH 0.01-db PASS-BAND RIPPLE
The cavities and terminating waveguides all have the same cross section
and Cavity 1 is nearest the generator

first been calculated, as from Eq. (15.03-1) or (15.03-4). The equivalent
power ratio is proportional to the stored energy, and so is proportional
to the group delay, over the pass-band region (Sec. 6.15).

The dissipation loss and the group delay both increase with the
average increase in stored energy, so that they are closely proportional
throughout the pass band. Thus, only the *average* increase in stored
energy over the pass-band region may be deduced from the universal curves,
Figs. 6.15-1 through 6.15-10. On the other hand, the power-handling
capacity is linked with the *greatest* increase in stored energy in any
section or resonator. The universal curves indicate in a general way how
the equivalent power rises toward the band edges, and the frequency at
which the maximum occurs (which is almost the same frequency for each
cavity). The cavity nearest the load does not have a maximum near the
band edge (Figs. 15.03-3 and 15.03-4), while the greatest increase in
equivalent power relative to midband occurs generally in the cavity
nearest the generator. It is probably safe to assume that the ratio of
the maximum-to-the-midband-equivalent-power-ratio is never more than twice
the ratio of the maximum-to-the-midband-group-delay. For example in
Fig. 15.03-3 the equivalent power peaks at 2.25 times its value at midband
in the second cavity, whereas the group delay rises by a factor of
0.6/0.38 = 1.6 (Fig. 6.15-2) from its midband value to its maximum value.
A similar comparison for the filter in Fig. 15.03-4 with the corresponding
group delay curves (Fig. III-19, Ref. 43) gives factors of 4.1 and 2.25.

It seems reasonable to assume then that the group delay curves Figs. 6.15-1 to 6.15-10 can be used to predict the equivalent power rise toward the band-edges, provided that a safety factor is used to allow for the greater rise in the cavities nearer the generator; this safety factor is probably always less than 2. (Compare 2.25/1.6 = 1.4 and 4.1/2.25 = 1.8 in the above two examples.)

Connection with External Q *of a Single Cavity,* Q_e—A symmetrical single-cavity resonator is shown in Fig. 15.03-5. The quantity c^2 is the power coupling coefficient defined by

$$c^2 = \frac{P}{P'} \qquad (15.03-6)$$

$$= \frac{4S}{(S + 1)^2} \qquad (15.03-7)$$
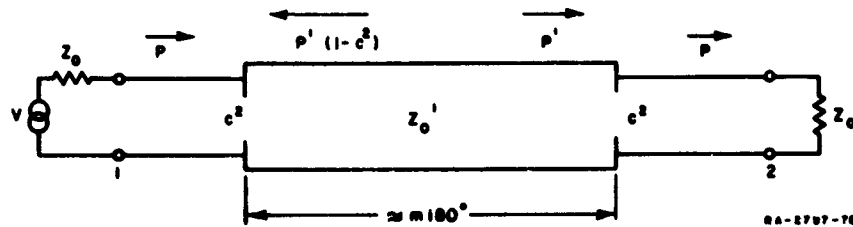
FIG. 15.03-5 SINGLE-CAVITY FILTER

where S is the internal VSWR, equal to the discontinuity-VSWR $V_1 = V_2$ in this case (Chapter 6). Defining Q as the ratio of 2π-times-the-energy-stored to the energy-dissipated-per-cycle,[41, 42] the external Q due to loading by only *one* coupling aperture can be shown to be

$$Q_e = \pi m \frac{(S + 1)^2}{2S} \left(\frac{\lambda_{g0}}{\lambda_0}\right)^2 = \frac{2\pi m}{c^2} \left(\frac{\lambda_{g0}}{\lambda_0}\right)^2 \qquad (15.03-8)$$

911

where λ_{g0} is the midband guide wavelength of the cavity mode and λ_0 is the free-space wavelength. The number m is again the length of the cavity measured in half guide wavelengths; m is an integer for stepped-impedance filters (Chapter 6), and Eq. (15.03-8) is then exact; m is close to an integer for narrow-band, reactance-coupled filters, and Eq. (15.03-8) is then a close approximation.

Note that Q_e is *defined* for a singly loaded cavity. The doubly loaded external Q, Q'_e, of the cavity shown in Fig. 15.03-5 is just half as much:

$$Q'_e = \frac{Q_e}{2} \quad . \tag{15.03-9}$$

Equation (15.03-8) can be solved for S in terms of Q_e, and the resulting expression substituted into Eq. (15.03-4) then yields P'_e/P_e. A particularly simple formula results for narrow-band filters ($S \gg 1$, $c \ll 1$), and then

$$\frac{P'_e}{P_e} = \frac{2Q_e}{\pi m} \left(\frac{\lambda_0}{\lambda_{g0}}\right)^2 \quad . \tag{15.03-10}$$

Proof of Eq. (15.03-1)—It can be seen from Eqs. (6.09-2) and (6.14-10), which hold for narrow-band filters that when $g_0 = 1$

$$S_k = \frac{4}{\pi} \frac{\omega'_1}{w_e} g_k \quad . \tag{15.03-11}$$

For narrow-band filters of fractional bandwidth w, whose line-resonators are m half-wavelengths long,

$$w = \frac{w_e}{2m} \left(\frac{\lambda_0}{\lambda_{g0}}\right)^2 \quad . \tag{15.03-12}$$

Substituting Eqs. (15.03-11) and (15.03-12) into Eq. (15.03-4) yields Eq. (15.03-1).

SEC. 15.04, A HIGH-POWER TUNABLE NARROW-BAND TE_{011}-MODE FILTER

This section discusses the design and performance of a narrow-band, high-power filter that uses cylindrical TE_{011} mode resonators.[*] This type of filter can be designed to have a narrow pass band together with a very low midband insertion loss. Furthermore, as can be seen by reference to Fig. 15.03-2, it has a considerably higher midband pulse-power capacity than filters constructed from other types of resonators. Hence, it is ideal for use with high-power transmitters in suppressing spurious emissions that have frequencies close to the center frequency. Its main disadvantage is that it has spurious pass bands at frequencies relatively close to the main pass band; these spurious pass bands occur when the cavities resonate in other modes. However, by using the techniques described below, the insertion loss of these spurious pass bands can be kept quite high over an appreciable frequency band.

Figure 15.04-1 shows the measured insertion loss of the experimental three-cavity TE_{011} mode filter which was constructed from aluminum and is tunable from 1250 to 1350 Mc. The coupling apertures in the filter were adjusted so that the product of the external Q of the end cavities and the coupling coefficient between cavities was approximately equal to unity. Thus the frequency response of the filter is approximately equal to that of a filter designed from an equal-element low-pass prototype. In air at atmospheric pressure, the theoretical midband pulse-power capacity of the filter is limited by voltage breakdown within the cavities and can be determined from Fig. 15.03-2 to be about 2.25 Mw. The pulse-power capacity at the edges of the pass band is reduced to about 1 Mw for the reasons discussed in Sec. 15.03. A dimensioned drawing of the filter is shown in Fig. 15.04-2.

The measured midband attenuation of the filter as a function of tuning frequency is shown in Fig. 15.04-3. These values of attenuation were measured by the substitution method with the filter terminated at either end with pads whose VSWR was about 1.10. Hence it is believed that the mismatch loss would introduce a maximum error of 0.04 db in the measurements. The theoretical unloaded Q for the cavities, assuming a conductivity for the aluminum of 40 percent of that of annealed copper, ranges from 53,000 at 1250 Mc to 47,000 at 1350 Mc. The measured values of Q_u as determined from the midband attenuation and the 3-db bandwidth of the filter using Eqs. (4.13-11) and (4.13-3) are 27,300, 55,700 and 28,400 at

913
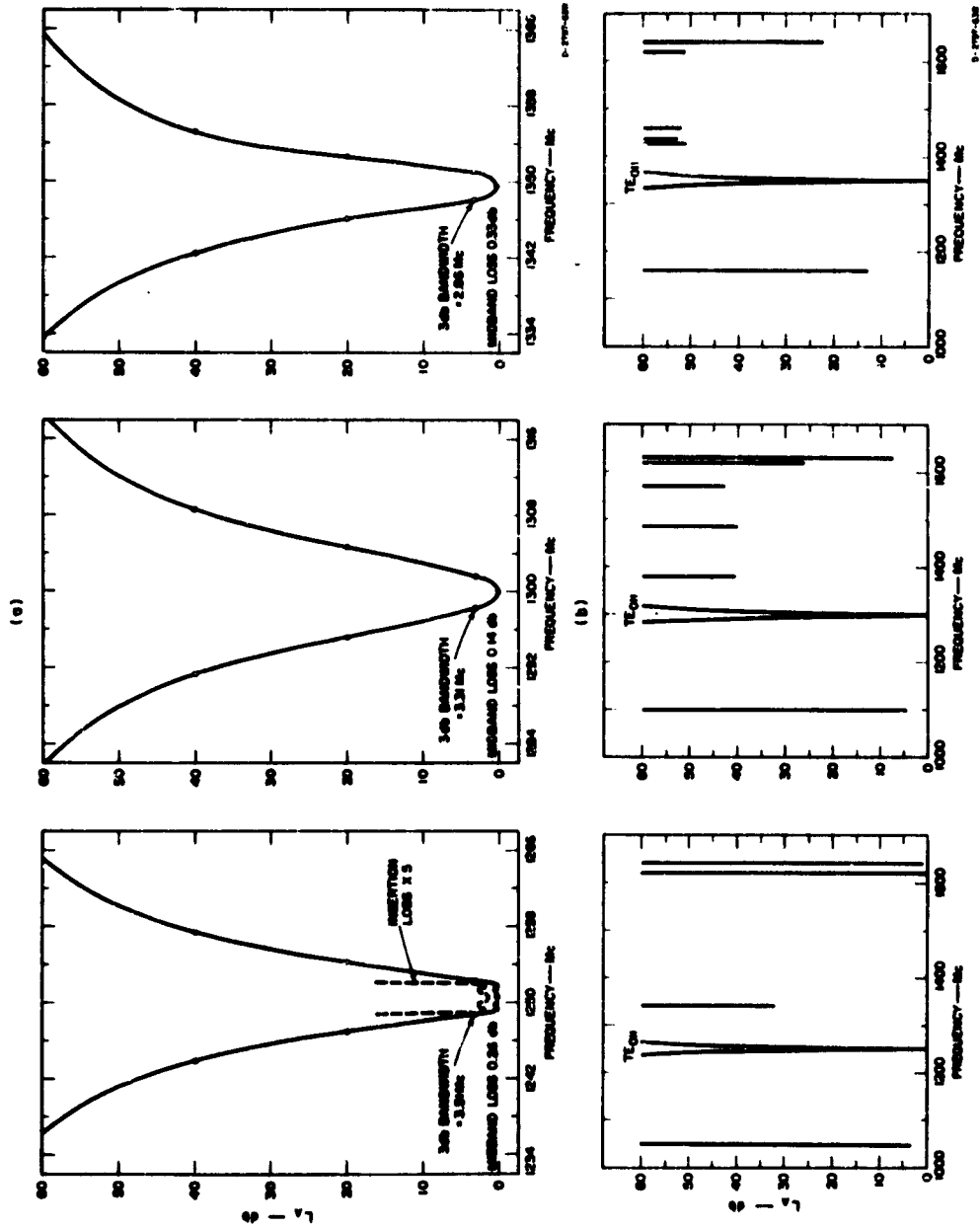
SOURCE: Technical Note 2, Contract AF 30(602)-1998, SRI
(See Ref. 38 by E. M. T. Jones)

FIG. 15.04-1 MEASURED ATTENUATION OF THE EXPERIMENTAL THREE-CAVITY TE$_{011}$ MODE FILTER

THREADED STUD (TYP)

CAVITY TUNING NUT (TYP)

EXTERNAL COUPLING APERTURE 2.75 x 3.25 FOR BOTH END CAVITES

L-BAND WAVEGUIDE (RG-69/U, 6.50 x 3.25 I.D.)

PINS & SCREWS LOCATION

$\frac{3}{16}$ (TYP)

$\frac{1}{2}$

5.118

$\frac{1}{8}$ (TYP)

$\frac{1}{4}$ (TYP)

2.50

$-2.75-$

2.00

11.50

12.50

$\frac{3}{8}$

$\frac{1}{8}$

SECTION A-A

$\frac{3}{8}$ R (TYP)

$\frac{1}{2}$ (TYP)

$\phi 3$

$\phi 2$

$\phi 1$

A

A

B

B

PLUNGER STEM SLOTTED FOR KEYWAY (3 PLACES)

KEY (3 PLACES)

CAST ALUMINUM CYLINDER

INTERNAL COUPLING APERTURE 3.25 x 2.00 (2 PLACES)

13.00

12.00

3.25

12.50

11.50

12.50

10.50

12.50

0.020

0.020

0.025

$\frac{3}{8}$

$\frac{1}{4}$

SHORT CIRCUITING FINGERS PLACED AROUND THE PLUNGER CIRCUMFERENCE (3 PLACES)

SECTION B-B

NOTE:
ALL DIMENSIONS IN INCHES

FIG. 15.04-2 DIMENSIONED DRAWINGS OF THE EXPERIMENTAL THREE-CAVITY TE_{011} MODE FILTER

RB-2797-80

915

FIG. 15.04-3   MEASURED MIDBAND ATTENUATION VERSUS
            TUNING FREQUENCY

1250, 1300, and 1350 Mc, respectively. The variation in the measured
value of Q_u may be due to measurement inaccuracies or to unsuspected
losses in the absorbing material mounted behind the tuning plungers as
described later on in this section.

Design Technique for TE_{011} *Mode Filters*—The method used in designing
this type of filter involves a combination of theoretical and experimental
techniques. The low-pass prototype of the filter is shown in Fig. 15.03-1(c);
a schematic diagram of the filter is shown in Fig. 15.04-4; and finally,
the narrow-band design equations are presented in Table 15.04-1. These
design relations were derived using Bethe's small-aperture coupling theory
by a procedure similar to that outlined in Secs. 8.07 and 8.14 for the
design of narrow-band rectangular-cavity filters. In the present filter,
the apertures used are rectangular in shape and have a length $l_{k,k+1}$
measured in a direction parallel to the unperturbed magnetic field at the
aperture, a height $h_{k,k+1}$, measured in a direction perpendicular to the
unperturbed magnetic field at the aperture, and a thickness $t_{k,k+1}$.

The theoretical static magnetic polarizabilities $(M_1)_{k,k+1}$ of the
various apertures, assuming zero thickness and no large-aperture effects,
were determined by extrapolating the values for the rectangular aperture
given in Fig. 5.10-4(a). The extrapolated value was taken as

$$\frac{(M_1)_{k,k+1}}{(l_{k,k+1})^3} = 0.061 + 0.197 \frac{h_{k,k+1}}{l_{k,k+1}} \quad . \quad (15.04-1)$$

916

The estimated actual magnetic polarizability $(M_1')_{k,k+1}$ taking into account both the thickness and frequency corrections were then determined from Eq. (5.10-6), which in the present instance takes the form

$$(M_1')_{k,k+1} = \frac{(M_1)_{k,k+1}}{1 - \left(\frac{2l_{k,k+1}}{\lambda}\right)^2} \times 10^{-\left[\frac{1.3464\,t_{k,k+1}}{l_{k,k+1}}\sqrt{1-\left(\frac{2l_{k,k+1}}{\lambda}\right)^2}\right]}$$

(15.04-2)

Because the apertures are cut in cylindrical walls, they are thicker at the edges than in the center. A thickness $t_{k,k+1}$, which is an average of these two values, is used in Eq. (15.04-2).

The accuracy of the values of magnetic polarizability computed from Eq. (15.04-2) were found to be quite high. This can be seen from an inspection of Fig. 15.04-5 which shows the measured external Q of the cavities compared with the theoretical values computed by solving Eq. (5) in Table 15.04-1 for $(Q_e)_A$. It is also seen from an inspection of Fig. 15.04-6 which shows the measured coupling coefficient k between the
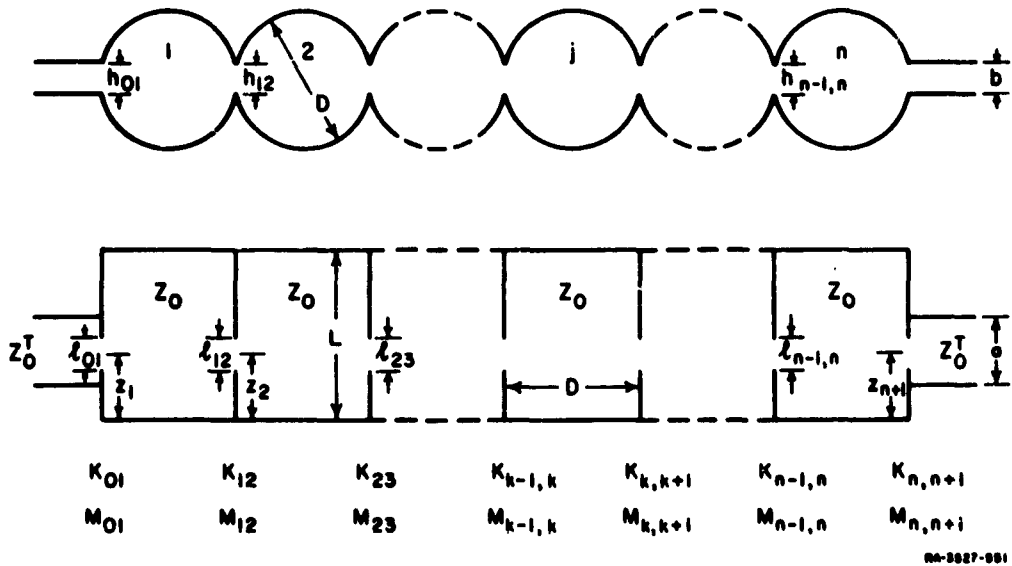

FIG. 15.04-4   A DIRECT-COUPLED TE$_{011}$ MODE FILTER HAVING n RESONATORS

Table 15.04-1

TE$_{011}$-MODE DIRECT-COUPLED CAVITY FILTERS
AND THEIR RELATION TO LOW-PASS PROTOTYPES

The prototype parameters g_0, g_1, ..., g_{n+1} are as defined in
Fig. 15.03-1(c) (or Sec. 4.04), while ω_1', ω_0, ω_1, and ω_2 are as
defined in Fig. 15.03-1(b). Figure 15.04-4 defines the filter
dimensions.

$$(Q_e)_A = \frac{g_0 g_1 \omega_1'}{w} = \text{external } Q \tag{1}$$

$$k_{k,k+1}\Big|_{k=1 \text{ to } n} = \frac{w}{\omega_1'\sqrt{g_k g_{k+1}}} = \text{coupling coefficient} \tag{2}$$

$$(Q_e)_B = \frac{g_n g_{n+1}\omega_1'}{w} = \text{external } Q \tag{3}$$

where

$$w = \frac{\omega_2 - \omega_1}{\omega_0} \quad \text{and} \quad \omega_0 = \frac{\omega_2 + \omega_1}{2} \tag{4}$$

$$(N_1')^2_{01} = \frac{L\lambda^T_{g0} ab D^4}{(Q_e)_A \, 47.5\lambda_0^2 \sin^2\left(\frac{\pi z_1}{L}\right)} \tag{5}$$

$$(N_1')_{k,k+1} = \frac{LD^4 k_{k,k+1}}{3.78\lambda_0^2 \sin^2\left(\frac{\pi z_k}{L}\right)} \tag{6}$$

$$(N_1')^2_{n,n+1} = \frac{L\lambda^T_{g0} ab D^4}{(Q_e)_B 47.5\lambda_0^2 \sin^2\left(\frac{\pi z_{n+1}}{L}\right)} \tag{7}$$

or alternatively, in terms of normalized impedance inverter
parameters

$$\frac{K_{01}}{Z_0'} = \sqrt{\frac{w\pi Z_0'\lambda^2_{g0}}{2\omega_1' Z_0'\lambda^2_0 g_0 g_1}} \tag{8}$$

Table 15.04-1 *concluded*

$$\frac{K_{k,k+1}}{Z_0} = \frac{w\pi\lambda_{g0}^2}{2\omega_1'\lambda_0\sqrt{\delta_k\delta_{k+1}}}$$

(9)

$$\frac{K_{n,n+1}}{Z_0^T} = \sqrt{\frac{w\pi Z_0\lambda_{g0}^2}{2\omega_1' Z_0^T\lambda_0^2\delta_n\delta_{n+1}}}$$

(10)

where

$$\frac{Z_0}{Z_0^T} = \frac{0.528D^4}{L\lambda_{g0}^T ab \, \sin^2\left(\frac{\pi z_1}{L}\right)}$$

(11)

$$(M_1')_{01} = \left(\frac{K_{01}}{Z_0^T}\right)\frac{\lambda_{g0}^T ab}{4\pi}$$

(12)

$$(M_1')_{k,k+1} = \left(\frac{K_{k,k+1}}{Z_0}\right)\frac{D^4}{23.7L \, \sin^2\left(\frac{\pi z_k}{L}\right)}$$

(13)

$$(M_1')_{r,n+1} = \left(\frac{K_{n,n+1}}{Z_0^T}\right)\frac{\lambda_{g0}^T ab}{4\pi}$$

(14)

where a, b, D and L are defined in Fig. 15.04-4, and

$$\lambda_{g0} = \frac{\lambda_0}{\sqrt{1-\left(\frac{\lambda_0}{0.821D}\right)^2}} = \begin{bmatrix} \text{guide wavelength in a} \\ \text{cylindrical waveguide of} \\ \text{diameter } D \text{ operating in the} \\ \text{TE}_{01} \text{ mode at frequency } \omega_0 \end{bmatrix}$$

(15)

$$\lambda_{g0}^T = \frac{\lambda_0}{\sqrt{1-\left(\frac{\lambda_0}{2a}\right)^2}} = \begin{bmatrix} \text{guide wavelength in a rec-} \\ \text{tangular terminating waveguide} \\ \text{of width } a \text{ operating in the} \\ \text{TE}_{10} \text{ mode at frequency } \omega_0 \end{bmatrix}$$

(16)

$$\lambda_0 = \begin{array}{l} \text{free space wavelength at} \\ \text{frequency } \omega_0 \end{array}$$
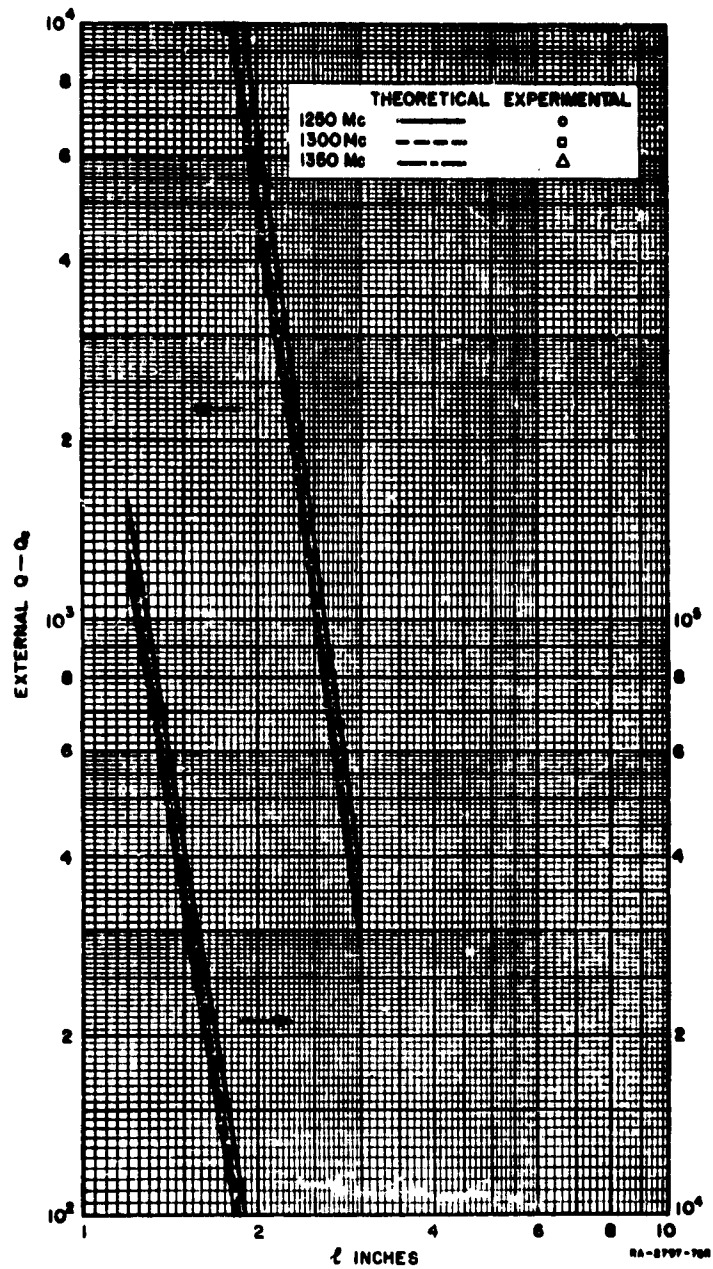
SOURCE: Technical Note 2, Contract AF 30(602)-1998 SRI
(See Ref. 38 by E. M. T. Jones)

FIG. 15.04-5   THEORETICAL AND EXPERIMENTAL VALUES OF
EXTERNAL Q, Q_e
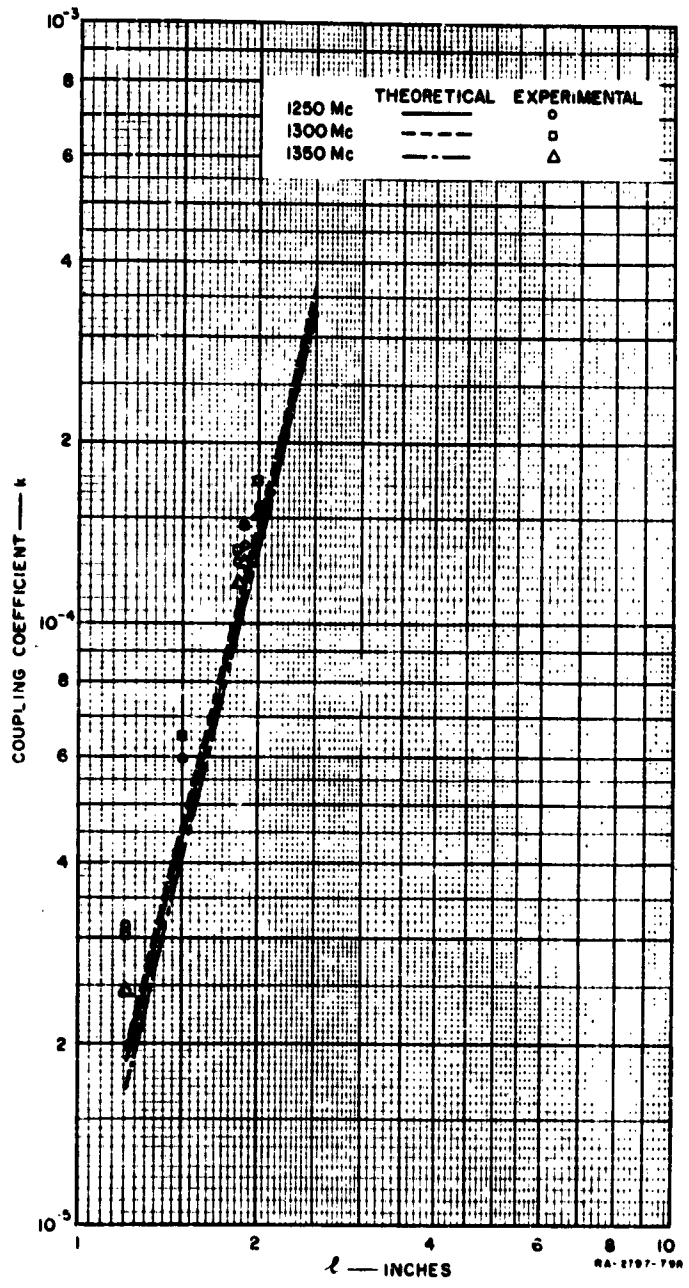
FIG. 15.04-6 THEORETICAL AND EXPERIMENTAL VALUES
OF THE COUPLING COEFFICIENT k

921

Table 15.04-2

MEASURED VALUES OF
k AND Q_e

f(Mc)	Q_e	k	kQ_e
1250	677	0.00137	0.93
1300	562	0.00176	0.99
1350	594	0.00180	1.07

cavities compared with the theoretical value computed by solving Eq. (6) in Table 15.04-1 for $k_{k,k+1}$. The values of external Q were determined from impedance measurements made on one of the end cavities operating as a singly-loaded resonator using the prescriptions in Sec. 11.02. After the apertures in the end cavities were adjusted to give the desired value of external Q the two end cavities were coupled together by means of a small iris. Measurements made on the frequency response of this pair of resonators then yielded the values of the coupling coefficient k using the prescriptions in Sec. 11.04. The final measured values of Q_e and k for the apertures whose dimensions are shown in Fig. 15.04-2 are listed in Table 15.04-2.

Techniques for Suppressing Spurious Modes—The diameter of the cavities was chosen so that, as the lengths of the cavities were varied to tune them from 1250 to 1350 Mc, the resonant frequencies of the other cavity modes were as far removed from that of the TE_{011} mode as possible. The inside diameter selected was 13 inches, which fixes the length of the unperturbed cavities at 10.23 inches when they are resonant at 1250 Mc, and 7.64 inches when they are resonant at 1350 Mc. The actual measured lengths of the cavities were found to differ significantly from these values, indicating that the coupling apertures had an appreciable perturbing effect on the resonant frequency. Figure 15.04-7 shows a mode chart for an unperturbed cylindrical resonator showing all the possible modes that can exist from 1050 Mc to 1725 Mc.

The terminating waveguides are oriented to couple strongly to those TE modes within the cavity that have components of magnetic field parallel to the cavity axes. TM modes, which have no components of magnetic field parallel to the cavity axes are only weakly excited from the terminating waveguides. It is noted, however, in Fig. 15.04-2 that the length l of the internal coupling apertures along the circumference of the cavity is greater than the aperture height parallel to the cavity axes. Therefore, TM modes inadvertently excited in the end cavities are very strongly coupled together through the internal coupling apertures. To reduce the internal coupling of the TM modes, and thereby reduce the spurious transmissions through the filter via these modes, a metal bar 0.25 inch wide

922

and 0.020 inch thick with rounded edges is placed across each internal coupling aperture parallel to the cavity axes as shown. This bar has negligible effect on the coupling of the apertures to TE modes.

Several techniques are used to minimize coupling through the filter at frequencies other than the design frequency via the many TE modes which may be coupled by the apertures. One technique consists of positioning the coupling apertures so that they lie midway between the top
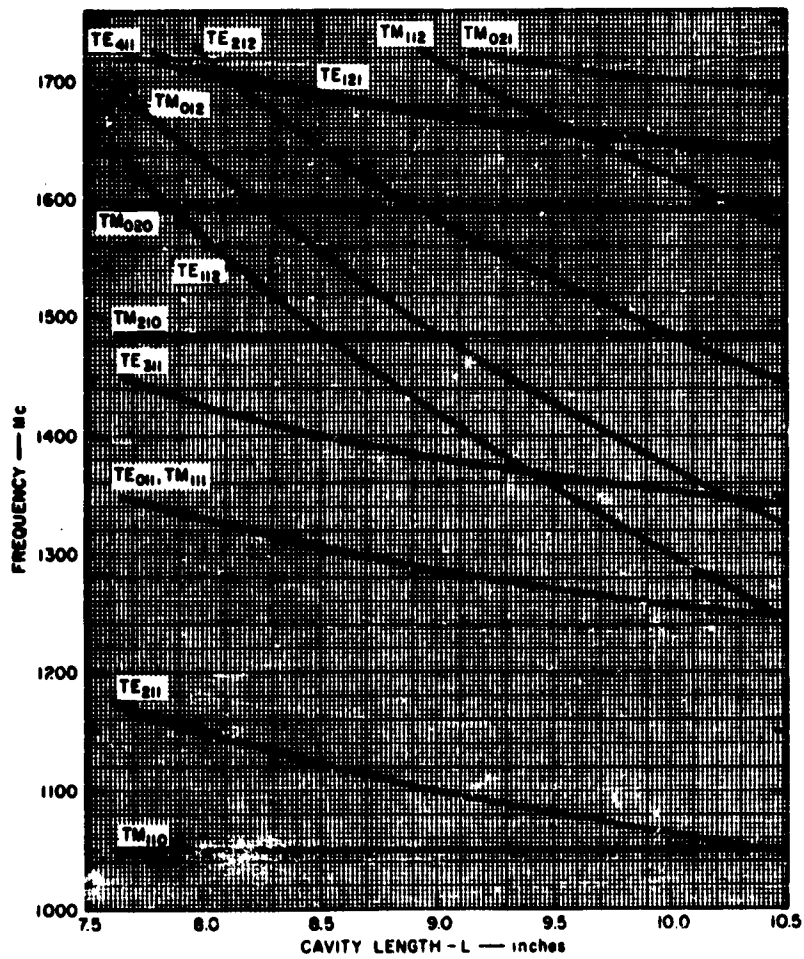
FIG. 15.04-7 MODE CHART FOR UNPERTURBED CYLINDRICAL RESONATOR

and bottom of the cavities when they are tuned to 1250 Mc. This procedure minimizes the coupling to the TE_{211} mode from the external waveguides, and also minimizes the coupling of this mode between cavities. In order to reduce the coupling of the TE_{311} mode between cavities, the coupling slots in each cavity are oriented at right angles to one another, resulting in the positioning of the cavities shown in Fig. 15.04-2.

In addition, radial transmission lines of different lengths are formed on the tuning plungers of each of the cavities as shown in Fig. 15.04-2. The radial transmission lines are formed by attaching undercut aluminum disks to the brass,contacting tuning plungers. In the two tuning plungers having the deepest chokes, two disks of resistive paper 0.0035 inch thick and having a resistance of 2000 ohms per square are placed between the brass,contacting tuning plungers and the undercut aluminum disks. In these cavities nylon screws are used to hold the two parts of the tuning plungers together. The resistive sheets lowered the unloaded Q of the undesired modes in these two cavities, without appreciably affecting the unloaded Q of the desired TE_{011} mode. The resistive paper was not placed in the tuning plunger having the shallowest radial line because in that case the paper lowered the unloaded Q of the TE_{011} mode also.

These radial transmission lines shift by different amounts the resonant frequencies of the undesired modes in each cavity, and, as explained above, lower the unloaded Q of unwanted modes in two of the cavities. Hence, the transmission via these higher-order modes is greatly reduced. The shift in resonant frequency in an end cavity, produced by the two deepest radial line chokes on some of the modes that are near in frequency to the TE_{011} mode is illustrated in Fig. 15.04-8. It is seen that these chokes do not cause the tuning curves of any of the unwanted modes to cross that of the TE_{011} mode. The chokes in the tuning plungers also have the advantage that they slightly shift the resonant frequency of the TM_{111} mode which, in an unperturbed cylindrical resonator, is always degenerate with the TE_{011} mode. The grooves at the outer edge of the bottom plates of the cavities have a depth of 0.125 inch and a width of 0.500 inch and are also for the purpose of shifting the frequency of the TM_{111} mode.

The usual technique for suppressing the effects of spurious modes on echo boxes or frequency meters operating in the TE_{01n} mode is to place absorbing material in the cavities in such a position that it couples

924

strongly to all modes except the TE_{01_a} modes[44] and therefore greatly reduces their unloaded Q, Q_u. Hence, such a dissipatively loaded cavity when used as a transmission device has a very low transmission for all modes except the TE_{01_a} modes, or when used as a reaction device produces only a negligible reaction in the feeding line except at the resonant frequency of the TE_{01_a} mode. One place where the lossy material is often put is behind the tuning plunger which is made non-contacting. The walls of the cavity can also be made in the form of a helix with lossy material between the turns. This lossy material, particularly when placed behind
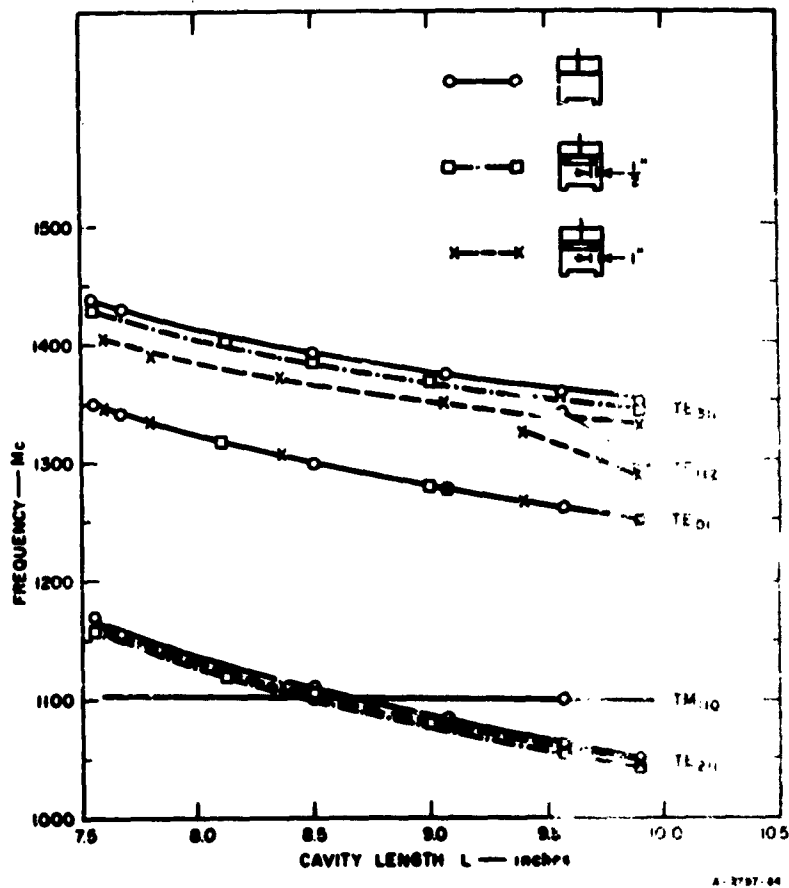
FIG. 15.04-8   MODE CHART FOR THE END CAVITY ILLUSTRATING THE
SHIFT IN MODE RESONANT FREQUENCY CAUSED BY
COUPLING APERTURES AND RADIAL LINE CHOKES

assumed sinusoidal electric field distribution (in the plane of the aperture) along its length, given by

$$E_1 \cos \frac{\pi u}{l} \qquad (15.04\text{-}3)$$

where E_1 is the peak electric field in the plane of the aperture. The exact expression for the amplitude E, the peak electric field excited in the rectangular guide, is

$$E = \frac{4lh \cos \frac{\pi l}{2a}}{\pi ab \left(1 - \frac{l^2}{a^2}\right)} E_1 \qquad (15.04\text{-}4)$$

The peak electric field in the plane of such an aperture can also be calculated approximately from another formula which has more utility in the calculation of electric fields in the internal apertures. The expression in mks units is

$$E_1 = \frac{\pi \omega_0 \mu_0 M_1' \Delta H}{2hl} \qquad \text{volts/meter} \qquad (15.04\text{-}5)$$

where, ω_0 is the angular frequency, $\mu_0 = 1.257 \times 10^{-6}$ henries/meter, M_1' is the magnetic polarizability of the aperture and ΔH is the difference between the magnetic fields on either side of the aperture. The magnetic field H_0 on the cavity side of an external aperture is much greater than the magnitude of the H-field of the external waveguide. Therefore, for the external apertures, $H_0 \approx \Delta H$.

The peak electric field $E_{k,k+1}$ in the plane of an internal window of polarizability $M'_{k,k+1}$ connecting Cavities k and $k+1$, is given by

$$E_{k,k+1} = \frac{\pi \omega_0 \mu_0 M'_{k,k+1} \Delta H_{k,k+1}}{2l_{k,k+1} h_{k,k+1}} \qquad (15.04\text{-}6)$$

where $l_{k,k+1}$ and $h_{k,k+1}$ are the length and height of the rectangular coupling aperture between Cavity k and Cavity $k+1$. It is tedious and

difficult to evaluate $\Delta H_{k,k+1}$ exactly, since its value depends on both
the magnitude and phase of the magnetic field on either side of the
aperture. A conservative design estimate is to assume that $\Delta H_{k,k+1}$ is
equal to the difference between the magnetic field in the two cavities
when they are in phase opposition.

In order that the fringing fields perpendicular to the plane of the
aperture and at its edges do not become excessive, it is necessary to use
thick coupling apertures, and to round the edges of the apertures. As
shown in Fig. 15.04-2, it is the aperture edges parallel to the u axis
(in Fig. 15.04-9) that must be rounded. The aperture edges parallel to
the v axis need not be rounded. The magnetic polarizability of the
apertures is quite insensitive to the rounding of the corners.

For an infinitesimally thin aperture with dimensions of $l = 2.75$
inches and $h = 3.25$ inches, exciting a rectangular waveguide with dimen-
sions of $a = 6.5$ inches and $b = 3.25$ inches, Eq. (15.04-4) predicts a
peak electric field E_1 in the plane of the aperture equal to 1.94 E. The
actual thick aperture in the experimental filter had the same l and h
dimensions and, in addition, the inner edge of each aperture was rounded
with a 0.325-inch radius along the l dimensions. Reference to Fig. 15.02-5
shows that the maximum electric field E_1' near the rounded corners is
1.85 E_1. (Note that E_1 is the peak field in the *plane* of the aperture,
while E_1' is the peak field regardless of direction.) Therefore, the maxi-
mum electric field E_1' near the external coupling apertures when exciting
a wave of amplitude E in the external guide is $E_1' = 3.59 E$. The pulse-
power capacity of the external coupling aperture is thus only 0.0776 times
that of the external guide. Using a relation taken from Table 15.03-1
(that the pulse-power capacity P_a' of the external guide is 76.4 λ/λ_g mega-
watts for air at standard temperature and pressure) it is found that the
peak pulse-power capacity of the external coupling apertures at midband,
where the filter is matched, is 4.06, 4.24, and 4.37 megawatts at fre-
quencies of 1250, 1300, and 1350 Mc, respectively, which is greater than
that of the resonators.

The ratio of the peak electric field in infinitesimally thin internal
coupling apertures (i.e., apertures between resonators) to that in infini-
tesimally thin external coupling apertures (i.e., apertures between end
resonators and the terminating guides) can be calculated from Eq. (15.04-6).
Since the edges of the actual apertures in the filter were all rounded by

the same amount, this ratio should also apply approximately for the actual apertures. The result is, using the final values of $l = 2.75$ and $h = 3.25$ for the external apertures and $l = 2.00$ and $h = 3.25$ for the internal apertures,

$$\frac{E'_{int}}{E'_{ext}} = \frac{M_{int}}{M_{ext}} \frac{(\Delta H)_{int}}{(\Delta H)_{ext}} 1.375 \quad . \qquad (15.04\text{-}7)$$

In this expression E'_{int} and E'_{ext} are the peak electric fields at the internal and external apertures, while $(\Delta H)_{int}$ and $(\Delta H)_{ext}$ are the differences between the H-fields on opposite sides of the internal apertures and on opposite sides of the external apertures. To an excellent approximation, $(\Delta H)_{ext} = H_{ext}$ where H_{ext} is the peak H-field in the center of the external apertures. In Eq. (15.04-7) M_{ext} is the polarizability of the external aperture which has calculated values of 4.60, 4.67, and 5.17 at frequencies of 1250, 1300, and 1350 Mc, respectively. The polarizability M_{int} of the internal apertures has calculated values of 1.275, 1.288, and . 347 at frequencies of 1250, 1300, and 1350 Mc, respectively. Making the conservative assumption that $(\Delta H)_{int}$ is equal to $2H_{ext}$, one finds that the pulse-power capacity of the internal apertures is 7.0, 7.35, and 8.53 megawatts at 1250, 1300, and 1350 Mc, respectively. Reference to Fig. 15.03-3 shows that the fields in the second and third cavity rise to about 1.4 times their midband values, for ω' of 1.4. Therefore at this frequency $(\Delta H)_{int}$ increases to about 1.4 times its assumed midband value. Consequently the pulse-power capacities of the internal apertures would be reduced to about one half their midband value, which still is higher than the pulse-power capacity of the filter cavities themselves.

SEC. 15.05, HIGH-POWER WAFFLE-IRON FILTERS

This section describes the design and measured performance of two L-band model waffle-iron filters (Sec. 7.05). In the one developed first,[46] the principal requirement was for a very wide stop band, to stop all harmonics from the second to the tenth, inclusive. This structure consisted of three waffle-iron filters in cascade with overlapping stop bands. In the second model[43] the emphasis was on power handling and pass-band width. This was achieved by changing from square to circular teeth, changing the end sections, and paralleling four identical filters. This increased the power handling capacity more than five times. There is no
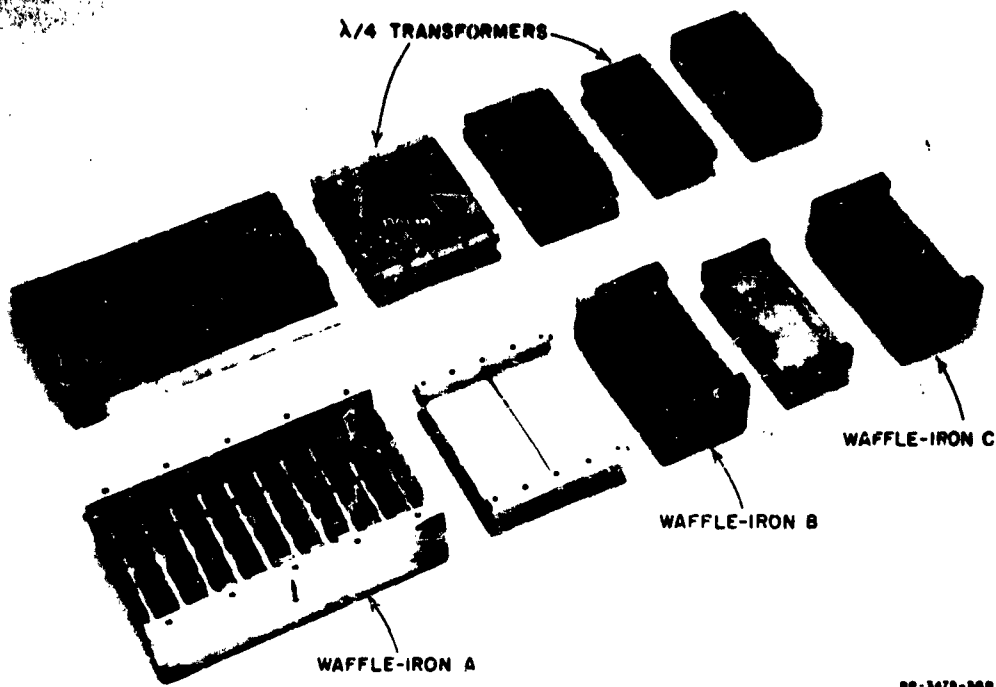
reason why the best features of both models could not be combined to produce a filter with a wide stop band (second to tenth harmonic), wide pass band (VSWR < 1.2 over almost all of L-band), and a pulse-power capacity of approximately 8 megawatts in air at atmospheric pressure, but such a model has not yet been built. The two separate models will now be described.

Waffle-Iron Filter with Stop Band up to Tenth Harmonic[6]— In this structure three different waffle-iron filters with overlapping stop bands are connected in series to give a combined stop band which extends from 2.2 Gc to 13.7 Gc where the attenuation is 60 db or greater for all possible propagating modes. This stop band includes the second through tenth harmonic of frequencies in the pass band of 1.25-1.35 Gc. In the pass band, the waffle-iron filter is matched to a WH650 waveguide using quarter-wavelength stepped transformers (Chapter 6). The pulse-power capacity without breakdown was measured in the presence of a cobalt-60 radioactive source to be 1.4 megawatts in air at atmospheric pressure using pulses 2 microseconds long and a repetition rate of 60 pulses per second.

Figure 15.05-1 is a photograph of the filter in the disassembled condition showing the quarter-wavelength transformers used to connect the various waffle-iron sections together. The transformers used to connect the waffle-iron filter to the WH650 guide are not shown.

The theoretical staggered image stop bands of the filters are shown in Fig. 15.05-2. The design of Waffle-Iron A has been previously described as the first example in Sec. 7.05 under the heading: *"Design Using Cohn's Corrugated Filter Data."* It was made ten sections long in order to achieve a theoretical stop-band attenuation of about 80 db.
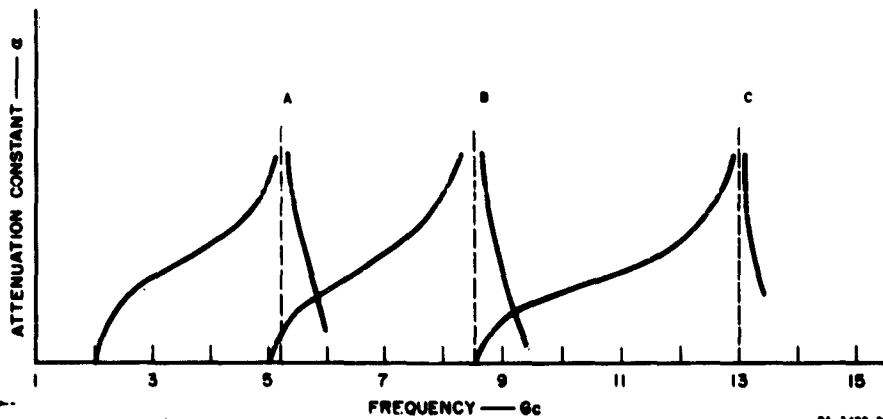
Waffle-Iron B and Waffle-Iron C were designed using the technique described in Sec. 7.05 under the heading: *"Design Using the T-Junction Equivalent Circuit of Marcuvitz."* Waffle-Iron B was made seven sections long in order to achieve a theoretical stop-band attenuation of more than 60 db above 5.75 Gc while Waffle-Iron C was made nine sections long in order to achieve a theoretical stop-band attenuation of more than 60 db above 9.25 Gc. Figure 15.05-3 shows a typical high-power waffle-iron filter section illustrating the notation used to specify the dimensions, while Table 15.05-1 shows the dimensions of each of the three waffle-iron filters.

λ/4 TRANSFORMERS

WAFFLE-IRON C

WAFFLE-IRON B

WAFFLE-IRON A

RP-3478-96R

FIG. 15.05-1   DISASSEMBLED WAFFLE-IRON FILTER AND CONNECTING
QUARTER-WAVE TRANSFORMER SECTIONS

FIG. 15.05-2   ATTENTUATION CONSTANTS OF WAFFLE-IRON FILTERS

931

Table 15.05-1

DIMENSIONS OF WAFFLE-IRON FILTERS

WAFFLE IRON FILTER	DIMENSIONS (Inches)					NUMBER OF SECTIONS		LENGTH (Inches)	RADIUS OF ROUNDED CORNERS (Inches)
	b'	b''	b	l	l'	In Width	In Length		
A	0.280	0.210	1.61	0.510	0.790	5	10	13.0	0.063
B	0.280	0.210	0.986	0.231	0.360	11	7	4.137	0.063
C	0.280	0.210	0.700	0.150	0.256	16	9	3.654	0.045

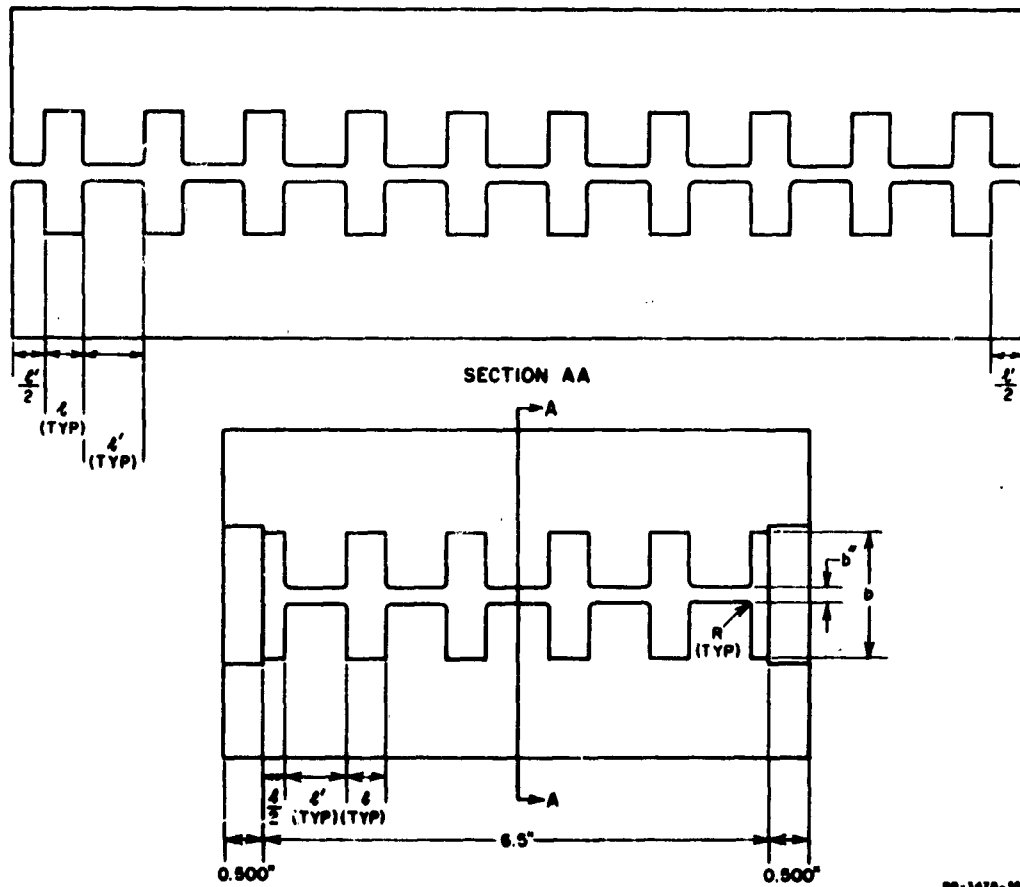SOURCE: Technical Note 2, Contract AF 30(602)-2392, SRI (See Ref. 45 by E. D. Sharp)

SECTION AA

SOURCE: Technical Note 2, Contract AF 30(602)-2392, SRI (See Ref. 45 by E. D. Sharp)

FIG. 15.05-3 TYPICAL L-BAND WAFFLE-IRON FILTER CROSS-SECTIONS

The corners of the bosses in each of the filters were rounded to reduce the electric field at these positions. The radius of curvature used in each case is shown in the table. For Waffle-Iron A and Waffle-Iron B which have $b'' < l$, it is appropriate to use Fig. 15.02-5 to determine the field strength at the rounded corners. Reference to this figure shows that the maximum electric field at the rounded corners is only 1.4 times its value at the center of the tooth. For Waffle-Iron C, $l < b''$ and it is more appropriate to use Fig. 15.02-7 to determine the field strength. Reference to this figure shows that the maximum electric field at the corners is 1.58 times its value at the center of the boss.

The height of the waveguides necessary to present an image match to each waffle-iron section was computed using the procedures outlined in Sec. 7.05 In addition, measurements of the image impedance of each filter were made using Dawir's method, which is described in Sec. 3.09. The results of these measurements are presented in Fig. 15.05-4 in terms of the height of the terminating guide necessary to achieve an image match. The height of the quarter-wave transformers necessary to match the waffle-iron sections to each other and to the terminating waveguides over a 1250- to 1350-Mc band were determined from these data and the quarter-wave-transformer tables of Sec. 6.04. The height of the single-section quarter-wave transformer between Waffle-Iron B and Waffle-Iron C is 0.341 inch. The dimensions of the two-section quarter-wave transformer between Waffle-Iron A and Waffle-Iron B are shown in Fig. 15.05-5, while the dimensions of the transformers at either end of the filter are shown in Fig. 15.05-6.

The measured VSWR of the assembly is shown in Fig. 15.05-7, while the stop-band insertion loss is shown in Fig. 15.05-8.

The performance of a single section S-band waffle-iron operating in both the evacuated and pressurized condition has also been described by Guthart and Jones.[46]

Waffle-Iron Filter with Increased Pass-Band Width and Increased Power-Handling Capacity[43]—The principle of the waffle-iron filter with wide pass-band width (and wide stop-band width) was explained at the end of Sec. 7.05. A photograph of this filter was shown in Fig. 7.05-10, and its dimensions were given in Sec. 7.05. The principle behind the increased power-handling capacity of the round (as opposed to square) teeth will now be explained.

933
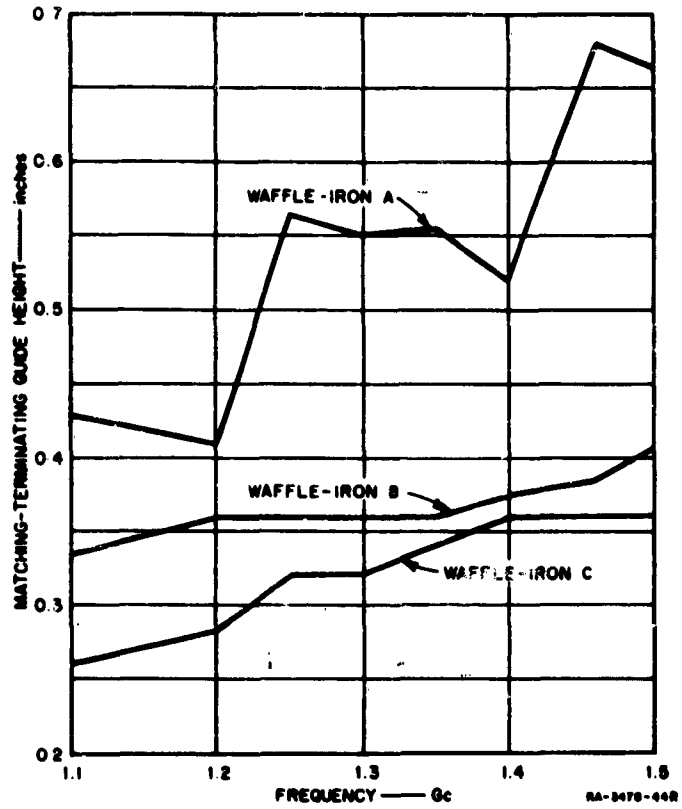
FIG. 15.05-4 MEASURED WAFFLE-IRON IMAGE IMPEDANCE

934
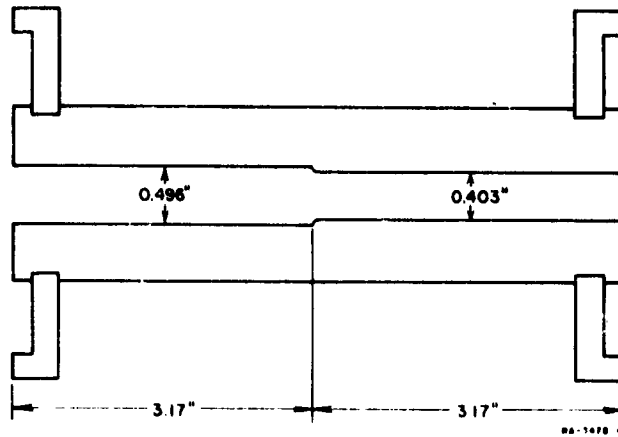
FIG. 15.05-5   CROSS-SECTION OF TRANSFORMER BETWEEN
WAFFLE IRON FILTERS A AND B
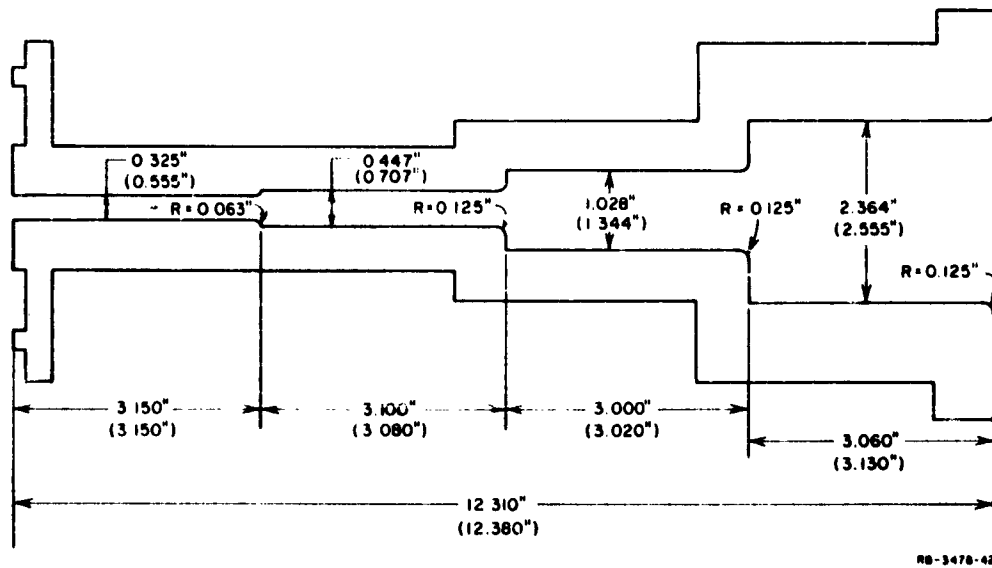
FIG. 15.05-6   CROSS-SECTIONS OF INPUT AND OUTPUT TRANSFORMERS (DIMENSIONS
WITH AND WITHOUT PARENTHESES ARE FOR TRANSFORMERS THAT
MATCH WAFFLE IRONS A AND C RESPECTIVELY, TO L-BAND WAVEGUIDE)
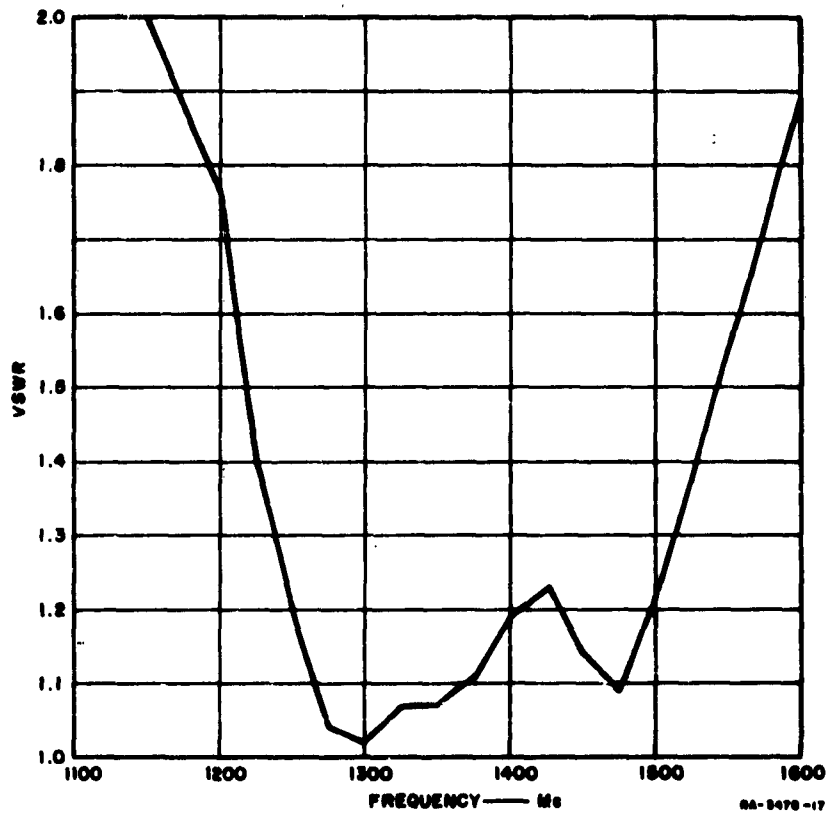
FIG. 15.05-7   VSWR OF WAFFLE-IRON FILTER ASSEMBLY
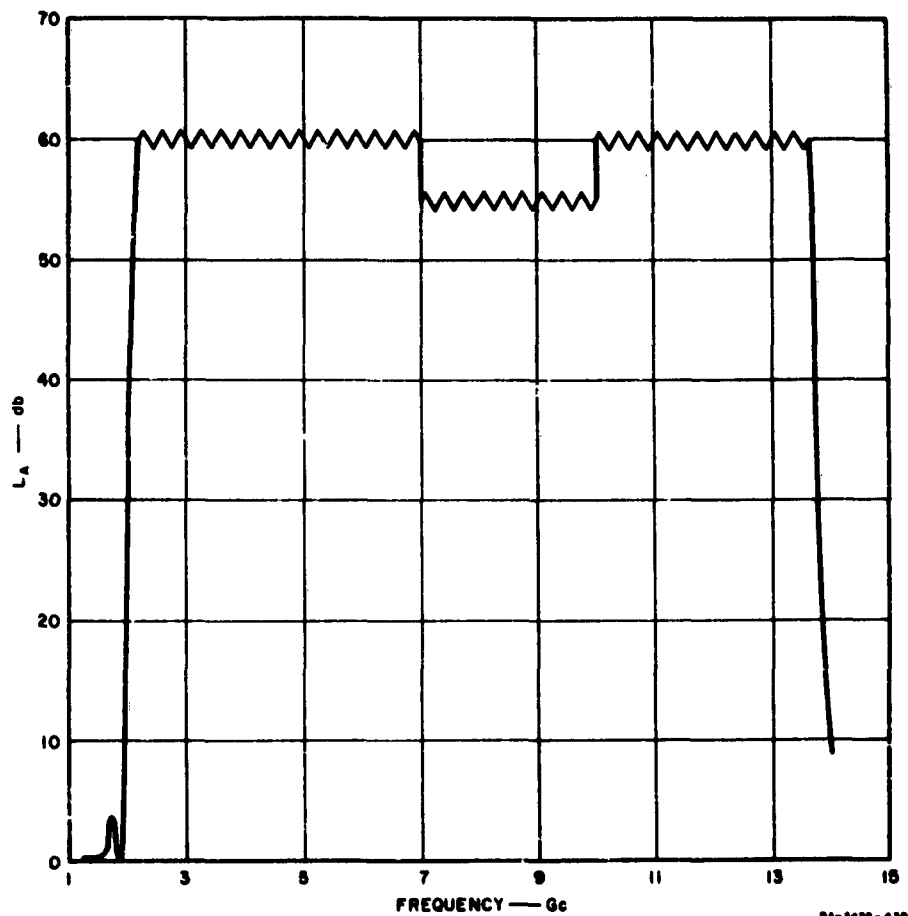
FIG. 15.05-8 ATTENUATION OF WAFFLE-IRON FILTER ASSEMBLY

The filter shown in Fig. 15.05-1 was tested at high power until
arcing occurred. It was then opened and examined: strong burn marks
were found on the four corners of the teeth in the center three longi-
tudinal rows. (There were no burn marks on the two rows of teeth along
the side wall.) Rounding the edges alone would leave a ridge at the
four corners, which had therefore been rounded off into approximately
spherical corners; but this still remained the weakest part of the filter
from the standpoint of power-handling capacity. To spread the field more
evenly, it was argued that a circular tooth should be better than a

937

square tooth, since it has only one edge and no corners. To arrive at a quantitative comparison, the following reasoning was used.

Cohn[35] has analyzed the fields near two-dimensional rounded corners. With the dimensions of both the round and square teeth, his results should still hold closely for the fields near the line-edges of the teeth. One curve in Fig. 15.05-9 is taken from Fig. 15.02-5, and shows the maximum field near a rounded edge with circular boundary. It is shown as a function of the ratio $2R/b''$, where R is the radius of the rounded edge and b'' is the spacing between teeth (Fig. 15.05-3). To calculate the maximum field near the spherically rounded corners of the square teeth, we proceed as follows.[a]
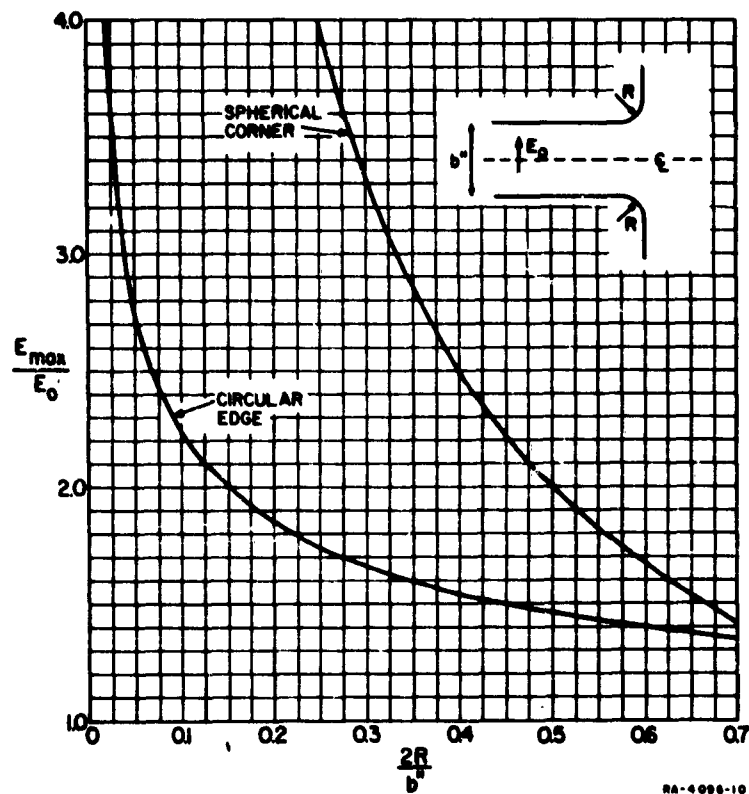
FIG. 15.05-9   MAXIMUM FIELD INTENSITIES NEAR CIRCULAR EDGE
OF ROUND TEETH AND NEAR SPHERICAL CORNERS OF
SQUARE TEETH

The plane of symmetry between teeth may be regarded as being at ground potential. The field intensity well inside the region between teeth is denoted by E_0. Then the potential V of a tooth is

$$V = \pm E_0 b''/2 \quad .$$

(15.05-1)

The field E_{max} on the surface of an isolated sphere of radius R and at a potential V above ground is

$$F_{max} = \frac{V}{R} = \frac{E_0 b''}{2R} \quad .$$

(15.05-2)

Therefore,

$$\frac{E_{max}}{F_0} \approx \frac{b''}{2R}$$

(15.05-3)

approximately, for the three-dimensional corners on the square teeth, when the corners have spherical contours. Equation (15.05-3) is also plotted against $2R/b''$ in Fig. 15.05-9 and is a rectangular hyperbola. For the filters under consideration

$$\frac{2R}{b''} = \frac{0.126}{0.210} = 0.6 \quad ,$$

(15.05-4)

and Fig. 15.05-9 shows that F_{max}/E_0 is 1.415 for the circular edge, and 1.667 for the spherical corner. Therefore, the waffle-iron filter with circular teeth should handle about

$$\left(\frac{1.667}{1.415}\right)^2 = 1.39$$

(15.05-5)

times as much power as the waffle-iron filter with square teeth. With four waffle-iron filters in parallel and circular teeth, as in Fig. 15.05-10, the filter should handle about $4 \times 1.39 = 5.56$ times the power of the single filter in Fig. 7.05-10, corresponding to about 15 percent of the power handled by WR650 L-band rectangular waveguide.
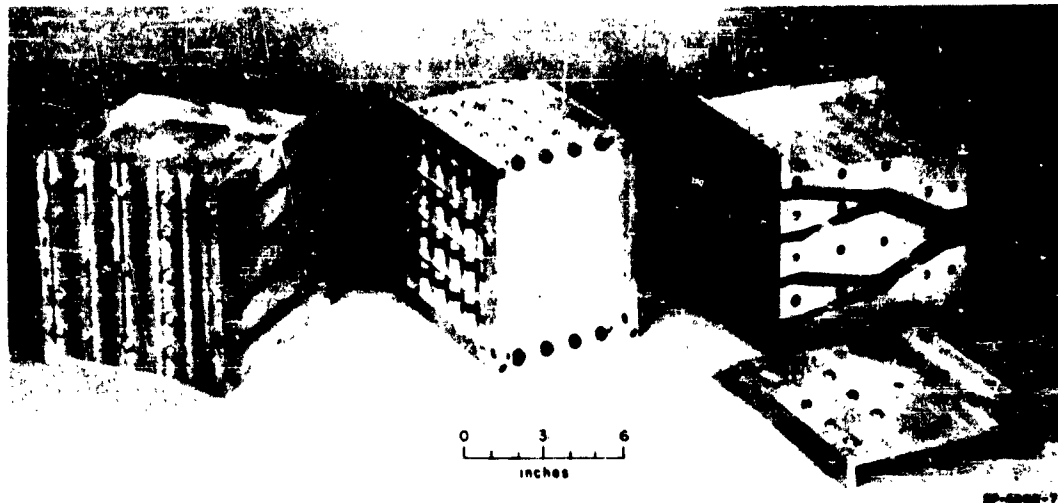
939

FIG. 15.05-10   HIGH-POWER WAFFLE-IRON FILTER USING ROUND TEETH
AND FOUR FILTERS IN PARALLEL
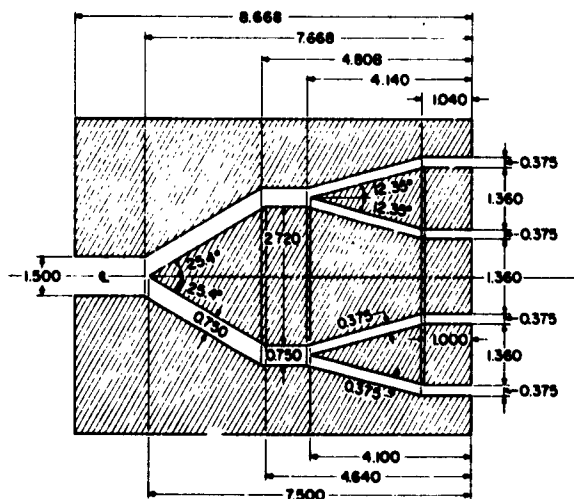
WAVEGUIDE, WIDTH, a = 6.500"   NO SCALE

FIG. 15.05-11   DIMENSIONS OF POWER-DIVIDERS SHOWN
IN FIG. 15.05-10

This four-waffle-iron filter was tested in the presence of a cobalt-60 radioactive source in air at atmospheric pressure, using pulses 2.5 microseconds long with a repetition rate of 200 pulses per second. At 6.3 megawatts pulse power (the maximum power available) there was still no sign of arcing. Based on the above calculation and 1.4 megawatts for the single-waffle-iron square-toothed filter of Fig. 15.05-1, the filter in Fig. 15.05-10 should handle $5.56 \times 1.4 = 7.8$ megawatts under the same conditions.

It was pointed out at the beginning of Sec. 15.02 that the pulse-power capacity referred to short pulses. The reader should use caution when applying these results to longer pulses. Both the square-toothed and the round-toothed waffle-iron filters were subjected to pulses 110 microseconds long, at a rate of 30 pulses per second. The pulse-power capacity with the 110-microsecond pulses was only about one-third of that with the 2-microsecond pulses. Furthermore, it appeared that arcing arted about 50 microseconds after the beginning of the pulse.

The dimensions of the power dividers for the high-power waffle-iron filter in Fig. 15.05-10 are given in Fig. 15.05-11. Each of the four parallel filters has the same dimensions as were given in Sec. 7.05 for the single filter shown in Fig. 7.05-10.

The VSWR of the filter shown in Fig. 15.05-10 is shown in Fig. 15.05-12, including both power dividers in the measurements. The solid line is for the original filter in which the three one-eighth-inch plates supporting the round teeth (Fig. 15.05-10) were solid plates from end to end. Later these plates were modified by cutting large circular holes between teeth, as shown in Fig. 15.05-13, which also shows the shelf-like construction of the filter in more detail. The reason for the holes was to allow coupling between the four parallel filter units, so that propagation through the various waffle iron filters could not get out of phase, and thus to forestall any possible trapped resonance around a plate due to poor tolerances or other imperfections. (No such resonance was ever actually observed with or without coupling holes.) The VSWR of the filter with coupling holes is shown by the dotted line in Fig. 5.05-12. The VSWR is better than 1.2 over almost the whole of L-band, with or without coupling holes, and better than 1.1 over two considerable portions of it.

The stop-band performance is shown in Fig. 15.05-14 together with that of Waffle-Iron Filter A (which has square teeth, has ten sections,
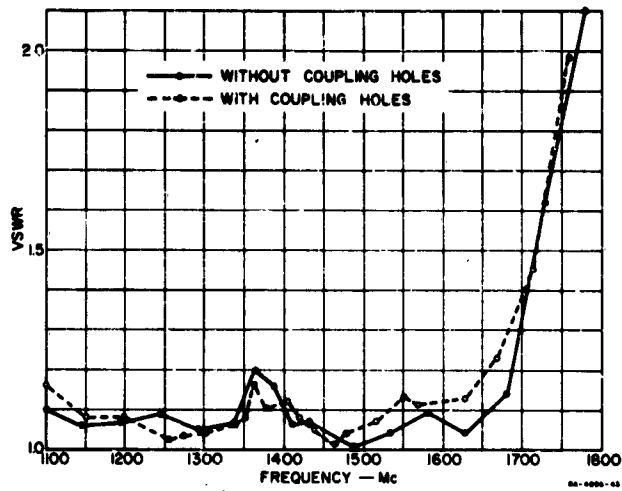
941

FIG. 15.05-12   VSWR OF FILTERS IN FIGS. 15.05-10 AND 15.05-13
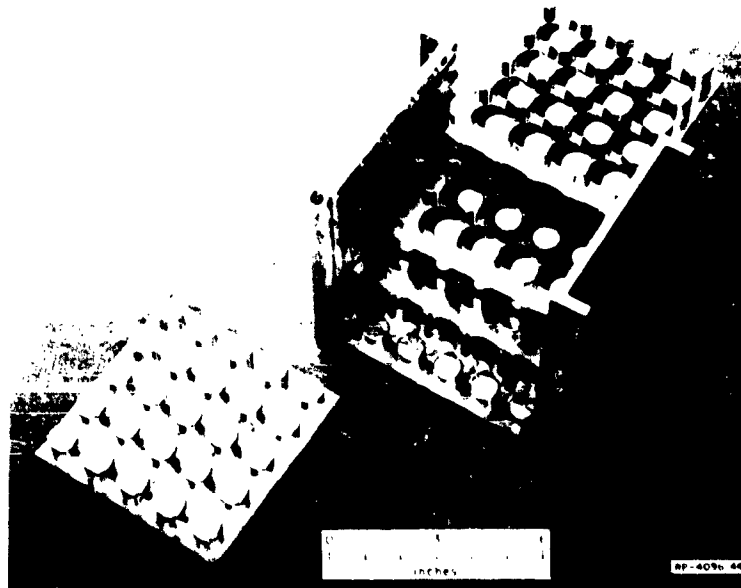
FIG. 15.05-13   SHELF-LIKE CONSTRUCTION OF FILTER IN FIG. 15.05-10
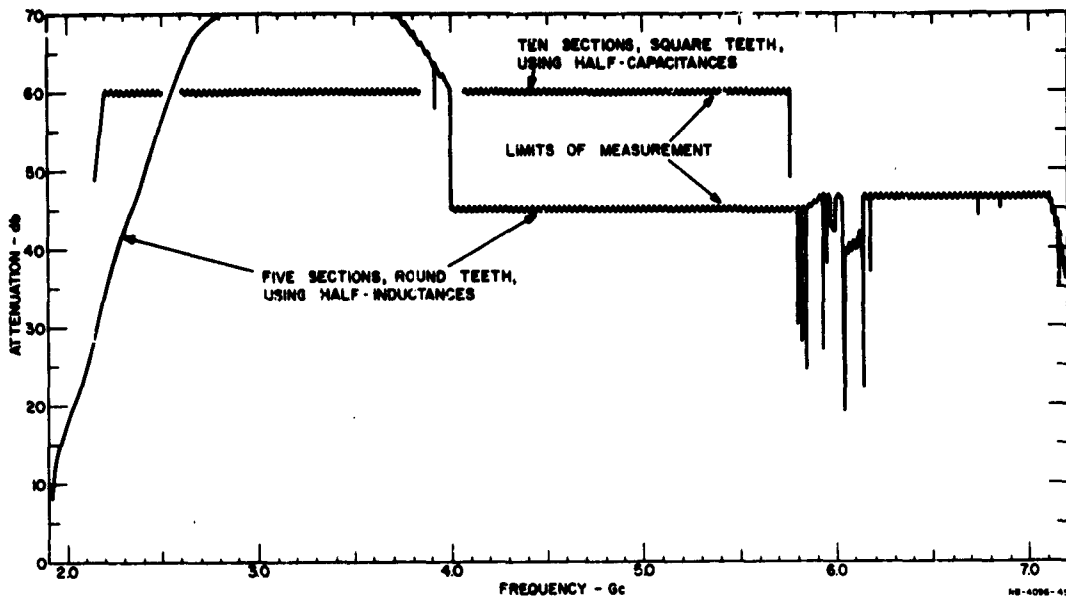
942

FIG. 15.05-14   ATTENUATION OF TWO WAFFLE-IRON FILTERS

and begins with half-teeth). After allowance is made for the fact that one is
a five-section and one is a ten-section filter, there is no noticeable differ-
ence in the stop-band performance. However, some difficulty was experienced
as a result of imperfect contact at the coupling flange. Since TE_{01} and other
TE_{0n} modes can propagate through the waffle-iron filter in the higher part of
the stop band, one must make sure that TE_{01} and other TE_{0n} modes are not excited
where the waffle-iron sections begin. Normally these modes are not excited be-
cause of the symmetry of the structure, and they are cut off in the low-height
waveguide matching sections so that none can reach the filter proper. However
if the waffle-iron filter and the low-height waveguide matching sections are
made in separate pieces and then connected, imperfect contact at the flanges may
set up the unwanted modes. Then any conversion from propagating TE_{m0} modes in
the exterior waveguide to propagating TE_{0n} modes in the filter proper, and sub-
sequent re-conversion at the output, will cause spurious pass bands. A few very
sharp and narrow spurious responses were observed, and were found to improve
with better flange fitting. To avoid the need for excessive care in mating
flanges, six one-eighth-inch-diameter rods were passed across the filter, as
shown in Fig. 15.05-15, which completely eliminated all spurious responses in
the stop band.
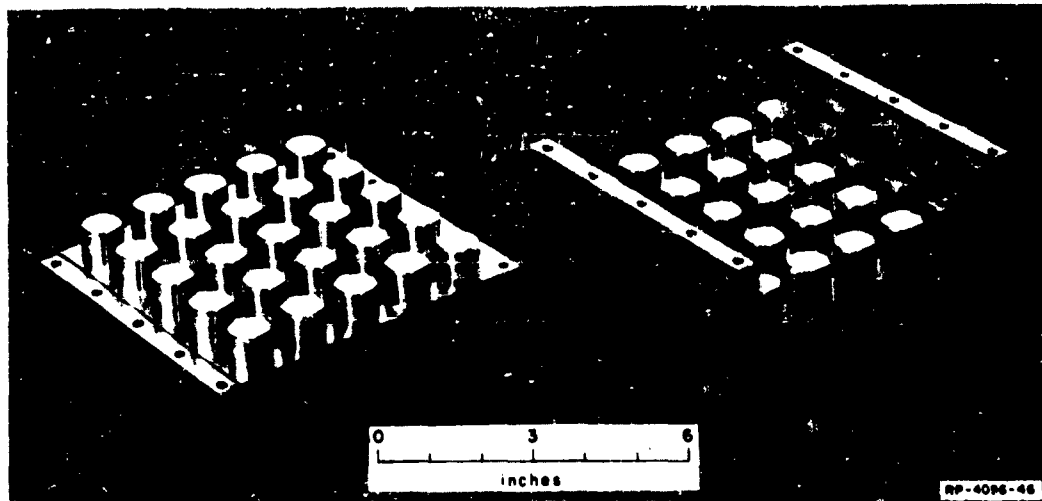
943

FIG. 15.05-15 WAFFLE-IRON FILTER WITH THIN RODS TO SUPPRESS TE_{01} MODE EXCITED
BY IMPERFECT CONTACT OR MISALIGNMENT OF FLANGES

SEC. 15.06, DISSIPATIVE WAVEGUIDE FILTERS

Dissipative low-pass waveguide filters are extensively used to
suppress the spurious harmonic radiation from high-power transmitters
because they are well matched in both the pass and stop bands and hence
preclude resonances between the transmitter and the filter that might be
damaging to the transmitting tube.[a,b] They usually have maximum attenu-
ation at the second and third harmonic frequencies with lesser attenuations
at higher frequencies. Most designs can handle essentially the full
waveguide pulse-power without recourse to pressurization. It is also
relatively easy to pressurize them if necessary in order to make them
compatible with other components in a system.

Figure 15.06-1 is a sketch of a portion of a typical dissipative
waveguide filter. It is seen to consist of a central waveguide that is
aperture coupled to an array of secondary waveguides, which stand on all
four sides of the central waveguide, and each of which is terminated in
a matched load. The width a_2 of the secondary waveguides is small enough

944

so that they are below cutoff in the pass band of the filter and hence
at these frequencies power can propagate down the central waveguide with
an attenuation that is ordinarily less than 0.1 db. In order to achieve
this low, pass-band attenuation the tips of the spear-shaped loads in the
secondary waveguides are placed approximately a distance a_2 (equal to
one-half of the TE_{10}-mode cutoff wavelength in the secondary waveguide)
from the apertures so that the fringing fields at the apertures do not
interact with the loads. In the stop band, which exists at frequencies
above the pass band, the side waveguides can propagate and harmonic power

TYPICAL LOAD

WAVEGUIDES TERMINATED
WITH MATCHED LOADS
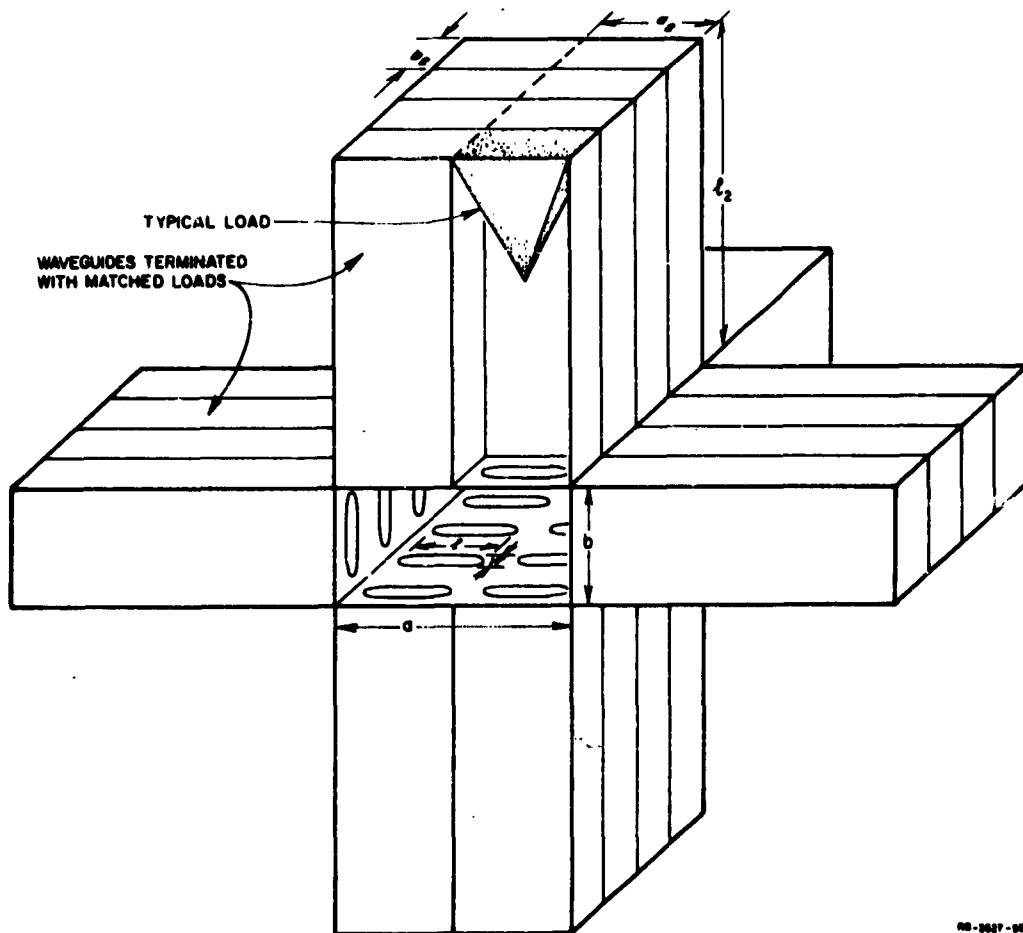
FIG. 15.06-1 TYPICAL CONSTRUCTION OF A DISSIPATIVE WAVEGUIDE FILTER

propagating down the central waveguide is coupled into the side waveguides where it is dissipated in the matched terminations.

The coupling apertures for the secondary waveguides are usually long and narrow slots as shown, and maximum attenuation in the central waveguide occurs at the frequency at which the aperture lengths l are about one-half a free-space wavelength. The center-to-center spacing of the apertures, along the length of the waveguide, is usually made less than half a free-space wavelength at the highest frequency of operation of the filter in order to avoid multiple reflections from the apertures which would raise the stop-band VSWR. The coupling apertures cannot couple equally well to all possible modes in the central waveguide, which can propagate a rapidly increasing number of modes as the frequency is increased. When slots are used, as shown in Fig. 15.06-1, the slots attenuate most strongly those modes with currents trying to cross the slots (i.e., having transverse magnetic fields in the case of Fig. 15.06-1); the secondary waveguides are then effectively in series with the central waveguide. Furthermore, the attenuation is greatest when the centers of the coupling apertures are located at the positions of maximum transverse magnetic field (maximum longitudinal wall current). The attenuation of a mode measured in db at a particular frequency is also approximately inversely proportional to its impedance in the central w... ide (which for TE modes and a given a/b ratio is proportional to the ... of guide wavelength to free-space wavelength). Therefore, a ! ... rder mode having the coupling apertures of the secondary waveguides arranged so that the mode will suffer maximum attenuation may still be less strongly attenuated than a lower-order mode having a lower guide impedance. Greater attenuation by the secondary waveguides along the broad wall of the central guide is obtained when the impedance of the guide is reduced by reducing its height, b.[a] However, this procedure also reduces the pulse-power capacity of the filter since the pulse-power capacity is directly proportional to b.

In the filter shown in Fig. 15.06-1 the secondary waveguides along the broad wall of the central waveguide would couple strongly to the second-harmonic power propagating in the TE_{20} mode. They also couple just about as strongly to the second-harmonic power propagating in the TE_{10} mode. The waveguides along the narrow wall of the central waveguide couple most strongly to second-harmonic power propagating in the TE_{01} mode.

If the double array of side waveguides along each broad wall of the central waveguide in Fig. 15.06-1 are replaced by triple arrays, the filter would be most effective in suppressing power propagating at the third harmonic frequency. For this reason some dissipative filters have a double array of waveguides along a portion of the broad wall and a triple array along the rest of the wall.

In order to provide a good match between the dissipative filter and the terminating waveguides it is customary to linearly taper the lengths of the coupling apertures at each end of the filter. When about a dozen apertures are tapered at each end of the filter the resulting pass-band VSWR is usually less than 1.20.

An S-Band Dissipative Filter—A filter which is typical of dissipative filters in general, has been developed by V. Price, *et al.*[*] The configuration of the side waveguides in this filter is as shown in Fig. 15.06-1; however, a cylindrical pressure vessel surrounds the filter so that it can be operated at a pressure of 30 psig (pounds per square inch, gauge). The filter, which is made of aluminum, is fabricated in the following fashion. First, the coupling apertures are milled in the central waveguide. Then a number of aluminum stampings are made which, when assembled in the fashion of an egg-crate, form the side waveguides. The side waveguides and the central waveguides are then clamped together and permanently joined to each other by immersion in a dip brazing tank. The specifications for such a filter are given in Table 15.06-1, and its attenuation characteristics are shown in Figs. 15.06-2, 3 and 4.

Table 15.06-1

SPECIFICATIONS OF AN *S*-BAND DISSIPATIVE-FILTER EXAMPLE

Rows of slots on each broad wall	2
Rows of slots on each narrow wall	1
Number of full-length slots on both broad walls	272
Number of full-length slots on both narrow walls	136
Number of linearly tapered matching slots at each end of each row of slots	16
b_2, height of side waveguides	0.26 inch
a_2, width of side waveguides	1.39 inches
l_2, length of narrow-wall side waveguides	2.6 inches
l_2, length of broad-wall side waveguides	2.4 inches
l, length of coupling apertures	1.30 inches
w, width of coupling apertures	0.10 inch
Over-all filter length including flanges	36 inches
Outside diameter of pressure vessel surrounding filter	9.25 inches
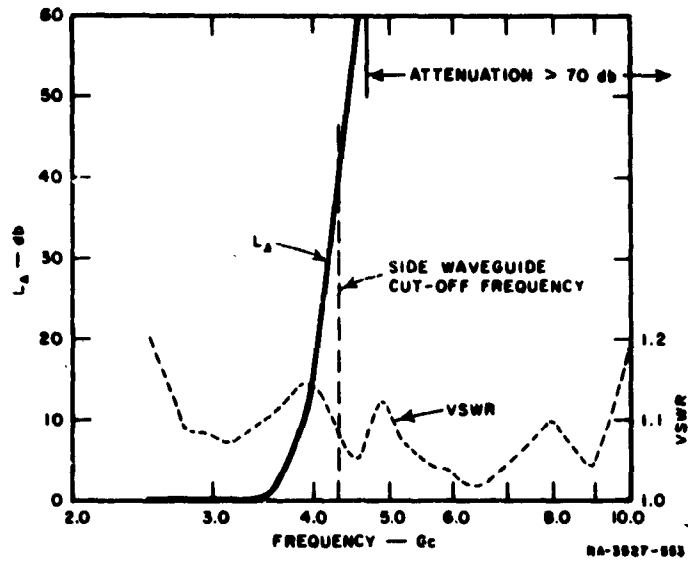
947

FIG. 15.06-2 TE$_{10}$-MODE ATTENUATION AND VSWR OF S-BAND DISSIPATIVE
FILTER WHOSE DIMENSIONS ARE GIVEN IN TABLE 15.06-1
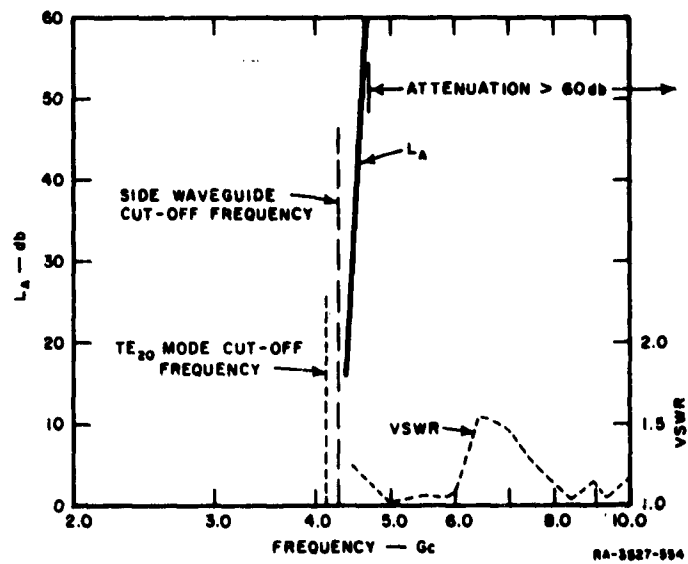
FIG. 15.06-3 TE$_{20}$-MODE ATTENUATION AND VSWR OF DISSIPATIVE FILTER
WHOSE DIMENSIONS ARE GIVEN IN TABLE 15.06-1

948
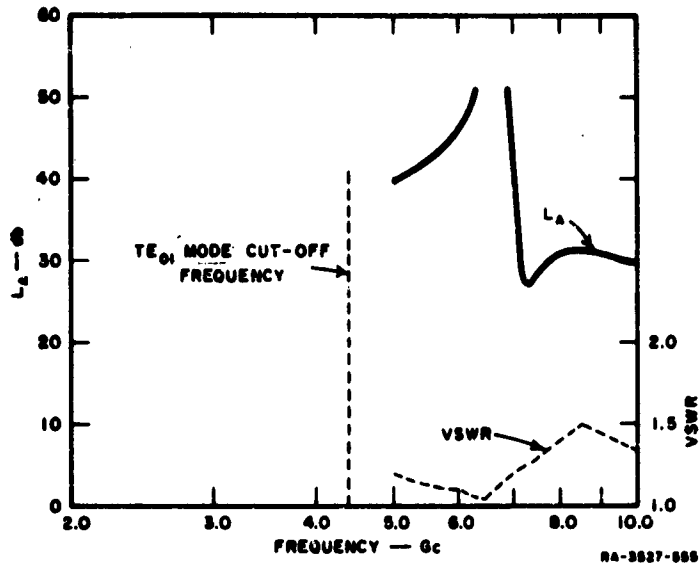
FIG. 15.06-4   TE$_{01}$-MODE ATTENUATION AND VSWR OF
DISSIPATIVE FILTER WHOSE DIMENSIONS
ARE GIVEN IN TABLE 15.06-1

Other types of harmonic-absorbing waveguide filters with secondary
waveguides have also been built. One of the more promising variations
on this theme has been the use of circular instead of rectangular
secondary waveguides, open-ended into the rectangular central waveguide.
The secondary guides may or may not be loaded with dielectric material,
but in any case must be cutoff in the pass band, and have to start propa-
gating at some frequency below the second harmonic.

SEC. 15.07, DISSIPATIVE COAXIAL-LINE FILTERS

Dissipative low-pass filters can also be constructed in coaxial line
to suppress the spurious power from high-power transmitters. Their
principle of operation is essentially the same as that of the waveguide
dissipative filters discussed in Sec. 15.06. The stop-band attenuation
per unit of length of the TEM mode in a typical coaxial dissipative
filter is greater than that of the lowest mode in a typical waveguide
dissipative filter because the characteristic impedance of the central

transmission line is lower. However, the pulse-power capacity is less
for a coaxial filter because the pulse-power capacity of the best coaxial
line is less than that of standard waveguide in the same frequency range.

Experimental models of coaxial dissipative filters have been built
by E. G. Cristal.[50] One model has a pass-band cutoff frequency of 1.7 Gc
and a characteristic impedance of 50 ohms. The inside diameter of the
outer conductor is 1.527 inches while the diameter of the inner conductor
is 0.664 inch. Twenty-one rectangular-slot pairs were cut in the
0.049-inch-thick coaxial line wall and were spaced 0.400 inch apart
center to center. The width of each slot was 0.25 inch, and each slot
subtended an angle of 150 degrees at the axis. In addition, ten smaller
slots were cut in the coaxial line in the regions ahead of and behind
the twenty-one main slots; the added slots were arranged to form a tapered
sequence so as to improve the impedance match in the pass band.

The secondary waveguides were 0.375 inch high and 3.5 inches wide,
corresponding to a cutoff frequency of 1.7 Gc. The length of the secondary
waveguides is about 12 inches, but this length could be reduced. Each of
the secondary waveguides was terminated with resistive Teledeltos* paper.
(Each load was found to be able to dissipate at least three watts average
power without cooling.) Figure 15.07-1 shows a sketch of the filter
(without the tapered slots). Its measured attenuation to the dominant
TEM mode is shown in Fig. 15.07-2, for several values of the coaxial line
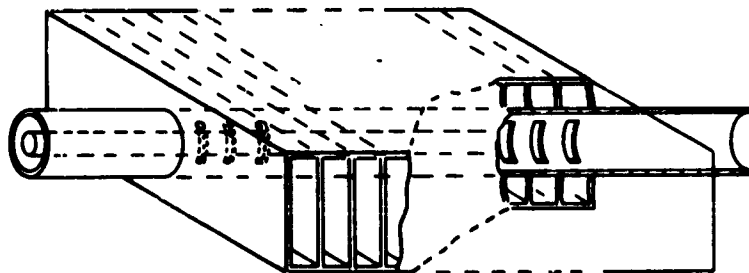
RA-692,521-86

FIG. 15.07-1   COAXIAL LEAKY-WAVE FILTER

* Obtainable from Micro Circuits Co., New Buffalo, Michigan.
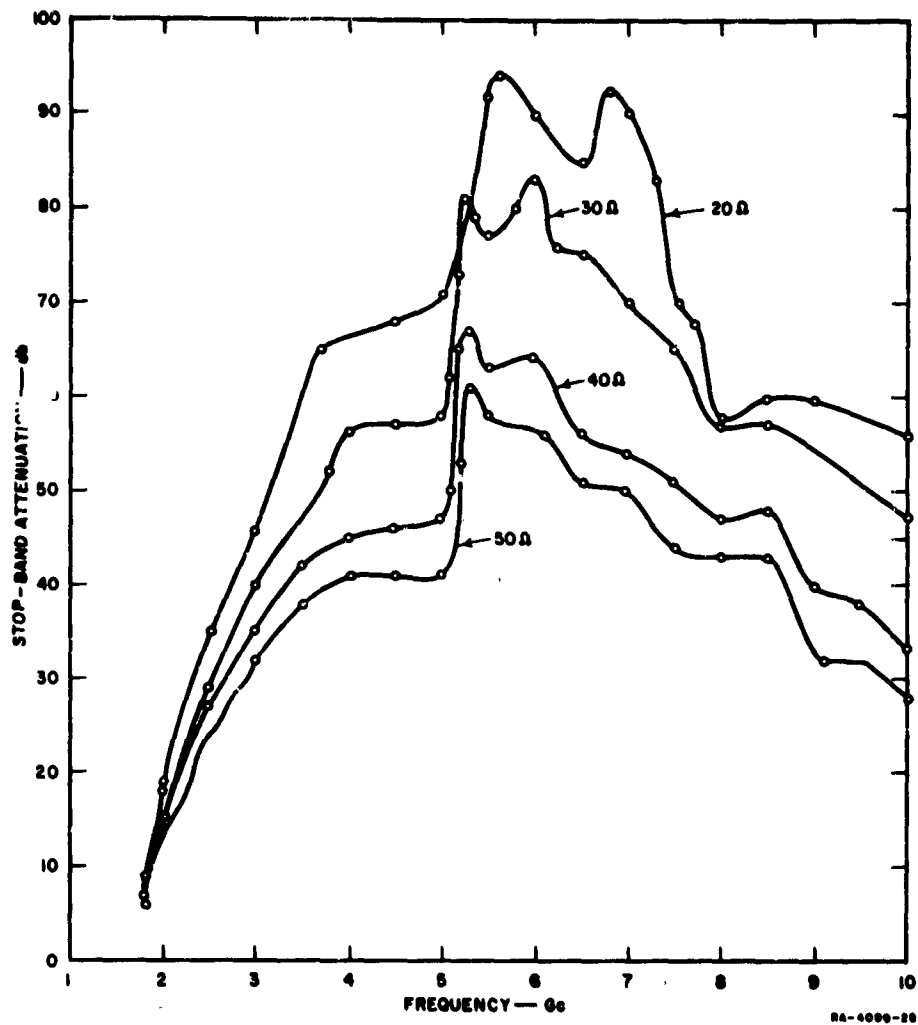
FIG. 15.07-2   ATTENUATION OF EXPERIMENTAL COAXIAL LEAKY-WAVE
FILTER TO A TEM WAVE FOR VARIOUS LINE IMPEDANCES

impedance, from 50 ohms to 20 ohms.   The impedance was adjusted by
changing the diameter of the inner conductor from 0.664 inch (for 50 ohms)
on up.   It can be seen from Fig. 15.07-2 that the attenuation to the TEM
mode is substantial over a very wide frequency band, for all line imped-
ances, and that the attenuation increases as the impedance decreases.

The TE_{11} mode propagates above 3.5 Gc.   A TE_{11} mode launcher was
constructed and the attenuation of the coaxial leaky-wave filter was

measured to two polarizations of the TE_{11} mode: in one polarization the currents try to cross the slots and are attenuated strongly, the over-all attenuation being about equal to that for the TEM mode. In the other polarization, the slots do not perturb the current flow so much, and the coupling through the slots is much weaker; the measured attenuation in db was about one-fifth of that for the orthogonal TE_{11} polarization and the TEM mode. One way to ensure high attenuation for the TE_{11} mode in all polarizations is to use two filters in cascade, but arranged with their transverse geometry orthogonal. At the time of this writing, other possibilities are still under consideration.

The shape and size of single slots were varied experimentally in order to determine the configuration for maximum coupling in the stop band. For example, dumbbell slots can be made to resonate at lower frequencies than plain rectangular slots, and thus give slightly stronger coupling near the cutoff frequency, but it is doubtful whether the small improvement is worth the mechanical complication for most applications. A numerical analysis for some idealized cases was also undertaken to discover the dependence of the stop-band attenuation on the various parameters involved. The slots were closely spaced in every case. Doubling the number of slots and secondary waveguides per unit length did not appreciably increase the attenuation, when the slot widths and waveguide heights had to be halved to allow for twice as many slots. The greatest attenuation and the flattest frequency response resulted from the widest slots (slot width equal to waveguide height).

The VSWR of the 50-ohm filter in the nominal pass band of 1.2 to 1.4 Gc was found to be less than 1.09. In the stop band, the VSWR for the TEM mode was less than 1.5 from the second to the fifth harmonic, inclusive.

REFERENCES

1. R. D. Campbell, "Radar Interference to Microwave Communication Services," *Elec. Eng.*, Vol. 77, pp. 916-921 (October 1958).

2. A. H. Ryan, "Control of Microwave Interference," *IRE Trans.*, PGRFI-1, pp. 1-10 (May 1959).

3. M. P. Forrer and K. Tomiyasu, "Effects and Measurements of Harmonics in High-Power Waveguide Systems," 1957 *IRE National Convention Record*, Part 1, pp. 263-269.

4. V. G. Price, "Measurement of Harmonic Power Generated by Microwave Transmitters," *IRE Trans.*, PGMTT-7, pp. 116-120 (January 1959).

5. C. C. Cutler, "Spurious Modulation of Electron Beams," *Proc. IRE*, Vol. 44, pp. 61-64 (January 1956).

6. R. L. Jepsen, "Ion Oscillations in Electron Beam Tubes; Ion Motion and Energy Transfer," *Proc. IRE*, Vol. 45, pp. 1069-1080 (August 1957).

7. A. D. Sutherland, "Relaxation Instabilities in High-Perveance Electron Beams," *IRE Trans.*, PGED-7, pp. 268-273 (October 1960).

8. Y. Koike and Y. Kumagai, "An Experiment of Ion Relaxation Oscillation in Electron Beams," *Proc. IRE*, Vol. 49, pp. 525-526 (February 1961).

9. O. Doehler, "Space Charge Effects in Traveling-Wave Tubes Using Crossed Electric and Magnetic Fields," *Proceedings of the Symposium on Modern Advances in Microwave Techniques*, Brooklyn, N.Y., November 8-10, 1954, Polytechnic Institute of Brooklyn, N.Y., Vol. 4, pp. 101-121 (1955). See especially pp. 115-119.

10. R. W. Gould, "Space Charge Effects in Beam-Type Magnetrons," *J. Appl. Phys.*, Vol. 28, pp. 599-605 (May 1957).

11. G. Novick and V. G. Price, "Measurement and Control of Harmonic and Spurious Microwave Energy," General Electric Microwave Lab., Palo Alto, California, Final Report, Phase III, Contract AF 30(602)-1670, ASTIA Document No. AD-214430 (May 15, 1959). RADC TR-59-172.

12. V. C. Price, J. P. Rooney, R. H. Stone, "Measurement and Control of Harmonic and Spurious Microwave Energy," General Electric Microwave Laboratory, Palo Alto, California, Final Report, Change A, Contract AF 30(602)-1670 (March 1960).

13. V. G. Price, R. H. Stone, J. P. Rooney, "Measurement and Control of Harmonic and Spurious Microwave Energy," General Electric Microwave Laboratory, Palo Alto, California, Final Report, Phase II, ASTIA Document No. AD-214430 (March 1959).

14. L. A. MacKenzie, "Klystron Cavities for Minimum Spurious Output Power," Research Report No. EE418, School of Electrical Engineering, Ithaca, N.Y., Cornell University, (January 31, 1959).

15. K. Tomiyasu and M. P. Forrer, "Diode Oscillation in High-Voltage Klystrons," *IRE Trans.*, PGED-8, pp. 381-386 (September 1961).

16. M. Chodorow, *et al.*, "Design and Performance of a High-Power Pulsed Klystron," *Proc. IRE*, Vol. 41, pp. 1584-1602 (November 1953). See especially p. 1601.

17. K. Tomiyasu, "On the Possibility of Drift-Tunnel Oscillations in High Power Klystrons," *Proc. IRE*, Vol. 49, pp. 1207-1208 (July 1961).

18. J. A. Ruetz and W. H. Yocom, "High-Power Traveling-Wave Tubes for Radar Systems," *IRE Trans.*, PGMIL-5, pp. 39-45 (April 1961).

19. D. G. Dow, "Behavior of Traveling-Wave Tubes Near Circuit Cutoff," *IRE Trans.*, PGED-7, pp. 123-131 (July 1960).

20. L. Young, E. G. Cristal, E. Sharp, and J. F. Cline, "Techniques for the Suppression of Spurious Energy," Final Report, SRI Project 3478, Contract AF 30(602)-2392, Stanford Research Institute, Menlo Park, California (March 1962). RADC-TDR-62-164.

21. K. Tomiyasu, "On Spurious Outputs from High-Power Pulsed Microwave Tubes and Their Control," *IRE Trans.*, *PGMTT*-9, pp. 480-484 (November 1961).

22. E. N. Torgow, "Hybrid Junction-Cutoff Waveguide Filters," *IRE Trans.*, *PGMTT*-7, pp. 163-167 (January 1959).

23. E. G. Cristal, L. Young, and B. M. Schiffman, "Suppression of Spurious Frequencies," Quarterly Progress Report 3, SRI Project 4096, Contract AF 30(602)-2734, Stanford Research Institute, Menlo Park, California (January 1963)

24. B. J. Duncan and B. Vafiades, "Design of Full Waveguide Bandwidth High-Power Isolator," *IRE Trans.*, *PGMTT*-6, pp. 411-414 (October 1958).

25. L. Young, "The Application of Branch-Guide Couplers to the Suppression of Spurious Frequencies," *Proceedings of the IRE-PGRFI* Fourth National Symposium on Radio Frequency Interference, San Francisco, California (June 1962).

26. L. Gould, "Handbook on Breakdown of Air in Waveguide Systems," Microwave Associates Report, Contract NObsr-63295 (Navy Department, Bureau of Ships), (April 1956). See also L. Gould and L. W. Roberts, "Breakdown of Air at Microwave Frequencies," *J. Appl. Phys.*, Vol. 27, pp. 1162-1170 (October 1956).

27. D. Dettinger and R. D. Wengenroth, "Microwave Breakdown Study," Final Engineering Report, Wheeler Laboratories, Great Neck, New York, Contract NObsr-52601, ASTIA No. AD 11121 (January 1953).

28. G. K. Hart and M. S. Tannenbaum, "High Power Breakdown of Microwave Components," IRE Convention Record, Part 8, pp. 62-67 (March 1955).

29. G. K. Hart, F. R. Stevenson and M. S. Tannenbaum, "High Power Breakdown of Microwave Structures," IRE Convention Record, Part 5, pp. 199-205 (March 1956).

30. W. S. Boyle, P. Kisliuk and L. Germer, "Electrical Breakdown in High Vacuum," *J. Appl. Phys.*, Vol. 26, pp. 720-725 (June 1955).

31. H. A. Wheeler and H. L. Bachman, "Evacuated Waveguide Filter for Suppressing Spurious Transmission from High-Power S-Band Radar," *IRE Trans.*, *PGMTT*-7, pp. 154-162 (January 1959). Correction to above article, *IRE Trans.*, *PGMTT*-7, 3, p. 369 (July 1959).

32. M. P. Forrer and C. Milazzo, "Duplexing and Switching with Multipactor Discharges," *Proc. IRE* 50, pp. 442-450 (April 1962).

33. H. A. Wheeler, "Pulse Power Chart for Waveguides and Coaxial Line," Wheeler Monograph No. 16 (April 1953).

34. G. L. Ragan, "Microwave Transmission Circuits," M.I.T. Rad. Lab. Series, Vol. 9 (McGraw-Hill Book Co., New York, N.Y., 1946).

35. S. B. Cohn, "Rounded Corners in Microwave High Power Filters and Other Components," Tech. Note 1, SRI Project 2797, Contract AF 30(602)-1998, Stanford Research Institute, Menlo Park, California (June 1960). Also published as "Rounded Corners in Microwave High-Power Filters," *IRE Trans.*, *PGMTT*-9, pp. 389-397 (September 1961).

36. H. E. King, "Rectangular Waveguide Theoretical CW Average Power Rating," *IRE Trans.*, *PGMTT*-9, pp. 349-357 (July 1961).

37. W. W. Macalpine, "Heating of Radio Frequency Cables," *Electrical Communication* 25, pp. 84-99 (March 1948).

38. E. M. T. Jones, "A Three-Cavity High-Power L-Band Filter Tunable from 1250-1350 Mc," Tech. Note 2, SRI Project 2797, Contract AF 30(602)-1998, Stanford Research Institute, Menlo Park, California (February 1961).

39. S. B. Cohn, "Design Considerations for High Power Microwave Filters," *IRE Trans.*, *PGMTT*-7, pp. 149-153 (January 1959).

40. L. Young, "Peak Internal Fields in Direct-Coupled-Cavity Filters," *IRE Trans.*, *PGMTT*-8, pp. 612-616 (November 1960).

41. L. Young, "Analysis of a Transmission Cavity Wavemeter," *IRE Trans.*, *PGMTT-8*, pp. 436-439 (July 1960).

42. L. Young, "Q-Factors of a Transmission Line Cavity," *IRE Trans.*, *PGCT-4*, pp. 3-5 (March 1957).

43. L. Young, *et al.*, "Suppression of Spurious Frequencies," Quarterly Progress Reports 1 and 2, SRI Project 4096, Contract AF 30(602)-2734, Stanford Research Institute, Menlo Park, California (July and October 1962).

44. E. L. Ginston, *Microwave Measurements*, p. 366 (McGraw Hill Book Co., Inc., New York City, New York, 1957).

45. E. D. Sharp, "A High-Power, Wide-Band Waffle-Iron Filter," Tech. Note 2, SRI Project 3478, Contract AF 30(602)-2392, Stanford Research Institute, Menlo Park, California (January 1962). RADC-TDR-62-183. To be published in *IRE Trans.*, *PGMTT*.

46. H. Guthart and E. M. T. Jones, "A High-Power S-Band Waffle-Iron Filter," Tech. Note 4, SRI Project 2797, Contract AF 30(602)-1998, Stanford Research Institute, Menlo Park, California (March 1961). Also published as "A High Power S-Band Filter," *IRE Trans.*, *PGMTT-10*, pp. 148-149 (March 1962).

47. V. Mat, "Absorptive Filters for Microwave Harmonic Power," *Proc. IRE.* Vol. 47, pp. 1762-1769 (October 1959).

48. V. G. Price, *et al.*, "Harmonic Suppression by Leaky-Wall Waveguide Filter," 1959 IRE WESCON Convention Record, Part 1, pp. 112-118.

49. V. G. Price, J. P. Rooney, and R. H. Stone, "Measurement and Control of Harmonic and Spurious Microwave Energy," Final Report, Change A, Contract AF 30(602)-1670, RADC TR-60-77, General Electric Microwave Laboratory, Power Tube Department, Palo Alto, California (March 1960).

50. E. G. Cristal, "Some Preliminary Experimental Results on Coaxial Absorption Leaky-Wave Filters," *Proceedings of the IRE-PGRFI Fourth National Symposium on Radio Frequency Interference*, San Francisco, California (June 1962).

    A more detailed treatment is given in "Coaxial Absorption Leaky-Wave Filter," Tech. Note 4, SRI Project 3478, Contract AF 30(602)-2392, Stanford Research Institute, Menlo Park, California (February 1962), RADC-TDR-62-184; and in Quarterly Progress Report 3, SRI Project 4096, Contract AF 30(602)-2734 (January 1963), Ref. 23.

OTHER REFERENCES ON HIGH-POWER FILTERS

A high-power filter using radial lines and uniform line discontinuities to increase the power capacity, is described by:

51. J. H. Vogelman, "High-Power Microwave Filters," *IRE Trans.*, *PGMTT-6*, pp. 429-439 (October 1958). See also *IRE Trans.*, *PGMTT-7*, pp. 461-465 (October 1959).

A branching filter with the circuit of Fig. 15.01-3(a), but using waveguide high-pass filters, is described by:

52. L. Young and J. Q. Owen, "A High Power Diplexing Filter," *IRE Trans.*, *PGMTT-7*, pp. 384-387 (July 1959).

The measurement of harmonic power should precede the choice and design of filter. One method is described by:

53. E. D. Sharp and E. M. T. Jones, "A Sampling Measurement of Multimode Waveguide Power," *IRE Trans.*, *PGMTT-10*, pp. 73-82 (January 1962), and another method is given in Ref. 4.

The former gives the harmonic power levels; the latter gives the spectral as well as the mode distribution, but requires a digital computer to compile the data.

A way to change the mode distribution with time, and then by time-averaging measure the spectral distribution of the harmonic output from a transmitter, has been described by:

54. V. G. Price and W. A. Edson. "Mode Scattering Technique for Interference Measurements," *IRE-PGRFI Fourth National Symposium on Radio Frequency Interference*, San Francisco, California (June 1962).

Electrical Breakdown in Vacuum is treated by:

55. L. Cranberg, "The Initiation of Electrical Breakdown in Vacuum," *J. Appl. Phys.*, Vol. 23, pp. 518-522 (May 1952), and

56. W. S. Boyle, P. Kisliuk, and L. H. Germer, "Electrical Breakdown in High Vacuum," *J. Appl. Phys.*, pp. 720-725 (June 1958).

The following is a tutorial paper:

57. S. C. Brown, "High-Frequency Gas-Discharge Breakdown," *Proc. IRE*, Vol. 39, pp. 1493-1501 (December 1951).

Further data on high-power, wide-band waffle-iron filters will be found in:

58. L. Young and B. M. Schiffman, "New and Improved Types of Waffle-Iron Filters," to be published in *Proc. IEE* (London).

CHAPTER 16

MULTIPLEXER DESIGN

SEC. 16.01, INTRODUCTION

As was discussed in Sec. 1.02, filters connected in parallel or in series are often needed in order to split a single channel carrying many frequencies into a number of separate channels carrying narrower bands of frequencies. Similar filter groups are often required also for the inverse process of summing a number of channels carrying different bands of frequencies so that all of the frequencies can be put in a single broad-band channel without loss of energy (which would otherwise occur due to leakage of energy from any one of the input channels into the other input channels).

Figure 16.01-1 shows a three-channel multiplexer which would use three separate band-pass filters, one to provide the 2.0- to 2.6-Gc channel, a second to provide the 2.6- to 3.3-Gc channel, and a third to provide the 3.3- to 4.0-Gc channel. It might at first appear that the design of this multiplexer could easily be accomplished by designing the filters using any of the band-pass filter design procedures previously discussed in this book, and then connecting the filters in parallel. However, though the procedures previously discussed are useful for multiplexer design, they should be used along with special techniques in order to avoid undesirable interaction between the filters, which could result in very poor performance.
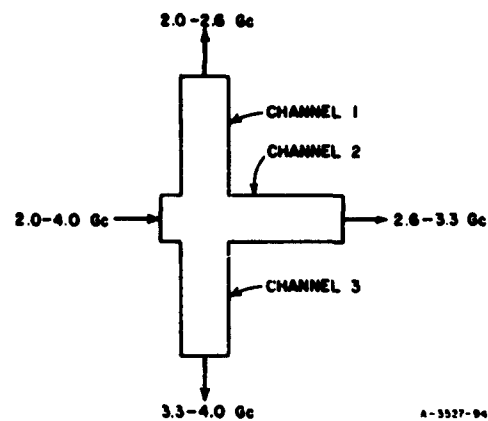
FIG. 16.01-1 A THREE-CHANNEL MULTIPLEXING FILTER GROUP

957

Most of the discussions in this chapter relate to the problem of design so as to eliminate such undesirable interaction effects. However, the constant-resistance-filter approach discussed in the next section avoids this problem entirely by using directional-filter units which have matched, constant-resistance input impedances at all frequencies so that in theory no interaction effects should occur.

SEC. 16.02, MULTIPLEXERS USING DIRECTIONAL FILTERS

The directional filters discussed in Chapter 14 have a constant-resistance input impedance provided that their output ports are terminated in their proper resistance terminations. Filters of this sort, when all designed for the same terminating resistance, can be cascaded as shown in Fig. 16.02-1 to form a multiplexer which in theory completely avoids the filter interaction problem mentioned in Sec. 16.01.
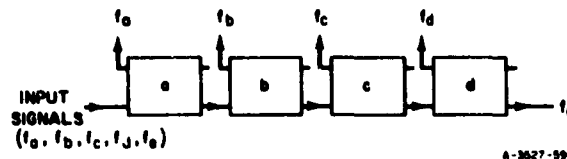
FIG. 16.02-1   EXAMPLE OF DIRECTIONAL FILTERS USED
FOR MULTIPLEXING

Each filter provides the proper termination for its neighbor, so that to the extent that there are no residual VSWR's due to design and manufacturing imperfections, the system is reflectionless. In Fig. 16.02-1, Filter a removes all of the energy at frequency f_a, but passes on the energy at all other frequencies. Filter b removes the energy at frequency f_b and so on.

The use of directional filters for multiplexing is a conceptually simple and elegant way of solving the multiplexer problem. In many cases it is also a very practical way of dealing with multiplexing problems, though by no means always the most practical way. Each filter will generally have some parasitic VSWR, which will affect the system significantly if many filters are to be cascaded. However, probably

the greatest practical drawback of directional filters is that each
resonator of each filter has two different orthogonal modes, and if
more than one or two resonators are required per filter, the tuning of
the filters may be difficult. Although an effort is made to tune the
two modes of each resonator independently with separate sets of tuning
screws, the tuning screws for one mode generally have some effect on
the other mode, so that some iteration in the tuning process is generally
required. Thus, if there are more than, say, two resonators per filter,
the fact that the two modes in each resonator must be tuned separately,
along with unavoidable interaction effects in the tuning mechanism, can
make the tuning process quite time consuming.

Figure 16.02-2 shows another form of directional filter which also
has the constant-resistance input properties exhibited by the filters
in Chapter 14.[1,2,3] In this circuit two hybrid junctions are used, such
as the 3-db couplers in Sec. 13.03, the 3-db branch-guide couplers
treated in Secs. 13.12 and 13.13, short-slot hybrids, or Magic-T's. In
the case of the Magic-T, an extra quarter-wavelength of line is required
on one of the side ports of the hybrid in order to give the desired
90-degree phase difference between the outputs of the side ports of the
hybrid. In Fig. 16.02-2, the required phase relations for transmission
between the various ports is indicated by arrows and numbers.
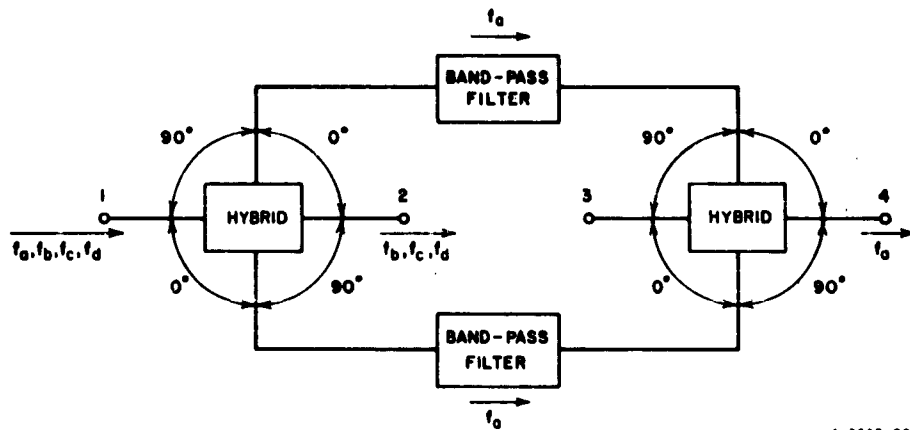
A-3527-597

FIG. 16.02-2 A TYPE OF DIRECTIONAL FILTER FORMED FROM TWO BAND-PASS
FILTERS AND TWO HYBRIDS

959

Besides the hybrid junctions, the circuit in Fig. 16.02-2 also uses two identical band-pass filters which are designed to pass some frequency f_a, which the circuit is to separate from other frequencies. Thus, if four frequencies f_a, f_b, f_c, and f_d are introduced at Port 1, the energy at frequency f_a is divided equally between the two side arms of the hybrid on the left, it passes through the two band-pass filters, and on into the side arms of the hybrid on the right. Because of the phase relations of the two components, the signal cancels to zero at Port 3, and all of the energy at frequency f_a emerges from Port 4. Meanwhile the other frequencies f_b, f_c, and f_d are reflected by the band-pass filters and they re-enter the side arms of the hybrid on the left. Because of the phase relation, the components cancel at Port 1 and all of the energy at these frequencies emerges from Port 2. The over-all performance of this circuit is just like that of the directional filters in Chapter 14, and filter circuits of this type may also be cascaded as indicated in Fig. 16.02-1.

The circuit in Fig. 16.02-2 will usually be much easier to adjust than the directional filters in Chapter 14, if there are very many resonators per filter. The two identical band-pass filters can be tuned separately, and the performance of the hybrid junctions is not particularly critical. For example, if the power split of the hybrid junction is not equal, and, say, is so bad that twice as much power comes out one side arm as comes out the other, the net result if both hybrids are identical will be to introduce only 0.5 db of attenuation in the transmission from Port 1 to Port 4. The circuit in Fig. 16.02-2 has the drawback, however, of being physically quite complicated and in many cases quite bulky.

In summary, directional filters with their constant-resistance input properties provide attractive possibilities for use in multiplexers. However, they also have appreciable practical drawbacks. In any given design situation their merits and drawbacks should be weighed against those of other possible multiplexer techniques.

SEC. 16.03, MULTIPLEXERS USING REFLECTING NARROW-BAND
FILTERS, WITH GUARD BANDS BETWEEN CHANNELS

If the channels of a multiplexer are quite narrow (say, of the order of 1 percent bandwidth or less) and if the channels are separated by guard bands which are several times the pass-band width of the

960

individual filters (or more), then various relatively simple decoupling techniques should work quite well for preventing harmful interaction between filters.

One method is shown in Fig. 16.03-1.[1,4] In this figure a three-channel waveguide multiplexer is shown; the individual filters are of the iris-coupled type discussed in Secs. 8.06 and 8.07. At frequency f_a, the filter on the right has a pass band while the other two filters are in their stop bands. Since the filters are of relatively narrow bandwidth, the first resonator of both the upper and the lower filter is relatively loosely coupled to the main waveguide, hence the input coupling irises of these two filters introduce only small reactive discontinuities in the main waveguide. These discontinuities will disturb the response of the filter on the right a little, and if this is objectionable, it can be compensated for by small corrections in the tuning and input coupling of the first resonator of the filter on the right.
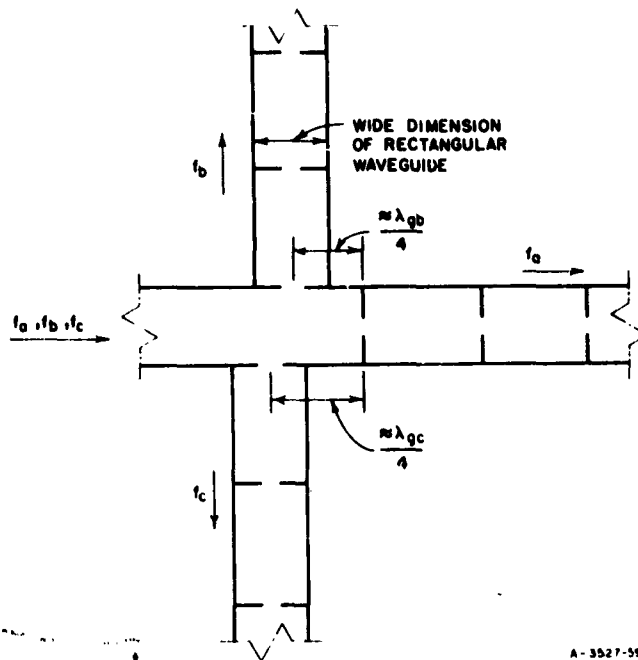
FIG. 16.03-1   A MULTIPLEXER WITH NARROW-BAND WAVEGUIDE
FILTERS MOUNTED SO AS TO ELIMINATE FILTER
INTERACTION

961

At frequency f_b the upper filter in Fig. 16.03-1 has a pass band while the other filters have stop bands and reflect small reactances to the main quide. If the upper filter is placed approximately one-quarter guide-wavelength (at frequency f_b) from the input iris of the filter on the right, the filter on the right will reflect an open circuit to the plane of the coupling iris. (Actually, because of the residual reactances, somewhat less than a quarter wavelength should be best.) Thus, the filter on the right will be completely decoupled, and the energy at frequency f_b will flow relatively undisturbed out through the upper filter. There will usually be some residual junction effects to disturb the performance of the upper filter a little. Again, these effects can be compensated for by small corrections in the input coupling iris size and in the tuning of the first resonator of the upper filter.

The lower filter is coupled to the main waveguide in a similar manner. If it is desired to add more channels, they can be mounted on the main waveguide at additional points corresponding to various odd multiples of $\lambda_g/4$ from the filter on the right in Fig. 16.03-1 (where λ_g is in each case the guide wavelength at the midband frequency of the filter in question).

Figure 16.03-2 shows another decoupling technique, which has been proposed by J. F. Cline.[6] Although the circuits have been drawn in lumped-element form, they can be realized in a variety of more or less equivalent microwave forms. In this case the filters are again assumed to be narrow band, with guard bands between channels. However, in this case decoupling between filters is achieved by a decoupling resonator adjacent to each filter. Since the filters are narrow band, their coupling to the main transmission line is quite loose, and the coupling between the decoupling resonator and the main line is also quite loose. Each decoupling resonator is tuned to the pass-band center frequency of its adjacent filter. Because of their loose couplings the filters and the decoupling resonators have very little effect on transmission when they are off resonance. Suppose that a signal of frequency f_2 enters the circuit. It will pass the f_1 filter and the f_1 decoupling resonator with very little reflection and go on to the f_2 filter and decoupling resonator. The decoupling resonator is a band-stop resonator and in the upper circuit of Fig. 16.03-2 the f_2 decoupling resonator circuit will short-circuit the entire circuit to the right, while in the case of the lower circuit of Fig. 16.03-2 the decoupling resonator open-circuits the entire circuit

SERIES CONNECTION

SHUNT CONNECTION

RA-3527-569
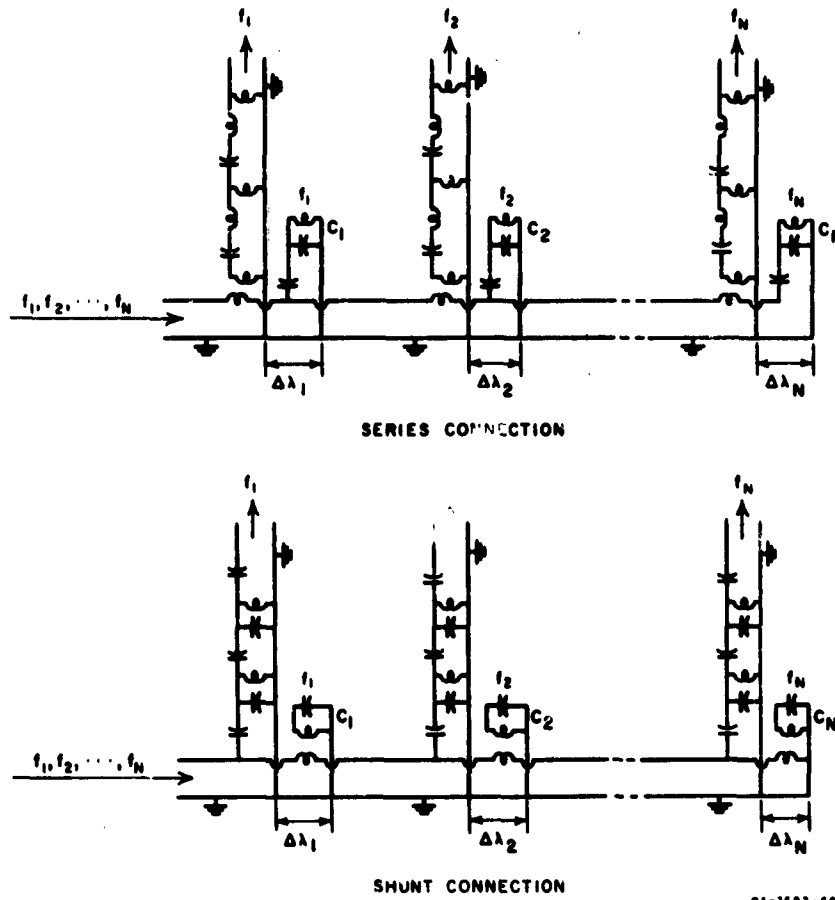
SOURCE: Final Report, Contract AF 19(606)-2247, SRI
(see Ref. 6 by J. F. Cline, et al.)

FIG. 16.03-2   MULTIPLEXERS USING DECOUPLING RESONATORS
In the upper structure filters with inductively coupled resonators are
used, while the decoupling resonators are capacitively coupled. In
the lower circuit the reverse is true.

963

to the right. In this manner the energy is channelled to the desired
filter with a minimum of interaction effects. Note that in this case
the spacing between filters is not critical, so that this multiplexing
technique is particularly useful where it must be possible to tune the
various filters over a range of frequencies. In the figure the spacing
$\Delta\lambda_k$ between each filter and its decoupling resonator is assumed to be
made as small as possible in order to avoid undesirable transmission-
line effects. Residual reflections in the system can be largely compen-
sated for by small adjustments of the tuning of the first resonator of
each filter, and of the coupling between the transmission line and the
input of each filter.

A possible way for utilizing the principle in Fig. 16.03-2 for
waveguide filters is suggested in Fig. 16.03-3. The band-pass filter
shown is of the iris-coupled type discussed in Secs. 8.06 and 8.07. The
decoupling resonator is of the waveguide band stop type discussed in
Chapter 12. The band-stop resonator presents a very large series
reactance when it is resonant, but this resonator is located a quarter-
guide-wavelength from the band-pass filter so that when looking right
from the band-pass filter a very large shunt susceptance will be seen
when the filter and band-stop resonator are resonant. The filter, being
series-connected will then receive all of the energy at frequency f_a,
and any circuits to the right will be completely decoupled. Just outside
of the pass band of the band-pass filter, the first resonator of the
band-pass filter will present reactances to the main waveguide which
are similar in nature to those presented by the band-stop resonator.
Thus at frequencies off f_a, the structure functions almost exactly like
a two-resonator band-stop filter of the form in Fig. 12.08-1, operating
in its pass band. It should be possible to design the band-stop res-
onator using the band-stop filter techniques discussed in Chapter 12.
(The band-pass filter is replaced mathematically by a band-stop resonator
having a similar off-resonance reactance characteristic, and the decoupling
resonator represents the second band-stop resonator.) Using this approach
the band-pass filter and band-stop resonator combination could present a
well-controlled low VSWR at frequencies off f_a, just as occurs in prop-
erly designed two-resonator band-stop filters.

The approach suggested in Fig. 16.03-2 and 16.03-3 looks especially
attractive if very many channels are to be multiplexed, because using
this approach the individual band-pass filter and decoupling resonator
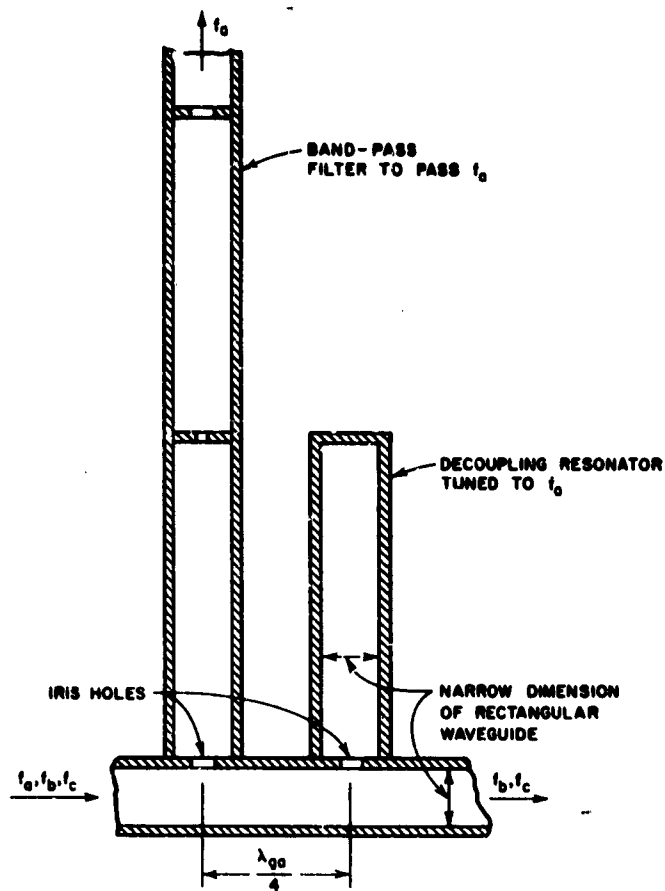
FIG. 16.03-3 A POSSIBLE METHOD FOR REALIZING DECOUPLING
RESONATORS IN A WAVEGUIDE MULTIPLEXER

units can be developed and tested separately, and then connected
together more or less as is convenient. Strip-line, coaxial-line, and
semi-lumped-element forms of these structures are also possible.

SEC. 16.04, MULTIPLEXERS WITH CONTIGUOUS PASS BANDS*

The multiplexers discussed in the preceding section were assumed
to have guard bands separating the various operating channel bands.

---

*The design equations and trial designs in this section were worked out by E. G. Cristal.

965

The multiplexers to be discussed in this section, however, are assumed to have contiguous channels so that channels which are adjacent have attenuation characteristics which typically cross over at their 3 db points. Most diplexers are simply two-channel versions of multiplexers, so the same principles apply to them. However, some additional comments with respect to diplexer design will be found in Sec. 16.05.

Figure 16.04-1 shows a schematic drawing which consists of N channels composed of specially designed band-pass filters. The channels are connected in parallel, and a susceptance-annulling network is added in shunt to help provide a nearly constant total input admittance Y_{TN} which approximates the generator conductance G_g, across the operating band of the multiplexer. Figure 16.04-2 shows the analogous case of a series-connected multiplexer. Since the series case is the exact dual of the shunt case, so that the same principles apply to both, our attention will be confined largely to the shunt case. However, it should be understood that the same remarks apply to series-connected multiplexers simply by replacing admittances by impedances, parallel connections by series connections, and the filters and annulling networks used for parallel connections by their duals.

The singly terminated low-pass filter Tchebyscheff prototypes discussed and tabulated in Sec. 4.06 are very useful for use in the design of band-pass filters for multiplexers of this type. Consider the singly terminated low-pass filter circuit in Fig. 16.04-3, which is driven by a zero-impedance generator at the right end and which has a resistor termination only at the left end. As was discussed in Sec. 4.06, the power delivered to the load on the left in this circuit is given by

$$P = |E_g|^2 \, \text{Re} \, Y_k' \qquad (16.04\text{-}1)$$

where Y_k' is the admittance seen from the generator. Thus if the filter has a Tchebyscheff transmission characteristic, Re Y_k' must also have a Tchebyscheff characteristic. Figure 16.04-4 shows typical Re Y_k' characteristics for Tchebyscheff filters designed to be driven by zero-impedance generators. Notice that in the figure a low-pass prototype filter parameter g_{n+1}'' is defined. This parameter will be referred to later with regard to the details of multiplexer design. However, it should be noted at this point that either g_{n+1}'' or its reciprocal corresponds to the geometric mean between the value of Re Y_k' at the top of the
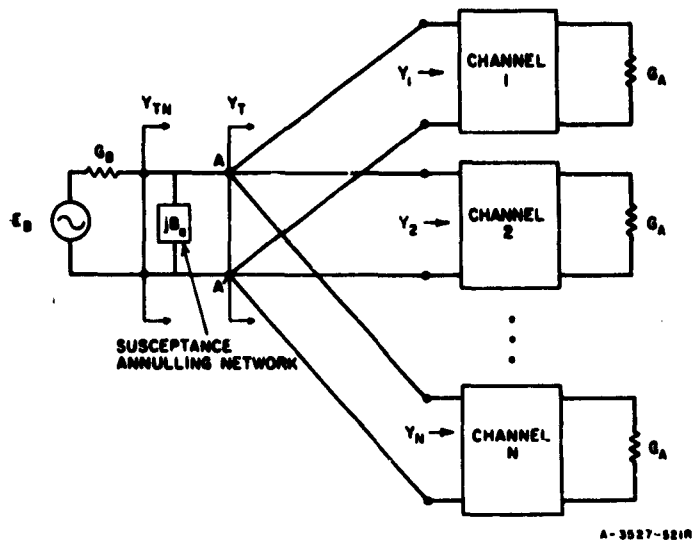
FIG. 16.04-1   A PARALLEL-CONNECTED MULTIPLEXER
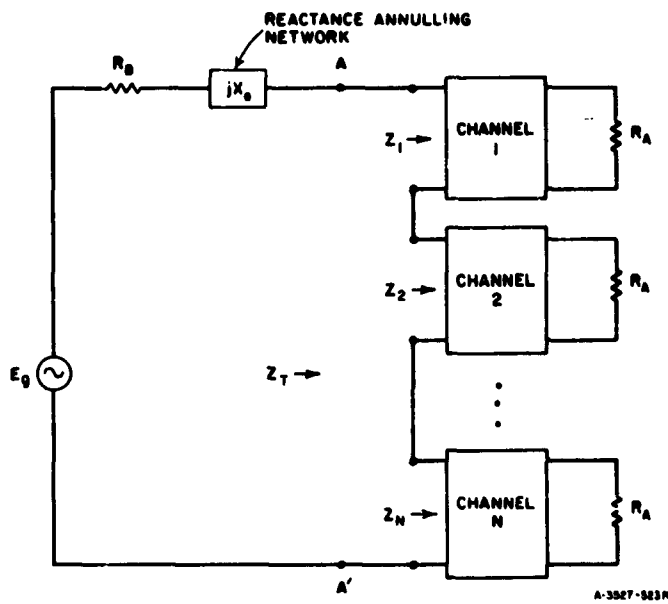
FIG. 16.04-2   A SERIES-CONNECTED MULTIPLEXER

967

$\omega_1' = $ PASS-BAND EDGE FREQUENCY
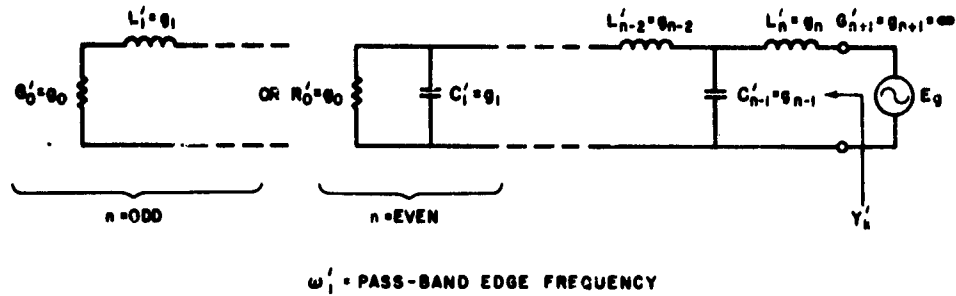
A-3527 527R

FIG. 16.04-3   A LOW-PASS PROTOTYPE FILTER DRIVEN BY A ZERO-IMPEDANCE
GENERATOR
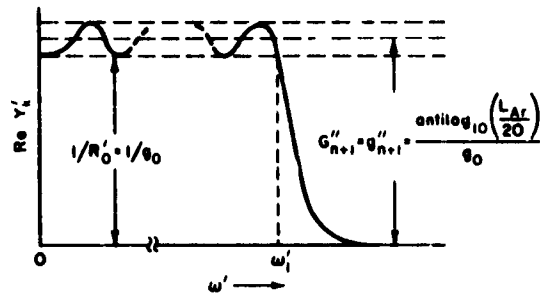
(a) CASE OF n EVEN

$L_{Ar} = $ TCHEBYSCHEFF ATTENUATION RIPPLE OF SINGLY
LOADED PROTOTYPE IN db
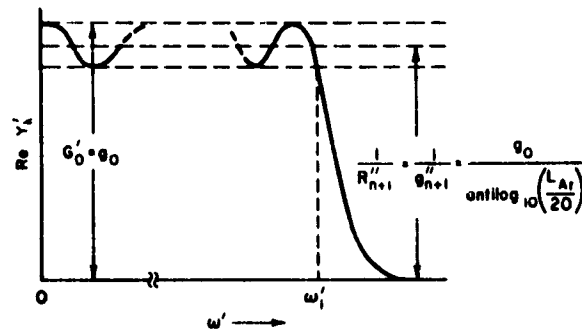
(b) CASE OF n ODD

A-3527-528R

FIG. 16.04-4   REAL PART OF THE INPUT ADMITTANCE
FOR TCHEBYSCHEFF FILTERS OF THE
TYPE IN FIG. 16.04-3

ripples and Re Y'_b at the bottom of the ripples. This admittance level
for the low-pass prototype is analogous to the terminating admittance
G_B in Fig. 16.04-1, for the actual multiplexer with band-pass filters.
That is, by the methods of this section the multiplexer is to be
designed to have a Tchebyscheff Re Y_{TN} characteristic with G_B equal to
the mean value of the ripples.

The principles of this design procedure are most easily understood
in terms of an example. Consider the comb-line filter in Fig. 16.04-5
(which can be designed by a modified version of the comb-line filter
design techniques discussed in Secs. 8.13 and 8.14). In this figure
the filter has been designed to include a fine-wire high-impedance line
at the right end, for coupling to the common junction of the multiplexer.
This type of coupling to the main junction has the advantage of relieving
possible crowding of the filters at the common junction. Other coupling
methods, such as series, capacitive-gap coupling, could also be used.
However, it should be noted that although numerous types of filter
structures and structures for coupling to the common junction are possible,
these structures must be of the sort which tends to give a small suscep-
tance in the stop bands, if the filters are to be connected in parallel.
If the filters were of the type to present large susceptances in their
stop bands, they would tend to short-circuit the other filters.

A four-resonator, 10-percent-bandwidth filter design was worked out
for a comb-line filter as shown in Fig. 16.04-5 using an $n = 4$ singly
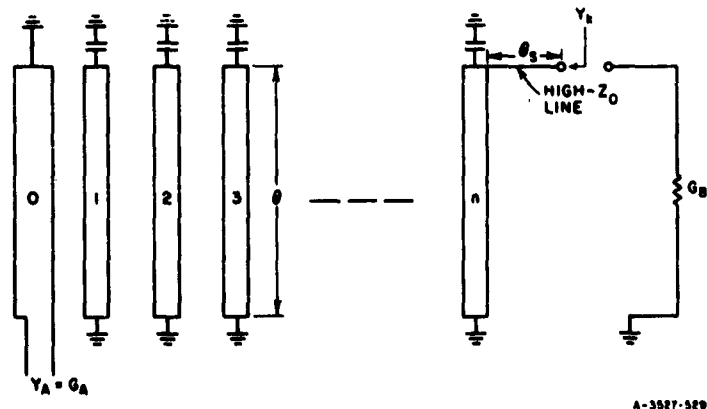
FIG. 16.04-5 A POSSIBLE COMB-LINE FILTER CONFIGURATION
FOR USE IN MULTIPLEXERS

969
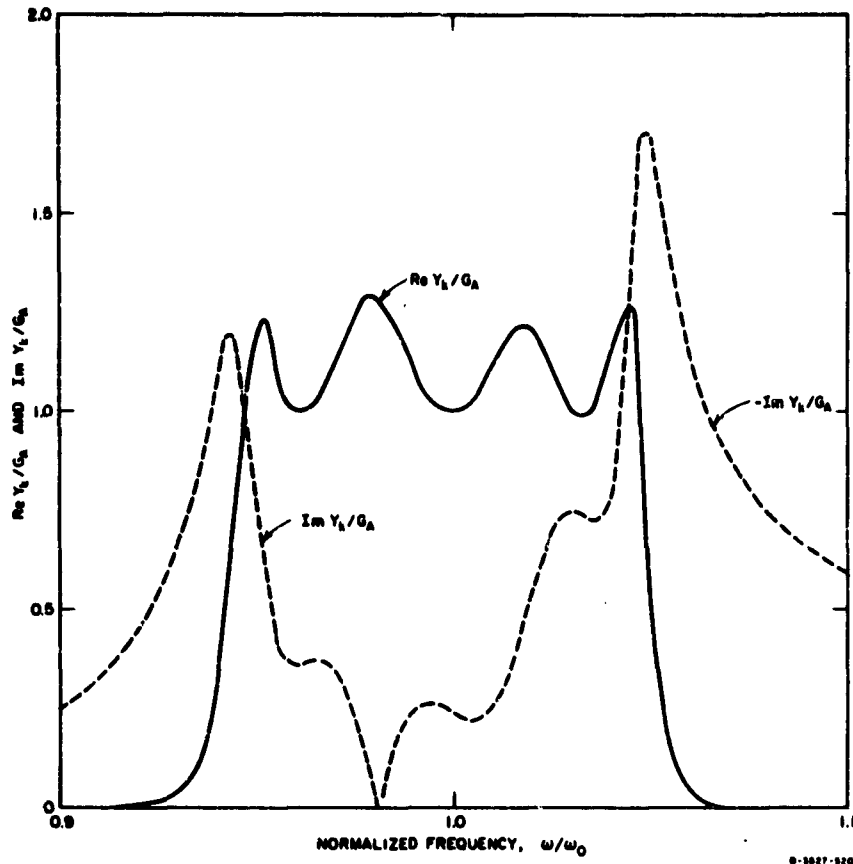
FIG. 16.04-6 COMPUTED INPUT ADMITTANCE CHARACTERISTIC OF A
COMB-LINE MULTIPLEXER FILTER AS SHOWN IN FIG. 16.04-5
This filter has four resonators

terminated prototype having 1-db ripple. (The prototype element values
were obtained from Table 4.06-2). This filter design was expressed in
an approximate form similar to that in Fig. 8.14-1, and its input
admittance Y_A was computed using a digital computer. The results are
shown in Fig. 16.04-6, normalized with respect to G_A. Note that
Re Y_A /G_A is very nearly perfectly Tchebyscheff, while in the pass band
the slope of Im Y_A/G_A is negative on the average. (Note that the right
half of the dashed curve is for negative values.)

    If band-pass filters with input admittance characteristics such
as that in Fig. 16.04-6 are designed to cover contiguous bands, and if
they are designed so that the Re Y_A/G_A characteristics of adjacent

970

filters overlap at approximately their Re Y_k/G_A = 0.5 points or slightly below, then their total input admittance $Y_T = Y_1 + Y_2 + Y_3 \ldots + Y_N$, when they are paralleled, will also have an approximately Tchebyscheff real-part characteristic. This was done in the example in Fig. 16.04-7(a). This figure shows the computed real-part characteristic for three paralleled, comb-line filters with contiguous pass bands, where the individual filters have input admittance characteristics as shown in Fig. 16.04-6 except for a shift in frequency. Figure 16.04-7(b) shows the corresponding $Im\ Y_T/G_A$ characteristic for this three-channel design.

Note that the $Im\ Y_T/G_A$ characteristic in Fig. 16.04-7(b) is negative on the right side of the figure, and that on the average the slope of the curve is negative throughout the operating band of the multiplexer. Since, by Foster's reactance theorem, the susceptance slope of a lossless network is always positive, the operating-band susceptance in Fig. 16.04-7(b) with its average negative slope can be largely cancelled by adding an appropriate lossless shunt branch (which will have a positive susceptance slope). In this case a susceptance-annulling branch could consist of a short-circuited stub of such a length as to give resonance at the normalized frequency ω/ω_0 = 1.02, where the $Im\ Y_T/G_A$ curve in Fig. 16.04-7(b) is approximately zero. Estimates indicate that if the stub had a normalized characteristic admittance of Y_a/G_A = 3.8502, the susceptance slope of the annulling network should be about right. Figure 16.04-8 shows the normalized susceptance Y_{TN}/G_A (Fig. 16.04-1) after the susceptance-annulling network has been added. Note that although $Im\ Y_{TN}$ has not been completely eliminated, it has been greatly reduced.

Since Re Y_{TN}/G_A = Re Y_T/G_A, the total input admittance Y_{TN} with the annulling network in place is given by Figs. 16.04-7(a) and 16.04-8. To the extent that Y_{TN} approximates a constant, pure conductance across the operating band, G_B and Y_{TN} in Fig. 16.04-1 will act as a resistive voltage divider, and the voltage developed across terminals $A - A'$ will be constant with frequency. Under these conditions the response of the individual filters would be exactly the same as if they were driven by zero-impedance generators (as they were designed to be driven). However, since Y_{TN} only approximates a pure constant conductance, the performance will be altered somewhat from this idealized performance.

The driving generator conductance G_B for the trial multiplexer design was given a normalized value of G_B/G_A = 1.15, which makes the

971
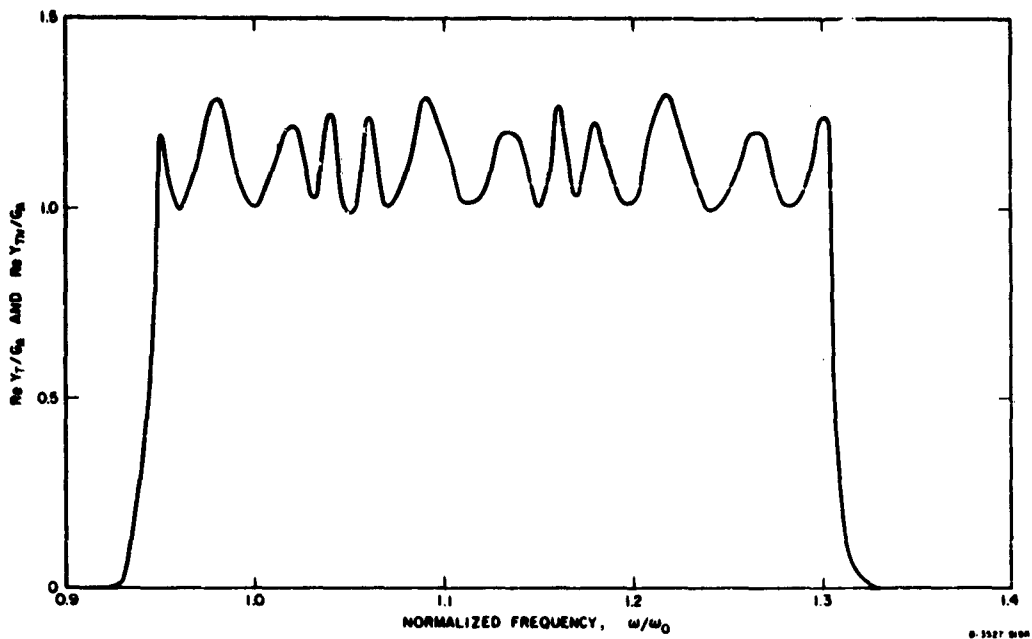
FIG. 16.04-7(a)   Re Y_T/G_A vs. FREQUENCY FOR THREE, PARALLELED,
COMB-LINE MULTIPLEXER FILTERS
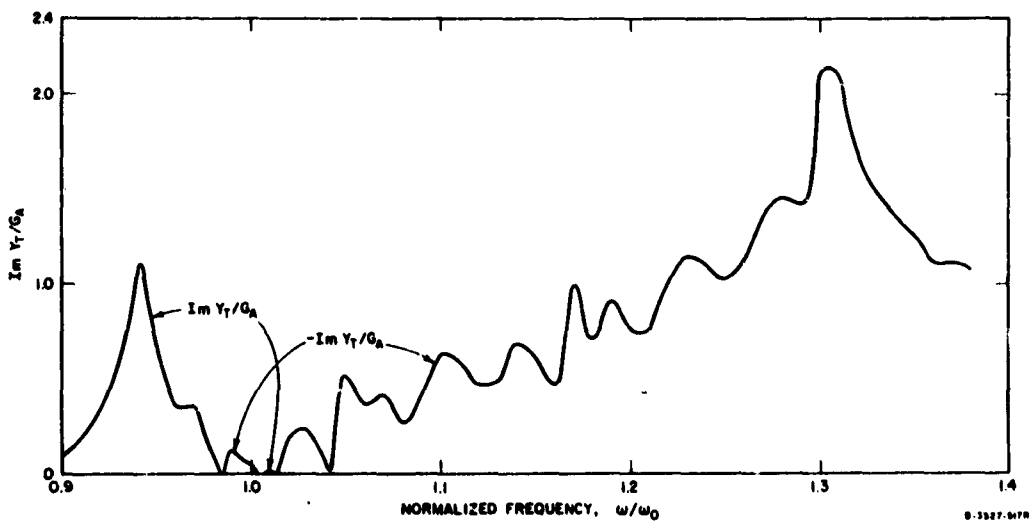
FIG. 16.04-7(b)   Im Y_T/G_A vs. FREQUENCY FOR THREE, PARALLELED,
COMB-LINE FILTERS
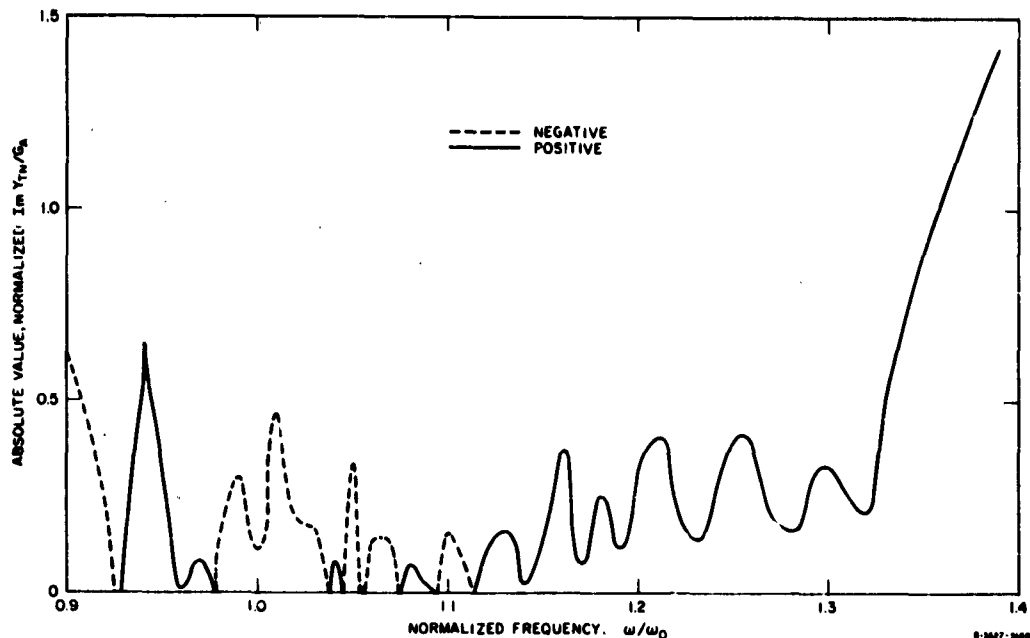
FIG. 16.04-8 Im Y_{TN}/G_A vs. FREQUENCY FOR MULTIPLEXER WITH COMB-LINE FILTERS

generator conductance equal to the mean value of the ripples in
Fig. 16.04-7(a). Figure 16.04-9(a) shows the computed response of the
multiplexer, while Fig. 16.04-9(b) shows the details of the pass-band
response in enlarged scale. Note that the attenuation characteristics
cross over at about the 3-db points, and that though the filters were
designed to have 1-db Tchebyscheff ripple when driven by a zero-impedance
generator, the pass-band attenuation is much less than that in the
completed multiplexer. This is due largely to the fact that adding the
generator internal conductance G_B tends to mask out the variations in
Re Y_{TN}. Also, choosing G_B to be equal to the mean value of Re Y_{TN} in
the operating band tends to reduce the amount of mismatch that will occur.

   Some Practical Details—The discussion of the example above has
laid out the principles of the multiplexer design technique under
consideration. Some steps will now be retraced in order to treat design
details.

   When designing the band-pass channel filters using singly termi-
nated prototype filters such as that in Fig. 16.04-3, the prototype
element values g_0, g_1, ..., g_n, g_{n+1} can be obtained from the tables

973
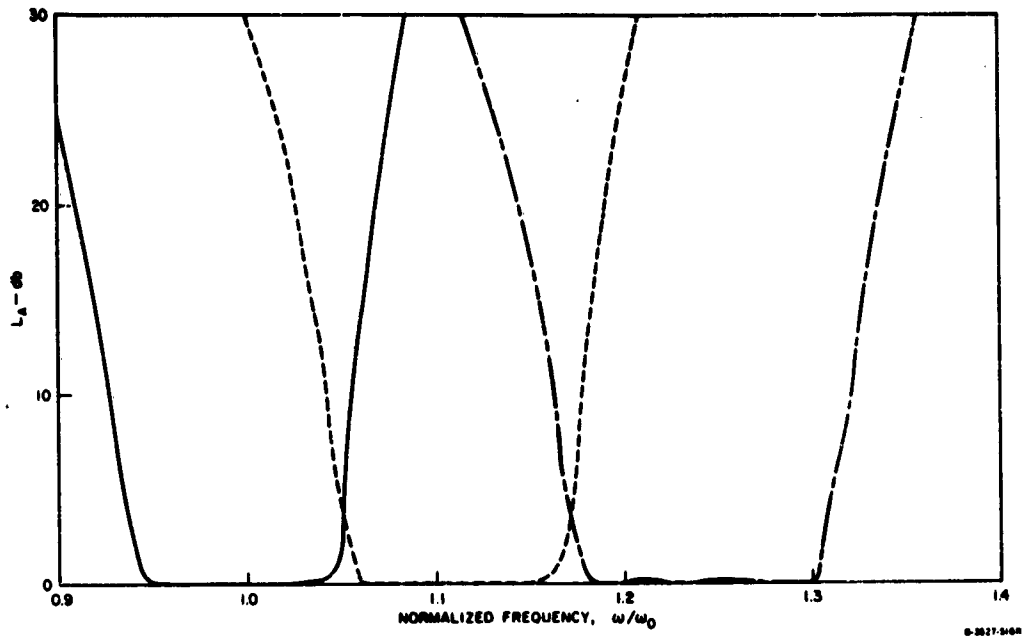
FIG. 16.04-9(a)   COMPUTED CHANNEL ATTENUATION OF MULTIPLEXER WITH
COMB-LINE FILTERS
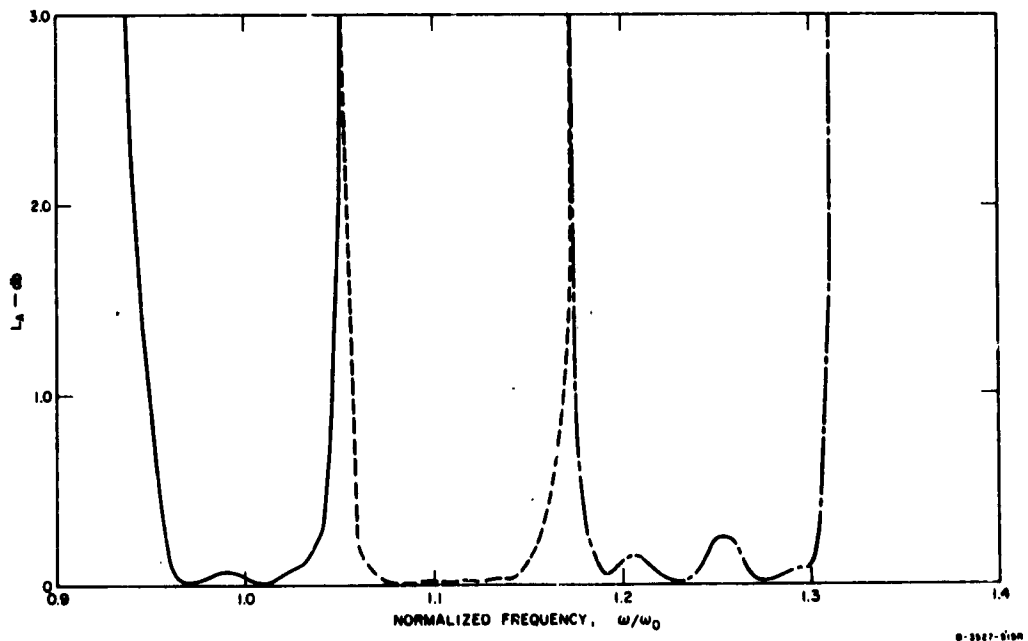
FIG. 16.04-9(b)   DETAILS OF PASS-BAND COMPUTED PERFORMANCE OF
COMB-LINE MULTIPLEXER

974

in Sec. 4.06. Note then in this case $g_{n+1} = \infty$ which corresponds to the infinite-internal-conductance of a zero-impedance voltage generator (or for the dual case, the impedance of an infinite-internal-impedance current generator). In the actual multiplexer the filters will be driven by a finite-internal-impedance generator, so it is convenient to replace $g_{n+1} = \infty$ by g_{n+1}'' defined in Fig. 16.04-4. As has been previously discussed, g_{n+1}'' (or its reciprocal) is a prototype parameter corresponding to the conductance G_B (or the resistance R_B for the dual series-connected case) of the termination to be used at the common junction of the multiplexer.

The band-pass filters for a multiplexer can be designed by the methods of Chapter 8 or Chapter 10, using any of a variety of structures. For example, if a lumped-element structure were desired it could be designed directly from the prototype in Fig. 16.04-3 using the mapping procedure summarized in Fig. 8.02-2(b). The resulting filter would be as shown in Fig. 16.04-10. Note that this filter starts out with a *series* resonator, which will cause the input admittance Y_k to be small in the stop band. This is necessary for a filter to be used in a parallel-connected multiplexer. The dual form of filter which has a *shunt* resonator at its input is appropriate for a series-connected multiplexer. In the cases of filters such as those in Fig. 8.02-3 or 8.02-4 in which the resonators are coupled by J- or K-inverters (Secs. 4.12, 8.02 and 8.03), it is necessary that the inverters next to the common junction of the multiplexer be of the J-inverter type (Fig. 8.03-2) if the filters are to be connected in parallel, and that they be of the K-inverter type (Fig. 8.03-1) if the filters are to be connected in series.
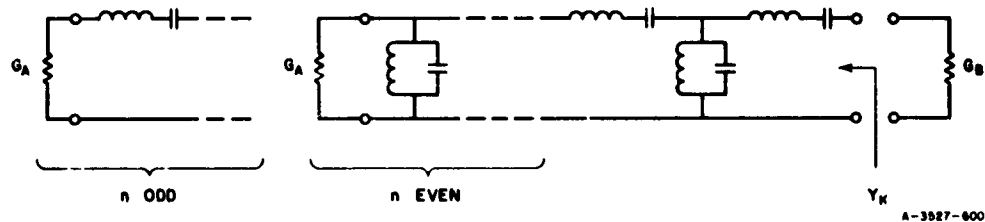
FIG. 16.04-10   A LUMPED-ELEMENT BAND-PASS CHANNEL FILTER .

Most of the design data in Chapters 8 and 10 applies directly to the design of multiplexers without any changes, at least for the case where the desired terminations of the multiplexer are all equal. Some exceptions are the design data in Figs. 8.09-1 and 8.13-1(b), and in Tables 10.02-1 and 10.06-1. These design procedures incorporate special matching end sections which have an effect like referring the desired Y_k (or Z_k) input characteristic through a length of transmission line, which will cause the real part of the input admittance (or impedance) to not have the desired shape. This problem can be overcome by replacing the matching section at the end of the filter which is to be connected to the multiplexer junction by a semi-lumped-element inverter. This is what was done in the case of the comb-line filter in Fig. 16.04-5, where a fine-wire coupling is shown at the right end. This point will be discussed further, later in this section.

After the low-pass prototype filter parameters have been specified there is no choice in the ratio G_A/G_B of the terminations if lumped-element filter designs of the form in Fig. 16.04-10 are to be used. Also, the ratio G_A/G_B is not unity for that case—a situation that could be inconvenient. However, in the case of designs using impedance inverters (as in the generalized cases in Figs. 8.02-3 and 8.02-4) the terminations can be specified as desired, and the J- or K-inverters will provide the necessary impedance transformations. For example, using the data in Fig. 8.02-4, G_A, G_B and the resonator slope parameters b_j can be chosen arbitrarily, and the impedance-matching conditions will automatically come out as is called for by the prototype parameters, g_0, g_1, g_2, $\cdots$ g_n, and g''_{n+1}.

Determination of Fractional Bandwidths So As To Give Desired Cross-Over Frequencies—Since it is usually desirable in the type of multiplexer under discussion for adjacent filters to cross over at their 3-db points, care must be taken in choosing the filter bandwidths to provide for this condition. By adapting Eqs. (4.03-4) and (4.03-5) an explicit expression for Re Y'_k for the singly loaded low-pass prototype filter can be obtained as a function of ω'. Then for n even

$$\left.\frac{\omega'}{\omega'_1}\right|_{\omega' > \omega'_1} = \cosh\left[\frac{1}{n}\cosh^{-1}\sqrt{\frac{1}{\epsilon}\left(\frac{1+\epsilon}{R'_0 \text{ Re } Y'_k} - 1\right)}\right] \qquad (16.04\text{-}2)$$

where

$$\epsilon = \left[\text{antilog}_{10}\left(\frac{L_{Ar}}{10}\right)\right] - 1 \quad , \qquad (16.04\text{-}3)$$

L_{Ar} is the db Tchebyscheff ripple of the prototype filter, R_0' is the termination in Fig. 16.04-3, and Re Y_k' and ω_1' are as indicated in Fig. 16.04-4. Having specified R_0' Re Y_k' = 0.5, corresponding approximately to the 3-db point, then the designer can solve for the corresponding normalized frequency ω'/ω_1'. From this the required fractional bandwidth can be obtained by using the low-pass to band-pass transformation appropriate for the filter structure to be used. For example, suppose that the desired cross-over points are f_a and $f_b > f_a$, and an appropriate mapping function is

$$\frac{\omega'}{\omega_1'} = \frac{2}{w}\left(\frac{f - f_0}{f_0}\right) \qquad (16.04\text{-}4)$$

where

$$f_0 = \frac{f_a + f_b}{2} \quad .$$

Then the required fractional bandwidth is

$$w = 2\left(\frac{f_b - f_0}{f_0}\right)\bigg/\left(\frac{\omega'}{\omega_1'}\right) , \qquad (16.04\text{-}5)$$

where ω'/ω_1' is specified for the desired 3-db point by use of Eq. (16.04-2), provided that n is even. If n is odd, Eq. (16.04-2) becomes

$$\frac{\omega'}{\omega_1'}\bigg|_{\omega' > \omega_1'} = \cosh\left[\frac{1}{n}\cosh^{-1}\sqrt{\frac{1}{\epsilon}\left(\frac{G_0'}{\text{Re }Y_k'} - 1\right)}\right] \quad . \qquad (16.04\text{-}6)$$

Coupling to the Common Junction—Although other means of coupling would have also been possible in the comb-line multiplexer example of this section it was assumed that the filters were coupled to the center junction by series inductances formed from high-impedance wire.

977

Figure 16.04-11 shows a
high-impedance wire and its
equivalent circuit when used
as a J-inverter. The comb-
line filter design equations
discussed in Secs. 8.13 and
8.14 were modified to use
this type of inverter at
one end of the filter. The
susceptance B at one side
of the inverter in
Fig. 16.04-11(b) was compen-
sated for by absorbing it
into Resonator n, while the
susceptance B on the other
side of the inverter was
effectively absorbed into
the susceptance-annulling
network. In this case the
high-impedance-wire type of
coupling was suggested

$$J_{n,n+1} = Y_s \csc \theta \cdot \sqrt{\frac{\theta_a L_n \omega}{\omega_1' \theta_n \theta_{n+1}''}}$$

$$B = Y_s \left[\tan \frac{\theta}{2} - \csc \theta \right]$$

(b)

A-3527-601

FIG. 16.04-11   USE OF A HIGH-IMPEDANCE WIRE
AS A J-INVERTER

because it would help prevent the common junction from being crowded.
However, it is desirable to keep the high-impedance wire quite short in
order to avoid unwanted resonances, while not having it so small in
diameter that it would increase the losses. Thus, in some narrow-band
cases, capacitive-gap couplings to approximate inverters as in
Fig. 8.03-2(b) will be preferable. Table 16.04-1 summarizes the equa-
tions used in the design of the filters for the example of Figs. 16.04-5
to 16.04-9(b).

Figure 16.04-12 shows the general form of another type of multi-
plexer structure once built by one of the authors. This multiplexer
split an octave band into three parts, and used capacitively coupled,
strip-line filters of the form in Fig. 8.05-4(a). Although the filters
used series-capacitance couplings everywhere except at the common junction
of the multiplexer, high-impedance wire coupling (i.e., series-inductance
coupling) was used at the common junction, as indicated in Fig. 16.04-12.
(In this case the wire was bent into a rectangle as shown.) The wire
plus a small section of the adjacent 50-ohm line were regarded as

Table 16.04-1

DESIGN EQUATIONS FOR COMB-LINE FILTERS WITH HIGH-Z_0 WIRE COUPLING
AT ONE END AS SHOWN IN FIG. 16.04-5

Choose a low-pass prototype filter and values for $G_A = Y_A$, $G_B = Y_B$, b_1/Y_A, ..., b_n/Y_A, θ_0, and θ_s.

NORMALIZED MUTUAL CAPACITANCES PER UNIT LENGTH

$$\frac{C_{01}}{\epsilon} = Y_A \frac{376.7}{\sqrt{\epsilon_r}} \left[\frac{w}{\omega_1'} \frac{(b_1/Y_A)}{g_0 g_1} \right]^{\frac{1}{2}} \tag{1}$$

$$\frac{C_{i,i+1}}{\epsilon} = Y_A \frac{376.7}{\sqrt{\epsilon_r}} \frac{w}{\omega_1'} \left[\frac{(b_i/Y_A)(b_{i+1}/Y_A)}{g_i g_{i+1}} \right]^{\frac{1}{2}} \tan \theta_0 \;, \quad i = 1,2, ..., n-1 \tag{2}$$

NORMALIZED ADMITTANCE OF HIGH-Z_0 COUPLING WIRE

$$\frac{Y_s}{Y_A} = \left[\frac{w}{\omega_1'} \frac{(b_n/Y_A)(Y_B/Y_A)}{g_n g_{n+1}} \right]^{\frac{1}{2}} \sin \theta_s \tag{3}$$

NORMALIZED SELF-CAPACITANCES PER UNIT LENGTH

$$\frac{C_0}{\epsilon} = \frac{376.7}{\sqrt{\epsilon_r}} \left(Y_A - \frac{C_{01}}{\epsilon} \frac{\sqrt{\epsilon_r}}{376.7} \right) \tag{4}$$

$$\frac{C_1}{\epsilon} = Y_A \left[\frac{376.7}{\sqrt{\epsilon_r}} \frac{2b_1}{Y_A} [\cot \theta_0 + \theta_0 \csc^2 \theta_0]^{-1} - \frac{(C_{12}/\epsilon)}{Y_A} - \frac{\sqrt{\epsilon_r}}{376.7} \frac{(C_0/\epsilon)(C_{01}/\epsilon)}{Y_A^2} \right] \tag{5}$$

$$\left(\frac{C_i}{\epsilon} \right) = \frac{Y_A \, 376.7}{\sqrt{\epsilon_r}} \left[2\frac{b_i}{Y_A} [\cot \theta_0 + \theta_0 \csc^2 \theta_0]^{-1} \right]$$

$$- \left[(C_{i,i+1}/\epsilon) + (C_{i-1,i}/\epsilon) \right] \quad \text{for} \quad i = 2,3, ..., (n-1) \tag{6}$$

$$\frac{C_n}{\epsilon} = \frac{-C_{n-1,n}}{\epsilon} + \frac{376.7 \, Y_A}{\sqrt{\epsilon_r}} \left[\frac{2(b_n/Y_A) - (Y_s/Y_A) [\cot \theta_s + \theta_s \csc^2 \theta_s]}{\cot \theta_0 + \theta_0 \csc^2 \theta_0} \right] \tag{7}$$

NORMALIZED LUMPED LOADING SUSCEPTANCES

$$\frac{\omega_0 C_i^s}{Y_A} = 2\frac{b_i}{Y_A} [\cot \theta_0 + \theta_0 \csc^2 \theta_0]^{-1} \cot \theta_0 \;, \quad i = 1,2, ..., n-1 \tag{8}$$

$$\frac{\omega_0 C_n^s}{Y_A} = \frac{Y_s}{Y_A} \cot \theta_s + \frac{2(b_n/Y_A) - (Y_s/Y_A) [\cot \theta_s + \theta_s \csc^2 \theta_s]}{\cot \theta_0 + \theta_0 \csc^2 \theta_0} \cot \theta_0 \tag{9}$$

979

SUSCEPTANCE
ANNULLING STUB

HIGH-II. .DANCE
WIRE COUPLINGS

CHANNEL 1
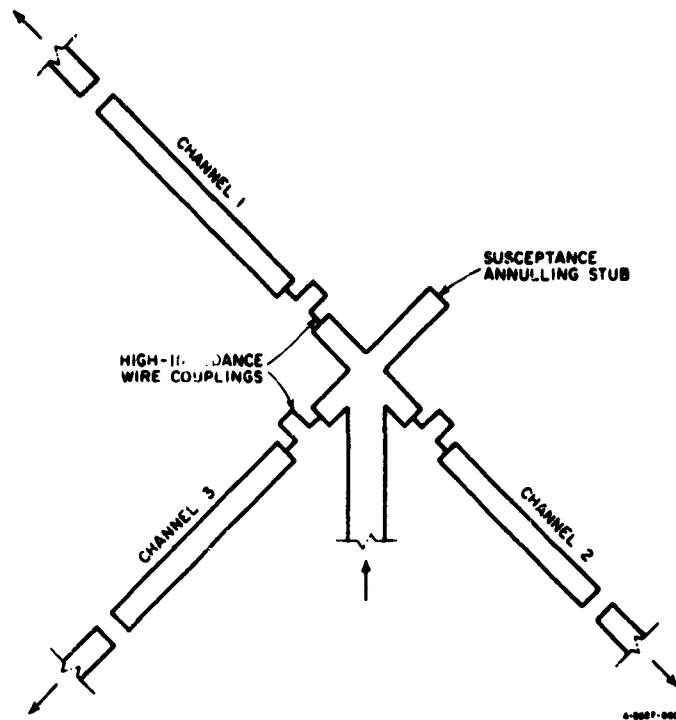
CHANNEL 3

CHANNEL 2

FIG. 16.04-12 A SCHEMATIC DRAWING OF A THREE-CHANNEL
MULTIPLEXER USING FILTERS OF THE TYPE
IN SEC. 8.05
Capacitive coupling is used except at the common
junction

comprising an inverter of the form in Fig. 8.03-2(c). This type of
coupling and point of view was used because it eliminated the undesirably
small capacitive coupling gaps that would otherwise have been needed,
and because in this particular type of filter it provided a convenient
reference plane for paralleling the filters. In this case only a small
capacitive stub was found to be required for susceptance annulling.
This result was partly due to the large band covered by the multiplexer
and probably partly due to the rather sizeable junction effects present
in this particular design at the common junction. The multiplexer was
designed for 1 db or less transducer loss in the pass bands, and achieved
this performance quite well. The input VSWR at the common junction was
2:1 or less across the entire octave operating band of the multiplexer,
which indicated that the desired contiguous pass-bands had been achieved.

Design of Annulling Networks—Solution of integral equations given by Bode[8] shows that if the real part of an admittance has the rectangular form defined by the equations

$$\text{Re } Y_T \; = \; 0 \text{ for } 0 \leq \omega < \omega_a$$

$$= \; G_A \text{ for } \omega_a < \omega < \omega_b \qquad\qquad (16.04\text{-}7)$$

$$= \; 0 \text{ for } \omega_b < \omega < \omega \qquad ,$$

then the minimum imaginary part is given by

$$\text{Im } Y_T \; = \; \frac{G_A}{\pi} \; \ln \left| \frac{1 + \dfrac{\omega}{\omega_0}\, w \, -\left(\dfrac{\omega}{\omega_0}\right)^2}{1 - \dfrac{\omega}{\omega_0}\, w \, -\left(\dfrac{\omega}{\omega_0}\right)^2} \right| \qquad\qquad (16.04\text{-}8)$$

where

$$\omega_0 \; = \; \sqrt{\omega_a \omega_b}$$

and

$$w \; = \; \frac{\omega_b - \omega_a}{\omega_0} \quad .$$

The imaginary part above is minimum in the sense that no shunt susceptance could be removed from the network without making the network non-physical.[8] When the filters for a parallel-connected multiplexer are designed by the methods of this section, after the filters are connected, the real part of the total input admittance can be approximated by Eq. (16.04-7), and to the extent that there is no shunt susceptance in the couplings to the common junction, the imaginary part can be approximated by Eq. (16.04-8). For example, Fig. 16.04-13 shows computed curves of Re Y_T and Im Y_T for a four-channel, lumped-element filter multiplexer design (the solid lines), along with corresponding approximations obtained using Eqs. (16.04-7) and (16.04-8). Note that the degree of agreement is quite good. In the case of Figs. 16.04-7(a),(b) the ripples in Re Y_T are larger so that the accuracy would be less good on that score. Also note from Fig. 16.04-7(b) that Im Y_T does not pass through zero near the middle of the operating
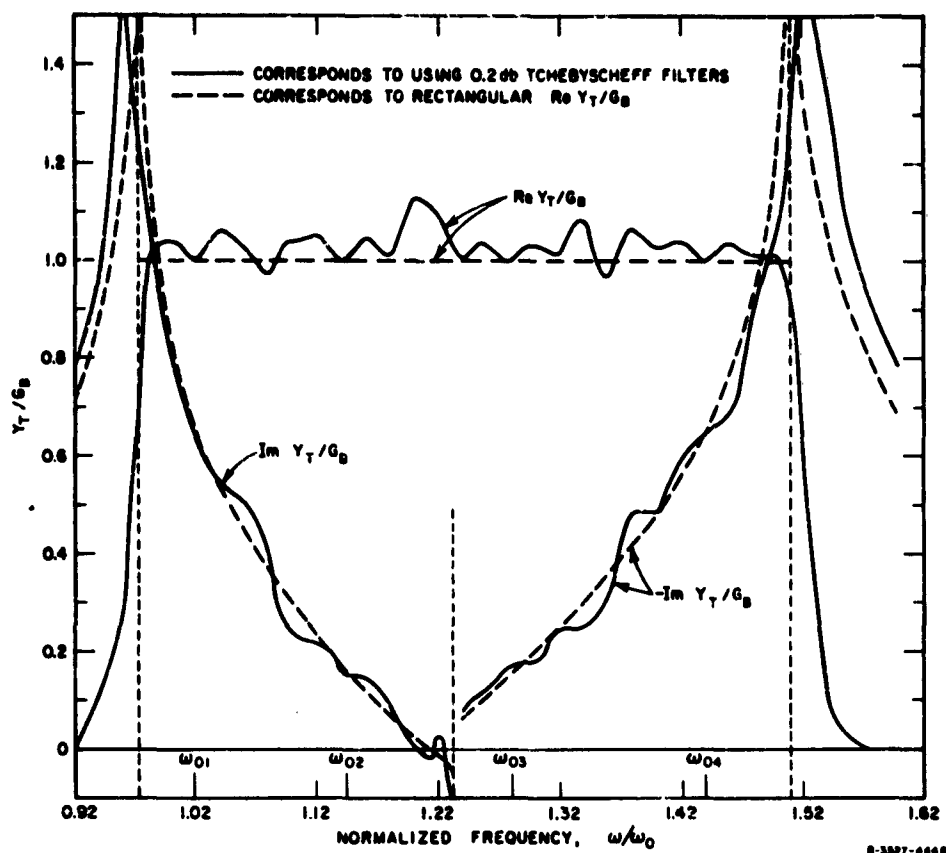
FIG. 16.04-13 Y_T FOR A LUMPED-ELEMENT MULTIPLEXER COMPARED WITH Y_T
FROM EQS. (16.04-7) AND (16.04-8)

range, as Eq. (16.04-8) indicates it should. This, however, is accounted
for by the residual shunt susceptance B indicated in Fig. 16.04-11(b),
for the high-impedance wire coupling to the common junction.

In many practical cases it may be desirable to design the susceptance-
annulling network after assembling the multiplexer and measuring the
admittance characteristic at the common junction (or the impedance
characteristic if the multiplexer is series-connected). In this manner
all significant effects due to the physical size of the common junction
can be accounted for. However, when such junction effects are relatively
small, Eq. (16.04-8) (plus a possible correction for any shunt susceptance
known to be present across the inputs of the filters) should give a very
useful estimate of what the imaginary part of Y_T will be. Having this

estimate, the susceptance-annulling network can then be designed. The
required annulling network for a parallel-connected multiplexer is
generally a parallel-resonant circuit having zero susceptance at the
frequency where $Im\ Y_T$ is zero.

In much of the above discussion the comments have been in terms of
admittances and parallel-connected multiplexers. It should be recalled
that the same remarks apply in an analogous way to impedances in a dual
series-connected multiplexer.

SEC. 16.05, DIPLEXERS WITH CONTIGUOUS PASS BANDS

Diplexers are basically two-channel multiplexers, hence they can be
designed by the same techniques discussed in Sec. 16.04. However, since
diplexers are frequently composed of low-pass and high-pass filters
rather than two band-pass filters, this case will be given some special
attention. Also, an alternate procedure for the design of diplexers
will be suggested.

Figure 16.05-1 shows a diplexer consisting of a low-pass filter and
a high-pass filter. Using the design viewpoint of Sec. 16.04, a singly
loaded prototype from Sec. 4.06 is used for designing the low-pass filter,
while the same prototype used with the mapping procedure in Fig. 7.07-2
can be used for design of the high-pass filter. The proper equal-ripple
band-edge frequencies needed to cause the filters to cross over at their
3-db points can be determined with the aid of Eqs. (16.04-2), (16.04-3),

A-3627-003
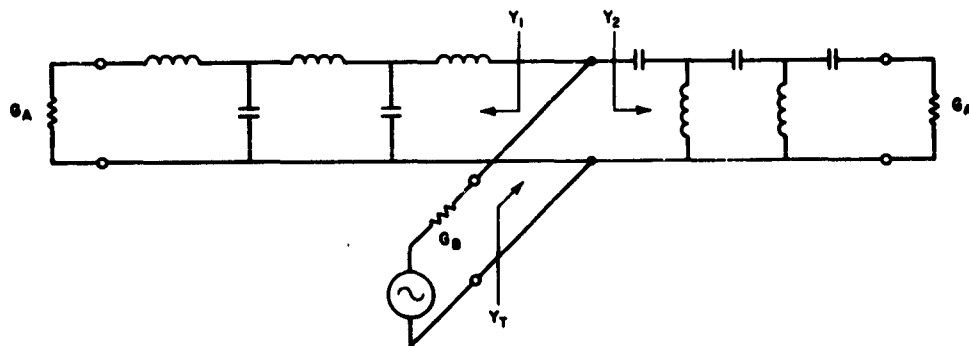
FIG. 16.05-1   A PARALLEL-CONNECTED DIPLEXER COMPOSED OF A
LOW-PASS AND A HIGH-PASS FILTER

and (16.04-6), along with the low-pass to high-pass mapping in Sec. 7.07. It can be shown that in this case the two filters will annul each others susceptances about as well as can be done, without any additional suscep-tance-annulling network. In fact, if the filters were designed from maximally flat, singly loaded prototypes, the imaginary part of the input admittance Y_T in Fig. 16.05-1 could be made to be exactly zero at all frequencies (at least for the idealized lumped-element case). The actual filters for a microwave diplexer such as this could in many cases be designed using the methods of Secs. 7.03 to 7.07.

In some cases it will be convenient to use a wide-band band-pass filter for the high-frequency channel, rather than a high-pass structure of the form in Fig. 16.05-1. In this case the susceptances of the two filters will not annul each other as well. Using Bode's integral equations,[8] if the two filters are designed so that the real part of their input admittance after parallel connection is approximately

$$\text{Re } Y_T \;=\; G_B \quad \text{for } 0 \lesssim \omega \lesssim \omega_b$$
$$\qquad\quad =\; 0 \quad \text{for } \omega_b < \omega < \infty \tag{16.05-1}$$

then the minimum imaginary part is given by

$$\text{Im } Y_T \;=\; \frac{G_B}{\pi} \; ln \left| \frac{\omega_b - \omega}{\omega_b + \omega} \right| \tag{16.05-2}$$

where the significance of the term "minimum" is as discussed with reference to Eq. (16.04-8). In this case the susceptance can be largely annulled by a series-resonant shunt branch having a susceptance of the form

$$B(\omega) \;=\; \frac{-1}{\omega_c L \left(\dfrac{\omega}{\omega_c} - \dfrac{\omega_c}{\omega} \right)} \tag{16.05-3}$$

where ω_c is slightly larger than ω_b and L is a constant (i.e., an inductance for a lumped circuit).

An Alternative Point of View for Diplexer Design—We will now consider an alternative approach to design of diplexers. This approach requires more guess work than is required for the approach suggested above, however,

it has a possible advantage for some situations in that it can be used
to modify conventional doubly terminated filters for use in diplexers.
The approach about to be described is in many respects equivalent to
the "fractional termination" method used for paralleling filters
designed on the image basis.[9] In the discussion to follow series con-
nection of the filters will be assumed, though the same technique applies
analogously to the dual case of parallel-connected diplexers.

Figure 16.05-2(a) shows a low-pass filter and a band-pass filter
with dotted lines indicating wires for connecting these filters in series.
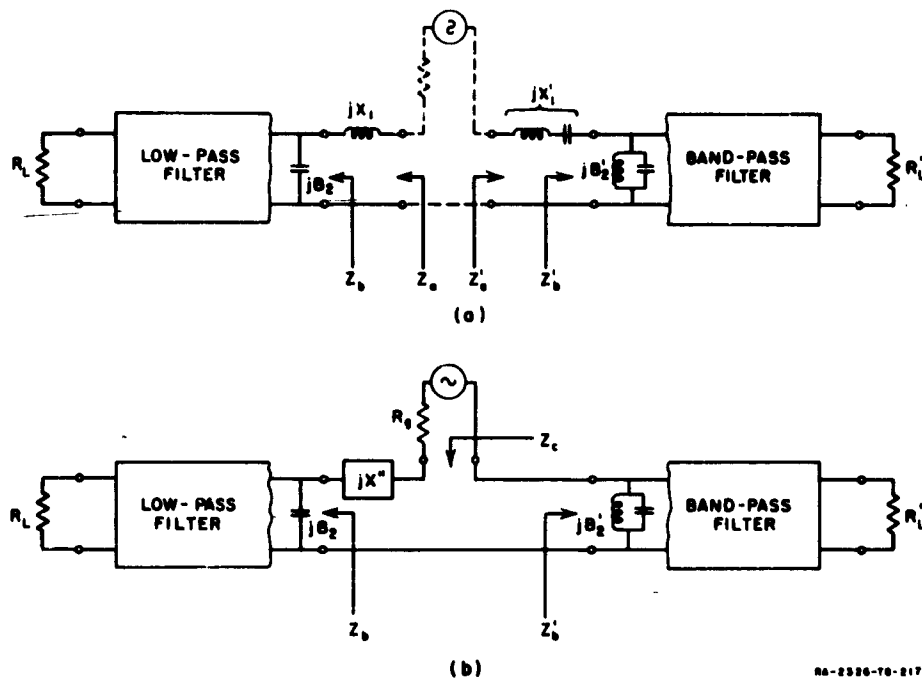
FIG. 16.05-2 FILTERS CONNECTED IN SERIES

If each of these filters were designed to operate normally with pure
resistance terminations at both ends, the two filter's performance would
be greatly disrupted by this connection. This disruption would be due
to the fact that although each filter exhibits a nominally resistive
input impedance in its individual pass band, each filter also exhibits
large reactive impedances in its stop band. Thus if the filters shown
in Fig. 16.05(a) have contiguous pass bands, the band-pass filter will

985

introduce a large reactive component in the terminating impedance seen
by the low-pass filter in the pass band of the low-pass filter, while
the low-pass filter will introduce a large reactive component to the
terminating impedance seen by the band-pass filter in the pass band of
the band-pass filter.

The large stop-band reactive components of the input impedances
Z_a and Z'_a of the filters in Fig. 16.05-2(a) are due largely to the
series reactances X_1 and X'_1 shown. If these are removed, the remaining
input impedances Z_b and Z'_b have the same real part characteristics but
much smaller stop-band reactances. Thus, to form a diplexer, jX_1 and
jX'_1 are removed and the remaining circuits are connected as shown in
Fig. 16.05-2(b). Next, an additional reactance jX'' is introduced to
further adjust the imaginary part of Z_c in order to cause

$$Z_c = Z_b + Z'_b + jX''$$
(16.05-4)

to approximate a pure resistance equal to R_a as nearly as possible.[*]
In the pass band of the low-pass filter $Z'_b + jX''$ represents, under the
conditions described above, a reactance about equivalent to jX_1 in that
band, so that the low-pass filter will operate very nearly in its normal
fashion throughout its pass band. Likewise, in the pass band of the
band-pass filter, $Z_b + jX''$ represents a reactance about equivalent to
jX'_1 in that band, so that the band-pass filter will operate very nearly
in its normal fashion throughout its pass band. However, the removal
of the series branches jX_1 and jX'_1 may result in some reduction in
stop-band attenuation of one or both filters.[†]

Figure 16.05-3 shows a diplexer that was designed by use of this
a roach. The low-pass channel was composed of the filter in Fig. 7.03-3(a)
cut off just to the right of the last capacitive disk on the right of the
filter. This corresponded to removing jX_1 in Fig. 16.05-2(a). The upper-
channel used a band-pass filter of the type discussed in Secs. 10.03
and 10.05. This filter was designed as though it were to have a series
stub at one end (making a series resonator). This was accomplished by
designing that end of the filter using the equations in Table 10.03-1,
while the other half of the filter was designed using the equations in

---

[*] This assumes that the normal terminating impedance next to Z_a and Z'_a for the individual
filters is R_g. It also assumes that the frequency responses of the filters are scaled to
intersect close to the 3-db points.

[†] The decrease in stop-band attenuation resulting from the removal of jX_1 and jX'_1 is largely
compensated for as a result of the input voltage reduction in the stop band of each filter
due to the series loading of the other filter.
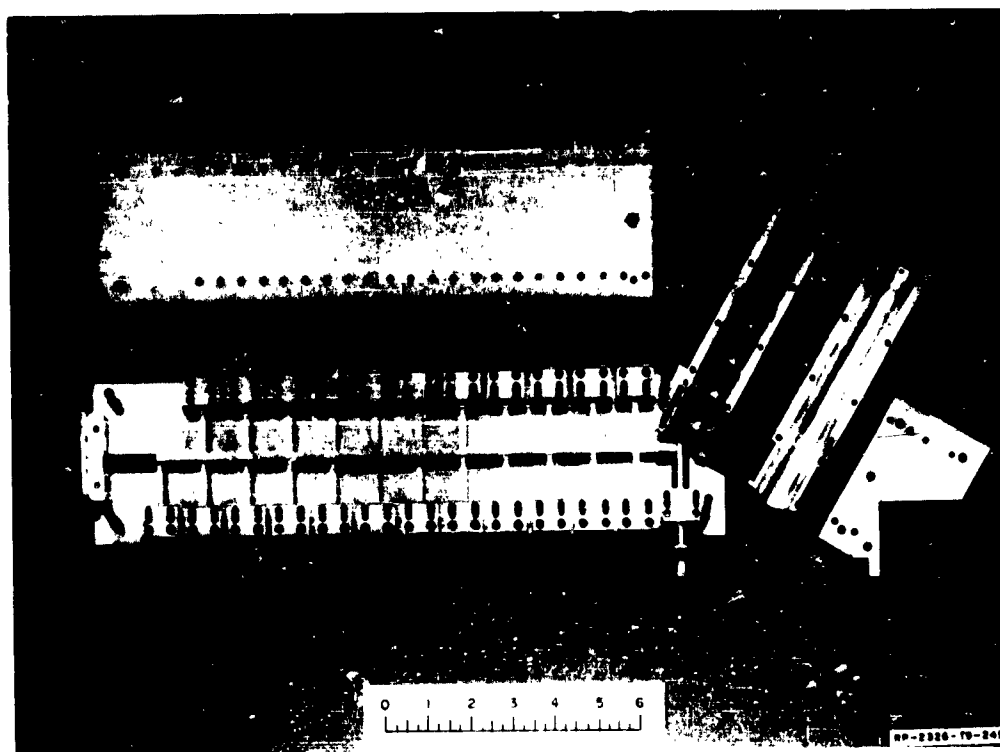
FIG. 16.05-3 PHOTOGRAPH OF A SERIES-CONNECTED DIPLEXER WITH THE
COVER PLATES REMOVED
This diplexer uses a low-pass and a band-pass filter

Table 10.05-1. In the actual diplexer the series stub was not included,
which was analogous to removing the series resonator jX_1' in Fig. 16.05-2(a).
Then the impedances of the two filters connected in series (with react-
ances jX_1 and jX_1' removed) was computed, and the desired form of
reactance-annulling network jX'' was determined. It was found that a
desirable annulling network should have a reactance of the form

$$X'' = \frac{-1}{\omega_c C\left(\dfrac{\omega}{\omega_c} - \dfrac{\omega_c}{\omega}\right)} .$$

(16.05-5)

Note that Eq. (16.05-5) is the dual of that in Eq. (16.05-3), which is
to be expected since the former case is for a parallel connection while
the later is for a series connection.

987

Figure 16.05-4 shows how the series connection was achieved in the diplexer in Fig. 16.05-3. The input line to the common junction passes within the end shunt stub of the band-pass filter. The center conductor of the input line connects to the center conductor of the coaxial low-pass filter, while the outer conductor of the input line connects to the band-pass filter. In this way a series connection is obtained.[*] The annulling reactance jX'' is obtained by using a disk to form a radial line in series with the low-pass filter. The common-junction for the series connection of the diplexer is the region marked A in the figure.

Figure 16.05-5 shows the measured performance of the low-pass channel of this diplexer, while Fig. 16.05-6 shows the performance of the high-pass channel. As can be seen from the figures, low pass-band attenuation with a sharp cross-over was obtained.

Either of the two diplexer design methods described above can be used with good results. The method where the filters are designed from singly loaded low-pass prototype filters has an advantage of involving less guess work for precise designs, and it should be capable of superior performance when very low pass-band attenuation and very precise cross-over characteristics are required. The alternative point of view for diplexer design described above may not be capable of quite as good results because the individual filters were originally designed to be doubly terminated and were later modified. As such, the filters do not have quite as favorable impedance properties for interconnection as do singly terminated filters. However, the alternative method does have the possible advantage that the individual filters can be constructed and tested first as conventional doubly terminated filters.

---

[*] This technique of feeding the multiplexer by a coaxial line within the shunt stub of the band-pass filter was suggested by S. B. Cohn.

METAL DISKS WITH DIELECTRIC
RIMS TO FORM LOW-PASS FILTER
SHUNT CAPACITANCES

SHORT-
CIRCUIT
BLOCK

Z_3 STUB →

BAND-PASS
FILTER

Z_3 STUB →

SHORT
CIRCUIT BLOCK

ROODS TO FORM
SERIES
INDUCTANCES

LOW-PASS FILTER

30°

DISK TO FORM jx''
IN RADIAL LINE

CENTER CONDUCTOR
OF SERIES INPUT LINE

HOLLOW TUBE TO FORM
STUB Z_2 WITH SERIES
INPUT LINE INSIDE

SHORT CIRCUIT BLOCK

GROUND PLANE SPACING
INCREASED IN THIS REGION

INPUT

FIG. 16.05-4 A PARTIAL VIEW OF A SERIES-CONNECTED DIPLEXER CONSTRUCTION

989
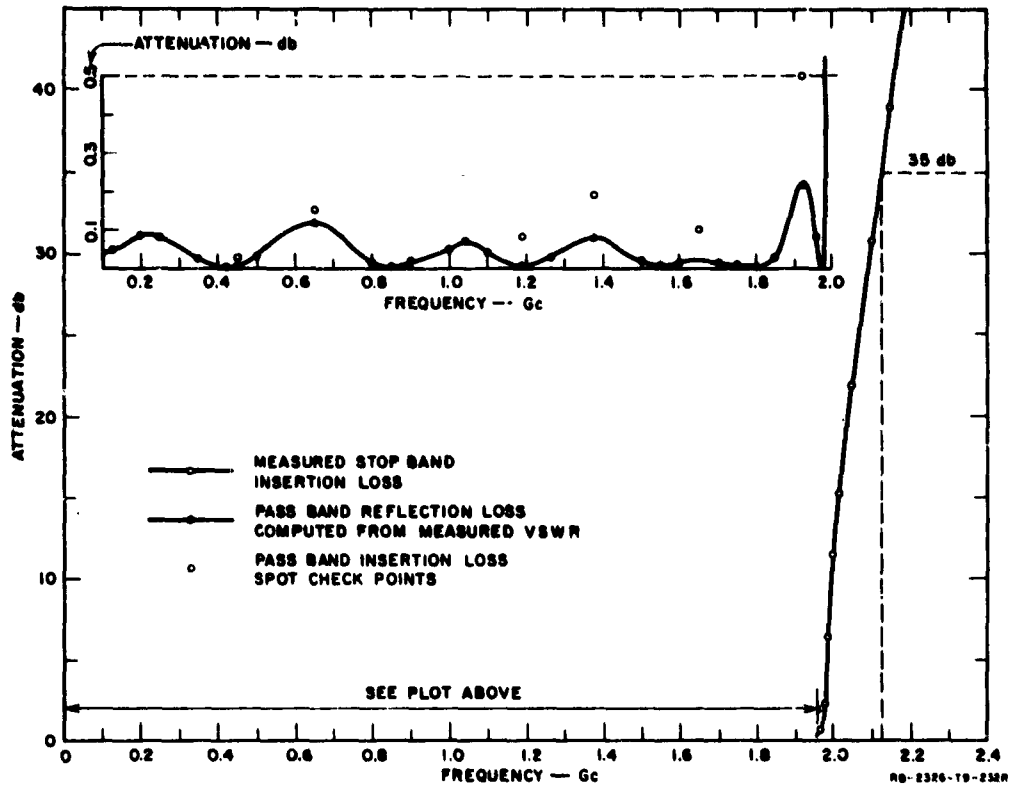
FIG. 16.05-5 MEASURED TRANSMISSION CHARACTERISTICS OF THE LOW-PASS
CHANNEL OF THE DIPLEXER IN FIG. 16.05-3
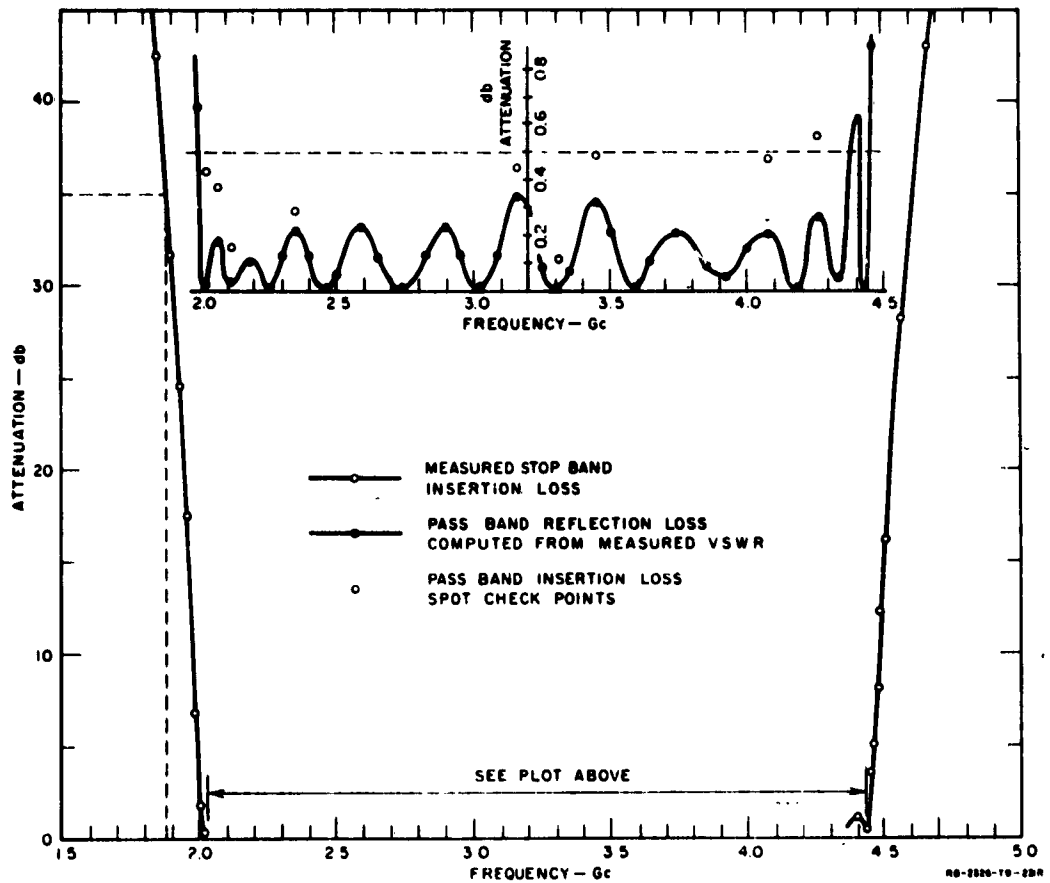
FIG. 16.05-6 MEASURED TRANSMISSION CHARACTERISTICS OF THE BAND-PASS
CHANNEL OF THE DIPLEXER IN FIG. 16.05-3

991

REFERENCES

1. G. C. Southworth, *Principles and Applications of Waveguide Transmission*, pp. 306-317, D. Van Nostrand Co., Inc., New York City (1950).

2. D. Alstadter and E. O. Houseman, Jr., "Some Notes on Strip Transmission Line and Waveguide Multiplexers," *1958 IRE Wescon Convention Record*, Part 1, pp. 54-69.

3. E. A. Marcatili and D. L. Bisbee, "Band-Splitting Filter," *BSTJ*, Vol. XL, pp. 197-212 (January 1961).

4. G. L. Ragan, *Microwave Transmission Circuits*, MIT Rad. Lab. Series, Vol. 9, pp. 708-709, McGraw-Hill Book Co., Inc., New York City (1948).

5. N. Marcuvitz, *Waveguide Handbook*, MIT Rad. Lab. Series, Vol. 10, pp. 360-363, McGraw-Hill Book Co., Inc. (1951).

6. J. F. Cline et al, "Design Data for Antenna-Multicoupler Systems," Final Report, SRI Project 2183, Contract AF 19(604)-2247, Stanford Research Institute, Menlo Park, California (September 1959).

7. W. J. Getsinger, E. G. Cristal, and G. L. Matthaei, "Microwave Filters and Coupling Structures," Quarterly Report 6, Part III, SRI Project 3527, Contract DA 36-039 SC-87398, Stanford Research Institute, Menlo Park, California (August 1962).

8. H. W. Bode, *Network Analysis and Feedback Amplifier Design*, p. 335, D. Van Nostrand Co., Inc., New York City (1945).

9. E. A. Guillemin, *Communication Networks*, Vol. II, pp. 356-371, John Wiley and Sons, Inc., New York City (1935).

MECHANICALLY AND MAGNETICALLY TUNABLE MICROWAVE FILTERS

SEC. 17.01. INTRODUCTION

This chapter will deal mainly with band-pass filters such as might be desired for use as receiver preselectors; however, some discussion of band-stop magnetically tunable filters will be included. Although there are a variety of simple means for shifting the resonant frequency of the resonators of a filter, if it is desired to maintain constant bandwidth and response shape as the filter is tuned, the problem becomes fairly complex (Sec. 17.02). The design data given in this chapter are slanted primarily toward designing filters with relatively constant response shape and bandwidth as the filter is tuned. Fortunately, in the case of magnetically tunable filters, the resonators inherently tend to give constant bandwidth, although there will be some change in response shape as the filter is tuned.

Figure 17.01-1 shows the two types of mechanically tunable filters that are specifically discussed in this chapter. The filter shown at (a) uses coaxial resonators that are tuned by sliding their inner conductors out or in, while the filter shown at (b) is tuned by a sliding wall on one side of each resonator cavity. The constancy of the bandwidth and response shape for filters of these types is improved by proper choice of the locations of the coupling apertures and loops, as is discussed in Secs. 17.03 and 17.04.

Certain materials that exhibit ferrimagnetic resonance have a high-Q resonance and can be easily coupled in to and out of using strip-line, coaxial-line, or waveguide circuitry. The resonant frequency of such ferrimagnetic resonators is controlled by a DC biasing magnetic field. Thus, it becomes possible to tune such resonators electronically by placing the filter in the field of an electromagnet, and then controlling the current in the electromagnet by electronic means. Section 17.05 outlines the general properties of ferrimagnetic resonators that are important to their use in microwave filters. Section 17.06 discusses means for determining the crystal axes of ferrimagnetic resonators—a problem of

993
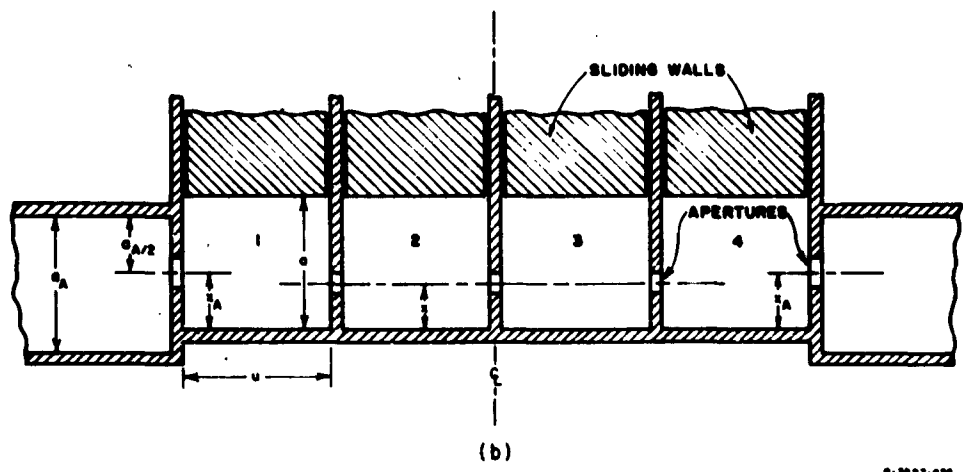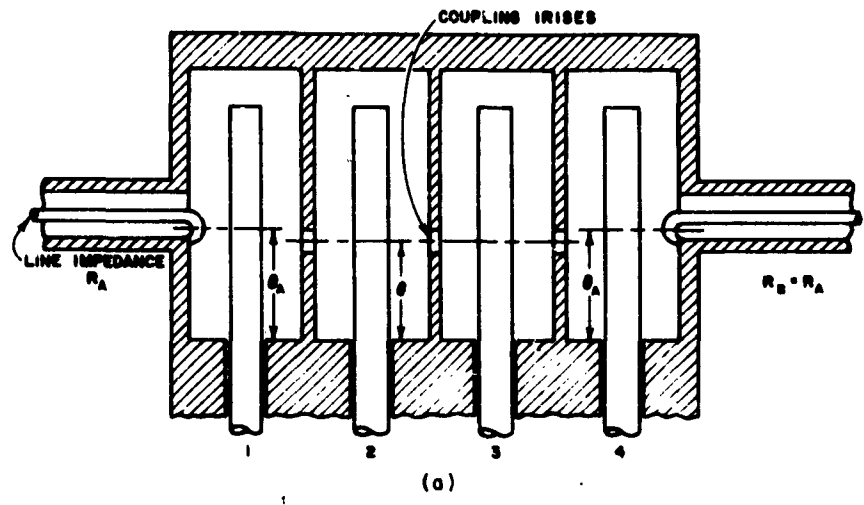
FIG. 17.01-1 COAXIAL AND WAVEGUIDE MECHANICALLY TUNABLE BAND-PASS FILTERS

considerable practical importance since the resonant frequency of ferri-
magnetic resonators is influenced by the orientation of the crystal axes
of the material, with respect to the biasing DC magnetic field.

Figure 17.01-2 shows several of the magnetically tunable filter
structures discussed in Secs. 17.07 to 17.09. The structure shown at (a)
utilizes input and output strip lines that are completely separated by a
dividing wall except for a small coupling slot next to the short-circuited
ends of the strip lines. There is negligible coupling between the two
strip lines when they are without the ferrimagnetic resonators; however,
when ferrimagnetic resonators such as spheres of single-crystal yttrium-
iron-garnet (YIG) are added as shown in the figure, good transmission from
one strip line to the other occurs, provided that the proper biasing mag-
netic field H_0 is applied. The filter shown at (a) will give a two-
resonator response, while that shown at (b) will give a three-resonator
response. A waveguide two-resonator filter is shown at (ᴄ).

A magnetically tunable directional filter is shown in Fig. 17.01-3.
This filter is very similar in principle to the waveguide directional
filters discussed in Sec. 14.02, except that the fixed-tuned electro-
magnetic resonators used in the filters in Sec. 14.02 are·here replaced
by magnetically tunable ferrimagnetic resonators consisting of spheres of
YIG (or of some other suitable material). Besides being magnetically
tunable, the filter in Fig. 17.01-3 differs from those in Sec. 14.02 in
one other important way. As a result of the non-reciprocal properties of
ferrimagnetic resonators, the filter in Fig. 17.01-3 has circulator action
at resonance as well as directional filter action. For example, at reso-
nance, energy entering Port 1 will go to Port 4, but energy entering at
Port 4 will go to Port 3. (The filters in Fig. 17.01-2 do not have this
property.) Directional filters of this type are discussed in Sec. 17.10.

Magnetically tunable band-stop filters are also of practical interest.
One possible form for such filters is the strip-line filter structure shown
in Fig. 17.01-4. This filter uses three YIG resonators placed between the
strip line and one of the ground planes. This filter could be designed to
produce a narrow stop band that can be moved in frequency by controlling
the biasing magnetic field. Band-stop magnetically tunable filters are
discussed in Sec. 17.11.

COUPLING SLOT — DIVIDING WALL

H_0 H_0

OUTLINE OF COUPLING SLOT

(a) TWO-RESONATOR CONFIGURATION

H_0 H_0 H_0

W W

TUNING ROD

(b) THREE-RESONATOR CONFIGURATION

STEPPED WAVEGUIDE TRANSFORMERS
BETWEEN STANDARD- AND
REDUCED-HEIGHT GUIDE

H_0

AXIAL COUPLING SLOT IN
COMMON WALL BETWEEN GUIDES

RESONATORS

(C) WAVEGUIDE TWO-RESONATOR FILTER
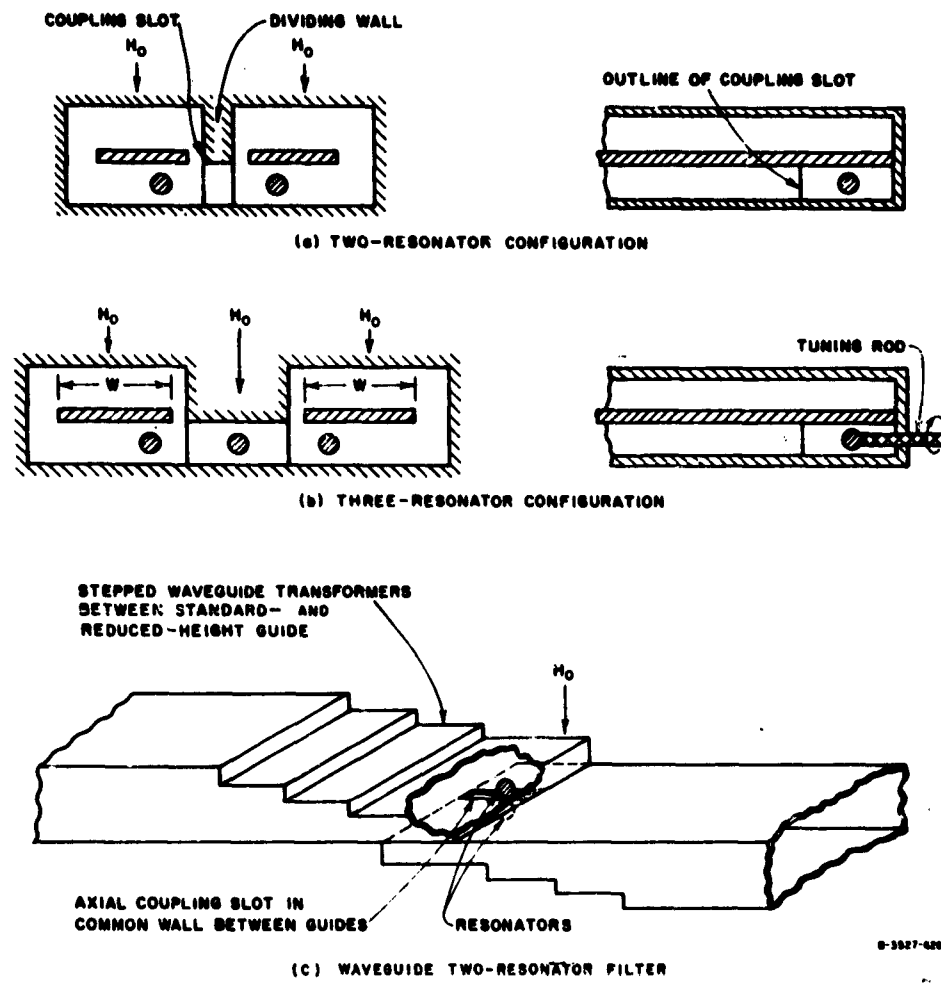
FIG. 17.01-2   MAGNETICALLY TUNABLE STRIP-LINE AND WAVEGUIDE BAND-PASS
FILTERS USING SPHERICAL FERRIMAGNETIC RESONATORS
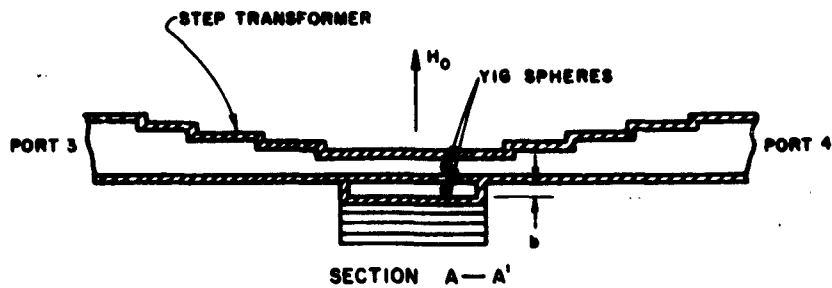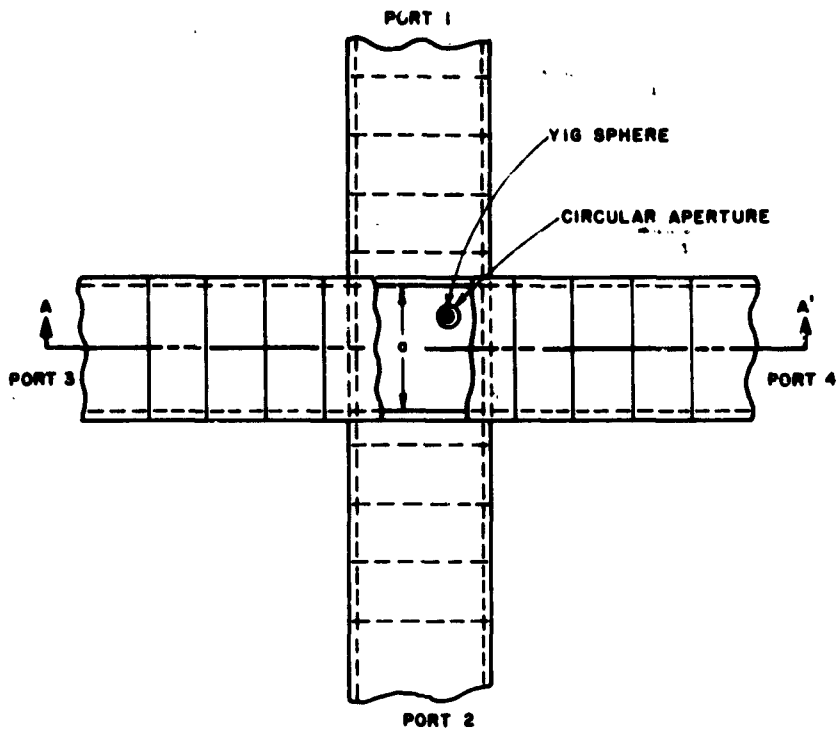
FIG. 17.01-3   A MAGNETICALLY TUNABLE DIRECTIONAL FILTER
HAVING CIRCULATOR ACTION

997
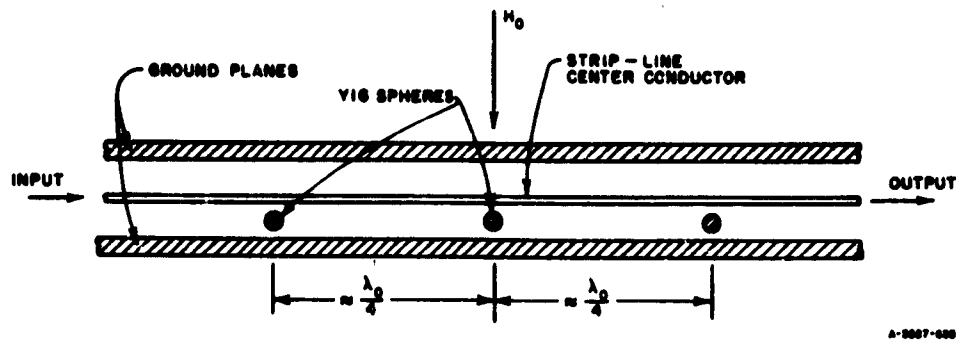
FIG. 17.01-4 A MAGNETICALLY TUNABLE STRIP-LINE BAND-STOP FILTER

The tuning of microwave resonators by use of variable-capacitance diodes or by use of ferroelectric materials might at first seem to be attractive. However, these possibilities are not considered in this chapter because at the time of this writing the Q's of available varactor diodes and of ferroelectric materials are not sufficiently high at micro- wave frequencies to provide very satisfactory means for electronic tuning of microwave-filter resonators.

SEC 17.02, THEORY OF IDEAL, TUNABLE BAND-PASS FILTERS

Although almost any kind of filter can be tuned by varying the lengths of the resonators, or by introducing variable capacitive or inductive loading of some form in the resonators, there are considerations besides resonator tuning that limit the types of structures desirable for use as tunable filters. Generally, it will be desired that the filter response shape will remain more or less constant as the filter is tuned. If steps are not taken to assure constant response shape, it is possible that a filter might have a good Tchebyscheff response at one end of the tuning range, but at the other end have a response of considerably different shape and bandwidth (and possibly with a sizeable reflection loss in the pass band). Thus, we shall now want to explore the factors that must be con- sidered if constant response shape (and also constant bandwidth) are to be maintained as a filter is tuned. Since tunable filters are generally of narrow bandwidth, it will be convenient to use the external Q's of the end resonators and the coupling coefficients between adjacent resonators as the basic design parameters (Sec. 8.02).
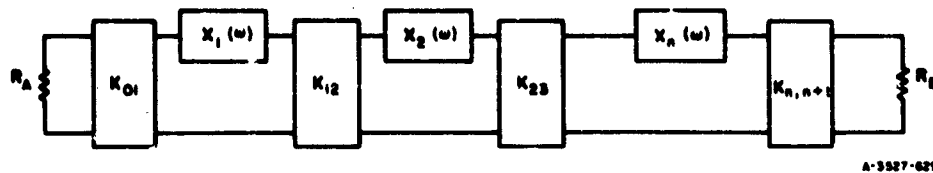
**FIG. 17.02-1 A GENERALIZED FILTER CIRCUIT USING SERIES RESONATORS
AND IMPEDANCE INVERTERS**

Figure 17.02-1 shows a generalized filter circuit with series
resonators coupled by impedance inverters (Sec. 8.02). By Fig. 8.02-3,
the external Q's of the end resonators of this circuit are

$$(Q_e)_A \ = \ \frac{\alpha_1}{K_{01}^2/R_A} \ = \ \frac{g_0 g_1 \omega_1'}{w} \tag{17.02-1}$$

$$(Q_e)_B \ = \ \frac{\alpha_n}{K_{n,n+1}^2/R_B} \ = \ \frac{\omega_1' g_n g_{n+1}}{w} \tag{17.02-2}$$

and the coupling coefficients between resonators are

$$k_{j,j+1} \bigg|_{j=1 \text{ to } n-1} = \ \frac{K_{j,j+1}}{\sqrt{\alpha_j \, \alpha_{j+1}}} \ = \ \frac{w}{\omega_1'\sqrt{g_j g_{j+1}}} \tag{17.02-3}$$

In Eqs. (17.02-1) to (17.02-3), the $K_{j,j+1}$ are impedance inverter
parameters, the α_j are resonator slope parameters defined by

$$\alpha_j \ = \ \frac{\omega_0}{2} \left. \frac{dX_j(\omega)}{d\omega} \right|_{\omega = \omega_0} \tag{17.02-4}$$

where X_j is the reactance of resonator j, and ω_0 is the resonant frequency.
The parameters g_0, g_1, ..., g_{n+1}, ω_1' are parameters of the low-pass proto-
type filter from which the band-pass filter is designed, and w is the
fractional bandwidth of the band-pass filter as measured to the points ω_1
and ω_2 on its response, corresponding to ω_1' on the low-pass prototype
response (Sec. 8.02).

999

Examining Eqs. (17.02-1) to (17.02-3) we see that for the type of response to be preserved (i.e., for maximally flat, Tchebyscheff, or some other response properties to be preserved) the external Q's must vary inversely with the fractional bandwidth w, while the coupling co-efficients must be directly proportional to w. Usually it is desired that the absolute bandwidth be kept constant. Thus, if Δf is the desired fixed bandwidth in cycles per second, f_0 is any given tuning frequency of the filter, and $(f_0)_a$ is the mean tuning frequency (i.e., the center fre-quency of the tuning range), then it is usually desired that

$$w = \frac{\Delta f}{f_0} = \frac{w_a (f_0)_a}{f_0} \qquad (17.02\text{-}5)$$

where

$$w_a = \frac{\Delta f}{(f_0)_a} \qquad (17.02\text{-}6)$$

is the mean fractional bandwidth. Inserting Eq. (17.02-5) in Eqs. (17.02-1) to (17.02-3) gives

$$(Q_e)_A = \frac{g_0 g_1 \omega_1' f_0}{w_a (f_0)_a} \qquad (17.02\text{-}7)$$

$$(Q_e)_B = \frac{\omega_1' g_n g_{n+1} f_0}{w_a (f_0)_a} \qquad (17.02\text{-}8)$$

and

$$k_{j,j+1} \bigg|_{j=1 \text{ to } n-1} = \frac{w_a (f_0)_a}{\omega_1' f_0 \sqrt{g_j g_{j+1}}} \qquad (17.02\text{-}9)$$

where all quantities on the right are constants except for f_0. From these equations we see that in order to give a constant response shape and band-width as the filter is tuned, the external Q's must vary directly with the tuning frequency f_0, while the coupling coefficients must vary inversely with the tuning frequency.

1000

The most commonly used tunable filters use inductive couplings, and the impedance inverters may be regarded as being of the form in Fig. 17.02-2. In the case of a narrow-band filter (tunable filters are usually narrow band), all of the reactances in the inverter circuit of Fig. 17.02-2 would be very small. The negative, series reactances are therefore small compared with the reactances that they are connected to, and hence have little effect in the filter except to cause a slight shift in the resonant frequency of the resonators. Thus, to a good approximation, we may represent the circuit in Fig. 17.02-1 by the circuit in Fig. 17.02-3 if the K-inverters are of the form in Fig. 17.02-2 and if the bandwidth is reasonably narrow (say, of the order of a few percent or less). Then by Fig. 17.02-2,
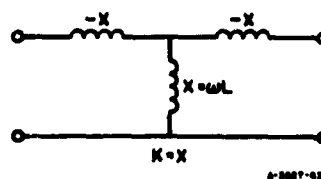
FIG. 17.02-2   A FORM OF K-INVERTER CORRESPONDING TO SHUNT-INDUCTIVE COUPLINGS

$$K_{j,j+1} = X_{j,j+1} = \left(X_{j,j+1}\right)_a \frac{f_0}{\left(f_0\right)_a} \qquad (17.02\text{-}10)$$
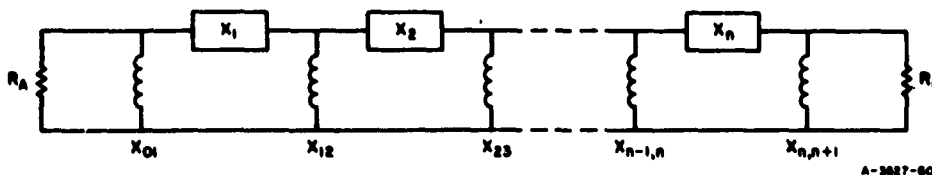
FIG. 17.02-3   A FILTER CIRCUIT WITH SHUNT-INDUCTIVE COUPLINGS

where $\left(X_{j,j+1}\right)_a$ is the reactance of the $j, j + 1$ coupling inductance at the mean tuning frequency $\left(f_0\right)_a$. Inserting Eq. (17.02-10) into Eqs. (17.02-1) to (17.02-3) gives

$$\left(Q_e\right)_A = \frac{\alpha_1 R_A \left(f_0\right)_a^2}{\left(X_{01}\right)_a^2 f_0^2} \qquad (17.02\text{-}11)$$

$$(Q_e)_B = \frac{x_n R_B (f_0)_a^2}{(X_{n,n+1})_n^2 f_0^2} \tag{17.02-12}$$

$$k_{j,j+1}\bigg|_{j=1 \text{ to } n-1} = \frac{(X_{j,j+1})_a f_0}{\sqrt{x_j x_{j+1}} (f_0)_a} \tag{17.02-13}$$

Comparing Eqs. (17.02-11) and (17.02-12) with Eqs. (17.02-7) and (17.02-8) we see that, to maintain constant response shape and bandwidth, the resonator slope parameters x_1 and x_n must vary as

$$x_1 = (x_1)_a \left[\frac{f_0}{(f_0)_a}\right]^3$$

$$x_n = (x_n)_a \left[\frac{f_0}{(f_0)_a}\right]^3 \tag{17.02-14}$$

where $(x_1)_a$ and $(x_n)_a$ are the slope parameter values at the mean tuning frequency $(f_0)_a$. Now, comparing Eqs. (17.02-9) and (17.02-13), we see that to maintain constant response shape and bandwidth

$$x_j\bigg|_{j=1 \text{ to } n} = (x_j)_a \left[\frac{f_0}{(f_0)_a}\right]^2 \tag{17.02-15}$$

where the $(x_j)_a$ are again the slope parameter values at $(f_0)_a$. Note that Eqs. (17.02-14) and (17.02-15) appear to be contradictory since Eq. (17.02-14) says that x_1 and x_n must vary as $(f_0)^3$ while Eq. (17.02-15) says they must vary as $(f_0)^2$. These two requirements are not, however, irreconcilable, since Eq. (17.02-14) refers to the slope parameters of Resonators 1 and n as seen from the coupling reactances X_{01} and $X_{n,n+1}$, while Eq. (17.02-15) relates to the slope parameters of Resonators 1 and n as seen from the between-resonator reactances X_{12} and $X_{n-1,n}$. Thus, as will be evident from the discussions in Sec. 17.03 and 17.04, it may be possible to approximately satisfy both Eqs. (17.02-14) and (17.02-15) at the same time by making the X_{01} and $X_{n,n+1}$ coupling reactances at the ends of the filter couple into Resonators 1 and n at points on the resonator

structures different from those of couplings X_{12} and $X_{n-1,n}$. In this
manner the slope parameters seen by the end couplings will be different
from those seen by the couplings between resonators.

Perhaps the most familiar type of series resonator is that consisting
of an inductance and capacitance in series, which gives

$$X_j = \omega L_j - \frac{1}{\omega C_j} = \omega L_j - \frac{L_j \omega_0^2}{\omega} \quad . \tag{17.02-16}$$

By Eq. (17.02-4)

$$x_j = \omega_0 L_j \quad . \tag{17.02-17}$$

If the resonators are tuned by varying the C_j while the L_j remains fixed,
then

$$x_j = (x_j)_a \frac{f_0}{(f_0)_a} \tag{17.02-18}$$

which does not have the frequency variation of either Eq. (17.02-14) or
Eq. (17.02-15). It is easily shown that if C_j is held fixed and the
filter is tuned by varying the L_j, then

$$x_j = (x_j)_a \frac{(f_0)_a}{f_0} \tag{17.02-19}$$

which deviates even more from the desired type of frequency variation.

From the above discussion we see that a simple series L-C resonator
cannot give the desired $(f_0)^2$ or $(f_0)^3$ variation of the resonator slope
parameters unless the resonators are tuned by varying both the L_j and
the C_j at the same time. However, Fig. 17.02-4 shows a resonator circuit
that could approximate the desired frequency variations while being tuned
by varying only a series capacitance. In this case a parallel resonant
circuit has been added, which adds a pole of reactance at frequency ω_∞.
Thus, as the resonator is tuned to higher frequencies, the resonator slope
parameter increases more rapidly than it would if the pole of reactance
were not there.

(a)

(b)

A-3527 609
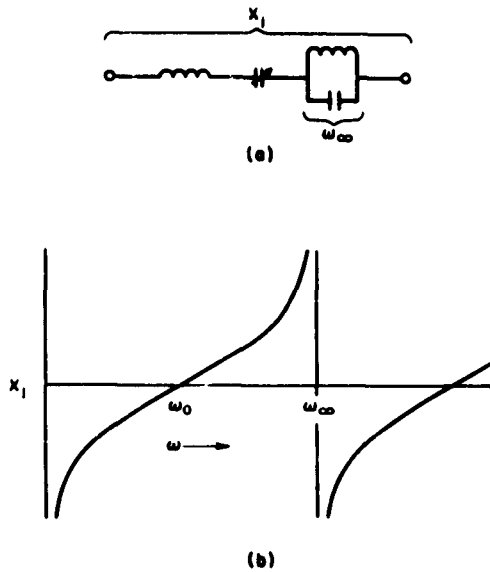
FIG. 17.02-4   A TUNABLE RESONATOR
AND ITS REACTANCE
CHARACTERISTIC

Although the form of the resonator circuit in Fig. 17.02-4 is not
of much interest for microwave filters, the discussion illustrates the
types of considerations and possible solutions involved in the design
of tunable filters with constant response shape and bandwidth. The dis-
cussion above has been in terms of filters with series resonators and
shunt inductive couplings; however, by use of the data in Figs. 8.02-3,
8.02-4, 8.03-1, 8.03-2 and 8.03-3, the same type of reasoning can be
applied for the derivation of the required parameter properties for
numerous other types of filters. Of course, Eqs. (17.02-7) to (17.02-9)
apply to all filters as long as constant response shape and bandwidth
are required.

Another factor to be considered in the design of tunable filters is
the choice of low-pass prototype filters to be used. Since the filters
used are usually of narrow bandwidth, the equal-element low-pass proto-
types discussed in Sec. 11.07 are often a desirable choice. As is dis-
cussed in Sec. 11.07, filters designed from equal-element prototypes can
give very nearly the absolute minimum midband dissipation loss for given

1004

resonator unloaded Q's, and for a given amount of attenuation required at some frequency a specified frequency interval from the mid-pass-band frequency.

For many narrow-band inductively coupled filters such as that in Fig. 17.02-3, a useful low-pass to band-pass mapping (Sec. 8.04) to use is

$$\frac{\omega'}{\omega'_1} = \frac{2}{w}\left(\frac{\omega - \omega_0}{\omega}\right) \qquad (17.02\text{-}20)$$

where

$$w = 2\left(\frac{\omega_2 - \omega_1}{\omega_2 + \omega_1}\right) \quad , \qquad (17.02\text{-}21)$$

$$\omega_0 = \frac{2\omega_2\omega_1}{\omega_2 + \omega_1} \quad , \qquad (17.02\text{-}22)$$

ω' and ω are the frequency variables of the low-pass prototype and band-pass filters, respectively, and ω_1 and ω_2 are the band-pass filter band-edge frequencies corresponding to ω'_1 for the low-pass prototype.

SEC. 17.03, MECHANICALLY TUNABLE COAXIAL BAND-PASS FILTERS

Figure 17.03-1 shows a form of coaxial, mechanically tunable filter, which has been used a good deal.[1] The resonators operate in the TEM mode and are a quarter-wavelength long at resonance. One end of each resonator is open-circuited while the other is short-circuited, and tuning is accomplished by sliding the round center conductor back and forth through the short-circuiting region at the lower end of each resonator. The coaxial input and output lines are coupled to the first and last resonators, respectively, by magnetic coupling loops, while the resonators are coupled to their neighbors by inductive irises. The cross-sectional shape of the resonators is approximately coaxial; however, the region between resonators is flattened so that the coupling irises will not be so thick.

The filter in Fig. 17.03-1 is of the inductively coupled type shown in generalized form in Fig. 17.02-3 and analyzed in Sec. 17.02. As was discussed in connection with Eqs. (17.02-14) and (17.02-15), a somewhat different frequency variation of the resonator slope parameters is usually
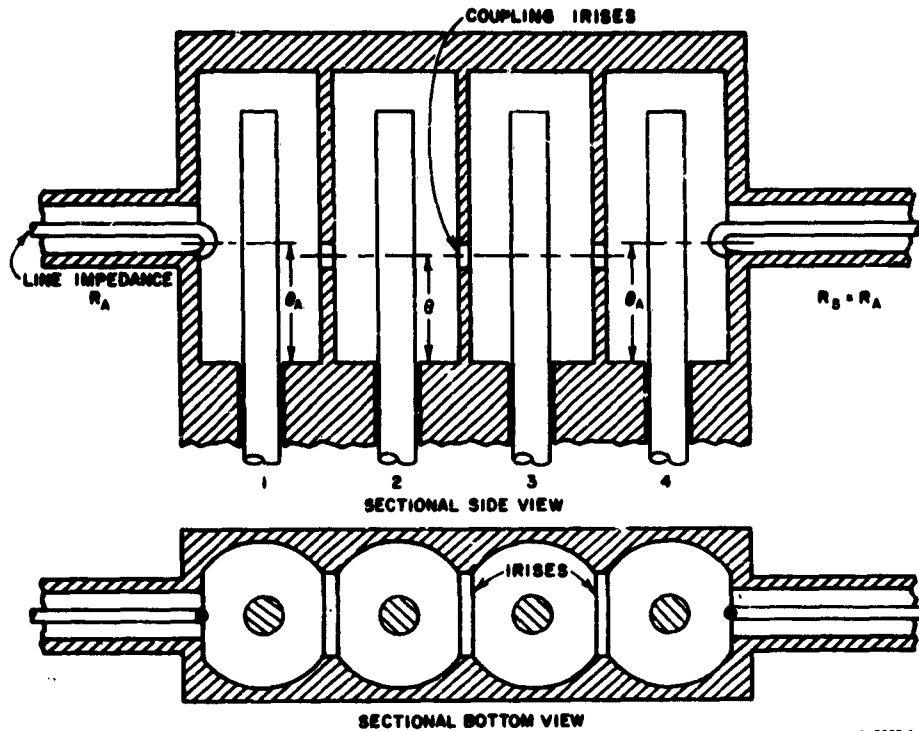
FIG. 17.03-1   A FOUR-RESONATOR MECHANICALLY TUNABLE TEM-MODE FILTER

desired in determining $(Q_e)_A$ and $(Q_e)_B$ as compared with the frequency variation of the resonator slope parameters desired for determining the coupling coefficients $k_{j,j+1}$.   In the filter structure in Fig. 17.03-1 the desired difference is achieved in an approximate fashion by locating the input and output coupling loops an electrical distance θ_A from the short-circuited ends of the resonators which is different from the electrical distance θ which the inductive coupling irises are located from the short-circuited ends of the resonators.

Figure 17.03-2(a) shows an equivalent circuit used for calculating $(Q_e)_A$.   In the figure

$$X_1 = Z_0 \left[\tan \theta_A - \cot \left(\frac{\pi}{2} - \theta_A \right) \right] \qquad (17.03\text{-}1)$$

where Z_0 is the characteristic impedance of the resonator line. The resonator reactance slope parameter is then

$$\alpha_1 = \frac{\omega_0}{2} \frac{dX}{d\omega}\bigg|_{\omega_0} = \frac{\pi}{4} Z_0 \sec^2 \theta_A \qquad (17.03\text{-}2)$$

and by Eq. (17.02-11) the external Q at end A is

$$(Q_e)_A = \frac{\pi}{4} \frac{Z_0 R_A}{(X_{01})^2 \dfrac{f_0^2}{(f_0)_m^2} \cos^2 \left[(\theta_A)_m \dfrac{f_0}{(f_0)_m} \right]} \qquad (17.03\text{-}3)$$

where the subscript m indicates a quantity evaluated at the mid-tuning-range frequency $(f_0)_m$. Of course, an analogous equation applies for $(Q_e)_B$.

(a)

(b)

A-3927-611
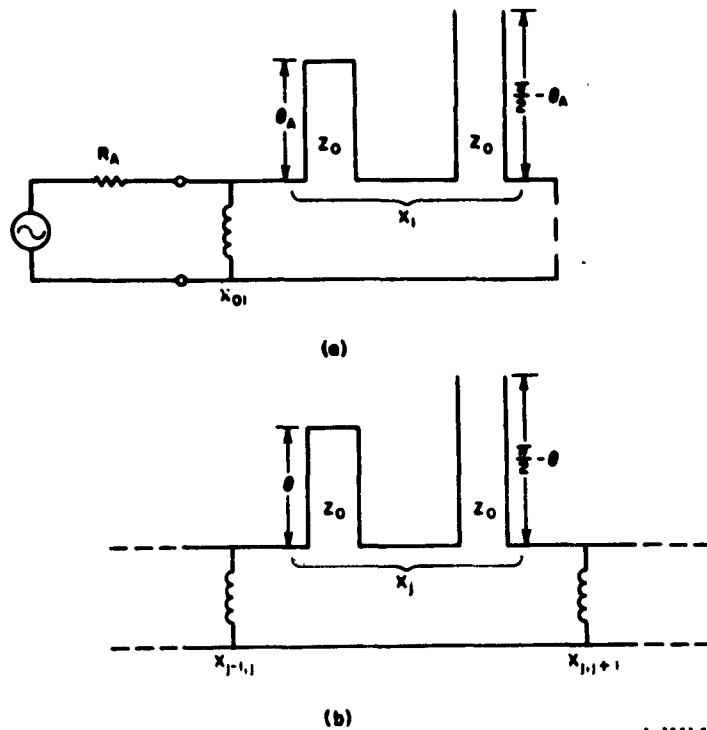
FIG. 17.03-2 RESONATOR EQUIVALENT CIRCUITS USED IN COMPUTING $(Q_e)_A$ AND $k_{i,i+1}$

1007

Figure 17.03-2(b) shows the resonator equivalent circuit used in computing the coupling coefficients between resonators. Using Eq. (17.02-13), analogously to the derivation above we obtain

$$k_{j,j+1} = \frac{4(X_{j,j+1})_a \, f_0 \, \cos^2 \, [(\theta)_a \, f_0/(f_0)_a]}{\pi Z_0 (f_0)_a} \qquad . \qquad (17.03\text{-}4)$$

Now as indicated by Eqs. (17.02-7) to (17.02-9), for constant response shape and bandwidth we desire that

$$(Q_e)_A = \left[(Q_e)_A\right]_a \frac{f_0}{(f_0)_a} \qquad , \qquad (17.03\text{-}5)$$

$$(Q_e)_B = \left[(Q_e)_B\right]_a \frac{f_0}{(f_0)_a} \qquad . \qquad (17.03\text{-}6)$$

and

$$k_{j,j+1} = (k_{j,j+1})_a \frac{(f_0)_a}{f_0} \qquad . \qquad (17.03\text{-}7)$$

If we equate Eqs. (17.03-5) and (17.03-3) for $f_0/(f_0)_a = 0.7$ and for $f_0/(f_0)_a = 1.3$, and solve for $(\theta_A)_a$, we find that $(\theta_A)_a = 0.9675$ radian. If we equate Eqs. (17.03-4) and (17.03-7) at the same frequencies and solve for $(\theta)_a$ we then find that $(\theta)_a = 0.8534$ radian.

From Eqs. (17.03-5) and (17.03-7) we see that both $(Q_e)_A$ and $1/k_{j,j+1}$ should ideally be directly proportional to the frequency, if constant response shape and bandwidth are desired. Figure 17.03-3 presents normalized curves for these quantities vs. $f_0/(f_0)_a$ for the values of $(\theta_A)_a$ and $(\theta)_a$ given above. We see that the external Q curve deviates most from the desired linear variation, which means that the response shape will change somewhat as the filter is tuned. The quantity $N/k_{j,j+1}$ follows the desired linear variation more closely, but it also deviates some from the desired line. Since the coupling coefficients between resonators have the dominant effect on bandwidth, the deviation in the $N/k_{j,j+1}$ curve from the desired line will cause some variation of the bandwidth. Although the deviations from ideal performance indicated in Fig. 17.03-3 are sizeable, they are probably acceptable for most applications. Also, the curves in
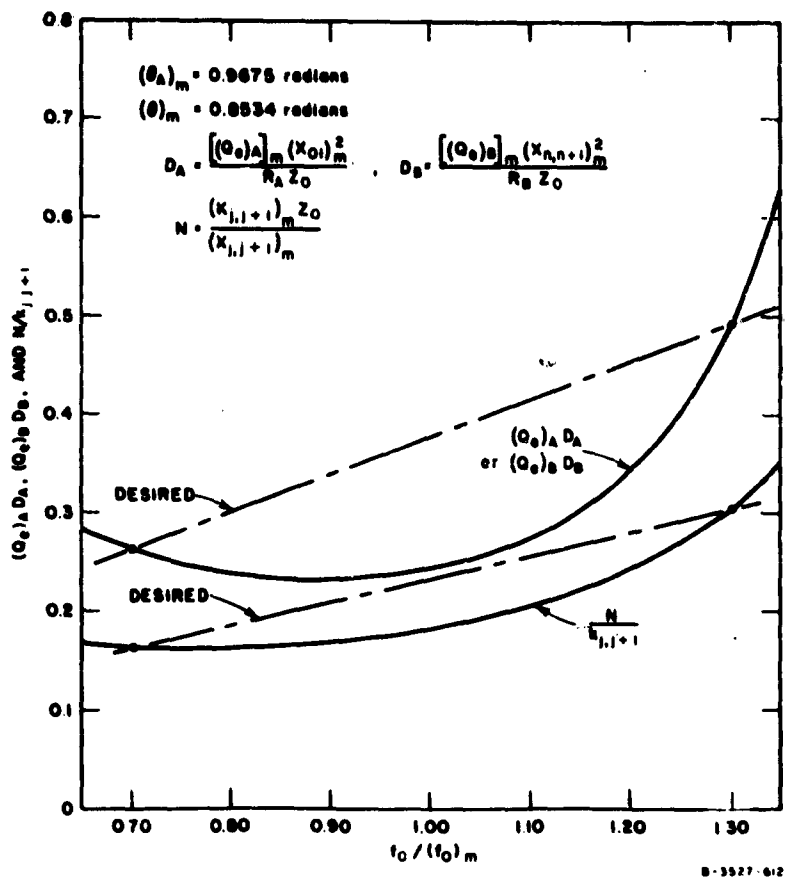
FIG. 17.03-3 NORMALIZED CURVES INDICATING THE FREQUENCY
VARIATION OF NORMALIZED $(Q_e)_A$, $(Q_e)_B$, AND
$1/k_{j,j+1}$ FOR A FILTER OF THE FORM SHOWN IN
FIG. 17.03-1

Fig. 17.03-3 apply to a design with a tuning range of over an octave.
The deviations from ideal performance can, of course, be kept much
smaller if smaller tuning ranges are sufficient.

Summary of Design Procedure—Let us now summarize how filters of the
sort in Fig. 17.03-1 can be designed.

The design process is carried out at the mid-tuning-range frequency
$(f_0)_m$. In order to obtain nearly optimum resonator Q's, the resonators
should have a line impedance of approximately $Z_0 = 76$ ohms (see Fig. 5.03-2).
Use the values of $(\theta_A)_m$ and $(\theta)_m$ in Fig. 17.03-3, or if tighter control on
the response is required and the required tuning range is smaller than an

1009

octave, solve for values of $(\theta_A)_a$ and $(\theta)_a$ as described above, in order to give a closer approximation over a smaller tuning range.

The coupling reactances can be computed by combining Eqs. (17.03-3) and (17.03-4) with Eqs. (17.02-1) to (17.02-3) to obtain

$$(X_{01})_a = \frac{1}{\cos{(\theta_A)_a}}\sqrt{\frac{\pi Z_0 w_a R_A}{4 g_0 g_1 \omega_1'}} \qquad , \qquad (17.03\text{-}8)$$

$$(X_{j,j+1})_a \bigg|_{j=1 \text{ to } n-1} = \frac{\pi Z_0 w_a}{4 \cos^2{(\theta_a)}\,\omega_1'\sqrt{g_j g_{j+1}}} \qquad (17.03\text{-}9)$$

$$(X_{n,n+1}) = \frac{1}{\cos{(\theta_A)_a}}\sqrt{\frac{\pi Z_0 w_a R_A}{4 g_n g_{n+1}\omega_1'}} \qquad (17.03\text{-}10)$$

where w_a is the fractional bandwidth $\Delta f/(f_0)_a$ to the pass-band edge points corresponding to ω_1' for the low-pass prototype.

As a rough guide in the design of the loop couplings at each end of the filter, the following reasoning can be used.[1] If I is the current in Resonator 1 or n at an electrical distance $(\theta_A)_a$ from the short-circuit end of the resonator, then the magnetic field at a radial distance r from the center axis of the coaxial resonator is $H = I/(2\pi r)$. This field will excite a voltage of $jA\mu_0\omega H = jA\mu_0\omega I/2\pi r$ in a loop of area A located at a mean radius r from the axis of the coaxial line. Thus, the mutual reactance of such a loop in a coaxial line is

$$X = \frac{A\mu_0\omega}{2\pi r} \qquad (17.03\text{-}11)$$

where, if r is in inches and A is in square inches, $\mu_0 = (0.0254)\,4\pi 10^{-7}$ henries/inch. This formula can serve as a guide for the initial design of the coupling loop but in practice experimental adjustments as described in Sec. 11.02 will probably be desirable. Reference 1 points out that in order to reduce the self reactance of the coupling loops (excess reactance can cause the tuning of the end resonators to track differently than that of the interior resonators), it is desirable for the coupling loop to be faired into the side wall as much as possible, as is suggested in

Fig. 17.03-1; under such conditions Eq. (17.03-11) may be a poor
approximation.

Using Bethe's small-aperture theory the apertures between the
resonators should have magnetic polarizabilities of approximately

$$M_{j,j+1} = \frac{\lambda_a a^2 (X_{j,j+1})_a}{60} \tag{17.03-12}$$

where a is the nominal radius of the inside of the outer conductor of
the resonators and λ_a is the wavelength at the mean tuning frequency
$(f_0)_a$. The sizes of the apertures can then be determined from the M_1
polarizability data in Fig. 5.10-4(a), (the M_1 rather than the M_2 data
is used since the lengths of the coupling irises are to be in the cir-
cumferential direction). Approximate corrections for the size and
thickness t of the apertures can be made by obtaining trial aperture
lengths $\ell_{j,j+1}$ using Eq. (17.03-12) and Fig. 5.10-4(a), and then computing
compensated polarizabilities

$$(M_{j,j+1})_{comp.} = M_{j,j+1} \left[1 - \left(\frac{2\ell_{j,j+1}}{\lambda_a}\right)^2\right] 10^{\left(\frac{1.36t}{\ell_{j,j+1}}\right)\sqrt{1-\left(\frac{2\ell_{j,j+1}}{\lambda_a}\right)^2}} \tag{17.03-13}$$

from which improved aperture lengths are obtained using Fig. 5.10-4(a).
For greatest accuracy the experimental procedures described in Sec. 11.02
to 11.04 should be used to check the aperture sizes.

One possible source of trouble in the practical operation of filters
of the type under discussion lies in the fact that the resonator rods
must slide freely while still maintaining a good short-circuit at one end.
Sliding contact fingers can be used to help ensure a good short-circuit
connection, but the non-contacting short-circuit connections in
Fig. 17.03-4 are found to be preferable.[1] The design in Fig. 17.03-4(a)
uses a very low impedance section, which is a quarter-wavelength long at
frequency $(f_0)_a$. In this design the resonator rod is supported by a di-
electric bearing surface at the left. The low-impedance line section is
effectively open-circuited at its left end and, as a result, tends to
reflect a very large susceptance at its right end. The design in
Fig. 17.03-4(b) is similar, but it uses an additional high-impedance line
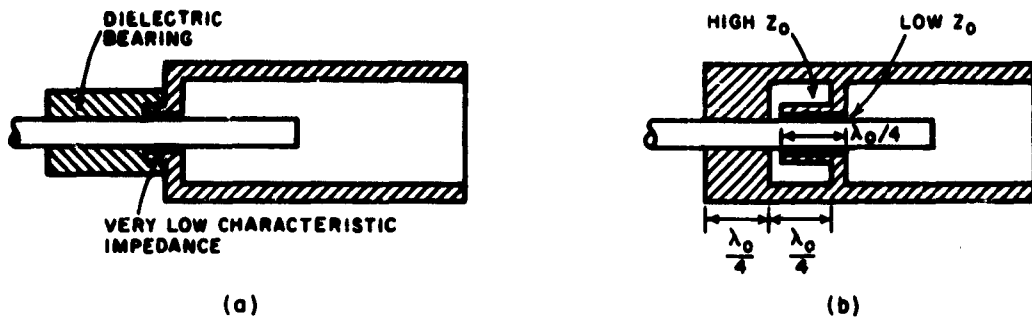
DIELECTRIC
BEARING

VERY LOW CHARACTERISTIC
IMPEDANCE

(a)

HIGH Z_0 LOW Z_0

$\frac{\lambda_0}{4}$

$\frac{\lambda_0}{4}$ $\frac{\lambda_0}{4}$

(b)

A-3627-631

FIG. 17.03-4   TWO POSSIBLE DESIGNS FOR THE SHORT-CIRCUIT AND BEARING PORTION
OF MECHANICALLY TUNABLE COAXIAL RESONATORS

section to reflect a very high impedance to the open-circuited end of
the low-impedance line section.   In this type of design the resonator
rod can be supported by a metal bearing.   Although this type of choke
joint design is frequency sensitive to some extent, it can be made to
work very well over as much as a five-to-one tuning range. [1]

SEC. 17.04, WAVEGUIDE MECHANICALLY TUNABLE BAND-PASS FILTERS

Figure 17.04-1 shows a waveguide mechanically tunable filter which
is in many respects analogous to the coaxial type of filter discussed in
Sec. 17.03.   This filter consists of rectangular cavity resonators that
are tuned by moving one of the side walls.   The resonators are coupled
by apertures which are located so as to come as close as possible to
giving the desired frequency variations of the external Q's and the
coupling coefficients.   As in the filter of Sec. 17.03, the coupling
apertures between resonators are positioned differently from the apertures
coupling to the input and output guides.

The analysis of the filter in Fig. 17.04-1 proceeds similarly to that
discussed in Sec. 17.03.   In this case the resonator slope parameters are
given by

$$\alpha_j \;=\; \frac{\pi}{2}\, Z_0 \left(\frac{\lambda_g}{\lambda}\right)^2 \qquad\qquad (17.04\text{-}1)$$

1012

when the analysis is carried out on a frequency basis. (See Sec. 8.14 for a discussion of the differences between waveguide filter design on a frequency basis vs. design on a reciprocal-guide-wavelength basis.) In Eq. (17.04-1) Z_0 is the guide impedance and λ_g and λ are the guide and free-space wavelengths at resonance. The coupling reactances and the effects of different guide dimensions for the terminating guides as compared to the dimensions of the cavity resonators can all be obtained from Fig. 5.10-6. Thus, using Eqs. (17.04-1) and (17.02-10) to (17.02-13), along with the data in Fig. 5.10-6 gives

$$(Q_e)_A = \frac{ab a_A b_A \lambda_{gA} u^3}{4\pi\lambda^2 M_{01}^2 \sin^2 \frac{\pi x_A}{a}} \tag{17.04-2}$$

$$k_{j,j+1}\bigg|_{j=1 \text{ to } n-1} = \frac{M_{j,j+1}\lambda^2 \sin^2 \frac{\pi x}{a}}{abu^3} \tag{17.04-3}$$

$$(Q_e)_B = \frac{ab a_A b_A \lambda_{gA} u^3}{4\pi\lambda^2 M_{n,n+1}^2 \sin^2 \frac{\pi x_A}{a}} \tag{17.04-4}$$

RESONATOR DIMENSIONS — a WIDE, u LONG, b HIGH
TERMINATING GUIDES — a_A WIDE, b_A HIGH
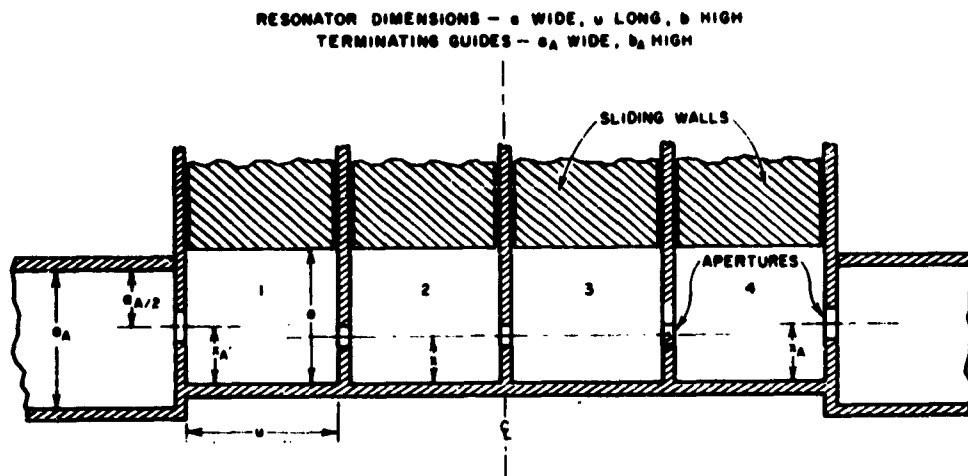
FIG. 17.04-1   A FOUR-RESONATOR MECHANICALLY TUNABLE WAVEGUIDE FILTER

where the $M_{j,j+1}$ are the horizontally directed magnetic polarizabilities of the coupling apertures, λ is the free-space wavelength at the resonant frequency f_0,

$$\lambda_{gA} = \frac{\lambda}{\sqrt{1 - \left(\frac{\lambda}{2a_A}\right)^2}} \qquad (17.04\text{-}5)$$

is the wavelength in the terminating guides, a_A, b_A, a, b, u, $\bar{x}_A$, and x are dimensions defined in Fig. 17.04-1, and where

$$a = \frac{u}{\sqrt{\left(\frac{2u}{\lambda}\right)^2 - 1}} \qquad (17.04\text{-}6)$$

is required in order to give resonance at the tuning frequency f_0 corresponding to the free-space wavelength λ.

As for the filter in Sec. 17.03, for constant response shape and bandwidth we desire the external Q's and coupling coefficients to vary with frequency as in Eqs. (17.03-5) to (17.03-7). Forcing Eqs. (17.03-5) to (17.03-7) to agree with Eqs. (17.04-2) to (17.04-4) at two frequencies $(f_0)_1$ and $(f_0)_2$ leads to equations of the form

$$\frac{Q_e\big|_{f_0=(f_0)_1}}{Q_e\big|_{f_0=(f_0)_2}} = \frac{(f_0)_1}{(f_0)_2} \qquad (17.04\text{-}7)$$

for the external Q's, and of the form

$$\frac{k_{j,j+1}\big|_{f_0=(f_0)_1}}{k_{j,j+1}\big|_{f_0=(f_0)_2}} = \frac{(f_0)_2}{(f_0)_1} \qquad (17.04\text{-}8)$$

for the coupling coefficients. These can be solved to obtain x_A and x just as θ_A and θ were solved for in the case of the filter in Sec. 17.03. However, in the present case there are other degrees of freedom available, which result from the fact that there is a choice in the proportions of

1014

the cavities and of the terminating guides.[2]
If, however, we specify $(f_0)_1/(f_0)_m$, $(f_0)_2/$
$(f_0)_m$, a_A, u and the wavelength λ_m at the
mean tuning frequency $(f_0)_m$, then the required
x_A and x values can be computed.

Table 17.04-1 shows normalized values
for x_A and x which will cause Eqs. (17.04-7)
and (17.04-8) to be satisfied for $(f_0)_1/$
$(f_0)_m = 0.90$ and $(f_0)_2/(f_0)_m = 1.10$. The
choice of cavity length u is controlled by
the λ_m/u parameter at the left. At the right
is shown the corresponding ratio a/u for the filter when tuned to the
mean tuning range frequency $(f_0)_m$.

Figure 17.04-2 shows plots of normalized external Q vs. $f_0/(f_0)_m$ for
the various cases listed in Table 17.04-1. Notice that the curves approach
the desired linear variation most closely when λ_m/u is made small.
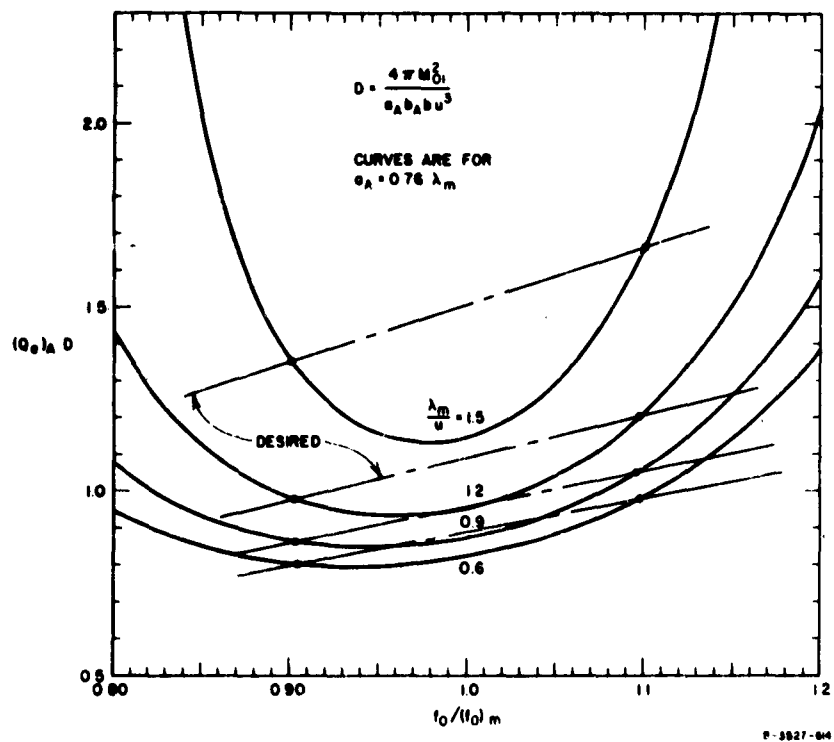
FIG. 17.04-2 CURVES OF NORMALIZED EXTERNAL Q vs. f_0 $(f_0)_m$
FOR PARAMETER VALUES IN TABLE 17.04-1
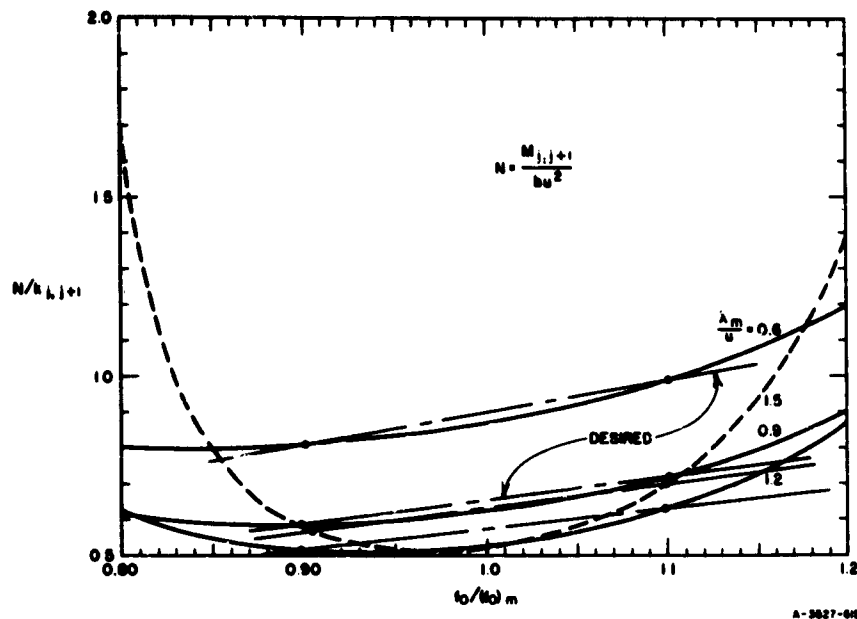
FIG. 17.04-3 CURVES OF NORMALIZED RECIPROCAL COUPLING
COEFFICIENT vs. $f_0/(f_0)_m$ FOR RESONATOR
PARAMETER VALUES IN TABLE 17.04-1

Figure 17.04-3 shows a corresponding plot of normalized reciprocal coupling
coefficient $vs.$ $f_0/(f_0)_a$. Here again the desired linear variation is ap-
proximated most closely if Λ_a/u is small. However, Fig. 17.04-4 shows a
plot of the corresponding values of a/u $vs.$ $f_0/(f_0)_a$ where it should be
recalled that u is constant while the cavity width a is varied to achieve
the desired tuning frequency. Note that the small values of Λ_a/u, which
gave the most desirable results in Figs. 17.04-2 and 17.04-3, correspond
to tuning characteristics that have very large changes in resonant fre-
quency f_0 for very small changes in cavity width a. Thus, as has been
discussed by Sleven,[2] in designing a tunable filter of this type one should
not insist on any greater uniformity of bandwidth and response shape than
is really necessary, since this uniformity is bought at the price of
criticalness in the tuning adjustment of the resonators.

Summary of Design Procedure — The first step in the design of a filter
of the type in Fig. 17.04-1 is to select a value for Λ_a/u using Figs. 17.04-2
to 17.04-4 while keeping the above points in mind. Some idea of the

variations in bandwidth that will result from the deviations of the reso-
nator coupling coefficients can be gained from the fact that the $k_{j,j+1}$
are directly proportional to the *fractional* bandwidth of the filter. The
choice of the external Q's of a multi-resonator filter affects the shape
of the pass band of a filter much more than it affects the bandwidth.
With a two-resonator filter, steadily increasing the size of the external
Q's tends to result in a Tchebyscheff response with an increasingly large
hump in the middle. Steadily decreasing the external Q's of such a filter
decreases and finally eliminates the hump in the middle of the response
and eventually leads to an "undercoupled" response (called *undercoupled*
because the coupling between resonators is quite loose as compared to the
coupling between the terminations and the resonators). Analogous effects
occur in filters with more resonators. The above points should be of some
help in assessing the effects of deviations from the ideal external Q and
coupling characteristics vs. frequency. More exact pictures of these
effects can be obtained by working back from the external Q and coupling
coefficient values at various frequencies by solving for the corresponding
sets of low-pass prototype element values g_0, g_1, $\cdots$, g_{n+1} using
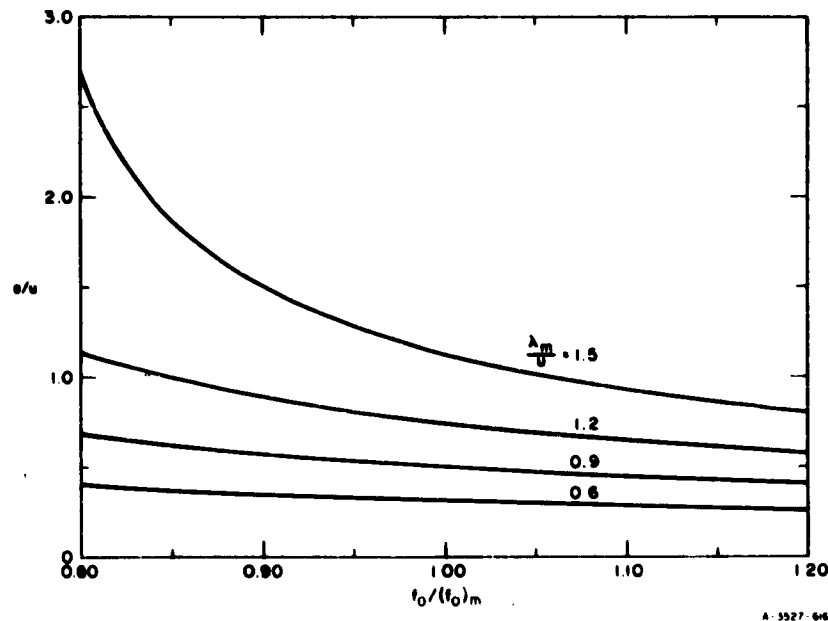
FIG. 17.04-4 a/u vs. $f_0/(f_0)_m$ FOR RESONATOR PARAMETER VALUES
IN TABLE 17.04-1

Eqs. (17.02-1) to (17.02-3) and then comparing these values with the
various tabulated designs in Sec. 4.05, or by actually computing the
responses corresponding to these sets of element values.

Having arrived at a suitable compromise choice for λ_a/u, then x_A/u
and x/u are obtained from Table 17.04-1 or by calculation as described
above. Having specified a mean tuning frequency $(f_0)_a$, the corresponding
free-space wavelength λ_a can be computed along with u, x_A, and x. The
desired external Q's and coupling coefficients are computed from the low-
pass prototype parameters by use of Eqs. (17.02-7) to (17.02-9). Then
using Eqs. (17.04-2) to (17.04-6) with $\lambda = \lambda_a$, the magnetic polarizabilities
M_{01}, M_{12}, ..., $M_{n,n+1}$ are obtained.

After the designer has obtained the required polarizabilities, the
dimensions of the apertures can be obtained from the data in Sec. 5.10.
If rectangular or elongated apertures are used, their length should be in
a direction parallel to the a dimension of the cavities in Fig. 17.04-1.
Corrections for aperture length $\ell_{j,j+1}$ and thickness t can be made as dis-
cussed at the end of Sec. 17.03 by use of Eq. (17.03-13). If round aper-
tures are used, the same procedure applies, except that the polarizability
is given by the approximate formula

$$M_{j,j+1} = \frac{d^3_{j,j+1}}{6} \qquad (17.04-9)$$

(where $d_{j,j+1}$ is the diameter of the aperture) and Eq. (17.03-13) becomes

$$(M_{j,j+1})_{comp} = M_{j,j+1} \left[1 - \left(\frac{1.7d_{j,j+1}}{\lambda_a} \right)^2 \right] 10^{\left(\frac{1.6t}{d_{j,j+1}} \right) \sqrt{1 - \left(\frac{1.7d_{j,j+1}}{\lambda_a} \right)^2}}$$

$$(17.04-10)$$

If high accuracy in the design is desired, the aperture sizes can be
checked using the experimental procedures described in Secs. 11.02 to
11.04.

SEC. 17.05, PROPERTIES OF FERRIMAGNETIC RESONATORS*

There are a number of single-crystal materials that have possible use as ferrimagnetic resonators in magnetically tunable microwave filters. Some materials of interest at the time of this writing are

(1)   Yttrium-iron-garnet (YIG)

(2)   Gallium-substituted yttrium-iron-garnet (GaYIG)

(3)   Lithium ferrite

(4)   Barium ferrite.

The YIG material listed above has proved the most useful to date and has been successfully used in constructing a variety of magnetically tunable microwave filters such as those described by Carter.[3,4,5,6]

In this book the detailed theory of ferrimagnetic resonance will not be treated. Such theory can be found in various references.[7,8,29] However, in this section a qualitative description of ferrimagnetic resonance will be presented along with some basic formulas and concepts useful in the design of magnetically tunable filters.

Description of the Resonance Phenomenon—Let us suppose that a dc H-field of strength H_0 is applied to a single-crystal YIG sphere in a horizontal direction, and then the direction of the H_0 field is rapidly switched to the vertical direction as shown in Fig. 17.05-1(a). The YIG material contains unpaired electrons which yield magnetic moments as a result of their spins. When the dc H-field is rapidly switched to the vertical position, these spin magnetic moments will precess about the vertical H-field H_0 at a rate of roughly (if H_0 is in oersteds)

$$ (f_0)_{Mc} \approx 2.8\, H_0 \qquad Mc \ . \qquad (17.05\text{-}1) $$

As time elapses the trajectory of the electron-spin magnetic moments will spiral in toward the direction of the H_0 field until the spins will ulti-mately end up parallel to the H_0 field. If the fields around the sphere are sampled while this process is going on, a circularly polarized RF field will be observed about the sphere like that which would be created if the

---
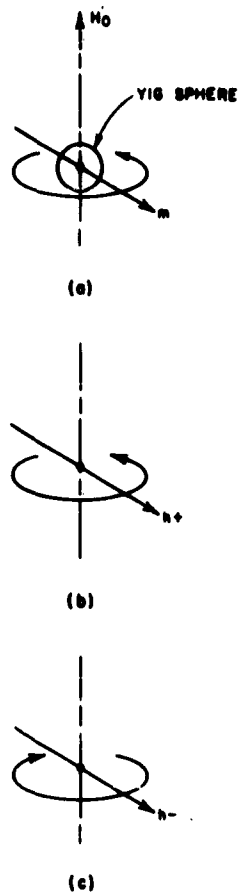
FIG. 17.05-1 A YIG SPHERE WITH A
CIRCULARLY POLARIZED
RF MAGNETIC MOMENT IS
SHOWN AT (a). EXTERIOR
CIRCULARLY POLARIZED
RF MAGNETIC FIELDS ARE
SHOWN AT (b) AND (c)

sphere contained a magnetic dipole rotating at the resonance rate given approximately by Eq. (17.05-1). This rotating dipole moment is pictured by Fig. 17.05-1(a). The circularly polarized magnetic field seen to be emanating from the sphere would die out exponentially with time in the same way that transient voltages and currents die out in a resonant circuit having dissipation loss.

Let us now consider another experiment. If the H_0-field is on and a circularly polarized RF H-field is applied as indicated by the rotating h^+ vector in Fig. 17.05-1(b), the RF field will have no effect on the sphere unless the frequency is at or very near the ferrimagnetic resonance frequency, which was given approximately by Eq. (17.05-1). When the circularly polarized applied field is at or very near the ferrimagnetic resonance frequency, circularly polarized RF H-fields will build up about the sphere in much the same way as the H-field will build up in the inductance of an L-C tuned circuit excited at its resonant frequency.

If a circularly polarized field with the circular polarization in the opposite direction, as indicated by the rotating vector in Fig. 17.05-1(c), is applied, the sphere will not respond even if the signal is at the ferrimagnetic resonance frequency. Thus it is seen that the resonance phenomenon is nonreciprocal.

If a linearly polarized RF H-field is applied to the sphere in a direction perpendicular to the biasing field H_0, it will be found that the

sphere will respond by emanating a circularly polarized RF H-field, provided that the linearly polarized field is at or very near the ferrimagnetic resonance frequency. The reason for this is that any linearly polarized field may be regarded as being the sum of two circularly polarized fields of equal strength rotating in opposite directions. Thus one of the circularly polarized components of the linear field will excite the sphere. Because of this, depending on the manner in which ferrimagnetic resonators are used, the transmission characteristics of the filter may be either reciprocal or nonreciprocal.

Parameters of Ferrimagnetic Resonator Materials—Several parameters characterize the various types of materials that can be used to construct ferrimagnetic resonators:

(1) Saturation magnetization, M_s

(2) Line width ΔH, or unloaded Q, Q_u

(3) Anisotropy field constant, K_1/M_s

(4) Curie temperature, T_c.

The saturation magnetization M_s is a function of the number of electron spins in the material per unit volume. The larger the M_s, the easier it is to couple from an exterior strip-line or waveguide circuit to a ferrimagnetic resonator.

The line width ΔH is defined in various ways, but it is basically the width of the resonance in oersteds as the signal frequency is held constant and the applied dc field is varied. For filter applications the line width ΔH is usually defined as the difference between the two values of biasing field (at each side of resonance) for which the imaginary part of the intrinsic susceptibility of the material equals the real part, while frequency is held constant. Looking at the same resonance phenomenon from the viewpoint of holding the biasing field constant and varying the frequency, we measure the unloaded Q of the resonator. With ΔH defined as above, for a spherical resonator

$$Q_u - \frac{f_0(10^{-6})}{2.8\ \Delta H} \qquad (17.05\text{-}2)$$

where f_0 is the resonant frequency in cycles per second and ΔH is the line width in oersteds. The unloaded Q of YIG will increase with frequency up

to around 5 or 10 Gc, but the curve of Q_u vs. frequency then levels out.[9] However, useful Q's appear to be possible up to at least 60 Gc.[10]

The line width (or unloaded Q) that will be measured for a ferrimagnetic resonator will depend upon both the material itself and the shape and surface finish of the material. In order for the line width to be narrow (and for the unloaded Q to be high) the internal field within the material must be uniform. Assuming that the applied H_0-field is uniform before the material is inserted, in order for the resonator material to have a uniform H-field within itself after being inserted within the biasing field, the resonator must be spheroidal or ellipsoidal.[7,8,29] Further, in order to achieve the narrowest possible line width (and highest possible unloaded Q), it is necessary that the surface of the resonator be very highly polished. Even when a ferrimagnetic resonator is spheroidal or ellipsoidal and is highly polished, its line width may still be degraded by the presence of metallic walls near the resonator. Some of this degradation, however, is unavoidable in most filter structures

The first-order anisotropy field constant K_1/M_s is important because of the lattice structure of single-crystal material. The lattice structure makes the material easier to magnetize along some crystal axes than along others. Because of this, the ferrimagnetic resonance frequency of a ferrimagnetic resonator will be influenced to some extent by the orientation of the crystal axes with respect to the biasing field H_0. As will be discussed below, the first-order anisotropy field constant K_1/M_s is used in computing the resonant frequency for various orientations of the crystal lattice with respect to the biasing field. There is also a second-order constant, but it is so small as to be unimportant for the applications herein.

The Curie temperature T_c is the temperature at which the saturation magnetization drops to zero.* Resonator operation at temperatures close to or above T_c is not possible.

Table 17.05-1 presents values for the parameters discussed above for various materials. Note that the saturation magnetization is given in gaussian units and is listed as $4\pi M_s$ gauss. This is the most commonly used unit for saturation magnetization. These values could be converted to mks units by use of the conversion

$$(\mu_0 M_s \text{ in webers/meter}^2) = (4\pi M_s \text{ in gauss})10^{-4} \qquad (17.05\text{-}3a)$$

---

*For ferrimagnetic materials this temperature is also known as the Néel temperature.[29]

or

$$(M_s \text{ in ampere-turns/meter}) = 79.5(4\pi M_s \text{ in gauss}) . \quad (17.05\text{-}3b)$$

Also recall that

$$(H_0 \text{ in ampere-turns/meter}) = 79.5(H_0 \text{ in oersteds}) . \quad (17.05\text{-}4)$$

Note that in Table 17.05-1 the $\Delta H = 0.22$ oersted line width listed (which is for a very high-quality YIG resonator) corresponds to an unloaded Q of 6500 at 4 Gc. This line width was measured in a waveguide with the spherical resonator some distance from any metallic walls. In practical filters the YIG resonators must be closer to metal walls, and the disturbing effects of the currents in the walls may reduce the unloaded Q to 2000 or less.

Table 17.05-1

PROPERTIES OF SINGLE-CRYSTAL FERRIMAGNETIC MATERIALS
FOR MAGNETICALLY TUNABLE FILTERS[6]

MATERIAL	$4\pi M_s$ (AT ROOM TEMPERATURE) (gauss)	K_1/M_s (AT ROOM TEMPERATURE) (oersteds)	ΔH (AT ROOM TEMPERATURE) (oersteds)	T_c (°C)
Yttrium-Iron-Garnet[†] (YIG)	1750	-43	0.22 (4 Gc), (Ref. 3)	292
Gallium-Substituted[†] Yttrium-Iron-Garnet (GaYIG)	50 - 1750 600 950 ± 50	-- -55.8 -41.7	-- -- 0.7 - 2.0 (at 4.4 Gc)	-- 160 206
Lithium Ferrite	3550 ± 40 (Ref. 11)	--	3[§](5 Gc)	--
"Planar" Ferrite "Zn_2Y" $(Ba_{12}Zn_2Fe_{12}O_{22})$	2850 (Ref. 12)	4950 (Ref. 12)	16 (X-band), (Ref. 12)	--

[*] These values of ΔH were measured in cavities. The line width may vary considerably from sample to sample and will be larger when measured in a closed-in filter structure.

[†] These materials were supplied by Microwave Chemical Laboratory, New York, N.Y.

[§] Private communication to P. S. Carter, Jr., from J. W. Nielsen, Airtron Division of Litton Industries, Morris Plains, New Jersey.

The value of ΔH may vary considerably from sample to sample of a given type of material, depending on how perfect the crystal structure is. However, M_s, K_1/M_s, and T_c are physical constants for a given type of material, and should vary only slightly from sample to sample. As will be discussed later, M_s and K_1/M_s do vary with temperature.

Determination of the Resonant Frequency—Three factors may cause the resonant frequency of a ferrimagnetic resonator to differ from the frequency indicated by Eq. (17.05-1):

(1) The shape of the resonator

(2) Crystalline anisotropy

(3) Interaction with currents in metallic walls close to the ferrimagnetic resonator.

The shape of the resonator can affect the resonant frequency because the shape affects the intensity of the demagnetizing field within the resonator.[7,8,29] Assuming that the biasing field H_0 is in the z direction, and x and y are rectangular coordinates perpendicular to H_0, then for any ellipsoidal resonator the resonant frequency (neglecting anisotropy effects) is given by

$$(f_0)_{Mc} = 2.8 \sqrt{[H_0 - (N_x - N_z)(4\pi M_s)][H_0 - (N_z - N_y)(4\pi M_s)]} \quad \text{Mc}$$

$$(17.05-5)$$

where N_x, N_y, and N_z are demagnetizing factors[7,8] in the x, y, and z directions, H_0 is in oersteds and $4\pi M_s$ is in gauss.

For a sphere

$$N_x = N_y = N_z = \frac{1}{3} \quad , \quad (17.05-6)$$

and Eq. (17.05-5) becomes

$$(f_0)_{Mc} = 2.8 \, H_0 \quad \text{Mc} \quad , \quad (17.05-7)$$

which is identical to Eq. (17.05-1).

We may consider a long thin rod and a very thin disk as limiting cases of ellipsoids. For an infinitely thin rod parallel to H_0,

$$N_x = N_y = \frac{1}{2} \quad \text{and} \quad N_z = 0 \quad . \quad (17.05-8)$$

For an infinitely thin disk in the plane of H_0 and the y axis,

$$N_x = 1, \quad \text{and} \quad N_y = N_z = 0 \quad . \quad (17.05-9)$$

If the disk lies in the plane of the x and y axis, then

$$N_x = N_y = 0 \quad \text{and} \quad N_z = 1 \quad . \qquad (17.05\text{-}10)$$

Thus, it can be seen that the shape of the resonator can have considerable effect on the resonant frequency. However, of the possible ellipsoidal shapes that can be used, the sphere is generally the most practical since it is the easiest to prepare with precision.

Materials such as YIG and GaYIG, which have cubic crystal structure, have three types of principal crystal axes: the [100], the [110], and the [111] axes.[13] Even though there are only three kinds of principal axes, there are three [100] axes, six [110] axes, and four [111] axes in each single-crystal. For a given applied biasing field H_0, the resonant frequency of a ferrimagnetic resonator will be influenced by the direction of these axes relative to the direction of the applied field. The opposite extremes of this effect occur when the [111] or the [100] axis is parallel to the H_0 field, when the [110] axis is parallel to H_0 an intermediate effect results. For a *sphere* of cubic crystal material with a [111] axis parallel to the H_0 field, Eq. (17.05-7) becomes

$$(f_0)_{Mc} = 2.8 \left(H_0 - \frac{4}{3} \frac{K_1}{M_s} \right) \quad \text{Mc} \quad , \qquad (17.05\text{-}11)$$

while if a [100] axis is parallel to H_0

$$(f_0)_{Mc} = 2.8 \left(H_0 + 2 \frac{K_1}{M_s} \right) \quad \text{Mc} \qquad (17.05\text{-}12)$$

where H_0 and K_1/M_s are in oersteds. For YIG or GaYIG, K_1/M_s is negative and Eq. (17.05-11) gives resonance for a lower field strength than does Eq. (17.05-12). As a result, for materials such as YIG and GaYIG which have negative K_1/M_s, the [111] axes are known as *easy* axes while the [100] axes are known as *hard* axes. If K_1/M_s is positive, the roles of these axes are reversed. For YIG, the difference in resonant frequencies given by Eqs. (17.05-11) and (17.05-12) is about 401 Mc, which is, of course, a significant difference. Figure 17.05-2 shows curves of the resonant frequency *vs.* biasing field strength for the [100], [110], and [111] axes parallel to the biasing field.

$f_{[111]} - f_{[100]} = 401$ Mc

$f_{[100]} = 2.8 \times 10^6 \left\{H_0 - 86\right\}$

$f_{[110]} = 2.8 \times 10^6 \left\{(H_0 - 43)(H_0 + 86)\right\}^{1/2}$

$f_{[111]} = 2.8 \times 10^6 \left\{H_0 + 57.2\right\}$

H_0 — kilooersteds

A-2326-330R
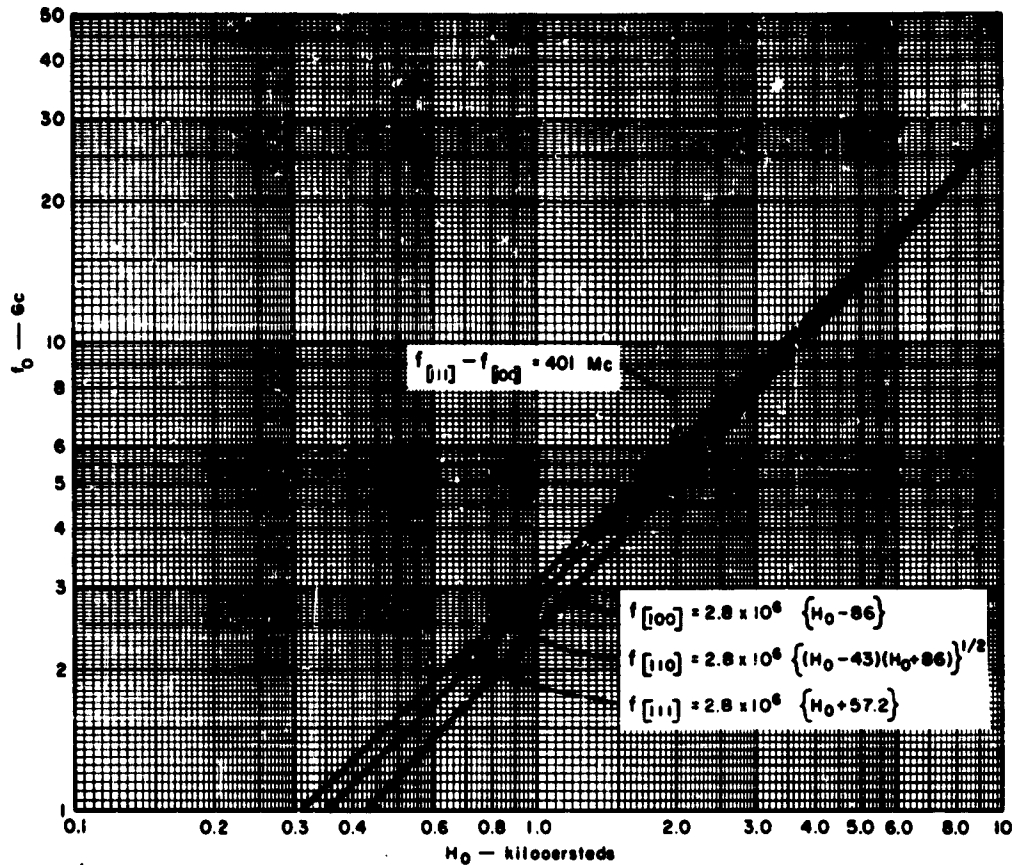
FIG. 17.05-2   RESONANT FREQUENCY OF YIG SPHERE vs. APPLIED dc FIELD
WITH FIELD ALONG THE [100], [110], OR [111]
PRINCIPAL AXES

If a sphere of ferrimagnetic material with cubic crystal structure
is rotated about a [110] crystal axis that is perpendicular to H_0, the
value of biasing field H_0 required to give resonance at $(f_0)_{Mc}$ megacycles
is

$$H_0 = \frac{(f_0)_{Mc}}{2.8} - \left(2 - \frac{5}{2}\sin^2\theta - \frac{15}{8}\sin^2\theta\right)\frac{K_1}{M_s} \qquad \text{oersteds}$$

(17.05-13)

where θ is the angle between H_0 and that [100] axis which becomes parallel
to H_0 as the sphere is rotated about the given [110] axis. This manner of
rotation will cause the sphere at different times to have a [100] or a

1026

[111] axis parallel to H_0, and the field strength for resonance will cover the largest possible range as the resonator is rotated.
Figure 17.05-3 presents measured data, due to Y. Sato and P. S. Carter, Jr.,[6] which show how the measured field strength for resonance at 3000 Mc varies as a YIG sphere is rotated about an [110] axis that is perpendicular to H_0.

As was mentioned above, the metallic boundary conditions seen by ferrimagnetic resonators can also alter their resonant frequencies. If all of the resonators see the same boundary conditions, this effect should cause no trouble. However, if one or more of the resonators see different boundary conditions (such as generally occurs in a filter with three or more YIG resonators) then some means for compensating for the detuning effects of the metallic boundaries is desirable. A successful way of doing this has been found: spherical resonators are mounted in such a way that they can be rotated about [110] axes that are perpendicular to H_0, as was done in making the measurements in Fig. 17.05-3. Using this technique, the resonators can be tuned by rotating their mounting shafts until angular positions relative to each other are obtained that will give synchronous tuning.

Minimum Tuning Frequency—As a ferrimagnetic resonator is tuned to lower and lower frequencies, the applied field H_0 to give resonance gets
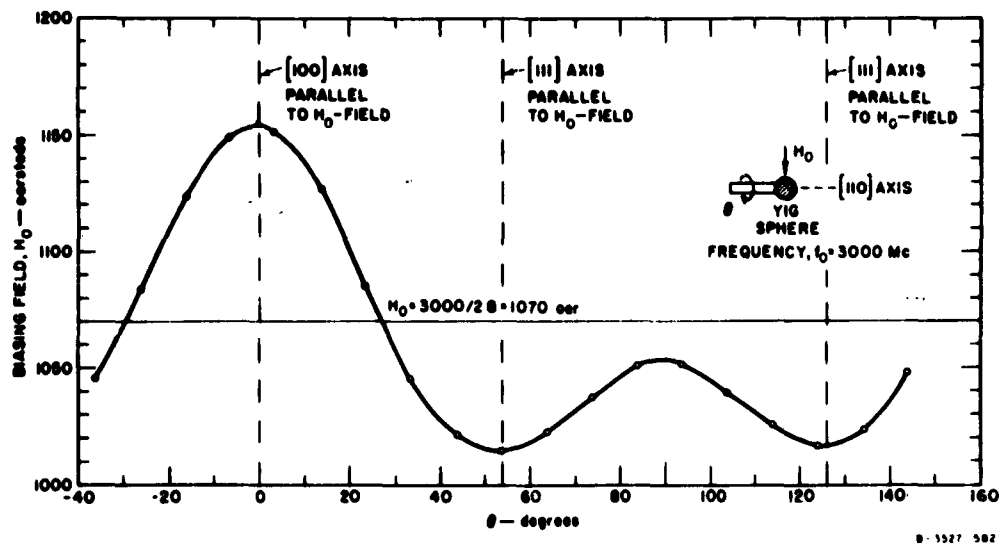

FIG. 17.05-3   FIELD STRENGTH TO GIVE RESONANCE AT 3000 Mc AS A YIG SPHERE
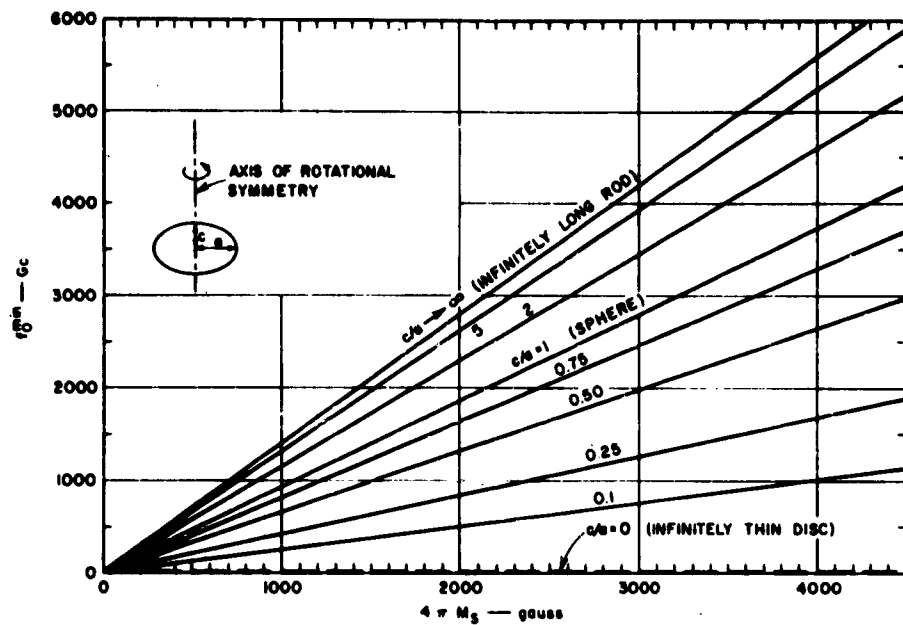IS ROTATED ABOUT A [110] AXIS WHICH IS PERPENDICULAR TO H_0

FIG. 17.05-4   APPROXIMATE MINIMUM RESONANT FREQUENCIES OF
FERRIMAGNETIC ELLIPSOIDS HAVING VARIOUS AXIS
RATIOS

smaller and smaller. When the applied field becomes so low as to be
approximately equal to or less than the demagnetizing field, the reso-
nator will cease to function. Since the demagnetizing field is deter-
mined by M and the demagnetizing factors (which are a function of the
shape of the resonator), the minimum resonant frequency is determined by
M_s and the resonator shape. Figure 17.05-4 shows plots of the minimum
resonant frequency f_0^{min} in gigacycles vs. $4\pi M_s$ in gauss for various
ellipsoidal shapes. Note that for YIG, which has $4\pi M_s = 1750$ gauss, the
minimum resonant frequency for a spherical sample is approximately 1630 Mc.
(In practice, the minimum frequency is found to be a little higher than
this.) In theory, by using flat, disk-like ellipsoidal shapes the minimum
resonant frequency could be reduced greatly. However, in practice, disk-
shaped resonators do not appear to work very well, possibly because of the
difficulty in obtaining disk-like resonators that are sufficiently perfect
ellipsoids.

A more practical way of obtaining lower minimum resonant frequencies
appears to be to use spheroidal resonators of single-crystal material

1028

having a lower value of $4\pi M_s$. At this time the gallium-substituted YIG materials appear to be the most promising in this respect. For example, the GaYIG material with $4\pi M_s = 600$ gauss listed in Table 17.05-1 should give a minimum resonant frequency of around 700 Mc for a spherical sample. The possible disadvantages of such materials are that the lower values of M_s will make coupling from the external circuit to the spheres more difficult, and the line widths of the material may not be as narrow as those obtainable with ordinary YIG.
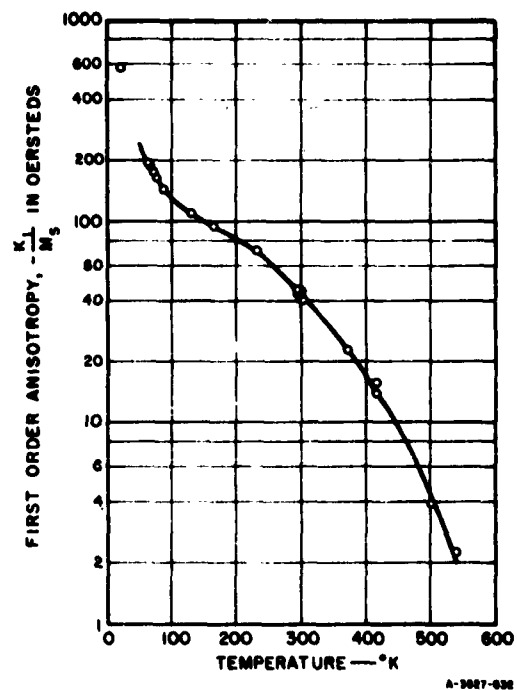
Temperature Effects—Temperature will affect the values of K_1/M_s, M_s, and ΔH. Of these effects probably the changes in K_1/M_s are potentially the most troublesome. Figure 17.05-5 shows some measured data due to Dillon[14] for $-K_1/M_s$ vs. temperature in degrees Kelvin for YIG. Note that the anisotropy constant varies considerably with temperature. By Eq. (17.05-11), if the [111] axis is parallel to H_0 the change in resonant frequency Δf_0 due to a change $\Delta|K_1/M_s|$ in the anisotropy field constant is

$$(\Delta f_0)_{Mc} = 3.73 \Delta\left|\frac{K_1}{M_s}\right| \quad Mc \quad (17.05-14)$$

while if the [100] axis is parallel to H_0

$$(\Delta f_0)_{Mc} = 5.6 \Delta\left|\frac{K_1}{M_s}\right| \quad Mc \quad (17.05-15)$$

where $\Delta|K_1/M_s|$ is in oersteds. From Fig. 17.05-5, for a change in temperature from 100°F to 200°F (i.e., 311°K to 466°K), $\Delta|K_1/M_s| = 31$ oersteds. Then the changes in resonant frequency given by Eqs. (17.05-14) and (17.05-15), are 115 and 173 Mc, respectively. Thus, we see that the shift in resonant frequency can be quite significant if the change in temperature is large.


SOURCE: *Physical Review* (see Ref. 14 by J. F. Dillon, Jr.)

FIG. 17.05-5   MEASURED VARIATION OF $-K_1/M_s$ vs. TEMPERATURE FOR YIG

It should be possible to 'eliminate the effect of temperature on the resonant frequency by orienting the crystal axes in certain directions. Note that in Fig. 17.05-3 the resonant frequency in megacycles is given by 2.8 H_0 when the sphere is oriented at the plus or minus 27 degree points. With these orientations, the anisotropy effects are cancelled out, and the resonant frequency should be independent of temperature.

Figure 17.05-6 shows some measured data of $4\pi M_s$ vs. temperature, which was obtained from work of Kooi, Stinson, Moss, Bradley, and Freiberg.[15]

Note that the saturation magnetization decreases as the temperature increases. As will be seen from the discussion in Sec. 17.07, the external Q's of a filter will be proportional to $1/M_s$, while the coupling coefficients between resonators are proportional to M_s. As a result, the bandwi_th of the filter will be proportional to M_s while the response shape (i ., its Tchebyscheff character, for example) should remain unchanged as M_s is varied. Of course, if M_s is decreased (and the bandwidth
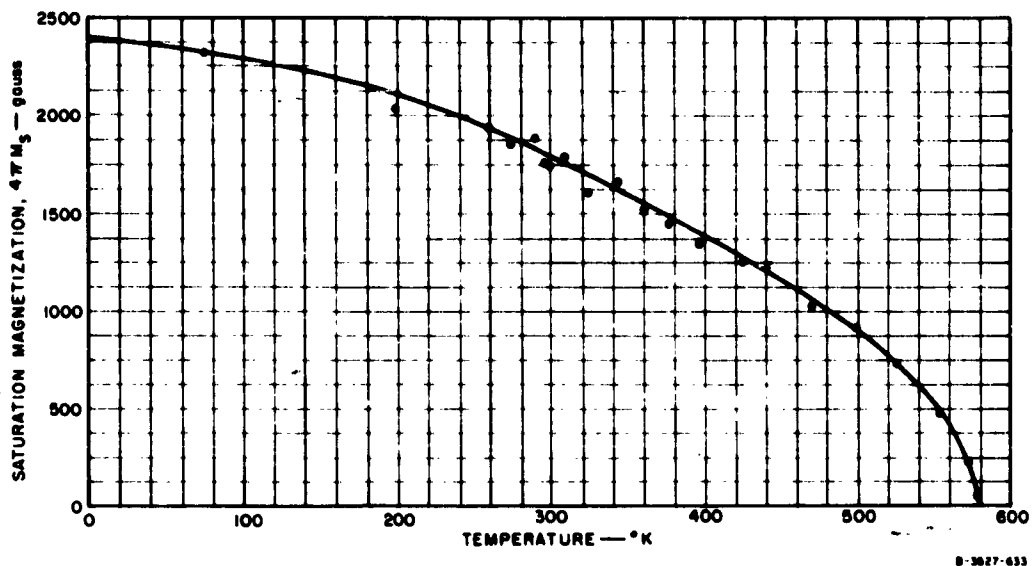
FIG. 17.05-6   MEASURED VARIATION OF SATURATION MAGNETIZATION WITH
TEMPERATURE FOR YIG

is decreased), the pass-band dissipation loss will increase, as is always the case when a filter's bandwidth is narrowed; if the resonator unloaded Q's are held constant.

Data from Spencer, LeCraw, and Linares[16] indicates that for very pure, well-polished YIG, the line width should vary approximately proportionally to the *absolute* temperature, at least in the room temperature range. Since the line width controls the unloaded Q of the resonators, this will have some influence on the dissipation loss of the filter. However, unless the temperature ranges covered are very large, this effect should not be of great importance in most practical situations.

Higher-Order Magnetostatic Modes—In the desired "free-precessional" resonant mode of ferrimagnetic resonators, all of the electron spins precess with the same phase. However, if either the applied biasing H-field or the RF H-field is not uniform, higher-order modes can occur in which the phases of the precessions in parts of the sphere will be different from the phases in other parts. This causes the ferrimagnetic resonator to have more than one resonant frequency for a given value of biasing H-field.[17] Because of the metallic material required near ferrimagnetic resonators in order to couple to them, there are almost always some disturbing effects which will tend to excite higher-order magnetostatic modes. However, if care is taken to keep the magnetic fields as uniform as possible, it should in most cases be possible to keep spurious responses due to higher-order modes at a level of 30 or more db below the level of the main response.

Besides designing the structure so as to keep the fields as uniform as possible, another important measure is to keep the ferrimagnetic resonator as small as possible. Fletcher and Solt[18] have found that if other factors are held equal, the coupling to higher-order magnetostatic modes depends on the ratio D_a/λ where D_a is the diameter of the sphere and λ is the wavelength at the frequency in question. The smaller D_a/λ, the less coupling there will be to higher-order modes. Thus, it is desirable to make ferrimagnetic resonators as small as possible—consistent with considerations of obtaining adequate coupling from the external circuit to the desired resonance of the resonators.

Power Limiting Effects—When the power passing through a ferrimagnetic resonator becomes sufficiently large, the insertion loss of the resonator will begin to increase greatly as a result of nonlinear effects.[19] Because

of this property of ferrimagnetic resonators, ferrimagnetic resonance filters also find application as limiters. Depending on the circuit design, type of resonator material, and frequency range, the limiting level may be much less than a milliwatt or up to around 10 watts.[20,21,22,23,3,4] A treatment of the theory of ferrimagnetic limiting is, however, beyond the scope of this discussion.

SEC. 17.06, DETERMINATION OF THE CRYSTAL AXES OF SPHERICAL FERRIMAGNETIC RESONATORS

The crystal axes of ferrimagnetic resonators can be determined by X-ray techniques, but fortunately there are simpler and easier methods. When a spherical ferrimagnetic resonator is placed within a strong magnetic field, it will automatically try to align itself so that one of its "easy" axes will be parallel to the applied field. If all of the resonators of a ferrimagnetic-resonator filter see the same boundary conditions (such as is usually the case in two-resonator ferrimagnetic filters) then aligning the resonators on their easy axes by this method is usually sufficient. After the easy axis of a resonator is determined by use of a strong magnetic field, the resonator is cemented to a small dielectric mount in the desired position.

As was discussed in Sec. 17.05, the easy axis is the [111] axis for yttrium-iron-garnet (YIG) or gallium-substituted yttrium-iron-garnet (GaYIG), both of which have negative anisotropy constants. In some cases, it may be desirable to rotate a resonator sphere about a [110] axis in order to obtain a tuning effect of maximum size, or in order to orient the resonator to a direction where anisotropy effects will be cancelled out, to make the tuning of the resonator independent of temperature. In order to locate a [110] axis, special procedures are required.

A technique for determining crystal axes other than the easy axes has been described by M. Auer.[24] His procedure involves geometric construction to determine the location of other axes after two easy axes have been determined. P. S. Carter, Jr. and Y. Sato[5,26] have extended Auer's method by devising an aligning jig which accomplishes the desired results very quickly and simply.

Briefly, the device of Carter and Sato[5,26] works as follows. The magnet is placed on a rotating mount as shown in Fig. 17.06-1 so that the field can be oriented in any desired direction with respect to the jig that holds
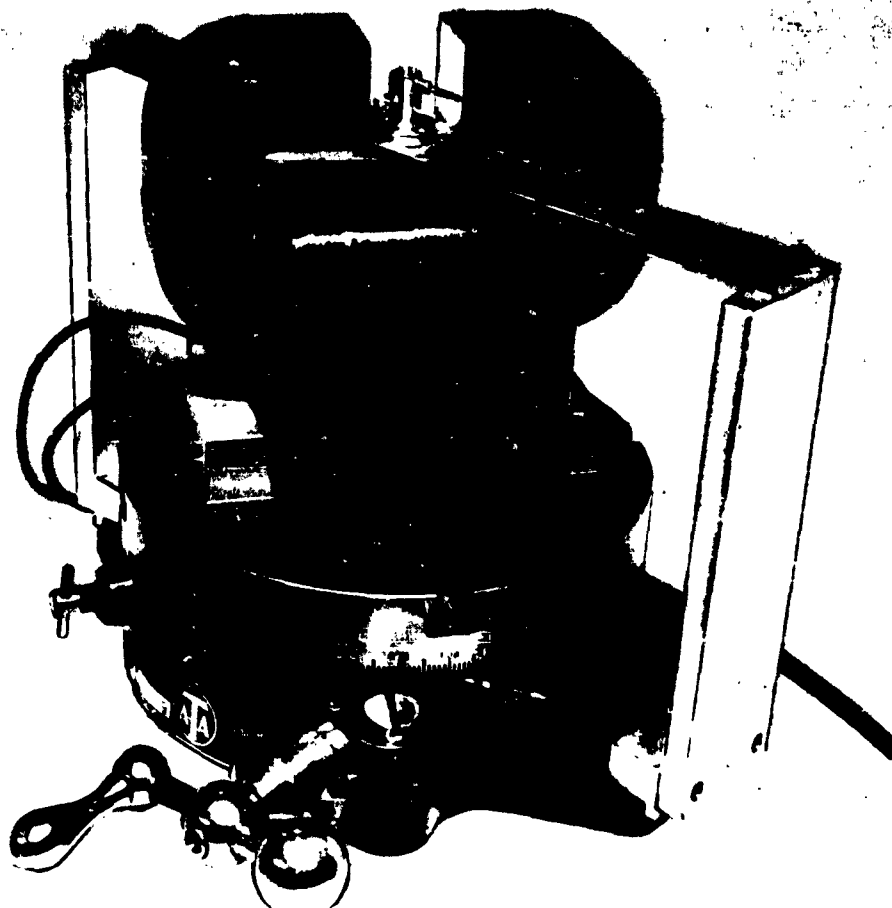
A-3527-404

FIG. 17.06-1 DEVICE FOR ORIENTING FERRIMAGNETIC CRYSTALS USING A
ROTATABLE ELECTROMAGNET AND ALIGNING JIG

the spherical crystal. The crystal is first mounted so that it is free
to turn until an easy axis (of which there are four in a cubic crystal
with negative anisotropy) comes into coincidence with the direction of
the magnetic field. After this first orientation is completed, the sphere
is attached (using some easily soluble glue, wax, etc.) to a wire which is
in line with the determined easy axis and which is placed in a radial hole

1033

FIG. 17.06-2   ALIGNING JIG SHOWING YIG SPHERE ATTACHED TO WIRE ALONG
ONE EASY AXIS AND QUARTZ ROD ALONG [110] AXIS

in the side of the aligning jig as shown in Fig. 17.06-2. This wire is
free to turn in the radial hole under the influence of the small torques
exerted on the ferrimagnetic sample by an applied dc field. This step
locates and retains one of the easy axes, and permits the sphere to
rotate about this axis.

   The next step is to rotate the magnet by an amount that depends on
the crystal axis which one is trying to locate. To determine the [110]
axis (the face diagonal) requires (as shown in Fig. 2 of Ref. 20) that
we locate a second easy axis displaced from the first by 70½ degrees.
This second angle is accurately located by means of the milling head

1034

protractor. The ferrimagnetic sphere rotates on che wire to which it was
attached in the previous step, so that the second easy axis is now placed
along the dc field. The final step is to attach the sphere to a dielectric .
rod along the [110] axis. A radial hole is located in the side.of the
alignment jig along the bisector of the angle between the two easy axes.
The radial hole, and the dielectric rod that it holds in position, are
shown in Fig. 17.06-2. The sample is attached to the dielectric rod (or
other holder) with a drop of cement and the wire is taken off.

SEC. 17.07, DESIGN OF MAGNETICALLY TUNABLE BAND-PASS FILTERS
          WITH TEM-MODE INPUTS AND OUTPUTS, AND A DISCUSSION
          OF GENERAL DESIGN PRINCIPLES

Figure 17.07-1 shows a possible form of single-resonator magnetically
tunable filter. This filter uses two coupling loops, oriented perpendicu-
larly to each other to minimize the coupling between them. One loop is
within the other, and a spherical ferrimagnetic resonator is so placed as
to be at the center of both loops. (In the picture shown, the loops would
have to be somewhat egg-shaped, with the long dimension of the y loop in
the x direction and the long dimension of the x loop in the z direction,
in order that both loops will have equal coupling to the sphere and still
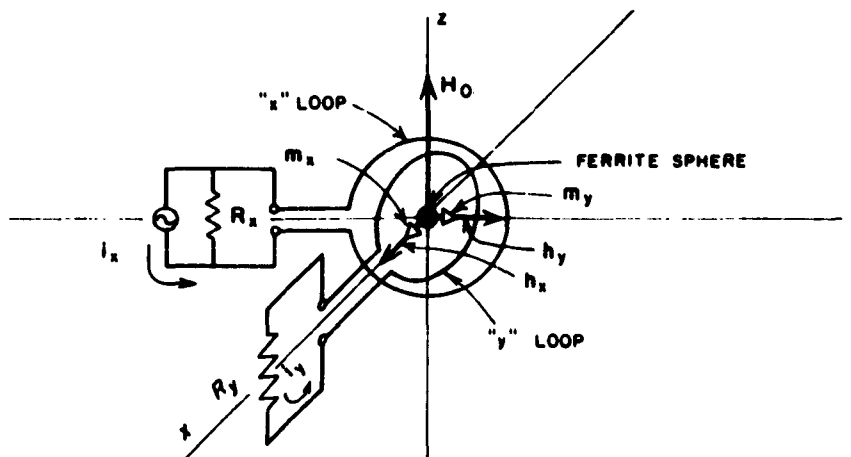
RA-2326-TB-189RR

FIG. 17.07-1 A SINGLE-RESONATOR MAGNETICALLY TUNABLE FILTER
             USING LOOP COUPLING

not touch each other.) The biasing H_0-field is parallel to the plane of both loops. When a signal at the ferrimagnetic resonant frequency is applied to the x loop, resonance will be excited in the sphere causing resulting HF magnetic dipole moments in both the x and y directions. The dipole moment in the y direction will create a magnetic field, which will couple to the y loop and result in transmission to the R_y termination. When the signal applied to the x loop is not at the ferrimagnetic resonance frequency, there will be no coupling between the x and y loops except for a small unavoidable amount of stray coupling.

Successful single-resonator filters have been built in the form shown in Fig. 17.07-1, but this type of structure has certain disadvantages. One is that the stray coupling is larger than in some other possible structures, and the other is that the HF magnetic fields are not very uniform, which will tend to excite higher-order magnetostatic modes. Both of these disadvantages can be combated by making the loops and the sphere as small as is practically feasible.

FIG. 17.07-2 A SINGLE-RESONATOR STRIP-LINE MAGNETICALLY TUNABLE FILTER

Figure 17.07-2 shows a strip-line single-resonator magnetically tunable filter structure. In this structure a dividing wall separates the two strip-lines and decreases the coupling between them. Note that the lines are at right angles to each other, which will further tend to reduce any stray coupling. In this case the sphere is placed in a hole in the wall separating the two strip-lines, and at resonance the circularly polarized magnetic moment excited in the sphere will cause coupling from one strip-line to the other. This structure still has a non-uniform HF field in the sphere as a result of being half on one side of the dividing wall and half on the other. For this reason, in order to minimize difficulties with higher-order modes, the sphere should be quite small (i.e., of the order of a fiftieth to a hundredth of a

wavelength in diameter). Kotzebue[25] has constructed coaxial filters which
are very similar to the strip-line filter shown in Fig. 17.07-2.

Figure 17.07-3 shows a type of two-resonator strip-line structure
with which Carter has obtained very good results.[4] In this structure,
each sphere is mounted close to the short-circuited end of the input or
output strip-line structure. Thus, the large RF H-field in the vicinity
of the short-circuits gives relatively good coupling between the strip
lines and the spheres. Coupling between spheres is obtained by use of a
long slot having its long dimension parallel to the axis of the strip
lines. This orientation of the slot causes minimum disturbance of the
currents and fields about the strip lines, while furnishing maximum iso-
lation between the strip lines. Thus, the coupling between strip lines
is extremely small when the spheres are not resonant. However, when the
spheres become resonant, the circularly polarized RF dipole moment in

FIG. 17.07-3   A TWO-RESONATOR MAGNETICALLY
TUNABLE FILTER WITH COUPLING
THROUGH TOP AND BOTTOM WALLS

1037

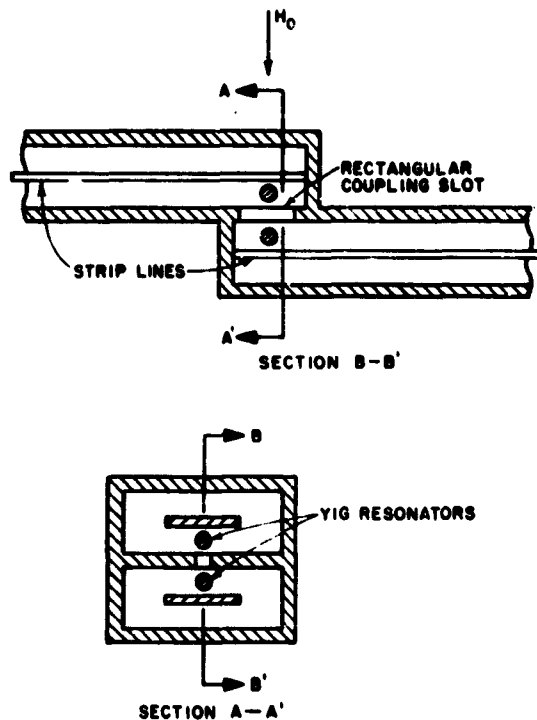the spheres provides a component of RF H-field which will couple through
the elongated slot very easily, and good coupling is obtained between
spheres. This structure has the advantage of providing relatively uniform
RF H-fields so that higher-order magnetostatic modes are not so easily ex-
cited, and high off-resonance isolation is not difficult to obtain. As
compared with the structures in Fig. 17.07-4, which are about to be dis-
cussed, the structure in Fig. 17.07-3 has the disadvantages of requiring
a larger magnet air gap and of not being quite as suitable for the design
of filters with more than two resonators.

Figure 17.07-4 shows two side-wall coupled filter configurations which
are similar to that in Fig. 17.07-3 except that the spheres are coupled
through the side wall of the structure instead of through the top and
bottom wall. One advantage of this structure is that the input and output
strip-lines can lie in the same plane, and as a result the magnet air gap
required can be minimized. Another advantage of this structure is that
additional spheres can be added as shown in Fig. 17.07-4(b) to give a
filter with more than two resonators, while all of the resonators see very
nearly the same boundary conditions. As can be seen from the discussion

(a) TWO-RESONATOR CONFIGURATION

(b) THREE RESONATOR CONFIGURATION
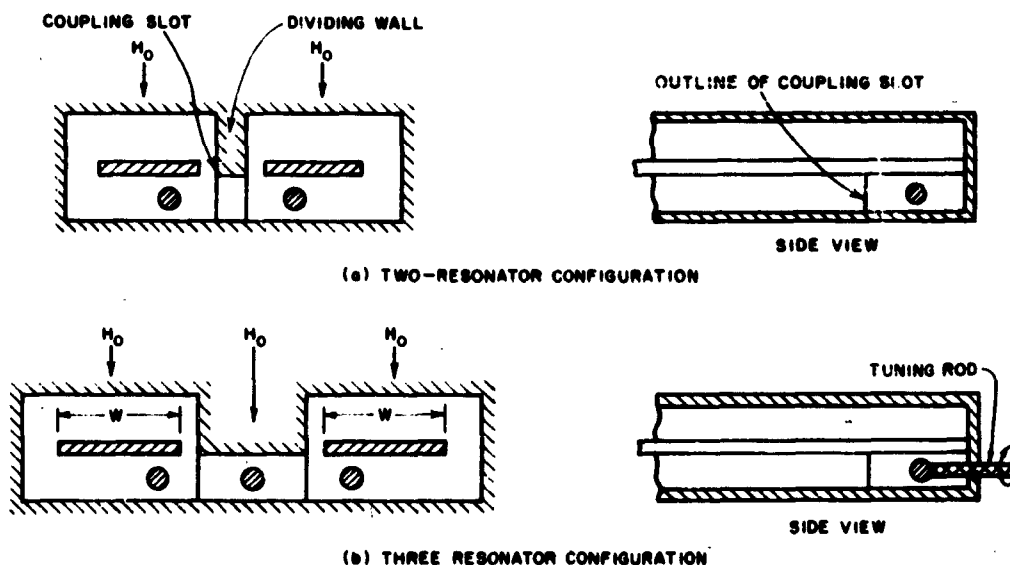
FIG. 17.07-4 TWO- AND THREE-RESONATOR MAGNETICALLY TUNABLE FILTERS
WITH COUPLING THROUGH THE SIDE WALLS

in Sec. 17.05, it is necessary for all spheres to see the same boundary conditions, and for all spheres to have the same orientation of their crystal axes with respect to H_0 if the spheres are all to have the same resonant frequencies for any given H_0 and given temperature. Although the structure in Fig. 17.07-4(b) gives relatively uniform boundary conditions for all spheres, some means for tuning the spheres is desirable in order to correct the small tuning errors that may be present. In Fig. 17.07-4(b) provision for rotating the spheres about a [110] axis (as discussed in Sec. 17.05) is suggested. A disadvantage of the structure in Fig. 17.07-4(a) as compared to that in Fig. 17.07-3 is that in the structure in Fig. 17.07-4(a) it may be necessary to place the spheres toward the inner edges of the strip-lines in order to obtain adequate coupling between spheres. This puts the spheres in a region of less uniform RF H-field, which makes them more vulnerable to higher-order modes.

All of the filters in Figs. 17.07-1 to 17.07-4 are reciprocal, except for a gyrator action* which is present in the circuits in Fig. 17.07-1 and 17.07-2.[3,6] For purposes of analysis the circuits in Figs. 17.07-1 to 17.07-4 may be thought of as operating like the filter with magnetically coupled resonators shown in Fig. 17.07-5. When the coupled coils are replaced by their T-equivalents, the circuit in Fig. 17.07-5 becomes of the form in Fig. 17.02-3, except for a small amount of residual self-inductance in series with the terminations R_A and R_B. Fortunately, the properties of ferrimagnetic resonators are such that they give nearly constant bandwidth as the filter is tuned, without resorting to special measures such as were required in the design of the filters in Secs. 17.03 and 17.04. There will be some change in response shape, however.

As with most any kind of narrow-band, band-pass filter, the desired response shape and bandwidth can be obtained by starting with a low-pass prototype filter and a specified desired fractional bandwidth w, and then computing the external Q's and coupling coefficients required for the band-pass filter, by use of Eqs. (17.02-1) to (17.02-3). The tabulated maximally flat or Tchebyscheff low-pass prototypes in Sec. 4.05 can be used, but the equal-element prototypes discussed in Sec. 11.07 should be of special interest for this application. The rate of cutoff of the filter can be

---

* This causes 180 degrees more phase shift in one direction of transmission than in other directions of transmission. This gyrator action results from the fact that in the circuits in Figs. 17.01-1 and 17.01-2 the input and output lines couple to orthogonal components of the circularly polarized magnetic moment within the sphere.
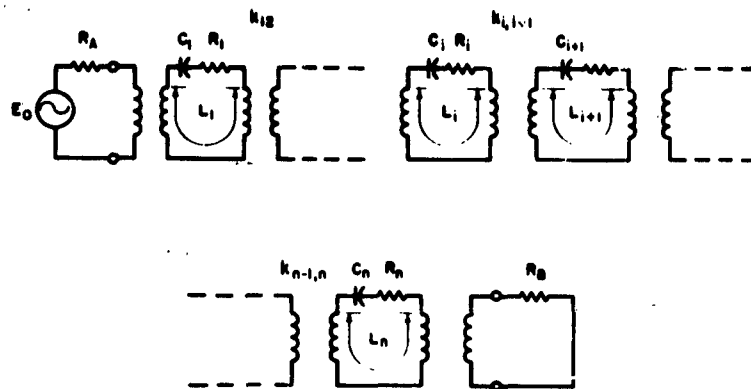
FIG. 17.07-5   EQUIVALENT CIRCUIT OF A FILTER HAVING n
FERRIMAGNETIC RESONATORS

estimated by use of the mapping defined by Eqs. (17.02-20) to (17.02-22)
along with the charts in Sec. 4.03, or by use of the data in Sec. 11.07.
The midband dissipation loss to be expected can be estimated by use of
the methods of Secs. 11.06 or 11.07.

Once the filter design has been fixed in terms of determining the
required number of resonators, determining the required external Q's of
the end resonators, and determining the coupling coefficients of the
couplings between resonators, the designer can focus his attention on the
physical parameters of the circuit required to realize these coupling
properties. Let us now consider the design of the structure after the
desired values for the external Q's and coupling coefficients have been
determined.

Design for Prescribed External Q's—Carter[3] has derived approximate
expressions for the external Q of ferrimagnetic resonators in various
coupling structures. For a loop of radius r meters having a sphere of
volume V_s cubic meters at its center, the external Q is

$$Q_e = \frac{4r^2 R_A}{\mu_0 V_s \omega_s} \left[1 + \left(\frac{\omega L_s}{R_0} \right)^2 \right] \qquad (17.07\text{-}1)$$

where R_A is the terminating resistance connected to the loop, L_s is the
self-inductance of the loop in henries, $\mu_0 = 1.256 \times 10^{-6}$ henries/meter
is the permeability of air, and

1040

$$\omega_a = \gamma \mu_0 M_s \qquad\qquad (17.07\text{-}2)$$

where $\gamma = 1.759 \times 10^{11}$ (mks units) is the gyromagnetic ratio. The quantity $\mu_0 M_s$ in webers/meter^2 can be obtained from $4\pi M_s$ in gauss by use of Eq. (17.05-3a). For YIG, ω_a is about $3.08\ (10^{10})$.

A corresponding equation for a YIG sphere mounted near a short-circuiting wall in a strip-line structure of impedance Z_0' is given in Fig. 17.07-6 along with curves that apply when $Z_0' = 50$ ohms and when the resonator is made from YIG. Note that the curves give Q_e for a given center conductor to ground-plane spacing d and sphere diameter D_a, both given in inches. If these curves are to be used for a resonator of some material other than YIG, or with a uniform strip-line of some impedance other than 50 ohms, the values obtained from the chart should be scaled as indicated by the equation

$$Q_e\Big|_{scaled} = Q_e \frac{(M_s)_{YIG}}{(M_s)_{used}} \frac{50}{(Z_0')_{used}} \qquad\qquad (17.07\text{-}3)$$

where $(Z_0')_{used}$ is the actual line impedance used and $(M_s)_{YIG}/(M_s)_{used}$ is the ratio of the saturation magnetization of YIG to that of the material actually used. The equation in Fig. 17.07-6 (upon which the curves are based) was computed assuming that the strip-line was bounded on each side by a magnetic wall (which implies that there are no fringing fields), and that the fields about the strip-line are perfectly uniform. Of course, if the strip-line is so narrow that the sphere projects into fringing fields, this approximation will not be good.

Figure 17.07-7 shows computed and experimental data obtained by Carter[3] in order to check out the equation in Fig. 17.07-6. These data were taken at 3000 Mc using the structure shown. Note that the sphere for each test was mounted about 0.125 inch from the short-circuit. It was found that moving the sphere too close to the short-circuiting wall would disrupt the sphere's performance, while putting the sphere too far from the wall would introduce excess reactance that would decouple the sphere. Note in Fig. 17.07-7 that the agreement between theory and measurement is reasonably good.

Other experimental work due to Carter[4] showed that the presence of an adjacent coupling slot such as that in the filter in Fig. 17.07-3 has

a decoupling effect on the input circuit which tends to raise the external Q about 20 percent or somewhat more from its value when the slot is not there. Therefore, some allowance should be made for this effect when designing for the strip-line and sphere dimensions to realize a required external Q.

$$Q_e = \frac{(120\pi)^2 d^2}{\mu_0 \, \omega_m V_m Z_0'}$$

$Z_0' = 50\,\Omega$

$d = 0.075$ in.
0.087
0.100
0.125
0.150
0.175
0.200

D_m — inches
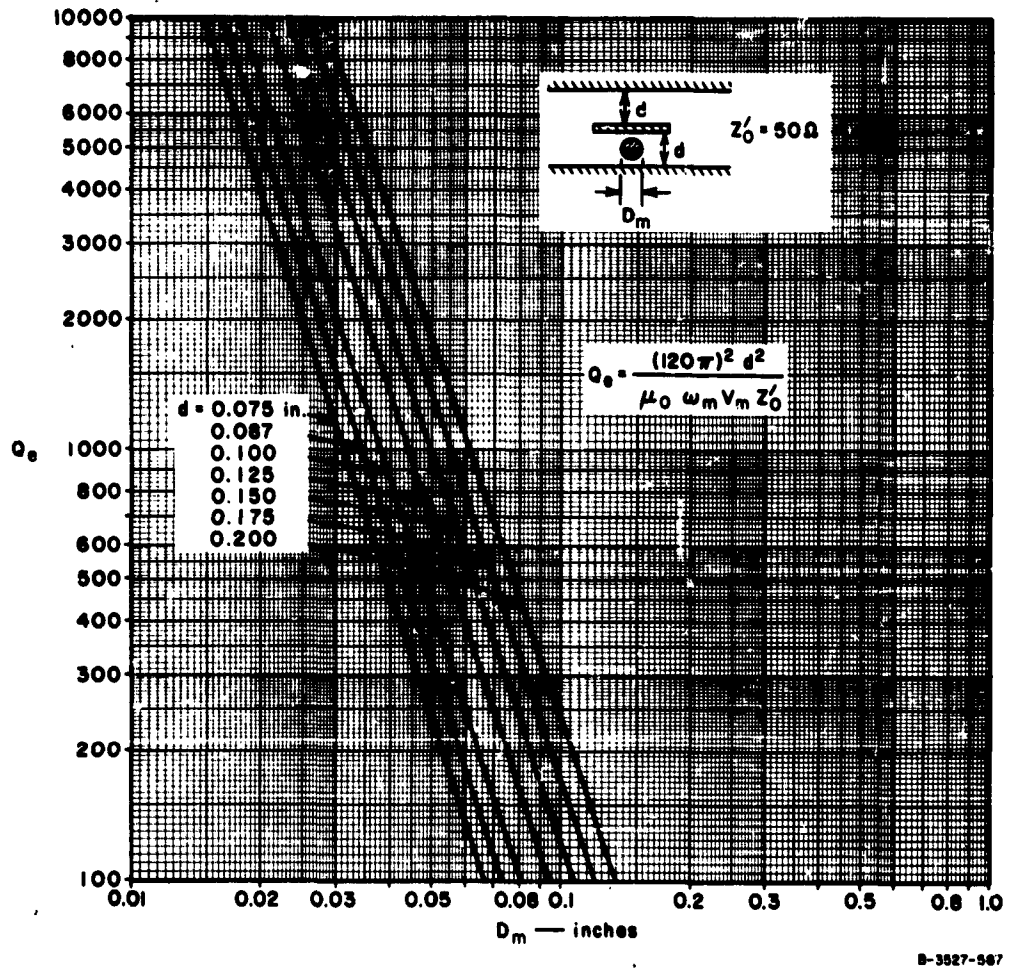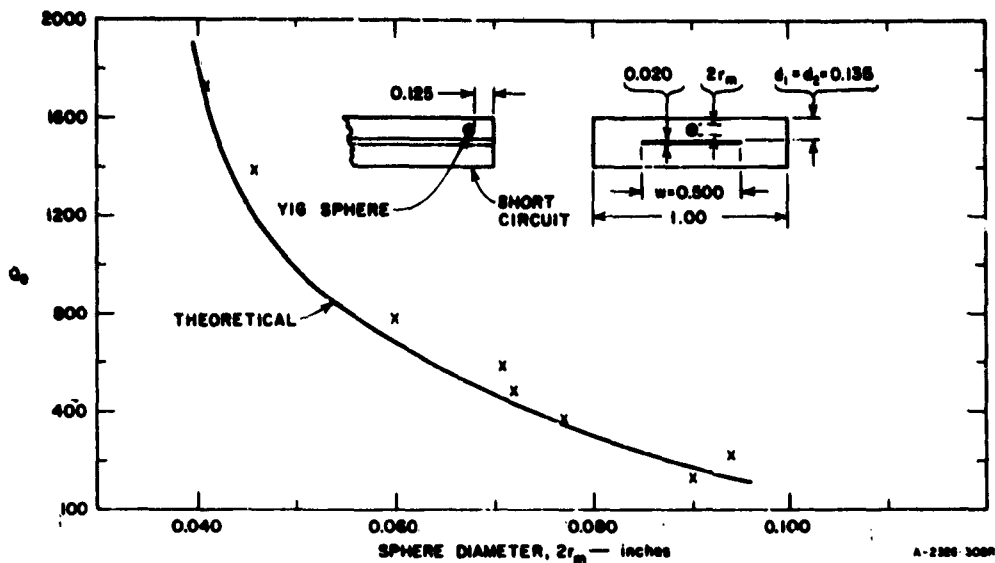
B-3527-567

FIG. 17.07-6 Q_e vs. SPHERE DIAMETER FOR SPHERICAL YIG RESONATOR IN SYMMETRICAL STRIP TRANSMISSION LINE
In the equation shown μ_0 is the permeability of the region about the sphere, $\omega_m = \gamma \mu_0 M_s$, $\gamma = 1.759 \times 10^{11}$ in mks units, V_m is the volume of the sphere, and Z_0' is the impedance of the strip line ($Z_0' = 50$ ohms for the graph).

FIG. 17.07-7   THEORETICAL AND EXPERIMENTAL VALUES OF Q_e OF YIG RESONATOR
USING STRIP-TRANSMISSION-LINE

Note in the equation in Fig. 17.07-6 that the external Q is inversely
proportional to the line impedance Z_0'. This is because for a given sphere
size and ground-plane-to-center-conductor spacing d, the narrower the strip-
line, the more concentrated the RF H-field is assumed to be in the vicinity
of the sphere. (The presence of fringing fields disrupts this picture when
the strip becomes narrow, however.) The equation and curves in Fig. 17.07-6
assume that the strip line is uniform and that it is terminated in its
characteristic impedance. However, if a short length of line of impedance
Z_0' is used in the vicinity of the sphere, and this line is terminated in a
much lower resistance R_A, it should be possible to obtain lower values of
external Q than would be possible otherwise. Thus, if Q_e is the external
Q when the line is terminated in a resistance $R = Z_0'$, then the external Q
when termination is changed to R_A is approximately

$$Q_e\big|_{corrected} = Q_e\,\frac{R_A}{Z_0'} \qquad\qquad (17.07\text{-}4)$$

1043

This, of course, assumes that the line section of impedance Z'_0 (to which the sphere is coupled) is short compared to a quarter wavelength, so that there will not be excessive reactance effects due to the Z'_0 line section not being matched. As seen by Eq. (17.07-4), the coupling can be made tighter (i.e., the corrected value of Q_e can be made lower) if R_A is made small. This result will be seen to be in agreement with Eq. (17.07-1). Thus, in cases where difficulty is being experienced in obtaining a sufficiently low value of Q_e, decreasing the size of R_A may be a satisfactory way of obtaining the desired result. If the external load impedance is not suitable for this, a step transformer can be used to present the desired R_A value to the resonator.

The procedures described in Sec. 11.02 will be found to be convenient for experimentally checking external Q values, as well as unloaded Q values.

Design for Prescribed Coupling Coefficients Between Resonators—The calculation of the spacing of ferrimagnetic resonators and the dimensions of intervening apertures in order to obtain specified coupling coefficients is a relatively difficult problem and no such procedures are presently available. However, it is quite practical to experimentally determine the proper sphere spacings and aperture sizes by use of the two-resonator test procedures described in Sec. 11.04. Some of the results shown in Sec. 17.08 should serve as a useful guide in estimating the approximate sphere spacings and aperture sizes to be expected.

Besides the consideration of obtaining adequate coupling between spheres, other considerations are the obtaining of sufficiently high isolation off resonance, and the maintenance of sufficient separation between the spheres so that the spheres will not cause each other to see non-uniform biasing H-fields (which could help excite unwanted modes). The experimental results obtained from the examples in Sec. 17.08 should be helpful guides with regard to both of these points. With regard to the spacing of the spheres, spacing their centers by about three times their diameters appears to be satisfactory.

Effects of Scaling the Filter Parameters—It should be useful to know the effect on the external Q's of the end resonators and on the coupling coefficient between resonators of changing the dimensional scale of the circuit, the saturation magnetization M_s, and the operating frequency range. Such information should help the designer in relating information obtained from a given filter design to other filter designs having somewhat different parameters.

1044

As previously discussed in this section, the equivalent circuits in Fig. 17.02-3 can be used in analyzing filters with ferrimagnetic resonators. Hence, Eqs. (17.02-11) to (17.02-13) also apply and we may restate them here in the form

$$(Q_e)_A = \frac{R_A \alpha_1}{(X_{01})^2} \qquad (17.07\text{-}5)$$

$$k_{j,j+1} = \frac{X_{j,j+1}}{\sqrt{\alpha_j \alpha_{j+1}}} \qquad (17.07\text{-}6)$$

$$(Q_e)_B = \frac{R_B \alpha_n}{(X_{n,n+1})^2} \qquad (17.07\text{-}7)$$

where the $X_{j,j+1}$ are mutual reactances and the α_j are resonator slope parameters. The mutual reactances can be assumed to be of the form

$$X_{j,j+1} = \omega_0 \mu_0 W_{j,j+1} \qquad (17.07\text{-}8)$$

where ω_0 is the radian frequency at resonance, μ_0 is the permeability of air in henries/unit length, and $W_{j,j+1}$ is a scale factor depending on the dimensions of the circuit. The parameter $W_{j,j+1}$ has the dimension of length. Then by Eq. (17.07-5) and (17.07-8)

$$(Q_e)_A = \frac{R_A \alpha_1}{\omega_0^2 \mu_0^2 (W_{01})^2} \qquad (17.07\text{-}9)$$

Now Carter[26] has shown that in general, if a ferrimagnetic resonator is coupled by way of a linearly polarized RF magnetic field h, then

$$Q_e = \frac{R_A}{\mu_0 V_s (U_{01})^2 \omega_a} \qquad (17.07\text{-}10)$$

where V_s is the volume of the sphere,

$$\omega_a = \mu_0 \gamma M_s , \qquad (17.07\text{-}11)$$

γ is the gyromagnetic ratio, and

$$U_{01} = \frac{h}{I_A} \qquad . \qquad (17.07\text{-}12)$$

where h is the RF field seen by the resonator due to current I_A flowing in the lead P_A. The parameter U_{01} is seen to have dimensions of $1/(\text{length})$. Equating Eqs. (17.07-10) and (17.07-9), and solving for the resonator slope parameter α_1 gives

$$\alpha_1 = \frac{\omega_0^2 \mu_0 (W_{01})^2}{V_a (U_{01})^2 \omega_a} \qquad . \qquad (17.07\text{-}13)$$

Assuming that $\alpha_j = \alpha_1$, by Eqs. (17.07-6), (17.07-8), and (17.07-13) we obtain

$$k_{j,j+1} = \frac{\omega_a (U_{01})^2 W_{j,j+1} V_a}{\omega_0 (W_{01})^2} \qquad . \qquad (17.07\text{-}14)$$

Checking the dimensionality of Eq. (17.07-14) we find that

$$k_{j,j+1} = \frac{A \omega_a}{\omega_0} = \frac{A \mu_0 \gamma M_a}{\omega_0} \qquad (17.07\text{-}15)$$

where A is a dimensionless factor which is determined only by the *relative* proportions of the various parts of the circuit, but which is independent of the dimensional scale of the circuit.

From a somewhat different point of view, it would appear that changing the M_a of the resonators ought to be like changing the number of turns in the coils in the circuit in Fig. 17.07-5. In that case the mutual reactance X_{01} for coupling to the load ought to be proportional to M_a, while the mutual reactances $X_{j,j+1}$ for coupling between resonators ought to be proportional to $(M_a)^2$. An analysis from this point of view was worked out in a manner similar to that described above. This analysis also led to Eq. (17.07-15), which helps to verify its correctness.

A number of useful conclusions can be drawn from the above analysis:

(1) Scaling the circuit up or down in size will have no effect
on the coupling coefficients between resonators, although
by Eqs. (17.07-10) to (17.07-12) it can be seen that the
external Q's of the end resonators will be affected. The
Q_e will vary as $1/(\text{size})$.

(2) The coupling coefficients between resonators will vary as
$1/\omega_0$ but the external Q's are independent of frequency.
Since the coupling coefficients predominate in determining
bandwidth, the bandwidth of a filter with ferrimagnetic
resonators will tend to remain constant as it is tuned (see
Sec. 17.02), but the response shape will change. A filter
with moderate-sized Tchebyscheff ripples at the center of
the tuning range will tend to have larger ripples when
tuned at the lower edge of the tuning range, and may tend
toward a nearly maximally flat response when tuned at the
upper edge of the tuning range.

(3) The coupling coefficients are directly proportional to M_s
while the external Q's are inversely proportional to M_s.
Thus as can be seen with the aid of Sec. 17.02, any change
in M_s will alter the filter bandwidth in proportion to the
change in M_s while the response shape should remain un-
affected. One qualification to this statement needs to
be made with regard to dissipation loss. Since the dis-
sipation loss effects are influenced by bandwidth (see
Secs 11.06 and 11.07), there may be some change in re-
sponse shape for this reason.

(4) Because the external Q varies as $1/(\text{size})$, as the circuit
is scaled in size, and because the coupling coefficients
vary as $1/\omega_0$, the obtaining of adequate coupling between
the end resonators and the external circuits, and the
obtaining of adequate coupling between adjacent resonators,
will become increasingly difficult as the operating fre-
quency is increased. Ferrimagnetic materials with
especially large values of M_s should be helpful for use
in the higher microwave ranges.

At the time of this writing, the above conclusions have not been
systematically checked by experimental means; however, they do appear to
be consistent with available experimental evidence. In particular, the
measured responses of the filters worked on by Carter[3,4,5,6] bear out the
second of the above conclusions very well.

SEC. 17.08, RESULTS OF SOME TRIAL MAGNETICALLY TUNABLE BAND-PASS FILTER DESIGNS HAVING STRIP-LINE INPUTS AND OUTPUTS*

Several trial magnetically tunable filter designs will now be described. Since part of the design process involves cut and try (namely the determination of the spacings of the resonators and the sizes of the coupling apertures), these designs should provide helpful guide lines for additional designs.

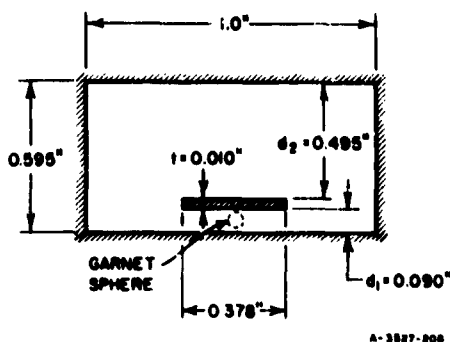*A Trial Two-Resonator YIG Filter Design Using Top and Bottom Wall Coupling*—Figure 17.08-1 shows the cross section of the strip-lines which were used in the design of a magnet-ically tunable filter of the form in Fig. 17.07-3. In this case, the strip line was made unsymmetrical in an effort to obtain tighter coupling to the spheres for given line impedance. The smaller spacing d_1 between the strip line and the bottom wall should give a greater flux density and tighter coupling to the sphere for a given line impedance. However, using a larger upper wall spacing d_2 increases the magnet air gap required, and other means for obtaining a tight coupling to the sphere appear at this time to be preferable. (The use of a step transformer to lower the terminating impedance seen by the resonator is recommended, as discussed in Sec. 17.07.)

FIG. 17.08-1 STRIP-LINE DIMENSIONS FOR AN EXPERIMENTAL FILTER OF THE FORM SHOWN IN FIG. 17.07-3

In this case the external Q's were computed using the formula

$$Q_e = \frac{120 \ \pi W' \ (d_1/d_2) \ (d_1 + d_2)}{\mu_0 \omega_a V_a} , \qquad (17.08-1)$$

where

$$W' = \frac{377}{Z_0'} \frac{d_1 d_2}{(d_1 + d_2)} \qquad (17.08-2)$$

---

* These designs are due to P. S. Carter, Jr.[4,6]

is the *effective* width of the line if it had no fringing capacitance
and Z_0' is the impedance of the line. All other quantities are as de-
fined in Fig. 17.08-1, or as were defined in connection with Eq. (17.07-1),
(17.07-2), and Fig. 17.07-6. The actual strip width W to give a Z_0' =
50-ohm line with fringing capacitance was estimated using the fringing
capacitance data in Sec. 5.05.

This trial filter design used 0.074-inch-diameter YIG spheres mounted
on 0.010-inch-thick dielectric plates, as indicated in Fig. 17.08-2. The
coupling slot between the spheres (see Fig. 17.07-3) was 0.105 inch wide
and 0.320 inch long, while the metal wall separating the input and output
strip line structures was 0.125 inch thick, as indicated in Fig. 17.08-2.
It was found desirable to use a relatively thick dividing wall in order
to separate the spheres enough that they would not disturb the biasing H_0
field seen by each other. Each sphere was mounted with its center 0.160 inch

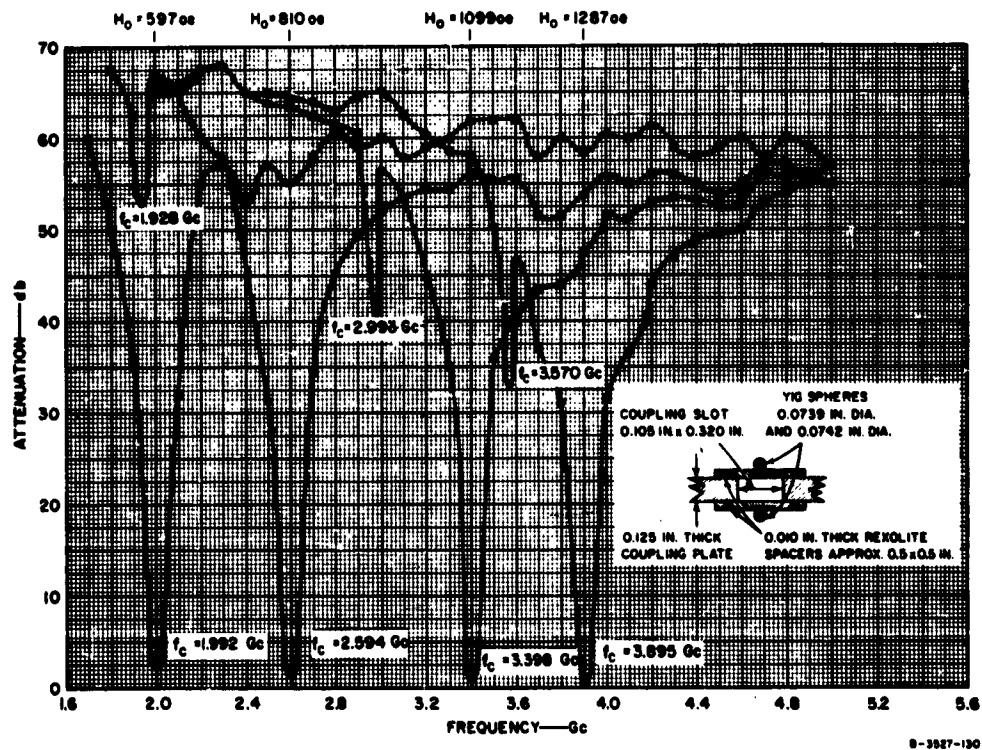

FIG. 17.08-2 MEASURED RESPONSE FOR A TRIAL TWO-RESONATOR FILTER
OF THE FORM SHOWN IN FIG. 17.07-3
The responses for four different values of biasing H_0 field are superimposed.

1049

from the vertical short-circuit wall terminating its strip line. The estimated external Q computed using Eqs. (17.08-1) and (17.08-2) was 105, while measured values obtained without the coupling slot averaged about 125. As might be expected, cutting the coupling slot in the wall between the two spheres tended to increase the external Q's, so that the measured values averaged around 170. The size of the coupling slot was determined by cut and try increases in the coupling-slot width until a Tchebyscheff response with small ripple was obtained.

Tests on one of the resonators gave a measured unloaded Q value which ranged from about 550 at 2 Gc to 1255 at 3.90 Gc, when tested in the strip-line structure before the coupling slot was cut. After the 0.105-inch by 0.302-inch slot was present, these values were, interestingly enough, raised to 710 and 1810, respectively. This same resonator when tested in waveguide had an unloaded Q of 3800 at 2.6 Gc, and 6,600 at 4.0 Gc.[4] The considerably lower Q's in the strip-line structure are due to the deleterious effects of the relatively confining metallic boundaries seen by the sphere.

The spheres were mounted so that they had a [111] axis (*i.e.*, an easy axis) parallel to H_0. Figure 17.08-2 shows the measured attenuation characteristics of the filter obtained for four values of biasing field H_0. Note that the off-resonance attenuation is quite high, although there is a spurious response below the pass band in each case. The higher the pass-band frequency, the lower the attenuation at the spurious response, until when the filter is tuned around 4.5 Gc, the spurious response merges with the pass-band response. The minimum attenuation of this filter was 2.8 db when tuned at 2.0 Gc, 1.8 db at 2.6 Gc, 1.3 db at 3.4 Gc, and 0.8 db at 3.9 Gc.

A Side-Wall Coupled Two-Resonator YIG Filter Design—Figure 17.08-3 shows the dimensions of an experimental filter of the sidewall-coupled type in Fig. 17.07-4(a). Note that the dividing wall with its aperture was made easily removable, so that various wall thicknesses and aperture sizes could be tried. The YIG spheres were mounted on dielectric rods so that they could be rotated about a [110] axis in order to achieve synchronous tuning. This type of tuning was provided mainly because it was planned that this filter would later be converted to a three-resonator filter, and it appeared desirable to include means for tuning the resonators with respect to each other.
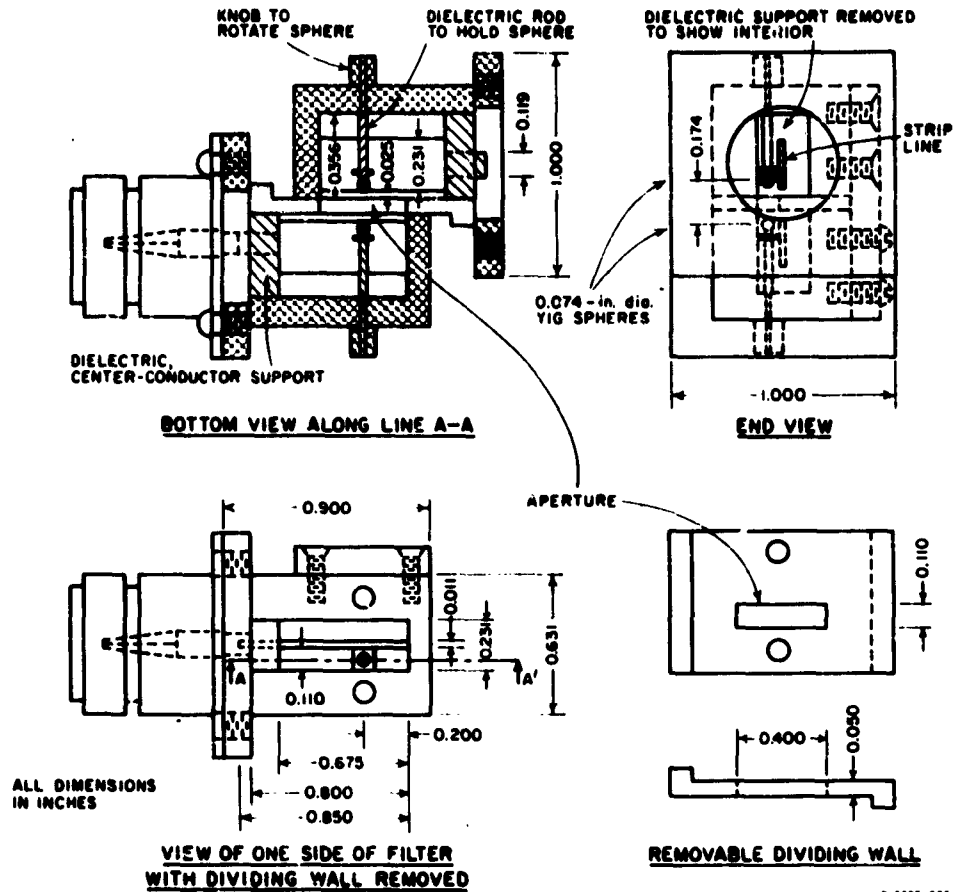
**FIG. 17.08-3   DETAILS OF A TWO-RESONATOR YIG FILTER
OF THE FORM SHOWN IN FIG. 17.07-4(a)**

Note that the strip lines in Fig. 17.08-3 are closer to the dividing wall than to the outer walls. This was done so that adequate coupling could be maintained between spheres while still keeping the spheres under the strip lines. The strip lines were designed to give a desired impedance of $Z_0' = 50$ ohms by first computing C_0/ϵ, the required normalized capacitance per unit length, by use of

$$\frac{C_0}{\epsilon} = \frac{376.7}{\sqrt{\epsilon_r}\, Z_0'} \tag{17.08-3}$$

1051

where ϵ_r is the relative dielectric constant of the medium of propagation. Then, referring to Fig. 17.08-4, desired values for t, b, $S_1/2$ and $S_2/2$ were selected, and the corresponding line width W required to give the desired line impedance Z_0' was computed using the formula

$$\frac{W}{b} = \frac{1}{2}\left(1 - \frac{t}{b}\right)\left[\frac{C_0}{2\epsilon} - \left(\frac{C_{f0}'}{\epsilon}\right)_1 - \left(\frac{C_{f0}}{\epsilon}\right)_2\right] \quad . \quad (17.08\text{-}4)$$

where $(C_{f0}/\epsilon)_1$ and $(C_{f0}/\epsilon)_2$ are normalized fringing capacitances obtained from Fig. 5.05-10(a) using $s/b = S_1/b$ and $s/b = S_2/b$, respectively.
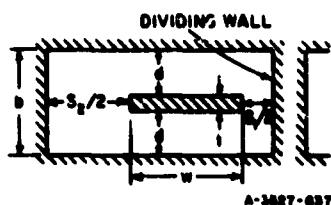

FIG. 17.08-4 DEFINITION OF THE STRIP-LINE PARAMETERS FOR THE FILTER SHOWN IN FIG. 17.08-3

This trial filter used 0.074-inch-diameter YIG spheres, while the spacing d between the strip-line and the adjacent ground planes was 0.110 inch. By Fig. 17.07- these dimensions are seen to yield a theoretical value of external Q of about 150, which is satisfactorily low. Measured values of Q_e in this structure ranged from 212 to 236. These relatively high measured values are no doubt due largely to the spheres being located near the edges of the strip lines instead of at their centers. The size of the coupling aperture was held constant while various thicknesses of the dividing wall in Fig. 17.08-3 were tried until a response with a small Tchebyscheff ripple was obtained

Table 17.08-1 along with Figs. 17.08-5 and 17.08-6 show the measured performance of this filter. The data in Fig. 17.08-6 were taken by holding the frequency constant and varying the biasing magnetic field. As can be seen from Fig. 17.08-6, the spurious response below the pass band is more severe than is the

Table 17.08-1

MEASURED CHARACTERISTICS OF TWO-RESONATOR SIDE-WALL-COUPLED FILTER IN FIG. 17.08-3

f_c (Gc)	$(L_A)_{min}$ (db)	VSWR (minimum)	Q_u (CALCULATED FROM MEASURED DATA)	H_0 (oersteds)	$\Delta f_{3\,db}$* (Mc)	$\Delta f_{30\,db}$* (Mc)
2.000	4.0	1.9	--	714.7	26	117
3.000	1.2	1.01	1500	1070	20	113
4.000	1.0	1.48	2050	1427	25	121

* The bandwidths given are measured to the 3-db or 30-db points below $(L_A)_{min}$.

main spurious response in the case of the top- and bottom-wall coupled
filter whose response is shown in Fig. 17.08-2. The larger spurious
response in Fig. 17.08-6 is believed to be due to having the spheres so
close to the edge of the strip-lines. By using a thinner dividing wall
between strip lines, it is possible to move the spheres further back
under the strip lines, but a thinner dividing wall was found to reduce
the off-resonance isolation of the filter. Note from Fig. 17.08-5 and
Table 17.08-1 that the 3-db and 30-db bandwidths of the filter are nearly
constant as the filter is tuned, while the response changes from an over-
coupled response at the lower end of the tuning range to an under-coupled
response at the upper end of the tuning range. These results are in agree-
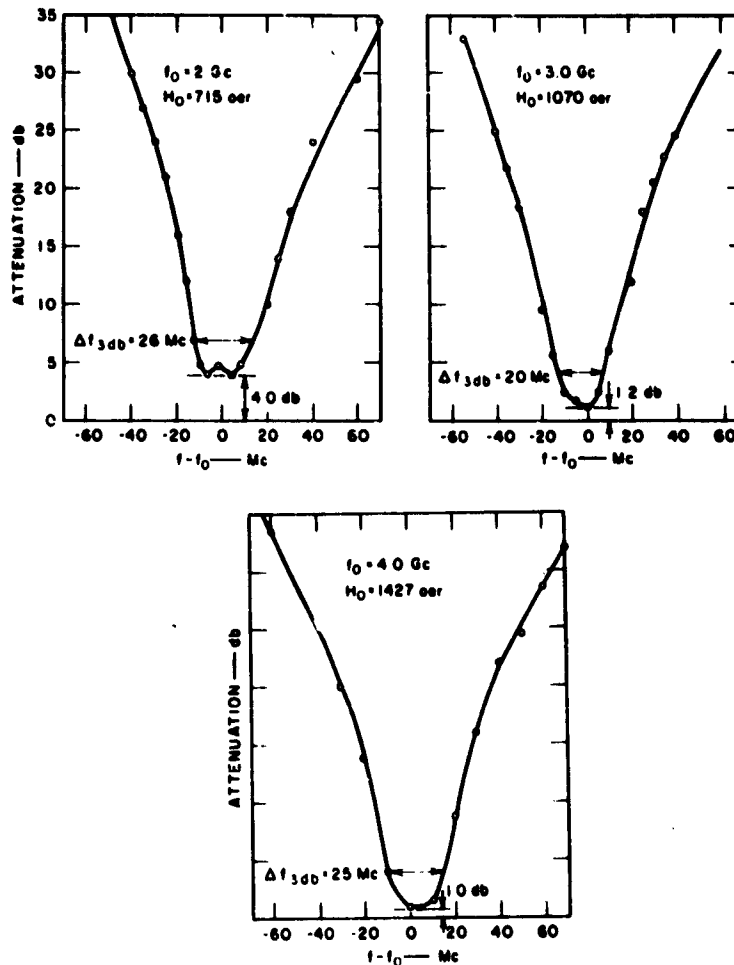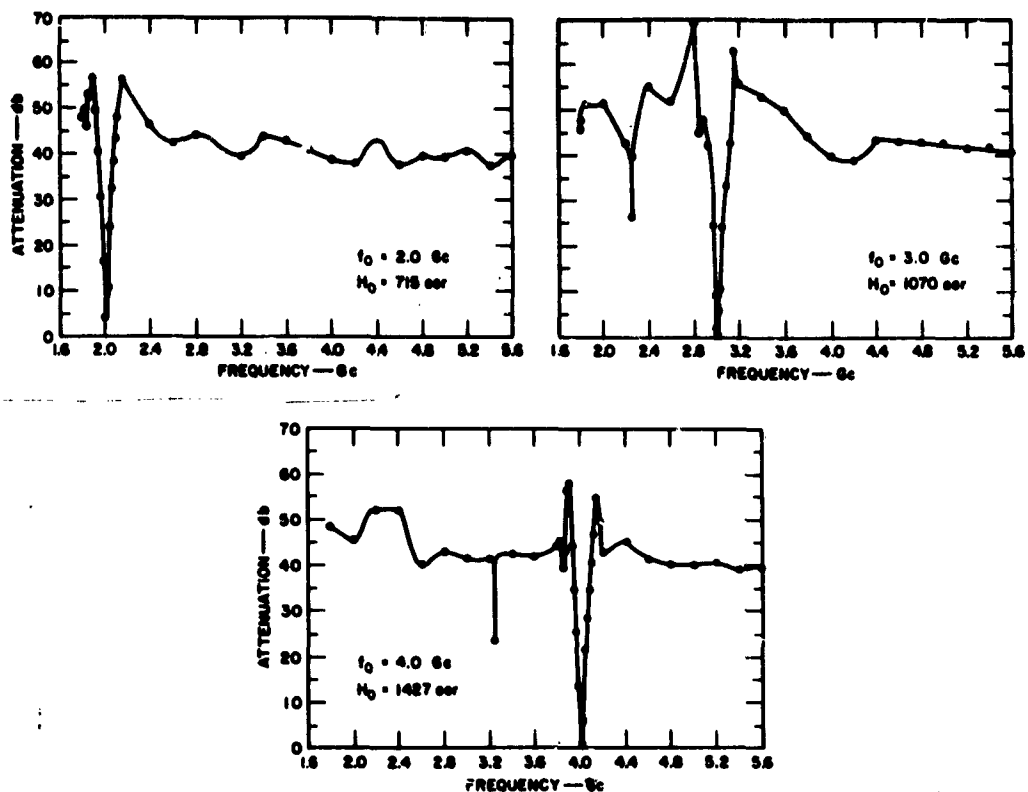ment with the conclusions listed at the end of Sec. 17.07.

FIG. 17.08-5   PASS-BAND CHARACTERISTICS OF THE TWO-RESONATOR
              FILTER SHOWN IN FIG. 17.08-3

1053

FIG. 17.08-6 STOP-BAND CHARACTERISTICS OF THE TWO-RESONATOR FILTER
SHOWN IN FIG. 17.08-3

One decided advantage of side-wall coupled filters of this type is
that they make possible the use of a magnet air gap of minimum size. A
more refined version of the filter in Fig. 17.08-3 has been built which
requires a magnet air gap of only 0.260 inch. This filter was constructed
to split in half horizontally in the plane of the strip-lines. The upper
and lower half were machined from separate blocks of brass, and the divid-
ing wall was machined integral with the rest of the structure.
Figure 17.08-7 shows this filter with half partially removed. The rec-
tangular tabs protruding from both sides of the middle of the filter
were included for possible use in mounting the filter in a magnet.

A Trial Three-Resonator YIG Filter—The filter in Fig. 17.08-3 was
modified to make it into a three-resonator filter of the form in

Fig. 17.07-4(b). This was done by removing the original dividing wall
and inserting the thicker wall shown in Fig. 17.08-8. Note that this
wall contains an additional 0.074-inch-diameter YIG sphere, and there
is also provision for rotating the added sphere about a [110] axis.
The height of the aperture in this dividing wall is 0.110 inch, the
same as the spacing d between the strip lines and the adjacent ground
planes. Thus, this third sphere will see boundary conditions very
similar to those seen by the spheres under the strip lines. The thick-
ness of the dividing wall was chosen so that the center-to-center spac-
ings of the three spheres would be the same as the center-to-center
spacings of the spheres in the two-resonator version. In order to
optimize the response shape, some adjustment of this spacing of the
spheres would be desirable, but the spacing used was found to give
reasonably good results. Figure 17.08-9 shows the assembled trial
three-resonator filter without a magnet.
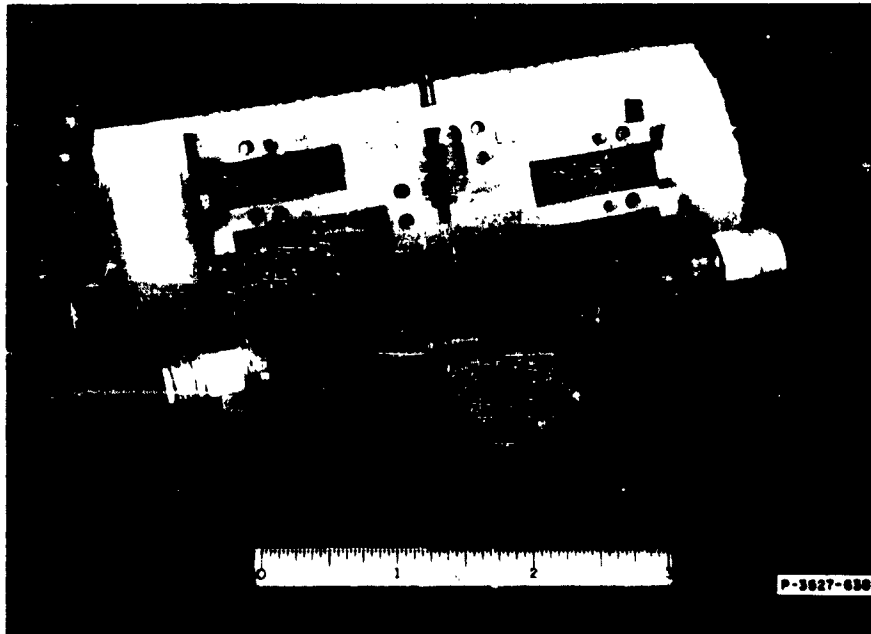
FIG. 17.08-7   A MORE REFINED VERSION OF THE FILTER SHOWN IN FIG. 17.08-3
WITH ITS UPPER HALF PARTIALLY REMOVED
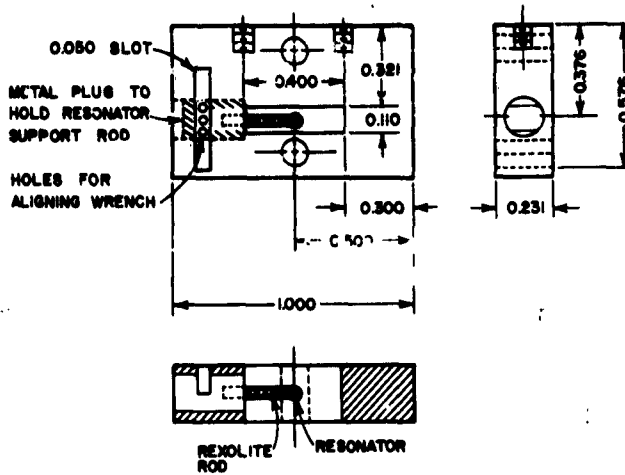This filter requires a magnet air gap of only 0.260 inch

1055

FIG. 17.08-8 DIVIDING WALL FOR THE THREE-RESONATOR
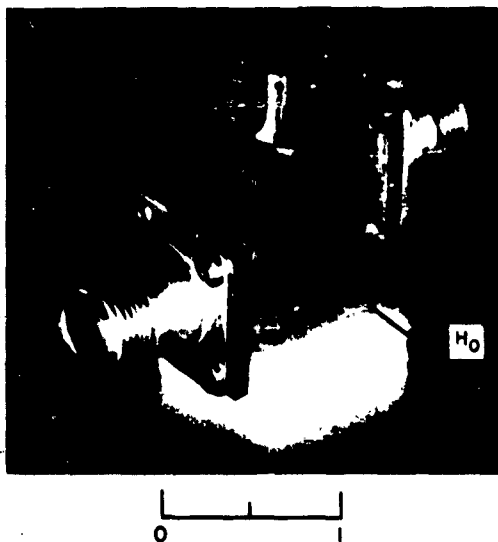VERSION OF THE FILTER SHOWN IN FIG. 17.08-3

FIG. 17.08-9 PHOTOGRAPH OF THE ASSEMBLED
THREE-YIG-RESONATOR FILTER
SHOWN WITHOUT A MAGNET
The required orientation of the biasing
field H_0 is indicated by an arrow.

The two end resonators were first tuned to be in about the middle of
their tuning range, when the filter was operated as a two-resonator filter.
The tuning rods were then cemented, and a third resonator was added and
tuned by rotating it so as to give a symmetrical response. In this type
of filter it would be desirable to adjust the resonators in such a way as
to be close to the orientation which would cancel out the temperature
effects of anisotropy. Otherwise, if all of the spheres do not have the
same orientations of the crystal axes, and if there are sizeable changes
in temperature, the resonators may suffer appreciable mistuning with re-
spect to each other.

Table 17.08-2 along with Figs. 17.08-10 and 17.08-11 show the measured
performance of the filter. The data in these figures were again taken by
holding the frequency constant
and varying the magnetic field.
This procedure is in most re-
spects equivalent to holding
the field constant and vary-
ing the frequency, and the
use of this procedure per-
mitted much more rapid test-
ing of the filter. Note
that the stop-band attenua-
tion level has been greatly
improved in this filter while
the pass-band attenuation has
been increased only a little.

Table 17.08-2

MEASURED CHARACTERISTICS OF THE THREE-RESONATOR
YIG FILTER SHOWN IN FIG. 17.08-9

f_c (Gc)	$(L_A)_{min}$ (db)	$\Delta f_{3 db}$ (Mc)	$\Delta f_{30 db}$ (Mc)	VSWR (minimum)	H_0 (oersteds)
2.0	3.5	32.9*	91.4	2.50	610
2.5	1.7	34.2	90.1	--	867.1
3.0	1.7	33.6	90.6	1.23	990
4.0	1.4	30.9	87.2	1.10	1310
4.5	1.6	24.0	89.1	--	1586.8
7.0	1.6	29.6	--	--	--

* The bandwidths given are measured to the 3-db or
30-db point below $(L_A)_{min}$.

One of the important things demonstrated by this trial three-resonator
filter is that the resonators can be kept in tune with each other as the
H_0-field is varied. An earlier trial three-resonator filter[4] was not so
successful in this regard. It is believed that the similar boundary con-
ditions seen by all three spheres in filters of the type in Fig. 17.07-4(b)
are important for maintaining synchronous tuning.

The 30-db bandwidth of the filter stays quite constant over the tuning
range, just as for the two-resonator version. The ratio of the 30-db band-
width to the 3-db bandwidth runs around 2.8 for the three-resonator filter
design as compared to around 5 for the two-resonator filter design. Al-
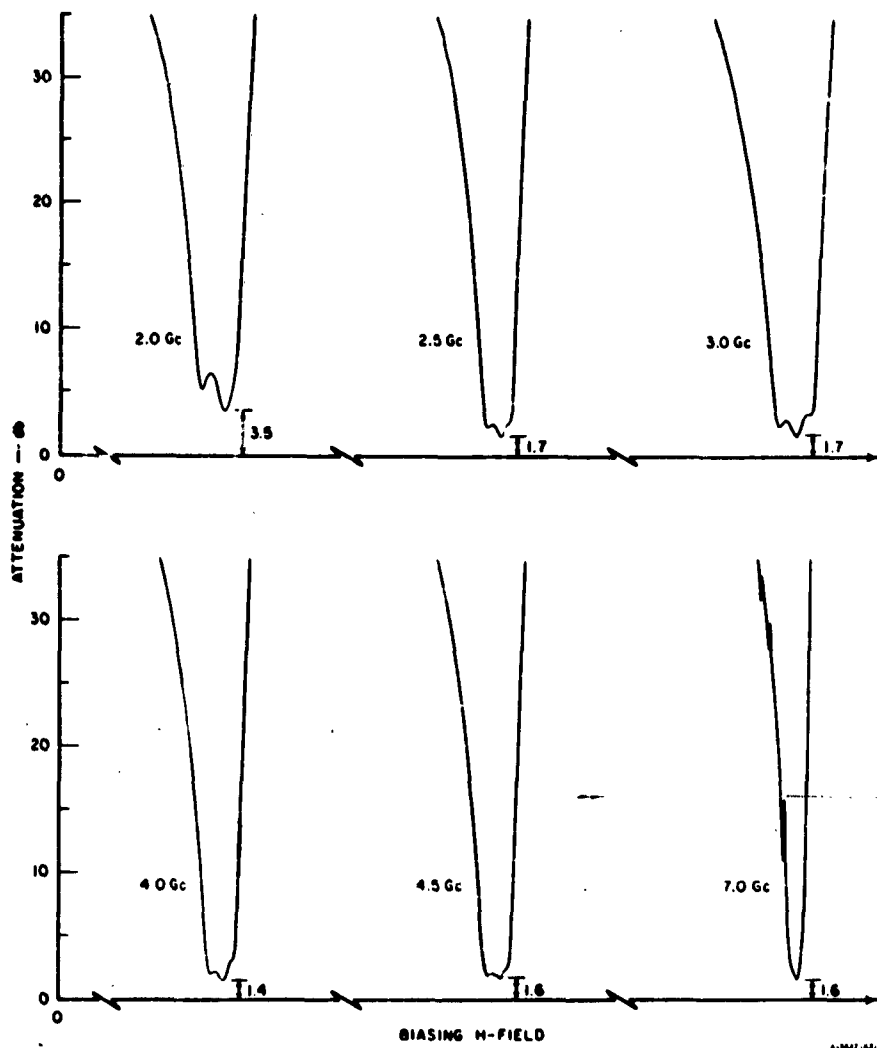though the cutoff rate was considerably sharper for the three-resonator

1057

FIG. 17.08-10 ATTENUATION vs. BIASING H-FIELD FOR THREE-YIG-RESONATOR
FILTER SHOWN IN FIG. 17.08-9
These curves were obtained using a recorder and a swept magnet
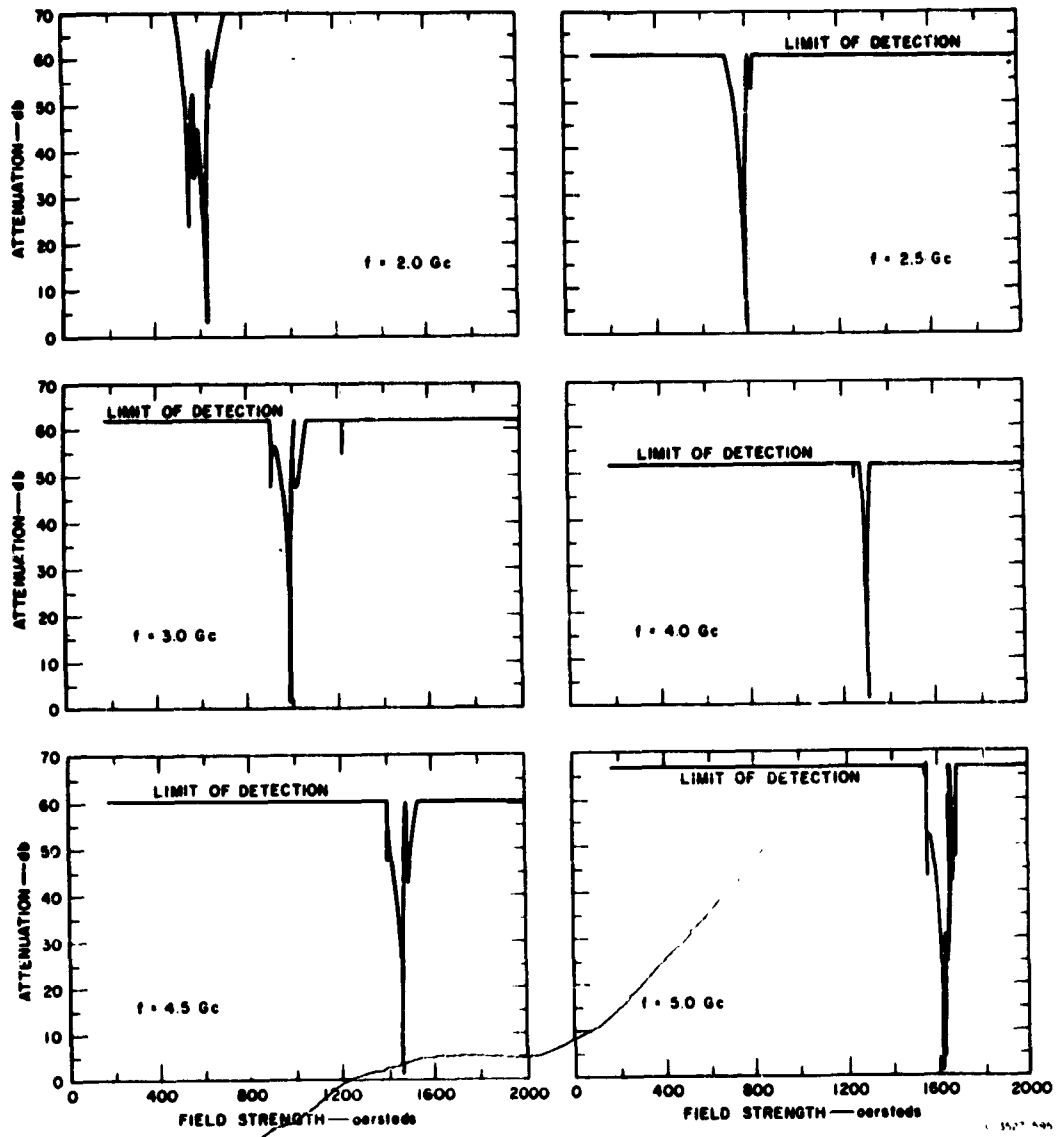power supply.

FIG. 17.08-11   THE STOP-BAND ATTENUATION CHARACTERISTICS vs. BIASING
H-FIELD FOR THE FILTER SHOWN IN FIG. 17.08-9

design, the performance of this particular filter was probably not optimum in this respect because of a small amount of mistuning and because no effort was made to optimize the shape of the pass-band response for this condition. Filters designed to correspond to equal-element prototypes (Sec. 11.07) would probably be desirable for most tunable filter applications. Such filters would result in very nearly minimum midband dissipation loss for a given specified 30-db (or other specified level) stop-bandwidth. In the case of the two- and three-resonator filters discussed herein, the three-resonator design has a 30-db bandwidth which is about 23 percent less than that for the two-resonator design, but with somewhat larger midband attenuation. Further optimization of the design to correspond to an equal-element prototype at a given tuning frequency, should make it possible to reduce the midband loss somewhat at least at that tuning frequency.

SEC. 17.09, MAGNETICALLY TUNABLE BAND-PASS FILTERS WITH
              WAVEGUIDE INPUTS AND OUTPUTS

Figure 17.09-1 shows a two-resonator waveguide filter which is analogous to the strip-line filter in Fig. 17.07-3. Ferrimagnetic resonator spheres are placed near short-circuit walls in the waveguides so that the spheres see strong magnetic fields. The spheres are coupled through an elongated coupling slot with its length parallel to the waveguide axes. With this orientation of the slot, there is very little coupling between guides except when resonance in the spheres is excited.
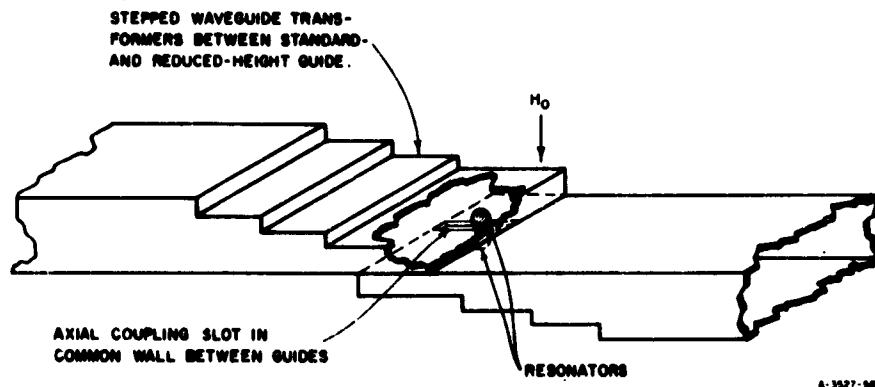

FIG. 17.09-1 TWO-RESONATOR FILTER USING OVERLAPPING WAVEGUIDES
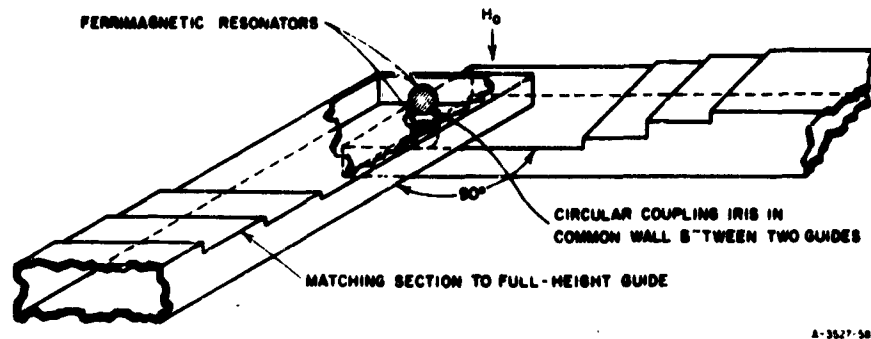   AND ELONGATED AXIAL COUPLING SLOT

FIG. 17.09-2 TWO-RESONATOR FILTER USING WAVEGUIDES AT RIGHT ANGLES
AND A CIRCULAR COUPLING IRIS

The spheres are placed in reduced-height waveguide in order to obtain
adequate coupling between the spheres and the waveguides, and also to
reduce the size of the magnet air gap required. Step transformers are
used to transform the impedance of the standard terminating guides to
that of the reduced-height guide sections.

Figure 17.09-2 shows another possible waveguide configuration, a
single-resonator version of which has been discussed by Kotzebue.[25] This
configuration differs from that in Fig. 17.09-1 mainly in that off-
resonance isolation is obtained in this case by using a round coupling
hole which will permit both linear components of the circularly polarized
fields generated by the spheres at resonance (see Sec. 17.05) to be
coupled from one sphere to the other. In this case the guides are placed
at right angles to each other in order to increase the off-resonance iso-
lation. With the guides so oriented, the filter will have the same attenu-
ation characteristic for both directions of transmission, but it will have
180 degrees more phase shift for one direction of transmission than for the
other.[6,3] In the case of the filter in Fig. 17.09-1, both the attenuation
and phase characteristics are independent of the direction of transmission.

The design process for a waveguide filter with ferrimagnetic reso-
nators closely parallels that for the strip-line cases discussed in
Sec. 17.07. Carter[3] has derived an equation for the external Q'of a ferri-
magnetic resonator mounted in waveguide, and this equation is given in
Fig. 17.09-3. In this equation λ_g is the guide wavelength, λ is the free-
space wavelength, a and b are guide dimensions indicated in the figure,

1061

Q_e   10000
8000   P-BAND, a=0.622in., b=0.311in.
6000   X-BAND, a=0.90in., b=0.40in.
5000
4000   C-BAND, a=1.872in., b=0.872in.
3000   S-BAND, a=2.84in., b=1.34in.

2000

$$Q_e = \frac{60\pi\,ab}{\mu_0\,\omega_m V_m}\left(\frac{\lambda_g}{\lambda}\right)$$

Q_e   1000
800

600
500
400   f = 7.5 Gc   f = 2.35 Gc
        8.2   2.65
300   10.0   3.00
        13.2   4.15
        f = 11.0 Gc   f = 3.6 Gc
200   13.0   4.0
        19.0   4.8
                            6.4

100
0.01   0.02 0.03 0.05 0.08 0.1   0.2   0.3   0.05   0.8 1.0
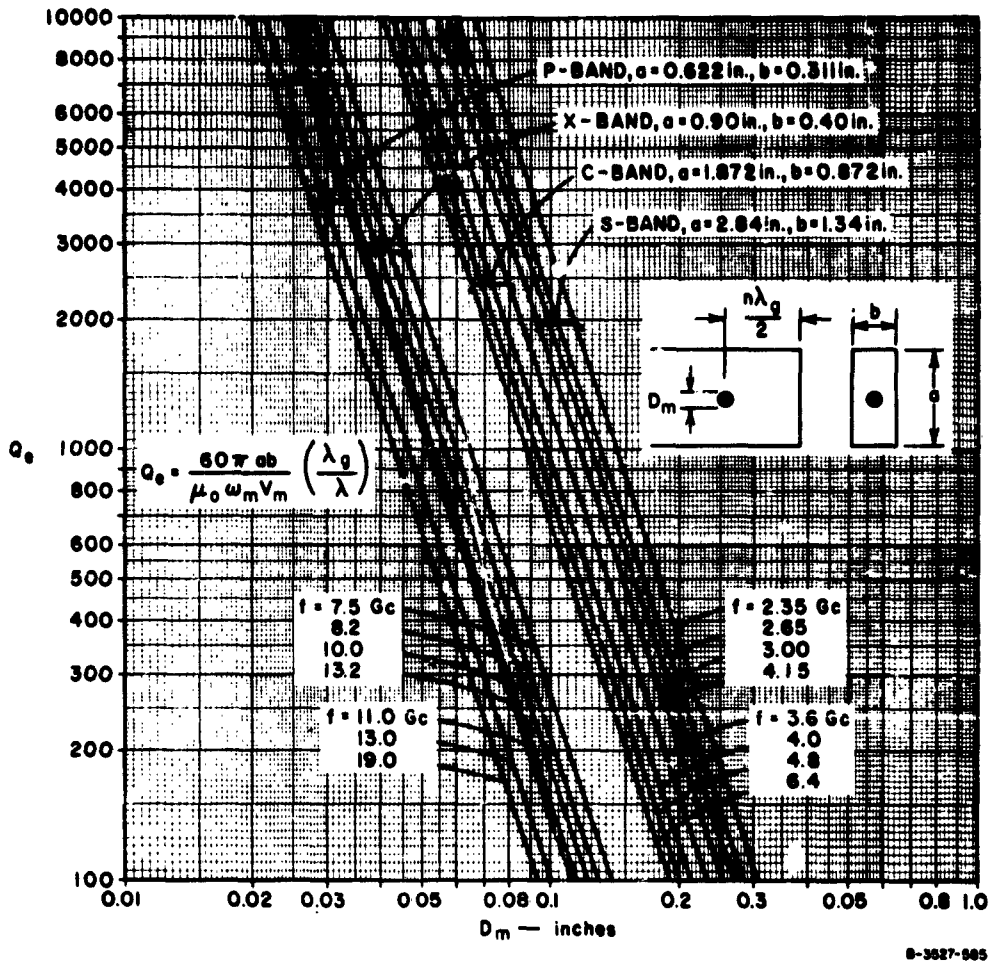
D_m — inches

B-3527-565

FIG. 17.09-3 Q_e vs. SPHERE DIAMETER OF SPHERICAL YIG RESONATOR LOCATED AT A
HIGH-CURRENT POSITION IN SHORT-CIRCUITED TE_{10} RECTANGULAR WAVEGUIDE
In the equation shown, μ_0 is the permeability of the region about the sphere,
$\omega_m = \gamma \mu_0 M_s$, $\gamma = 1.759 \times 10^{11}$ in mks units, and V_m is the volume of the sphere.

and the other parameters are the same as was discussed in connection with
Eqs. (17.07-1) and (17.07-2). Figure 17.09-3 also shows curves of Q_e
vs. sphere diameter for YIG spheres ($4\pi M_s = 1750$ gauss) in various standard
height waveguides. To scale the values of Q_e in Fig. 17.09-3 to correspond
to other than standard height waveguides use the relation

$$Q_e\big|_{b'} = Q_e\big|_b \frac{b'}{b} \qquad (17.09\text{-}1)$$

where b is the height of the standard guide, b' is the actual height to
be used, and $Q_e|_b$ and $Q_e|_{b'}$, are the external Q's for the guides of height
b and b', respectively. To scale data in Fig. 17.09-3 to correspond to
materials other than YIG use

$$Q'_e = Q_e \frac{M_s}{M'_s} \qquad (17.09\text{-}2)$$

where M_s/M'_s is the ratio of the saturation magnetization of YIG to that
of the material to be used, Q_e is the external Q for YIG as obtained from
Fig. 17.09-3, and Q'_e is the external Q for the ferrimagnetic material
actually used.

Figure 17.09-4 shows computed and measured data for the external Q
of YIG spheres in one-quarter height X-band waveguide. Notice that the
agreement between theory and experiment is quite good. However, as for
the strip-line cases discussed in Secs. 17.07 and 17.08, the presence of
an adjacent coupling hole or slot can be expected to increase the external
Q of a resonator, typically by a factor of 20 percent or somewhat more.

The determination of the proper spacing between spheres and the size
of the intervening coupling aperture can be determined as discussed in
Secs. 17.07 and 17.08. Approximate designs can be obtained by scaling
the sphere spacings and aperture sizes in the examples in Sec. 17.08,
using the principles discussed in Sec. 17.07. It is generally desirable
to make the aperture somewhat undersized to start out with (i.e., somewhat
narrow if it is an elongated slot), and then its size can be increased
until the desired pass-band shape (or coupling coefficient) is obtained.

As was discussed in Sec. 17.05, the coupling to magnetostatic modes
in a ferrimagnetic resonator tends to increase as the frequency increases.
The work of Fletcher and Solt[16] indicates that this coupling depends
strongly on the sphere diameter as compared to a wavelength. Thus, for
the same level of spurious-response activity, filters designed to operate
at X-band or higher should use smaller resonator spheres than filters
designed for S-band, if other factors are equal.
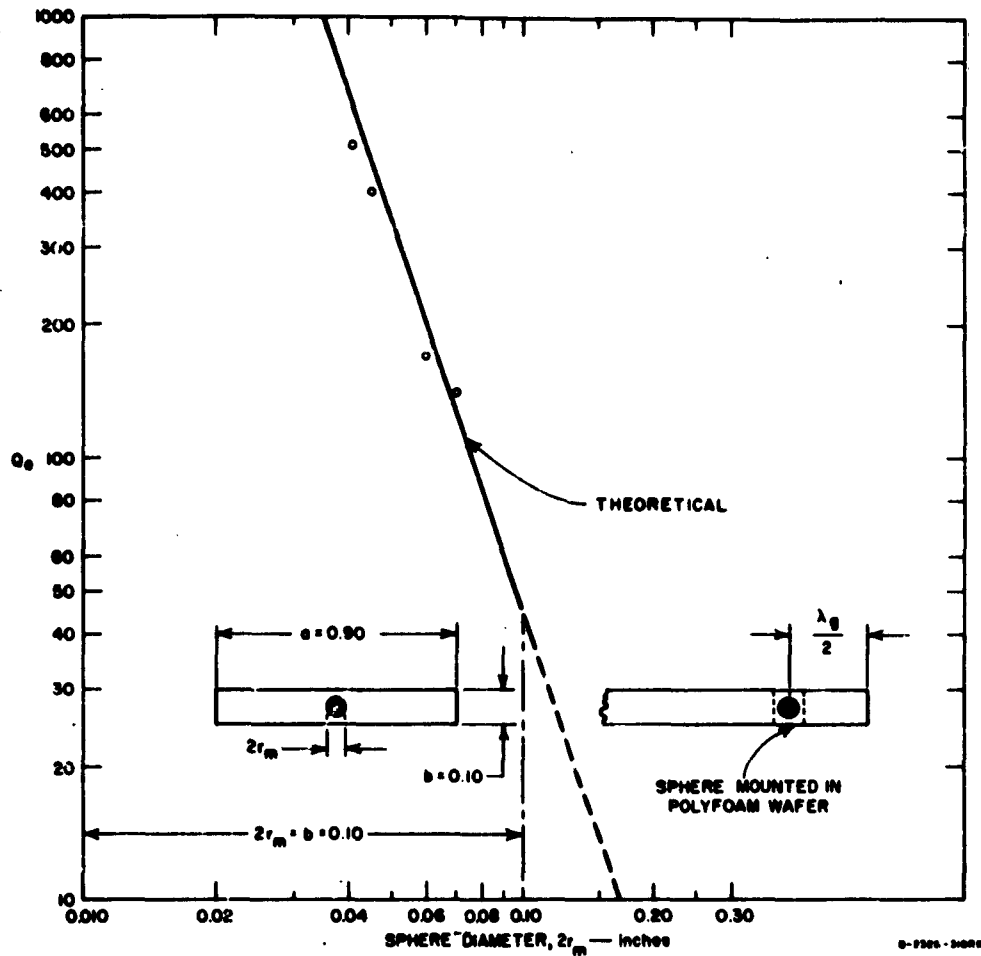
FIG. 17.09-4 THEORETICAL AND EXPERIMENTAL Q_e OF YIG RESONATORS IN REDUCED
(One-Quarter) HEIGHT, STANDARD-WIDTH X-BAND WAVEGUIDE AT 10 Gc

SEC. 17.10, MAGNETICALLY TUNABLE DIRECTIONAL FILTERS HAVING CIRCULATOR ACTION

Figure 17.10-1 shows a waveguide directional filter of a type dis-
cussed in Chapter 14. This filter uses cylindrical resonators with
circular apertures, which all together can propagate circularly polarized
TE_{11} modes at resonance. The first and last apertures are cut in the
adjacent TE_{10}-mode rectangular waveguide at points where the H-field is

1064

circularly polarized at the resonant frequency of the cavities. As a result of the circular polarization in the resonators and coupling apertures, when the cavities become resonant, power flows from Port 1 through the resonators and out Port 4, while in theory no power emerges from Port 2 or 3. Off of resonance all of the power flows straight through from Port 1 to Port 2. Figure 17.10-2 shows the measured attenuation characteristics for transmission from Port 1 to Ports 2, 3, and 4 for a two-resonator filter of the type in Fig. 17.10-1. The input VSWR at Port 1 is also shown. In theory this type of filter will always present a matched impedance looking into any one of its ports if the other three ports are terminated in waveguide loads of unity VSWR.
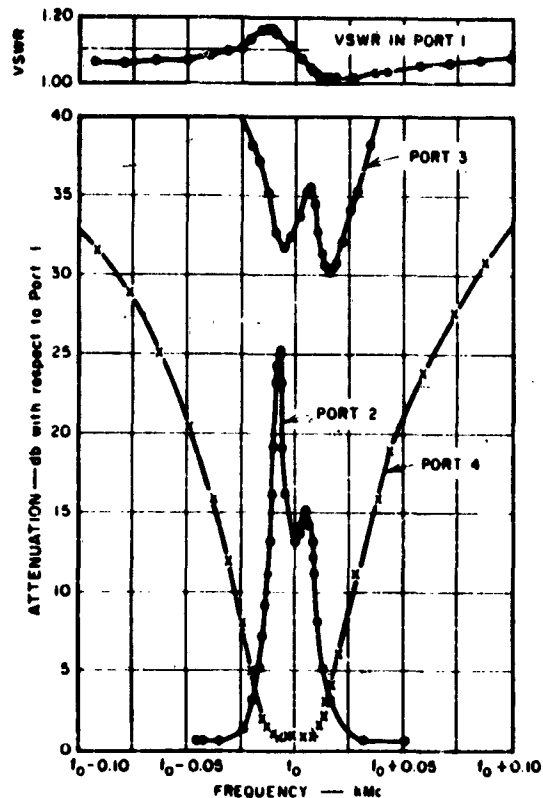
Figure 17.10-3 shows a magnetically tunable two-resonator directional filter which is potentially capable of producing the same attenuation characteristics shown in Fig. 17.10-2 when the input is at Port 1. As was indicated in the case of the filters in Figs. 17.09-1 and 17.09-2, the spherical YIG ferrimagnetic resonators are

FIG. 17.10-1 A TWO-RESONATOR, FIXED-TUNED WAVEGUIDE DIRECTIONAL FILTER

placed in reduced-height waveguide in order to increase the coupling between the waveguides and the spheres, and step transformers are used to match between the reduced-height guide and the standard height terminating guides. The YIG spheres are placed in the waveguide at points in the guides where the RF H-field will be circularly polarized. Now at ferrimagnetic resonance the circularly polarized RF H-field in the first guide will excite a strong circularly polarized magnetic moment in the first sphere (see Sec. 17.05). This magnetic moment will in turn produce an intense circularly polarized H-field which will couple through the circular aperture to the second sphere. An intense circular polarized magnetic moment will then be excited in the second sphere which will cause energy to be radiated out Port 4. Thus we see that the filter in

FIG. 17.10-2 MEASURED PERFORMANCE OF A
TWO-RESONATOR WAVEGUIDE
DIRECTIONAL FILTER OF THE
FORM SHOWN IN FIG. 17.10-1

Fig. 17.10-3 will operate essentially the same as the filter in
Fig. 17.10-1 when power is fed in Port 1. The main difference is that
the filter in Fig. 17.10-1 uses circularly polarized resonances in
electromagnetic resonators while the filter in Fig. 17.10-3 uses circu-
larly polarized resonances in *ferrimagnetic* resonators.

If power is fed into Port 4 of the filter in Fig. 17.10-1 it will
exhibit the same general transmission properties indicated in Fig. 17.10-2,
except for the curve marked for Port 4 now applies to Port 1, etc. This
is necessary since the filter in Fig. 17.10-1 is a reciprocal device.
However, as was noted in Sec. 17.05, ferrimagnetic resonators are not
reciprocal circuit elements. As a result, if power is fed into Port 4
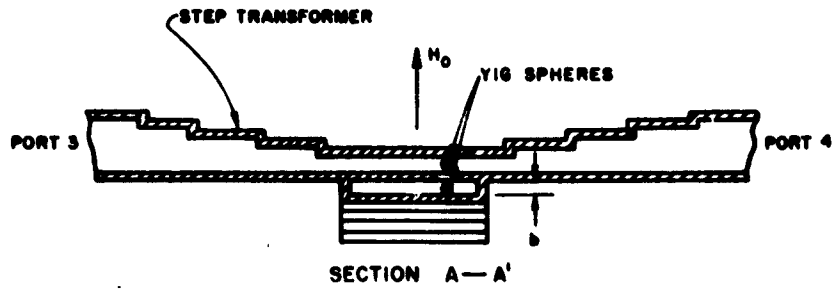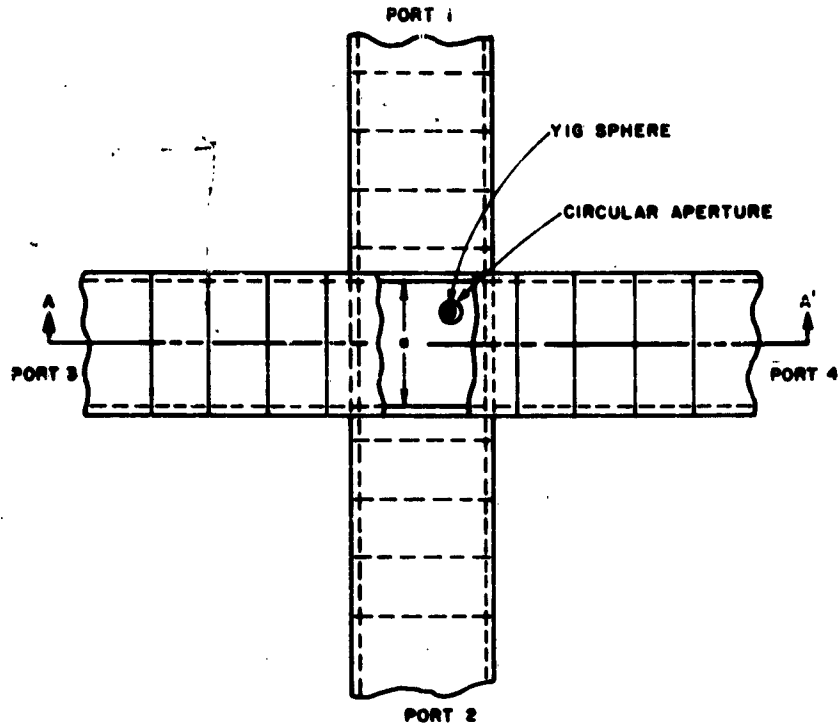
FIG. 17.10-3 A MAGNETICALLY TUNABLE DIRECTIONAL FILTER
THAT HAS CIRCULATOR ACTION

1867

of the filter in Fig. 17.10-3, the circularly polarized H-fields will have the wrong direction of polarization to excite resonance, and the power will emerge from Port 3 instead of going to Port 1 as it does in the case of the filter in Fig. 17.10-1. Thus, at resonance we can get transmission from Port 1 to Port 4, from Port 4 to Port 3, from Port 3 to Port 2, and from Port 2 to Port 1. Therefore at resonance this device can be used as a circulator. If the direction of the biasing H_0 field is reversed, then the directions for transmission at resonance would all be reversed, i.e., power could flow from Pu t 4 to Port 1 at resonance, etc. Thus, this device can also be used as a magnetically controlled switch.

The amount of reverse isolation between, say, Ports 4 and 1 at resonance depends on how nearly perfectly polarized the H-fields seen by the resonators are. For example, if the resonators are located at points in the waveguides so that they see elliptically polarized fields, if the main transmission is from Port 4 to Port 3 there will also be some transmission through the resonators to Port 1. This is because any elliptically polarized field can be regarded as being composed of two circularly polarized fields with opposite directions of rotation, and the component with the proper direction of circular polarization to excite the spheres will pass through to the other guide.

Patel[27] has made an extensive analysis of single-resonator filters of the type in Fig. 17.10-3. In his filters a single YIG sphere was so placed in the center of the coupling aperture between guides as to be half in the upper guide and half in the lower guide. Among other things, he made a study to determine the optimum location of the sphere in the waveguide to obtain the best possible circular polarization of the RF H-fields over a waveguide band. This is an important consideration since for any given position of the sphere, perfect circular polarization can only be obtained at one frequency, and it is desirable that the ellipticity of the H-fields at the upper and lower edges of the desired frequency tuning range be minimized. Patel's study shows that the optimum compromise location for the ferrimagnetic resonator is approximately $a/4$ from the side wall of the waveguide, where a is the width of the waveguide. Figure 17.10-4 shows experimental points and theoretical curves obtained by Patel for a single-resonator filter of the type in Fig. 17.10-3, which illustrates how the forward and reverse insertion loss at resonance vary. The upper dashed curve shows how the theoretical reverse isolation at
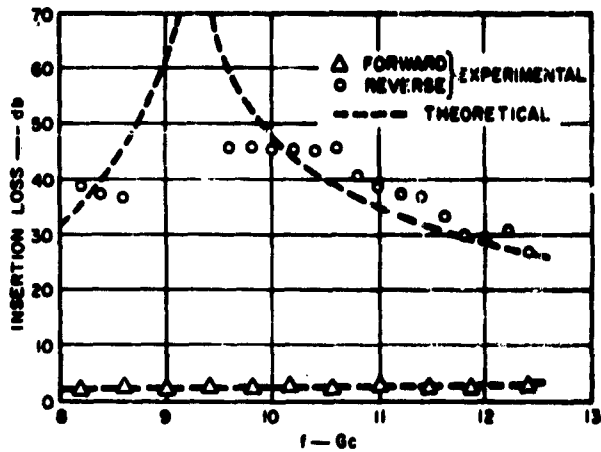
FIG. 17.10-4 THEORETICAL AND EXPERIMENTAL INSERTION LOSS IN
FORWARD DIRECTION (Port 1 to Port 4) AND REVERSE
DIRECTION (Port 4 to Port 1) FOR A SINGLE-RESONATOR
FILTER OF THE FORM SHOWN IN FIG. 17.10-3
The magnetic field was adjusted to give resonance at each
test frequency.

resonance varies as a function of the tuning frequency, as a result of
the ellipticity of the H-field polarization. Note that the theoretical
isolation goes to infinity at around 9.3 Gc where the polarization is
circular. The lower dashed curve shows the forward insertion loss at
resonance as the filter is tuned across the band. Even though, when the
H-field does not have perfect circular polarization, there will be some
leakage of power out Port 2 at resonance (when power is fed in Port 1),
this source of power loss is small, and the insertion loss indicated in
this figure is mostly due to dissipation loss in the resonator.

The design of magnetically tunable directional filters can be carried
out in much the same fashion as was described for the cases treated in
Secs. 17.07 to 17.09. Patel[27] gives, for the external Q of a ferrimagnetic
resonator in a directional filter, the formula

$$Q_e = \frac{Z_0}{\mu_0 \omega_m V_m (k_x^2 + k_y^2)}$$
(17.10-1)

1069

where in mks units $\omega_m = \gamma \mu_0 M_s$, $\gamma = 1.759 \times 10^{11}$, $\mu_0 = 1.256 \times 10^{-6}$ henry/meter, and M_s is the saturation magnetisation in ampere-turns/meter. [See Eqs. (17.05-3a,b) for conversion to other units.] The quantity V_s is the volume of the ferrimagnetic resonator and

$$k_x = \frac{\pi}{2a} \sin \frac{\pi x}{a} \qquad (17.10-2)$$

$$k_y = -\frac{\pi}{2a} \left(\frac{\lambda_s}{2a} \right) \cos \frac{\pi x}{a} . \qquad (17.10-3)$$

The ratio of $|k_x/k_y|$ is equal to the ratio of the RF H-field strength seen by the resonator in a direction transverse to the axis of the guide containing the resonator, to the RF H-field strength seen by the resonator in the direction parallel to the axis of the guide, while a is the width of the guide, x is the distance from the center of the resonator to the side of the guide, and λ_s is the guide wavelength. To give circularly polarized excitation of the resonator, $|k_x| = |k_y|$ is required.

Patel does not give an explicit definition of the guide impedance Z_0 in Eq. (17.10-1). However, it can be shown that for $x = a/2$ (which gives $k_x = \pi/2a$ and $k_y = 0$), Eq. (17.10-1) should reduce to Carter's equation shown in Fig. 17.09-3. Making use of this fact, we conclude that Eq. (17.10-1) can be restated as

$$Q_e = \frac{60 \pi a b}{\mu_0 \omega_m V_s \left[\left(\sin \frac{\pi x}{a} \right)^2 + \left(\frac{\lambda_s}{2a} \cos \frac{\pi x}{a} \right)^2 \right]} \left(\frac{\lambda_s}{\lambda} \right) . \qquad (17.10-4)$$

Using $x = a/4$, as appears to be desirable from Patel's work, and letting $\lambda_s/(2a) = 0.870$ as is typical for the center of a waveguide operating frequency band, then

$$Q_e = 1.14 \ (Q_e \text{ obtained using Fig. 17.09-3}). \qquad (17.10-5)$$

Thus, using Eq. (17.10-5), along with Fig. 17.09-3 used in the manner described in Sec. 17.09, the proper waveguide dimensions and sphere sizes required to give desired external Q values can be estimated. As was

discussed in Sec. 17.07, the presence of the coupling aperture between resonators will tend to raise the external Q somewhat (perhaps about 20 percent), so some allowance should be made for this fact when determining the sphere dimensions.

When the designer has determined the diameter of the ferrimagnetic resonators and the desired waveguide dimensions, if step transformers such as those shown in Fig. 17.10-3 are required, the desired design can be obtained using the data in Tables 6.02-2 through 6.02-5, and Tables 6.04-1 through 6.04-4. Correction for the fringing capacitances at the step discontinuities should be made using the procedure described in Sec. 6.08.

The required diameter of coupling aperture between resonators for a filter such as that in Fig. 17.10-3 can be determined experimentally by making the hole relatively small to start out with, and then increasing its size until desired shape of response is obtained. If the value of external Q for the resonators was chosen so as to correspond to a given low-pass prototype filter and a specified fractional bandwidth, then it should be possible to obtain the desired response shape and bandwidth by increasing the size of the coupling aperture between the resonators until the proper coupling coefficient is obtained between the resonators.

SEC. 17.11, MAGNETICALLY TUNABLE BAND-STOP FILTERS

Figure 17.11-1 shows a possible form of strip-line, magnetically tunable, band-stop filter having a narrow stop band with high attenuation.
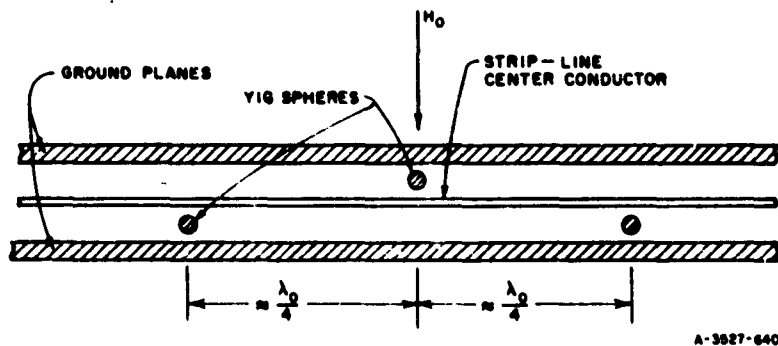

FIG. 17.11-1   A MAGNETICALLY TUNABLE STRIP-LINE
BAND-STOP FILTER
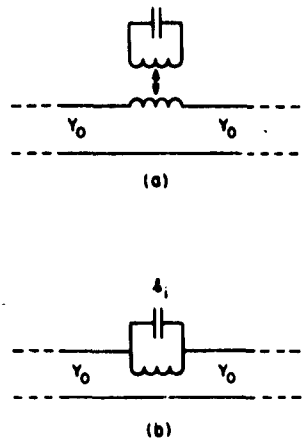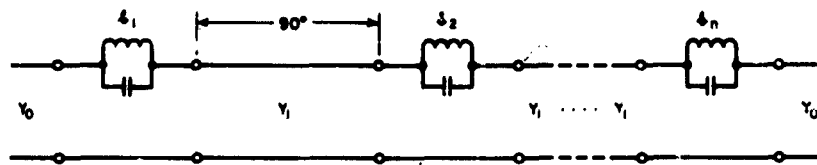
1071

(a)

(b)

A-3527-641

FIG. 17.11-2 EQUIVALENT CIRCUITS OF A
YIG SPHERE COUPLED TO A
STRIP LINE AS SHOWN IN
FIG. 17.11-1
In this figure resonator losses
are neglected

In this filter spheres of ferri-
magnetic material such as YIG
are placed between the strip-
line center conductor and an
adjacent ground plane, so that
the magnetic field about the
strip line will couple to the
spheres. Each sphere then has
mutual inductance coupling to
the transmission line as sug-
gested by the equivalent circuit
in Fig. 17.11-2(a). (Note that
this equivalent circuit neglects
resonator dissipation loss.)
When the signal frequency and
the biasing magnetic field
strength H_0 are proper to excite
resonance in the spheres the
equivalent circuit of the coupled resonator is as shown in Fig. 17.11-2(b),
where within practical limits the slope parameter b_i of the resonator can
be controlled by the choice of sphere diameter and by the magnitude of the
saturation magnetization of the ferrimagnetic material. The ferrimagnetic
resonators of the filter in Fig. 17.11-1 can be tuned by varying the biasing
magnetic field strength H_0. The second resonator is shown above the strip-
line while its neighbors are shown below the strip-line in order to minimize
possible undesirable interaction between resonators. Whether this is neces-
sary or not will depend on the relative size of the spheres and of the ground-
plane spacing as compared to the wavelengths in the operating frequency range.

From the equivalent circuit in Fig. 17.11-2(b) it is seen that the mag-
netically tunable filter under consideration is of the type discussed in
Sec. 12.04 and shown in Fig. 12.04-2, which is repeated in Fig. 17.11-3.
Filters designed from the data in Fig. 17.11-3 will usually be most practical
if they are designed to have a constant main-line characteristic admittance
which equals the termination admittance Y_0. Under this condition, in
Fig. 17.11-3(a)

$$Y_0 = Y_1 = \frac{1}{g_0 g_{n+1}} , \qquad (17.11-1)$$

1072

$$\frac{\ell_i}{Y_0} = \frac{1}{\omega_1' g_0 g_1 w}$$
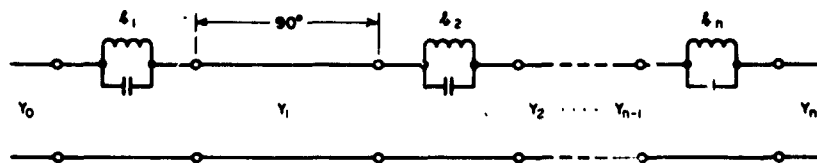
$$\frac{\ell_i}{Y_0}\bigg|_{i=even} = \left(\frac{Y_1}{Y_0}\right)^2 \frac{g_0}{\omega_1' g_i w}$$

$$\frac{\ell_i}{Y_0}\bigg|_{i=odd} = \frac{1}{\omega_1' g_0 g_i w}$$

If $n = even$, $\left(\frac{Y_1}{Y_0}\right)^2 = \frac{1}{g_0 g_{n+1}}$

If $n = odd$, $Y_1 = Y_0$

(a)

$$\frac{\ell_i}{Y_0} = \frac{1}{\omega_1' g_0 g_1 w}$$

$$\frac{\ell_i}{Y_0}\bigg|_{i=even} = \left(\frac{Y_1 Y_3 \ldots Y_{i-1}}{Y_0 Y_2 \ldots Y_{i-2}}\right)^2 \frac{g_0}{\omega_1' g_i w}$$

$$\frac{\ell_i}{Y_0}\bigg|_{\substack{i=odd \\ i \neq 1}} = \left(\frac{Y_2 Y_4 \ldots Y_{i-1}}{Y_1 Y_3 \ldots Y_{i-2}}\right)^2 \frac{1}{\omega_1' g_0 g_i w}$$

If $n = even$, $\frac{Y_0}{Y_n} = \left(\frac{Y_0 Y_2 \ldots Y_{n-2}}{Y_1 Y_3 \ldots Y_{n-1}}\right)^2 \frac{1}{g_0 g_{n+1}}$, or

If $n = odd$, $\frac{Y_0}{Y_n} = \left(\frac{Y_1 Y_3 \ldots Y_{n-2}}{Y_2 Y_4 \ldots Y_{n-1}}\right)^2 \frac{g_0}{g_{n+1}}$

(b)

B-3527-229

FIG. 17.11-3 BAND-STOP FILTER WITH SERIES BRANCHES AND QUARTER-WAVE COUPLINGS: (a) EQUAL LINE ADMITTANCES, Y_1; (b) GENERAL CASE OF UNEQUAL CONNECTING-LINE ADMITTANCES

1073

a condition which is obtained for any of the maximally flat low-pass prototypes in Sec. 4.05, or for any of the Tchebyscheff prototypes having n odd in that section. Using the data in Fig 17.11-3(a) the normalized resonator slope parameters b_j/Y_0 can be calculated, where in the figure w is the fractional bandwidth of the stop band to the band-edge points corresponding to ω_1' for the low-pass prototype (see Sec. 12.?)

After the normalized resonator slope parameters b_j/Y_0 have been computed, the required ferrimagnetic resonator parameters can be computed by use of data given earlier in this chapter. Note in Fig 1 11.2 that if a short-circuit were placed across the transmission line just to the right side of the resonator, assuming that the line to the left the resonator is terminated in its characteristic admittance Y_0, the Q of the circuit would be

$$ (Q_e) . \qquad \frac{b_j}{Y_0} \qquad\qquad (17.11-2) $$

Note that operating the resonators in the circuit in Fig 17.11.1 individually with a short circuit at one side of the sphere under test, and with a matched transmission line at the other side, is exactly the condition under which the external Q data in Fig 17.07-6 and Eqs. (17.07-3) and (17.07-4) apply. Thus, using the reference external Q values given by Eq. (17.11-2) along with the data in Sec 17.07, the required resonator diameters for given M_s values can be determined. If the unloaded Q's of the resonators are known, the peak stop-band attenuation of the filter can be computed by use of the data in Sec 12.03. If the unloaded Q's are not known, they can be measured by placing the resonator spheres one at a time in a short-circuited strip-line structure close to or at a short circuit and making measurements as described in Sec 11.? This procedure can, of course, also provide an experimental verification of (Q_e).

One obvious disadvantage of the type of filter in Fig 17.11.1 is that its design is based on the assumption that its resonators are spaced a quarter-wavelength at resonance. If the filter is tuned over a very large range its response may deviate appreciably from the ideal since the resonator spacings are $\Lambda_0/4$ at only one frequency. The most serious effect may be that the peak attenuation might fall below acceptable levels in some parts of the tuning range. However, if the performance requirements are not very severe, or if the tuning range is relatively small, filters of the type in Fig. 17.11.1 may be quite satisfactory

1074

BROADBAND
TRANSFORMER
SECTION

GARNET SPHERES   (a) SIDE VIEW
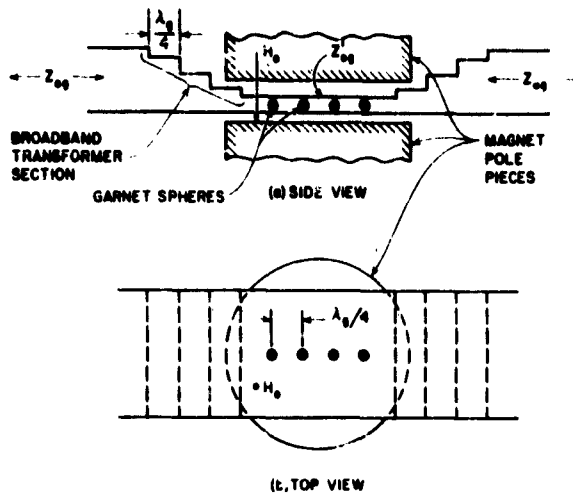
MAGNET
POLE
PIECES

(b) TOP VIEW

FIG. 17.11-5   A FOUR-RESONATOR MAGNETICALLY
TUNABLE WAVEGUIDE BAND-STOP
FILTER

Though a detailed design procedure for filters of the type in
Fig. 17.11-4 has not been worked out at the time of this writing, the
design equations in Fig. 17.11-3(b) should prove helpful. The quarter-
wavelength connecting lines of admittance Y_i operate as impedance in-
verters (Sec. 8.03) having inverter parameter $K_i = 1/Y_i$. The equations
in Fig. 17.11-3(b) allow for a range of choice for these inverter param-
eters. Now by Fig. 8.03-1(d) we see that a length of line with a shunt
capacitor in the middle can operate as an impedance inverter. Thus, for
purposes of determining the proper sphere sizes, etc., the circuits be-
tween spheres in Fig. 17.11-4 can be characterized in terms of impedance
inverters of the form in Fig. 8.03-1(d). After the designer has worked
out the basic low-pass filter structure design he can compute values for
the K_i and $Y_i = 1/K_i$. Then the equations in Fig. 17.11-3(b) can be used
to compute the required normalized resonator slope parameters. Finally,
the required sphere sizes can be computed from the b_i/Y_0 by procedures
such as were discussed above.

The discussion in this section has so far been phrased in terms of
strip-line structures. However, the same principles also will apply to
the design of waveguide band-stop filters. Figure 17.11-5 shows a multi-
resonator waveguide band-stop filter. Judging from experience with

1076

cavity-type waveguide band-stop filters (Sec. 12.08), some difficulty might be expected due to coupling directly from one resonator to the next. In order to avoid this problem, the waveguide height and sphere size should both be kept very small compared to one-quarter wavelength. It should be possible to design waveguide filters of the form in Fig. 17.11-5 using the same procedure described for the filter in Fig. 17.11-1 except that Fig. 17.09-3 and Eqs. (17.09-1) and (17.09-2) should be used in place of Fig. 17.07-6 and Eqs. (17.07-3) and (17.07-4).

Waveguide filters analogous to the strip-line filter in Fig. 17.11-4 are also possible. These filters could take the general form of the corrugated waveguide filters discussed in Sec. 7.04, with YIG spheres inserted in the high-impedance sections of the corrugations.

REFERENCES

1. Harvard Univ. Radio Research Laboratory Staff, *Very High-Frequency Techniques*, McGraw-Hill Book Co., Inc., New York (1947), pp. 769-795.

2. R. L. Sleven, "Design of a Tunable Multi-Cavity Waveguide Band-Pass Filter," *1959 IRE National Convention Record*, Part 3, pp. 91-112.

3. G. L. Matthaei, ..., P. S. Carter, Jr., *et al.*, "Design Criteria for Microwave Filters and Coupling Structures," Chap. 28, Final Report, SRI Project 2326, Contract DA 36-039 SC-74862, Stanford Research Institute, Menlo Park, California (January 1961). An abbreviated version of this material will be found in the paper: P. S. Carter, Jr., "Magnetically Tunable Microwave Filters Using Single-Crystal Yttrium-Iron-Garnet Resonators," *IRE Trans. PGMTT*-9, pp. 252-260 (May 1961).

4. P. S. Carter, Jr., L. Young, G. L. Matthaei, and E. M. T. Jones, "Microwave Filters and Coupling Structures," Third Quarterly Progress Report, Part II, SRI Project 3527, Contract DA 36-039 SC-87398, Stanford Research Institute, Menlo Park, California (October 1961).

5. G. L. Matthaei, Leo Young, and P. S. Carter, Jr., "Microwave Filters and Coupling Structures," Fifth Quarterly Progress Report, Part IV, SRI Project 3527, Contract DA 36-039 SC-87398, Stanford Research Institute, Menlo Park, California (May 1962).

6. B. M. Schiffman, P. S. Carter, Jr., and G. L. Matthaei, "Microwave Filters and Coupling Structures," Seventh Quarterly Progress Report, Part III, SRI Project 3527, Contract DA 36-039 SC-87398, Stanford Research Institute, Menlo Park, California (October 1962).

7. J. Smit and H. P. Wijn, *Ferrites*, John Wiley and Sons, Inc., New York (1959).

8. R. F. Soohoo, *Theory and Application of Ferrites*, Prentice-Hall, Inc., Englewood Cliffs, N. J. (1960).

9. P. S. Carter, Jr., and C. Flammer, "Unloaded Q of Single Crystal Yttrium-Iron-Garnet Resonators as a Function of Frequency," *IRE Trans. PGMTT*-8, pp. 570-571 (September 1960).

10. D. Douthett and I. Kaufman, "The Unloaded Q of a YIG Resonator from X-Band to 4 Millimeters," *IRE Trans. PGMTT*-9, pp. 261-262 (May 1961).

11. J. W. Nielsen, D. A. Lepore, J. Zaeimer, and G. B. Townsend, "Effect of Mechanical, Thermal, and Chemical Treatment of the Ferrimagnetic Resonance Linewidth on Lithium Ferrite Crystals," *Jour. Appl. Phys.*, Vol. 33S, pp. 1379S-1380S (March 1962).

12. C. R. Buffler, "Resonance Properties of Single-Crystal Hexagonal Ferrites," *Jour. Appl. Phys.*, Vol. 33S, pp. 1360S-1362S (March 1962).

13. J. E. Artman, "Microwave Resonance Relations in Anisotropic Single Crystal Ferrites," *Proc. IRE*, Vol. 44, pp. 1284-1293 (October 1956).

14. J. F. Dillon, Jr., "Ferrimagnetic Resonance in Yttrium Iron Garnet," *Phys. Rev.*, Vol. 105, Second Series, pp. 759-760 (January 15, 1957).

15. C. Kooi, D. Stinson, R. Moss, F. Bradley, L. Freiberg, "Microwave Ferrites," Report LMSD-5036, Lockheed Missile Systems Division, Sunnyvale, California (1 July 1958).

16. E. G. Spencer, R. C. LeCraw, and R. C. Linares, Jr., "Low-Temperature Ferromagnetic Relaxation in Yttrium Iron Garnet," *Phys. Rev.*, Vol. 123, Second Series, pp. 1937-1938 (September 15, 1961).

17. P. C. Fletcher and R. O. Bell, "Ferrimagnetic Resonance Modes in Spheres," *Jour. Appl. Phys.*, Vol. 30, pp. 687-698 (May 1959).

18. P. C. Fletcher and I. H. Solt, Jr., "Coupling of the Magnetostatic Modes," *Jour. Appl. Phys.*, Vol. 30, pp. 181S-182S (April 1959).

19. H. Suhl, "The Nonlinear Behavior of Ferrites at High Microwave Signal Levels," *Proc. IRE*, Vol. 44, pp. 1270-1284 (October 1946).

20. R. W. DeGrasse, "Low-Loss Gyromagnetic Coupling Through Single Crystal Garnets," *J. Appl. Phys.* Vol. 30, pp. 155S-156S (April 1959).

21. F. J. Sansalone and E. G. Spencer, "Low-Temperature Microwave Power Limiter," *IRE Trans.* MTT-9, pp. 272-273 (May 1961).

22. F. C. Rossol, "Power Limiting in the 4 kMc to 7 kMc Frequency Range Using Lithium Ferrite," *Proc. IRE*, Vol. 49, p. 1574 (October 1961).

23. F. R. Arams, M. Grace, and S. Okwit, "Low-Level Garnet Limiters," *Proc. IRE*, Vol. 49, pp. 1308-1313 (August 1961).

24. Martin Auer, "Novel Method to Orient Ferrimagnetic Single-Crystal Spheres," *IRE Trans.* PGMTT-10, p. 88 (January 1962).

25. K. L. Kotzebue, "Broadband Electronically-Tunable Microwave Filters," *1960 IRE WESCON Convention Record*, Part 1, pp. 21-27.

26. P. S. Carter, Jr., G. L. Matthaei, and W. J. Getsinger, "Design Criteria for Microwave Filters and Coupling Structures," Technical Report 8, Part II, SRI Project 2326, Contract DA 36-039 SC-74862, Stanford Research Institute, Menlo Park, California (October 1959).

27. C. N. Patel, "Magnetically Tunable Nonreciprocal Band-Pass Filters Using Ferrimagnetic Resonators," *IRE Trans.* PGMTT-10, pp. 152-161 (May 1962).

28. Y. Sato and P. S. Carter, Jr., "A Device for Rapidly Aligning and Mounting Ferromagnetic Single Crystals Along any Desired Axis," *IRE Trans.* PGMTT-10, pp. 611-612 (November 1962).

29. B. Lax and K. J. Button, *Microwave Ferrites and Ferrimagnetics*, McGraw-Hill Book Co., Inc., New York (1961).

DISTRIBUTION LIST

ORGANIZATION	NO. OF COPIES	ORGANIZATION	
OASD (R & E) Attn: Technical Library Room 3E1065 The Pentagon Washington 25, D.C.	1	Commanding Officer Harry Diamond Laboratories Attn: Library, Room 211, Building 92 Washington 25, D.C.	1
Chief of Research and Development OCS, Department of the Army Washington 25, D.C.	1	Corps of Engineers Liaison Office U.S. Army Electronics Research and Development Laboratory Fort Monmouth, New Jersey	
Commanding General U.S. Army Materiel Command Attn: R & D Directorate Washington 25, D.C.	1	AFSC Scientific/Technical Liaison Office U.S. Naval Air Development Center Johnsville, Pennsylvania	1
Commanding General U.S. Army Electronics Command Attn: AMSEL-AD Fort Monmouth, New Jersey	1	Commanding Officer U.S. Army Electronics Materiel Support Agency Attn: SELMS-ADJ Fort Monmouth, New Jersey	

Director, U.S. Naval Research
  Laboratory
Attn: Code 2027
Washington 25, D.C.
	1	Marine Corps Liaison Office
		U.S. Army Electronics Research and
		  Development Laboratory
		Attn: SELRA/LNR	

Commander, Aeronautical Systems Division Attn: ASAPRL Wright-Patterson Air Force Base, Ohio	1	Fort Monmouth, New Jersey	

		Commanding Officer
		U.S. Army Electronics Research and
		  Development Laboratory
		Attn: Director of Research or
		  Engineering
		Fort Monmouth, New Jersey	

Hq, Electronic Systems Division Attn: ESAL L. G. Hanscom Field Bedford, Massachusetts	1		

Commander, Air Force Cambridge
  Research Laboratories
Attn: CRO
L. G. Hanscom Field
Bedford, Massachusetts
	1	Commanding Officer
		U.S. Army Electronics Research and
		  Development Laboratory
		Attn: Technical Documents Center
		Fort Monmouth, New Jersey	

Commander, Air Force Command and
  Control Development Division
Attn: CRZC
L. G. Hanscom Field
Bedford, Massachusetts
	1	Commanding Officer
		U.S. Armay Electronics Research and
		  Development Laboratory
		Attn: SELRA/ADJ (FU #1)
		Fort Monmouth, New Jersey	

Commander, Rome Air Development Center Attn: RAALD Griffiss Air Force Base, New York	10	Advisory Group on Electron Devices 346 Broadway New York 13, New York	
Commander, Armed Services Technical Attn: TISIA Arlington Hall Station Arlington 12, Virginia	2	Commanding Officer U.S. Army Electronics Research and Development Laboratory Attn: SELRA/TNR Fort Monmouth, New Jersey	
Chief, U.S. Army Security Agency Arlington Hall Station Arlington 12, Virginia		1 (FOR RETRANSMITTAL TO ACCREDITED BRITISH AND CANADIAN GOVERNMENT REPRESENTATIVES)	
Deputy President U.S. Army Security Agency Board Arlington Hall Station Arlington 12, Virginia			